Chem Soc Rev

ROYAL SOCIETY OF CHEMISTRY

REVIEW ARTICLE

View Article Online
View Journal

Cite this: DOI: 10.1039/d0cs00239a

Naphthalene diimides: perspectives and promise

Sheshanath V. Bhosale, *[a] Mohammad Al Kobaisi,[b] Ratan W. Jadhav,†[a] Pranay P. Morajkar, †[a] Lathe A. Jones †[b] and Subi George [c]

In this review, we describe the developments in the field of naphthalene diimides (NDIs) from 2016 to the presentday. NDIs are shown to be an increasingly interesting class of molecules due to their electronic properties, large electron deficient aromatic cores and tendency to self-assemble into functional structures. Almost all NDIs possess high electron affinity, good charge carrier mobility, and excellent thermal and oxidative stability, making them promising candidates for applications in organic electronics, photovoltaic devices, and flexible displays. NDIs have also been extensively studied due to their potential real-world uses across a wide variety of applications including supramolecular chemistry, sensing, host–guest complexes for molecular switching devices, such as catenanes and rotaxanes, ion-channels, catalysis, and medicine and as non-fullerene accepters in solar cells. In recent years, NDI research with respect to supramolecular assemblies and mechanoluminescent properties has also gained considerable traction. Thus, this review will assist a wide range of readers and researchers including chemists, physicists, biologists, medicinal chemists and materials scientists in understanding the scope for development and applicability of NDI dyes in their respective fields through a discussion of the main properties of NDI derivatives and of the status of emerging applications.

Received 12th April 2021

DOI: 10.1039/d0cs00239a

rsc.li/chem-soc-rev

1 Introduction

Innovation in organic materials science is becoming an increasingly important tool to address important worldwide problems in broad areas such as energy, materials science, the environment, and biomedicine. As such, the synthesis of new organic functional molecules and their adaptation for high

[a] School of Chemical Sciences, Goa University, Taleigao Plateau, Goa-403 206, India. E-mail: svbhosale@unigoa.ac.in
[b] Centre for Advanced Materials and Industrial Chemistry (CAMIC), School of Science, RMIT University, GPO Box 2476, Melbourne, Victoria 3001, Australia
[c] New Chemistry Unit (NCU), Jawaharlal Nehru Centre for Advanced Scientific Research (JNCASR), Jakkur PO, Bangalore-560064, India
† These authors contributed equally.

Sheshanath V. Bhosale

Professor Sheshanath V. Bhosale completed his doctorate degree in supramolecular chemistry under the supervision of Prof. J. H. Fuhrhop from Freie University, Berlin, Germany. He pursued his postdoctoral studies with Prof. S. Matile at the University of Geneva, Switzerland, under the auspices of a Roche Foundation Fellowship. This was followed by a stay at Monash University, Australia, for five years as an ARC-APD Fellow. He worked at RMIT University, Melbourne as an ARC-Future Fellow. Currently, he is working at Goa University, India as a UGC-FRP Professor. His research interest is in the synthesis of π-functional materials for sensing, biomaterials and supramolecular chemistry applications.

Mohammad Al Kobaisi

Dr Mohammad Al Kobaisi was born in 1971 in Iraq and received his PhD under the supervision of A/Prof. Colin Rix and Prof. David Mainwaring from RMIT University in 2007, investigating the design of selective adsorbent polymers for sensing applications. Currently, he is a senior researcher at Swinburne University of Technology. His main interest is in materials engineering, especially biopolymer hydrogels in drug delivery and vaccine formulation. He also collaborates in the field of functional organic materials in photonic sensing and supramolecular self-assembly.

performance materials has continued to gain traction in the last few decades. Several key classes of molecules have been synthesised to this end based on the diimide structure, as the nitrogen functionality in conjunction with aromatic linkers and functional groups enables the introduction of functional properties to a vast family of derivatives for applications that span modern materials science and applied chemistry. In the last three decades, rylene diimides (RDIs) (**1**) have become one of the most important classes of compounds for these applications.[1] There are various classes of RDIs, such as pyromellitic diimides (PMIs), 1,4,5,8-naphthalenediimides (NDIs) (also known as naphthalene carbodiimides) (**2**), perylene tetracarboxylic diimides (PDIs) (**3**) and other larger diimides (Fig. 1).[2]

NDIs have been shown to be the most interesting class of molecules due in part to the electronic properties of the large electron deficient aromatic core, which is supplemented by an ability to self-assemble into structures through non-covalent interactions.[3] This has allowed NDI derivatives to be utilised as functional materials, as their electronic and physical properties are more suited to applications than PMIs and PDIs, and multiple properties including solubility and electronic and supramolecular behaviour can be controlled through functionlization.[4]

NDIs substituted at the diimide nitrogen are often used as electron acceptors and as supramolecular building blocks for molecular assemblies and supramolecular arrays.[5] For example, *N*-functionalisation at the diimide position with an

Ratan W. Jadhav

Mr Ratan W. Jadhav, born in Ambegaon, Tq. Deoni, completed his MSc in organic chemistry with distinction from Rajarshi Shahu College, Latur, India. He also qualified various competitive exams such as UGC-JRF fellowship, SET and GATE. Currently, he is pursuing his PhD degree under Prof. Sheshanath V. Bhosale at the School of Chemical Sciences, Goa University, Goa, India. He has recently been promoted to senior research fellow under UGC-NET. The research topic of his PhD is the use of various small molecules for supramolecular self-assembly and photocatalysis applications.

Pranay P. Morajkar

Dr Pranay P. Morajkar received his PhD from the University of Lille 1 in collaboration with University of Bordeaux 1 (France) in 2012. He served as a CNRS post-doctoral researcher at the LRGP-ENSIC-University of Lorraine (France) and as a Research Scientist at Khalifa University of Science and Technology (UAE). Presently, he is an Assistant Professor at the School of Chemical Sciences, Goa University wherein his research focuses of nanostructured materials for energy and environmental applications. He is the recipient of Early Career Research Award by S.E.R.B, Startup research grant from UGC (India) and Indo-European S&T INNO-INDIGO research grant.

Lathe A. Jones

Dr Lathe A. Jones obtained his PhD from the University of Queensland (Australia) and has held research positions at the University of Manchester (UK), La Universidad de Zaragoza (Spain), and CIDETEC (Spain). He is currently a senior lecturer at RMIT University and Deputy Director of CAMIC (Centre for Advanced Materials and Industrial Chemistry). His research interests are in applied chemistry, particularly electrochemistry, industrial chemistry, and supramolecular chemistry.

Subi George

Prof. Subi J. George obtained his BSc degree in Chemistry from Mahatma Gandhi University, Kerala and MSc degree in Organic Chemistry (First Rank) from Mahatma Gandhi University, Kerala. Prof. Subi George obtained his PhD in Organic Chemistry from National Institute for Interdisciplinary Science and Technology, Trivandrum. He is currently a professor at Jawaharlal Nehru Centre for Advanced Scientific Research (JNCASR), Jakkur, Bangalore, India. His research interests are in supramolecular chemistry and organic materials, supramolecular polymers, organic phosphors, and circularly polarized luminescent (CPL) materials. Due to his contribution to research, recently he got Shanti Swarup Bhatnagar Award.

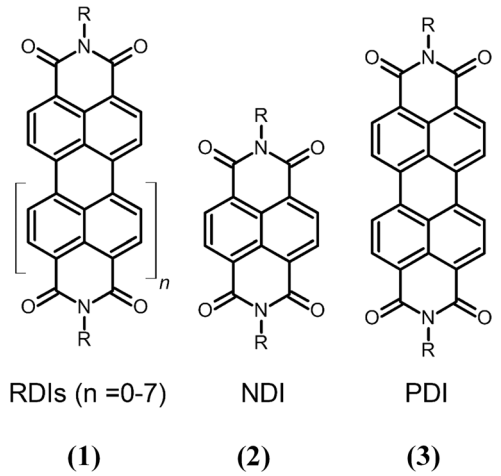

Fig. 1 Chemical structure of possible homologues of rylene diimide.

aromatic group produces a non-emissive dye, whereas alkyl substitution at the diimide produces white-blue emission.[3,6] Manipulation of the core[7] of NDIs can lead to colorful, conducting, functional aromatic molecules with variable photophysical properties, which can be tuned by the incorporation of different functional groups on the core structure.

Since the key report on core substituted NDIs (cNDIs) by Würthner in 2002,[8] new classes of NDIs have been created for functional materials with varying photophysical properties to supplement the core unsubstituted NDIs discovered by Vollmann *et al.* in the early 1930s.[9] Since then, NDIs have found great versatility because of their tendency to form n-type semiconductor materials, which is not possible with other RDIs.[10] Furthermore, NDI functionalization through the diimide nitrogen or *via* core-substitution varies the absorption and emission properties, allowing the derivatives to act as either donors or acceptors in a controlled manner.

The flat, compact aromatic core of NDI dyes enables aggregation into larger structures, which when combined with their electron deficient nature is of both fundamental and applied interest, as the self-organization affects the properties of the NDI in the resulting supramolecular structures and systems. The self-assembly and self-organization occurs through π–π interactions of the aromatic core which affects the electronic and optical properties, and can be used to tune properties that match the application being studied. Thus, both NDI and cNDI structures are finding applications in various research fields including materials science, supramolecular chemistry, sensing, catalysis, artificial photosynthesis, energy, solar cell devices, and biomedicine.[2b,3b,7a]

In this review, we will begin with recent developments in the synthesis of new NDI derivatives. The various synthetic strategies to obtain NDI derivatives will be explored and the new structures related to their chemical, physical and redox properties. Thereafter, fundamental research efforts on NDIs and cNDIs in the field of supramolecular chemistry will be discussed in depth, focussing not only on the self-organization of the structures, but also the roles of stimuli such as organic solvents, pH, and temperature, to name a few. In the following sections, we will describe non-covalent interactions in a variety of mechanically interlocked molecules such as catenanes, rotaxanes, and pseudorotaxanes including recent applications in molecular motors. We will then provide a brief discussion on the use of various NDI derivatives in sensing, including ion sensing, ion channels, pH sensing, and the detection of biologically important molecules.

Due to their electron accepting capacity and conducting properties, NDIs have been used in photovoltaic and optical devices. We will discuss how the donor–acceptor nature of NDI derivatives in bulk heterojunctions is crucial in determining the photovoltaic properties and how bilayer heterojunction solar cells consist of p–n active layers of NDIs. We will then explore the use of NDI derivatives to fabricate fused macrocycles, donor–acceptor derivatives, and bulk-heterojunction devices and finally their use in perovskite solar cells.[7c] We will also discuss new polymer derivatives prepared from NDIs for organic field-effect transistors (OFETs) and their use as acceptors in organic photovoltaic (OPV) cells.[11]

NDIs are finding use in a range of medicinal applications including as anticancer agents, for electrochemical detection and imaging, and in medicinal chemistry, which will be discussed. We will finally explore hybrid materials of NDIs with metals to prepare Metal Organic Frameworks (MOFs) and their applications, along with the use of the surface of aromatic NDIs for homogeneous and heterogenous catalysis, showing the extraordinarily broad range of applications of these classes of compounds.[12] This review will thus impart our view for future development in the field, and the future promise of NDIs and cNDIs for real-world applications.

2 Molecular design and synthesis

One reason NDIs have attracted so much attention is their versatile synthesis, leading to a large library of derivatives. Symmetric NDIs can be prepared through a simple one-pot reaction from commercially available 1,4,5,8-naphthalenetetracarboxylic acid dianhydride (NDA) *via* condensation with a primary amine in a high boiling point solvent such as isopropanol or DMF.[2b] Ghadhiri and co-workers synthesised unsymmetrical NDIs in two steps: by hydrolysing NDA using KOH to produce tetracarboxylic acid, followed by re-acidification with H_3PO_4 to pH 6.2 to form the monoanhydride, then the addition of 1 equiv. of a primary amine to produce a monoimide, followed by the addition of a second primary amine to the anhydride intermediate under reflux in DMF, producing an unsymmetrical NDI.[13] Recently, Koz *et al.* synthesised an unsymmetrically substituted NDI derivative in two steps: firstly NDA is converted to a monoimide by reaction with dodecylamine, with the formation of diimide with ethyl 3,4-diaminobenzoate occurring in the presence of $Zn(OAc)_2$ in quinolone.[14] Until 2002, NDIs were mostly functionalised and studied at the diimide positions, despite having four available positions (2, 3, 6, and 7) on the NDI core, as it was suggested in

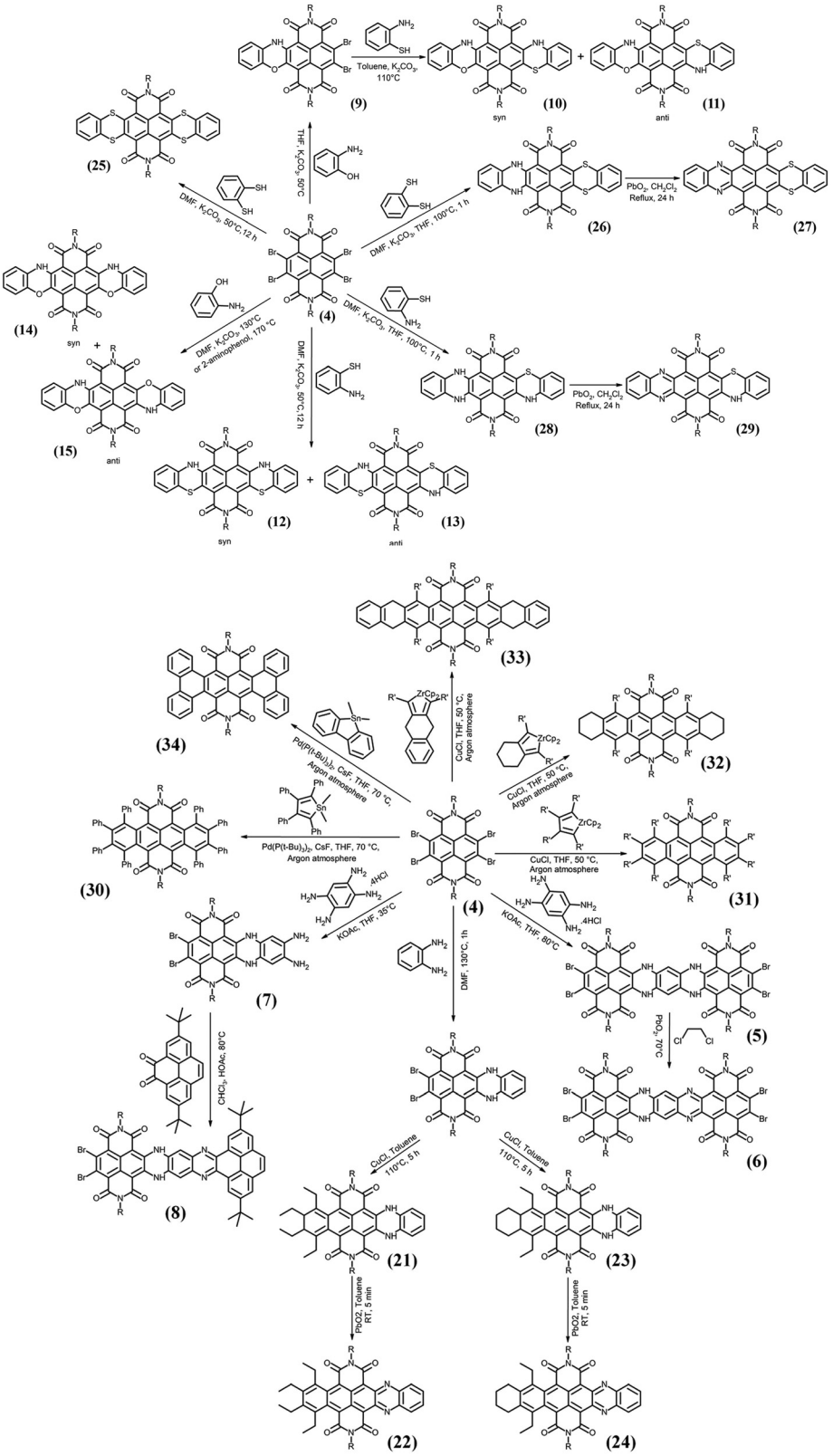

Fig. 2 Synthetic methods to produce core-expanded and heterocyclic core-expanded derivatives of NDI.[15–18,20]

the 1990s that the core-substitution of NDIs with aryl functionalities did not significantly change any of its properties. This situation changed after a report by the Würthner group, which showed that the core-substitution of an NDI with heteroatom

(N, O, or S) donor substituents could produce a range of colors, representing a variation in optical properties required for different applications.[8] We reviewed this area in depth for the novel synthetic pathways.[3b,6] In this section, we have described some classic structures of importance, along with recently developed methods for the synthesis of NDI structures.

An early study by the Zhao group reported very interesting hydroazaheptacene tetraimide derivatives (**5–8**), which showed red to NIR absorption, and exhibited well-defined J-type aggregates in solution as well as thin films.[15] In another report, the group synthesised a series of *anti*- and *syn*-isomers of heterocyclic hexacene diimides (**9–15**) containing NH and O/S.[16] Interestingly, *anti*- and *syn*-isomer mixtures were recovered from the synthetic reactions, where only the *anti*-isomer dehydrogenated to afford quinoidal structures, making it easy to isolate the *syn*-isomer. Furthermore, the *anti*-isomer was obtained by reducing the quinoidal oxidation products. Wang and co-workers synthesised diazapentacene diimides using double cross-coupling of unilateral 4Br-NDI derivatives (**4**) with zirconacyclopentadienes, yielding dihydrodiazapentacene diimide derivatives (**17**) and (**18**) in 24% and 45% yields, respectively. Further dehydrogenative aromatization in the presence of PbO_2 afforded hydroazaheptacene tetraimides (**19**) and (**20**) in high yields at room temperature.[17] The Wang group synthesised a series of heterocyclic acene NDIs (**21–24**) by simple condensation reactions of 4Br-NDI with *o*-phenylenediamine, 1,2-benzenedithiol, and 2-aminothiophenol, respectively.[18] These novel heterocyclic acene diimides exhibited bathochromic-shifted absorption and a significant increase in the energy of the occupied orbitals, which led to the conversion of the usually n-type NDI material into a p-type semiconductor. This group has also reviewed the chemistry of π-extended NDIs *via* heterocyclic core-substitution (**25–29**).[19] Wang and co-workers synthesised a series of near-infrared absorbing tetracene-cNDIs by direct double ring extension of electron deficient 4Br-NDI with zirconacyclopentadiene, and they have also shown that the reaction of 4Br-NDI with 9-stannafluorene produces TBNDI (**30–34**) in the presence of $Pd(P(t\text{-}Bu)_3)_2$ and CsF, affording tetrabenzotetracene diimides. Importantly, all of the synthesised molecular skeletons were shown to be promising candidates for n-type semiconductors.[20]

Amino core-substituted NDIs have been extensively studied in the context of electronics, sensors, and supramolecular chemistry due to their π-stacking ability. However, there were no previous reports of reactions of alkynyl-substituted NDIs with amines, which are of interest, as π-core NDIs substituted with ethynyl groups would provide intermediates for the synthesis of π-conjugated molecules such as oligomers and polymers (Fig. 3). To this end, Takai and Takeuchi reported for the first time the synthesis of NDIs (**35**, **36**) with terminal alkynes, and further addition of diisopropylamine (DIPA) produced (**36**)-DIPA and (**36**)-(DIPA)2.[21] Typically, Sonogashira coupling of Br-NDI with trimethylsilylacetylene in the presence of CuI and $Pd(PPh_3)_2Cl_2$ gives TMS-protected ethynyl NDI, and KF can be used to remove the TMS group, producing (**35**) in 69% yield, and with a similar pathway (**36**) was produced in 78% yield. Further step-wise addition of DIPA with (**36**) produced the (**36**)–DIPA mono-adduct; however, for the formation of the bisadduct (**36**)–(DIPA)2 in 95% yield, a relatively large excess of DIPA was required. Another report by Wang and co-workers described a one-pot reaction involving an oxidative homocoupling reaction of 1,6-di((trimethylsilyl)ethynyl)NDIs to produce well-defined oligo-butadiynylene NDIs (**37**, **38**) in excellent yields under mild conditions, *i.e.* CuI and DMF at room temperature.[22] A very interesting synthesis procedure has been reported by the joint work of the Li, Nagri, Marder and Wang group who prepared hybrid rylene trimeric systems bearing perylene diimide (PDI) as a central moiety, and functionalised the core of PDI with stannyl NDI (**36**) using Stille cross-coupling and C–H transformation.[23] Another interesting example was reported by the Chi group involving a thiophene-fused tetracene diimide with an $FeCl_3$ mediated oxidative cyclodehydrogenation reaction, producing a novel dye (**39–43**) with a low band gap of 1.52 eV and amphoteric redox behaviour.[24] Seferos and co-workers developed new synthetic routes to thionated-core-substituted NDIs (**44**) using microwave irradiation in the presence of excess Lawesson's reagent, and they further extended their study to the postpolymerization thionation of NDI-based polymers to afford a series of polymers with varying degrees of thionation in high yield *via* selective polymerisation.[25]

Takimiya *et al.* synthesised thiophene-fused NDIs (**45–47**). *N*,*N*′-dioctyl-2,6-bis(trimethylsilyl)ethynyl-NDI (**48**) with $Na_2S{\cdot}9H_2O$ in ethanol led to a thiophene annulation reaction giving a 42% yield of *N*,*N*′-dioctyl-NDTI (**45**).[26] Furthermore, they functionalised thiophene with various halogenation reactions such as bromination and chlorination, and subsequently performed C–C bond formation using Suzuki reactions.[27] In another report, they synthesised mono-thiophene-annulated NDIs (**49**, **52**) *via* a two-step C–H activation.[28] Firstly rhodium catalysed the direct C–H iodination of an NDI (**55**), followed by an efficient direct arylation of the NDI in high yield.[29] Coupling of a mono-thiophene-annulated NDI with a benzene, a pyrene core or other bromide derivatives in the presence of the $Pd_2dba_3/P(o\text{-anisyl})_3$ catalyst and Cs_2CO_3/PivOH base in mesitylene produced all the NDI derivatives in ~80% yield. Gu and Liu reported the synthesis of cNDI-based coplanar conjugated molecules *via* a condensation reaction of 2,6-dibromo-NDI with aryl ethylenes using the Heck–Mizoroki reaction.[30] They revealed that two different series of products were obtained: one is diolefination products (**53**, **54**) and the other is hydroxylated and mono-olefination products (**53**), and all the products could be controlled depending on the choice of the catalyst and base used in the reactions (Fig. 4).

In an interesting study, the Langford group reported the design and synthesis of new di-, tri-, and tetra-core-substituted NDIs by means of reactions of 2Br-NDI, 3Br-NDI and 4Br-NDI allyl ethers, giving allyl-NDI and diallyl-NDI (**56**), which further deallylated (**57**) in the presence of strong and soft Lewis acids, *i.e.* metal and non-metal-based.[32] Typically, deallylated products (**57**, X = Br, Y = Z = H) were obtained in 50–80% yields in the presence of hard $SnCl_4$ and CF_3COOH; however,

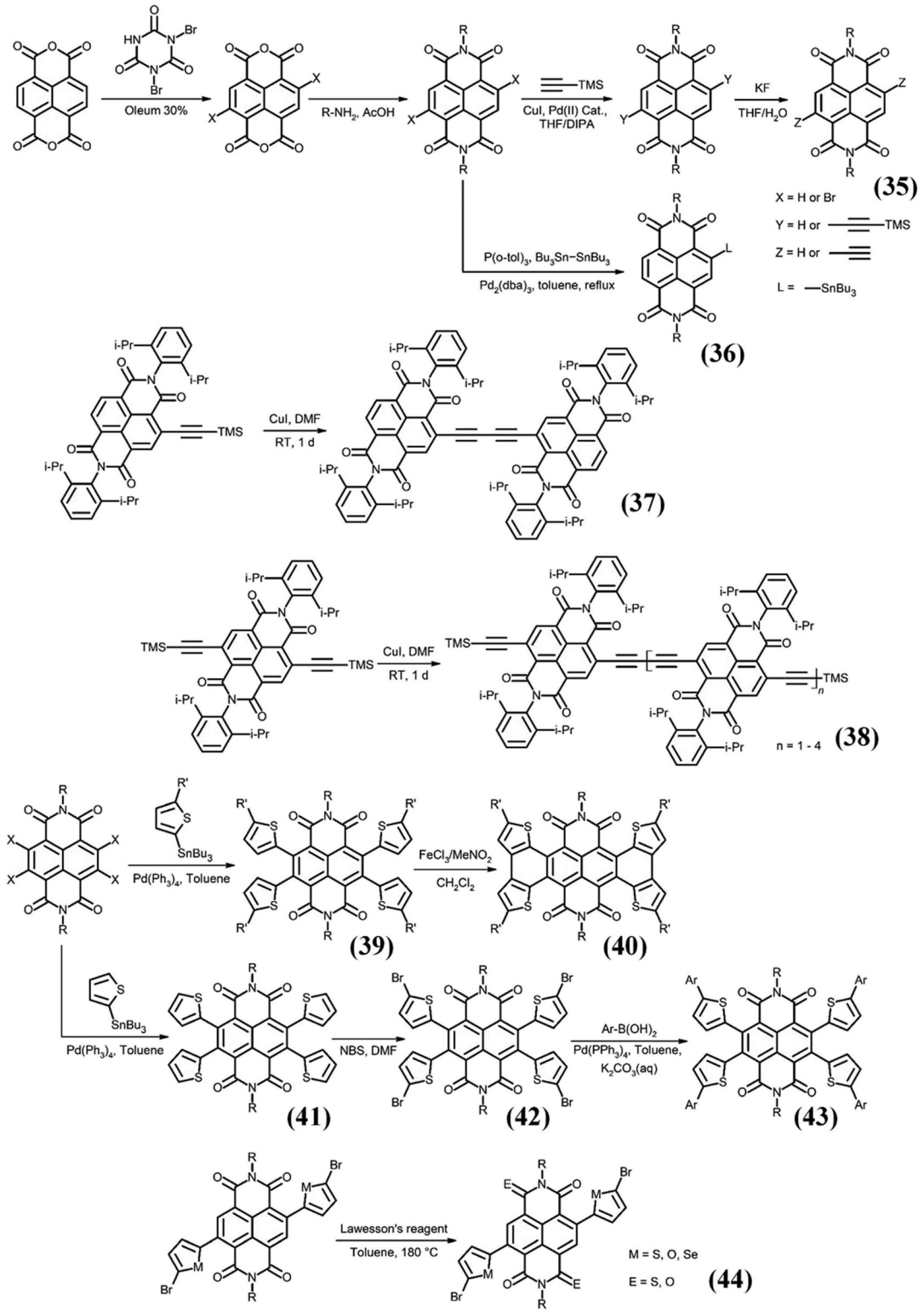

Fig. 3 The reaction scheme of catalyst-free ethynyl-π-extended NDI based electron acceptors,[21,23] oligo-butadiynylene–NDIs,[22] and thiophene-fused tetracene diimide with a low band gap,[24] and microwave synthesis of thionated NDI-based small molecules and polymers.[25]

treatment of allyl-NDI with the soft L Pd^0 under similar conditions produced the same in 85% yield. Furthermore, these deallylated NDIs were used for ring-closing metathesis to form furan-fused NDIs (**58**) and (**59**), and eventually these derivatives may be useful for the development of π-extended systems. In another report, this group explored the oxidation of NDI by ruthenium(III) chloride and sodium periodate at 35 °C, giving the corresponding diones (**60**) in good yields. However, further

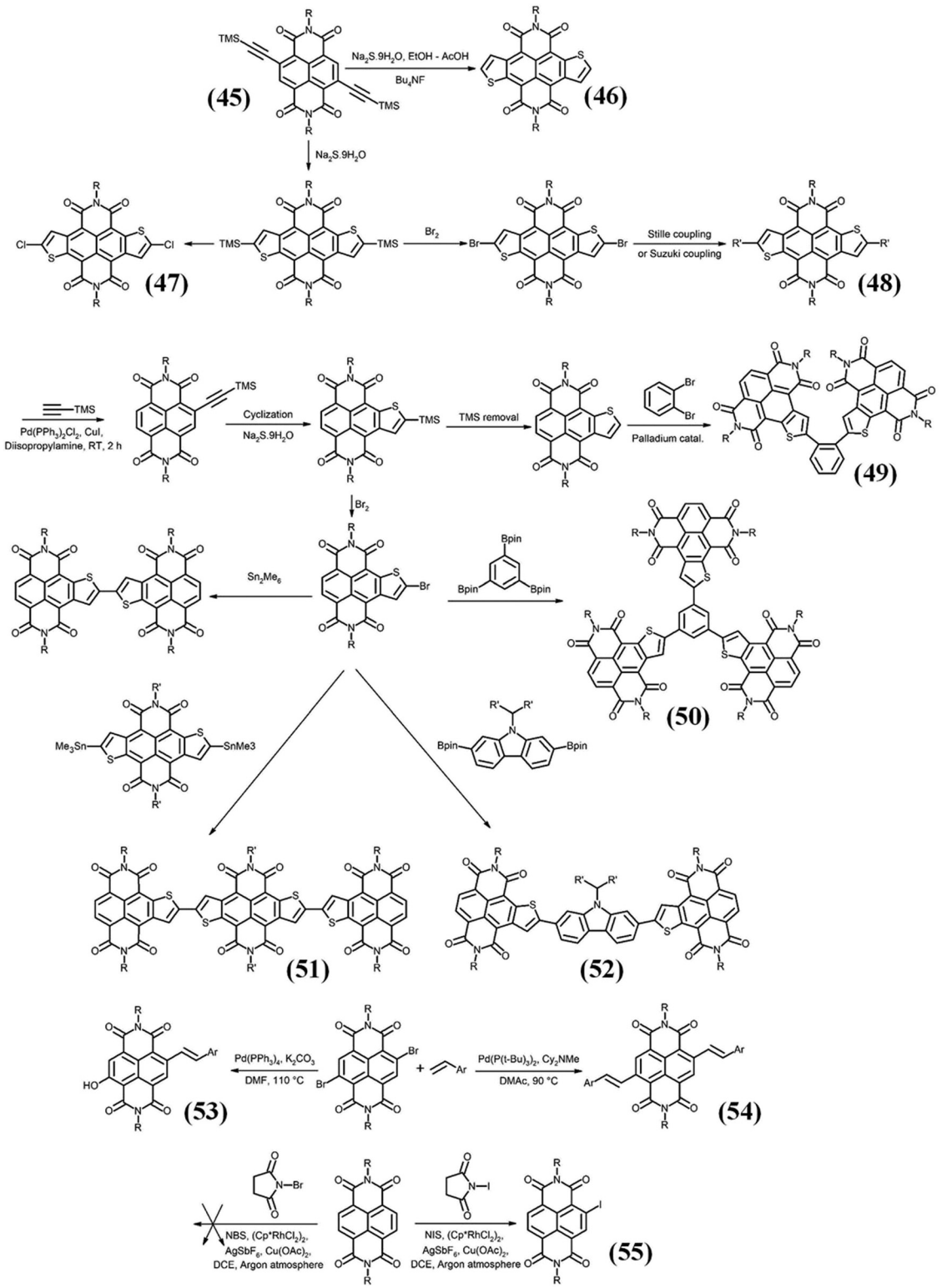

Fig. 4 Allyl and di-allyl NDIs react with hard and soft LAs to form deallylated and rearranged products. Synthesis of NDI-furan derivatives from tri- and tetrasubstituted NDIs.[26] Synthesis of 1,4-dione, reactions of NDI diones,[29] and general synthesis of the cyclophanes used in this study.[30] Reaction scheme of the Py_2-NDI-2X compounds.[31]

oxidation does not occur even at a longer reaction time and a higher temperature in the presence of an oxidant.[33] Further, reaction of (**60**) with $NaBH_4$ yielded dialkene (**61**) which was converted to bis-hemiacetal (**62**) in the presence of ethanol. The (**60**) derivative was converted to isoindole (**63**) by reaction with 1,2-ethylenediamine.

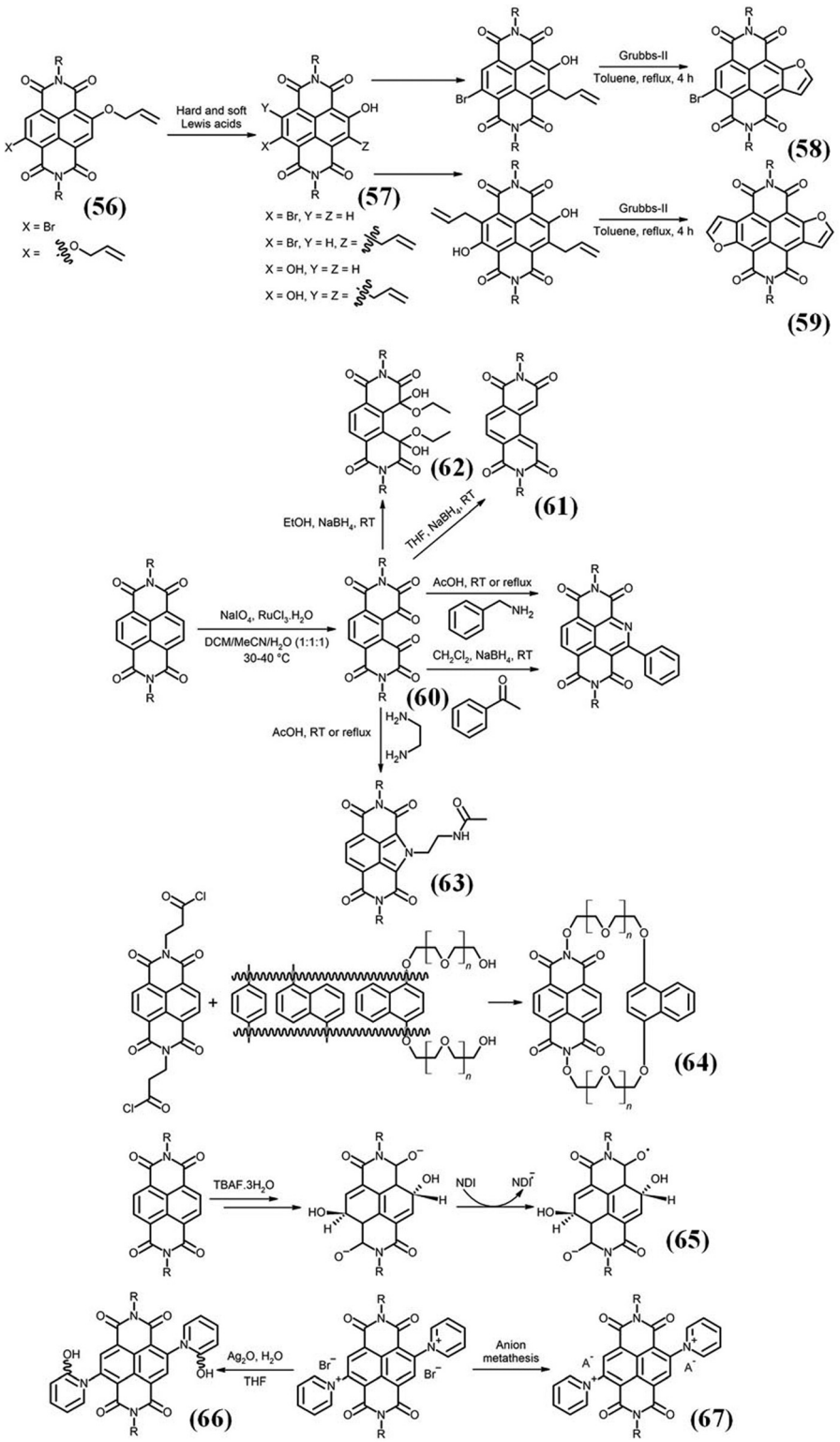

Fig. 5 Synthesis of NDI–furan derivatives from tri- and tetrasubstituted NDIs,[32] unusual products from the oxidation of NDI,[33] cyclophanes bearing NDI and dialkoxyaryl groups,[34] the proposed reaction mechanism when TBAF was added to NDI,[35] and highly *p*-acidic dipyridinium-NDI salts.[36]

A series of NDI cyclophanes (**64**) were synthesised, which demonstrate π–π interactions between π-electron-rich naphthalene and π-electron-deficient NDI chromophores, and these derivatives were used for fluoride anion sensing (Fig. 5).[34] Xu and co-workers used the anion–π interaction for the first time to reduce NDI to $NDI^{-\bullet}$ (**65**) using a fluoride anion (F^-) with NDI in polar aprotic THF, where F^- produces hydroxide, which plays an important role in the reduction process.[35] Using

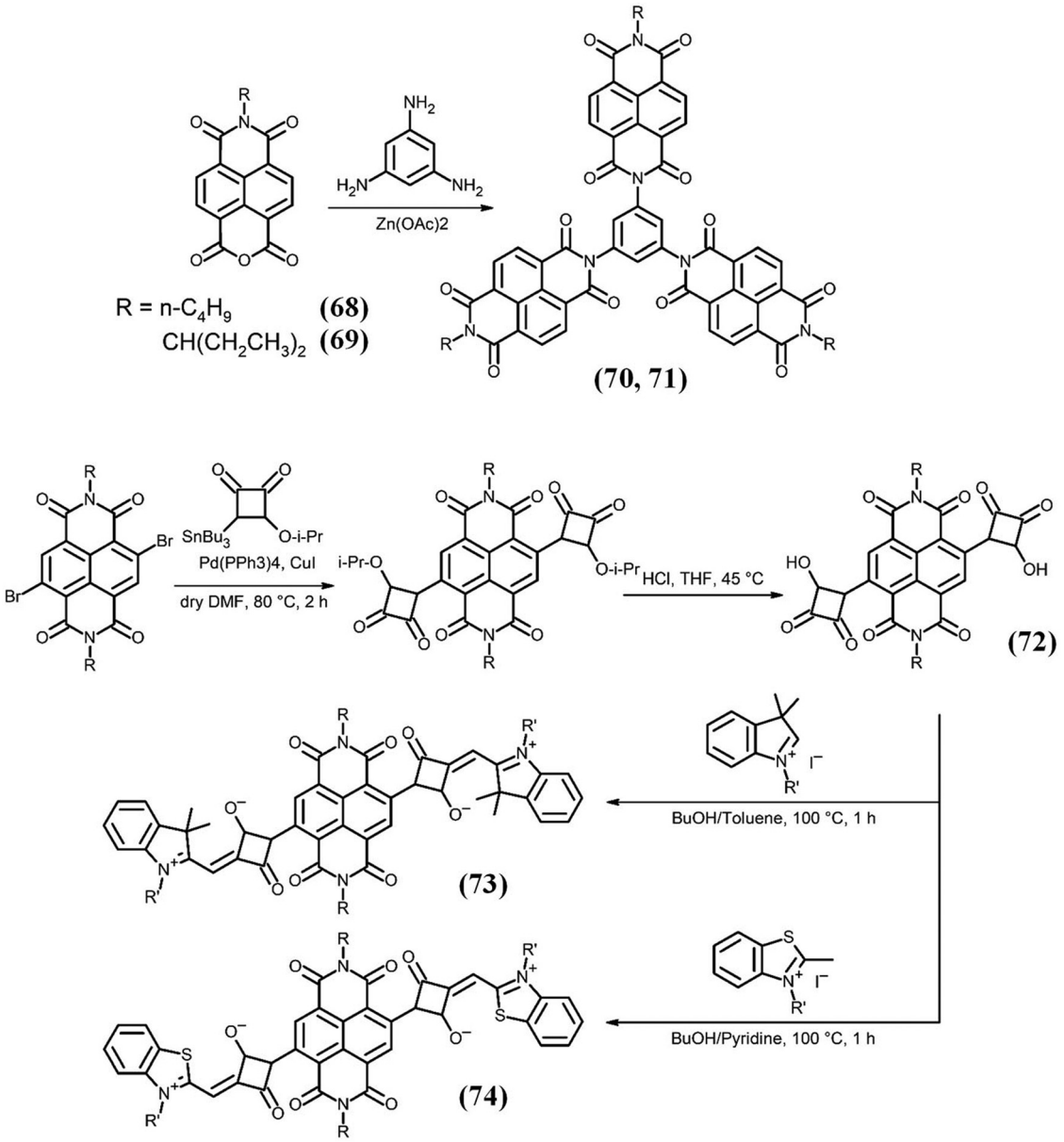

Fig. 6 Synthesis of a star-shaped analogue with a benzene core and three NDI side-arms,[37] and functional dyes with a squaraine–NDI hybrid structure.[38]

similar strategies, Wu and co-workers synthesised 2,6-bipyridyl-NDI (**66**) and studied anion–π interactions on the highly π-acidic Py_2-NDI^{2+} (**67**) system with halides and PF_6^-.[36]

Yin and co-workers synthesised two novel star-shaped NDI derivatives bearing a central 1,3,5-triaminobenzene core and three NDI side arms.[37] In typical reactions, NDA was treated with primary alkyl amines to synthesize (**68**) and (**69**) in 20 and 30% yields, respectively. Imidization of (**68**) and (**69**) with 1,3,5-triaminobenzene produced the target molecules (**70**) and (**71**) in 10% and 20% yields, respectively. Interestingly, both the derivatives displayed a bathochromic shift in their absorption as thin films in comparison to solution. Thus, they will be useful as non-fullerene acceptors for organic semiconductors. In another example, Maeda *et al.* synthesised NDI hybrid structures containing the squaraine chromophore at the 2,6-position of the core of NDI (**72**) using Stille coupling reactions of 3-stannylcyclobutenediones and 2Br-NDI.[38] Interestingly, the absorption band of the novel dyes (**73**, **74**) exhibited a bathochromic shift in the solid state, indicating that J-aggregates engaged in excitonic coupling.

Tam and co-workers synthesised a series of bis(triphenylphosphonium)-NDIs (BTPP-NDI) from (**75**) in the presence of triphenylamine using triphenyl phosphine as a catalyst in dioxame (Fig. 7).[39] Furthermore, they studied anion–π and anion–π-radical interactions as (**76**) was oxidized using bromine to give (**77**). The derivatives (**78**, **79**, **81** and **82**) were obtained by anion metathesis. Reaction of (**76**) with silver nitrate yielded (**83**) and subsequent reduction using excess

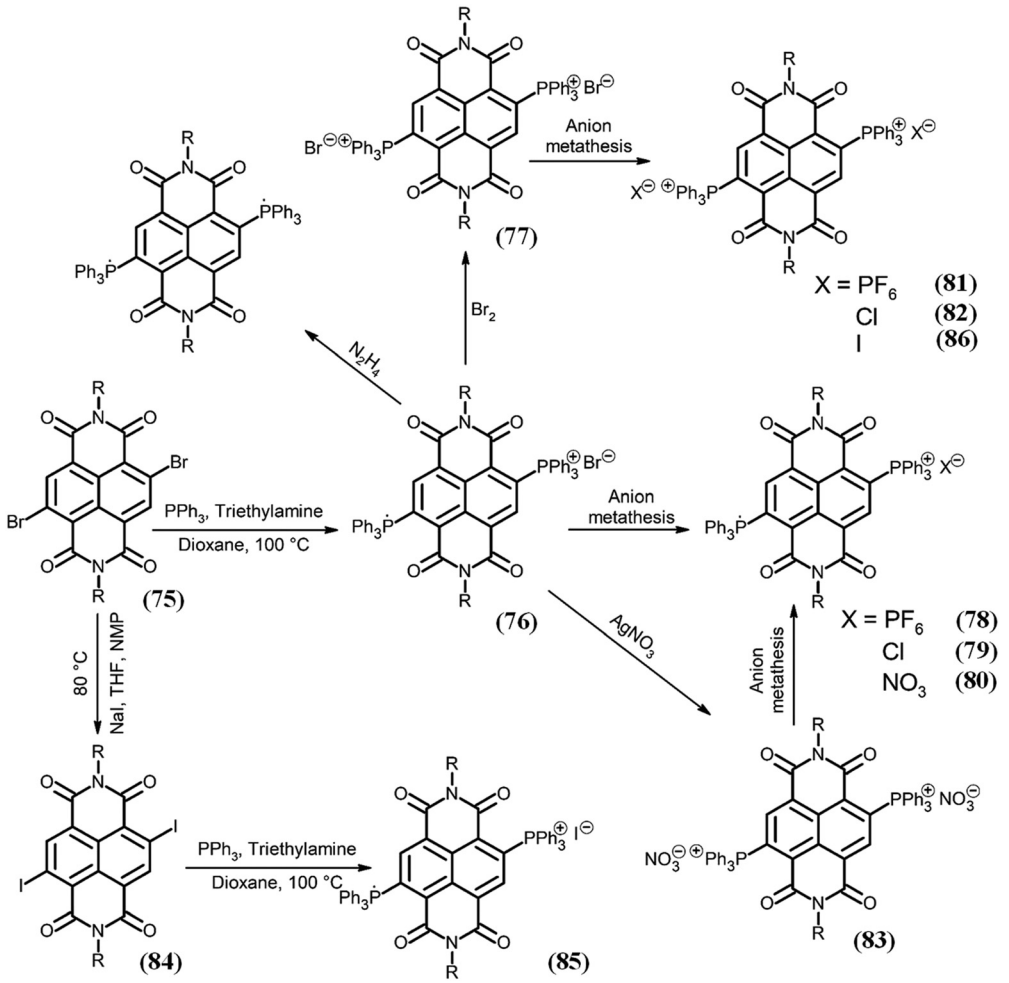

Fig. 7 Synthesis of the BTPP-NDI compounds.[39]

triethylamine yielded (**80**). The derivative **75** was reacted with sodium iodide to give **84**, which in similar conditions produced (**85**). Interestingly, to produce (**86**) having iodine as counter ion using anion metathesis with sodium iodide shown to be tedious method, thus, other methods are used to produce good yield of NDI **77** and **85**, respectively. This study may provide an understanding of organic ferromagnets and p-doped conductors.

Schab-Balcerzak and co-workers synthesised novel NDI derivatives bearing an end-capped anthracene bridged with imine linkages (**87–90**) as shown in Fig. 8. These derivatives were prepared by condensation of 9-anthracenecarboxaldehyde and diamines with NDI using Schiff base linkers.[40] Ledwon and co-workers used multistep synthesis to obtain a new class of π-conjugated copolymers bearing NDI side groups. The backbone of the polymer containing a donor–acceptor system contained thiophene and carbazole as a donor (**91**) and benzothiadiazole as an acceptor unit, and the polymerization was performed using the Suzuki/Stille reaction.[41] Very interesting derivatives of NDIs have been reported by the Miyake group, where they have performed reductive aromatization to achieve an excellent yield of tetrapivaloxy-2,7-diazapyrene (**92**) from NDI (**93**) *via* Ni-catalysed cross-coupling reactions, which was subsequently transformed into tetraaryl-2,7-diazapyrenes using excess Ni-catalyst with arylboronic acids. These novel 2,7-diazapyrenes (**92**) displayed a significantly higher intrinsic electron mobility than the corresponding pyrene.[42]

To achieve strong absorbance in the visible spectrum for NDIs, functionalisation is required not only on the diimide, but also at the core. In this regard, Champness and co-workers investigated tertiary amine substitution onto the core of NDIs *via* mono-, di- and tetra-substituted morpholine substitution (**94–96**) as illustrated in Fig. 9.[43] As expected, mono-substituted NDI gave a 91% yield and di-substituted NDI gave an 81% yield, with the tetra-substituted NDI giving a considerably lower yield (3%) because of decomposition.

In general, when core-substitution of NDIs is performed with heteroatoms (N, S or O), halogens (Cl, Br or I) are required at the 2, 3, 6, and 7 positions of NDI, though 2-, 6- or even 2, 3, 6, and 7-substitution of NDI has been demonstrated in the literature,[3b] with 2,3-substitution more rarely being described. For the first time, Höger developed a new and efficient synthetic route for 2,3-diamino substituted NDIs (**97–99**) from non-halogenated NDIs *via* vicinal diamination of arylene diimides

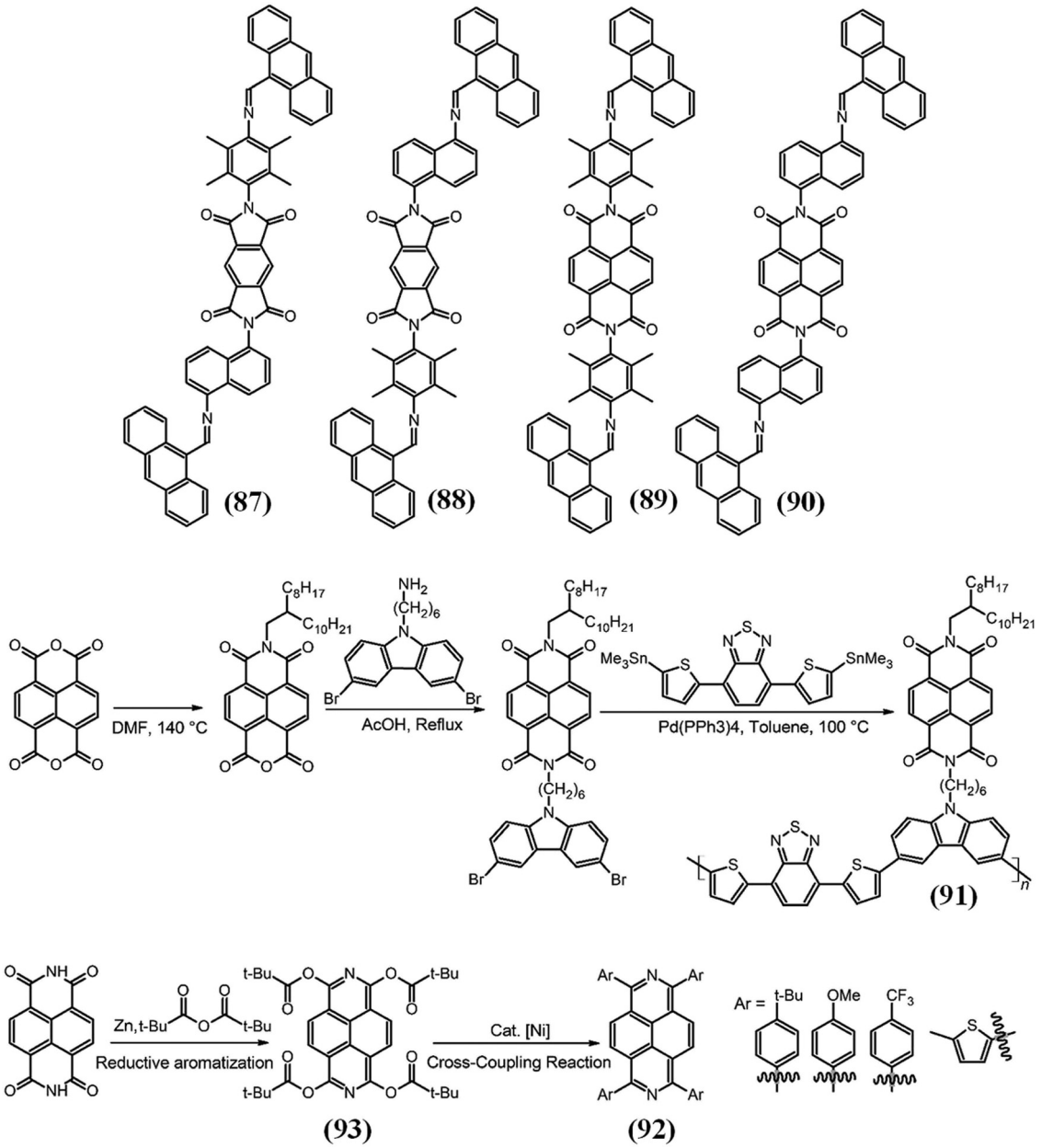

Fig. 8 Molecular structures of azomethine diimides end-capped with anthracene moieties,[40] the synthesis of aromatic diimide side groups on the π-conjugated polymer,[41] and the synthesis of 2,7-diazapyrenes *via* reductive aromatization of NDI.[42]

with 1,2-diamino compounds in the presence of $CuBr_2$ in water (Fig. 10).[44] Wang and co-workers described the direct perfluoroalkylation (**100**) of non-core-substituted NDIs.[45]

Water-soluble high quantum yield chromophores with favourable optical properties are required in key applications such as detection and imaging of biological molecules in cellular systems. NDI and cNDI have excellent absorption and emission properties; however, their water insoluble nature can limit their use. Recently, the Würthner group synthesised a series of highly water soluble NDIs containing either glutaric acid or 2-dimethylaminoethyl moieties at the diimide position as a water solubilising group (**101**, **102**) and amino substituents at the core of NDI (**103**, **104**).[46] Importantly, the amino-substituted NDI exhibited a fluorescence quantum yield of 39% in water (Fig. 11).

An NDI bearing two chlorine atoms on the core has been shown to be an excellent candidate for sensing of gaseous primary amines and biogenic diamines. Earlier, the same group reported regioselectivity in nucleophilic substitution of 4Br-NDI with aniline to give (**105–109**), showing the effect of reaction solvents and additives (Fig. 12).[47]

In a chlorinated solvent, the 2,7-diamino-3,6-dibromo-NDI isomer was formed regioselectively without an additive, whereas in DMF the 2,3-diamino-6,7-dibromo isomer was formed

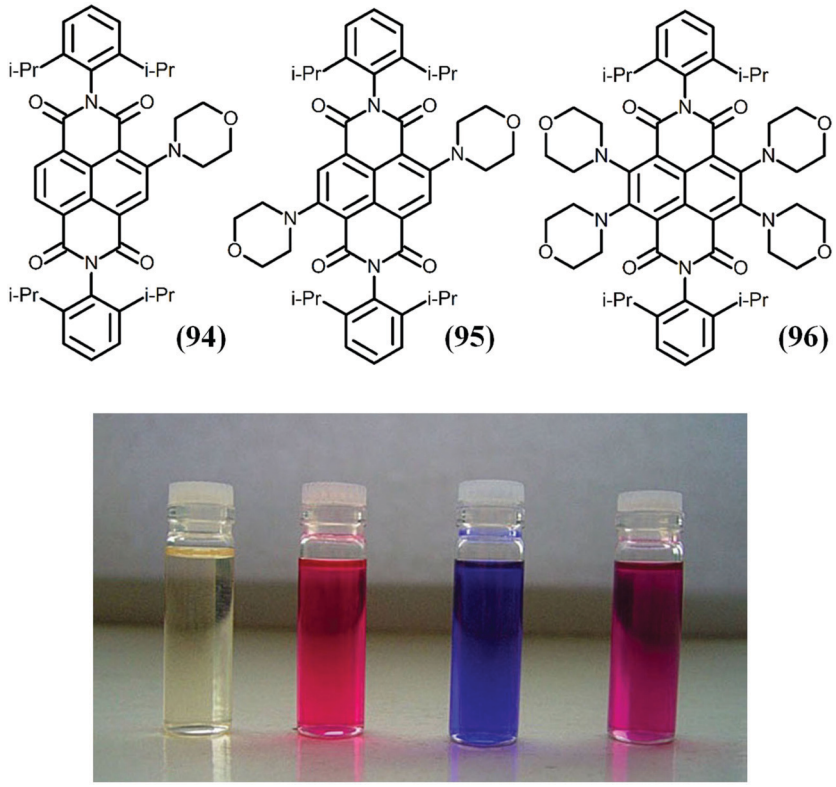

Fig. 9 Mono- (**94**), di- (**95**) and tetra- (**96**) morpholine-substituted NDIs reported by Champness *et al.* and the solutions of the NDI species in $CHCl_3$ solution (from left to right: NDI and (**94–96**)).[43] This figure has been adapted from ref. 43 with permission from John Wiley and Sons, copyright 2017.

under similar reaction conditions. Tetrabutylammonium fluoride (TBAF) additive plays a major role in regioselectivity, as in DCM without TBAF the 2,7-diamino isomer was the major product, while with TBAF the 2,3-diamino isomer was formed exclusively. It was thus shown for the first time that regioselectivity can be controlled by an additive and a solvent for the formation of 2,7-diamino-3,6-dibromo- and 2,3-diamino-6,7-dibromo-NDIs. Sommer and co-workers synthesised a series of NDI derivatives (**110**) *via* intermolecular photoinduced redox-doping of core-unsubstituted NDI with a dimethylaminopropyl chain at the diimide position (**111**), which upon photoirradiation reduces another core-substituted NDI derivative to form a radical anion (**110**).[48] They have also synthesised the novel copolymer PNDIFu2 (**112**), consisting of alternating NDI and bifuran (Fu2) units.[49] The use of the alternating Fu2 repeat unit allows flattened polymer backbones because of reduced steric interactions between the imide oxygen and Fu2 units, giving this polymer a stronger dichroic ratio and transport anisotropy in field effect transistors compared to analogous copolymers such as NDI–bithiophene (T2) (**113**), with a high electron mobility of 0.21 $cm^2 V^{-1} s^{-1}$. They have also synthesised a novel NDI-2,2′-bithiazole (2-BTz) copolymer (PNDI-2-BTz) (**114**) by direct arylation polycondensation, in which regioselective C–H activation at the 5-position of 2-BTz produces high molecular weight PNDI-2-BTz (**114**) in quantitative yield *via* the reaction of 2-BTz and 2Br-NDI in the presence of tris(*o*-anisyl)phosphine [P(*o*-anisyl)$_3$] as a ligand.[50] The PNDI-2-BTz (**114**) copolymer displayed high thermal stability and hypsochromically shifted charge transfer absorption when compared with the well-known bithiophene analogue PNDIT2. This makes PNDI-2-BTz an interesting candidate for organic electronic devices (Fig. 13).

Lee and Jin synthesised a series of n-type π-conjugated polymers, namely, NDI-T-1FP-T (**115**), NDI-T-2FP-T (**116**), and NDI-T-4FP-T (**117**), with various amounts of fluorine atoms (1F, 2F, and 4F) in their backbones. OFET performance was shown to improve by polyethylenimine (PEI) doping, the field-effect mobility was obtained as 0.51, 0.34, and 0.26 $cm^2 V^{-1} s^{-1}$, respectively, and NDI-T-4FP-T (**117**) doped with 4F showed unipolar n-channel behavior.[51] The Fujitsuka and Majima group synthesised two NDI dimers, NDI-*m*-NDI and NDI-*p*-NDI, bearing a 2-ethylhexyl group at one imide position where the other imide position was used to join two NDIs with a 2,5-dimethylphenyl group used as a spacer to minimize the π-conjugation with NDI and also to study fixed donor–acceptor electron transfer.[52] Gundogdu, Kim and Woo reported the synthesis, photovoltaic properties and charge dynamics of a series of donor–acceptor polymers in which they used P(NDI2OD-T2) (**118**) and its fluorinated analogue, P(NDI2OD-T2F) (**119**), as an acceptor polymer and PBDTTTPD as the donor polymer.[53] Interestingly, a PBDTTTPD:P(NDI2OD-T2)-based device produced a high open-circuit voltage (V_{OC}) of 1.03 V, but suffered from a low power conversion efficiency of 2.02%; however, the PCE of a PBDTTTPD:P(NDI2OD-T2F)-based PSC dramatically increases to 6.09% (V_{OC} = 1.00 V, J_{SC} = 11.68 mA cm^{-2}, and FF = 0.52). These results

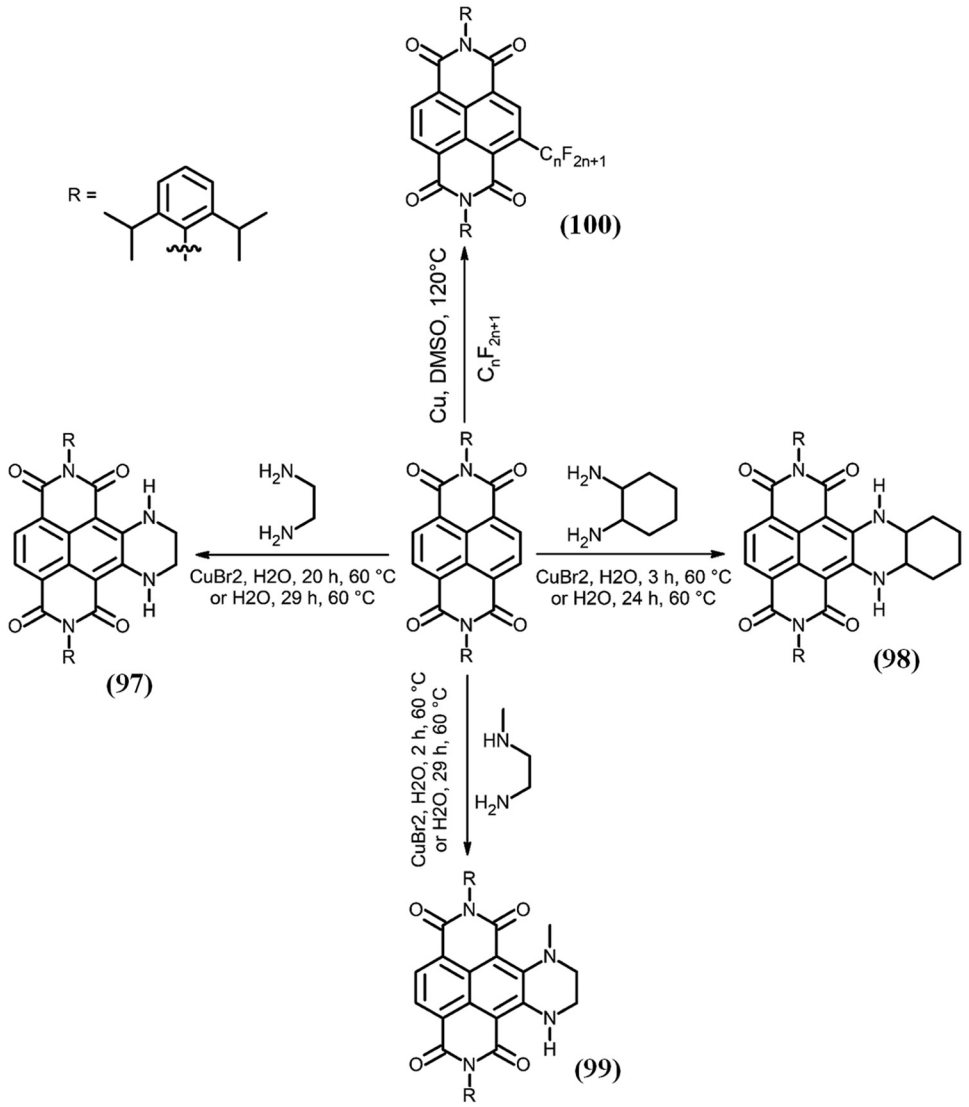

Fig. 10 Synthesis of 2,3-diamino[44] and perfluoroalkyl NDIs.[45]

demonstrated that fluorination removes the energetic barrier for hole transfer, promotes the formation of the donor/acceptor blend morphology, and suppresses phase separation. The Han and Heeney group synthesised a monomer containing two (tributylstannyl)vinyl groups, which was further copolymerized with five different electron-rich comonomers *via* Stille coupling reactions to produce high molecular weight polymers (**120**).[54] These new copolymers displayed red-shifted absorption in comparison to the analogous polymers without the vinylene spacer, all exhibiting ambipolar behavior in bottom-gate, top-contact organic thin-film transistors. Banerjee and co-workers synthesised novel sulfonated copoly(triazole imides) (**121**) with different ion exchange capacities *via* a click reaction (Fig. 14).[55] All the copoly(triazole imides) were soluble in various organic solvents and displayed good mechanical and thermal properties along with the ability to form flexible films. These polymers showed proton conducting behaviour in the range of 15–98 mS cm^{-1} at 90 °C in water.

We have reported for the first time the synthesis of a trimeric NDI system bearing two peripheral NDIs on the NDI central core (**122**) *via* a Suzuki coupling reaction between a mono-octyl-NDI containing boronic ester (**123**) at the imide position and dibromothiophene (**124**) at the 2,6-core position of the central NDI in a dioxane:water solvent mixture with a catalytic amount of $[Pd(dppf)Cl_2{\cdot}CH_2Cl_2]$ and cesium fluoride (CsF) as the base (Fig. 15).[56] This new NDI derivative was soluble in a range of common organic solvents (chloroform and dichlorobenzene), making it a candidate as a dye for organic semiconductors for the fabrication of solution-processable OPV devices. In another report, we have synthesised 2,6-cNDI bearing 2-methoxyethyl-2-cyanoacetate (**125**) and cyanopyridone (**126**) acceptor functionalities at the terminals and studied their role as non-fullerene acceptors in solution-processable OPVs, with results demonstrating that the cNDI bearing the cyanopyridone acceptor afforded the highest PCE of 6.10% when paired with the conventional donor polymer poly(3-hexylthiophene).[57]

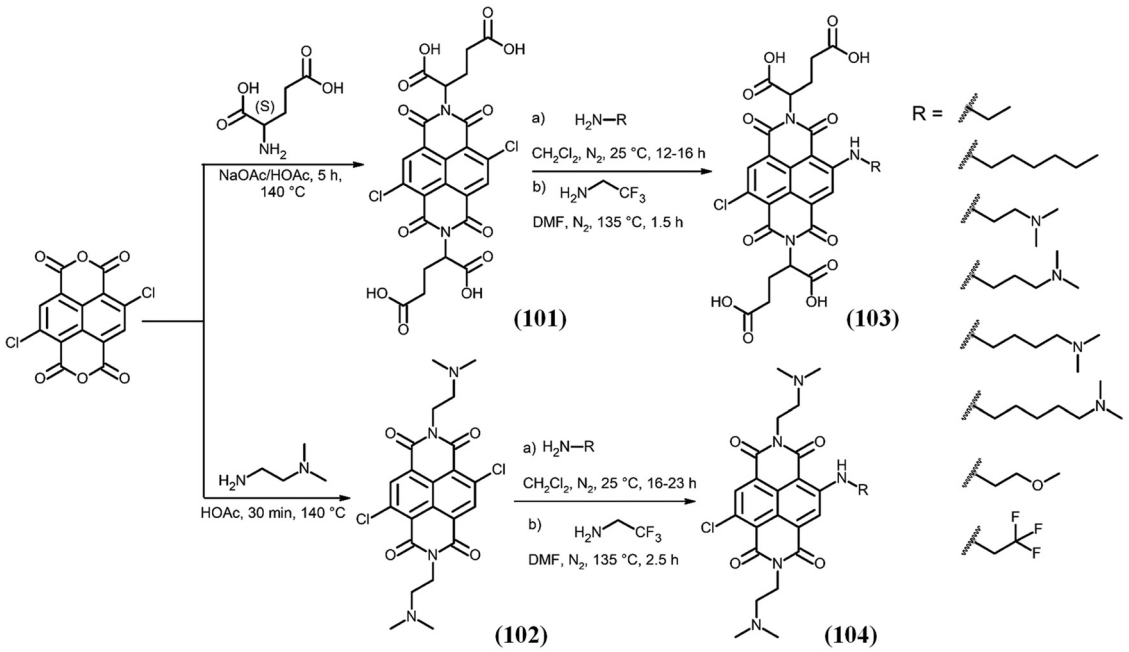

Fig. 11 Synthesis of core-dichlorinated precursor NDIs (**101** and **102**) and core monochloro–monoamino-functionalized NDIs (**103** and **104**).[46]

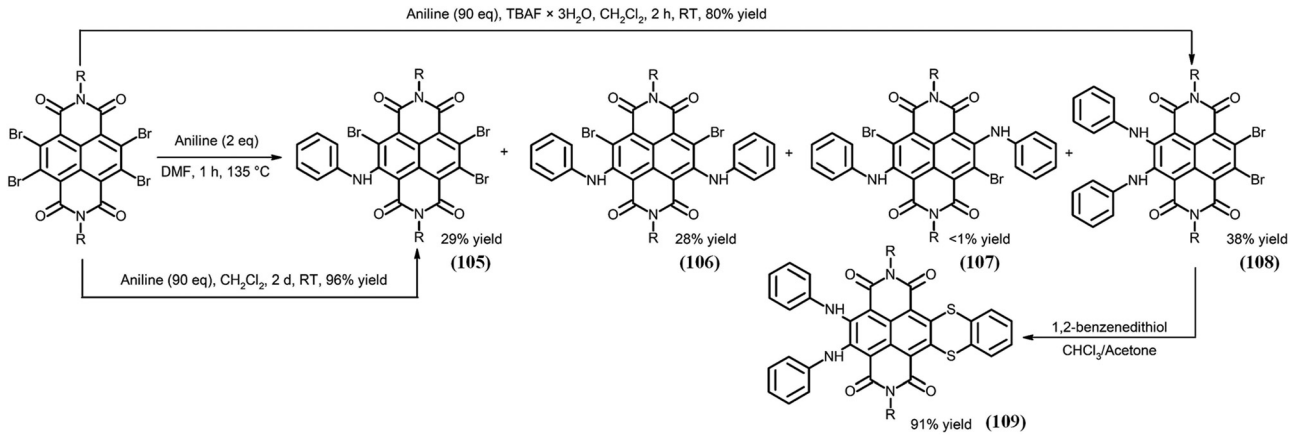

Fig. 12 Reactions of NDI-Br_4 with aniline under different conditions and derivatization of NDI.[47]

3 Physical and chemical properties of NDIs

NDI derivatives are planar, aromatic, chemically robust, optically active molecules with fascinating redox properties and high melting points. NDIs have favourable n-type conductor properties when compared with other rylene diimides or diketopyrrolopyrrole.[58] NDIs undergo single reversible one-electron reductions, either chemically and electrochemically, at modest potentials (E^1_{red} = −1.10 V *vs.* Fc/Fc^+ in CH_2Cl_2) to form stable radical/diradical anions in excellent yields, which can be characterised by the near-IR absorption band, *i.e.* >650 nm (λ_{ex} = ~450 nm), and also confirmed by strong SPR signals.[59] Therefore, in the last two to three decades, NDI derivatives have been explored as n-type optoelectronic materials.

Recently, the Lai and Muhammad group described the tuning of the non-linear optical properties of NDI derivatives containing sulphur atoms.[60] Bickelhaupt and co-workers studied the core-substitution effect on the optical properties of NDI using time dependent density functional theory (TDDFT) at ZORA-CAMB3LYP/TZ2P//ZORA-BP86/TZ2P with COSMO to simulate the effect of dichloromethane (DCM) solution.[61] An earlier report by Zhao and co-workers described the synthesis of three novel hydroazaheptacene tetraimide NDI derivatives (**127–129**) and studied their optical properties in the single-molecule state for the first time in chloroform and *n*-hexane solvents, observing red-shifted absorption bands with narrow

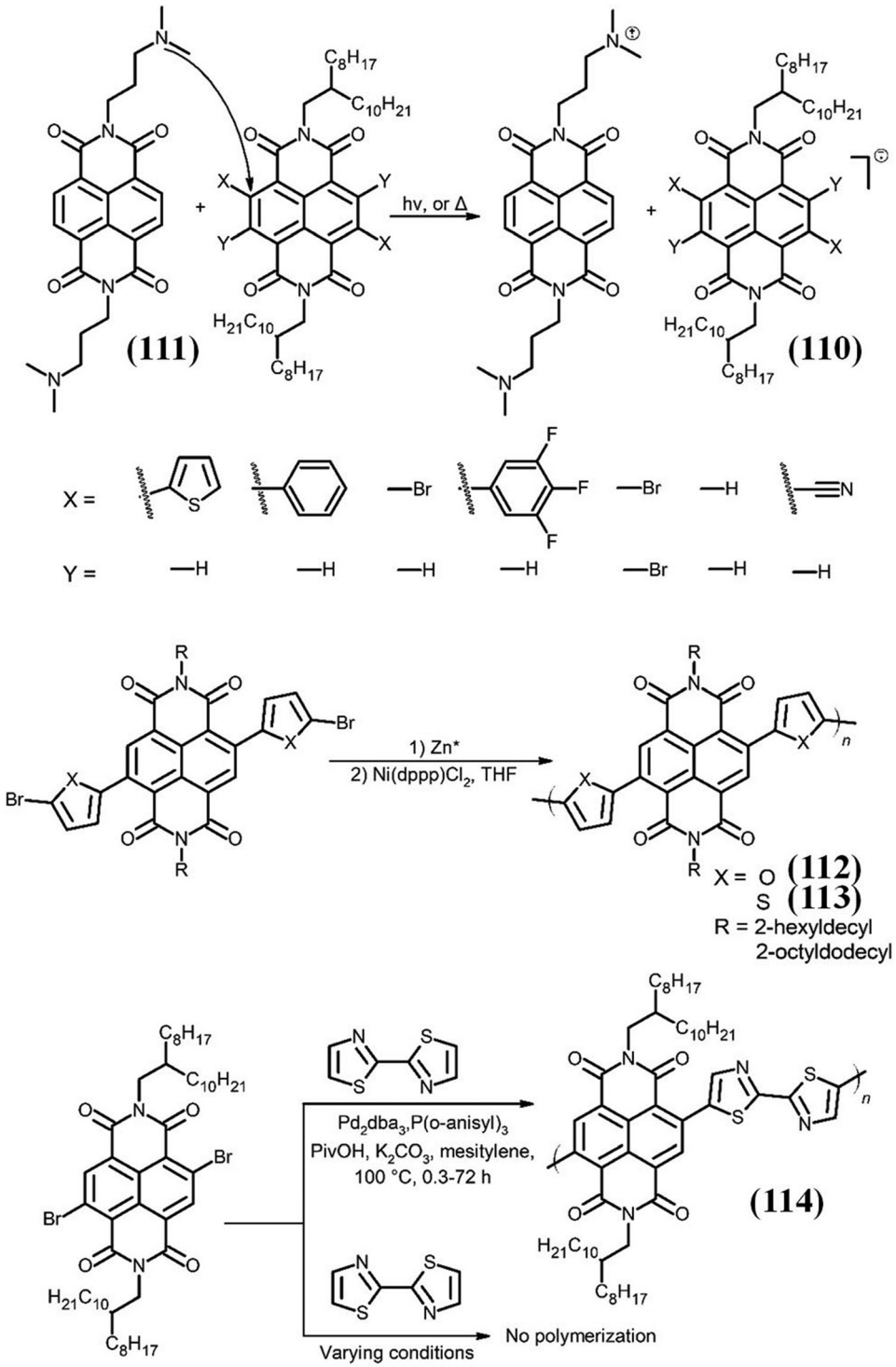

Fig. 13 Reaction scheme for the synthesis of PNDIFu2 and PNDIT2,[49] core-substituted NDIs blended with dimethylaminopropyl-NDI to investigate photo- or thermally-induced electron transfer depending on the NDI substitution pattern,[48] synthetic route for the DAP of 2-BTz and NDIBr2 for reaction conditions intended to copolymerize NDIBr2 and 5-BTz.[50]

band widths.[15] Amongst these, compounds (**127**) and (**129**) displayed absorption bands in the near-IR at 900 and 740 nm (assigned to 0–0 transition, *i.e.* $S_0 \rightarrow S_1$), which confirms J-aggregate formation (Fig. 16).

Karthäuser and co-workers studied the self-assembly behaviour and the electronic properties of 2,7-dibenzyl-NDI (BNTCDI) (**131**) using low-temperature scanning tunnelling microscopy (Fig. 17).[62] As expected, BNTCDI adsorbed

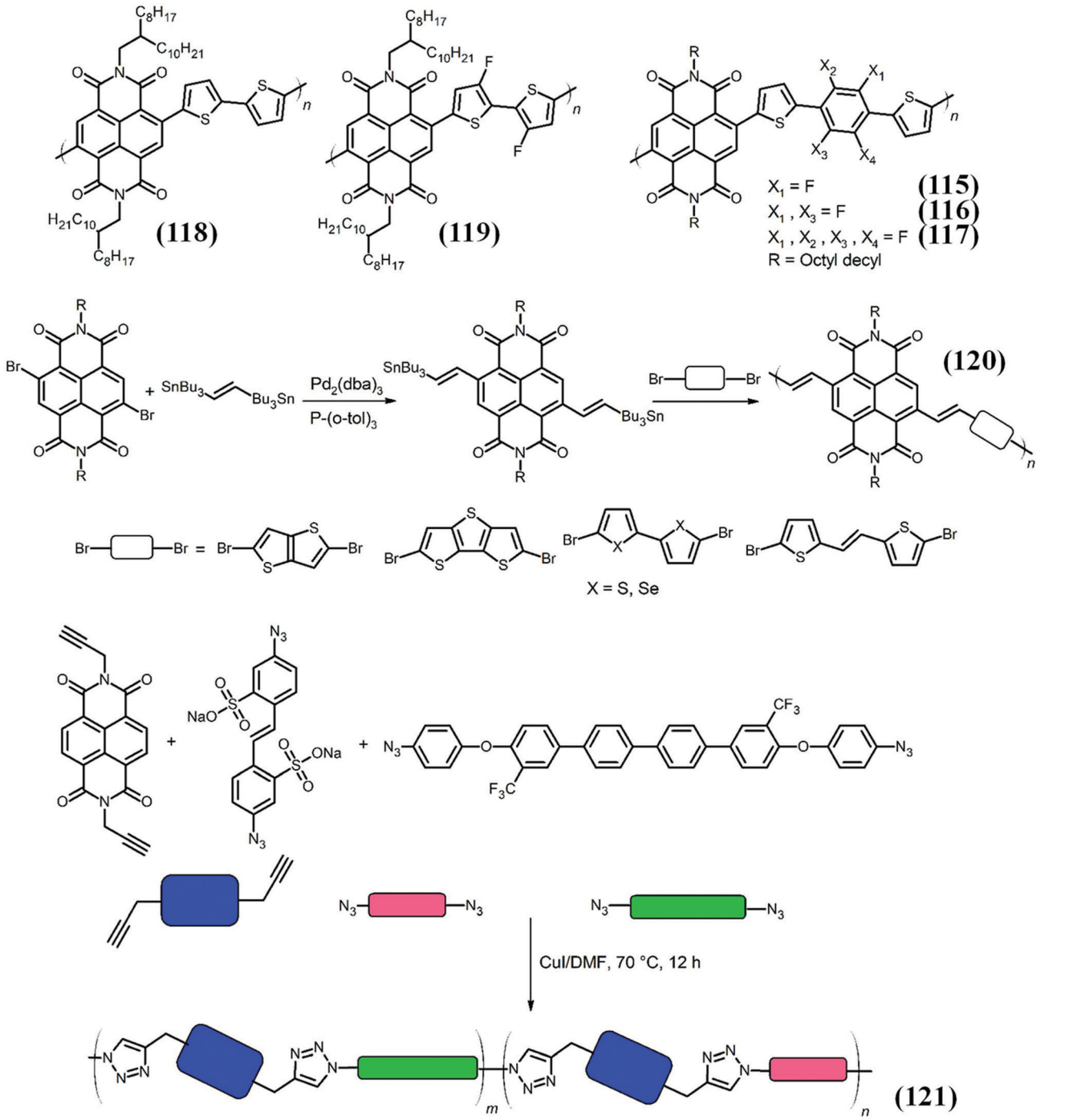

Fig. 14 Molecular structures of fluorinated NDI-based conjugated polymers,[51] poly[(*N*,*N*′-bis(2-octyldodecyl)naphthalene-NDI-2,6-diyl)-*alt*-5,5′-(2,2′-bithiophene)] (P-(NDI2OD-T2)) and its fluorinated analogue,[53] conjugated copolymers of vinylene flanked NDI,[54] and synthesis of PTNQSH-XX copoly(triazole imides).[55]

on Au(111) to form chain structures on the step edges at low coverages, and chains arranged side-by-side due to strong hydrogen bonding between neighbouring NDI backbones, allowing ordered double layers within the supramolecular structures to be observed. Importantly, within the chain structures, single molecules were visibly observed.

Draper and co-workers described the self-assembly of NDI gel based devices which showed remarkable photo- and electrochromic effects, with the formation of the NDI radical anion showing good cyclability and temperature stability in a low cost device.[63] Their further studies demonstrated stimuli responsive color changes in the device with a color change from transparent to black, caused by either photo- or electrochemical stimuli,

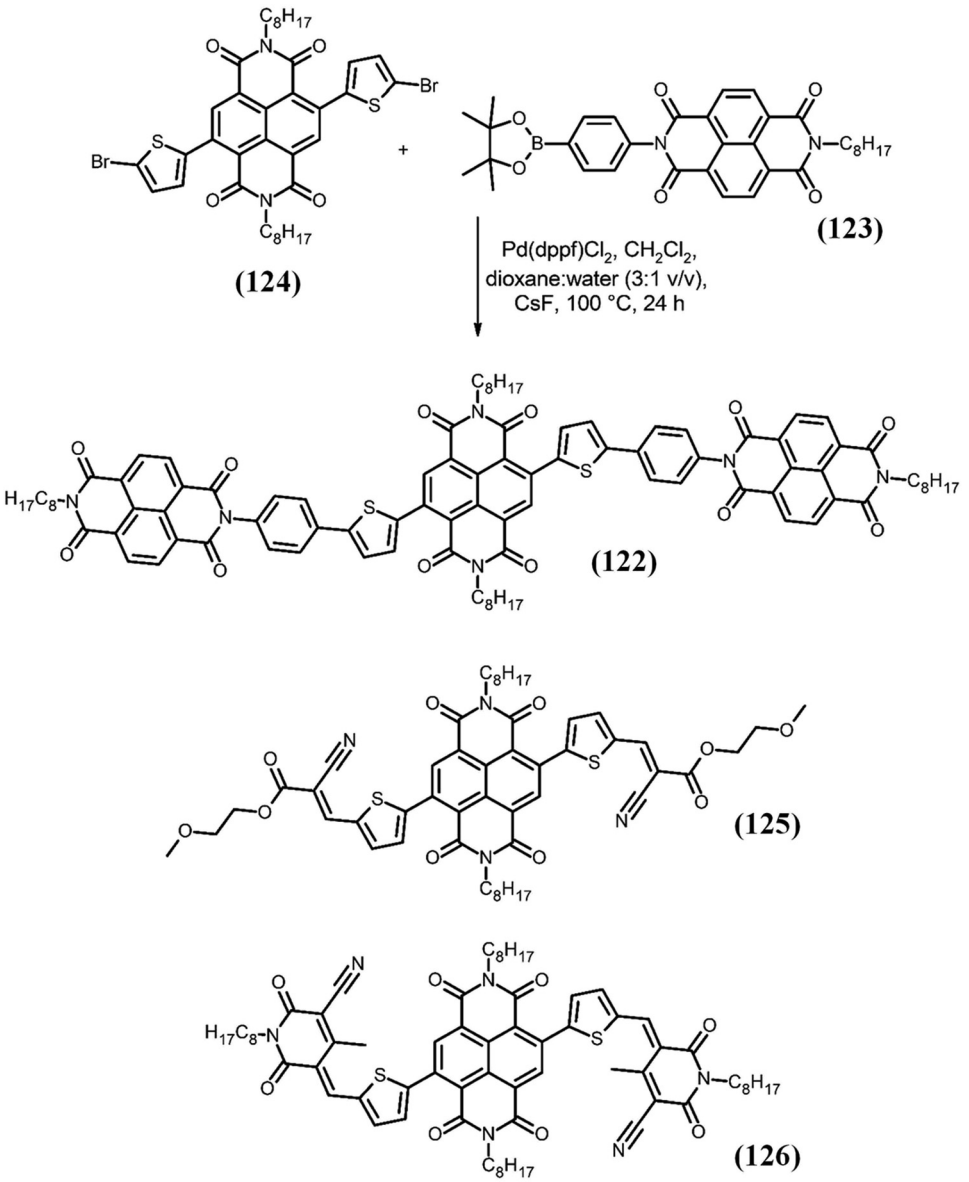

Fig. 15 Molecular structure of (**122**) and its synthetic protocol,[56] and the NDI core-based acceptors (**125**) and (**126**).[57]

and these color changes were stable for many cycles with no degradation in color intensity, nor in the speed of the response.

Lapkowskia and co-workers synthesised aliphatic–aromatic structures based on NDI units (**134–137**) and studied the optical, electrochemical, EPR and fluorescence properties.[64] The electrochemical properties of NDI based polymers show low-lying LUMO levels in open air-operating devices, ranging from −4.28 to −4.14 eV, and fluorescence quantum efficiencies reach up to 68% in the solid state as a blend with poly(methyl methacrylate). The Yin group synthesised two star-shaped molecules with NDIs attached as side arms to a central benzene moiety (Fig. 6).[37] Both molecules (**70**, **71**) showed a bathochromic shift in absorption in thin films when compared to the solution state and displayed two reversible reduction waves (at −0.93 and −1.33 V for (**70**) and −0.89 and −1.28 V for (**71**) (*vs.* AgCl/Ag)) with low-lying LUMO energy levels, *i.e.* −3.83 eV for (**70**) and −3.87 eV for (**71**). These properties demonstrated that different alkyl chains had little effect on the redox behaviour, and that both molecules are good electron acceptors which may be employed for n-type organic semiconductors. The Wang and Jiang group synthesised a series of diazapentacene NDI derivatives and studied their optical and electrochemical properties, showing that these molecules display high electron affinity (up to 4.39 eV) with small HOMO–LUMO band gaps, *i.e.* 1.26 eV, marking these derivatives as candidates for n-type semiconductors, as well as NIR (**22**, **24**) dyes (Fig. 2).[17] Earlier, the Zhao group demonstrated that dihydro- and tetrahydro-tetraazaacence NDIs bearing 6 or 7 laterally fused six-membered rings displayed halochromic and redox-switchable vis-NIR optical properties.[65] Interestingly, they also demonstrated that acid-assisted tautomerization of 2H-TAHDI (**147** and **148**) is also possible, and naked eye colour changes of

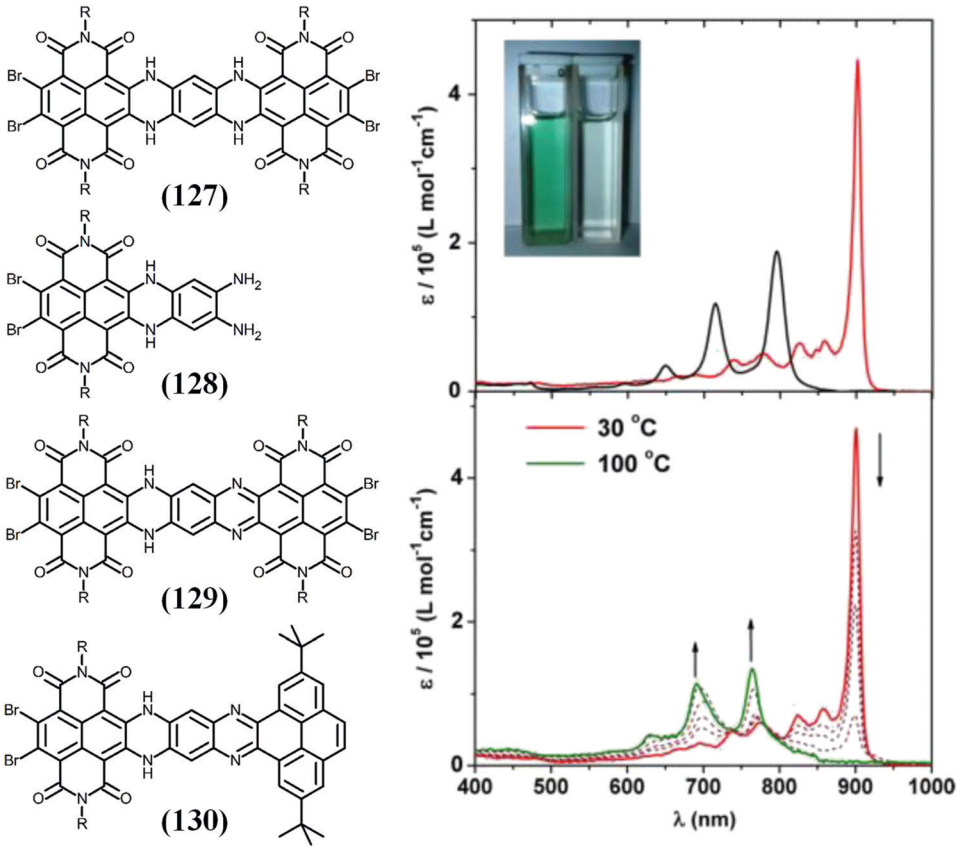

Fig. 16 Absorption spectra of (**127**) (1.0×10^{-6} M) in $CHCl_3$ (black) and *n*-hexane (red) at room temperature; the image shows solutions in $CHCl_3$ (left) and *n*-hexane (right); absorption of (**127**) in *n*-octane (1.0×10^{-6} M) at various temperatures (arrows indicate the direction of intensity change with increasing temperature).[15] This figure has been adapted from ref. 15 with permission from The American Chemical Society, copyright 2014.

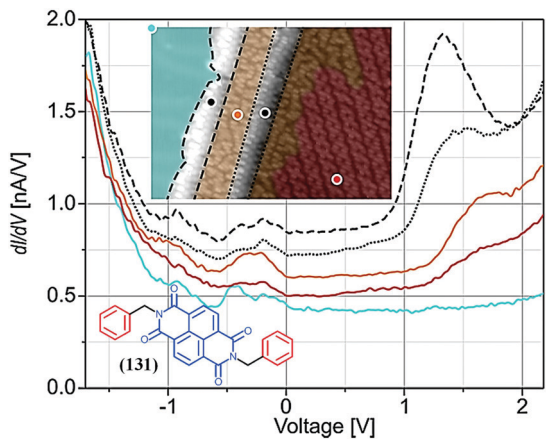

Fig. 17 STS measurement on BNTCDI (**131**) in double-layer structures (V_{bias} = −1.8 V, I_{set} = 1.0 nA, offset = 0.1 nA V^{-1}). Spectra obtained on the bare Au(111) surface (cyan), disordered double layers (orange), ordered double layers (red), and chain structures formed by molecules on the step edge (marked by dashed and dotted lines). Inset: STM image with color-coded areas to identify the positions where the spectra were taken.[62] This figure has been adapted from ref. 62 with permission from The American Chemical Society, copyright 2019.

4H-TAHDI (**145**) and 2H-TAHDI (**147**) *via* reversible redox and protonation–deprotonation processes could be observed. 2H-TAHDI (**145**) quantitatively reduced to 4H-TAHDI (**145**), and reverse oxidation of 4H-TAHDI (**145**) to 2H-TAHDI (**147**) using PbO_2/MnO_2 was shown to be possible (Fig. 19), enabling redox-switching in the future for NIR chromophores. Takimiya prepared electron deficient NDI derivatives based on thiophene fused NDI (**132**, **133**), which displayed a low-lying energy level LUMO (3.8–4.1 eV) with a high electron mobility (~ 0.8 cm^2 V^{-1} s^{-1}).[27] Both the NDI derivatives were shown to be very promising for n-type and ambipolar materials for OFETs and promising acceptors for OPVs, giving power conversion efficiencies (PCE) of up to 9%. Schab-Balcerzak has shown that azomethine bridged NDI derivatives with an anthracene end-cap have low LUMO energies between −3.96 and 4.24 eV with very low band gaps of 1.19 to 1.53 eV, indicating that these derivatives also can be used as n-type semiconductors.[40] A report by the Seferosa group shows the influence on the optical properties of the core-thionated NDI (**138–144**) and PDI, where as expected the thionated NDI gives a three orders of magnitude increase in electron mobility compared to the parent PDI derivatives, as well as a bathochromic shift in optical absorption and an increase in electron affinity (Fig. 18).[66]

The Kim and Wu group described the formation of the radical and diradical of NDI derivatives through chemical oxidation using the lead(IV) dioxide of hydroxyl aryl core-substituents

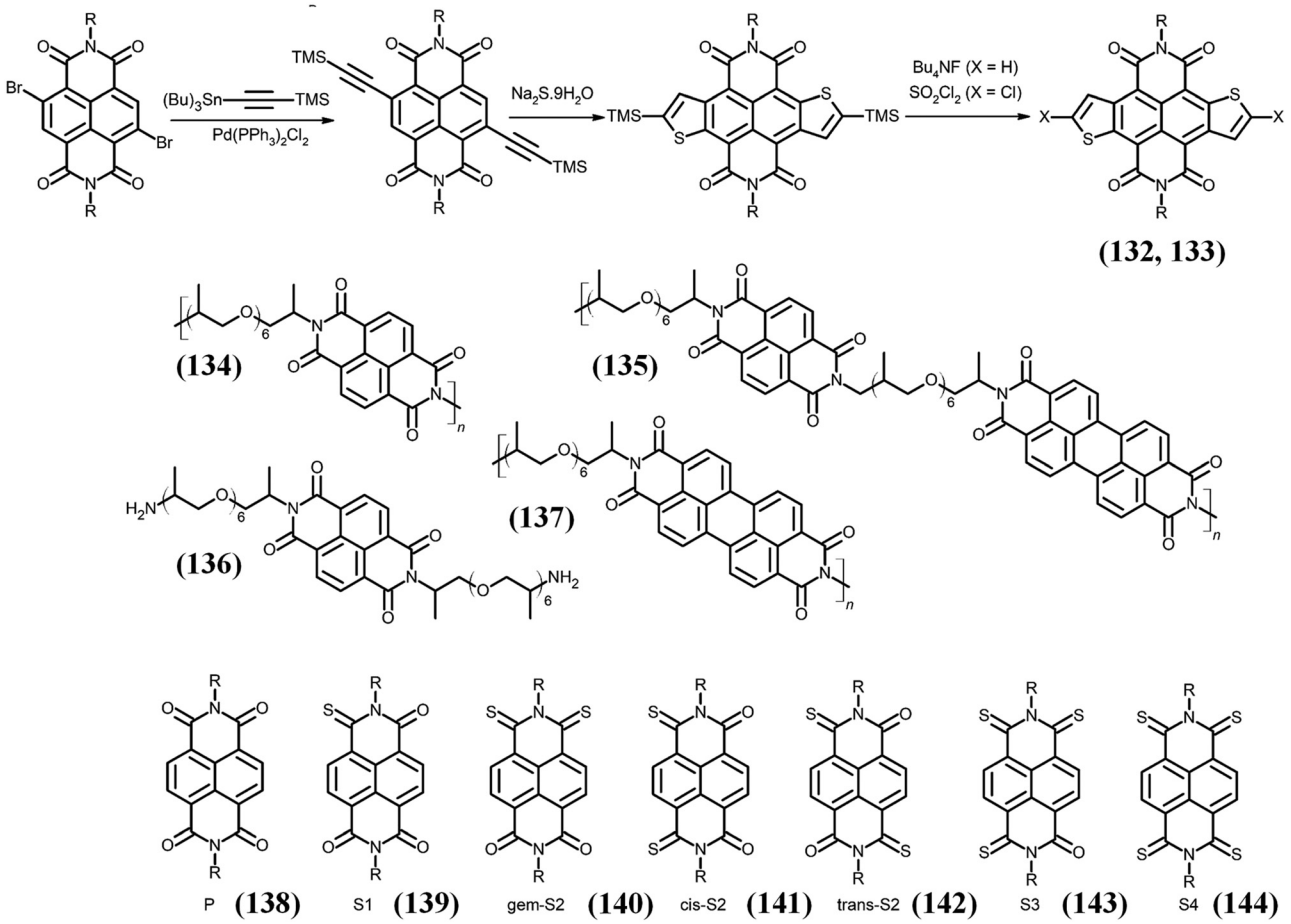

Fig. 18 Synthesis of *N*,*N*′-bis(2-cyclohexylethyl)-NDTI derivatives (**132**, **133**).[27] The molecular structure of aliphatic–aromatic polymers based on perylene or/and naphthalene diimide units,[64] and chemical structures of thionated naphthalene diimides (R = dodecyl).[66]

in (**149**) and (**150**), where the formation of radical species *via* deprotonation of the OH group of the core generates the corresponding $(\mathbf{149})^{-}$ and $(\mathbf{150})^{2-}$ anions, respectively, which were evaluated by NIR–UV–Vis absorption spectroscopy (Fig. 20).[67] Further superconducting quantum interference device characterisation and quantum calculations revealed a ground state NDI diradical with a singlet diradical character of $y = 0.69$.

The development of rigid organic materials having multiple redox states with emission properties is important for applications in organic electronics and photonic materials. PDI fluorophores have attracted attention because of their high fluorescence quantum yield in solution; however, they suffer from drawbacks such as aggregation-caused emission quenching in the assembled or solid state. To overcome this issue, the Wasielewski and Stoddart group synthesised two chiral isosceles triangles, in which they used one PDI fluorophore and two PMI or NDI units in a cyclic triangle (**151**). Interestingly, the triangle bearing two NDIs and one PDI displayed efficient intramolecular energy transfer from NDI to PDI subunits, in contrast to the triangle prepared from PMI and PDI.[68] However, both isosceles triangles show excellent fluorescence quantum yields, 10- to 40-fold larger than the triangle prepared from only PDI. Both the triangles showed reversible redox states, which is useful for molecular organic optoelectronics, energy storage, and energy-harvesting devices in the future. In another report, the group has synthesised two rigid chiral triangles having either two non-identical PMIs and one NDI or two NDIs and one PMI as a redox-active unit.[69] When compared with a triangle containing three identical NDIs or PMIs, the non-identical triangles formed one-dimensional supramolecular nanotubes by interaction-driven columnar stacking in DMF. They also showed that isosceles triangles can reversibly accept up to six electrons by cyclic voltammetry, and when used for rechargeable lithium-ion batteries the triangles with NDI subunits were superior to PMI in terms of the cell performance of the batteries.

Recently, we have shown that the optical properties of NDI acceptors can be tuned *via* the addition of the polymer P3HT in solution, both in the pristine state as well as in a blend film, with tuning of the HOMO and LUMO energy levels due to electron transfer.[56] As such, three NDI functionalities at the central and peripheral positions of a trimer exhibited two absorption peaks (*i.e.* 362 nm and 382 nm) at a high energy, together with a strong shoulder peak at 543 nm in solution. However, in a thin film, the absorption peaks were broader and

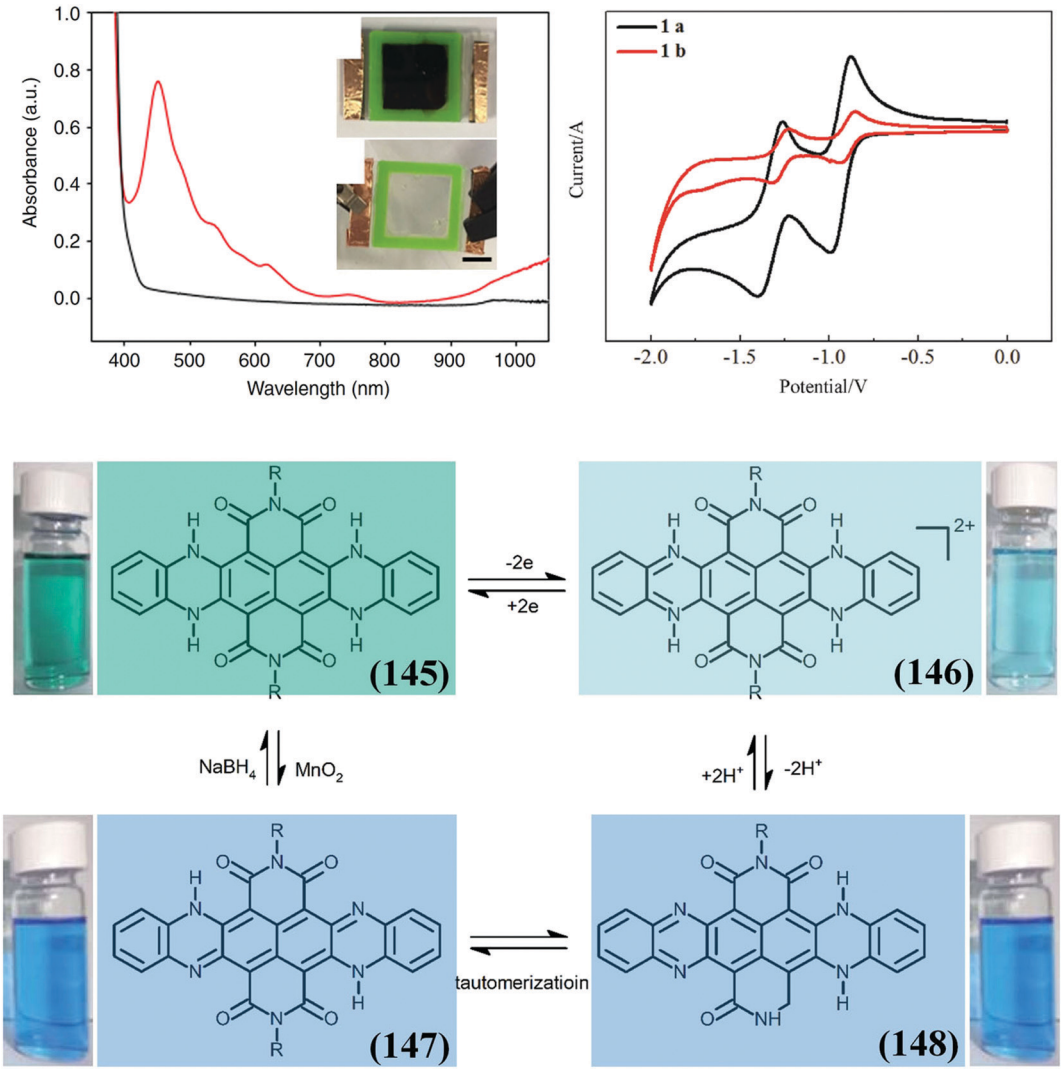

Fig. 19 Dual stimuli responsive behavior and UV-Vis absorption spectra of the (**193** in Fig. 37) gel prepared in a cell irradiated with UV light (red data and b) and after applying 0.6 V for 60 s (black data and c). The scale bar is 1 cm.[63] This figure has been adapted from ref. 63 with permission from Springer Nature, copyright 2018. Colour changes of 4H-TAHDI and 2H-TAHDI *via* reversible redox and protonation–deprotonation processes.[65] This figure has been adapted from ref. 65 with permission from The Royal Society of Chemistry, copyright 2010.

λ_{max} was red-shifted by ~51 nm, which was due to p–p stacking in solid state. The HOMO and LUMO energy levels were determined using photoelectron spectroscopy in air (PESA) on pristine films. The estimated HOMO was −5.70 eV, whereas the LUMO level was calculated to be −4.15 eV with a band gap of 1.55 eV. Furthermore, this novel trimeric derivative was shown to be an excellent n-type material, and when blended with the P3HT p-type semiconductor, the resulting bulk heterojunction solar cell device has an excellent power conversion efficiency of 7.65%. In a similar vein, Lee and co-workers synthesised triads using the acceptor–acceptor–acceptor (A–A′–A) molecular platform, with three different types of pendants (A′): benzothiadiazole (BTD-P), naphthalene diimide with octyl (NDI-O-P) or ethylhexyl groups (NDI-EH-P), or perylene diimide with ethylhexyl (PTCDI-EH-P).[71] Both NDI-EH-P and NDI-O-P showed absorption bands at 514 nm with identical spectra, which confirms that the alkyl chain does not have any influence on absorption. In comparison, BTDP displayed a UV-vis band at 445 nm and PTCDI-EH-P produced the longest λ_{max} of 587 nm, with the shift becoming more pronounced as the electron-deficiency of the pendant increases from BTD to NDI to PTCDI (**152–155**) as shown in Fig. 22. As expected, the solid state absorption in films showed a significantly red-shifted absorption compared with the solution spectrum, which is attributed to the formation of J-aggregates. This study demonstrated that simple triads can be used as a model system for future development of donor–acceptor systems. A report by Zerson and co-workers demonstrated for the first time that the properties of copolymers of bis-thiophene-NDI structures can be tuned in spin-cast films and annealed films, and this phenomenon was studied using atomic force microscopy.[72] This study that compares molecular arrangement along with electronic properties of polymers may be useful for applications where n-type mobility in organic field-effect transistors is important.

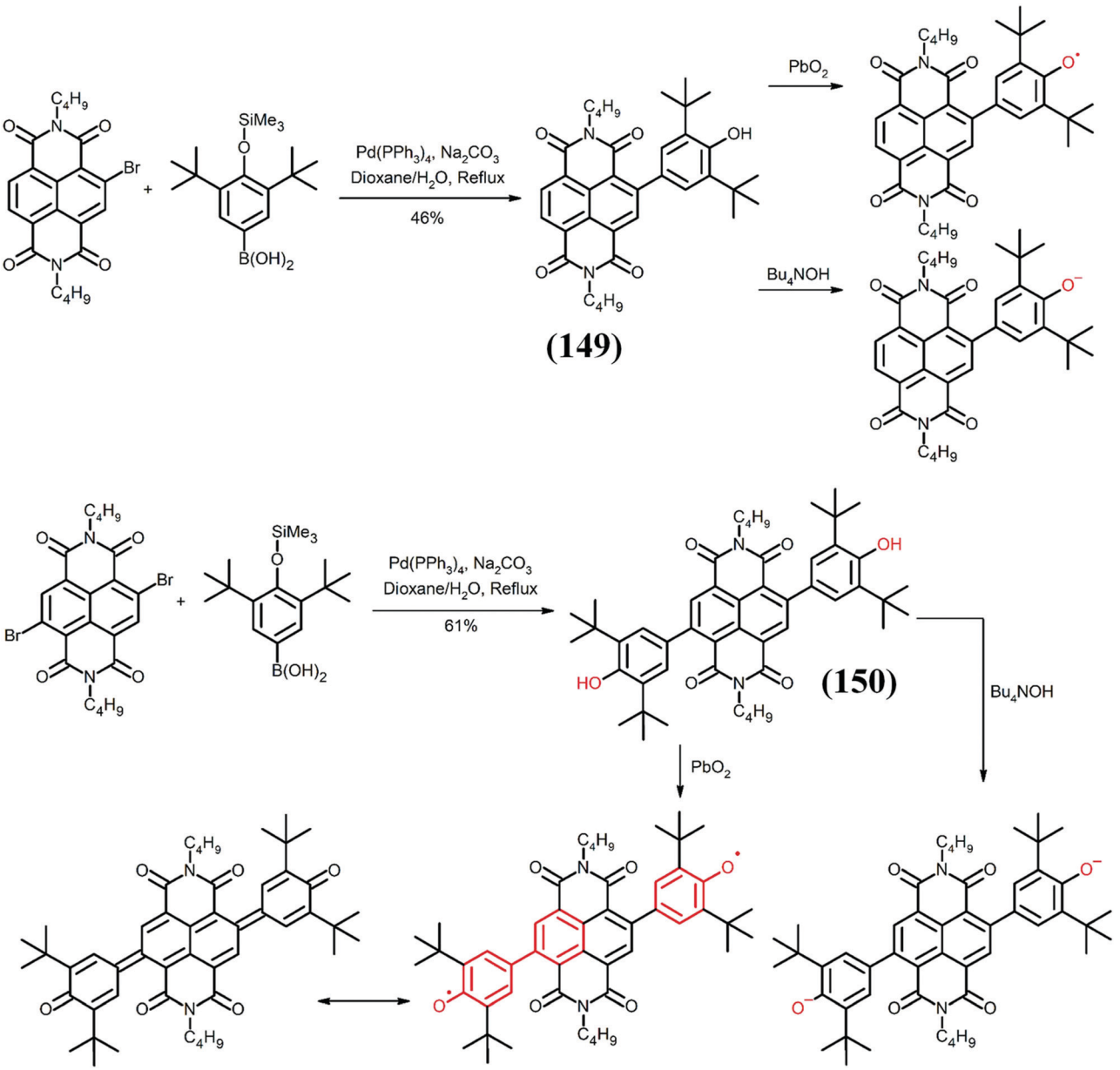

Fig. 20 Synthesis of (**149**) and (**150**) and their corresponding (di)anion and (di)radical species.[67]

Electron deficient NDI has the ability to be used for anion–p interactions, with one example being fluoride anion (F^-) sensing. In the literature, many reports show that a fluoride anion not only forms a complex with NDI, but is also involved in electron transfer processes, where F^- is oxidised to fluorine and NDI is reduced to an anionic species. However, a few reports state that oxidation of F^- is an unlikely mechanism. As such, Gabbaïï and co-workers studied in detail the use of F^- to reduce *N′N′*-di-(2,6-di-iso-propylphenyl)-NDI (**156**) in the presence of cobaltocene, a very well-known one-electron molecular reductant (Fig. 23).[73] In their study, they revealed that the deprotonated solvent acts as a reducing agent to generate NDI radicals, suggesting that the F^- ion does not act as a reducing agent in this instance.

Ayitou reported a reductive desulfurization reaction of NDI using thionating Lawesson's reagent, in which they found that, along with expected thionated NDI derivatives, a new naphtho-*p*-quinodimethane heterocyclic derivative (**159**) was isolated, showing broken/reduced symmetry (Fig. 24).[74] Experimental and theoretical modelling suggests that this derivative was formed *via* a six-membered oxathiaphosphenine ring intermediate instead of the usual four-membered oxathiaphosphetane ring. The UV-vis absorption of the new naphtho-*p*-quinodimethane derivative was red-shifted compared to the NDI starting material. The time-dependent photoluminescence study in a glass matrix produced an aromatic triplet excited state, along with radiative decay to the ground state with an ~395 μs lifetime upon excitation using a Xe lamp at an

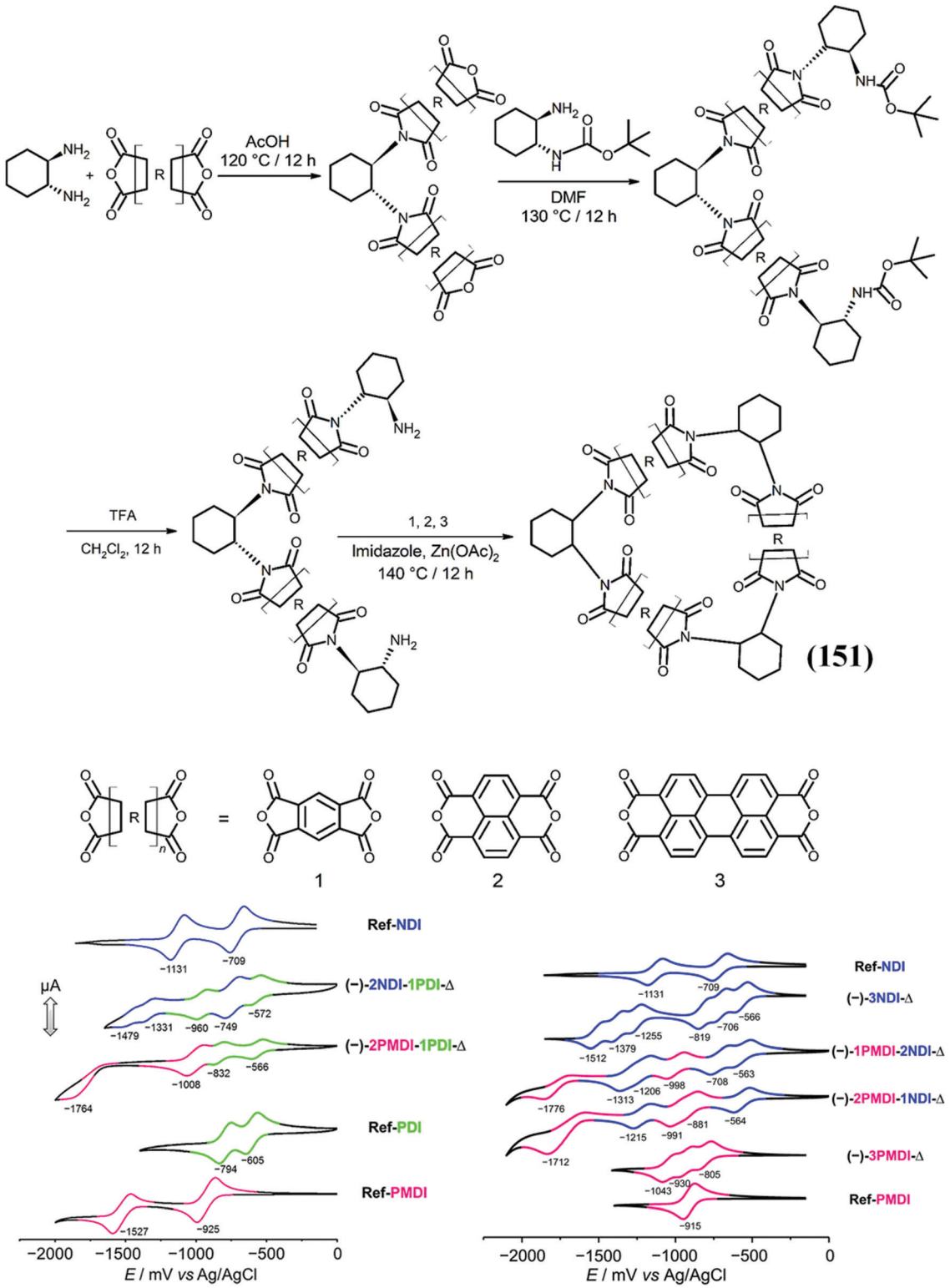

Fig. 21 Stereospecific stepwise preparation of chiral isosceles triangles[68,70] and the CVs (0.5 mM in CH_2Cl_2, 100 mM $TBAPF_6$, 50 mV s^{-1}, 298 K) of Ref-NDI, (−)-3NDI-Δ, (−)-1PMDI-2NDI-Δ, (−)-2PMDI-1NDI-Δ, (−)-3PMDI-Δ, and Ref-PMDI. Half-wave peak potentials ($E_{1/2}$) are shown in mV.[69] This figure has been adapted from ref. 69 with permission from The American Chemical Society, copyright 2016.

excitation wavelength of 470 nm. These results clearly demonstrated (anti)aromaticity according to Baird's rule of aromaticity.

The Papanikolas and Schanze group synthesised a series of acceptor–donor–acceptor assemblies bearing thiophene oligomers (T_n, n = 4, 6, 8, 10 and 12) (**160**) as donor and NDI as

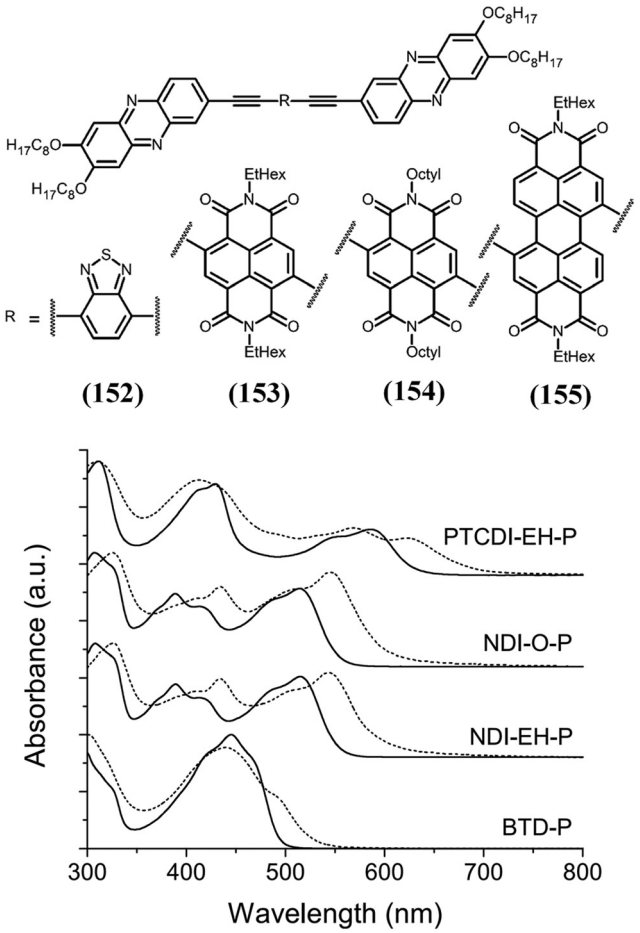

Fig. 22 Molecular structures of acceptor (A)–acceptor′ (A′)–acceptor (A) triads (**152–155**) and the UV-visible absorption spectra of BTD-P (**152**), NDI-EH-P (**153**), NDI-O-P (**154**), and PTCDI-EH-P (**155**). Solid line: in DCM (5 μM), broken line: film.[71] This figure has been adapted from ref. 71 with permission from The American Chemical Society, copyright 2019.

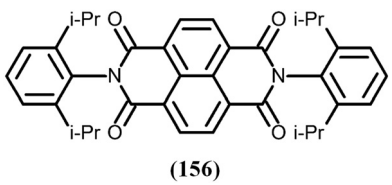

Fig. 23 The molecular structure of *N′N′*-di-(2,6-di-iso-propylphenyl)-NDI (**156**).[73]

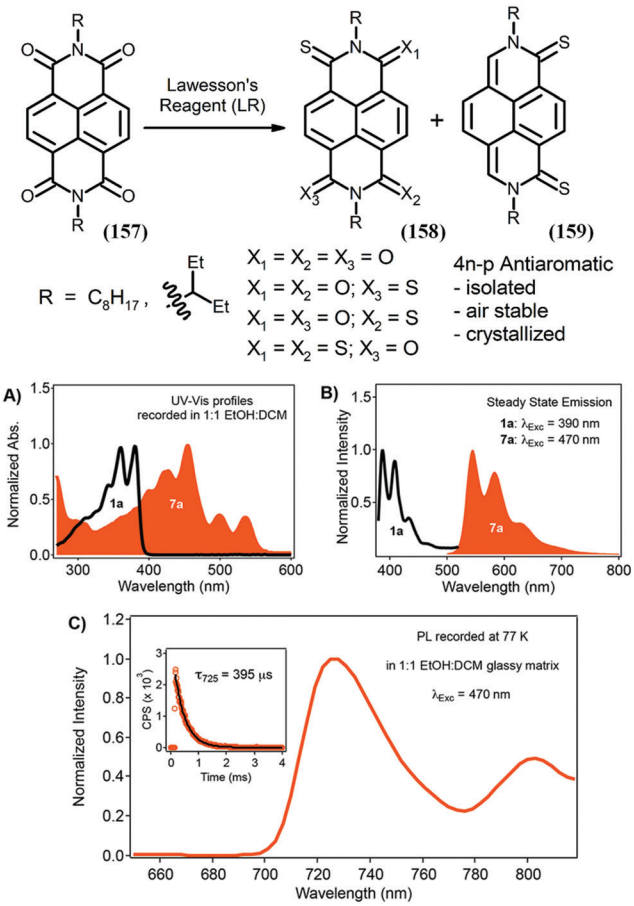

Fig. 24 Thionation of NDI using Lawesson's reagent: isolation of thionated NDIs (**158**) and antiaromatic naphtho-*p*-quinodimethyl bis-thioamide (**159**). (A) UV-vis profiles of (**157**) and (**159**) in 1 : 1 ethanol : dichloromethane (EtOH : DCM). (B) Steady-state emission profiles of (**157**) and (**159**) with optical density (O.D.) = 0.15 at excitation wavelengths of 390 and 470 nm, respectively. (C) Time-dependent and gated (90 μs delay) photoluminescence of (**159**) in a 1 : 1 EtOH:DCM glassy matrix at 77 K with pulsed excitation using a Xe lamp (pulse length: ~20 μs). (Inset) Phosphorescence decay trace of (**159**) after pulsed excitation at 77 K.[74] This figure has been adapted from ref. 74 with permission from The American Chemical Society, copyright 2017.

acceptor end groups.[75] Femtosecond transient absorption spectroscopy studies revealed ultrafast charge separation after excitation of the thiophene donor, leading to charge separation and producing NDI anions ($NDI^{\bullet -}$) and a thiophene cation ($T_n^{\bullet +}$), along with charge separation, followed by rapid recombination with length-dependent long-range electron-transfer (Fig. 25).

Imaging individual molecular orbitals of NDI on Pt(111) by means of STM and DFT studies is challenging, but is helpful to better understand the properties of the derivatives. To this end, Atodiresei and co-workers studied 2,7-dibenzyl-NDI (**161**) adsorbed on Pt(111), where two methylene groups of the benzyl side arms were introduced on both sides of the diimide, which induces a steric hindrance (Fig. 26). The molecule is thus slightly lifted from the surface because without steric hindrance the four oxygen atoms of NDI weakly chemisorb as a molecular planar structure on any metallic surface.[76] Thus, the benzyl side arms of (**161**) induced non-planarity into the molecule, enabling imaging of NDI on Pt(111).

4 Supramolecular chemistry of NDIs

Supramolecular chemistry (chemistry beyond the molecule) is a concept derived from nature to construct complex molecular architectures.[77] One of the finest examples is the

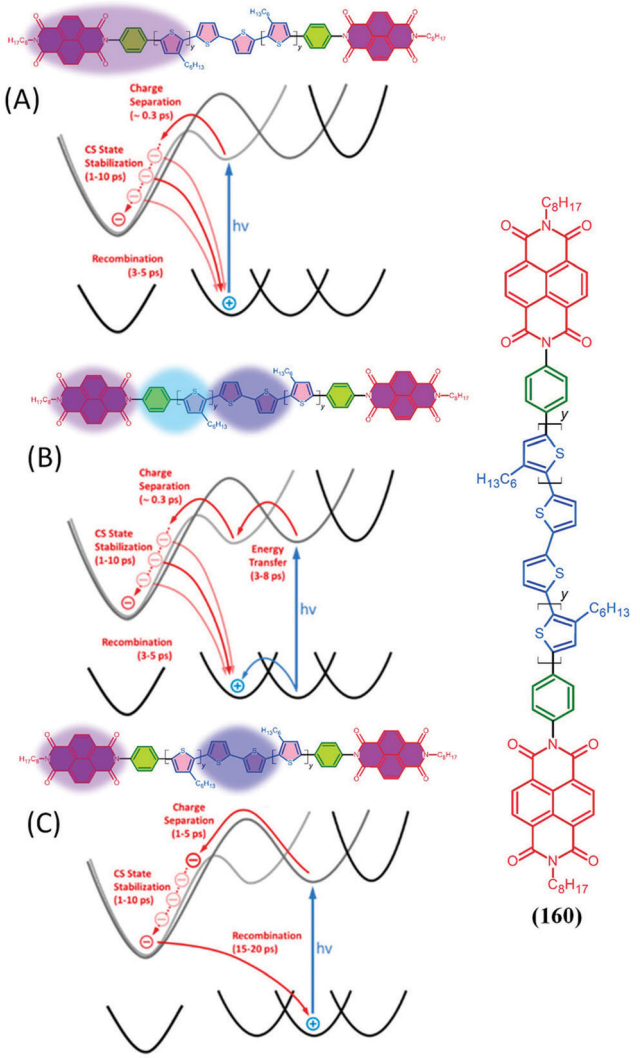

Fig. 25 Mechanism of charge separation and recombination for photo-excitation (A) at the end of the thiophene chain (red pentagons) and delocalized across phenylene bridge (green hexagons); (B) at the center of the thiophene chain where energy transfer is followed by ET; and (C) at the center of the thiophene chain where long-range ET occurs.[75] This figure has been adapted from ref. 75 with permission from The American Chemical Society, copyright 2018.

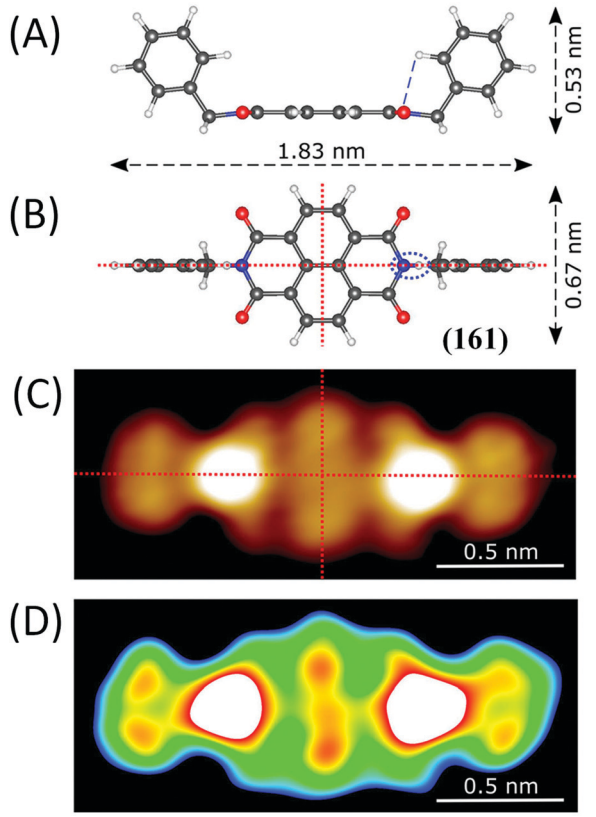

Fig. 26 Sketch of (**161**): (A) side view and (B) top view with indicated mirror planes. One hydrogen bond between a N atom of the NDI core and the next H atom of the phenyl ring (N···H distance: 0.262 nm) is indicated by a dashed blue line in the side view and an ellipsoid in the top view. (C) High-resolution UHV-STM image of a single (**161**) molecule; the mirror planes are indicated (U_{bias} = +0.5 V, I_{set} = 510 pA, T = 4.2 K). (D) Contrast enhanced illustration of (**161**).[76] This figure has been adapted from ref. 76 with permission from The American Chemical Society, copyright 2017.

photosynthetic reaction center (PRC) of purple bacteria, where various molecules such as bacteriochlorophyll, two bacteriopheophytins, and two quinones are arranged in a non-covalent manner along an axis of several membrane proteins, giving rise to long-lived charge separation. All the supramolecular thermodynamically stable structures at both the cellular and subcellular levels from nano-to-millimeter dimensions use the bottom-up/bioinspired approach. Supramolecular chemistry uses weak interactions such as π–π interactions, hydrogen bonding, and van der Waals forces to produce architectures of various sizes, shapes, and functions, similar to those of the working PRC molecular apparatus.[77,78] Using this approach, in the early 1960s, Pedersen, Lehn and Cram developed crown ethers,[79] cryptands[80] and spherands,[80] respectively, and were recognised with the Nobel prize in 1987. Supramolecular self-assembly also allows access to various architectures such as nanoballs, nanotubes, flower-like structures, nanoboxes, cavities, vesicles, and many other structures, which provide molecules with novel physical and chemical properties. For this purpose, various small organic molecules have been used such as porphyrins,[67] oligo(*p*-phenylenevinylene), and PDI, to name a few, because of their favorable optical and electronic properties. However, some of these materials suffer from the drawbacks of poor solubility, multistep synthesis and high cost.

Researchers are attracted toward the use of NDIs in supramolecular chemistry due to their relatively easy preparation, redox-activity, access to neutral and planar molecules as well as demonstrated n-type properties.[81] Furthermore, through core-substitution of NDIs their optical and electronic properties can be tuned in line with their structural features, which can be similar to naturally occurring acceptors of PRC.[82] Recently, NDIs and cNDIs based on various architectures such as worm-like morphologies, cages, catenanes and rotaxanes, nanotubes, nanowires, gels, and vesicles have been produced with applications in sensors, ion channels, organic solar cells,

and organic field-effect transistors and medicinal applications.[83] We have reviewed this part in depth in an earlier review, so here we outline further development of novel NDIs and cNDIs and their use in supramolecular chemistry for the construction of new architectures.

4.1 Nano- and micro-superstructures

In an earlier report, we designed and synthesised NDI derivatives bearing hydrophobic alkyl chains at one imide position, and at the other NDI imide position we placed para-nitroaniline, with (**162**) and without (**163**) an ethylenediamine spacer (Fig. 27).[84] This design incorporated three important features: (i) a hydrophobic alkyl chain with an affinity for non-polar solvents, (ii) an amide linkage using the ethylenediamine spacer, capable of intermolecular amide hydrogen bonding, and (iii) the core of the NDI which is capable of π–π stacking.

For stacking and aggregation of aromatic planar molecules, UV-vis absorption and fluorescence are the techniques that are used to probe assembly in solvent mixtures. Therefore, we firstly studied the self-assembly of both the amphiphiles (**162**, **163**) in chloroform with various amounts of MCH, where both derivatives in chloroform exhibit three peaks (*i.e.* 340, 358 and 380 nm), which are typical for π–π* transitions. (**162**) in a mixture of chloroform and MCH led to a decrease in peak intensity with loss of the fine structure, along with the appearance of a new band at 404 nm, caused by the aggregation of NDI-NA. The emission spectrum of NDI-NA in chloroform displayed three weak bands at 408 nm, 430 nm, and 462 nm. However, in a mixture of chloroform and MCH (0–95%), an enhancement of fluorescence was observed with a high quantum yield of ~22.8%, which is indicative of an aggregation induced emission enhancement (AIEE) effect. Field-emission scanning electron microscopy (FE-SEM) was used to visualise the self-assembled structures, showing that NDI-NA formed 10–100 nm thick multilayer sheets up to 20 mm in length from chloroform/MCH (v/v, 5 : 95), which then formed micelles from curved nanosheets, which further collapse to decrease surface energy and form microcups.

In another report, we synthesised an NDI bolaamphiphile containing the peptide (Tye-Glu) segment at both the diimide positions (**164**), and further employed this structure for supramolecular self-assembly through solvophobic control (Fig. 28). The NDI-peptide bolaamphiphile self-assembled into micro-flower-like structures from THF : MCH (4 : 6, v/v) solvent mixtures, while THF : water (2 : 8, v/v) produced grass-like architectures.[85] We concluded that intermolecular amide hydrogen-bonding between peptide linkages and the π–π interaction within the core of NDI prevented crystallization of the molecule, with fractal growth of the assembly producing various structures. We also reported on the synthesis of an NDI containing a dipeptide with an imide at one end and an amino head group at the other imide position, which self-assembled into uniform golf ball-like spheres with wrinkled surfaces.[86]

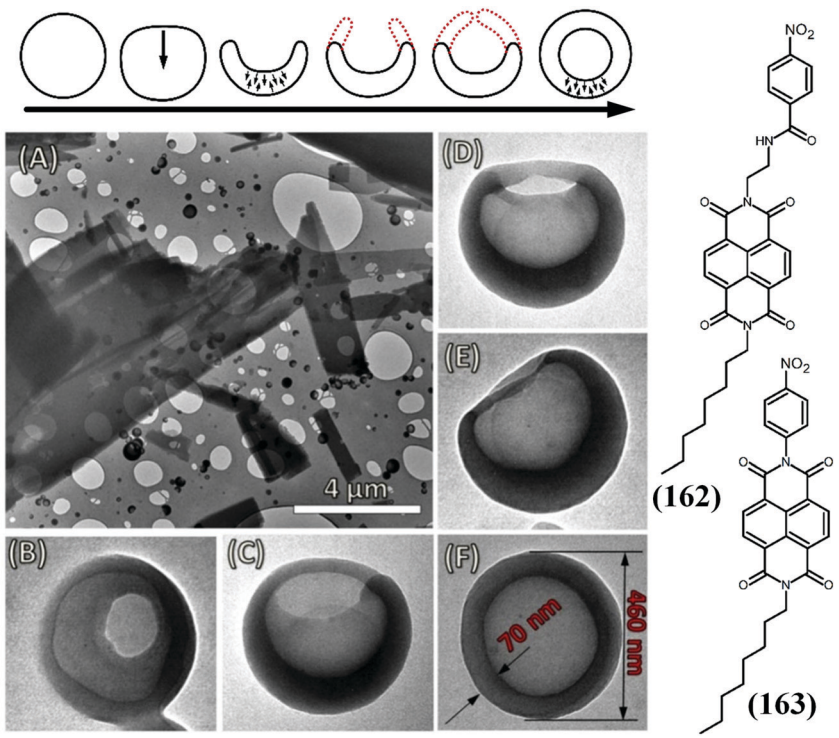

Fig. 27 NDI-NA molecules self-assembled into supramolecular microsheets *via* amide H-bonding, π–π stacking, and hydrophobic interactions. The microsheet bilayer detaches from other microsheets layer-by-layer upon solvent evaporation. Furthermore, the nanosheets are transformed into microcups, which turn into microcapsules (vesicles).[84] This figure has been adapted from ref. 84 with permission from John Wiley and Sons, copyright 2016.

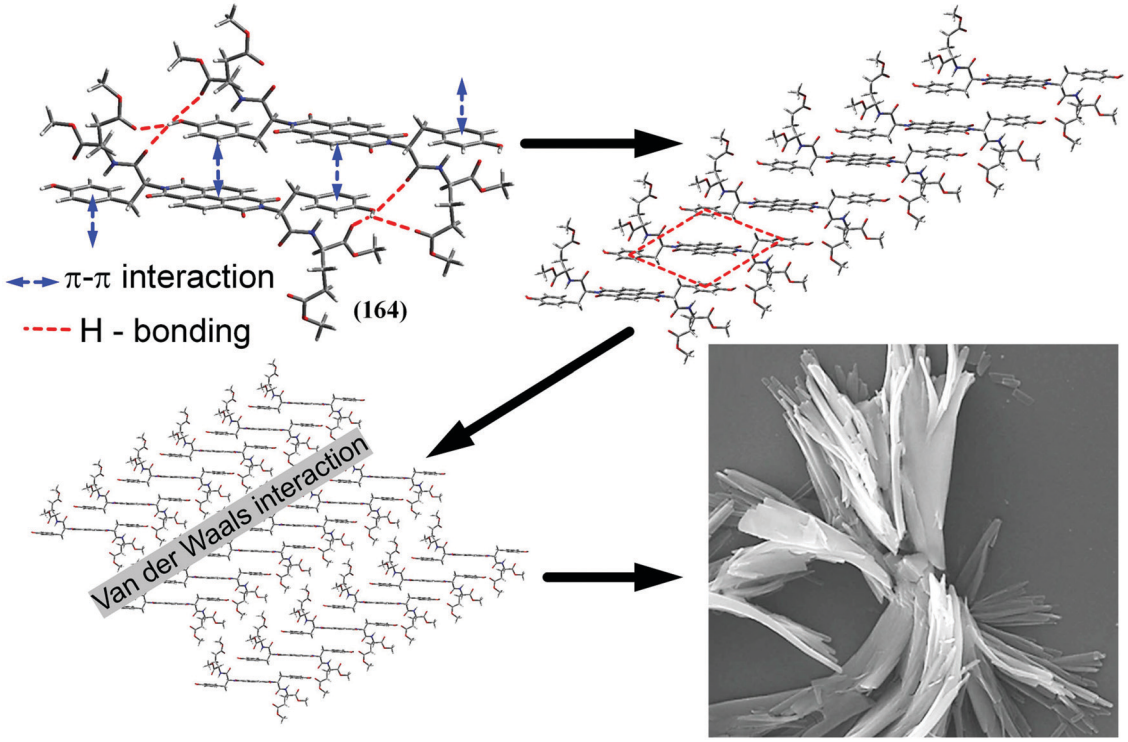

Fig. 28 The self-assembly of (**164**) to give the petals of a flower-like superstructure.[85] This figure has been adapted from ref. 85 with permission from John Wiley and Sons, copyright 2018.

We synthesised an NDI bearing four carbamate (boc protected ethylene diamine) groups (coded as NDI-carbamate) at both the diimide and 2,6-core positions and studied the self-assembly of this molecule in various solvent mixtures.[87] Typically, the NDI-carbamate self-assembled into various nanostructures with controlled structure such as nanobelts, nano-spheres, nano-corals, micro-flowers and grass-like structures from $CHCl_3$ with DMF, MCH, THF, H_2O and MeOH, respectively. The self-assembly and self-organization of the NDI-carbamate derived from the π–π interaction between NDI cores and the H-bonding between the carbamate moieties.

The Ghosh group reported the solvophobic controlled supramolecular assembly of a hydrophobic asymmetrical NDI bolaamphiphile containing a non-ionic hydrophilic OEG chain on one end and a pyridine group at the opposite end of the imide position (**165**).[88] Interestingly, the NDI-chromophore containing a hydrazide group located in the hydrophobic domain between the NDI and the hydrophilic-wedge led to supramolecular self-assembled vesicular structures in non-polar solvents such as tetrachloroethylene (TCE) as well as in aqueous medium, with critical concentrations around 0.3 mM, which was derived from both H-bonding and π–π interactions (Fig. 29). Importantly, in water, the NDI bolaamphiphile assembled due to head-to-head type-stacking, which yielded an unsymmetrical membrane with the pyridine groups located at the exowall. In acidic pH, a pyridinium ion was generated on the surface which showed effective anti-bacterial activity against Gram-positive *S. aureus* with a high HC_{50}/MIC value of >86. They have also studied the utility of surface pyridine groups on the vesicles for molecular recognition, which leads to the encapsulation/release of guest molecules with natural pH stimulus.

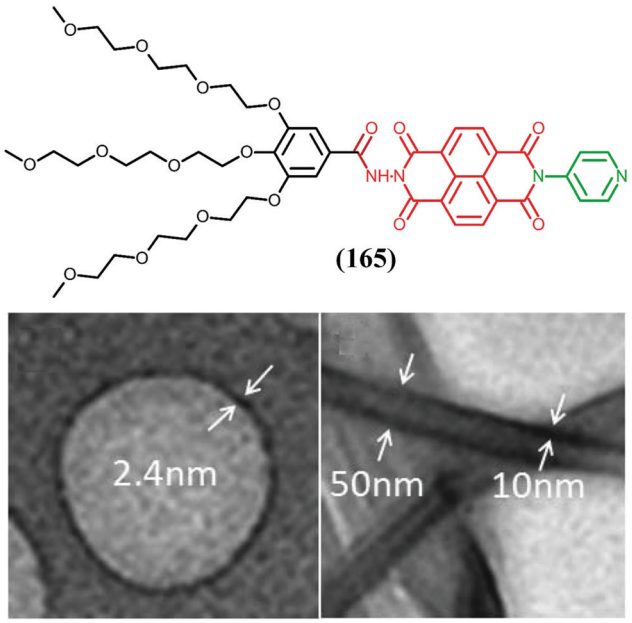

Fig. 29 Anionic NDI-amphiphile molecular structure and HRTEM images of (**165**) (left) in water and (right) in TCE. Samples were prepared by dropcasting a solution (C = 1.0 mM) on a carbon coated Cu grid, followed by removal of the solvent by using a blotting paper, and subsequently drying the grid at RT for 24 h before imaging.[88] This figure has been adapted from ref. 88 with permission from The Royal Society of Chemistry, copyright 2009.

We have also demonstrated the self-assembly of two components *via* charge-transfer (CT) complexation containing an electron donor, *i.e.* DAN (bearing phosphonic acid, *i.e.* (**167**) and (**168**)), and an electron acceptor, NDI (appended with diamine) (**166**), in aqueous medium.[89] In our design, NDI self-assembled with (**167**) *via* dispersive interactions (π–π and van der Waals interactions), which favored the directional growth of 3D flower nanostructures, as crystallization was prevented through CT complexation; however, (**168**) did not self-assemble because of the mismatching (**168**) structure because the amino groups of NDI could not interact with the phosphonic acid of (**168**), as shown in Fig. 30. The SEM and TEM images demonstrated the formation of flower-like structures through donor–acceptor (D–A) CT complex formation between NDI and (**167**). The formation of the CT complex of (**166–167**) was observable by the naked eye, as the pale-yellow NDI with colourless (**167**) in a 1 : 1 ratio gave a dark purple-reddish colour. Importantly, mixing in a 1 : 1 ratio of NDI with colourless (**168**) did not lead to any visual colour changes. In a recent report, de Carvasal *et al.*[90] synthesised the $(DAN–NDI)_3$ hexamer which self-assembled to form supramolecular foldamer nanotubes in water stabilized by donor/acceptor interactions and the solvophobic effect. Similarly, Gowd and co-workers described three-component assembly for the first time, in which a donor, pyrenebutyric acid (PBA), an acceptor, NDI molecules, and a block copolymer, polystyrene-*block*-poly(4-vinylpyridine) (PS-*b*-P4VP), were used to direct the supramolecular assembly approach.[91] The self-assembly of PBA and NDI in the presence of PS-*b*-P4VP produced structures of cylindrical morphology by means of hydrogen bonding and π–π interactions between aromatic cores, in which the hydrogen bonds of PBA with P4VP and aromatic interactions with NDI were visualised by TEM imaging (Fig. 31). Tovar and co-workers

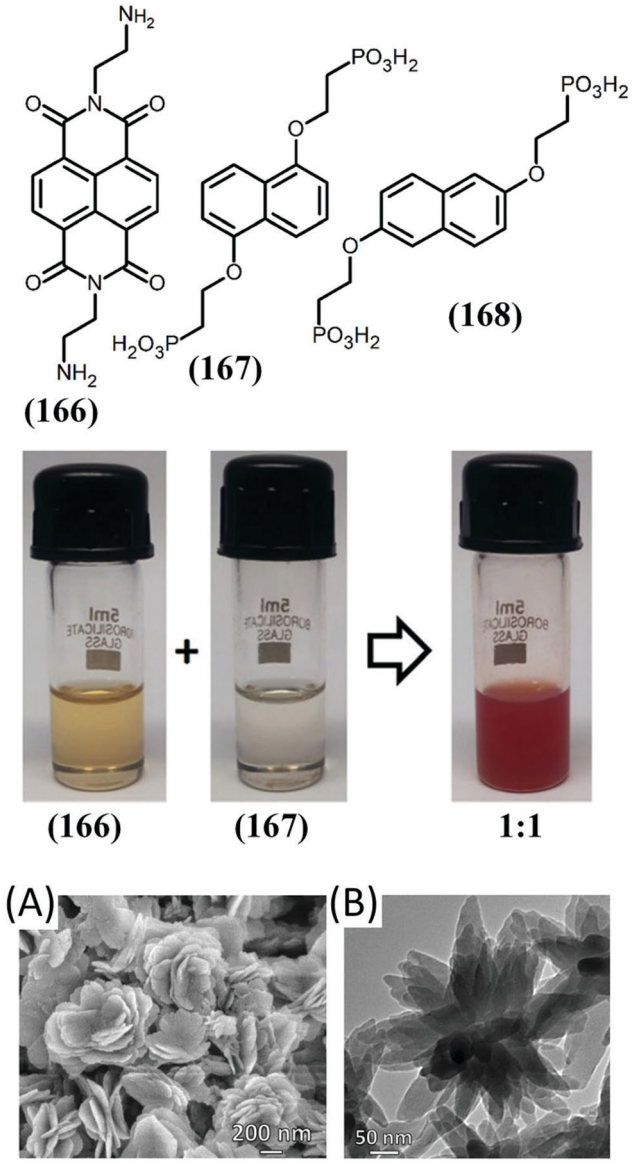

Fig. 30 The molecular structures of NDI (**166**) and phosphoric acid substituted naphthalane (**167** and **168**); the vial shows naked eye charge transfer complex of between **166** and **167** in ultrapure water solutions appear at a 10^{-5} M concentration and complex at a 1 : 1 molar ratio. Further, the flower-like self-assembly of the complex micrographs shown using scanning electron microscopy (A) and transmission electron microscopy (B).[89] This figure has been adapted from ref. 89 with permission from Springer Nature Research (NPG), copyright 2017.

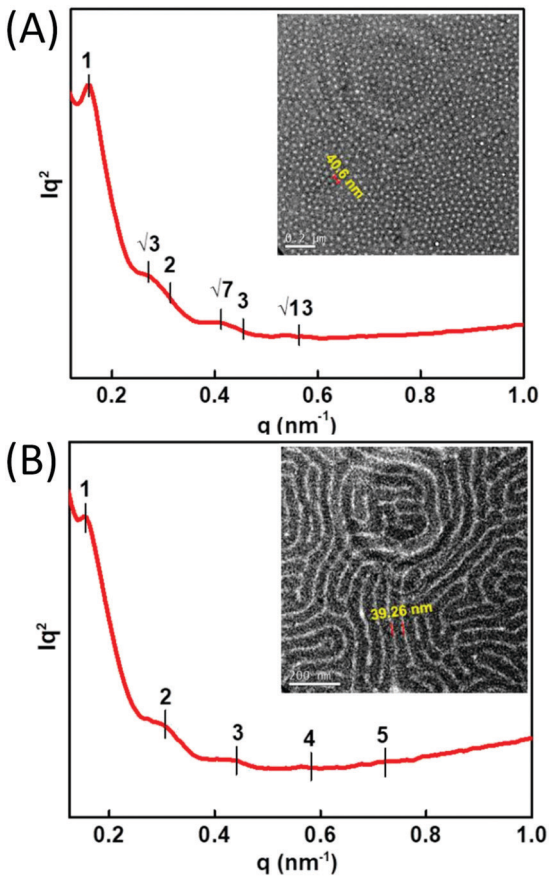

Fig. 31 Lorentz-corrected SAXS patterns of (A) PS-*b*-P4VP (PBA) 0.5 (inset: corresponding TEM image) and (B) PS-*b*-P4VP (PBA + NDI) (inset: corresponding TEM image).[91] This figure has been adapted from ref. 91 with permission from The American Chemical Society, copyright 2019.

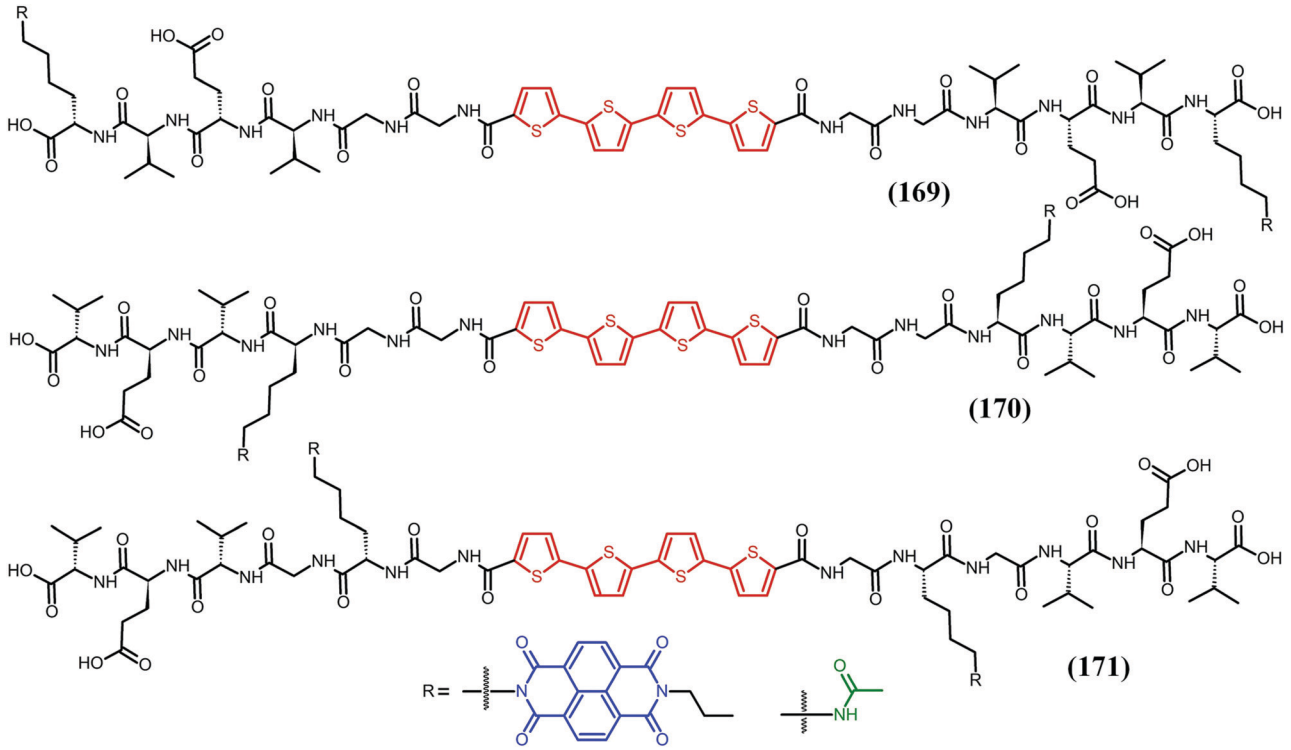

Fig. 32 Structures of donor–acceptor (DA-6, DA-3, and DA-2) and acylated control (C-6, C-3, and C-2) peptides, and the transmission electron micrograph of 25 : 75 DA-2 : C-2 assemblies.[92]

synthesised a series of donor–acceptor structures, with a peptide bearing a π-conjugated oligothiophene electron donor functionalised with NDI at the periphery as an electron acceptor *via* imidation with lysine side-chains (**169–171**) as shown in Fig. 32.[92] Interestingly, due to hydrogen bonding these molecules assembled into one-dimensional molecular wire-like structures in aqueous media. Furthermore, upon excitation of the oligothiophene donors, electron transfer to the peripherally attached NDI acceptor occurred promptly (<100 fs) and with a delay of 270 fs for assembled and unassembled dyads. Assembled donor–acceptor hybrids resulted in an enhancement of charge-separation and a 10- to 100-fold increase with a nanosecond time regime. The Ghosh group studied the multi-stimuli-responsive assembly of an amphiphilic copolymer with alternative donor (pyrene) (**172**)–acceptor (NDI) (**173**) functionalities within the copolymers through CT and hydrogen bonding (Fig. 33).[93] In another example, they described the

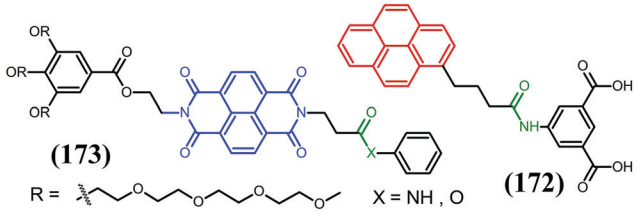

Fig. 33 Structure of the amide-appended donor and acceptor-type *p*-amphiphiles and the control molecule NDI-2.[93]

supramolecular self-assembly of diamino-substituted NDI through hydrogen-bonding within donor–acceptor–donor (D–A–D) configurations *via* J-aggregates, leading to nanotubular superstructures and gel formation in *n*-decane.[94] Maria and co-workers synthesised an NDI bearing thiophene at both diimide positions with a phenyl spacer (**174**). They have studied self-assembly under both thermodynamically and kinetically controlled conditions, producing 1D needles and nanofibers when the solvent slowly evaporated (Fig. 34).[95]

The Sakurai and Seki group synthesised an NDI containing a dodecyl alkyl chain at one imide position and triethylene glycol (TEG) chains on the other side with phenyl ring as a spacer (**175**). The resulting $NDI_{C12/TEGG0}$ assembled into a *p2mg* symmetry with a rectangular columnar mesophase through hydrophobic/hydrophilic nano-segregation of side chains.[96] This molecular design strategy using immiscible side chain pairs (forming hydrophobic/hydrophilic nano-segregation of side chains) enables stacking to form a columnar phase rather than other ordered micellar cubic, crystalline, or isotropic liquid phases when using dodecyl or TEG peripheral chains. Ghosh and co-workers reported the synthesis of NDI chromophores bearing two different hydrogen bonding groups, *i.e.* hydrazide (P1–50) (**176**) or amide (P2–50) (**177**), with hydrophobic/hydrophilic balance, which self-assembled into unsymmetrical vesicles and cylindrical micelles, respectively (Fig. 35).[97] Interestingly, variations in the hydrophobic/hydrophilic balance does not alter the self-assembled morphology, confirming that the assembly is primarily driven by directional molecular

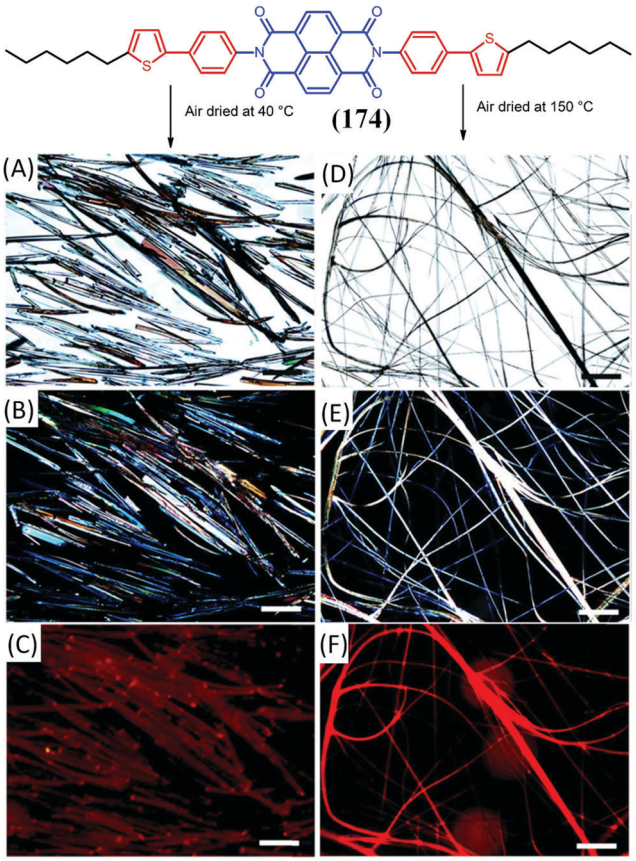

Fig. 34 Needle-shaped crystals (A–C) or crystalline nanofibers (D–F) are formed by deposition of a hot DMF solution of ThPh-NDI (**174**) onto a substrate held at 40 °C and 150 °C, respectively. Optical microscopy images of the two polymorphs under bright field (A and D) and cross-polarizer (B and E) light illumination, and epifluorescence (C and F). The scale bar is 10 μm.[95] This figure has been adapted from ref. 95 with permission from The American Chemical Society, copyright 2019.

interactions. It is important to mention that within these assemblies the H-bonded chain of the hydrazine (P1–50) (**176**) shielded the inner side of the assembled structure, with the anionic group remaining at the outer surface. To evaluate this, the group synthesised new NDIs (**178–180**) with small differences in the hydrogen bonding groups, *i.e.* a hydrazide and an amide, which self-assembled into vesicles and cylindrical micelles, respectively.[98] In another report they engineered NDI amphiphiles which assembled *via* J-aggregation through core π–π stacking, leading to the formation of thermally stable spherical micelles.[99] They have also synthesised NDI containing carboxylic acids which extend H-bonding, and spontaneously form open-chain polymers in MCH.[83] This and other hydrogen-bonding directed assemblies of NDI have been reviewed by Ghose;[100] herein, we outline a few interesting examples along with recent studies in the field.

Banerjee and co-workers prepared two NDI derivatives, one with a peptide (NDI-appended peptide, **181**) linkage and the second one having a covalently attached amino acid residue and a diamine group (pseudo-peptide, **182**). In both structures the intervening amide groups and centrally located imide have an identical molecular weight.[103] The only difference between these two molecules is the position of the amide groups, which influence the molecular assembly and gelation processes. Both molecules (**181**) and (**182**) are partially soluble in MCH and highly soluble in chloroform ($CHCl_3$). Taking advantage of this, the group has dissolved both derivatives in $CHCl_3$, followed by the addition of MCH. The molecule (**181**) immediately formed an organogel in mixtures of $CHCl_3$ and MCH (v/v, 5 : 95); however, (**182**) did not form a gel instantly, rather it formed a highly viscous transparent solution first and after 30–40 min at room temperature it formed an organogel. The lifetime and quantum yield of the (**181**) gel were shown to be higher than those of (**182**) under similar conditions; however, both (**181**) and (**182**) displayed semiconducting properties in their xerogel states as shown in Fig. 36. Thus, this study is an example for future development of organogels and their optoelectronic materials.

In a similar direction, Schmuck and co-workers used host–guest interactions between a multi-cationic dendrimer containing 16 guanidino-carbonyl pyrrole groups on its surface, and an NDI bearing dicarboxylic acid. When mixed in a 1 : 8 ratio, self-assembly occurred in a stepwise manner: firstly, into reverse micelles and then into reverse vesicles.[104] In another report, they studied the two-component self-assembly between the guanidinocarbonyl pyrrole tetra-cation and NDI-carboxylic acid in DMSO at neutral pH, in which firstly two building blocks form 1 : 2 ion pairs and further assemble into supramolecular networks of micrometer size through a hierarchical and cooperative process and π–π stacking of the NDI cores.[105] Importantly, they have also demonstrated that the disassembled supramolecular structure was reversibly triggered by pH. The D'Anna group synthesised an NDI bearing *N,N′*-bis-(1-alkyl-3-propylimidazolium)diiodide at both diimide positions, which formed H-aggregates that assembled into spherical disk-like structures.[106] One interesting example by the Gao and Li group described the formation of 2D crystallised monolayers of n-type NDI semiconductors on the 1-phenyloctane–HOPG interface in an ordered manner at the liquid–solid interface.[107] Colombani and co-workers synthesised NDI-polymers (**183** & **184**), with, nevertheless, **183** bearing a water soluble poly(ethylene oxide) (PEO; M_n = 2000 g mol^{-1}, D = 1.1) arm with the other imide position containing a bis(urea) (U_2) unit that leads to cooperative hydrogen bonds.[101] The derivative **183** instantly dissolves in water, and cryo-TEM allowed imaging of long nanocylinders with a monodispersed diameter of ~10 nm with a polydispersed length of several hundreds of nanometers. Qi and co-workers synthesised an NDI bearing benzo-21-crown-7 ether (**185**) at both the diimide positions and further studied the solvent-dependent self-assembly behavior.[108] Interestingly, among the solvents used, NDI-21-C-7 self-assembled into nanobelt-like structures in aqueous medium. The Hasegava and Wakamiya group synthesised an NDI bearing *tert*-butoxycarbonyl substituents which can be removed by thermal cleavage to control molecular orientation within thin films. They have synthesised an NDI containing the Boc moiety at both imide positions, which leads to a herringbone packing

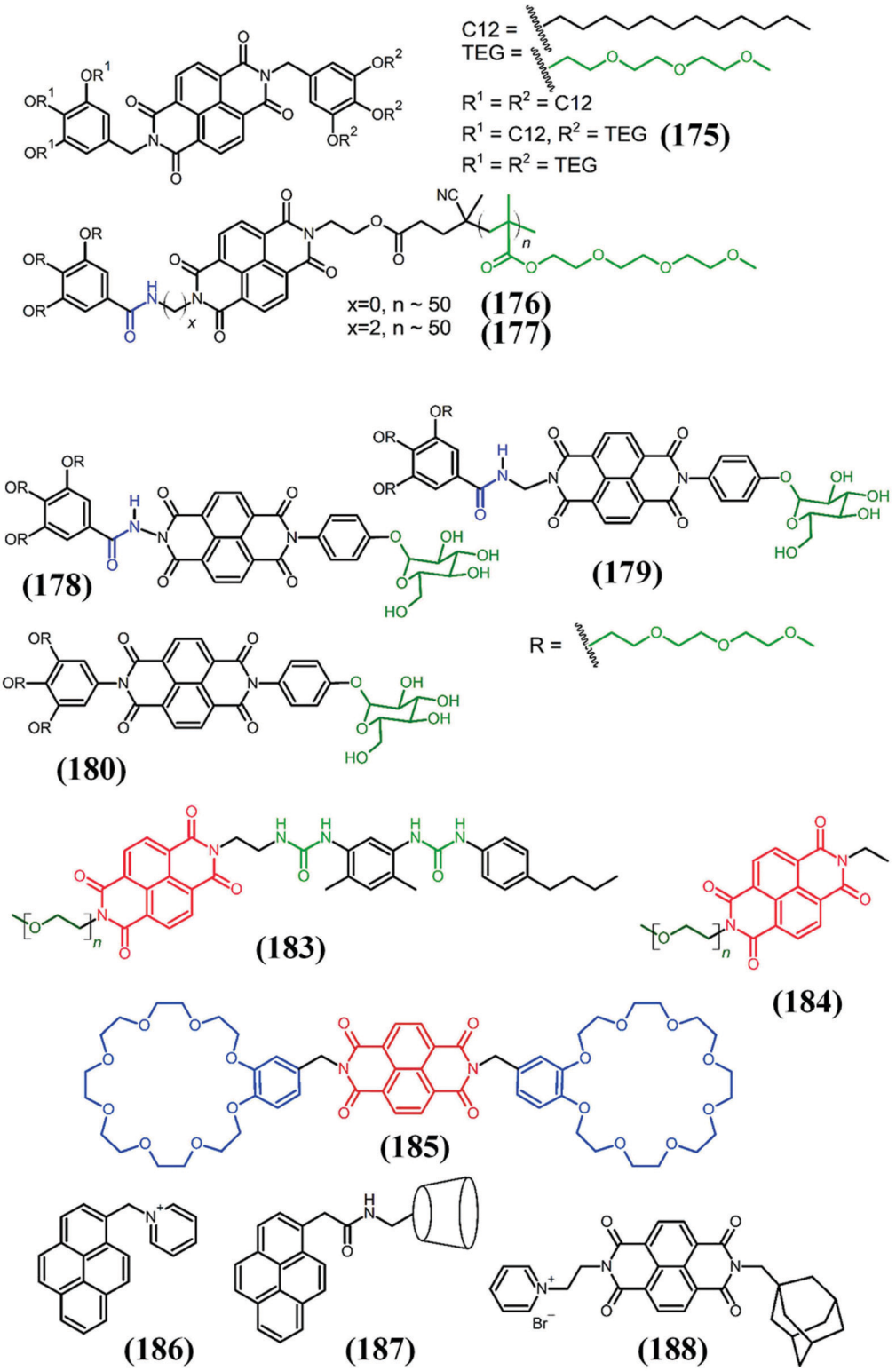

Fig. 35 Molecular structures of the perylenediimide (PDI) and naphthalene diimide (NDI) derivatives with hydrophobic and/or hydrophilic peripheral side chains (**175**).[96] Structure of the SEAMs and a schematic diagram showing directional molecular interaction-driven distinct self-assembly (**176**, **177**).[97] Structure of various NDI amphiphiles (**178–180**),[98] (**183**, **184**),[101] and (**186–188**).[102]

structure.[109] Interestingly, they also found for the first time that Boc groups can be eliminated at ~180 °C in the thin film with conversion of NDI-Boc to NDI-H, which was confirmed by the film thickness using a stylus-based surface profiler, showing a decrease in film thickness from 80 nm to 40 nm. Furthermore, FTIR spectroscopy was used to confirm NDI-H formation, and

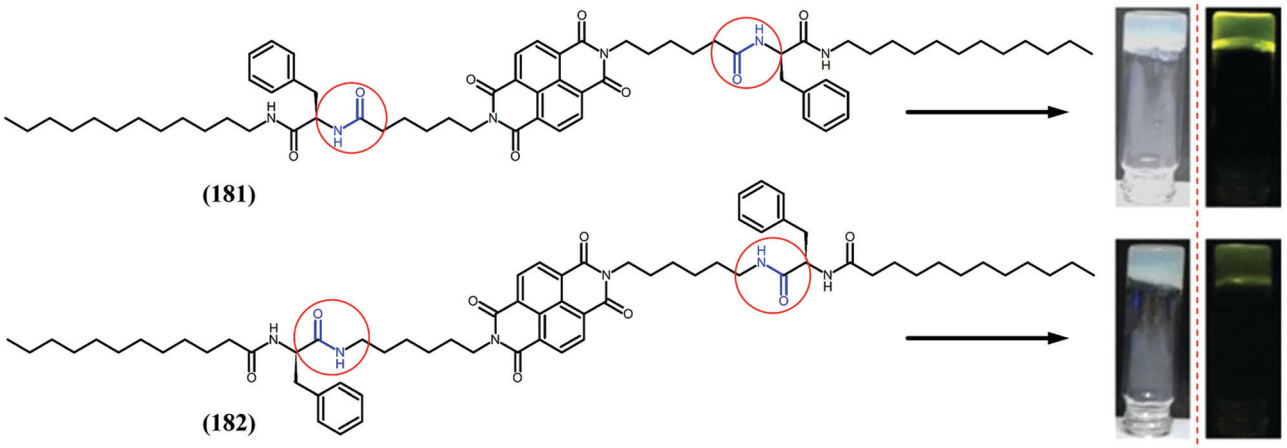

Fig. 36 Molecular structures of the gelator molecules (**181**) and (**182**), and the photographs of their corresponding organogels (2 mM) obtained from the chloroform–methylcyclohexane mixture (5 : 95), respectively [left side vials in daylight and right side vials under UV-lamp illumination at 365 nm].[103] This figure has been adapted from ref. 103 with permission from The Royal Society of Chemistry, copyright 2005.

UV-Vis absorption showed a red shift band of 11 nm, *i.e.* 390 (NDI-Boc) to 401 nm (NDI-H). NDI-H can be used as an electron-transport layer in the fabricated perovskite solar cells. Gopidas and co-workers exploited CT complexation between a pyrene (donor) (**186**) linked to β-cyclodextrin (β-CD) (**187**) and an NDI (acceptor) linked to adamantine (**188**), which when mixed together led to the inclusion of the NDI within β-CD and stabilised the CT complex.[102]

4.2 Gelation

In the last few decades, the fabrication and applications of supramolecular organogels has attracted significant attention. Several review articles have summarised the design and function of various gels; however, reports focusing on NDI organogels are lacking. Herein, we give a brief description of recently reported supramolecular organogels in terms of their design, concept and applications, the structures of which are shown in Fig. 37.[12b]

Draper and co-workers synthesised NDI organogel-based devices for applications in smart windows through a supramolecular self-assembly approach.[63] By means of photo- and electrochemical reduction of the NDI, radical anions are generated which undergo a color change from transparent to black when triggered by either photo- or electrochemical stimulation. On a similar path, Lin and co-workers described the formation of a hydrogel through a two-component self-assembly approach based on CT complexation between pyrenebutyric acid (donor) (**189**) and the NDI (acceptor) in aqueous medium, and they have also studied the influence of amino acid side chains on NDI-capped peptides such as NDI-Ser (**190**), NDI-Glu (**191**), and NDI-Lys (**192**) on one end and an octyl hydrophobic tail at the other end of the NDI.[110] Draper[63] reported an obvious color change from yellow to deep purple upon mixing pyrenebutyric acid (donor) and an NDI (acceptor) (**193**). These results demonstrated the formation of a CT complex through π-stacking in an aqueous medium. These types of material are useful for applications in smart windows. The Franco and Mba group reported the formation of red organogels through donor–acceptor CT complexation between pyrenebutyric acid (donor) (**189**, **194**) and an NDI (diphenylalanine dipeptide) (acceptor) (**195**, **196**) in various solvents such as *ortho*-dichlorobenzene, toluene, ethyl acetate and polar methanol.[111] The Chaudhuri group demonstrated the use of an NDI based gelator (**197–199**), which they applied in powder form to solidify heavy crude oil from water within 20 seconds.[112] The Shi group demonstrated the preparation of a neutral supramolecular self-assembly *via* donor–acceptor CT complexation (**199–201**) between pyrene (as a donor) having a pillar[5]arene (**200**) and an NDI (acceptor) (**199**) *via* a hierarchical orthogonal strategy through host–guest recognition.[113] In another report, Dasgupta, Ukil and Da synthesised asymmetric NDI-based hydrogelators by functionalising one end of the NDI with a C_6H_{13}-alkyl chain and the other end with a GKRGDS peptide chain (**202**), as GKRGDS has already been shown to play dual roles, as a structural component as well as a biological ligand for tumour homing and cell adhesion properties.[114] The NDI-peptide amphiphile formed a hydrogel at a low concentration (50 μM) *via* three important steps: π–π stacking of the NDI core, hydrophobic interaction between alkyl chains, and strong hydrogen bonding within the peptide chains. Furthermore, the hydrogel was found to be non-toxic in MTT assays, cell permeable and was able to be used for cell imaging. Ghosh and co-workers synthesised two NDI (**203**, **204**) derivatives having hydrophobic/hydrophilic balance, only differing by amide and ester groups. Interestingly, the NDI having an amide linkage formed hydrogels in water, whereas the NDI with the ester linkage formed micelles that were imaged by cryo-TEM. This result demonstrated that hydrogen-bonding plays an important role in the self-assembly.[115] This group also demonstrated core-substitution of the NDI with hydrophobic long-alkyl chains, with both the diimides bearing an octyl alkyl chain, leading to the J-aggregation of hydrophobic linear chains; however, cyclic alkyl (MCH, cyclohexane) chains did not lead to gelation.[116] They found that linear alkyl chains participate in nucleation

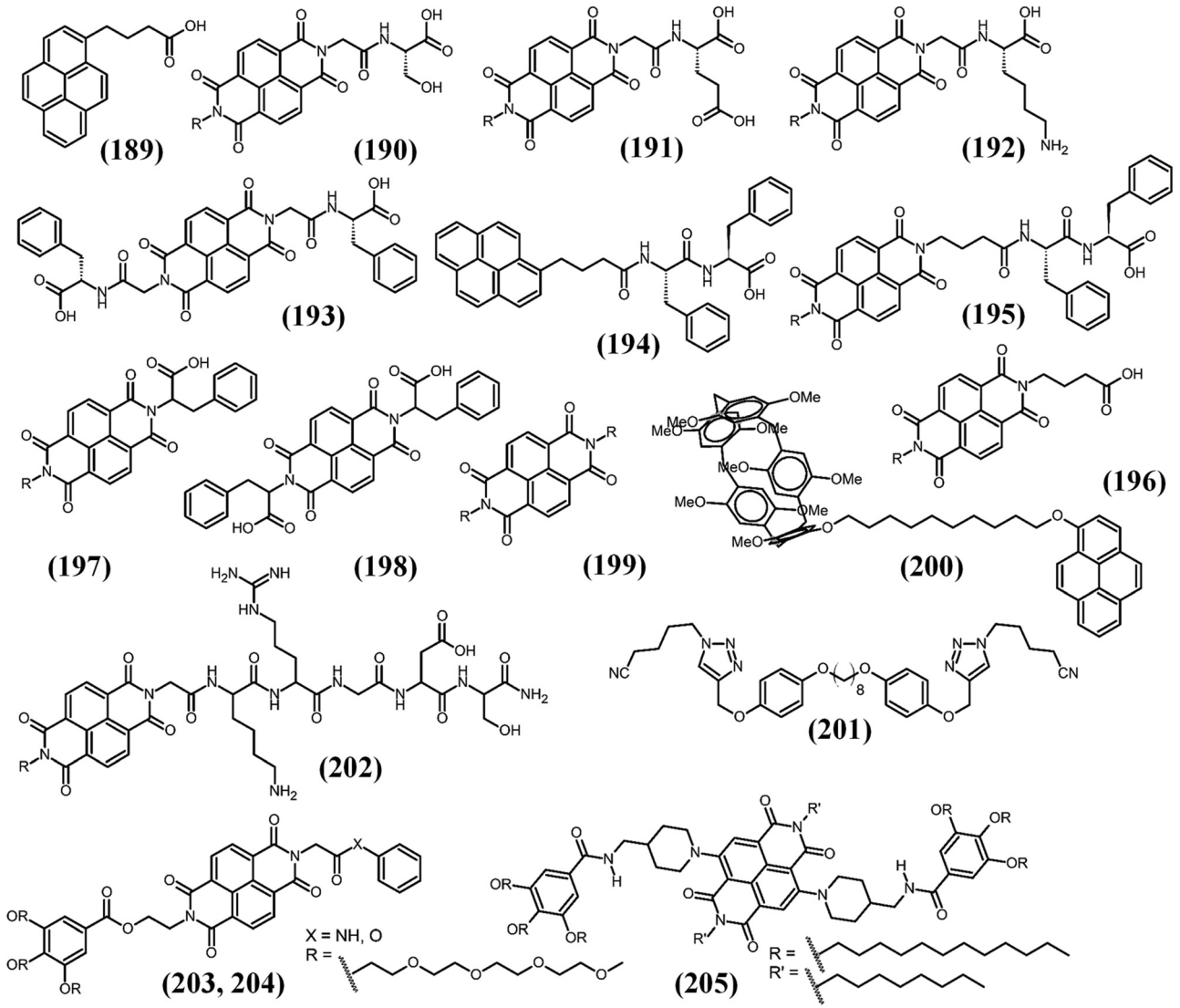

Fig. 37 Hydrogel forming NDI derivatives and counter gelling agent compounds.[63,110–116]

processes through an interaction with the alkyl chains of NDI (**205**), whereas due to mismatching of cyclic alkanes a gel was not produced. Long linear alkyl chains induce nucleation and elongation growth faster than shorter chains. Atomic force microscopy (AFM) provided evidence of the formation of fibril networks and short-length rods in MCH and decane, respectively.

Moraes *et al.*[117] reported an interesting silsesquioxane-NDI which was able to form gels using DMF as a dipolar aprotic solvent. The gelation process of the silsesquioxane-NDI is induced by π–π stacking of the NDI core and chain formation through hydrolysis and further polycondensation of the propyltriethoxysilane (PTES) moieties using the water molecule produced during the *N*-substitution reaction in dry DMF. This PTES-ND gel was able to give NDI-reduced moieties by photo- and thermo-excitation, lowering considerably the electrical resistance as in conventional synthetic metals.

4.3 Chiral self-assembly

The construction of bioinspired chiral nanostructures not only has the potential to improve our understanding of natural processes, but may also find application in various fields such as sensing, liquid crystals, and optical activity. There have been various aromatic core units used, including NDIs with amino/peptide functionality, that allow sophisticated control of the structure in solution due to π–π interactions. There have also been a few reports describing the controlled organization of helical structures *via* donor (naphthalene)–acceptor (optically active NDI) molecules with chirality derived through self-assembly of charge-transfer (CT) complexes. There are a few reports that describe the formation and induction of chirality into helical supramolecular nanostructures with achiral NDIs where various factors play a role such as solvent polarity, pH, and temperature, as well as through the use of chiral amino acids as examples illustrated in Fig. 38.[83]

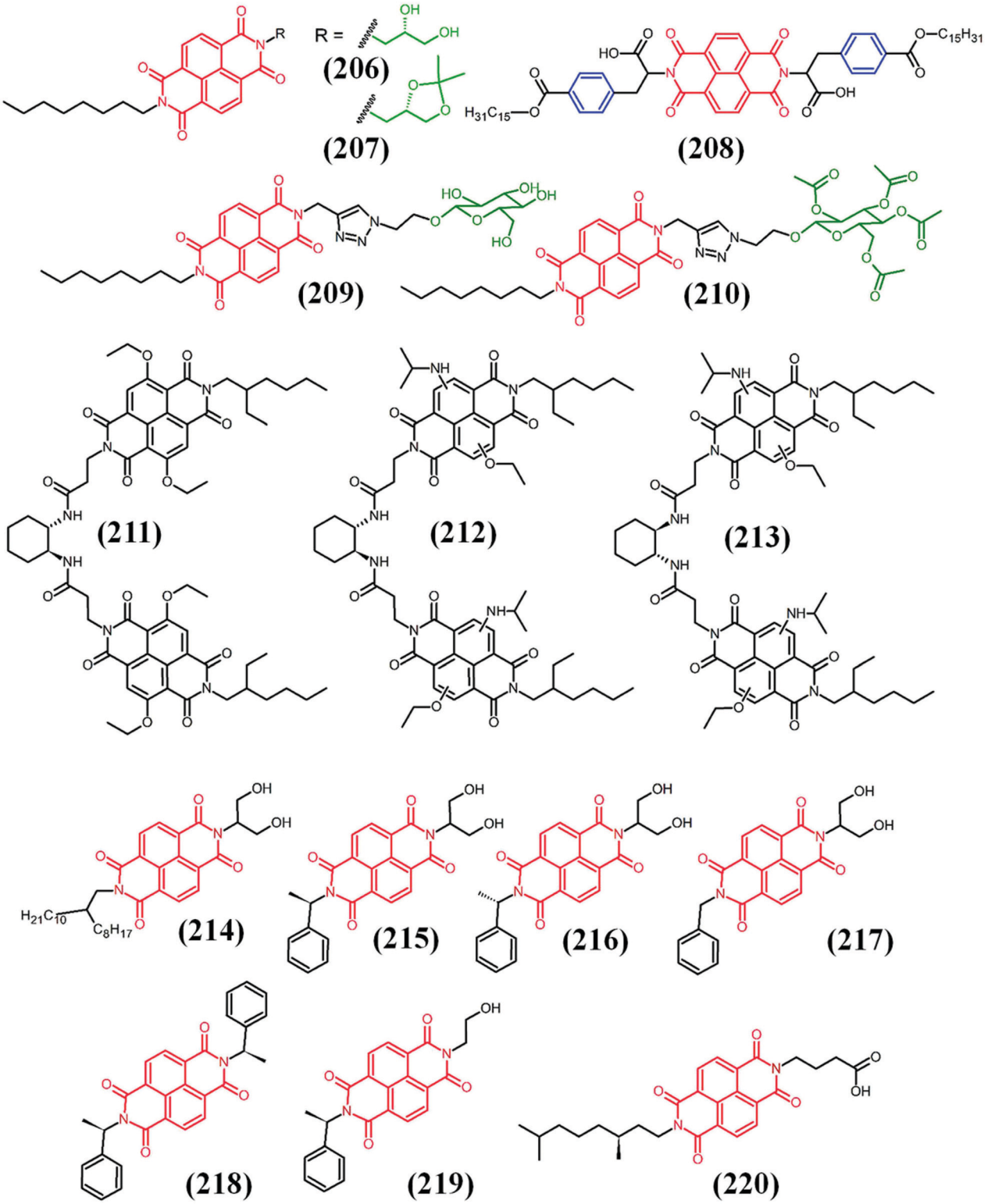

Fig. 38 Molecular structures of NDI derivatives designed for self-assembly/co-assembly into molecular superstructures.[118–123]

The Talukdar group demonstrated the formation of helical supramolecular structures of an NDI containing a 1,2-diol group *via* extended intermolecular hydrogen-bonding in MCH/$CHCl_3$ (95 : 5, v/v), in which the 1,2-diol-NDI (**206**) leads to excimer formation, observed by color changes, and compared it to (**207**) as a control compound.[118] Microscopy (TEM, AFM and SEM) results demonstrated the formation of micrometer long M-helical supramolecular structures and circular

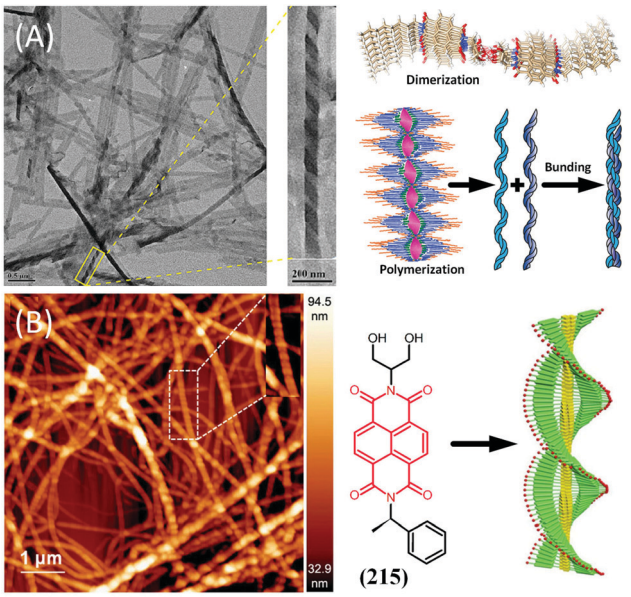

Fig. 39 (A) TEM image recorded after drop-casting the suspension of the gel of (**207**) and the scheme of the self-assembly geometry.[118] (B) AFM image of (**215**) superstructure diluted gel in TCE (*C* = 1.8 mm) spin-coated on a mica surface for imaging; and schematic representation of the proposed model for helical self-assembly.[122] This figure has been adapted from ref. 122 with permission from John Wiley and Sons, copyright 2018.

dichroism confirmed the chirality induced within the helical structures. Stefankiewicz and co-workers demonstrated the assembly and disassembly of NDI containing various sites (**208**) for multiple H-bonding, π–π stacking, and van der Waals interactions.[119] Furthermore, they controlled the morphology with solvents, for example, NDI derivatives assembled into helical nanotubes in $CHCl_3$/MCH, producing linear polymers and further aggregates with time. Interestingly, these morphologies could be disassembled by either the addition of THF or TEMP solvents, or changes in temperature. Similarly, Narayan and co-workers synthesised an NDI containing β-D-glucopyranoside (**209**, **210**) and also studied the influence on chiral assembly with acetylation/deacetylation.[120] George and co-workers synthesised two core-substituted NDIs with donor and acceptor moieties (**211–213**) on the core of NDIs, which self-assembled into helical fibers, and the assembled structure demonstrated energy transfer between donor–acceptor NDI molecules.[121] Furthermore, they explored the use of chirality-controlled energy transfer to visualise chirality driven self-sorting.[122] This group also demonstrated the assembly of an NDI bearing 1,3-dihydroxyl moieties at one end (**214–219**) and chiral alkyl chains of either the (*R*)- or (*S*)-isomers on the other end as the chiral dopant, and studied the impact of chirality on gelation and the effect of self-assembly on charge-carrier mobility. AFM microscopy images demonstrated the formation of chiral gelators (*R*)-NDI/(*S*)-NDI which self-assembled into M- and P-type helical fibrillar structures in tetrachloroethylene (TCE), but not in halogenated solvent ($CHCl_3$), due to hydrogen-bonding between the 1,3-dihydroxyl group and π–π stacking of the NDI cores (Fig. 39). The Meijer and Bari group reported circularly polarised luminescence (CPL) on an assembly formed by an NDI functionalised with a chiral carboxylic acid (**220**). A supramolecular ordered structure was formed due to hydrogen-bonding along with π–π interactions which were confirmed by excimer formation in chlorinated/hydrocarbon solvent mixtures.[123] Gao *et al.*[124] developed an optically active helical polyacetylene with π-conjugated building blocks bearing NDI moieties, where the π–π stacking of the NDI moieties is driven by chlorinated solvents and the helical conformation of the polymer backbone and the stacking pattern can be regulated by adding trifluoroacetic acid or specific solvents or anions.

We have demonstrated the formation of left (*M*-type) and right (*P*-type) helical-ribbons in THF/H_2O (40 : 60 v/v) using an NDI bearing tetraphenylethylene with L- and D-alanine as a spacer.[125] Firstly, solution based assembly was characterised by circular dichroism, which confirmed the handedness of the chiral structure, and SEM imaging allowed visualisation of the microstructures. In another report, we demonstrated controlled chiral supramolecular self-assembly from an achiral NDI containing a urea functionality from THF/MCH (60/40, v/v).[126] In this study we also demonstrated the influence of a bulky halogroup into the assembled structures. Ulijn and co-workers reported the use of an NDI bearing L- and D-enantiomers of tyrosine methyl ester on both the end diimides (**221**), which shows no chirality at all.[127] However, in the presence of the enzyme α-chymotrypsin biocatalytic self-assembly processes resulted in either transient or delayed chiral assembly with tunable right- or left-handed nanostructures. Typically, a hydrophilic amino acid leads to the formation of left-handed structures, whereas a hydrophobic amino acid resulted in delayed chirality with right-handed superstructures (Fig. 40).

4.4 Supramolecular structures *via* covalent bonds

Pérez and co-workers synthesised a series of NDI derivatives bearing terminal bisalkene moieties (**222**, **223**), which form mechanically interlocked rotaxane-like derivatives by the metathesis reaction using Grubbs catalyst, and extended to rotaxane-like structures wrapped around carbon nanotubes using supramolecular chemistry (Fig. 41).[128] Similarly, Sfrazzetto and Tuccitto prepared carbon nanoparticles covalently bonded to triazine, functionalised with an NDI through hydrogen-bonding, which was used as a messenger for artificial chemical communication.[129]

Taura *et al.*[130] designed and selectively synthesized double-stranded *hetero*-helicates bridged by spiroborate groups using electron-deficient NDI and PDI linkers, easily resolved by chiral HPLC to give *homo*-helicates. Their approach can be applied to prepare various other one-handed spiroborate-based double-stranded *hetero*-helicates with different functional linkers as well as more complicated macrocyclic supramolecules with an optical activity.

4.5 Organic crystals

Recently, crystal structures formed from at least two different molecules have received attention as these co-crystals allow tuning of optical properties including the lifetime and

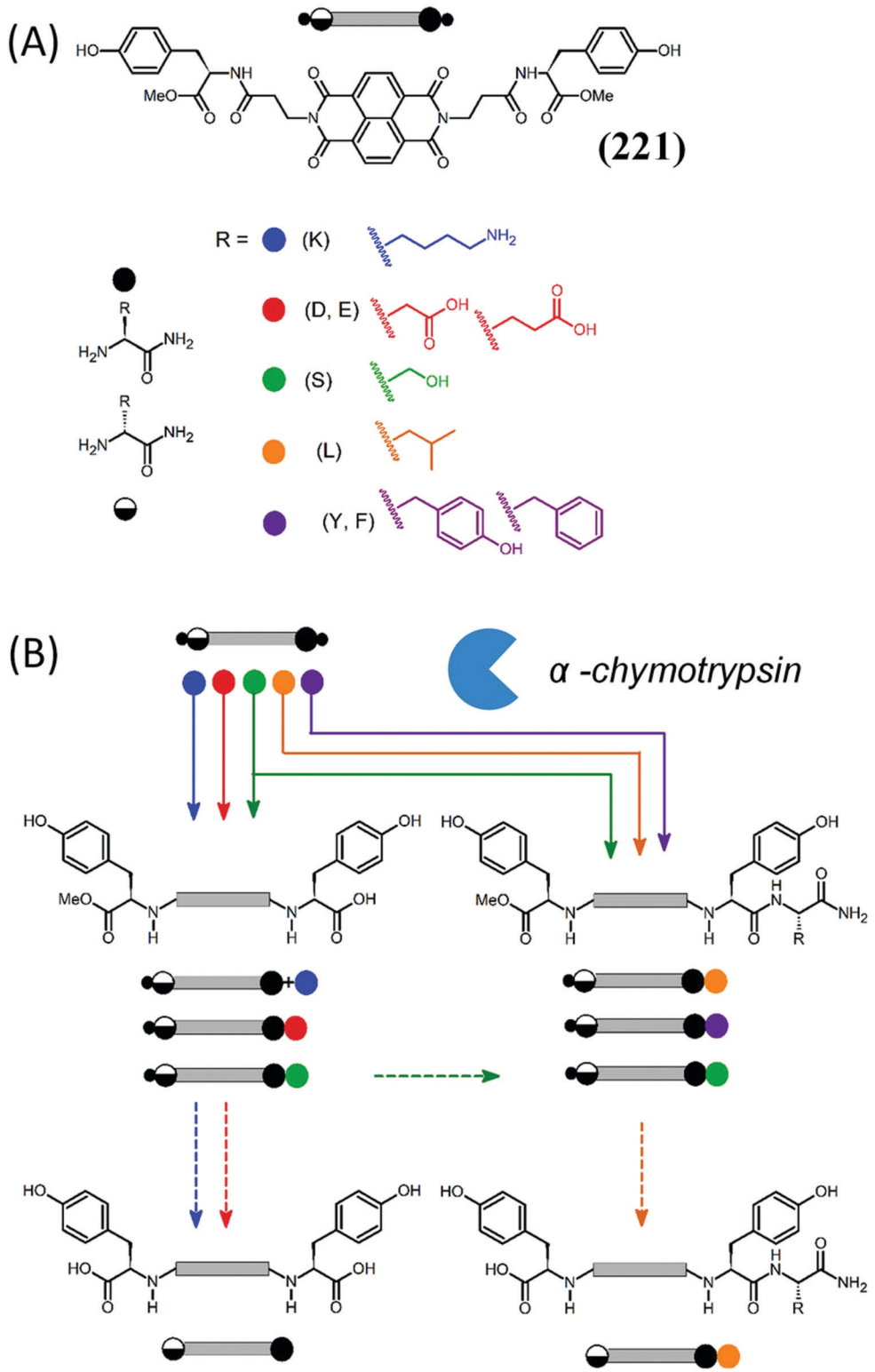

Fig. 40 Active amino acid encoding of biocatalytic self-assembly pathways. (A) Chemical structure of the meso molecule (**221**) (full spheres and half spheres represent L- and D-enantiomers, respectively) and various input amino acid amides (colour-coded spheres). (B) Time-dependent chemical transformation of (**221**) upon the action of α-chymotrypsin in the presence of various input amino acids (fast step: 3 h; slow step: 2 weeks) showing kinetic competition and pathway selection leading to hydrolysis or *trans*-acylation pathways or a combination thereof.[127] This figure has been adapted from ref. 127 with permission from Springer Nature (NPG), copyright 2018.

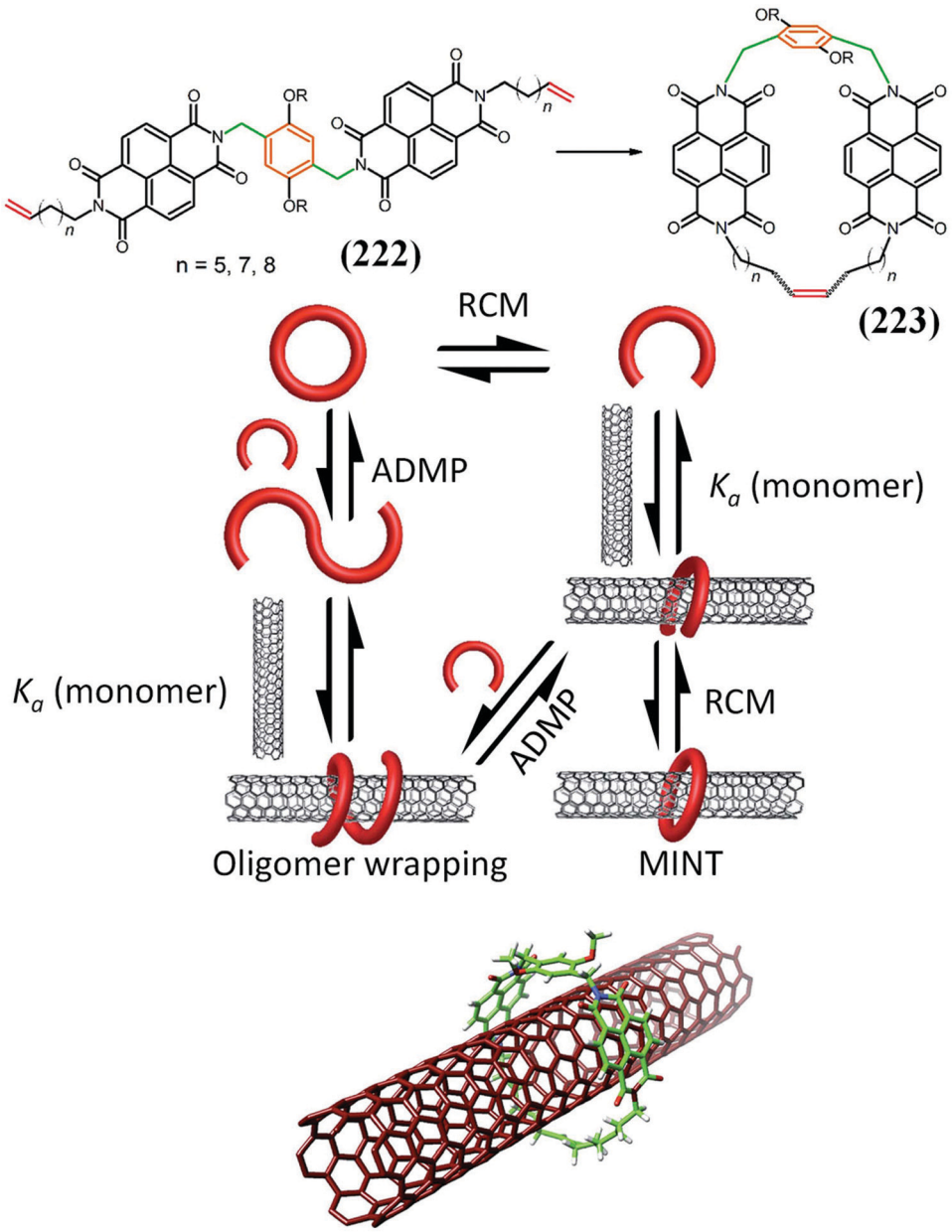

Fig. 41 The linear precursors (**222**) and macrocycles (**223**), and reaction pathways for the bimodal noncovalent functionalization of SWNTs to afford either oligomer-wrapped SWNTs or MINTs. Grubbs catalyst has been omitted for clarity.[128] This figure has been adapted from ref. 128 with permission from The Royal Society of Chemistry, copyright 2017.

quantum yield of the organic molecules involved. The properties of NDI are typically tuned by functionalisation at either the diimide or the core of the NDI. However, co-crystallisation of the NDI (acceptor) with various donor molecules may lead to interesting properties without core-substitution. For example, Groot stacked an NDI derivative in a *P*2/*c* supramolecular scaffold with alignment of the electric dipole moment, which may have various applications such as light harvesting or injection of charges in catalysis for water splitting.[131]

Liu *et al.* reported the luminescence properties of NDIs which can be modulated by supramolecular co-crystal formation through donor–acceptor interactions between the electron-deficient *N*,*N*′-di-(4-pyridyl)-NDI (**224**) molecules and electron-rich naphthalene derivatives (guest) (**225**) in a series of co-crystal complexes with colour tuneable emissions (Fig. 42A and B).[132] The Lin and Huang group reported tuning of the luminescence properties of NDI by supramolecular crystallisation with electron-rich DAN molecules, in which bis-pyridyl-NDI (**226**) acts as an acceptor and DAN as an electron donor. They were able to observe multi-color emission of NDIs with various naphthalene derivatives. The Hawes and Gunnlaugsson group synthesised picolyl ligands, *i.e.* *N*,*N*′-di(2-picolyl)NDI and *N*,*N*′-di(2-picolyl)-4,4′-oxybisphthalimide, and

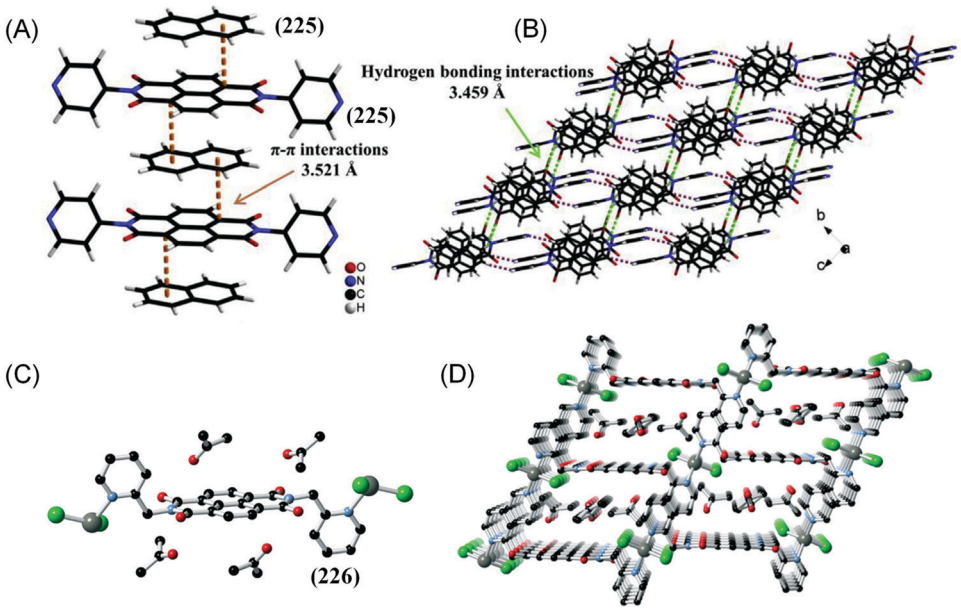

Fig. 42 (A) The crystal structure fabricated from the alternate stacking of (**224**) and naphthalene molecules (**225**); (B) the packing diagram of (**224–225**) viewed along the *b* axis. (For interpretation of the references to colour in this figure legend, the reader is referred to the web version of this article.)[132] (C) The interactions between lattice acetone molecules and the π-surface of (**226**) within the structure of (**226**). A single disordered contributor is represented for clarity. (D) Extended structure of compound (**226**) viewed parallel to the primary solvent channels. All hydrogen atoms are omitted for clarity.[133] This figure has been adapted from ref. 133 with permission from The Royal Society of Chemistry, copyright 1999.

undertook crystallographic studies on their coordination chemistry with d-block metal ions.[133]

Mukhopadhyay and co-workers reported the synthesis of very stable radical ions of diphosphonium NDI derivatives and further studied the influence of the anion–π interactions on the supramolecular self-assembled networks using single-crystal structure analysis.[134] Their findings revealed that self-assembled networks could be tuned by the counter anions. The oxygen atoms of imide carbonyl groups of the NDI core form hydrogen bonds with the aryl group of triphenyl phosphonium of the neighboring NDI, producing infinite networks. This study opens up a route towards switchable devices in the future. Similarly, D'Anna and co-workers described the influence of anions on the supramolecular self-assembly of NDI-diimidazolium salts.[135] George and co-workers described the effect of heavy atoms on the NDI for pre-organization where the NDI without a heavy atom (Br) displayed green excimer-like emission; however, with Br present red phosphorescence on visible light excitation was observed under ambient conditions in water.[136]

The Xu and Liu group[137] described the influence of water on the single-crystal-to-single crystal (SCSC) transformation using *N*,*N*′-bis-(4-pyridylmethyl)-NDI (**227**), through intermolecular π–π interactions and hydrogen bonding interactions (Fig. 43). These crystals in solid state showed selective adsorption and fluorescence changes for water sensing over methanol, ethanol, *n*-propanol, isopropanol, *n*-butanol, and benzene. The Zhu and Ma group described the formation of a new crystalline porous aromatic framework (PAF-10) *via* an imidization reaction of linear NDA with triangular tris(4-aminophenyl)amine, which is capable of selective separation of acetylene from ethylene at ambient temperature. Importantly, this crystalline material of PAF-10 was shown to have impressive long-term thermal and structural stability, even in the presence of various coordinating solvents and acids.

The Reddy group described a crystal engineering approach to synthesise ∼10 flexible plastic-like single crystals by means of supramolecular weak interactions such as van der Waals forces using spacers such as –*t*-Bu, –OMe, –Me, and –Cl/Br, along with π–π stacking and hydrogen bonding groups for the first time.[138]

Zhu *et al.*[139] synthesized NDI-based supramolecular networks comprising donor–acceptor units with photochromic properties using both solvothermal and solvent diffusion methods. The introduction of electron-rich solvent molecules into these superstructures gives rise to distinct ion pair–π interactions that effectively regulate the interfacial contacts between different electron-rich carbonyl oxygen donors and electron-deficient NDI centroid acceptors, and play a subtle modulating role in the intermolecular charge transfer and photoresponsive properties.

4.6 Surface 2D self-assembly

Two-dimensional crystalline organic frameworks constructed with a high degree of precision from organic chromophores *via* face-to-face stacking can create materials that allow charge transport through π–π stacking, with properties that are significantly different from those of their 3D counterparts. 2D crystalline organic assembled structures may be useful for energy conversion processes. In this regard, the Ghosh group

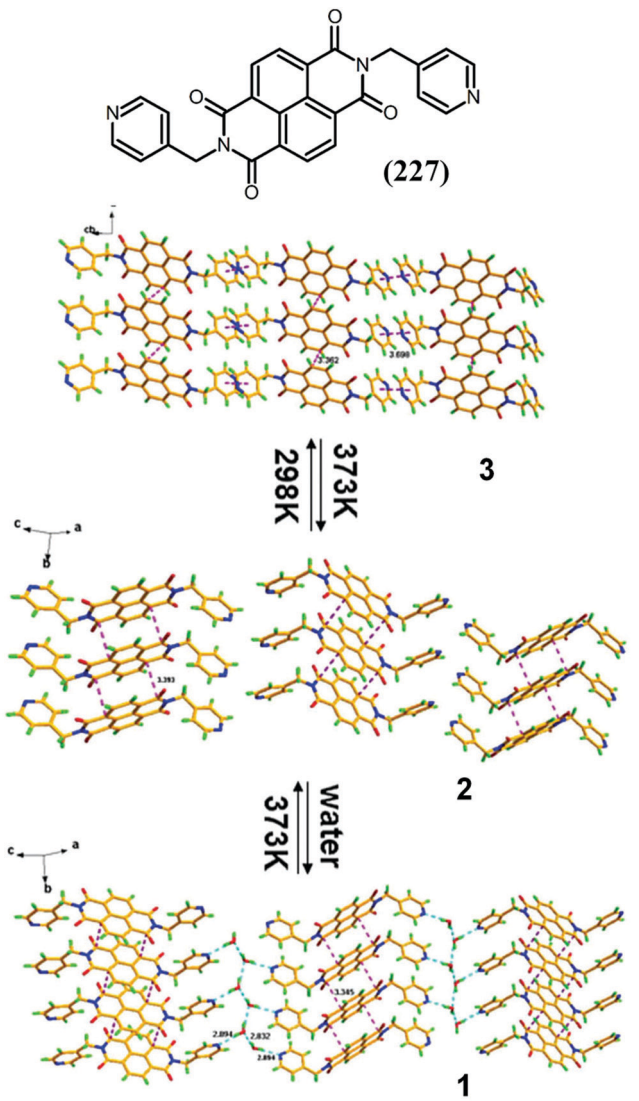

Fig. 43 Reversible single-crystal-to-single-crystal transformations between 1, 2 and 3 of (**227**).[137] This figure has been adapted from ref. 137 with permission from The Royal Society of Chemistry, copyright 2017.

synthesised photo-triggered 2D nanostructured materials through supramolecular assemblies of NDI bearing the photo-labile *ortho*-nitrobenzyl (ONB)-ester protected carboxylic acid (**228**), which produces the free COOH group (**229**) by photo-irradiation leading to ultra-thin (<2 nm height) nanosheets.[58] Interestingly, they also found that, by using the same monomer, a fibrillary network spontaneously assembled through J-aggregation. Wasielewski and Wu synthesised G-quadruplex organic frameworks (GQFs) constructed through guanine cyclic tetramers (**230**) using hydrogen-bonding assemblies (Fig. 44). In their study, they used as the electron-deficient NDI and PDI appended with the electron-rich guanines.[140] Their findings revealed that photo-induced electron transfer occurred from the guanine donor to the photo-excited NDI/PDI acceptors, enabling facile hole transport, which was evidenced by transient optical and microwave conductivity measurements. To change the electronic properties of the GQFs, they also co-crystallized guanine-functionalized pyrene derivatives (with high lying HOMOs), which led to charge-transfer (CT) complexes with NDI. In the future these types of 2D structures are candidates for photocatalytic reactions for the splitting of water.

Ma *et al.*[141] reported the synthesis of binary co-crystals with 1 : 1 mixed-stack arrangement by solvent evaporation or grinding of Me-NDI as the receptor and 1,4,8,11-tetramethyl-6,13-triethylsilylethynyl pentacene (TMTES-P) as the donor. These host–guest co-crystals showed host-dependent thermal response where the absolute sublimation by guest volatilization/decomposition can serve as molecular-scale capture and delivery control using non-covalent weak interactions.

4.7 Self-assembled triangles for rechargeable lithium-ion batteries

In recent years, batteries have been of continuing interest as an energy storage technology. Improvements in energy and power densities, life time, safety and cost effectiveness are required to meet global demand. Lithium (Li)-ion batteries have been successful and are generally based on transition metal oxide cathodes and graphite as anodes, though there remains scope for improvement. To this end, recent developments include the use of organic/polymer rechargeable Li-ion batteries that avoid the use of heavy metals. In this regard, NDI has been shown to be a candidate due to its n-type semiconductor properties.[3b,142] Taking advantage of this, Stoddart and co-workers synthesised thermally stable molecular triangular prisms by reacting a rigid NDA with (*RR*)- and (*SS*)-*trans*-1,2-diaminocyclohexane.[70] Interestingly, these triangles have three redox-active NDI units in a rigid, cyclic constitution and show delocalisation across the overlapping p-orbitals of the three NDIs in the triangle. As a result, it can store and release up to six electrons reversibly, providing a cell with a capacity of 146.4 mA h g^{-1} at a low current rate of 0.1C and a capacity of 58.1 mA h g^{-1} at an ultrahigh rate of 100C. Another report by the group described two rigid chiral triangles, which were made up of PMI and NDI redox active units.[69] These rigid triangles produced two types of intermolecular NDI-NDI and NDI-PMI forms in solid state through π–π-stacking, in contrast to the triangle formed by three identical NDI units.[69,70] Cyclic voltammetry (CV) of both the isosceles rigid triangles of NDI and PMI showed reversible acceptance of six electrons. They also found that an increase in the number of NDI units within the triangles, replacing PMI, improved the battery performance. This group also prepared two chiral isosceles triangles containing one PDI unit with either two NDI or PMI units in a cyclic triangle.[68] They found that the triangle containing NDI and PDI units showed excellent intermolecular energy transfer from the NDI to PDI units, and both the isosceles triangles exhibited reversible redox behaviour, making them useful for molecular optoelectronic devices in the future (Fig. 21). However, neither of the triangles have the capacity or voltage superior to inorganic cathode materials. Nevertheless, this investigation suggests that one could balance donor–acceptor systems to approach

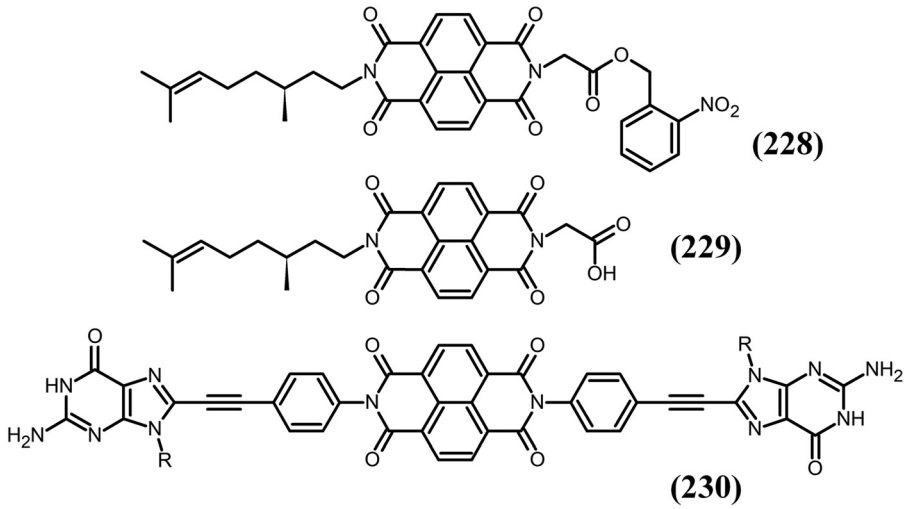

Fig. 44 The molecular structures of G-quadruplexes forming an organic framework.[58,140]

the performance of Li-ion batteries, and small molecules may contribute in the future in the field of energy-storage technologies.

5 Host–guest chemistry

Host–guest chemistry describes supramolecular complexes that are assembled from two or more molecules *via* non-covalent bonding such as hydrogen-bonding, ionic interactions, π–π interactions, and van der Waals forces. One of the best examples is the creation of the 3D structure of proteins in the biological world, where large molecules interact with one another to create globular structures. Synthetic examples include host–guest chemistry, such as the use of dendrimers in drug-delivery systems, where the drug acts as a guest and the dendrimer as a host *via* encapsulation, improving the drug delivery by sustained and selective release of the drug. Host–guest chemistry can also be used for chemical sensing applications, where the receptor site is covalently bound to an indicator, and when the analyte (guest) binds, the indicator changes color or undergoes a change in a similar physical property. Host–guest chemistry can be employed for environmental applications, where the host systems can be utilised to remove hazardous components by size selectively, such as calix[4]arene being used to trap a cesium ion. To study host–guest chemistry, various techniques have been used, and one of the most powerful spectroscopic techniques is nuclear magnetic resonance (NMR) which identifies the chemical shift of the proton of the host upon binding to the guest. Another two techniques that are also useful to study host–guest interactions are UV-vis absorption and fluorescence spectroscopy. NDI is a planar molecule and has been used as a building block in donor–acceptor charge transfer complexes, which is an important phenomenon in host–guest complexes to organise various structures such as foldamers, ion-channels, catenanes, and rotaxanes.[3b] This part has been reviewed in depth by us in 2016, and herein we will discuss recent and interesting examples of host–guest types of structures.

The first example to discuss in this section is the study by Gond and co-workers who used host–guest chemistry to construct a pillar[5]arene tetramer *via* cross-linked supramolecular polymers using charge-transfer complexes.[143] This group firstly synthesised two different pillar[5]arene dimers functionalised with NDI bridged pillar[5]arene (**231**) as an acceptor, naphthalene bridged pillar[5]arene (**232**) as a donor, and a neutral guest (**233**) bearing two 5-(1*H*-1,2,3-triazol-1-yl)pentanenitrile binding sites as a spacer (Fig. 45), and mixing these three molecules produced new cross-linked supramolecular polymers through charge transfer interactions and hierarchical self-assembly. They used ^{1}H NMR to understand host–guest interactions between the (**233**)⊂(**231**)·(**232**) tetramer in $CHCl_3$ at a 1 : 1 : 1 ratio, and further UV-vis absorption viscosity studies added to an understanding of the interactions. This design principle is similar to that reported in an earlier study by Zhang and co-workers[144] who assembled X-shaped superamphiphiles by using NDI and NAP based amphiphiles through host–guest interactions. Champness and co-workers described an interlocked handcuff, prepared using NDI and PDI to create dimeric structures linked through pillar[5]arene/imidazolium rotaxanes.[145]

Another interesting example was reported by the Rissanen and Heitz group who studied allosteric control of receptor properties using two flexible covalent cages (**234**, **235**).[146] Two zinc-porphyrins were connected by four linkers of varying size using 1,2,3-triazolyl ligands. An effective on/off encapsulation mechanism was demonstrated using Ag(I), which binds to the triazoles, opens the cages, and prompts the encapsulation of NDI or *N,N′*-di butyl-NDI. Here, allosteric control of the receptor properties of the molecular structures (**234**) and (**235**) was investigated (Fig. 46). It was shown that Ag(I) ions act as chemical effectors that trigger the encapsulation of neutral guest molecules. Thanks to the chemical nature of the Zn(II) porphyrins, the allosteric mechanism was shown to operate

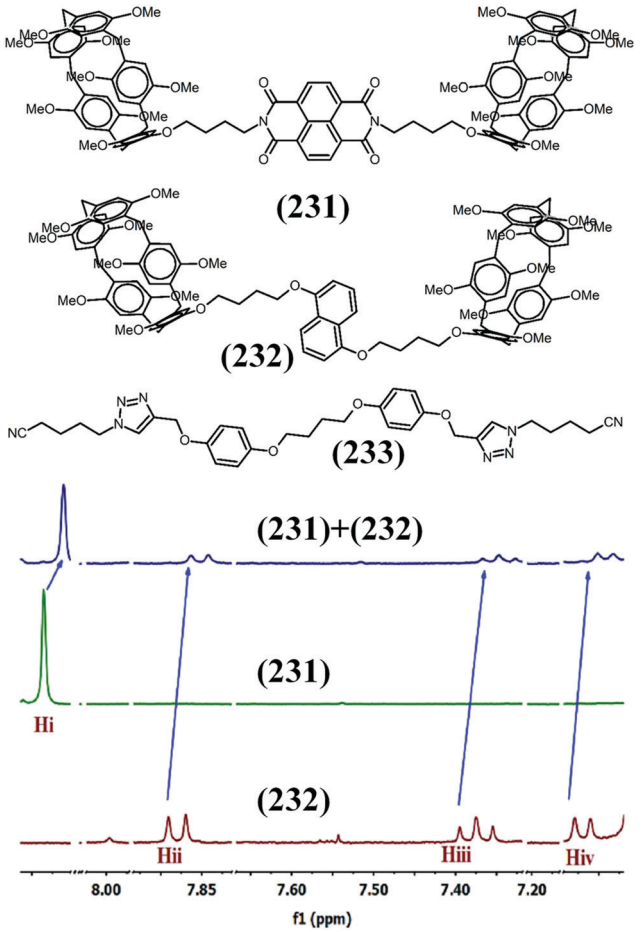

Fig. 45 The molecular structures of (**231**) host, (**232**) host, and (**233**); and the ^{1}H NMR of (**231**) host, (**232**) host, and a mixture of (**231**) + (**232**) host at a 1 : 1 ratio.[143] This figure has been adapted from ref. 143 with permission from John Wiley and Sons, copyright 2018.

both for the aditopic ligand, pyrazine, and for *N,N′*-di butyl-NDI. The X-ray structural analyses confirmed the open structure of silver(I)-complexed cage (**234**) as well as the encapsulation of pyrazine in this receptor.

Fujita and co-workers prepared a self-assembled box-shaped cage by mixing tris(4-pyridyl)-2,4,6-triazine (**236**), 2,2′,6,6′-tetramethyl-4,4′-bipyridine (**237**), and (en)Pd$(NO_3)_2$ (**238**) in aqueous solution where the inclusion of a mixture of a water-insoluble guest NDI (**239**) and corannulene (**240**) *via* donor–acceptor interactions was confirmed by ^{1}H NMR spectroscopy (Fig. 47).[147] The formation of an inclusion complex of 1 : 1 ratio of host–guest, *i.e.* cage-(NDI.corannulene) (**241**), was observed.

Du and co-workers prepared an octamethoxy-[8]-cycloparaphenylene cage bearing eight symmetrical methoxy groups (**242**) on the conjugated cyclic structure by platinum mediated reductive elimination.[148] They also studied the inclusion of NDI (**243**) within the cage, which was confirmed by ^{1}H NMR and the naked eye, where before inclusion of a guest NDI in CH_2Cl_2 gives blue emission (λ_{ex} = 365 nm), and after addition quenching of fluorescence was observed (Fig. 48). They also studied the electron transfer between the octamethoxy-[8]-cycloparaphenylene donor (**242**) and NDI as an electron acceptor (**243**).

The development of the next phase of nanotechnology depends upon the ability of scientists to construct man-made molecular machines, with controlled movement of individual molecules. In this regard, rotaxanes and catenanes have been developed which are mechanically interlocked molecules. Beer and co-workers designed and synthesised a multifunctional dynamic [3]rotaxane containing a four-station axle component bearing two peripheral fluorescent NDIs as electron-accepting units, with a centrally positioned electron-deficient fullerene bis-triazolium unit (**244**), along with two mechanically bonded ferrocenyl-functionalized isophthalamide anion binding sites (**245**).[149] In this design the macrocycles are dynamic, as recognition shuttling alters the position of the electron donor and acceptor axle components, which was confirmed by ^{1}H NMR, along with an on/off switchable emission response induced by anion (chloride) binding. They also described for the first time selective nitrate bonding to the [3]rotaxane host bearing

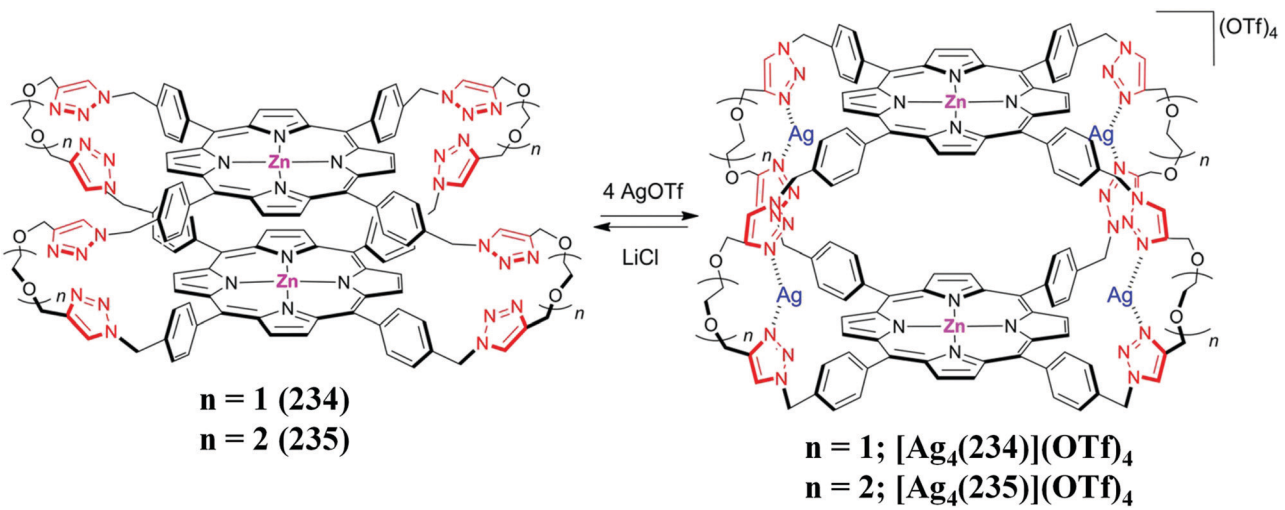

Fig. 46 The breathing motion of flexible zinc(II) porphyrin cages by reversible binding of silver(I) ions to the peripheral triazole moieties.[146]

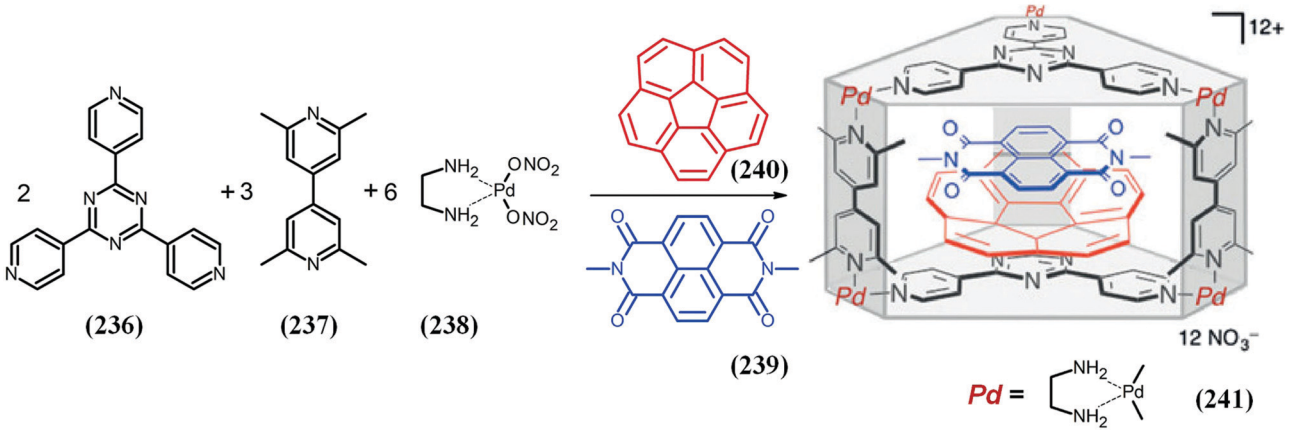

Fig. 47 Formation of the inclusion self-assembled box-shaped cage (**241**) structure of the studied guests corannulenes (**240**) and NDI (**239**) at 100 °C for 2 h in H_2O solvent.[147] This figure has been adapted from ref. 147 with permission from John Wiley and Sons, copyright 2015.

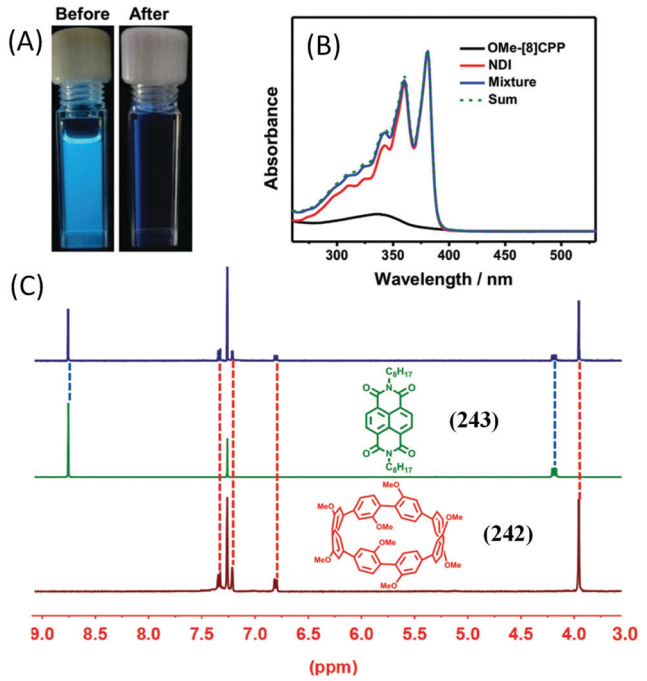

Fig. 48 (A) Photograph of the fluorescence of octamethoxy-[8]CPP (**242**) before and after the addition of NDI (**243**) in CH_2Cl_2 under a UV lamp (365 nm). (B) Absorption spectra of (**242**) (black line), (**243**) (red line), a mixture of octamethoxy-[8]CPP (**242**) and NDI (**242**) (blue line), and the sum of the absorption spectra of (**242**) and (**243**) (olive dash) in CH_2Cl_2. (C) ^{1}H NMR spectra of (**242**) (bottom, 6×10^{-3} M^{-1}), (**243**) (middle, 9×10^{-3} M^{-1}), and a mixture of (**242**) (6×10^{-3} M^{-1}) and (**243**) (9×10^{-3} M^{-1}) (top) in $CDCl_3$.[148] This figure has been adapted from ref. 148 with permission from The Royal Society of Chemistry, copyright 2019.

a bis-iodo triazolium-bis-NDI with a four-station axle component, over the more basic acetate.[150] In another example this group has synthesised two bistable halogen and hydrogen-bonded NDI [2]rotaxanes, in which the rotaxane shows superior halogen induced translational motion of the macrocyclic wheel.[151] In a similar fashion, another interesting example was described by Leret *et al.* where they functionalised a single-walled carbon nanotube with bisalkene NDI using Grubbs catalyst *via* ring closing metathesis, which produced rotaxane-like mechanically interlocked SWANT derivatives.[128] Briken and Isaacs described molecular clips of glycoluril as a selective receptor for cationic dyes in water *via* cation–π interactions.[152]

Khurana *et al.*[153] demonstrated the generation, stabilization and *in situ* redox reaction in benzimidazole appended NDI dye (BzNDI) and cucurbit[*n*]uril CB7 and CB8 host–guest complex. The complex gives emissive radical anions through the complexation of macrocycles in aqueous medium, and through the CB8 complexation it displayed a novel excimer emission band in the 523 nm region, which originated from the dimeric inclusion of BzNDI dyes into the CB8 cavity. This dynamic stability window of the radical anions has been used for the *in situ* reduction of Au^{3+} to generate stable AuNPs.

Wang and co-workers designed and synthesised [2]rotaxanes using a one-pot, two-step procedure *via* a donor–acceptor interaction between the electron acceptor and the electron rich naphthalene (NA) unit donor.[154] An NDI containing a dialkyne and a macrocyclic polyether NA form the pseudorotaxane complex, and a copper-catalysed azide–alkyne cycloaddition (CuAAC) click reaction was used as a stoppering process to produce the final rotaxane (**246–247**) as shown in Fig. 49. This method is a promising approach for the preparation of rotaxanes, as it requires a small amount of solvent, no heating, and a very short reaction time and provides an excellent yield. Furthermore, charge-transfer interactions were induced *via* shuttling within the [2]rotaxanes.

Takenaka and co-workers synthesised ferrocenyl-connected NDI (FND) derivatives connected with β-cyclodextrin (β-CD) and used them for electrochemical aberrant methylation detection.[155] In another report, the Gruenberg group synthesised a series of methyl-piperazine substituted NDIs with varying chain length between the NDI and the piperazine moieties (*i.e.* 2–5 CH_2 groups) and used these derivatives as molecular telomeric quadruplex-DNA receptors (Fig. 50).[156]

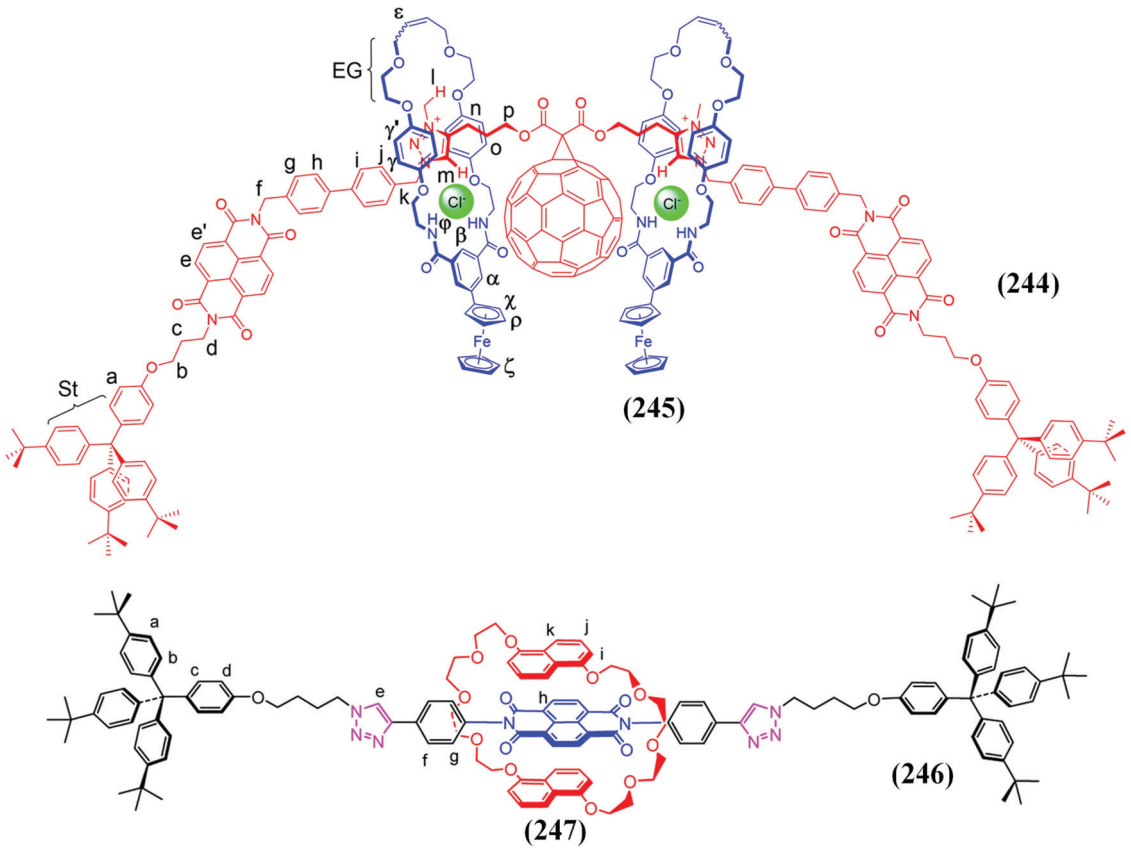

Fig. 49 Chloride templated [3]rotaxanes[149] and [2]rotaxanes.[154]

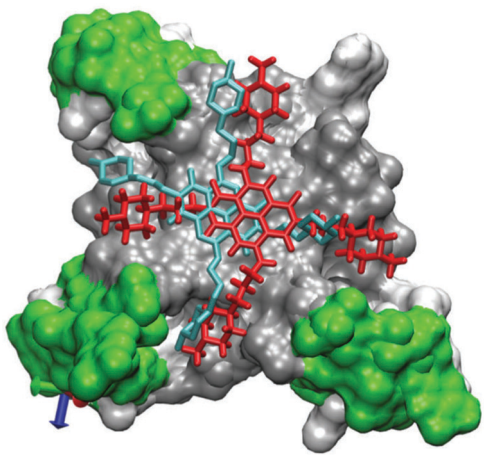

Fig. 50 Superposition of the crystal structure (light blue) with the global minimum found for ligand 2 intramolecular (red).[156] This figure has been adapted from ref. 156 with permission from The Royal Society of Chemistry, copyright 2015.

The Ghosh group synthesised polymeric foldamers bearing an n-type semiconducting NDI through hierarchical self-assembly of folded polyurethanes (PUs). Three different foldamers were prepared, differing only in the structure of the chain end functionality.[157] Their results are very exciting with respect to supramolecular electronics because of two advantages, the first being internal order in the folded conformation driven by directional H-bonding and the second being long range order by assembly of the foldamers.[158]

6 Sensors

The development of chemical sensors is of increasing interest in nano- and bio-technology enabling the determination of a diverse range of analytes such as anions, cations, organic volatiles, and toxic gases, not only in the human body but also in air, water, food, and environmental analysis. There has been tremendous development in this research area with a range of derivatives, but some of the organic molecules employed suffer from drawbacks such as tedious synthetic pathways.[159] In the last two to three decades, researchers have been using NDI analogues to improve the detection limit and sensitivity for both quantitative and qualitative sensing through the optical, calorimetric or naked eye detection of ions.[83,160]

NDIs and cNDIs are suitable to fabricate sensors as they are small organic planar molecules that can be easily synthesised with functional sensing groups, can be tuned in terms of fluorescence properties, and are soluble in a broad range of solvents. Importantly, cNDIs with electron donating groups on the core have rich electronic and spectroscopic properties, which makes them good candidates for sensing, especially because their near IR emission offers advantages for both

in vitro and *in vivo* biological sensing applications.[83] In earlier reviews, we give an in-depth discussion of NDIs in various sensing areas, and here we will illustrate development in the field with a few examples in the field of gas sensing, imaging, chemical sensing, photodetection, and vapochromic chemosensors.

6.1 Chemosensors

We have reported the synthesis of an aza-crown ether (1-aza-18-crown-6) core-substituted NDI (**248**, **249**), which displays an optical response toward calcium (Ca^{2+}) over other cations.[161] Both (**248**) and (**249**) produced violet colour and upon addition of Ca^{2+} selectively showed a colour change to faint yellow. In another report, we showed that, by placing 1-aza-18-crown-6 with aza-12-crown-4-ether (**250**) onto the core of NDI, selective detection of Li^+ over other monovalent cations such as Cs^+, Na^+ and K^+ was possible.[162] The UV-vis, fluorescence, CV, ^{1}H NMR and naked eye color changes clearly showed selective binding of Li^+, with a limit of detection of 5.0 mM. Interestingly Li^+ could be removed and NDI-12-C-4 could be re-used by simple addition of EDTA, followed by centrifugation. In a similar strategy the Bell group synthesised two new sensors based on NDI, substituted with aza-15-crown-5-ether (**251**) and aza-18-crown-6 ether (**252**), where (**251**) was found to bind to Ca^{2+}, while (**252**) was found to be selective towards sodium and potassium cations.[163] The development of this field is highlighted in Fig. 51.[161–169]

Li and co-workers studied ''turn-on'' fluorescence for Cu^{2+} ions *via* the synthesis of an NDI linked with 1,4,6,10-tetrathia-1,3-azacyclopentadecane at the 2-core position (**253**), which acts as a receptor for Cu^{2+}, and 6-core carbon piperidine attached to the other side of the core which acts as a strong electron donor.[164] This novel cNDI exhibited high selectivity, affinity and good sensitivity towards Cu^{2+} with a detection limit of about 4.0 μM, which is lower than the acceptable level of Cu^{2+} in drinking water ($\sim$20 μM). They also prepared test-strips on silica gel plates for the detection of Cu^{2+} ions. In another report, they synthesised an NDI bearing bis[2-(3,5-dimethylpyrazol-1-yl)ethyl]amine (**254**) at the core, which acts as an electron donor as well as a receptor site. Interestingly, this NDI derivative exhibited ''turn-on'' fluorescence for mercury ions (Hg^{2+}) with a detection limit of 1.3×10^{-6} mol L^{-1} and selectivity over other cations studied.[165] Due to a change from colourless to red emission, they were able to prepare test strips which could be used repeatedly, and demonstrated that this NDI derivative could be used for detection of Hg^{2+} in living cells. In another report, they functionalised the core of an NDI with 2-((pyridine-2-ylmethyl-amino)ethanol, which acts as an electron donor as well as a receptor moiety. This derivative was non-emissive in solution; however, upon formation of the complex NDI-Cd^{2+} produced strong red fluorescence and also displayed rapid quenching in response to S^{2-} ions with a limit of detection as low as 8.7 μM because of the high affinity between sulphide and Cd^{2+}. They synthesised a cNDI bearing 8-aminoquinoline (**255**) as an electron donor and receptor for Hg^{2+} by ''turn-on'' fluorescence, and the same molecule detected Cu^{2+} through a

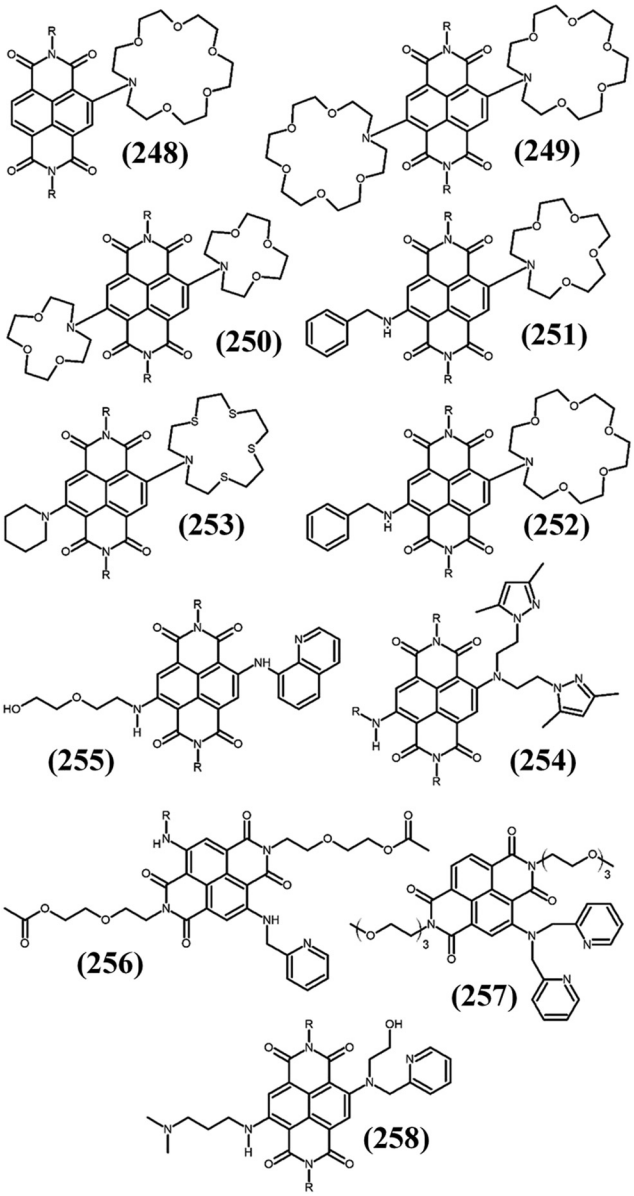

Fig. 51 Structures of aza-crown-cNDI and other NDI based chelating agents used for sensing.[161–169]

naked-eye color change from blue to green.[166] These changes can be attributed to twisted intramolecular charge transfer (TICT) in the excited state. Functionalisation of an NDI with 2-methylamino pyridine (**256**) enabled copper (Cu^{2+}) detection with a limit of detection as low as 0.97 μM in solution, and strip tests showed a 2.0 μM detection limit.[167] Wanichacheva and co-workers synthesised an NDI containing dipicolylamine as the receptor moiety at the core with 2-(2-(2-methoxyethoxy) ethoxy)ethan-1-amine at both the diimide positions (**257**) to solubilise the ligand in water as well as other aqueous-organic solvent mixtures.[168] The NDI-dipicolylamine sensor demonstrated significant fluorescence quenching by Cu^{2+} over interfering metal ions and colour changes could be seen by the naked eye. The sensor was also capable of detecting Cu^{2+} in 100% aqueous solution with a limit of detection as low as

0.7 ppb, which is lower than that recommended by the United States Environmental Protection Agency (USEPA) and the World Health Organization (WHO) for drinking water. In another work, Zong *et al.*[169] reported a red fluorescence probe based on NDI (**258**) that can detect the presence of sulphide anions with high selectivity and sensitivity. The fluorescence response is mainly due to the different kinds of excited states by coordination, which is related to the TICT process.

The Lin and Wei groups jointly undertook carboxyl functionalisation at the diimide position (**259**), and upon mixing with NaOH the complex soluble in water was shown to be selective for the detection of mercury(II) *via* ''turn-on'' fluorescence with a limit of detection of 1.18×10^{-6} M, and this derivative was also used to remove mercury(II) from water.[170] In another report they synthesised an NDI bearing a benzimidazole functionality at both the diimide positions (**260**), which displayed highly selective and sensitive fluorescence emission for cyanide ions CN^- with a detection limit of 8.32×10^{-7} M.[171] Importantly, the reversible binding of CN^- was also demonstrated by addition of H^+ allowing the sensor to be used again, and this process could be repeated many times without loss of activity. The Pina-Luis group synthesised an NDI bearing two 3-phenylboronic acid groups at the diimide positions (**261**) which showed high selectivity towards fluoride ions over other anions, where the two boronic groups acted as cooperative binding sites for the analyte.[172] This group also developed an AIE active supramolecular p-gel for fluorescence detection and separation of metal ions from water through the preparation of a yellow fluorescent π-gel of di-pyridine NDI (**262**) and tri-pyridine functionalised trimesic amide (**263**).[173] This p-gel was able to detect and separate Fe^{3+} and Cu^{2+} ions from water with detection limits of 6.60×10^{-8} M and 1.75×10^{-7} M, respectively. Furthermore, they studied a thin film based on AIE p-gel, which displayed excellent detection capability for Fe^{3+} and Cu^{2+} ions over other various interference cations. Campbell and co-workers prepared a mesoporous metal organic framework (MOF) based on the redox-active NDI chromophore (**264**), which exhibited selective fluoride sensing over other anions such as chloride, bromide and iodide (added as TBA salts), which could be seen by the naked eye with a reversible color change (red/orange to black).[174] They have also used NDI MOF based test strips, and the strips were a pale orange color, which turned dark brown after dipping into TBAF (F^-) solution. Iyer and co-workers appended imidazolium at the diimide position (**265**) of the NDI for nitro-explosive (picric acid) detection in aqueous medium and in the vapour phase, where fluorescence quenching occurred because of anion exchange and strong π–π interactions.[175] The detection of PA was also observed by single crystal X-ray structures, enabling visualisation of the NDMI and NDMI–PA complex for the first time. NDMI also self-assembled into flower-like structures, suitable for a device for vapor mode detection of PA which could be monitored by the LED_{off} and LED_{on} states. Li *et al.*[176] used the anion effect (Cl^-, Br^-, NO_3^-, ClO_4^-, BF_4^-) to construct devices using 1D supramolecular chains of *N*,*N*′-bis(4-pyridylmethyl)-NDI for iodide detection. The I^- anion interactions with pyridine rings quenched the Br^- induced 1D structure solution fluorescence intensity. The development of the sensing of ions using various NDI derivatives is illustrated in Fig. 52.

Kavitha *et al.*[177] used cysteine conjugated NDI coated on an etched fiber Bragg grating (eFBG) sensor for selective and rapid detection of mercury (Hg^{2+}) in drinking water. The sensor responds with a Bragg wavelength shift ($\Delta\lambda_B$) to the thiol–Hg^{2+} coordination interaction, displaying a dynamic range from 1 pM to 1 μM.

6.2 Vapochromic chemosensors

Low-cost sensors for the detection of organic volatiles and other toxic gases have received attention for the development of affordable techniques for environment protection and industrial safety and security. The current techniques used to detect gases and organic volatiles are based on high-performance liquid and gas chromatography; however, these techniques are quite expensive and time-consuming, leading to the need to develop new techniques or materials which are more convenient and simple. In this regard, we have prepared fluorescent porous metal–organic frameworks (PMOFs), with the network consisting of a central tetraphenylethene (TPE) bearing four pyridine periphery rings (coded as Py-TPE) coordinated to $ZnCl_2$ nodes, which crystallizes to produce large channels (13.4×17.5 Å). As the PMOF contains TPE central moieties, the aggregation induced emission (AIE) phenomenon was observed, with ''turn-on'' fluorescence in response to volatile organic aromatic compounds (VOACs) and quenching in response to nitro-substituted VOACs.

In recent years, single-crystal-to-single crystal (SCSC) transformations have become of interest as it allows not only visualisation of changes in the crystal structure during the transformation, but also allows an understanding of the interaction between the host and guest molecules. Xu and co-workers prepared supramolecular organic frameworks (SOFs) based on *N*,*N*′-bis(4-pyridylmethyl)-NDI, which demonstrated that the SCSC-process using an external stimulus such as temperature directly influences intermolecular π–π and hydrogen-bonding interactions.[137] Interestingly, this SOF displayed selective adsorption and sensing of water over other polar/non-polar organic solvents such as methanol, ethanol, *n*-propanol, isopropanol, *n*-butanol and benzene, which could be observed by means of fluorescence emission quenching.

The Ono and Hisaeda group synthesised derivatives by functionalising the diimide position of NDI with 3,5-di-*tert*-butylaniline, 2-aminodiphenylmethane, 2-aminobenzophenone (**266**) and tris(pentafluorophenyl)borane units.[178] Among them, the NDI bearing 2-benzophenone (**266**) displayed interesting vapochromic and vapofluorochromic behavior for VOACs (toluene, *p*-xylene, 4-fluorotoluene, and anisole) as shown in Fig. 53. They have also fabricated mini-sensors using NDI by functionalising the diimide position with two 2-benzophenone and two tris(pentafluorophenyl)borane units. Both these sensors allowed discrimination of benzene derivatives such as isomers of xylene, and detection could be seen by the naked eye based on their vapochromic/vapofluorochromic response.

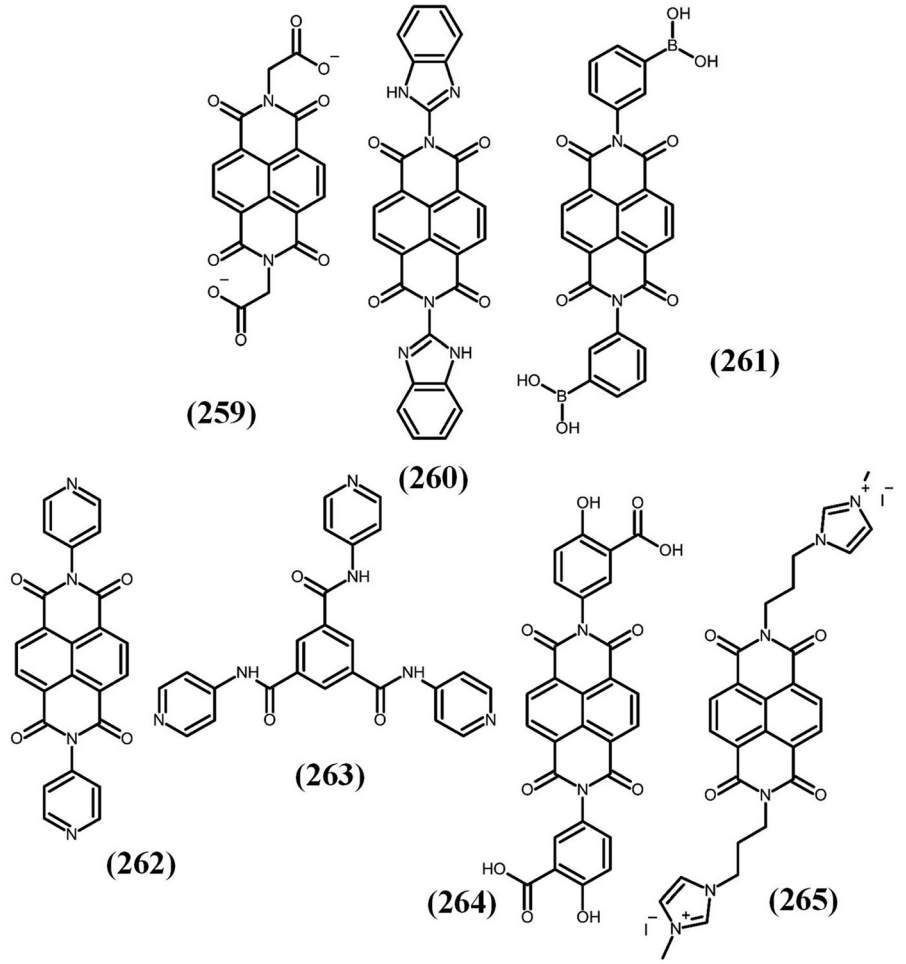

Fig. 52 NDI based chemosensors.[170–175]

In an earlier work, the Shinkai group demonstrated an NDI based low molecular weight gel for the selective sensing of isomers of dihydroxynaphthalene at millimolar concentrations with detection noticeable by visible colour changes.[179] On a similar path, the Peng and Fang group synthesised a 3,4,5-tris(dodecyloxy)benzamide NDI derivative (**267**), which is photochemically stable and highly fluorescent (Fig. 54). Due to the long alkyl chains at the diimide position of NDI, compatibility with organic solvents was achieved and gels were formed with nine solvents at low concentrations of 2.0% (w/v).[180] The gelator of (**267**) formed a fluorescent fibrillary structure in methylcyclohexane (MCH) *via* supramolecular self-assembly. This allowed a fluorescent film to be formed by spin-coating on a glass substrate, which was used for the detection of various VOCs, such as aniline and *o*-toluidine vapor. Interestingly, the sensing process is reversible, and these types of low molecular weight gels may thus be useful for the preparation of fluorescent sensing films to detect VOCs for real-world applications in the future.

Ali *et al.*[181] reported the development of a capacitive type humidity sensor employing NDI derivatives bearing imide side chains of different hydrophilicity as sensing layers. The developed sensors exhibited high sensitivity, good long-term stability, excellent reproducibility, and low hysteresis.

6.3 Imaging and biosensing of analytes

The development of fluorescence organic compounds capable of penetrating the cell with dual functionality, cell imaging and signalling, as well as acting as a binding unit (receptor) has attracted considerable interest. Among the various fluorophores used in these studies, NDI has become an interesting component in the last two to three decades because of its fluorescence and self-assembling capability for biomedical applications. NDI derivatives bearing peptide conjugates are capable of probing intracellular pH within the rough endoplasmic reticulum of living cells.[182] In this regard, Freccero and co-workers synthesised a water soluble non-fluorescence NDI dimer (**268**), which was prepared from the conjugation of two red tri-substituted NDIs (**269**) and a blue tetra-substituted NDI (**270**) *via* a $(CH_2)_7$-flexible spacer (Fig. 55).[183] Interestingly, the non-fluorescent NDI dimer ''turned on'' red/NIR fluorescence emission upon binding with G-quadruplex DNA. The fluorescence lifetime of the NDI dimer varies with the G-quadruplex and the weakly emitting ds-DNA, and thus the discrimination

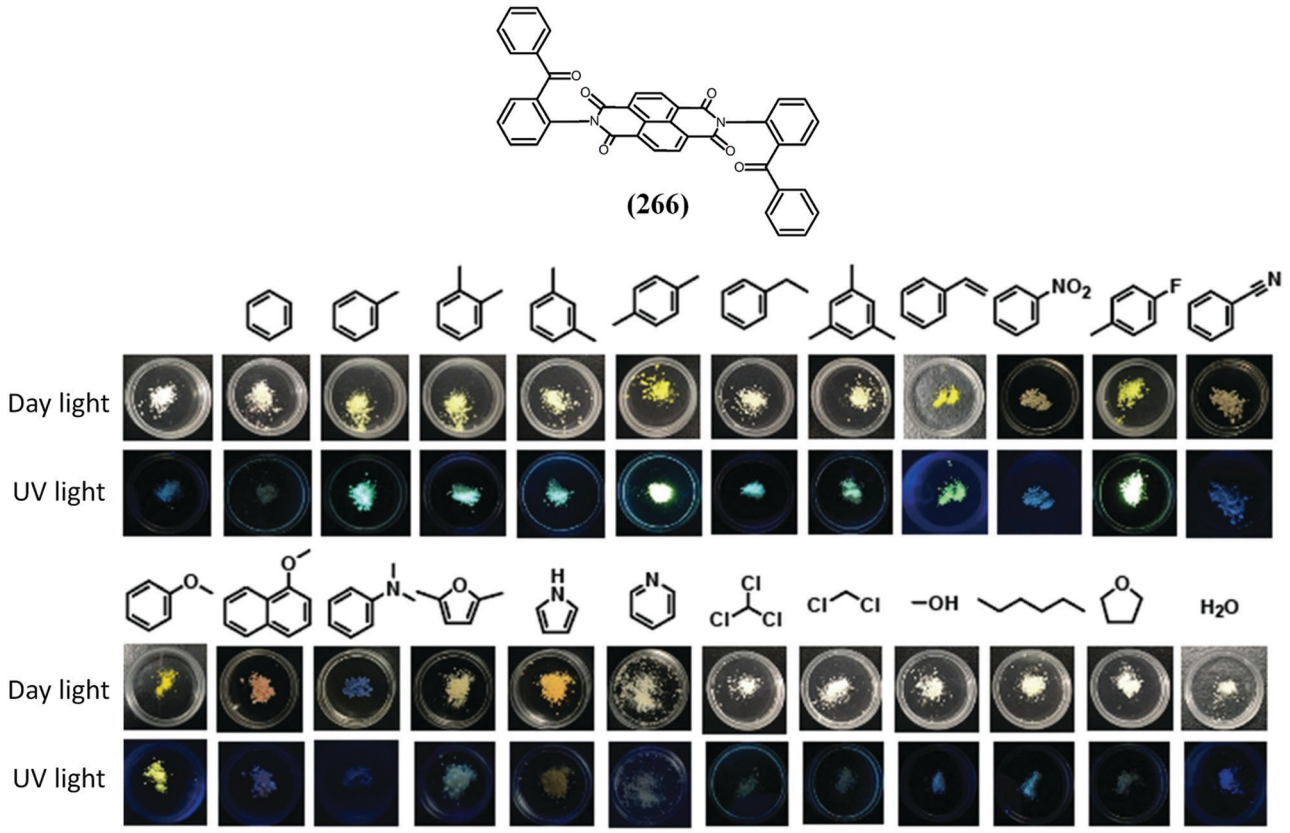

Fig. 53 Photographs of (**266**) and various guests in daylight (upper row) and under UV-light irradiation (365 nm, bottom row).[178] This figure has been adapted from ref. 178 with permission from The Royal Society of Chemistry, copyright 2013.

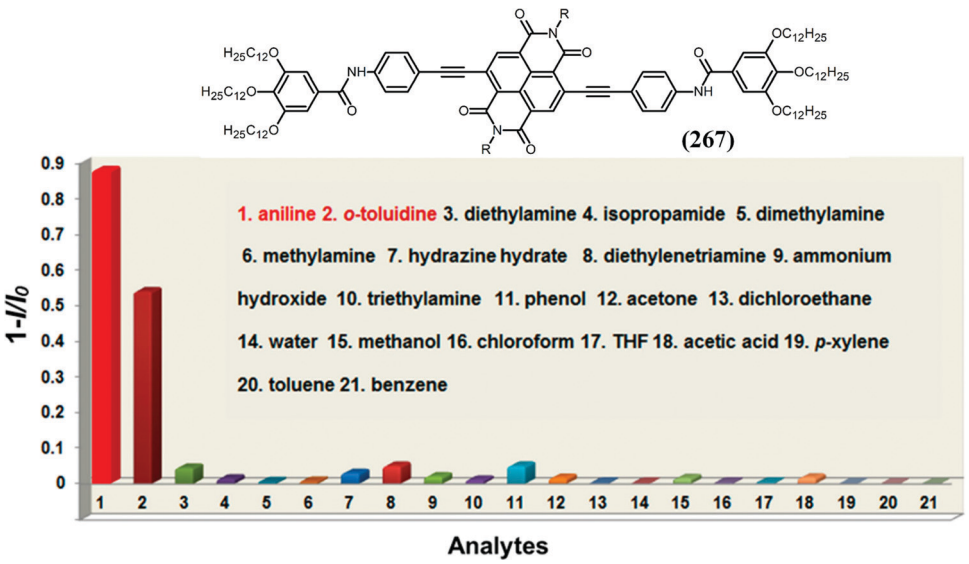

Fig. 54 Fluorescence response of (**267**)-functionalized film to different organic vapors at a concentration of 3060 mg m^{-3} (error of ±3%).[180] This figure has been adapted from ref. 180 with permission from The American Chemical Society, copyright 2016.

of G-quadruplex DNA in the presence of dsDNA using NDI dimer as a sensor was observed.

In another report, the Dasgupta, Ukil and Da group synthesised an asymmetric NDI-based hydrogelator by functionalisation at one end with a C_6H_{13}-alkyl chain and at the other end with a GKRGDS peptide chain. GKRGDS has already been shown to play a dual role, acting as a structural component as well as a biological ligand for tumor homing and cell adhesion

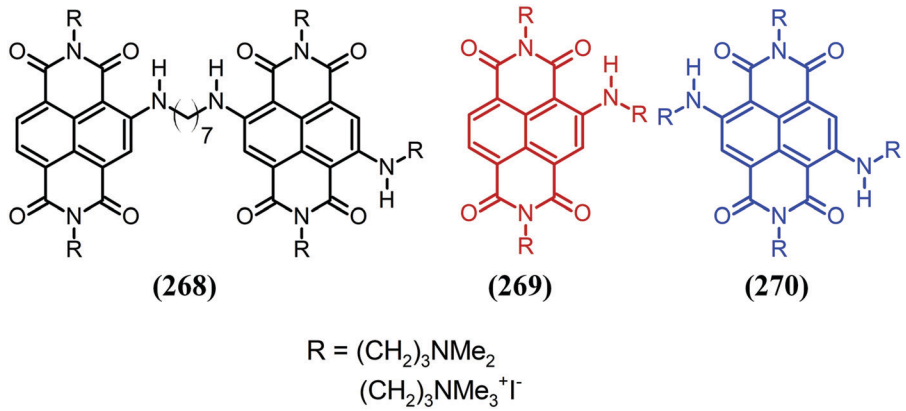

Fig. 55 Structure of dimeric (**268**) resulting from the merging of monomeric (**269**) and (**270**) and its quaternary ammonium iodide salt.

properties.[114] The NDI-peptide amphiphile formed a hydrogel with a lower concentration (50 μM) *via* three important steps: firstly π–π stacking of the NDI core, then hydrophobic interaction between the alkyl chains, and thirdly strong hydrogen bonding within the peptide chains. Furthermore, the hydrogel was found to be non-toxic in MTT assays and cell permeable.

Estrela and co-workers synthesised an NDI containing diferrocene at the diimide position through an amide linkage with an oligoethylene spacer (**271**). The diferrocene was used to bind a peptide nucleic acid (PNA)-DNA duplex and enable electrochemical sensing to monitor DNA recognition (a detection limit of 11.68 fM) through the ferrocene oxidation peak as shown in Fig. 56. The

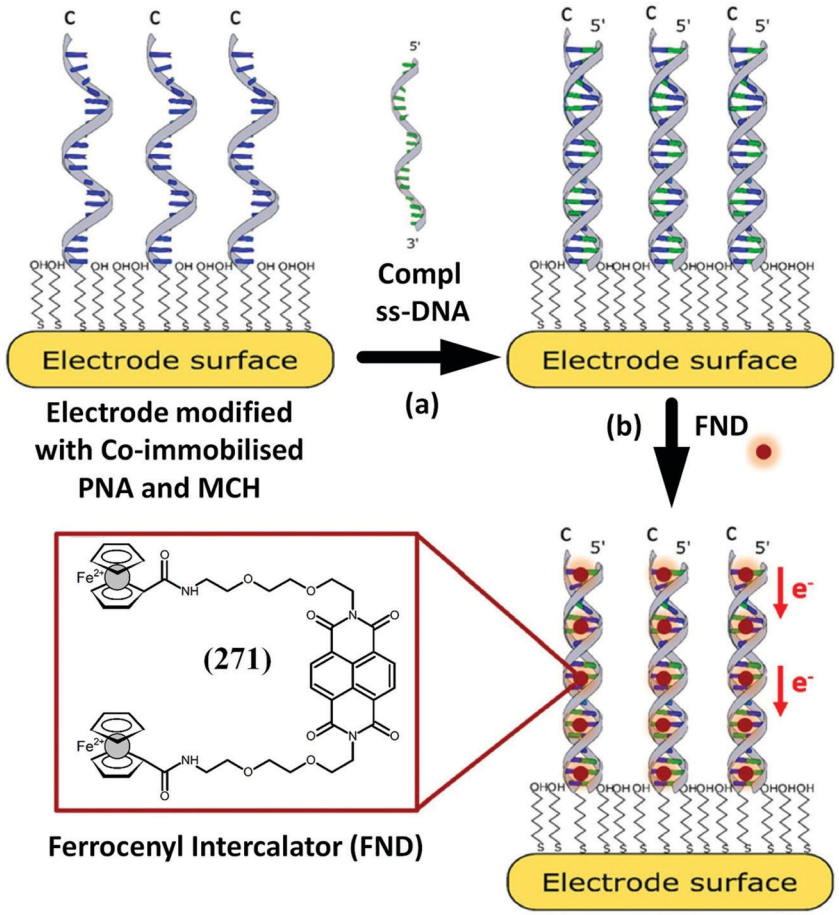

Fig. 56 Schematic illustration of the (**271**) based biosensor for the investigation of PNA–DNA hybridization: (a) PNA–DNA hybridization step and (b) (**271**) binding with the PNA–DNA duplex.[184] This figure has been adapted from ref. 184 with permission from John Wiley and Sons, copyright 2016.

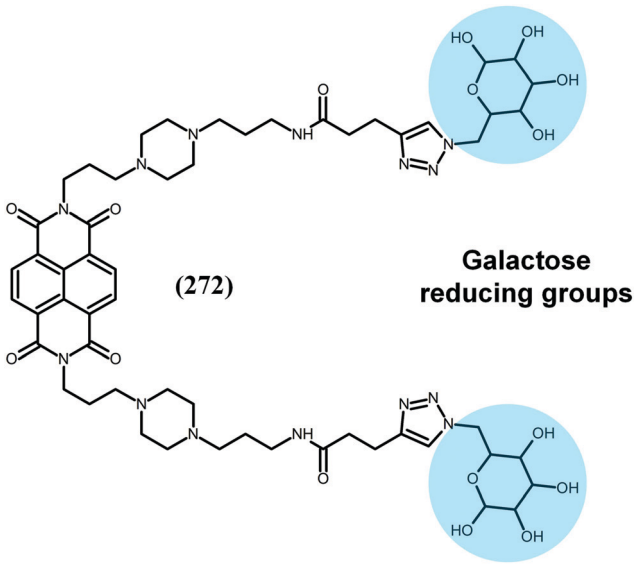

Fig. 57 The molecular structure of NDI based intercalators (**272**) with two terminal galactose moieties, which act as threads that form a stable complex with double-stranded DNA, and the galactose moieties act as reducing agents.[185]

chemically stable and planar NDI core was used to interact with nucleic acid sequences *via* π–π stacking interactions, making the probe a selective sensor for DNA.[184]

Yasuda and co-workers described the use of an NDI containing two galactose moieties (**272**), which intercalated to form a stable complex with double-stranded DNA and galactose moieties at both the diimide positions to reduce silver ions along the λDNA (Fig. 57).[185] Interestingly, metallized DNA nanowires were formed and they were also evaluated for electrical detection of biomolecules. The detailed mechanism is illustrated in Fig. 56.

The Wang group synthesised an NDI bearing spermine conjugate (NDIS) and studied the interaction with herring sperm DNA, in which NDIS interacts with DNA *via* intercalation and groove binding due to hydrophobic and hydrogen-bonding interactions.[186] The groove binding of NDIS with DNA was confirmed by the hypochromic effect observed in UV-Vis spectroscopy and quenching of the NDIS fluorescence. Another report by the Barone and Grunenberg group described functionalised NDI diimide and 2,6-core substitution with methylpiperazine rings, which was shown to be locked deep inside the quadruplex grooves, leading to a stronger electrostatic interaction with the receptor for G4-DNA.

Chakraborty *et al.*[187] used aggregation-induced emission (AIE) properties of NDI amphiphile derivatives for lipase sensing. They showed that benzylester linked C5 tailored NDI exhibits AIE with an emission maximum at 490 nm in the DMSO–water binary solvent system at f_w of 30% and above to gradually give fluorescent organic nanoparticles. They used this phenomenon in selective turn-off sensing of lipase against many other enzymes including esterase through hydrolysis of a benzyl ester linkage with a limit of detection of 10.0 ± 0.8 mg L^{-1}.

6.4 Photodetection

Organic photodetectors (OPDs) have encouraged researchers to use NDI derivatives due to their properties such as tuneable spectra and processability in solution, which may lead to large area detection due to ease of fabrication of lightweight and mechanically flexible devices. Conjugated polymers based on alternate donor–acceptors (D–A) with organic materials have shown to be an excellent choice because they possess high photo-responsivity from the UV-Vis to the NIR spectrum, and these polymers can use either two donor units and one electron acceptor or *vice versa*, which is advantageous for low dark current and high-performing OPDs.

In this regard, there has been much development, and a few important examples are illustrated in Fig. 58. For instance, the

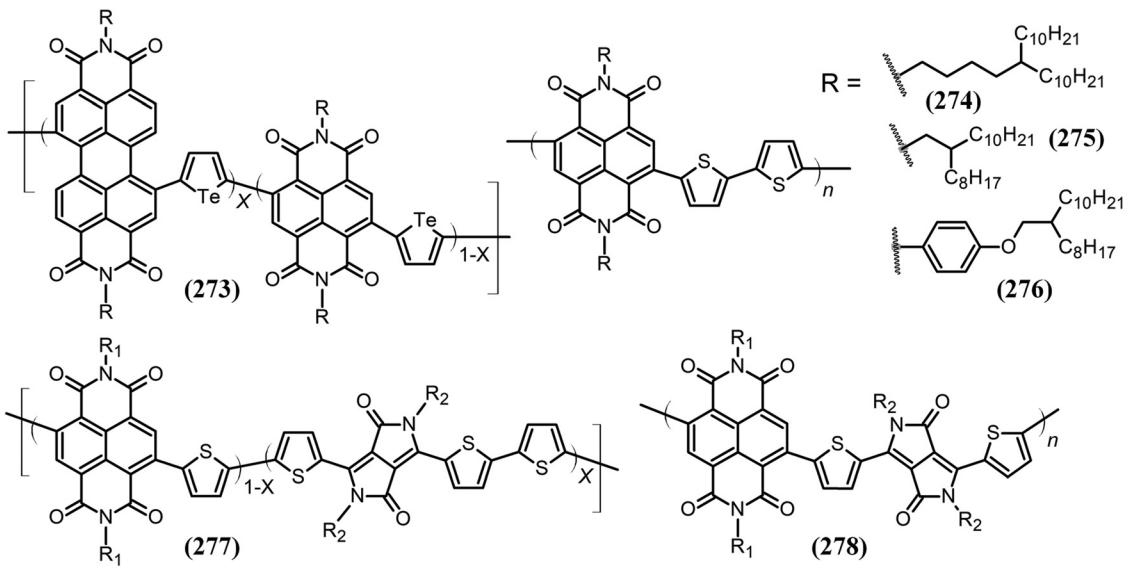

Fig. 58 Molecular structures of NDI based copolymer acceptors.[188–191]

Shen, Peng and Huang group synthesised a series of random copolymers based on one electron-donating tellurophene and two different electron-deficient PDI/NDI moieties (**273**). Importantly, all the polymers displayed excellent solubility in common organic solvents including chloroform, chlorobenzene, and dichlorobenzene.[188] Changing the proportion of the two electron-accepting moieties led to polymer films with tunable photophysical properties and photodetector performance. While studying a series of random copolymers, they found that the polymer with a 70/30 molar ratio of PDI/NDI gave the best photoinduced absorption and most favorable morphology. Finally, a photodetector based on P70 was shown to be highly responsive, *i.e.* about 19.1 A W^{-1} at 600 nm with excellent detectivity ranging from 350 to 600 nm, making this device amongst those showing the highest values for OPDs for UV-vis light detection in comparison with inorganic counterparts. The Qiao and Wang group synthesised a series of n-type semiconducting conjugated polymers containing NDIs with three different side chains, 5-decylpentadecyl (**274**), 2-octyldodecyl (**275**) and 4-(2-octyldodecyloxy)phenyl (**276**).[189] The results demonstrated that structural changes on the side chain influenced the packing of the structure, electron mobility and also the blend film morphology, thus influencing the properties of heterojunction polymer photodetectors. Nevertheless, the all-polymer photodetector exhibited a specific detectivity of over 10^{13} jones from the absorption region of 300–800 nm under −0.1 V bias, which is amongst the best detectivity values reported so far for UV-vis-NIR all-polymer photodetectors.

The Zhao, Hu and Gong group synthesised novel n-type low bandgap conjugated polymers (NDI-DPP) (**277**) by Stille coupling in toluene.[190] They mixed low bandgap conjugated polymers with SWCNTs for type II band alignment, enabling the SWCNTs to efficiently extract holes from the n-type conjugated polymer. Near-IR optical properties of both NDI-DPP and SWCNTs generated a NIR photo-response in OPDs with a high quantum efficiency of ≈80% in the visible region and ≈20% in the NIR region. Furthermore, when operating at room temperature, broadband OPDs exhibited responsivities (R) of ≈400 and 150 mA W^{-1} and detectivity over 6×10^{12} jones and over 2×10^{12} jones in the visible and NIR regions, respectively. Using a similar strategy, Qiao and Wang synthesised a series of random copolymers bearing two electron-withdrawing groups (NDI and DPP) with thiophene as a spacer (**278**). Interestingly, increasing the number of DPP-T segments in the copolymer led to a narrowing of the bandgap, with better film morphology and a lower dark current density, and a specific detectivity over 1012 jones in the range of 340–960 nm under −0.1 V bias.[191]

7 Optoelectronics, solar cells and storage

7.1 NDI based organic semiconductor technologies

In recent times, organic semiconductors have shown great potential for device scale applications such as in organic light-emitting diodes (OLEDS), organic field-effect transistors (OFETS), batteries and supercapacitors, and organic photovoltaic materials. Unlike the traditional inorganic semiconductors, these organic semiconductors offer great versatility due to flexibility, extended π-conjugation, and the degree to which they can be tuned by modifying the functional groups attached to the semiconducting core. Naphthalene diimide (NDI) is one such versatile π-conjugated molecule which can be easily functionalized at the N-atom position to produce highly active, redox, organic semiconductor molecular systems with enhanced electron or hole mobility, charge transfer characteristics, optical absorption–emission properties and microstructural superiority facilitating the fabrication of organic devices which are efficient, lightweight, flexible and self-healing.[192] Devices with memory storage and recognition properties[193] that are air stable,[194] economical and environmentally safe for application in optics, electronics and other semiconductor technologies can be envisioned with NDI derivatives.[105] Vener *et al.*[195] studied the charge carrier mobilities of *N*,*N*′-hexyl NDI and *N*,*N*′-cyclohexyl-NDI to compare and evaluate their efficient operation as organic electronic devices. Charge transport in high-mobility organic semiconductor crystals is considerably hindered by non-local electron–phonon interaction (NLEPI) transforming dynamic disorder induced by low-frequency (LF) vibrations into fluctuations of charge transfer integrals. They have shown that the contribution of various modes to the NLEPI correlates with their experimental Raman intensities, suggesting that LF Raman spectroscopy can be used to study NLEPI. Using molecular modelling, Xie *et al.*[196] showed that pyrene diimide (PyDI) is a more competitive core to assemble 1D n-type materials with desired charge transfer properties. A side-by-side inspection of binding energy and transfer integral surfaces revealed that intermolecular rotation can reduce repulsive interactions making the local energy minimum conformation coincide with the local maximum of electronic couplings. Mukhopadhyay *et al.*[197] studied the redox-active hybrid interface of silicon single crystal covalently functionalised with n-type NDI molecular systems. They showed that grafting NDI π–anion stacks on the Si surfaces gives a semiconducting Si surface where electron injection occurs at more positive potentials.

This section highlights some of the basic NDI based molecules/derivatives and their semiconducting and optical properties reported to date. The applications of these NDI based semiconducting compounds in OFETS/OTFTs, batteries/supercapacitors and solar cells in particular are vast and extensively researched, and hence separate sections are dedicated to highlight the progress in these areas, and a few interesting examples are discussed in Fig. 59.

The light absorption properties of organic semiconductors are extremely crucial for optoelectronic devices. Keeping this objective in mind, Higashihara and co-workers[198] synthesized several organic semiconducting polymers consisting of NDI functionalized with benzodithiophene or dithienopyrrole units (**279–282**). Extended intramolecular charge transfer was induced in these materials (*i.e.* shift in the peak from 739 nm in (**279**) to 785 nm in (**281**)) by incorporating a 3-hexylthiophene

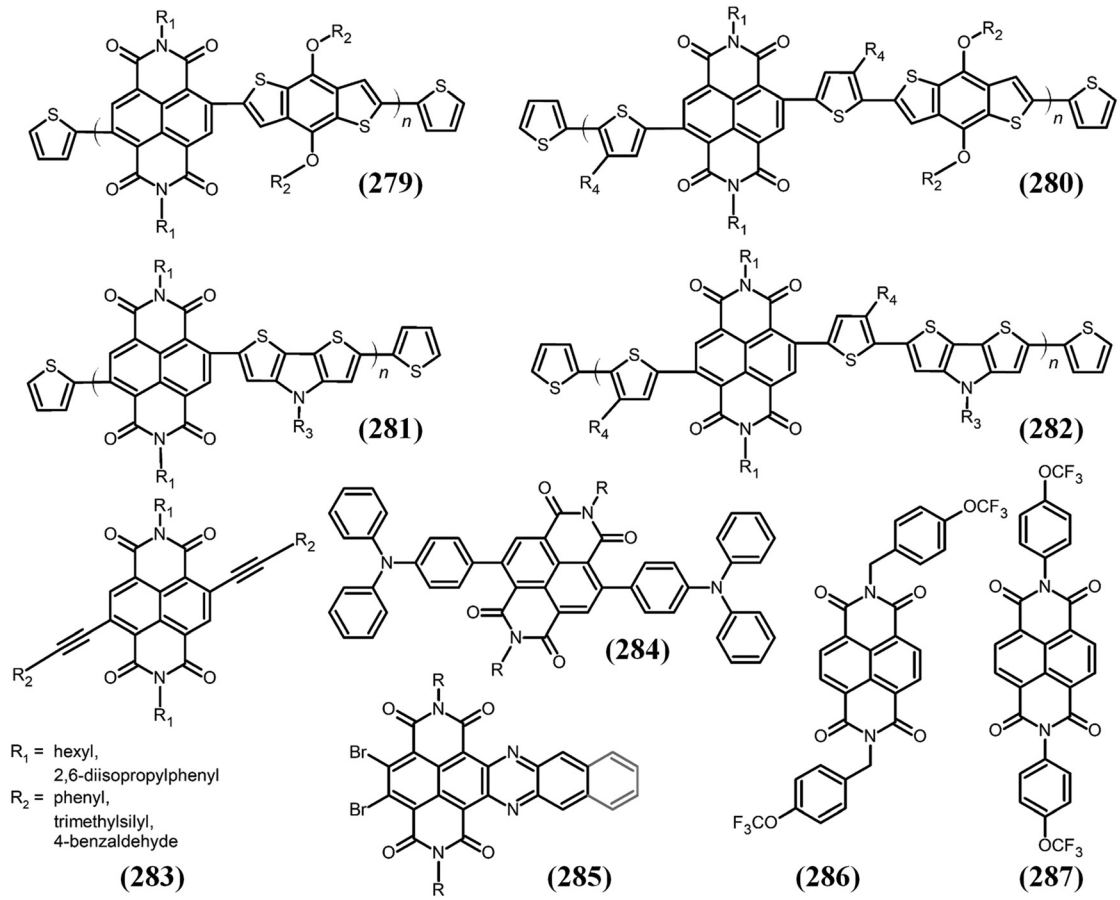

Fig. 59 The molecular structures of NDI-based semiconducting polymers (**279–282**) containing benzodithiophene or dithienopyrrole,[198] acetylene-substituted NDI (**283**),[199] triphenylamine disubstituted NDI (**284**),[200] (hydro)azaacene diimide derivatives (**285**),[65] *N,N′*-bis(4-trifluoromethoxybenzyl) NDI (**286**) and *N,N′*-bis(4-trifluoromethoxyphenyl) NDI (**287**).[201]

(3HT) spacer into the structure. As a result of the high-lying HOMO energy levels, (**280**) and (**282**) exhibited a 250 nm red-shift of the ICT peaks along with increased electron mobilities up to 1.5×10^{-2} cm^2 V^{-1} s^{-1} compared to (**279**) and (**281**). This behavior was attributed to the extended intermolecular orbitals overall and orientational effects of the polymer backbone. Acetylene-substituted naphthalene diimides (**283**) were prepared by Korzec and co-workers[199] using $PdCl_2$, Et_3N, and electrolytic copper powder. The synthesized NDI derivative exhibited green light fluorescence with quantum yields of *ca.* 6% in chloroform. A single-layer organic light-emitting diode (OLED) was later fabricated which exhibited orange or red electroluminescence. Data and co-workers[200] synthesized NDI core substituted triphenylamine (**284**) and demonstrated its use as a delayed fluorescence emitter in OLEDs upon thermal activation. Several dihydro- and tetrahydro-tetraazaacene diimides with laterally fused six membered rings (**285**) were synthesized by Zhao and co-workers.[65] These diimide derivates exhibited halochromic characteristics as well as redox-switchable vis-NIR optical properties. Meng and co-workers[201] synthesized *N,N′*-bis(4-trifluoromethoxybenzyl)-NDI (**286**) and *N,N′*-bis(4-trifluoromethoxyphenyl)-NDI (**287**) and used them as hole injection layers (HILs) in OLEDS. They found that NDI-BOCF$_3$ enhances hole injection, while NDI-POCF$_3$ hinders it.

Banerjee and co-workers[202] reported a two component hydrogel consisting of a mixture of NDI-conjugated peptide functionalized bola-amphiphile (**288**) and long alkyl chain primary amines, which exhibited rare J-aggregation induced bright yellow fluorescence in aqueous medium. This π-conjugated co-assembly consisted of a nanofibrillar network which exhibited enhanced fluorescence emission, long excited state lifetime, thermal stability, mechanical strength and semiconducting behavior with promising potential for optoelectronic and other semiconductor devices (Fig. 60).

Joon Hak Oh and co-workers[203] effectively used the chirality of a molecule to obtain supramolecular morphologies of NDI enantiomers (**289**, **290**) and cadmium iodide based coordination networks. The synthesized heterochiral micro/nanocrystals demonstrated photochromic properties. Doping of hydrazine into these semiconductors resulted in band gap reduction and hence increased the conductivity, which is beneficial for optoelectronic applications as illustrated in Fig. 61.

The influence of molecular design on a 2D surface crystallization process was studied by Li and co-workers[107] *via* scanning tunneling microscopy using semiconducting cores such as

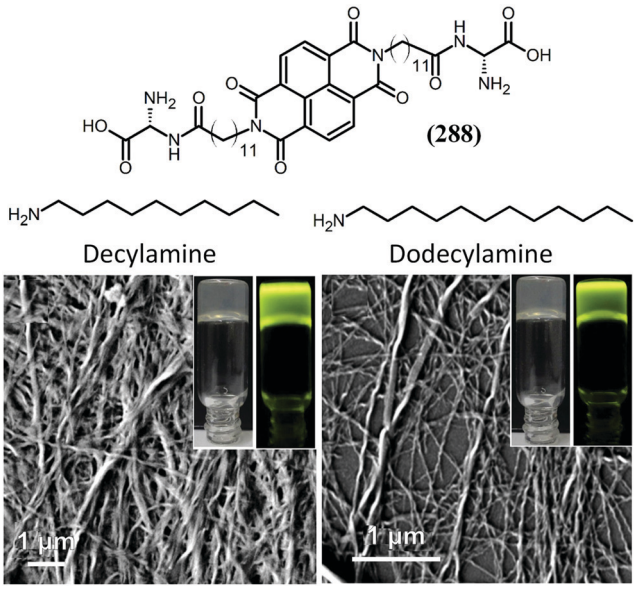

Fig. 60 Chemical structures of NDI-peptide (**288**), decylamine and dodecylamine, the FE-SEM images and photographs of two-component hydrogels of (**288**): amine at a 1 : 2 molar ratio in daylight (left side) and under a UV lamp (right side) (365 nm), respectively.[202] This figure has been adapted from ref. 202 with permission from The American Chemical Society, copyright 2016.

NDI (**291**), 2-perylene diimide (**292**), and tribenzo[*de*,*kl*,*rst*] pentaphene diimide (**293**) consisting of the same substituents and molecular symmetry, but differing in the length of the π-conjugated core. This study demonstrated that the surface chirality and 2D patterns were influenced by aromatic dimensions as well as the nature of the solvent, while the molecular symmetry could be effectively used to tune the long-range ordered 2D monolayer structure for n-type semiconductors (Fig. 62).

Liu and co-workers[204] investigated the effect of electron-transfer photochromism in coordination polymers made of NDI and dicarboxylate ligand, for example, $[Zn_2(DPNDI)(TPDC)_2]$ (**295**) and $[Cd_6(DPNDI)(TPDC)_6(DMF)_6]$ (**296**) as shown in Fig. 63. Due to the NDI moieties, complexes (**295**) and (**296**) exhibited photo-induced electron transfer and eye-detectable photochromic behaviour which could be further modulated by UV-Vis light irradiation.

Furthermore, electrochromic properties exhibited by novel NDI based metal–organic frameworks with MOF-74 (CPO-27) were demonstrated by Dincă and co-workers,[205] thus opening up a new doorway for the application of NDI based (**264**) MOFs in optoelectronic technologies (Fig. 64).

The efficiency of n-type organic semiconductors with the NDI core is significantly dependent on the efficiency of the n-doping functional groups. However, most of these n-dopants are unstable in air which renders these organic semiconductors ineffective for device scale applications. Leo and co-workers[206] utilized the air-stable precursor molecule *o*-MeO-DMBI-Cl (**298**) and investigated its efficiency for n-doping of *N*,*N*-bis(fluoren-2-yl)-NDI (**297**) *via* a thermal annealing process as shown in

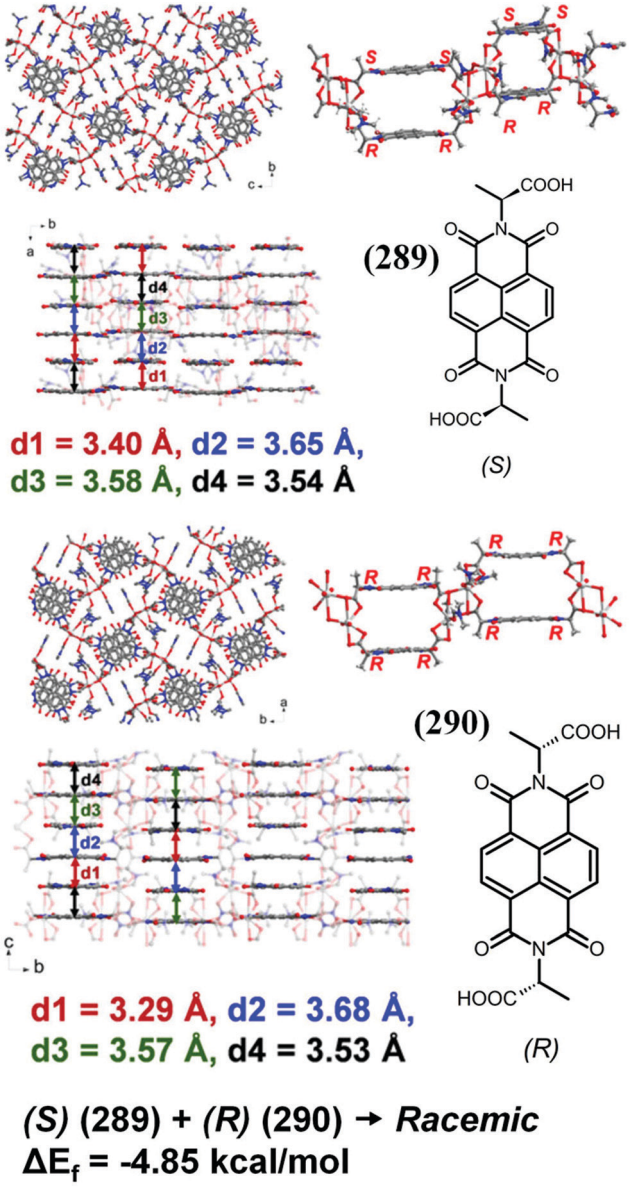

Fig. 61 Crystal structures of SCNs (*Rac*)-AlaNDI-Cd (**289**, **290**); the top left shows *a*-axis projection, the top middle shows unit description containing two AlaNDI units in a 1D chain with description of chirality, the top right shows polycatenation of 1D chains, the bottom left shows the π–π stacking scheme with centroid–centroid distances, and the bottom right shows chiral configuration in this SCN and (*R*)-AlaNDI-Cd (**290**); the top left shows *c*-axis projection, the top right shows unit description containing two AlaNDI units in a 1D chain with description of chirality, the bottom left shows the π–π stacking scheme with centroid–centroid distances, the bottom right shows chiral configuration in this SCN, and the bottom right shows polycatenation of 1D chains. Scheme on the right demonstrates the chemical structure of two enantiomeric AlaNDI ligands (**289**, **290**), which have coordination with cadmium in SCN.[203] This figure has been adapted from ref. 203 with permission from The American Chemical Society, copyright 2019.

Fig. 65. They concluded that the n-doping precursors can be tailor designed to achieve air-stable and highly conductive films for device scale applications. Bao and co-workers[207] also

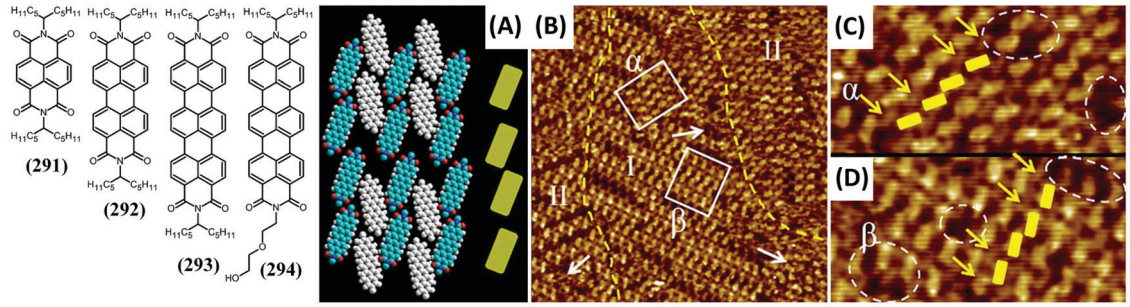

Fig. 62 The molecular structures of a series of n-type semiconductors (**291–294**) and the (A) tentative packing models of (**294**), and STM images of (**294**) (B–D) at the 1-phenyloctane–HOPG interface. Imaging conditions for panels (B–D): I_{set} = 300 pA, V_{bias} = −730 mV.[107] This figure has been adapted from ref. 107 with permission from John Wiley and Sons, copyright 2017.

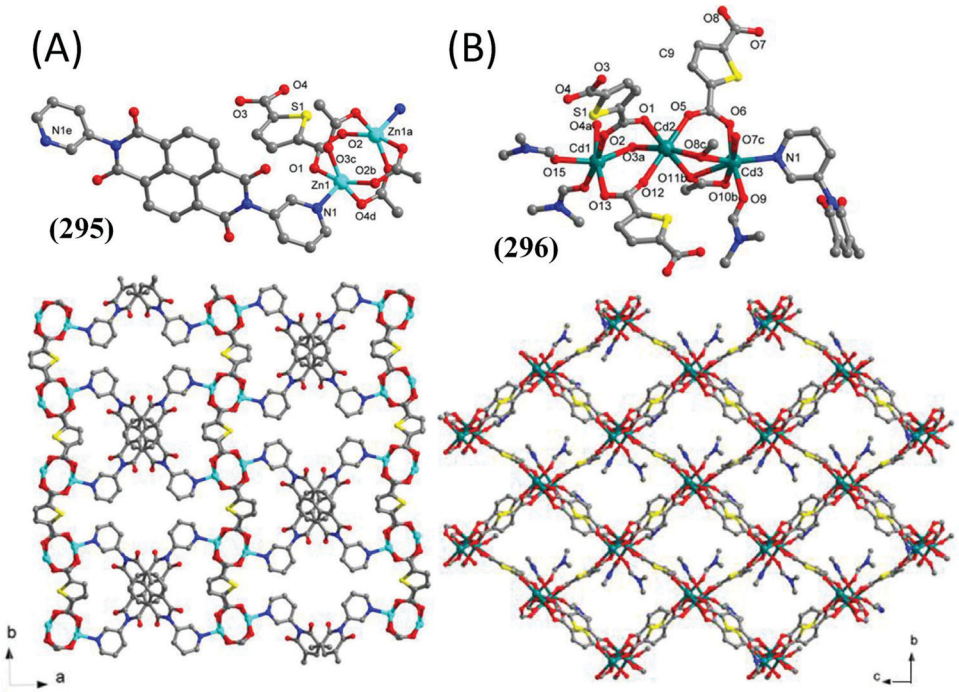

Fig. 63 The electron-deficient NDI based coordination polymers, dicarboxylate ligand, namely (A) $[Zn_2(DPNDI)(TPDC)_2]$ (**295**) **and** (B) $[Cd_6(DPNDI)(TPDC)_6(DMF)_6]$ (**296**) (DPNDI = *N*,*N*′-di(3-pyridyl)-NDI, H_2TPDC = thiophene-2,5-dicarboxylic acid, DMF = *N*,*N*′-dimethylformamide).[204] This figure has been adapted from ref. 204 with permission from Elsevier, copyright 2019.

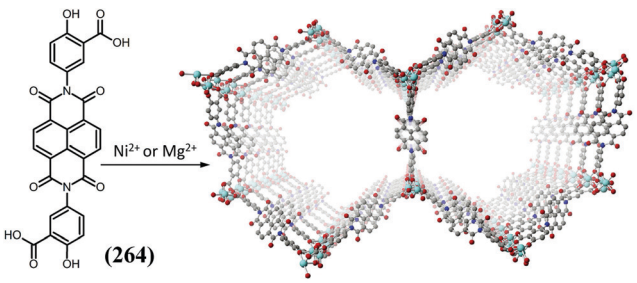

Fig. 64 A representation of the secondary building unit of the electrochromic NDI-based (**264**) mesoporous MOF. Teal, blue, red, and gray spheres represent metal (Mg or Ni), N, O, and C atoms, respectively. H atoms are omitted for clarity.[205b] This figure has been adapted from ref. 205*b* with permission from Elsevier, copyright 2016.

studied the effect of n-doping in NDI based molecules copolymerised with ethynylene, ethylene, and bithiophene (**274**) by dimeric dopants. They concluded that ethynylene based copolymers demonstrate the highest conductivity of 0.45 S cm^{-1} which is two orders of magnitude greater than bithiophene based copolymers. Tam *et al.*[208] reviewed n-doping strategies in organic semiconductors including NDI-based small molecules and polymers.

Gao and co-workers[209] managed to laterally extend the π-conjugation in NDI-2-(1,3-dithiol-2-ylidene) acetonitrile moieties by fusing the NDI core with benzo[*b*]thiophen-2-yl, naphthalen-2-yl and azulen-2-yl groups. As an outcome of the extended conjugation, an extension in NIR absorption up to 920 nm was achieved. These novel structures exhibited high

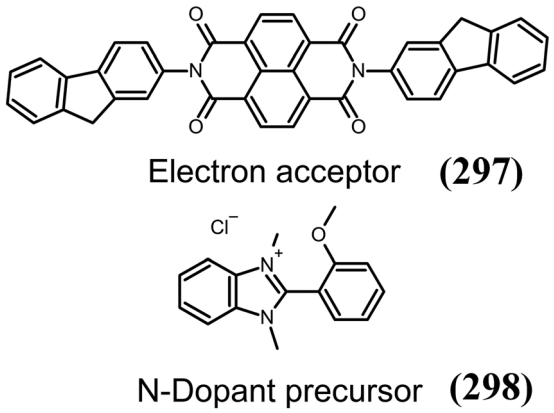

Fig. 65 NDI based acceptor (**297**) used to prepare organic semiconductors in combination with the N-dopant precursor (**298**).[206]

electron mobilities of up to 0.37 $cm^2 V^{-1} s^{-1}$ and extended NIR-absorption properties which make them potential n-type organic semiconductor materials. The effects of thionation and isomerization on the charge carrier mobilities of thionated naphthalene diimide crystals were studied using Marcus–Hush theory and quantum-chemical calculations by Zhao and co-workers.[210] Consistent with previous studies, it was found that, with an increase in the thionation degree of NDIs, the charge mobility of both electrons and holes was enhanced in particular. The *trans*-isomers of these derivatives exhibited larger hole mobility compared to *cis*-isomers.

Subsequently, near edge X-ray absorption fine structure (NEXAFS) and density functional theory studies were undertaken by McNeill and co-workers[211] leading to the understanding that, due to thionation of NDI, the transition from C 1s energy to LUMO drastically decreased with thionation, as a result of an increase in valence electron density of the carbon atoms due to replacement of oxygen by sulphur atoms. LUMO engineering of NDIs (Fig. 66) was found to be easily achievable in comparison to PDI and other fullerenes in a study conducted by Matile *et al.*[212] Moreover, substitution of aromatics and electron rich sulphides in NDI makes them more responsive and ideal to integrate anion–π interactions within functional systems, confirming the superiority of NDI based systems in semiconductor and optoelectronic technologies as illustrated in detail in Fig. 66.

Sommer and co-workers[49] utilized biomass derived bifuran as alternating repeating units to NDI in order to produce flattened polymeric NDI-bifuran (**323**) and NDI–bithiophene (**322**). PNDIFu2 exhibited a smaller π–π stacking distance of 0.35 nm, a strong dichroic ratio and transport anisotropy with a good electron mobility of 0.21 $cm^2 V^{-1} s^{-1}$. Density functional theory studies concluded that the limited charge transport in

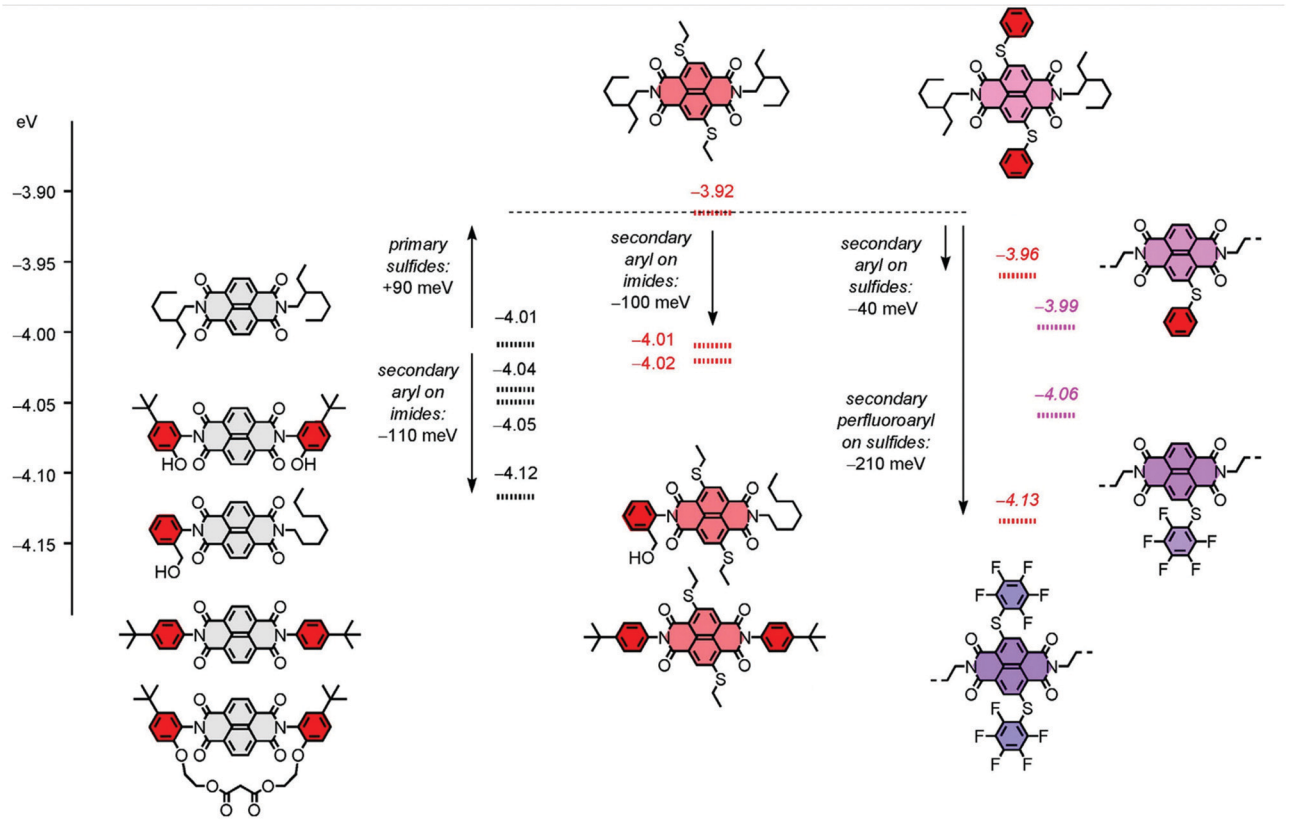

Fig. 66 Contributions from substituents in the NDI core and periphery to the energy of their LUMOs. E_{LUMO} values were obtained by differential pulse voltammetry (DPV) in CH_2Cl_2 and are reported in eV relative to −5.10 eV for Fc^+/Fc.[212] This figure has been adapted from ref. 212 with permission from John Wiley and Sons, copyright 2015.

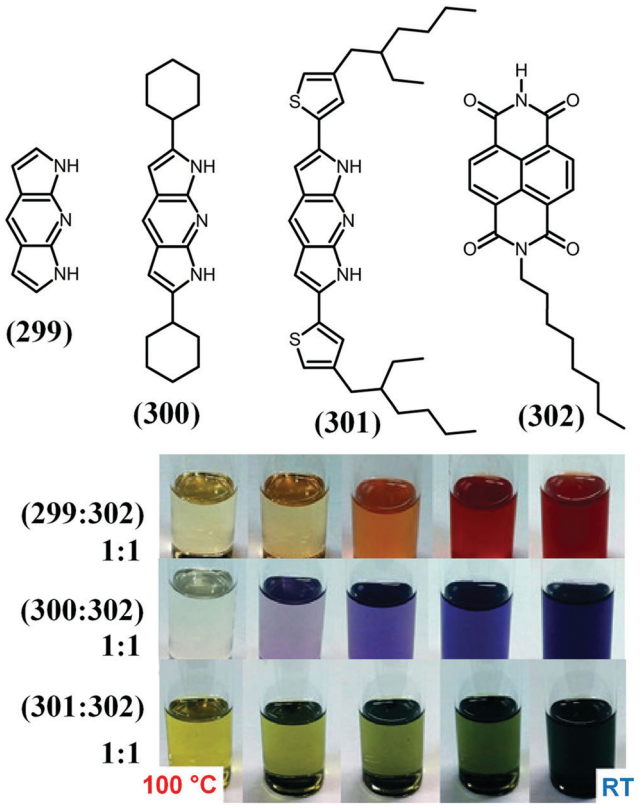

Fig. 67 The molecular structure of dipyrrolo[2,3-*b*:3′,2′-*e*]pyridine (P2P) electron donors (**299–301**) and the NDI based acceptor (**302**), and images of co-assembly solutions and their thermochromism in 1,1,2,2-tetrachloroethane.[213] This figure has been adapted from ref. 213 with permission from John Wiley and Sons, copyright 2016.

PNDIFu2 is a result of enhanced polaron localization in the molecular structure. Perepichka and co-workers[213] investigated the effect of complementary H-bonding across self-assembled dipyrrolopyridine (P2P) electron donors (**299–301**) and the NDI acceptor (**302**). This study concluded that the heteroatoms in the P2P/NDI assembly not only act as proton donors/acceptors but can also contribute to π-conjugation, which leads to perturbations of electronic levels due to H-bonding, as confirmed through concentration-dependent NMR and UV/Vis spectroscopic studies. As a result of this, charge-transfer (CT) absorption extends throughout the visible region (Fig. 67). Thus, this study provides a promising methodology for utilizing H-bonding-mediated self-assemblies of NDI based molecules for optoelectronic device applications.

Meng and co-workers[214] designed novel NDI based fluoro derivatives, namely, *N,N′*-bis(4-trifluoromethoxyphenyl)-NDI (NDI-POCF$_3$) and *N,N′*-bis(4-trifluoromethoxybenzyl)-NDI (NDI-BOCF$_3$). An interesting revelation made in this study is that while optical and electrochemical properties are similar in these two compounds, their electron mobility and molecular packing significantly differ. NDI-BOCF$_3$ in particular exhibits an air-stable electron mobility of 0.7 cm^2 V^{-1} s^{-1} which is attributed to the larger grain size and improved crystallinity.

Briseno *et al.*[215] designed an NDI-bithiazole-based copolymer, P(NDI2OD-BiTz), which exhibited an electron mobility of 0.11 cm^2 V^{-1} s^{-1} as a result of the optimized dihedral angle of 90° between acceptor units along polymer chains and highly ordered edge-on orientation. The unique feature of this study is that high electron mobility is achieved in spite of a non-planar backbone, contrary to those reported in the literature. Core substituted NDI based molecules have received a great deal of attention in recent times due to their tunable electron transport properties which can be exploited in optoelectronic devices.[212] For instance, Yao *et al.*[216] reviewed the development of core substituted NDI derivatives which were self-assembled into a series of 1D nanostructures such as nanotubes and nanoribbons *via* the controlled self-assembly of electron acceptor NDI and electron donor porphyrin molecules. Enhanced charge transport properties were measured using transient absorption spectroscopy, which were attributed to highly ordered and conductive π–π stacking of the chromophores.

DNA based nanoelectronics have been among the new developments in organic semiconductors, where NDI molecules and derivatives have played an important role in technology advancement. For example, a novel process to design a single silver nanowire based on DNA metallization utilizing NDI molecules with terminally labelled galactose moieties was reported by Yasuda *et al.*[185] The NDI molecules served as intercalators by forming a stable complex with DNA molecules, which allowed the DNA molecule to be electrostatically stretched and exhibited linear current–voltage characteristics with applicability in electronic devices. The significance of charge transfer effects in DNA devices based on NDI linked hairpins have recently been investigated by some research groups. One such interesting study is by Grozema and co-workers.[217] In this study they designed NDI capped hairpins to modify the energetics of charge injection and obtained a new 'deep-hole transfer' mechanism involving long-range hole migration *via* low energy states of the nucleobases (Fig. 68).

Subsequently, Burtman and co-workers [218] also demonstrated that in DNA nanoelectronic devices with NDI based molecules (**307**), the charge transport through the π-stacks of the NDI based system exhibited switching behaviour owing to the changes in its redox state and hence could partially explain the discrepancies across different charge transport models. In some studies, NDI based derivatives have found utility in thermoelectrics, dyads and microbial fuel cells, though such studies are at the very initial stages. For instance, to design a high-performance n-type thermoelectric (TE) device, Wang and co-workers [219] synthesized composites consisting of single walled carbon nanotubes (SWCNTs) and amino-substituted NDI (NDINE) (**308**). The n-type composite exhibited good performance with a power factor of 135 ± 14 μW m^{-1} K^{-2} and excellent air stability.

Liu *et al.*[220] synthesised binary composites of NDI-based polymer (PNDI2OD-T2) (**322**) and SWCNTs, both doped with the 1*H*-benzimidazole derivative (N-DMBI) to tune the thermoelectric (TE) properties of solution-processed semiconductors.

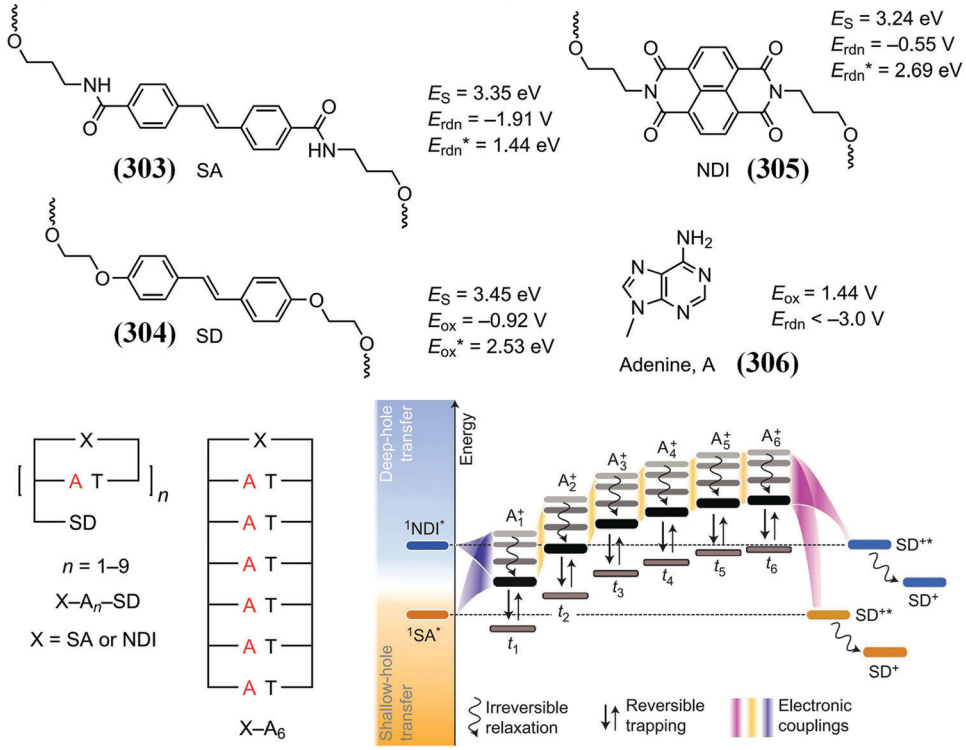

Fig. 68 Structures and energetics of stilbenedicarboxamide (SA) (**303**) and stilbenediether (SD) (**304**) molecular fragments usually used as hole donor and acceptor to probe charge transfer along DNA hairpins, which were replaced with NDI (**305**) to understand how the energetics of charge injection affect charge transfer. Representation of NDI- and SA-linked poly-A poly-T hairpins and capped hairpins with an SD capping group used to probe charge transfer in this study. The high-energy states represent lower-lying orbitals of the adenines (**306**) as we study hole transfer. Relaxation among those states progressively drives the hole to the lowest energy state, that is, the HOMO of each molecule, where trapping can occur.[217] This figure has been adapted from ref. 217 with permission from Springer Nature, copyright 2016.

They reported a power factor of 18.1 μW m^{-1} K^{-2} for an SWCNT loading of 45.5 wt%.

Kemerink and co-workers[221] designed [6,6]-phenyl-C61-butyric acid methyl ester (PCBM) and used the inverse-sequential doping method over the pre-casted dopant 4-(1,3-dimethyl-2,3-dihydro-1*H*-benzoimidazol-2-yl)-*N*,*N*-diphenyl-aniline film which resulted in a very high power factor (PF) ≈ 35 μW m^{-1} K^{-2} as well as remarkable conductivity. Upon the addition of a small fraction of core-cyanated NDI (**309**) into PCBM, a greater Seebeck coefficient was obtained, and the molecular structures are shown in Fig. 69.[218,219,221]

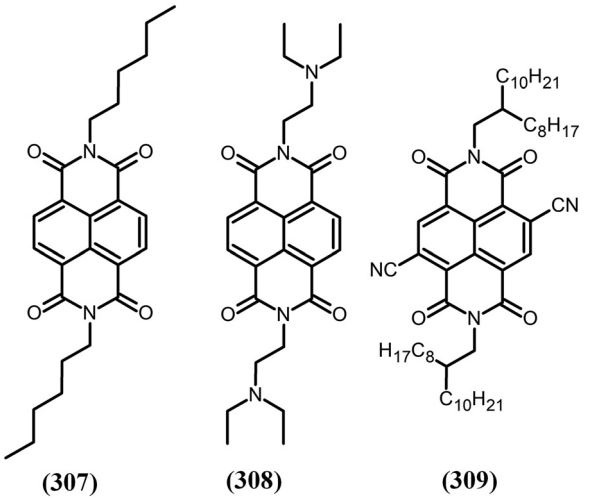

Fig. 69 Molecular structure of NDI derivatives used in thermoelectric composites: (**307**),[218] (**308**),[219] and (**309**).[221]

The use of NDI derivatives as dyads has also been reported. For example, the effect of increasing the degree of thionation of a series of NDI dyad systems (**310**, **311**) in comparison to pristine NDI systems was investigated by Champness *et al.* (Fig. 70).[222] They observed that thionation increases the electron affinity of the NDI acceptor dyad as well as accessibility of the reduced states, along with a decrease in the lifetime of the excited state.

Lambert and co-workers[223] designed a molecular dyad consisting of a triarylamine and an NDI acceptor bridged together (Fig. 71) by meta-conjugated diethynylbenzene (**312**, **313**). This bridge can be tuned with electron donating (OMe, Me) or electron withdrawing (Cl, CN) substituents. They concluded from this study that the kinetics of charge separation/recombination in this dyad were influenced by the functional groups in the bridge substituents. However, more research is needed to confirm the superiority and applicability of NDI based derivatives for dyad technology. Utilization of NDI derivatives in fuel cells has recently been reported by some research groups.

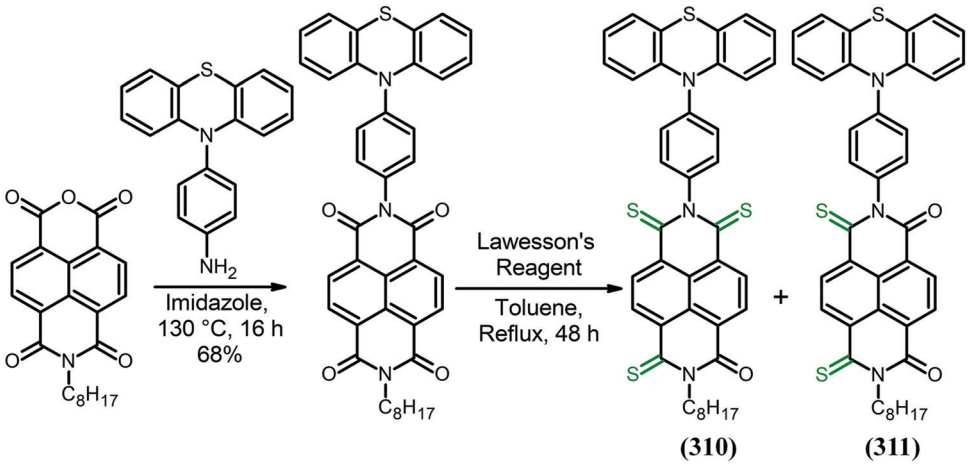

Fig. 70 Synthesis of thionated phenothiazine donor–acceptor NDI based molecules (**310**, **311**).[222]

Banerjee and co-workers[224] synthesized a series of fluorenyl and trifluoromethyl groups containing co-poly(ether imide)s (**314**) which were subsequently used to make NDI based polymers. Compound (**314**) exhibited high thermal and mechanical stability along with appreciable proton conductivity. One of the copolymers (DAN-80; IECw $\sim$2.27 meq g^{-1}) exhibited a proton conductivity of 149 mS cm^{-1}. Microbial fuel cell (MFC) tests were evaluated with DAN-80 wherein these novel polymers exhibited excellent performance on par with Nafion-117. The same group further extended their work by synthesizing trifluoromethyl and benzyl ether side groups containing the new sulfonated co-poly(ether imide) (**315**).[225] The membranes prepared from these NDI based copolymers exhibited high thermal, mechanical and hydrolytic stability. Composites of these polymers with cerium oxide resulted in enhanced peroxide stability and high proton conductivity of $\sim$244 mS cm^{-1}. The microbial fuel cell performance of these polymer composite members was also appreciable with a power density $\sim$576 mW m^{-1} which is comparable to that of Nafion® 117.

Xu and co-workers[226] used a 4,4-bibromomethenyl diphenylether cross-linker to synthesis several cross-linked sulfonated NDI based poly(imidebenzimidazole)s (**316**). The cross linking in fact reduced the conductivity as a result of blockage of the hydrophilic channel. Subsequently, the alkaline imidazole ring at the cross-linking center and a basic site to absorb phosphoric acid (PA) molecules were utilized. This resulted in a remarkable increase in the proton conductivity due to the doping of (**316**) with PA even higher than Nafion based membranes (Fig. 71). These membranes demonstrated excellent mechanical and chemical stability with a high tensile strength ranging from 47.2 to 55.5 MPa and remarkable water stability for device scale applications in a proton exchange fuel cell.

7.2 NDI based organic field effect/thin film transistors

A field effect transistor is a triad which controls the flow of current by the application of an electric field. It consists of a source, a drain and a gate. By applying a suitable voltage to the gate, the current flowing through the source to the drain can be controlled in order to act as either an amplifier or a switch. The most popular among all are the metal oxide semiconductor field effect transistors (MOSFETs). However, the use of expensive metal oxides and high input impedance due to limited charge carrier mobility have limited the applicability of MOSFETs. In recent times, organic field effect transistors (OFETs) and organic thin film transistors (OTFTS) have been considered promising in electronic devices because of their low energy consumption, large active area, flexibility and cost effectiveness. Over the years, several p-type and n-type organic field effect transistor materials have been developed. The n-type organic semiconductors made of pyromellitic diimides, anthracene diimides, PDIs and NDIs in particular have been found to exhibit significant advantages due to the rigid planar structure and delocalized π-electron mobility which is extremely important for electronic applications.[1,4b] However, these materials suffer from reduced stability and lifetime under ambient conditions due to electron scavenging by O_2.[227] Therefore, a great deal of research effort has been directed toward improving the charge carrier mobilities, solubility and stability of NDI based thin films for OFETs. Several synthetic strategies such as functionalization of NDI molecules with thiophene and halogens such as fluorine based organic molecules and their polymeric derivatives have been employed to lower the LUMO level and enhance the electron injection across the organic and electrode layer interface. Alkyl side chain engineering at the N-atom of NDI in particular (either linear or branched) and also the number of carbon atoms have been found to influence the thin film microstructure and in-plane anisotropy, both of which significantly influence the electron mobility as well as film stability. This section summarizes some of the important studies reported so far on NDI based OFETS, and some important examples are illustrated in Fig. 72 and 73.

NDI–thiophene based OFETS in their early development stages showed encouraging performance for device scale application. For instance, Hu and co-workers[228] successfully synthesized two isomeric azulene functionalized naphthodithiophene diimide (NDTI) triads (**317**, **318**), by connecting azulene units

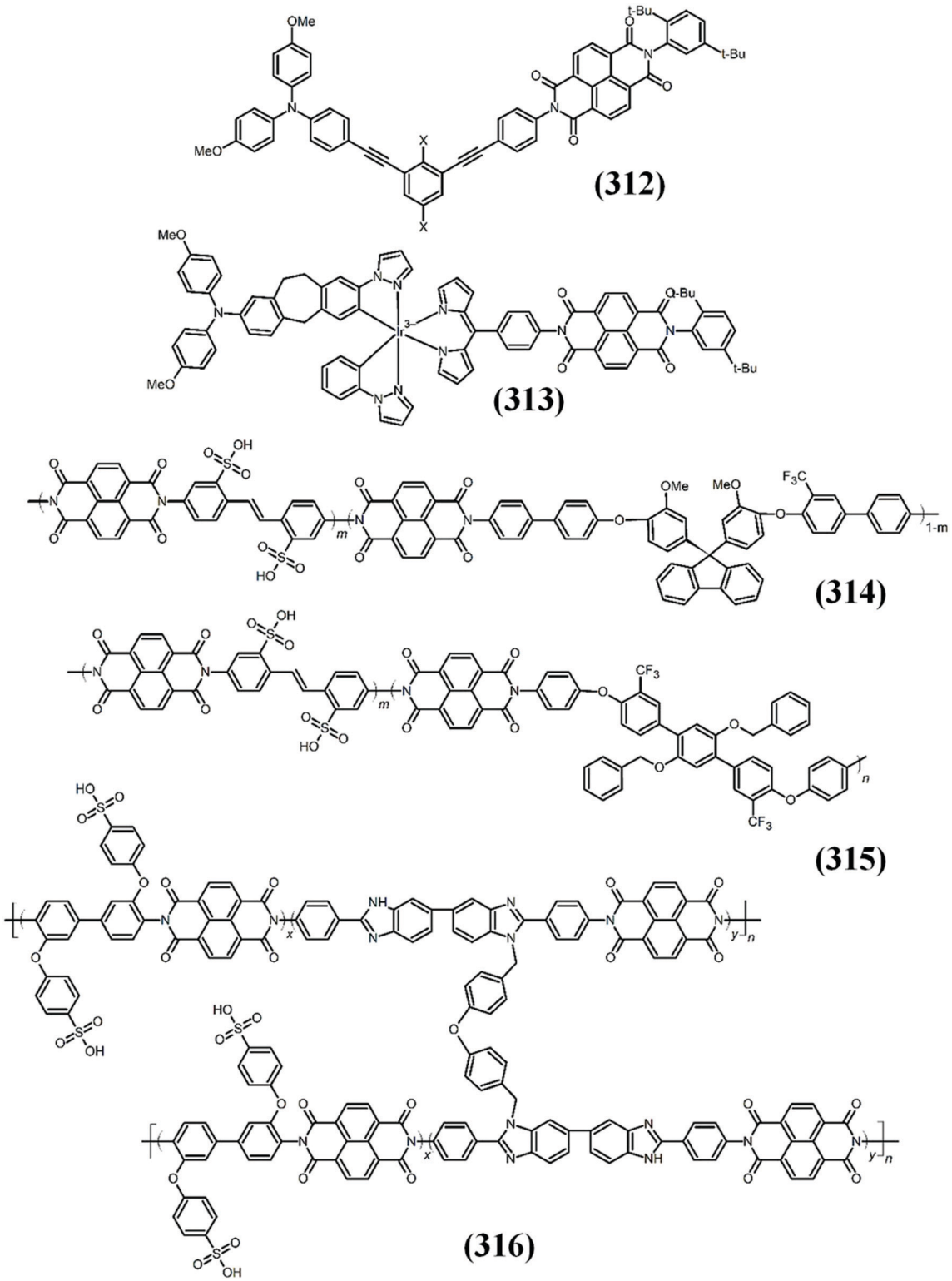

Fig. 71 Molecular structures of NDI derivatives and polymers used in microbial fuel cells: (**312**, **313**),[223] (**314**),[224] (**315**),[225] and (**316**).[226]

with NDTI at the 2- and 6-positions, respectively. The fabricated (**317**) bottom gate transistor exhibited ambipolar behavior with a high electron mobility of 0.32 $cm^2 V^{-1} s^{-1}$ and a hole mobility of 0.03 $cm^2 V^{-1} s^{-1}$. The unipolar characteristics in (**318**) had almost halved mobility values compared to (**317**) suggesting that the delocalization of HOMO and LUMO could be used in controlling polarity change in organic FETs. Kim and co-workers[229] reported the synthesis of a novel NDI-based molecule functionalized with a bithiophene linker unit (**319**) and demonstrated its utility in solution-processable n-channel

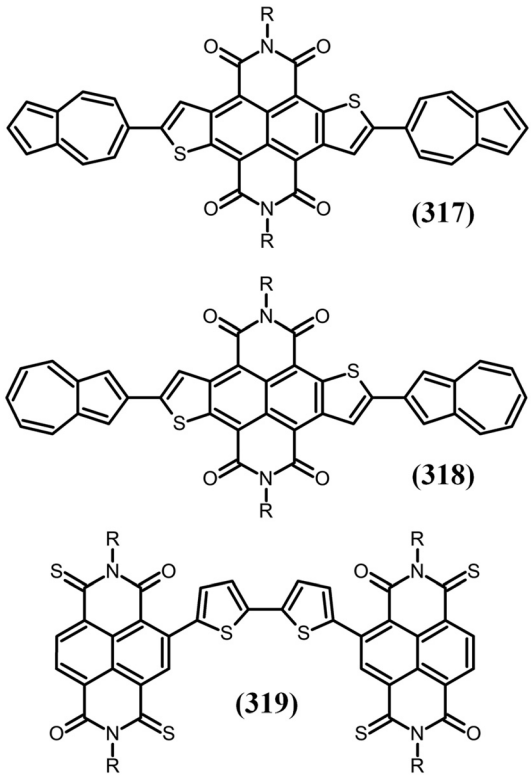

Fig. 72 NDI based small molecules for use in organic field-effect transistors; (**317**, **318**) isomeric azulene decorated NDI-based triads, in which two azulene units were connected with NDI at the 2-position of the azulene ring (**317**), whereas two azulene units were incorporated with NDI at the 6-position of the azulene ring in (**318**),[228] and NDI dimer with a bithiophene linker.[229]

OFETs. As a result of improved crystallinity, solubility, and π–π stacking, a high field-effect mobility of up to 0.016 $cm^2 V^{-1} s^{-1}$ was recorded in good agreement with previous studies on thiophene linked NDI derivatives. Since the handling of chlorine based solvents is a tedious task, especially in fabricating OTFTs, Ichikawa and co-workers[230] introduced a new wet-process for designing several NDI derivatives with alkyl chain substituents of varying lengths (NDI-C_n). The OTFT devices of NDI-C_n demonstrated a high electron mobility of 0.38 $cm^2 V^{-1} s^{-1}$ using 50 nm thick films.

Sommer and co-workers[231] carried out thionation of the n-type conjugated polymer PNDIT2 (**322**) using Lawesson's reagent (LR). They utilized NMR analysis and proved that steric hindrance of carbonyl groups in NDI is reduced due to the polymer backbone, resulting in regioselective thionation in the trans-configuration (**328**). The main limitation with PNDIT2 (**322**) is the miscibility issue with other polymers for fabricating films. To overcome this problem, the same research group[232] added the *meta* substituted monomer 1,3-bis(2-thienyl)benzene (TPT) (''kinked monomer'') into the PNDIT2 backbone. This improved the crystallinity and miscibility of P(NDI-*alt*-[T2-*co*-TPT]) (**333**) with a partial loss in conductivity. Hence, there exists plenty of scope to further improve the molecular design to achieve better electronic performance.

Antognazza and Caironi *et al.*[233] designed the first ever n-type water gated OFET using organic semiconductor NDI copolymers, namely (**322**) and (**332**), and a soluble fullerene derivative such as [6,6]-phenyl-C61-butyric acid methylester (PCBM). They found that PCBM exhibited a high electric double layer capacitance of 1 μF cm^{-2} and a mobility–capacitance of 7×10^{-3} μF $V^{-1} s^{-1}$. This material exhibited good cycling stability even in an aqueous environment. Kim and co-workers[234] developed NDI-based regioregular D–A_1–D–A_2 copolymers with varying side chains (**334–337**). As a result of this side chain engineering and lowering of the LUMO level, molecular packing order was improved and a high electron mobility of 1.05 $cm^2 V^{-1} s^{-1}$ in the case of poly(NDI-thieno[3,4-*c*]pyrrole-4,6(5*H*)-dione)-2-hexyldecyl (PNT-HD) (**337**) based thin-film transistors was observed. These molecules also exhibited appreciable performance in solar cells. Facchetti and co-workers[235] synthesized NDI based chlorinated polymers such as poly(*N,N*′-dialkyl-NDI–3,3′-dichloro-2,2′-bithiophene) (**338**). An appreciable electron mobility of 0.1 $cm^2 V^{-1} s^{-1}$ and low ambipolarity were recorded when these NDI derivates were used in thin-film transistors (OTFTs) with high stability even under high-humidity conditions (RH ∼ 60%) and upon submersion in water. Moreover, when these chlorinated NDI polymers were used as OTFTs, they exhibited excellent operational stability of >97% in a bias-stress test. Subsequently, conjugated NDI based polymers with (methylselenophen-2-yl)vinyl)selenophen (**332**) were compared to P(NDI-T2) (**322**) and P(NDI-3,3-dichloro-2,2′-bithiophene) (**338**), respectively, by Noh and co-workers.[236] These polymers, when tested in solid-state electrolyte-gated transistors, exhibited electron mobilities in the range of 10^{-2}–10^{-3} $cm^2 V^{-1} s^{-1}$ with a very low operating voltage (2 V). P(NDI–SVS) in particular displayed an excellent hole mobility of 0.14 ± 0.02 $cm^2 V^{-1} s^{-1}$ as a result of large hole accumulation due to the delocalized HOMO. Wang and co-workers[237] went a step ahead to innovatively synthesize novel platinum(II)–NDI based (**339**) copolymers which *via* a donor–acceptor (D–A) mechanism could serve as potential metallo-organic materials for OFETs. The two synthesized metallopolyyne polymers (P1 and P2) exhibited unipolar p-type transport with a mobility of 2.89×10^{-4} $cm^2 V^{-1} s^{-1}$. This study concluded that the number of thiophene molecules in the metallopolymer has a significant effect on improving film stability, solubility and charge mobility. Trapping of charge carriers has been a common challenge in the operational stability of n-channel OFETs. Jenekhe and co-workers[238] synthesized poly(NDI-*alt*-biselenophene) (**324**) and exploited its properties for non-volatile, high performance electronic memory storage devices. The (**324**)-based field-effect transistor memory devices exhibited excellent charge-trapping and de-trapping characteristics, with a remarkable cycling stability at a high current ratio of 10^3. It is worth mentioning here that NDI and bithiophene or dithienylethene (TVT) based copolymers (**330**) suffer from poor electron transport mainly due to the lack of electrical connections across the crystal domains. Park and co-workers[239] demonstrated that an interconnected network of small domains and short-range ordering achieved

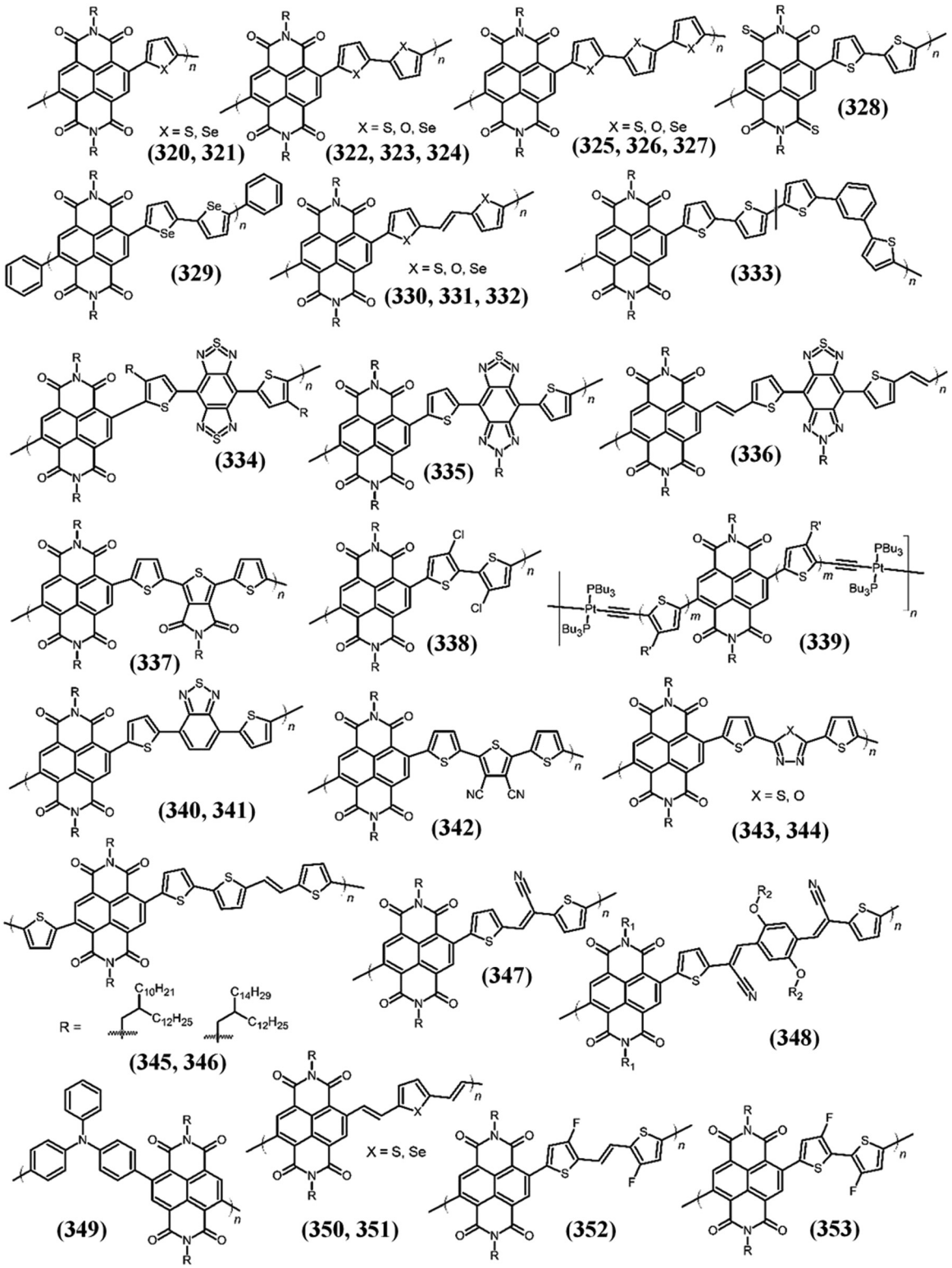

Fig. 73 The molecular structure of NDI–thiophene and selenophene based polymers used in organic field effect/thin film transistors.[53,231–235,237–240]

using fluorinated TVT (FTVT) units (**352**) can augment the intermolecular interactions across the polymer chains. This enhances the electronic conductivity and thermal stability of the material for device scale applications (Fig. 73).

McNeill *et al.* also studied the effect of increasing the number of sulfur groups on the NDI moiety (**354–359**) and the resulting OFET performance (Fig. 74).[241] They observed that S2-*cis* NDI (**355**) structures exhibited the highest mobility of

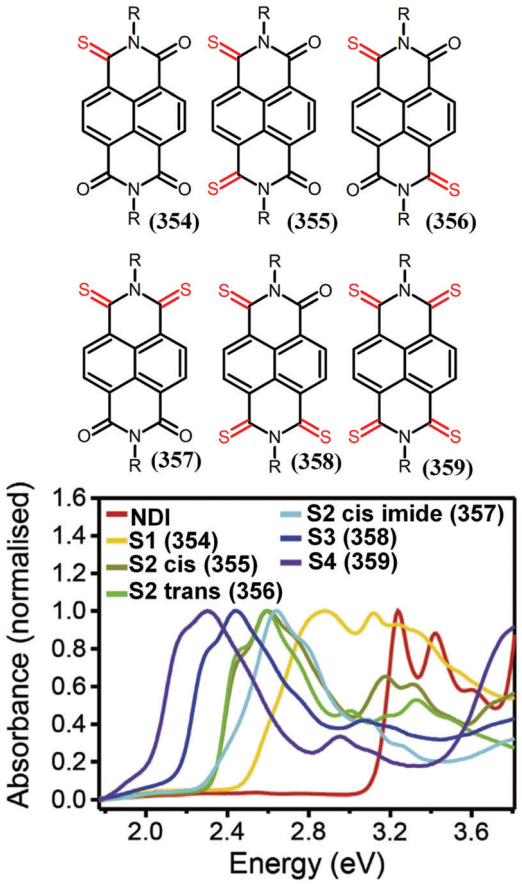

Fig. 74 Molecular structures of the full series of thionated NDI molecules (**354–359**), and the UV-Vis absorption spectra of the parent and 6 thionated molecules in solution.[241] This figure has been adapted from ref. 241 with permission from Elsevier, copyright 2018.

0.20 $cm^2\ V^{-1}\ s^{-1}$ compared to the rest of the synthesized molecules.

Alternatively, fluoroalkyl derivatives of NDI based systems have started to gain interest in the recent years due to their electron withdrawing ability, which lowers the LUMO energy levels of the NDI-based polymers. One such study by Li and co-workers[242] reported the synthesis of NDIs modified with *p*-fluorophenyl (NDI-FAN), *p*-chlorophenyl (NDI-ClAN), and *p*-fluorobenzyl (NDI-FBN), which demonstrated appreciable electron mobilities when tested as field effect transistors (OFETs). All materials displayed a high decomposition temperature and a low LUMO energy level facilitating air stable electron transport (Fig. 75). These synthesized molecules with *N*-octadecylphosphonic acid (ODPA) treated SiO_2/Si substrates exhibited electron mobilities of up to $1.8 \times 10^{-1}\ cm^2\ V^{-1}\ s^{-1}$. These results suggest that fluorinated *N*-substituents in organic OFETs could boost device performance considerably.

Bromo-NDIs were subjected to exchange reactions with fluorine to produce several novel difluoro- and tetrafluoro core substituted NDIs (**363–366**) by Müllen and co-workers (Fig. 76).[243] The OFETs fabricated with the fluoroderivatives exhibited n-channel field-effect with an improved mobility of $0.1\ cm^2\ V^{-1}\ s^{-1}$. The improved performance was attributed to a decrease in LUMO energy with an increasing degree of fluorination. Several partially fluorinated and hydroxy terminated NDI *N*,*N*′-derivatives (**367**) were synthesized by Katz and co-workers,[244] with high electron mobilities of $>0.01\ cm^2\ V^{-1}\ s^{-1}$ and $>0.001\ cm^2\ V^{-1}\ s^{-1}$, respectively. Jin and co-workers[51] synthesized NDI based π-conjugated polymers, namely the (**368**) series, by changing the number of fluorine atoms in the structure. It was concluded that, with the increase in the number of fluorine atoms, the charge transport properties were reduced. With the positive impact of the fluoro-alkyl derivatives of NDIs for OFETs, subsequent research development in fluoro-thiophene based NDI-OFETS has become increasingly popular. Meng and co-workers[245] synthesized *N*,*N*′-bis(4-trifluoromethylthiobenzyl)-NDI (**369**) and compared

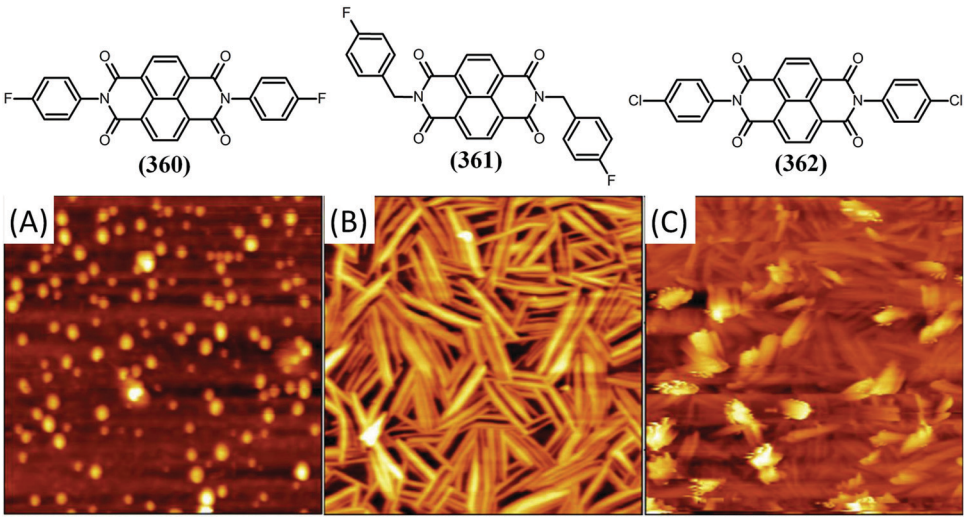

Fig. 75 The chemical structure of NDI derivatives containing halogen elements: NDI-FAN (**360**), NDI-FBN (**361**) and NDI-ClAN (**362**); and the AFM images (5 × 5 μm) of NDI-FAN (A), NDI-FBN (B) and NDI-ClAN (C) thin films on an ODPA/SiO_2 substrate at room temperature.[242] This figure has been adapted from ref. 242 with permission from Elsevier, copyright 2018.

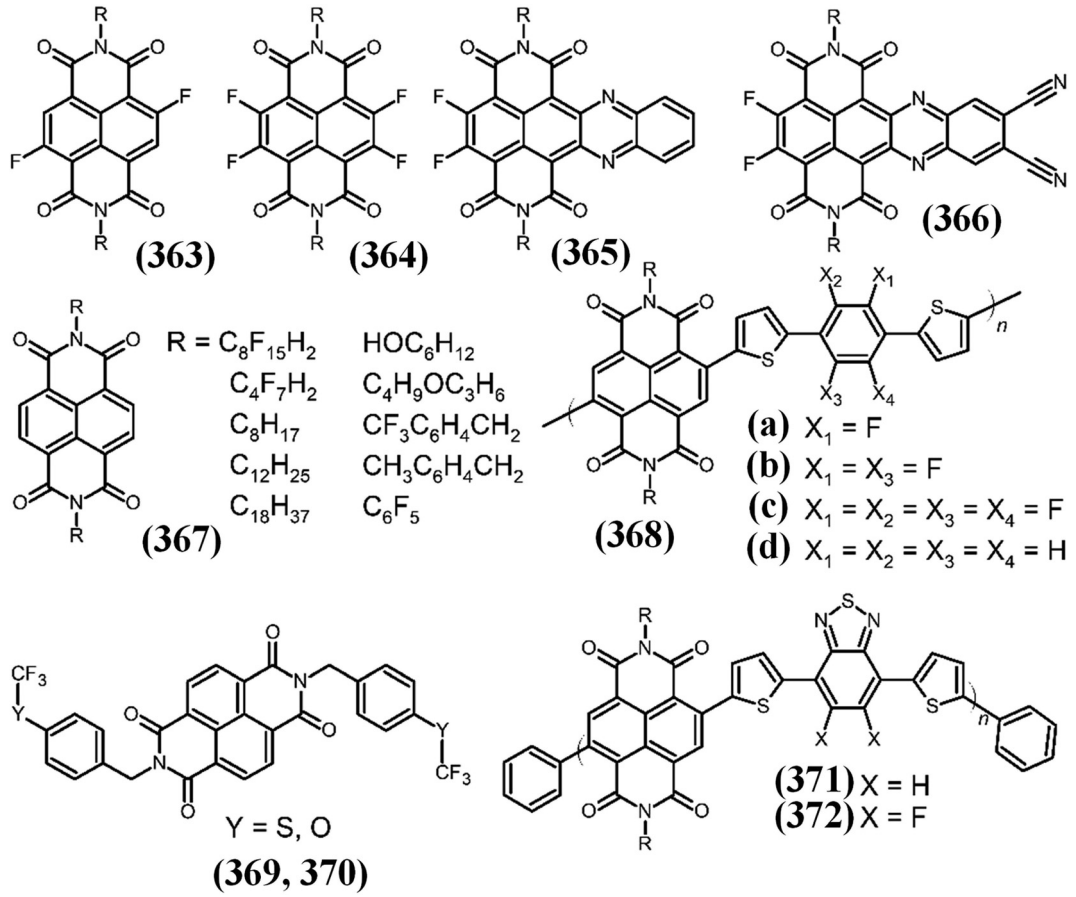

Fig. 76 The molecular structures of fluoro-NDI derivatives used in organic field effect/thin film transistors.[51,53,239,240b,l,v,243–247]

its structure and OFET performance with a similar compound, *N,N′*-bis(4-trifluoromethoxybenzyl)-NDI (**370**). Although the above two compounds displayed similar packing structures, the former had enhanced environmental stability but a lower electron mobility of 0.17 $cm^2\ V^{-1}\ s^{-1}$ compared to (**370**). The greater stability was attributed to the attachment of the trifluoromethanesulfenyl (SCF_3) group to the NDI, while the lower mobility is a result of a lack of crystallinity and thin film inhomogeneity. Baumgarten and co-workers[246] synthesized two conjugated copolymers consisting of an NDI and benzothiadiazole (BT) or an NDI and difluorinated BT (FBT) coded as (**371**) and (**372**), respectively. OFETs fabricated using (**372**) exhibited superior performance with an almost 5 times higher electron mobility of 0.258 $cm^2\ V^{-1}\ s^{-1}$ and a lower hole migration of 2.4×10^{-3} $cm^2\ V^{-1}\ s^{-1}$ compared to (**371**) which was attributed to the lower lying HOMO in (**372**) compared to (**371**).

Core expanded NDI based molecules have also shown potential as organic semiconductors, especially for n-type conduction. Interestingly, very few studies have been reported on core extended NDIs for p-type semiconductor applications. One such noteworthy study is by Würthner *et al.*[248] where they synthesized a novel NDI with laterally fused, highly electron-rich carbazole rings (**373**) which extend not only conjugation but the π-core as well (Fig. 77). Ambipolar transport characteristics with a large hole mobility of 0.56 $cm^2\ V^{-1}\ s^{-1}$ in bottom-gate transistors were observed, which was attributed

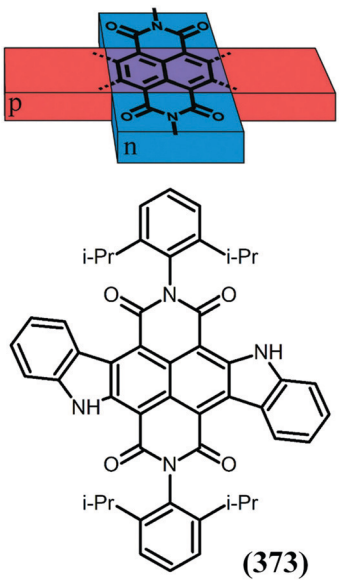

Fig. 77 Schematic representation of the concept of π-conjugated systems with direction-dependent p- or n-type semiconducting characteristics, and the molecular structure of the laterally core-expanded NDI (**373**).[248]

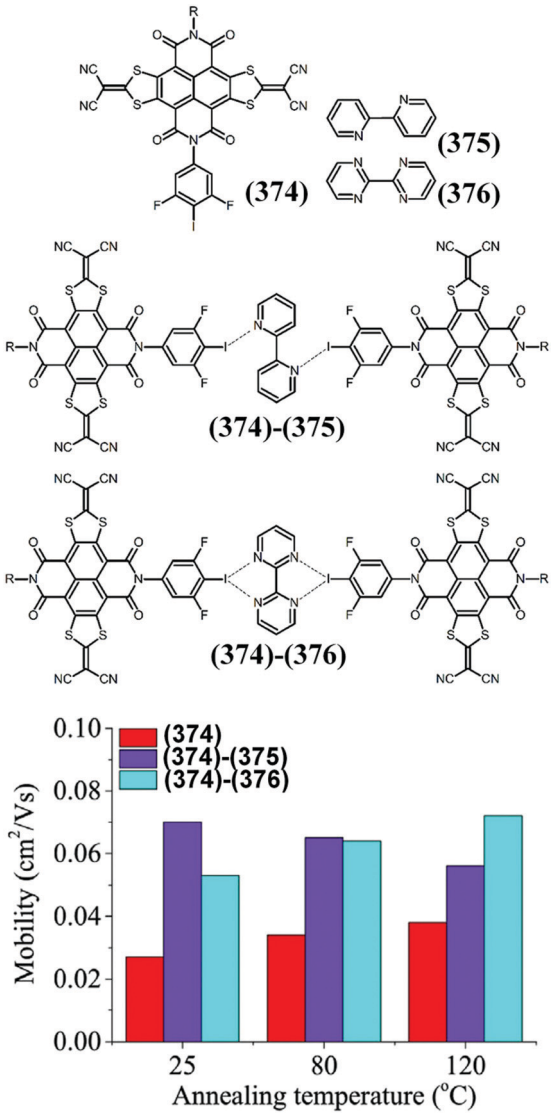

Fig. 78 Molecular structures of compounds (**374**), 2,2-dipyridine (**375**), 2,2-bipyrimidine (**376**), and two XB complexes (**374**)/(**375**) and (**374**)/(**375**).[249] This figure has been adapted from ref. 249 with permission from Elsevier, copyright 2018.

to intermolecular HOMO overlap by stacking of the extended π-core.

A supramolecular assembly of a core expanded NDI derivative (1) and a halogen bonded (XB) donor that could form extended structures with 2,2-dipyridine (**375**) and 2,2-bipyrimidine (**376**) was designed, synthesized and characterized using TGA, XPS, ^{19}F NMR and solid-state ^{13}C NMR techniques by Gao and co-workers (Fig. 78).[249] The XB complexes of (**374**)/(**375**) and (**374**)/(**376**) both exhibited an increased electron mobility of 0.027 $cm^2\ V^{-1}\ s^{-1}$ which is almost double that of the other NDI derivative (**374**).

A different approach to address the mobility issues of NDI based OFETs was adopted by Choi and Noha *et al.*[250] They investigated the effect of linear and branched polyethyleneimine (PEI) doping on poly[[*N*,*N*′-bis(2-octyldodecyl)-NDI-2,6-diyl]-*alt*-5,5′-(2,2′-bithiophene)] (**322**). Doping of PEI (0.1 wt%)

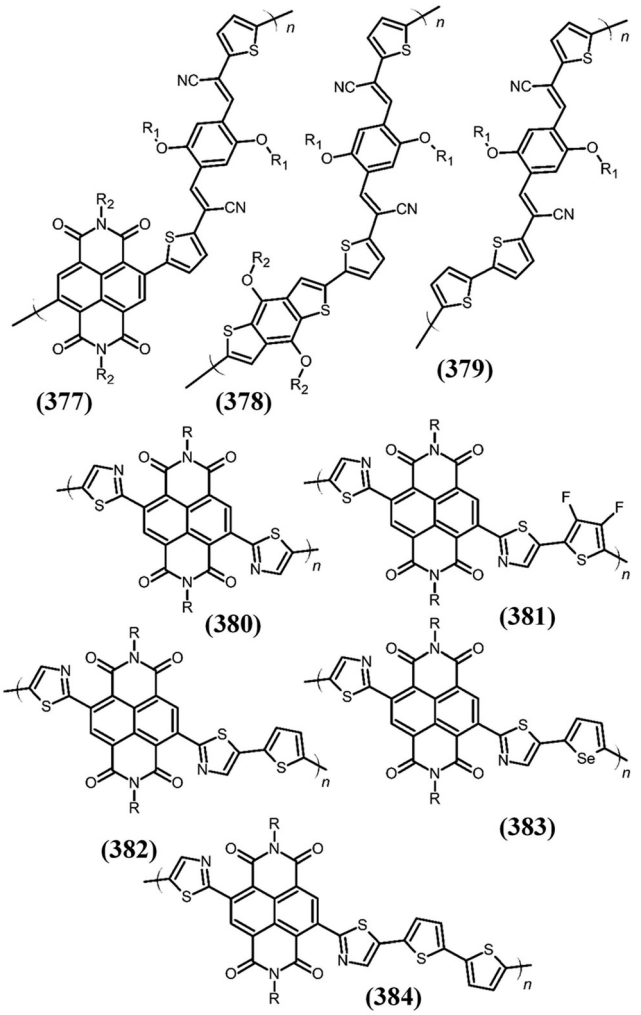

Fig. 79 Chemical structures of NDI-dicyanodistyrylbenzene (DCS)[251] and NDI–thiazole[252] copolymers.

in (**322**) OFETs exhibited an enhanced mobility of around 0.85 $cm^2\ V^{-1}\ s^{-1}$ and greater operational stability compared to the pristine material. Woo and co-workers[251] reported the synthesis of three dicyanodistyrylbenzene (DCS) copolymers (**377–379**). As a result of lowering of the LUMO energy level in (**377**) and dipole–dipole interaction induced crystalline ordering in the molecule, the hole/electron mobilities of the OFETs were improved, *i.e.* 0.064/0.014, 0.492/0.181, and 0.420/0.447 $cm^2\ V^{-1}\ s^{-1}$ in the case of (**378**), (**379**), and (**377**), respectively (Fig. 79).

Thiazole based NDI (TzNDI) conjugated polymers (**380–384**) were synthesized by Huang and co-workers.[252] As a result of lowering of the LUMO, these polymers exhibited n-type transport characteristics with the highest electron mobility (μ_e) of 0.57 $cm^2\ V^{-1}\ s^{-1}$ in the case of (**381**). Reichmanis and co-workers[252b] synthesized conjugated monomers and polymers (**380**) by linking 2,2′-bithiazole (BTz) to NDI units *via* a palladium-catalyzed Stille polycondensation reaction. The synthesized materials, especially (**380**), exhibited broad absorption at 540 nm and had a band gap of 1.8 eV. When

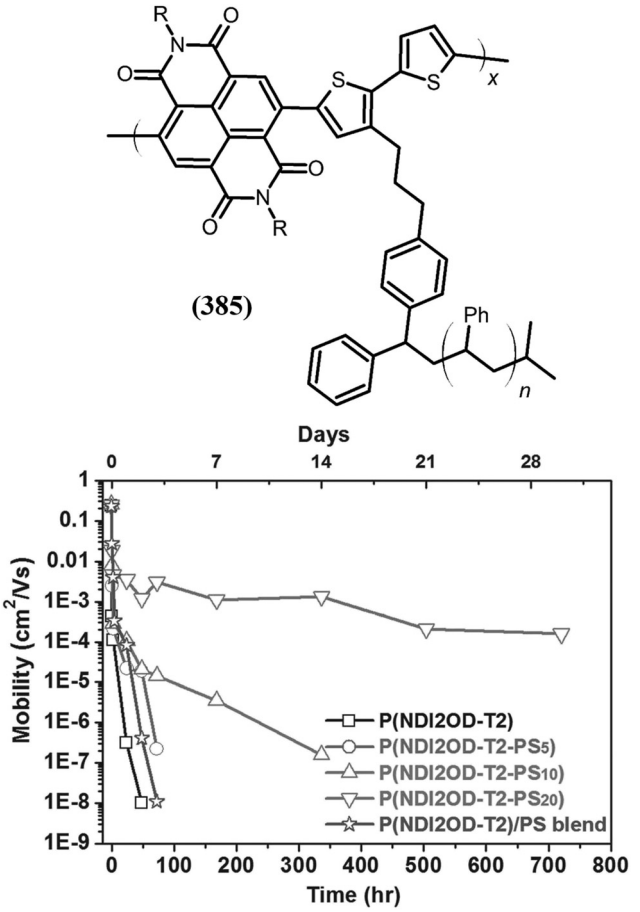

Fig. 80 Chemical structure of P(NDI2OD-T2-PS_x) (**385**) prepared *via* Stille coupling polymerization; the stability tests of the FET devices were performed under ambient conditions. The initial point is plotted based on the result obtained in a glove box after annealing the device at 170 °C. The star-symbol plot denotes the device based on the blending film of P(NDI2OD-T2) and pristine PS.[253] This figure has been adapted from ref. 253 with permission from John Wiley and Sons, copyright 2016.

used as OFETs, these polymers exhibited unipolar characteristics (n-type) with a mobility of 0.05 $cm^2\ V^{-1}\ s^{-1}$ (Fig. 79).

NDI-polystyrene (PS) conjugated polymers (**385**) of several weight percentages were synthesized by Bao and co-workers [253] *via* chain termination of living anionic polymerization reactions. A high electron mobility of $\approx$0.2 $cm^2\ V^{-1}\ s^{-1}$ was measured when these conjugated polymers were used as OFETs. The improved stability and high mobility were attributed to PS encapsulation of the polymer skeleton which prevented scavenging of electrons by O_2 and H_2O (Fig. 80).

Alkyl side chain engineering of NDI based monomers and conjugate polymers has been of interest for OFET applications. In one such noteworthy study, an n-type, core-expanded NDI fused with 2-(1,3-dithiol-2-ylidene)malononitrile groups (**386**) was reported for the first time by Zhu and co-workers.[254] These novel molecules with branched *N*-alkyl chains, when used as n-channel OFETs, exhibited a high electron motility of 0.51 $cm^2\ V^{-1}\ s^{-1}$ under ambient conditions. Furthermore, this group extended this study to several more (**386**) analogues and studied the effect of branched chain length and position of the substituent groups on the OFET performance.[255] They utilized synchrotron measurements and device optimization analysis and concluded that the molecular structure, molecular packing, and OTFT mobility are interrelated, and this is mildly influenced by chain length but greatly affected by the position of the substituent group. More critically, the packing structure is influenced by side chain position which increases the electron mobility from $\sim$0.001 to $>$3.0 $cm^2\ V^{-1}\ s^{-1}$. Exceptionally high electron mobilities of up to 3.50 $cm^2\ V^{-1}\ s^{-1}$ have been obtained by integrating the (**386**) core and three branched *N*-alkyl substituents at C11- and 6-positions with improved density and packing structure (Fig. 81).

Similar studies investigating the effect of long alkyl substitution at the *N* and *N*′ positions of NDI on the performance of thin-film transistors (TFTs) were carried out by Ichikawa *et al.*[256] Increased electron mobilities from octyl (NDI-C8) to pentadecyl (NDI-C15) (**387**) analogues were measured in agreement with earlier studies. Subsequently, the effect of linear side chains with increasing number of carbons from four (C4) to twelve (C12) (**388–393**) on NDI based OFET thin films were studied by McNeill and co-workers (Fig. 82).[257] They found that longer side chain lengths produce larger domain sizes of better film quality and a greater number of edge-on orientations of NDI, while shorter side chains resulted in tilted orientations of NDI with changes in lateral stacking which increases the electron mobility to $\sim$0.2 $cm^2\ V^{-1}\ s^{-1}$. Thus, by altering side chain lengths the microstructure of the material and OFET performance can be modulated. Bradley, Kim and co-workers[258] employed Sonogashira coupling polymerization reaction to produce various NDI analogues (**394–396**) bearing the *N*-octyldodecyl (OD) at diimide position and 2,5-positions hexadecyloxy (HO) chain attached 1,4-diethynylbenzene, P(NDIOD-HO) at the core of NDI, respectively. This triple bond conjugate polymer, when used in OFETs, gave the highest electron mobility of 0.016 $cm^2\ V^{-1}\ s^{-1}$ (Fig. 82). This performance is far greater than other ethylhexyl chain polymers and is attributed to the highly ordered nano-fiber-like surface structure with preferred edge-on orientation, which facilitated efficient in-plane charge transport.

McNeill[261] studied the effect of solvent on the microstructure and OFET performance of an NDI–thiophene-based copolymer (**322**) with 2-octyldodecyl *N*-substitutions and concluded that the electron mobility increases from 0.21 $cm^2\ V^{-1}\ s^{-1}$ to 0.56 $cm^2\ V^{-1}\ s^{-1}$ as the solvent quality reduces. The highest electron mobility of 1.5 $cm^2\ V^{-1}\ s^{-1}$ was recorded for toluene processed transistors which was attributed to the magnitude of the solution aggregation of (**322**) polymer chains. The effect of side chain engineering in NDI based copolymers was further investigated by Liu and Zhang *et al.*[240h] They synthesized (**322**) with different *N* and *N*′-alkyl substitutions to construct a polymer having an NDI–bithiophene skeleton and branching/linear chain *N* and *N*′- substitutions. This flexible OFET polymer exhibited an electron mobility of 1.52 $cm^2\ V^{-1}\ s^{-1}$ which was greater than other branched chain copolymers.

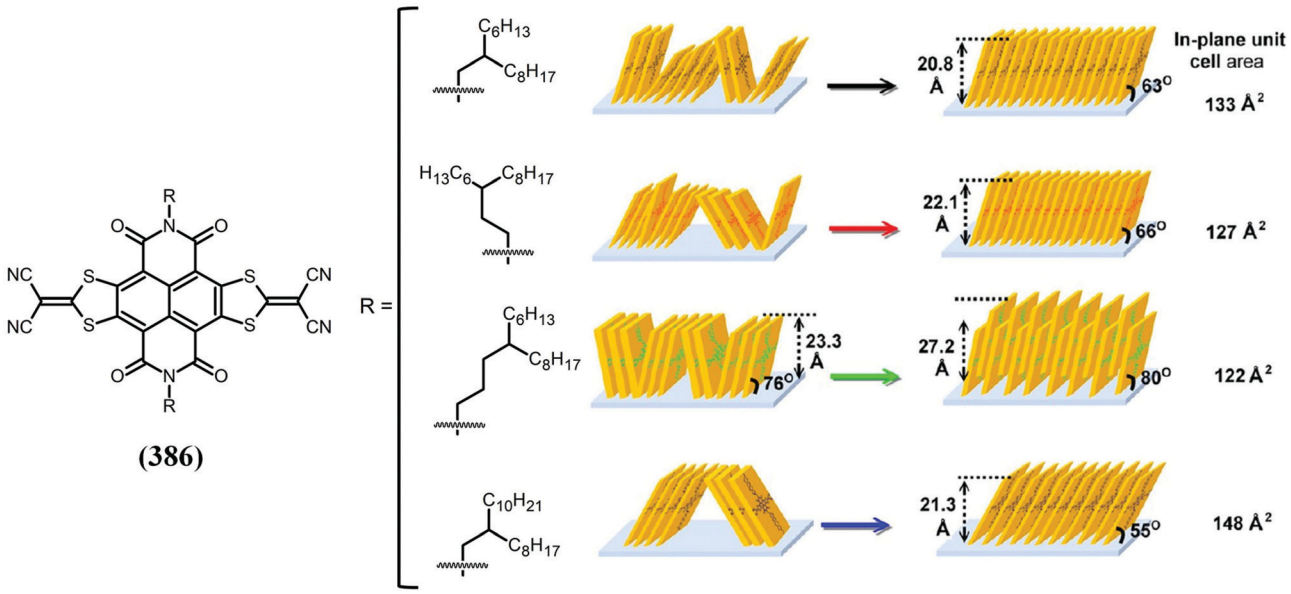

Fig. 81 The structure of NDI (**386**) fused with 2-(1,3-dithiol-2-ylidene)malononitrile groups bearing various branched *N*-alkyl substituents derivative and their self-assembled arrangement in thin films before and after thermal treatment.[255] Reprinted from ref. 255. This figure has been adapted from ref. 255 with permission from The American Chemical Society, copyright 2013.

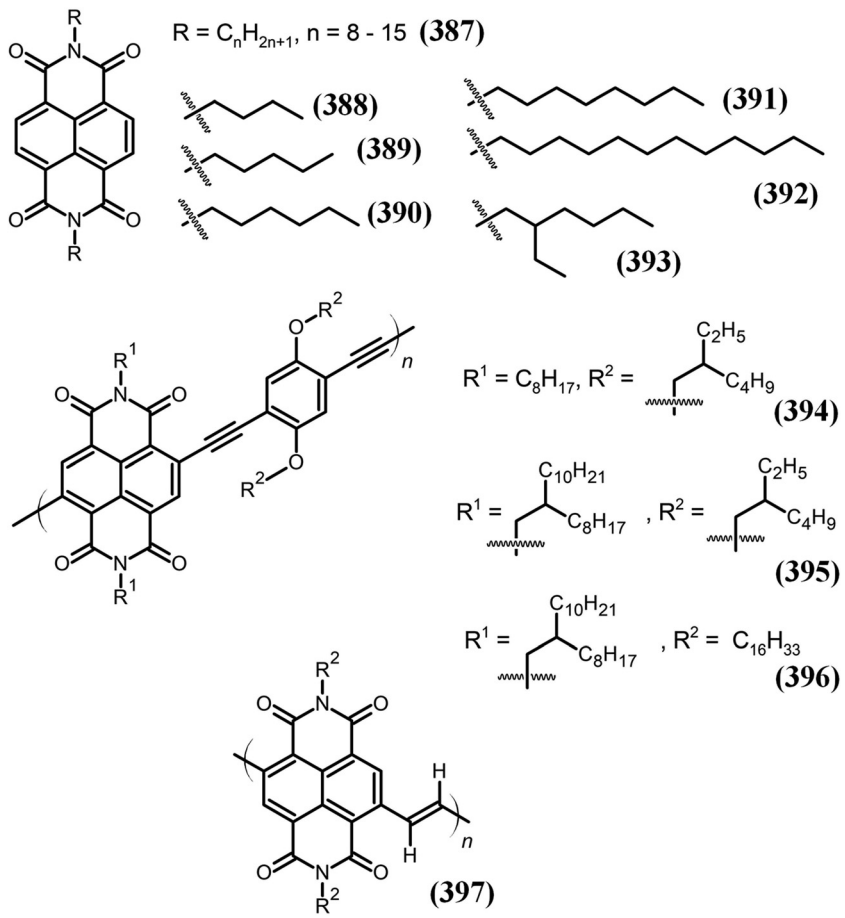

Fig. 82 Chemical structures of NDIs with *N*,*N*′ long normal alkyl chain substitutions,[256,259] NDIs with *N*,*N*′ short alkyl chain substitutions,[257] triple bond-conjugated NDI-based copolymers,[258] and poly(NDI-vinylene).[260]

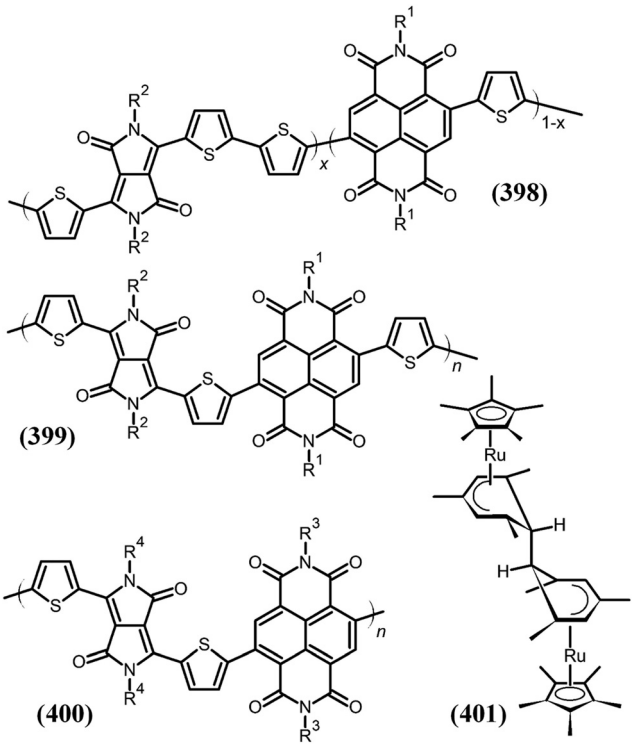

Fig. 83 The molecular structures of NDI and diketopyrrolopyrrole (DPP) based copolymers[262,263] and the $(RuCp^*Mes)_2$ dimer (**401**) dopant used in the (**400**) host.[263]

Kim, Cho and co-workers[240l] synthesized several flexible three NDI and three diketopyrrolopyrrole (DPP) polymers, namely (**322**), (**354**) and (**324**), for flexible field effect transistors. P(DPP-bithiophene) exhibited a high hole mobility of 1.51 $cm^2\ V^{-1}\ s^{-1}$, while the highest electron mobility of 0.85 $cm^2\ V^{-1}\ s^{-1}$ was recorded in the case of (**324**). This behavior was attributed to the synergistic effect of material crystallinity and improved interconnectivity across the fibrils of the polymers in OFETs. Similar observations regarding the OFET performance of the NDI and DPP based copolymers (**398**) with x = 0.1, 0.3, and 0.5 and (**399**) were made by Wan and co-workers.[262] Zang and co-workers[263] studied the effect of molecular electron doping in NDI and diketopyrrolopyrrole (DPP) copolymers (**400**) using a dimeric dopant such as $(RuCp^*Mes)_2$ (**401**), which resulted in enhanced electron mobility in an n-type OFET (Fig. 83). Yamashita *et al.*[264] achieved moderate ambient stability with $(RuCp^*Mes)_2$, which is in contrast to the unstable, n-doped state obtained with cobaltocene n-dopant. This air stability emerges from the suppression of the back electron transfer reaction by the highly cathodic $(RuCp^*Mes)_2$ with an effective redox potential of *ca.* −2.0 V *vs.* ferrocene.

Several research groups have focused on modifying NDI side chains with vinyl linkages in particular. For example, Tan and co-workers[260] synthesized an n-type conjugated polymer (PNV) (**397**) by connecting naphthalene diimide with a vinyl linkage. The synthesized material exhibited red emission with a photoluminescence efficiency of 33.4% along with an electron

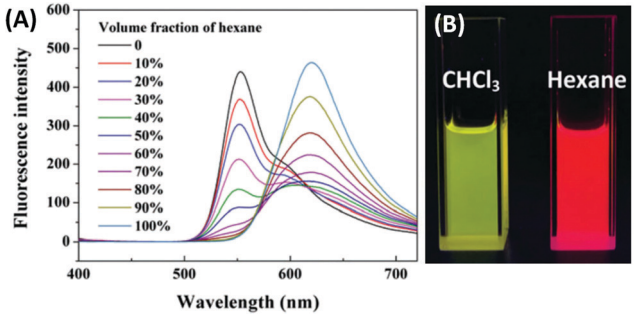

Fig. 84 (A) Emission spectrum variations of PNV in various volume fractions of hexane in solution (10^{-5} M) and (B) photograph of PNV (**397**) in $CHCl_3$ and hexane under 326 nm.[260] This figure has been adapted from ref. 260 with permission from The Royal Society of Chemistry, copyright 2017.

mobility of 1.5 × 10^{-3} $cm^2\ V^{-1}\ s^{-1}$ (Fig. 84). DFT studies suggested that the H-bonding between carbonyl and the vinyl group resulted in a steric competition effect, which could have resulted in enhanced emission and restricted electron mobility.

A novel NDI based copolymer with a selenophene vinylene selenophene donor group (**332**) was synthesized by Kim *et al.*[240m] The thin films prepared using this material exhibited 3D crystallinity under optimized annealing conditions which resulted in a high electron mobility of 2.4 $cm^2\ V^{-1}\ s^{-1}$ and appreciable ambient stability when used as an OFET. Jeng *et al.*[247a] prepared several urea/malonamide dendritic molecules as gate insulators for OTFTs. sNDI functionalized with fluorinated alkyl end groups were used as semiconductors, *i.e.* (**402**) and (**403**). An appreciable performance of both insulating dendrons and NDI derivates as semiconductors was observed and the molecular structures are shown in Fig. 85.

Subsequently, the same group extended their study to prepare a copolymer constituting NDI and bithiophene vinylene bithiophene having different pendant alkyl groups, *i.e.*, (**345**) and (**346**),[240k] *via* Stille coupling polymerization. The C28 OFET exhibited superior performance, giving an electron mobility of 0.019 $cm^2\ V^{-1}\ s^{-1}$ compared to C24 with a mobility of 0.015 $cm^2\ V^{-1}\ s^{-1}$ which was attributed to greater solubility and crystallinity. Noh and co-workers[240n] synthesised (**350**) and (**351**) and used them for OFETs. Electron mobilities of 0.043 and 0.7 $cm^2\ V^{-1}\ s^{-1}$ were measured for PNDI–TVT and PNDI–SVS, respectively. Nevertheless, several studies as discussed above focused on improving the electron mobility of the NDI based system *via* side chain engineering (**404**). Loo and co-workers[247b] succeeded in demonstrating that the existence of in-plane anisotropy is critical compared to a higher mobility along a particular crystallographic direction for polycrystalline materials. This study tuned the molecular packing of (**404**) in thin films *via* post-deposition processing to prepare triclinic and monoclinic polymorphs. The triclinic (**404**) exhibited an electron mobility that is almost double that of the monoclinic one, which was attributed to the smaller charge transport anisotropy due to in-plane molecular orientations in the former case. Ichikawa and co-workers[259] developed copolymers with ditridecyl alkyl chains (C13) substituted at *N* and *N′* positions of

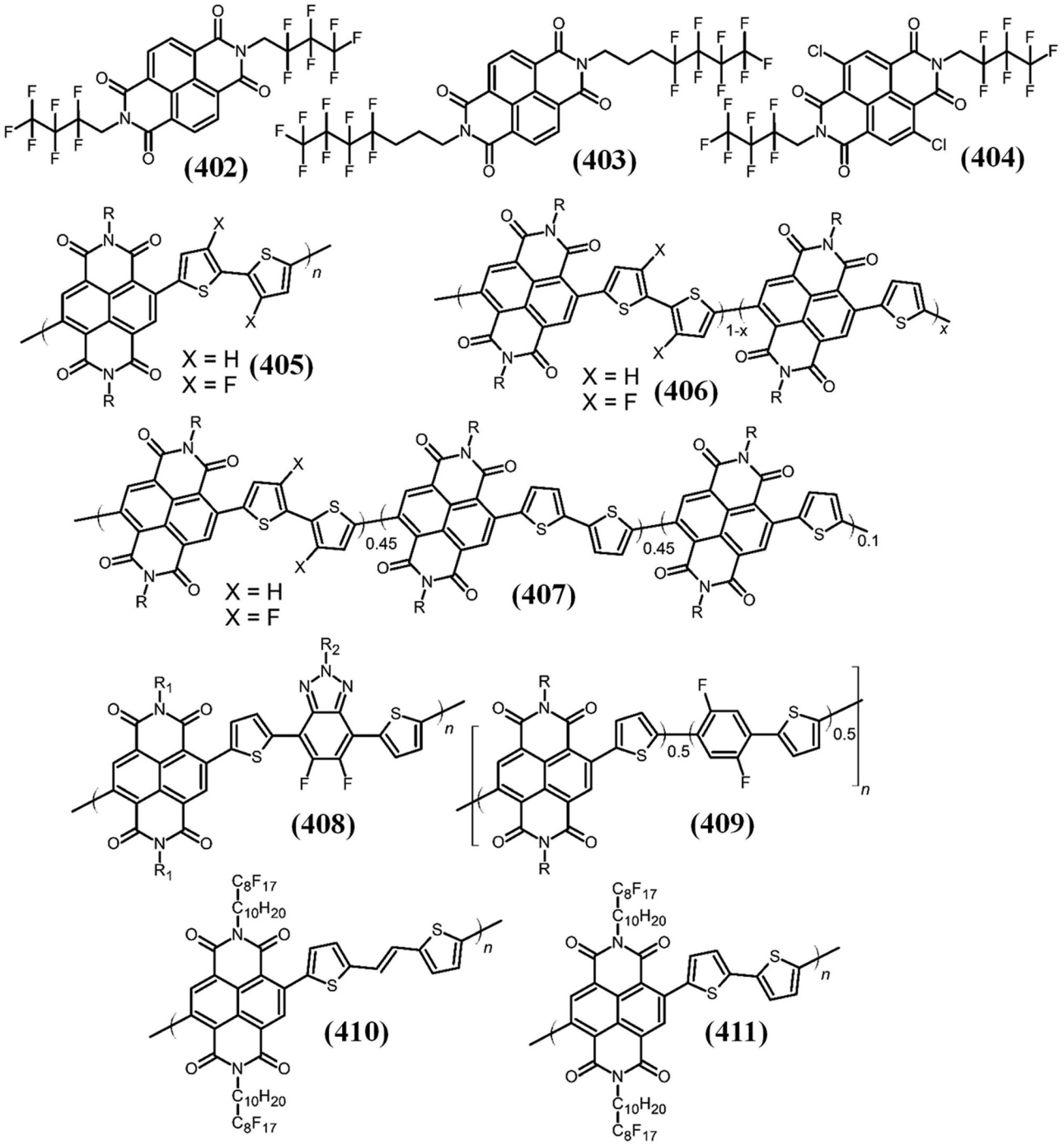

Fig. 85 The chemical structures of small molecule NDIs with different chain lengths of fluorinated alkyl end groups[247a] and fluorinated NDI based polymers.

NDI (**387**) and used them in thin film transistors using a solvent-free transfer-printing process. The films exhibited a high electron mobility of 0.3 $cm^2 V^{-1} s^{-1}$, thus providing a new pathway toward the development of high mobility thin film transistors without the use of any harmful solvents. Finally, some elongated hexagonal microstructures of single crystals of NDI functionalized with fluoroalkyl chains (**404**) were synthesized by Hu *et al.*[265] and used in single crystal field effect transistors (SCFETs) as shown in Fig. 86. It was concluded that, as a result of anisotropy along a certain plane, the electron mobility of these materials in SCFETs could reach values as high as 0.7 $cm^2 V^{-1} s^{-1}$ which is almost 70 times greater than that of organic thin film transistors.

An interesting study reported the fabrication of NDI based phototransistors. Wide-band gap, monocrystalline NDI derivatives with methylene-bridged aromatic side chains (**412**, **413**)

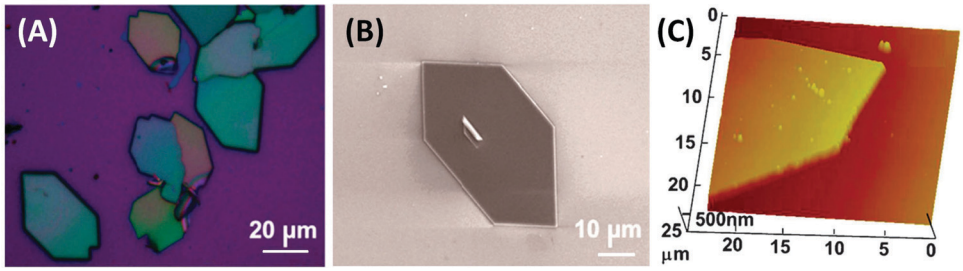

Fig. 86 (A) Large-area OM image of (**404**) single crystals, (B) SEM image of a single crystal and (C) AFM image of a part of an individual hexagonal single crystal.[265] This figure has been adapted from ref. 265 with permission from The Royal Society of Chemistry, copyright 2009.

were synthesized by Kwon and co-workers.[266] These organic phototransistors exhibited a remarkable electron mobility of 1.7 $cm^2 V^{-1} s^{-1}$ and a fast response to UV detection ($\sim$1 μW cm^{-2} limit). This excellent performance was attributed to the methylene-bridged aromatic side chain inducing enhanced face-to-face π–π stacking area between the NDI cores (Fig. 87).

NDI based organic semiconductor molecules have also found enormous utility as battery and supercapacitor electrode materials in recent times. The next section presents the summary of structure–activity relationship between functional groups in NDI derivatives and its effect on energy storage performance. Birajdar *et al.*[267] designed and synthesised fullerene bearing NDI core compounds and compared their application in thin film transistor devices, showing electron mobility values ranging from 8.33×10^{-5} to 3.58×10^{-4} $cm^2 V^{-1} s^{-1}$ depending on the number of C_{60} units and channel length. Blending has been used extensively to enhance the electron mobility in organic field-effect transistors (OFETs).

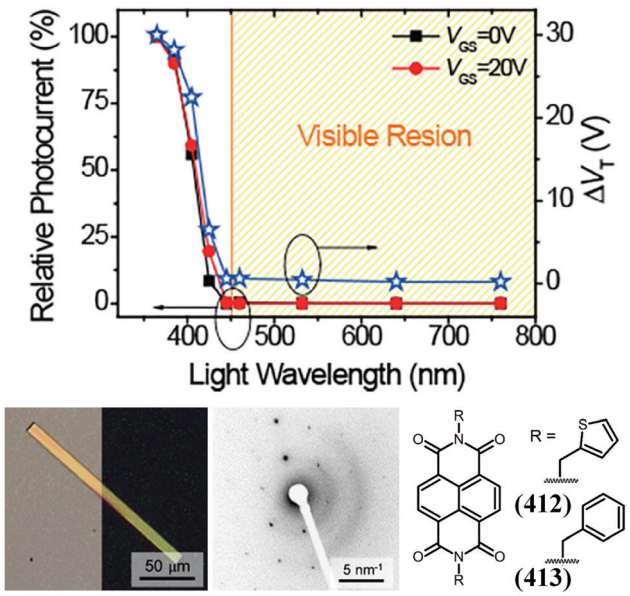

Fig. 87 Optical image of single crystalline (**413**) and selected area diffraction (SAED) pattern of (**413**), and relative photocurrent and V_T change of (**413**) under monochromatic light illumination with different wavelengths (100 μW cm^{-2}).[266] This figure has been adapted from ref. 266 with permission from The Royal Society of Chemistry, copyright 2018.

Yang *et al.*[268] reported the blending of P(NDI2OD-T2) and *N,N′*-bisbutyl-2,6-bis([2,2′]bithiophenyl-5-yl)-NDI on the premise that structural similarity produces more compatible blends where electronic coupling is maintained through intermolecular interactions and charge-transport pathways are established through orders in assembled self-similar structures. The optimization of the composition resulted in an electron mobility of up to $\approx$0.3 $cm^2 V^{-1} s^{-1}$, and the threshold voltage was reduced by 50%. Ohayon *et al.*[269] reported a family of donor–acceptor-type polymers based on the NDI-T2 backbone, where the NDI unit bears an ethylene glycol (EG) side chain in an attempt to produce n-type stable polymers when electrochemically doped in aqueous media to transduce biological events. They found that the substitution of the T2 core with an electron-withdrawing group, methoxy or an EG side chain leads to ambipolar charge transport properties, causing significant changes in film microstructure, thus impairing the n-type OECT performance. They also found that the distance of the EG from the backbone affects the film order and crystallinity, and subsequently electron mobility. Oh *et al.*[270] studied two NDI based molecular dimers, one with thiophene–vinylene–thiophene and the other with a selenophene–vinylene–selenophene linker donor unit for use as the n-type material in OFETs. They found that the selenophene containing compound displays lower backbone planarity and an electron mobility of 0.016 $cm^2 V^{-1} s^{-1}$ in comparison to 6.6×10^{-3} $cm^2 V^{-1} s^{-1}$ for the thiophene containing compound.

7.3 NDI based battery and supercapacitor electrodes

For almost a century, batteries have served as alternatives to fossil fuels as advanced energy sources. Lithium ion batteries in particular have been most successful in powering the day-to-day needs of humankind and can be found in several electrical appliances such as mobile phones and laptops. Fundamentally, a battery consists of a cathode and an anode, an electrolyte, a separator and two current collectors. The efficiency of a battery depends on the electrode kinetics and its stability over long cycling periods.[271] The traditionally used metal oxide cathodes and graphite/carbon anodes are approaching their performance limits for both batteries and supercapacitors. Hence, new advanced electrodes that can achieve a high energy/power density, light weight, a long charge–discharge

lifetime, economical price and environmental safety have become the focus of current research in battery technology.

Recently, organic redox active rechargeable lithium-ion batteries have exhibited promising potential for sustainable energy technology. These organic electrodes do not need transition metal oxides and are able to undergo reversible charge–discharge performance on demand. Several organic small molecules and polymers which are redox active have been synthesized over the past decade for Li ion battery electrodes. 1,4,5,8-Naphthalene diimide (NDI) in particular has emerged as one of the most promising redox active organic molecules for this application. Despite its high theoretical capacity, NDI has often been criticized for its solubility in common battery electrolytes, which results in electrode instability and poor cycling performance.[272] Therefore, several modifications such as synthesizing NDI based (i) polymeric redox active molecules, (ii) covalent organic frameworks and (iii) organic–inorganic hybrids with improved rate capacity and cycling stability have been developed so far. This section summarizes the progress and development of such NDI based organic redox materials for battery applications.

The early improvement in NDI based redox active molecules was initiated with the synthesis of *N*-substituted NDI sodium salts of carboxylic (**414**) and sulfonic acid (**415**), which were designed as active positive electrodes for lithium-half cells by Dolhem Bonnet *et al.*[273] The composite electrodes fabricated with the above two NDI derivatives and carbon black exhibited good electrochemical performance *vs.* Li^+/Li^0 with a specific capacitance of 147 mA hg^{-1} for dicarboxylate and 113 mA h g^{-1} for the disulfonate derivative. This study demonstrated the positive effect of small redox-active units on the cycling stability (99%) of organic molecules. However, the low number of cycles (−50 cycles) is too low for any device scale application and hence further optimization of the electrode is required. The above issues have been overcome in the work of Kothandaraman *et al.*[274] where they synthesized three different aromatic diimide lithium carboxylates, namely the dilithium salt of *N,N′*-bis(glycinyl)biphenyl diimide, the dilithium salt of *N,N′*-bis(glycinyl)pyromellitic diimide and the dilithium salt of *N,N′*-bis(glycinyl)naphthalene diimide (**416**) with three different aromatic cores, *i.e.* biphenyl, benzene and naphthalene, respectively. Among all, (**416**) demonstrated an exceptionally high stable capacity of 134 mA h g^{-1} at 2.24 V *vs.* Li/Li^+ beyond 125 cycles with negligible polarization effects (50 mV). The distinguishing feature of this material is that the Li intercalation/de-intercalation process is biphasic. The excellent electrochemical performance of (**416**) is attributed to (i) improved anion–dianion kinetics due to the presence of the $-CH_2COOLi$ group, (ii) reduction in the HOMO–LUMO band gap, (iii) greater electron affinity of the $-CH_2COOLi$ group and (iv) greater aromaticity of the naphthalene core. The same research group also tested the above synthesized diimides for Na ion battery applications. In this synthesis method the Li ions were substituted by Na ions to form disodium diimide carboxylates, the disodium salt of *N,N′*-bis(glycinyl)pyromellitic diimide (Na_2-BPDI) and the disodium salt of *N,N′*-bis(glycinyl)

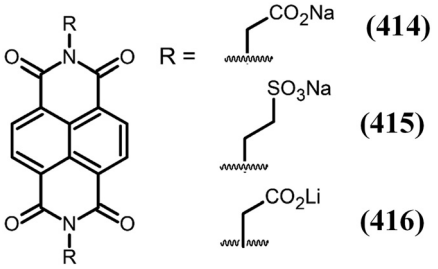

Fig. 88 Molecular structures of carboxylic and sulfonic *N*-substituted NDI salts.[273–275]

NDI (**414**). (**414**) exhibited superior performance over Na_2-BPDI with a capacity of 122 mA h g^{-1} which dropped to only 92 mA h g^{-1} over 50 cycles at a current density of 50 mA g^{-1}.[275] Thus, these extended conjugated systems seemed to be beneficial for alkali battery applications (Fig. 88).[273–275]

Although many studies in the literature claim excellent electrochemical performance for small organic redox molecules, a major drawback is that these organic molecules are largely not stable in non-aqueous electrolytes. This leads to poor cycling performance for battery applications. To overcome this limitation, Stoddart *et al.*[70] synthesized a very unique 3D molecular triangular prism using (−)-NDI-Δ (**417**) and its enantiomer (+)-NDI-Δ *via* a condensation reaction of naphthalene dianhydride with (*RR*)- and (*SS*)-*trans*-1,2-diaminocyclohexane, respectively. The triangular architecture with 3 NDI cores not only provided structural rigidity but also allowed cyclic electron delocalization through π orbital coupling. This allowed the exchange of 6 electrons per unit molecule during the Li^+ intercalation/de-intercalation process. These triangular NDIs exhibited an ultra-high rate capability with a capacity of 146.4 mA h g^{-1} at a low current rate of 0.1C and a capacity of 58.1 mA h g^{-1} at an ultra-high rate of 100C. Furthermore, a remarkable cycling capacity of 71.1 mA h g^{-1} after 300 cycles was obtained for triangular NDIs which could not be achieved in the case of the monomeric NDI derivative (Fig. 89). The superior electrochemical performance of triangular NDIs was attributed to (i) the intrinsic nanoporosity of 197 m^2 g^{-1} BET surface area, (ii) structural integrity, and (iii) enhanced electron delocalization effect due to the triangular geometry. This study opened up a new doorway towards designing higher dimensional organic structures for new generation energy technologies.

To address the stability and performance issues of several NDI based derivatives, Chen and co-workers[276] took a completely different yet fundamental approach (Fig. 90). They used NDI as a model molecule to optimize fundamental electrochemical parameters such as electrolyte compatibility, highest achievable capacity, stability, and rate capability in several organic electrolytes. By performing extensive experimental measurements and computational studies using DFT calculations, they found that the most important limiting factor to improve rate capacity and electrode stability is the electrode–electrolyte interaction. Using dimethyl ether as electrolyte and

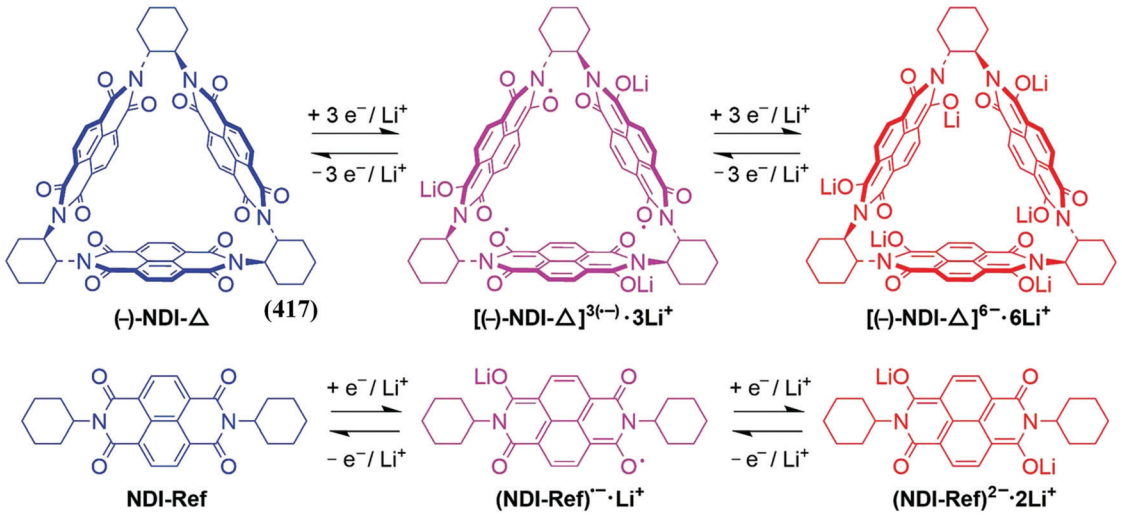

Fig. 89 Structural formulas and redox processes for (–)-NDI-Δ (**417**) and NDI-Ref. The redox reactions between (–)-NDI-Δ, $[(–)\text{-NDI-}\Delta]^{3(\bullet-)}3Li^+$, and $[(–)\text{-NDI-}\Delta]^{6-}6Li^+$. B) Redox reactions between NDI-Ref, $(\text{NDI-Ref})^{\bullet-}Li^+$, and $(\text{NDI-Ref})^{2-}2Li^+$, where each NDI unit is capable of undergoing two reversible one-electron redox processes. Molecular triangles composed of three NDI units undergo two reversible three-electron redox processes, amounting to a total of six electrons per molecule, whereas NDI-Ref can only accept two electrons.[70]

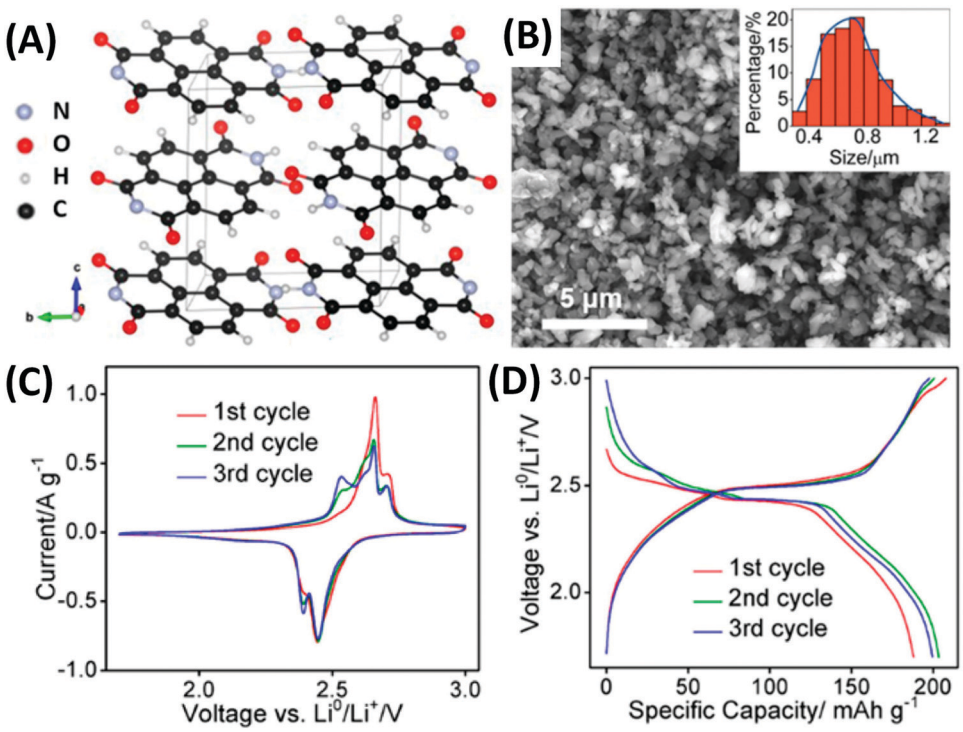

Fig. 90 (A) The crystal structures of NDI and (B) SEM images of NDI with the inset showing the particle size distribution, (C) CV plots of NDI electrodes in the first three cycles at a scan rate of 0.2 mV s^{-1}, and (D) voltage–capacity profiles of NDI electrodes in the first three cycles at C/5.[276] This figure has been adapted from ref. 276 with permission from The American Chemical Society, copyright 2018.

an active mass loading of 1–2 mg cm^{-2}, a remarkably high reversible capacity of 200 mA h g^{-1} and an excellent cycling stability of 96% after 400 cycles at 1C were obtained. This study provided a new life to the NDI based organic electrodes which were otherwise considered not suitable for battery applications.

Alternatively, some research groups succeeded in attaching the NDI moiety to organic polymeric chains so that the dissolution of organic electrodes in non-aqueous electrolytes can be reduced. One such study by Maniam and Nishide *et al.*[277] prepared pendent-type NDI polymers with a polynorbornene backbone consisting of *N*-phenyl (**418**) and *N*-4-nitrophenyl

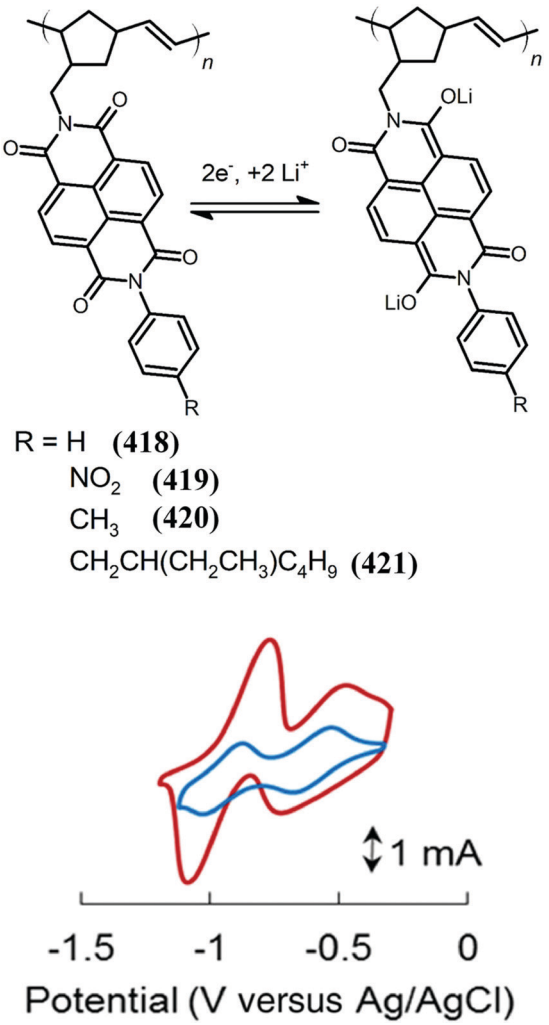

Fig. 91 The redox reactions of the NDI moieties on norbornene polymers and cyclic voltammograms of (**418**) (maroon) and (**419**) (blue) in 1 M TEAP/acetonitrile electrolyte at a scan rate of 10 mV s^{-1}.[277] This figure has been adapted from ref. 277 with permission from Springer Nature (NPG), copyright 2017.

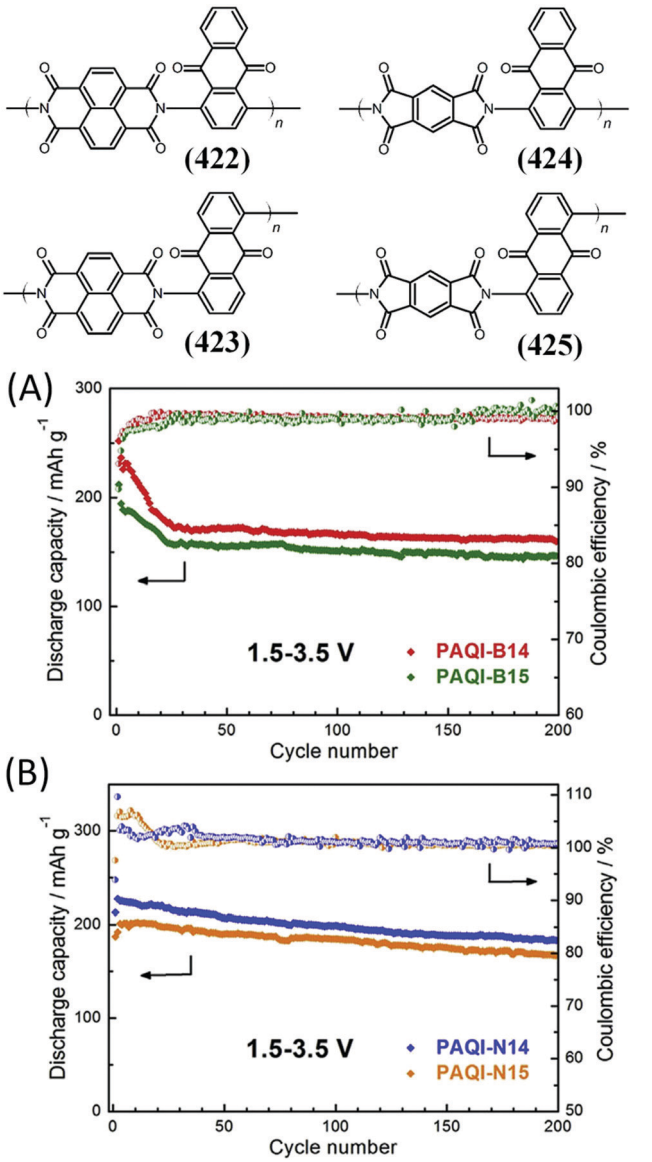

Fig. 92 The molecular structures of poly(anthraquinonyl imide)s (**422–425**) and cycling performance of (A) (**424–425**) and (B) (**422–423**) at 50 mA g^{-1}.[279] This figure has been adapted from ref. 279 with permission from Elsevier, copyright 2018.

(**419**) giving flexible hybrid battery materials. Furthermore, they have[278] independently synthesized some other derivatives where the phenyl group was replaced by a CH_3 (**420**) and a $CH_2CH(C_2H_5)C_4H_9$ (**421**) group (Fig. 91). Although the polymer functionalization could eliminate the solubility issues of the electrodes fabricated with the above molecules, these organic electrodes could retain only 80% of the initial capacity after 10 cycles in a Li-ion coin cell in the case of (**419**). On the contrary, (**418**) displayed high charge capacity (119 mA h g^{-1} at 1C) and remarkable cyclability over 500 cycles. The outcomes of this study are however at the early stages of research and the pendant type NDI polynorbornene composites seem to hold promising potential for future battery applications.

Another interesting study worth mentioning here is that by Cao *et al.*[279] who reported two isomeric pairs of poly (anthraquinonyl imide)s (PAQIs) (**422–425**) organic cathodes for Li-ion batteries (Fig. 92). The reversible four electron redox reaction and subsequent Li^+ insertion in and out of the (**422**, **423**) matrix served as a high capacity organic cathode material with a capacity of 202 mA h g^{-1} and approximately 80% capacity retention over 200 cycles. A comparative analysis of isomers (**422**) and (**423**) suggested that (**422**) exhibits a relatively low overpotential, a high discharge capacity, and greater cycle and rate performance, confirming that structural isomerism has a significant influence in boosting the electrochemical performance of such organic electrodes. The same group also tested the electrochemical performance of these PAQIs for Na ion batteries and obtained appreciable performance with a high reversible capacity of 190 mA h g^{-1} and a cyclic stability of 93% capacity retention up to 150 cycles.[280] Thus, PAQIs

could serve as promising organic electrode materials for both Na and Li ion batteries.

A redox active conjugated polymer, poly(fluorene-*alt*-NDI) (**426**), synthesized through Suzuki coupling reaction and its utilization as an n-type battery electrode material was reported by Lutkenhaus *et al.*[281] By performing Li^+ intercalation/de-intercalation studies, it was observed that (**426**) could retain 86% of its initial capacity of 18 mA h g^{-1} over 500 cycles while maintaining a 99.8% coulombic efficiency. Furthermore, (**426**) and carbon composite electrode exhibited the highest capacity of 39.8 mA h g^{-1} at 0.5C and 91% capacity retention over 500 cycles. The improved electrochemical performance was hypothesized to be a result of the resonance at the NDI unit and π-conjugation along the polymeric structure. Hou and co-workers[282] reported the synthesis of a copolymer, poly[ethylene-*N,N′*-bis(2-ethylhexyl)-NDI] (**427**), *via* Stille coupling reaction of 2,6-dibromo-*N,N′*-bis(2-ethylhexyl)-NDI and (*E*)-1,2-bis(tributylstannyl)ethene, and used it as a cathode material for lithium ion batteries. (**427**) could retain 85% of its initial theoretical capacity over 100 cycles at 0.1C, with a 98% coulombic efficiency. The activity demonstrated here is attributed to the low solubility of (**427**) and increased electrode stability. Further investigation on structural and electronic effects would be essential for further development.

While several reports discussed above were focused on improving the organic electrode stability in organic electrolytes, their practical applicability poses several challenges for device scale applications (Fig. 93). Therefore, in recent times, aqueous batteries have emerged as promising candidates for environmentally safe, economical and sustainable energy systems. Technological realization of such aqueous batteries needs naturally available, recyclable and less/non-toxic materials for developing organic battery electrodes. Gaubicher and co-workers[283] designed the first ever such organic electrode material that operates by simultaneous uptake and release of both cations and anions from the aqueous electrolyte. By coupling p-type bipyridinium and n-type NDI through a propyl linker, a new p/n type redox active material (MNV) (**428**) was fabricated which demonstrated a high oxidation potential (−0.47 V *vs.* saturated calomel electrode), fast reversible electrode kinetics, and excellent capacity (63 mA h g^{-1} at 4C) and cycling stability in Na^+ and Mg^{2+} electrolytes. This research group also provided support for a novel redox mechanism using UV-vis spectro-electrochemistry, operando synchrotron X-ray diffraction, and theoretical studies based on density functional theory calculations.

Extending this idea further,[284] the same group designed a novel di-block oligomer (DNVBr), by linking the NDI coupled to bipyridinium repeating units (**429**) *via* a propyl linker. Enhanced battery performance with DNVBr as the negative electrode due to simultaneous exchange of Na^+, Mg^{2+}, and Cl^- resulted in a high capacity of 105 mA h g^{-1} and unprecedented capacity retention over 6500 cycles in neutral electrolytes such as raw ocean water. These researchers even demonstrated a complete cell validation of over 1600 cycles using a commercial 2,2,6,6-tetramethylpiperidin-1-yl)oxyl (TEMPO) molecule, which exhibited an energy density of −40 W h kg^{-1}. On similar grounds, Nelson *et al.*[285] developed fast switchable p- and n-type redox polymer materials as battery electrodes. They synthesized the 3,3′-dialkoxybithiophene homo-polymer (as p-type) with glycol side chains and NDI-dialkoxybithiophene copolymers (**433**) (as n-type) with either a glycol or a zwitterionic side chain on the NDI unit, and combined them to form p- and n-type redox polymers p(ZI-NDI-gT2) (**433**). When both the above p- and n-type polymers were tested in a two-electrode cell, both materials exhibited reversible charging up to 1.4 V with high redox stability in NaCl solution, which was attributed to the formation of bipolaron states almost reaching the theoretical capacity. Since these materials can operate in water, it paves the way for utilization of sustainable and safe electrolytes for energy storage devices. Furthermore, organic–inorganic hybrids consisting of NDI (**430**) and reduced graphene oxide (NDI–RGO) were synthesized *via* a self-assembly strategy by Dongqing Wu and co-workers.[286] As a result of the non-covalent interactions between NDI and RGO in a 2-dimensional hybrid system, homogeneous distribution of NDI (**430**) across the RGO surface facilitated reversible Li^+ intercalation/de-intercalation across the electrode. An excellent reversible capacity of 200 mA g^{-1} was reported which dropped to only 170 mA h g^{-1} after 260 cycles with a columbic efficiency of 98%. On the contrary, pristine NDI (**430**) had a poor capacity of 10 mA h g^{-1} with loss of activity after merely 5 cycles under similar operating conditions. Demets and co-workers[287] innovatively incorporated *N,N′*-bis(4-aminophenyl)-NDI (**431**) into the lamellar morphology of vanadium pentoxide (V_2O_5) in varying amounts and synthesized hybrid intercalates. The imide moiety, being prone to form salts with lithium, induces enhanced Li^+ uptake and discharge by lamellar intercalation. This resulted in doubling of the ion uptake capacity (1.27 Li^+ per V_2O_5 unit *vs.* 0.66 for pure V_2O_5), and improved reversibility of the intercalation/de-intercalation process, while the specific charge capacity was doubled (188 mA h g^{-1} *vs.* 98 mA h g^{-1} for pure V_2O_5). Furthermore, the intercalation of imide into the V_2O_5 matrix improved its structural stability and hence cycling performance. An electroactive carbonyl-based poly(NDI-*alt*-benzoquinone) (**432**) has been reported by Troshin *et al.*[288] using 1,4,5,8-naphthalenetetracarboxylic dianhydride and 2,5-diaminobenzoquinone. Under optimized conditions, the (**432**)//Li cells achieved a capacity of 168 mA h g^{-1}, which was higher than those of $LiFePO_4$ and $LiCoO_2$ which are common inorganic materials used in battery applications. There exists plenty of scope for further research and development in this redox system as the theoretically achievable capacity is almost double the practically obtained one.

Jhulki *et al.*[289] reported a 2D imine-linked covalent organic framework (COF) containing NDI redox groups and 1,3,5-tris(4-aminophenyl)benzene (TAPB) for use as electrodes in lithium-ion batteries. The pores of this COF are among the largest reported, facilitating efficient Li^+ ion transport. Wang *et al.*[290] reviewed the design and application of molecular triangle macrocycles as an emerging class of organic molecules with interesting properties including their structural rigidity,

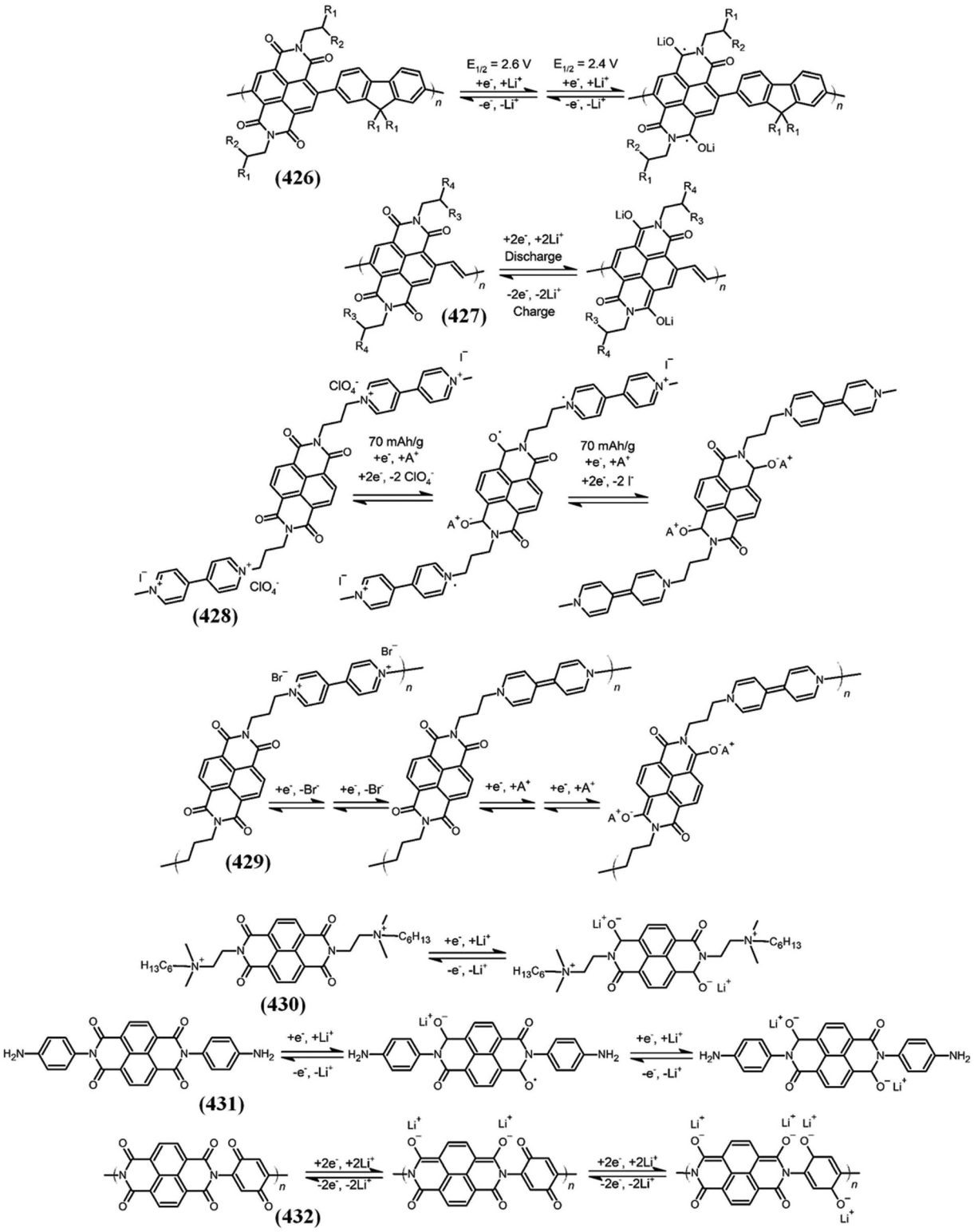

Fig. 93 Doping of poly(fluorene-*alt*-naphthalene diimide) (**426**) with Li^+ ions; upon the first reduction, one carbonyl oxygen is doped with a Li^+ ion, and upon the second reduction, a second carbonyl oxygen is doped. The reverse process takes place during oxidation. Voltages are *versus* Li/Li^+;[281] electrochemical redox mechanism of the (**427**) copolymer,[282] the anticipated electrochemistry of MNV (**428**) in an aqueous electrolyte,[283] the reversible one-electron reduction steps of both segments of (**429**) copolymer redox-active moieties,[284] electrochemical redox reactions of Li ions with NDI based on anhydride functional groups (**430**),[286] successive electrochemical reductions of *N*,*N*′-bis(4-aminophenyl)-NDI (**431**) in the presence of lithium ions,[287] and electrochemical lithiation and delithiation of (**432**).[288]

electron deficiency, through-space electronic communication, intrinsic chirality, energy storage, solid-state luminescence, and nonlinear optical response.

Very few research groups have utilized NDI based organic molecules for supercapacitor applications. There are a couple of noteworthy reports from the research of Malik *et al.*[291] and Kurungot and Asha *et al.*[240y] Malik and co-workers[291] synthesized a novel benzimidazole appended arylimide (pyromellitic, naphthalene and perylene) (**433**, **434**) based on covalent organic frameworks (COFs) such as (**433**). They found that NDI and the diaminobenzidine COF exhibited the highest binding affinity with CO_2, *i.e.* 127.87 cc g^{-1} at 195 K. Moreover, (**433**) exhibited an appreciable specific capacitance value of 66.56 F g^{-1} at 0.5 A g^{-1} in 1M H_3PO_4 solution, which is higher than other reported pristine NDI molecules. Conjugated copolymers of NDI and thiophene terminated oligophenylenevinylene as donor moieties (**348**) and (**348**) were synthesized by Kurungot and Asha *et al.*[240y] Both polymers exhibited π–π* transitions and intramolecular charge transfer (ICT) from thiophene to NDI in the region of 300–480 nm and 500–800 nm, respectively. A composite electrode of synthesized polymers and carbon nanotubes in 0.5 M H_2SO_4 electrolyte exhibited a high specific capacitance of 124 F g^{-1} for (**348**) with excellent cycling stability over 5000 cycles and nearly 100% retention. The measured energy and power density values were 2 W h kg^{-1} and 22 kW kg^{-1}, respectively, signifying the capabilities of NDI based polymers for supercapacitor applications. The latest trend in the development of organic battery electrodes focuses on photo/electroactive organic–inorganic hybrids. By innovatively incorporating NDI and triphenylamine (**435**) units in a novel covalent organic framework (NT-COF) (**436**), a 3D porous structure having a high specific surface area of 1276 m^2 g^{-1} was synthesized by Wang and co-workers.[292] As a result of the synergistic effect, an efficient intramolecular charge transfer from (**435**) to NDI was observed. Furthermore, the NT-COF also demonstrated a highly reversible electrochemical reaction when used as a battery electrode. This synergy between the NDI and (**435**) resulted in improved solar energy efficiency and accelerated electrode kinetics. A prototype for direct solar-to-electrochemical energy conversion and storage using NT-COF (**436**) as the cathode in a solar energy powered Li ion battery exhibited a decrease in charge voltage (−0.5 V), an increase in discharge voltage (−0.5 V), and an overall 38.7% increase in battery efficiency. Thus, it is very encouraging to note that several NDI based organic hybrid materials hold promising potential for development and realization of sustainable next generation battery technologies for the future.

Biradar *et al.*[293] reported dopamine *N*- and *N,N′*-functionalised NDIs and studied their application as composite electrode materials for supercapacitors and found a specific capacitance of 202.5 F g^{-1} (as measured by CV) and 195.9 F g^{-1} (as measured by galvanostatic charge/discharge) for the disubstituted NDI, while the monosubstituted NDI gave 142.8 and 137.2 F g^{-1} and the NDI gave 45.6 and 37.6 F g^{-1} in a potential window of 0 V to 1 V, respectively.

While imides have been at the forefront of organic redox electrodes for battery applications, their effectiveness is restricted due to limited accessibility to their active sites. Feng and co-workers[294] synthesized a crystalline 2D polyarylimide (2D-PAI) (**436**) and its composite with carbon nanotubes (CNTs) and utilized it as the cathode in Li ion battery applications (Fig. 94). The synthesized polyarylimide hybrid (2D-PAI@CNT) exhibited high rate capability and remarkable cycling stability (100% capacity retention after 8000 cycles), which far exceed those of the state-of-the-art polyimide electrodes. This exceptional electrochemical performance was attributed to the high stability of the cyclic imide linkage, and enhanced surface area due to well-defined accessible pores which facilitated access to the π-conjugated redox-active NDI units.

Several NDI based organic semiconductors have been extensively utilized in organic solar cells and have demonstrated encouraging preliminary success for device scale applications. The next section details available reports on NDI based molecules and their utilization in organic photovoltaics.

7.4 NDI based organic solar cells

The era of modern solid state photovoltaics (PV) began with the discovery of the photovoltaic effect in silicon in 1954. The high manufacturing cost of Si PVs has led to the interest in a new class of photovoltaics which are based on organic materials. Also known as polymer solar cells, they constitute several advantages over the classical Si based PVs in terms of being inexpensive, flexible, lightweight, and thus suitable for grid power generation. The efficient functioning of a polymer solar cell (PSC) depends largely on the choice of donor and acceptor which should have suitable optical, electronic and morphological properties. NDI and its polymeric derivatives offer unique physico-chemical properties such as structural planarity, delocalized π-electron mobility and tunable LUMO energy levels which make them a very efficient electron acceptor class of compounds for solar cells. When a p-type electron donor polymer and an n-type electron acceptor NDI based polymer are incorporated into the active layer in an all-polymer solar cell (all-PSC), excellent photovoltaic performance and high solar power conversion efficiencies (PCE) are achieved compared to fullerene-based solar cells. Therefore, several functionalized NDI based polymers such as cyanated polyphenylenevinylenes, benzothiadiazole containing polymers, aromatic diimides with side functional groups as (i) thiophenes, (ii) seleno-thiophene, (iii) fluorinated NDIs, and (iv) porphyrin based NDIs have been synthesized and characterized, and their photovoltaic performance has been reported.[4a,295] All-polymer solar cells have been recently reviewed by Zhang and Li,[296] yet here we provide a detailed literature survey of NDI-based polymers reported to date for organic solar cell applications.

The early work on the use of pristine NDI in a solar cell device was initiated by Song and co-workers[297] where, upon using NDI as an electron acceptor layer, they observed an improvement in the device performance of bulk-heterojunction PSCs. They chemically introduced NDI **437** onto an ITO surface as a cathode interlayer (CIL) using the

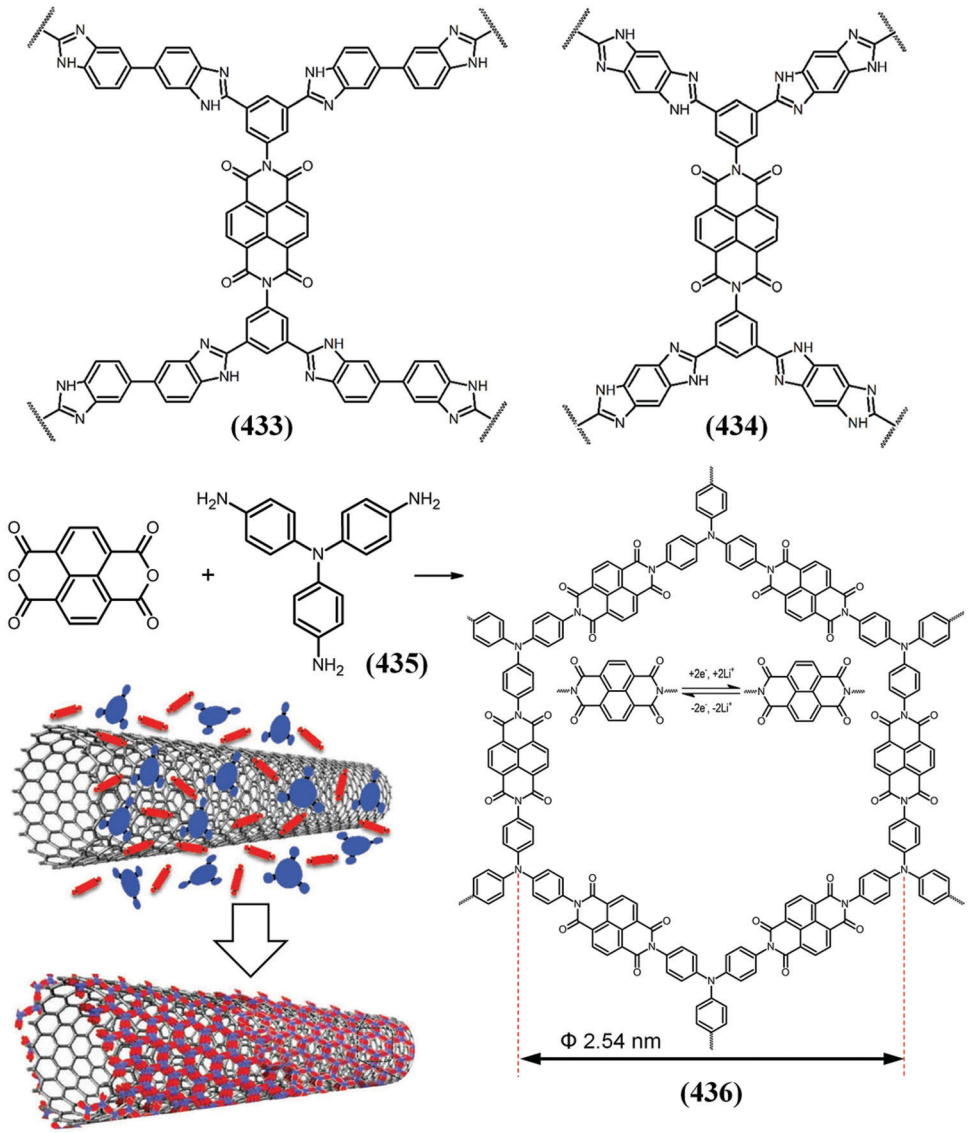

Fig. 94 The structure of the benzimidazole linked arylimide based porous crosslinked polymers[291] and the schematic illustration of the synthesis of crystalline 2D-PAI (**436**)@CNT and energy storage process.[292,294]

3-bromopropyltrimethoxysilane coupling agent (**438**). The modification led to a reduction in the work function of ITO from 4.70 to 4.23 eV (Fig. 95). The modified cathode was used in inverted polymer solar cells (PSCs) based on PTB7-Th:$PC_{71}BM$ which yielded a power conversion efficiency (PCE) of 5.87%.

In a work by Bentounsi *et al.*,[298] the practical aspect of hybrid dye-sensitized photoelectrochemical cells was addressed using click conjugation of propiolic ester substituted NDI on a NiO photocathode already coated with a diketopyrrolopyrrole dye bearing two azido groups. Transient absorption spectroscopy showed that optical excitation of the diketopyrrolopyrrole dye leads to an effective electron transfer chain from the NiO valence band to the NDI passing *via* the diketopyrrolopyrrole dye, resulting in a long-lived charge-separated state of 170 μs. This approach provides a strategy to design multicomponent hybrid dye-sensitized photoelectrochemical cells by chemistry on the electrode.

Subsequently, modifications to the NDI structure and tuning of its electronic properties were undertaken by several researchers. In one such noteworthy study, four non-fullerene NDI based acceptor materials were designed by Ali and co-workers (Fig. 96),[299] involving modifying the nature of the electron withdrawing groups at the end of A–D–A–D–A molecules (**441–445**). These new acceptor molecules exhibited strong absorption bands around 420 to 650 nm, a reduction in HOMO energies from −7.24 to −7.28 eV, enhanced %ETC of 35 to 65%, and a reduction in the excitation energy from 2.28 to 2.47. Kim and co-workers[300] designed NDI-based non-fullerene acceptor molecules (**446**, **447**) which exhibited high electron affinity and electron mobility, and a good energy match with polymer donor levels. The (**446**) based organic solar cell exhibited a high fill

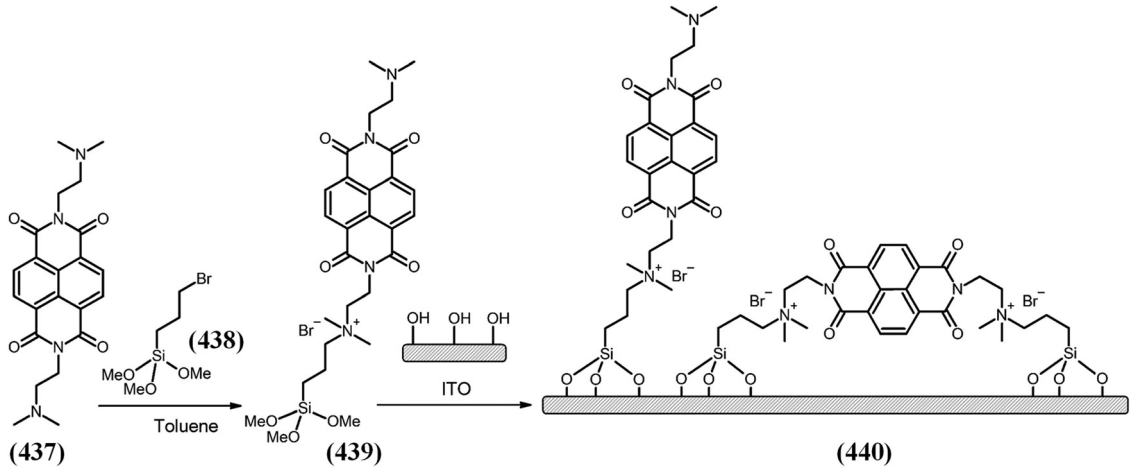

Fig. 95 The procedure of modifying ITO substrates with NDI-TMS.[297]

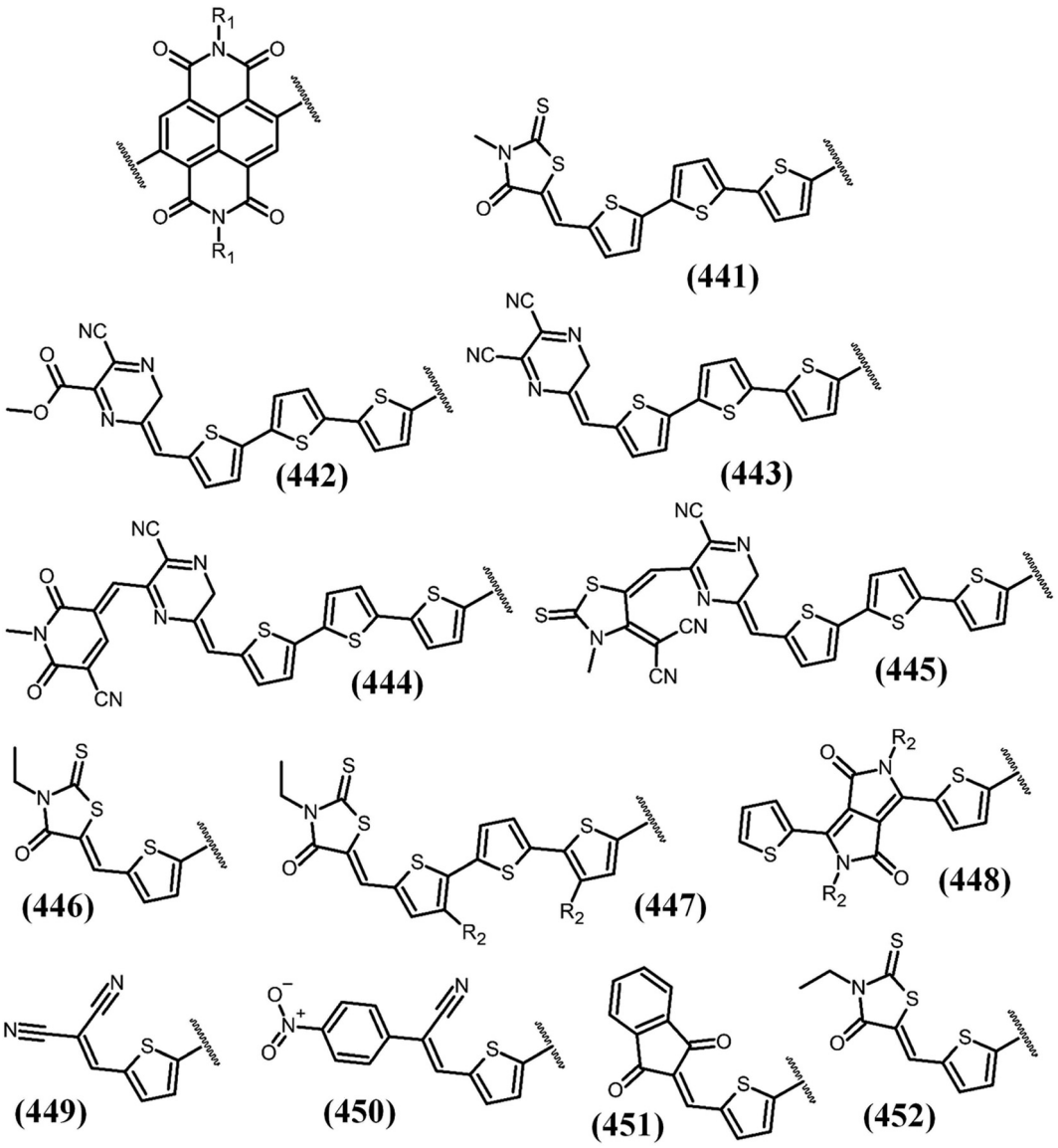

Fig. 96 Molecular structures of small organic NDI based core substituted non-fullerene used in solar cells: (**441–445**),[299] (**446**, **447**),[300] (**448–452**),[301] and (**449**, **450**).[302]

factor of 0.69 and an appreciable power conversion efficiency of 3.07%.

Ling and co-workers[303] designed several NDI-based terpolymers by varying the thiophene–NDI/selenophene–NDI ratio in a set of copolymers (**453**). Thiophene–NDI and selenophene–NDI copolymers were synthesized as references. Compared to the rest of the copolymers, the PBDT(T)TPD/0.5-NDI based solar cell demonstrated an improved short-circuit current density (J_{sc}) of 9.1 mA cm^{-2} along with a high open circuit voltage (V_{oc}) of 1.05 V. Furthermore, a high power conversion efficiency (PCE) of 5.4% was recorded for PBDT(T)TPD/0.5-NDI. Subsequently, thiophene functionalized NDI based polymers gained tremendous attention from researchers for solar cell applications. For instance, the optical and semiconducting properties of the NDI–bithiophene copolymer (**322**) was tuned *via* random incorporation of perylene diimide (PDI) as a co-acceptor (**454**) by Asha and co-workers.[304] These random copolymers exhibited an enhanced power conversion efficiency of 5.03% using an NDI-Th-PDI30 acceptor and a PTB7-Th donor combination as illustrated in Fig. 97.

Bao and co-workers[306] performed a detailed morphological analysis of polymer poly(3-hexylthiophene-2,5-diyl) (P3HT):fullerene (PCBM) and polymer (P3HT):poly(NDI–thiophene) (**320**) solar cells to understand the challenge of obtaining high performance all-polymer solar cells. In contrast to PCBM, PNDIT (**320**) has a lower tendency to form mixed phases with P3HT than PCBM, which may be a key to inhibit the donor polymer crystallization process, thus creating preferred small phase separations between the donor and acceptor polymers. Son and co-workers[307] synthesized five polymer donors with different molecular orientations, synthesized by random copolymerization of 5-fluoro-2,1,3-benzothiadiazole with different relative amounts of 2,2′-bithiophene (**456**) and dithieno[3,2-*b*;2′,3′-*d*]thiophene (**457**) to give (**458**). Solar cells were prepared by blending the polymer donors with an NDI-based polymer acceptor (**322**) or a [6,6]-phenyl C_{71}-butyric acid methyl ester ($PC_{71}BM$) (**459**) acceptor. (**456**) exhibited a PCE of (**456**):(**459**) = 5.98% and a PCE of (**456**):(**322**) = 3.40%. In contrast, (**458**) exhibited high EQEs (≈60%) and the highest PCE in both (**459**)-based and (**322**)-based devices (PCE of (**458**):(**459**) = 7.03%, PCE of (**458**):(**322**) = 6.01%). Subsequently, Zhou and co-workers[308] designed an n-type polymer of (**460**) based on asymmetric rylene diimide and thiophene. The highest power conversion efficiency of 4.70% was achieved for PTB7-Th:(**460**)-based devices, which is higher than those of the analogue polymers of (**461**) and (**462**). All the examples are illustrated in Fig. 98 and 99.

An all conjugated NDI based graft/block copolymer was synthesized by Chen and co-workers[311] using the Kumada catalyst-transfer polycondensation (KCTP) strategy (Fig. 99). The (**471–473**) polymers exhibited a low power conversion efficiency of 2.28% with an open circuit voltage (V_{oc}) of 0.61 V, a short circuit current density (J_{sc}) of 7.00 mA cm^{-2}, and a fill factor (FF) of 0.62.

Huang and co-workers[312] incorporated truxene units (**322**) to give (**474**) and paired with PTzBI-O which led to an excellent power conversion efficiency of 8% attributed to enhanced charge carrier mobilities, reduced recombination rate and film stability (Fig. 100).

A series of copolymers, consisting of NDI-2,2′-bithiophene and PDI-2,2′-bithiophene (**454**), were synthesized by Zhan and co-workers (Fig. 101).[315] An interesting observation made in this study is that the variation of the PDI/NDI ratio resulted in changes to the LUMO energy levels from 23.90 to 23.80 eV, while the HOMO energy levels reduced from 26.10 to 25.85 eV. Along with PTB7-Th the device with PTB7-Th/NDI100 (**322**) exhibited the highest power conversion efficiency of 4.67%, whereas the PTB7-Th/PDI100 (**454**, x = 1) yielded a conversion efficiency of 1.03%.

Leclerc and co-workers[240g] synthesized (**322**) with HOMO energy levels similar to that of commercial N2200 (**322**). An inverted all-polymer solar cell with these polymers along with PCE12 or PCE10 gave a superior power conversion efficiency (7.3%) compared to N2200 (**322**). Cao and co-workers[316] presented three n-type conjugated polymers; (**320**) with varying size *N*-alkyl substitutions. The introduction of asymmetric alkyl side chains improved the intermolecular packing, leading to stronger aggregation and crystallization in the resulting polymers with an impressive PCE of 6.89% in the case of *N*-2-butyloctyl-*N*′-2-octyldodecyl, which outperformed the value of

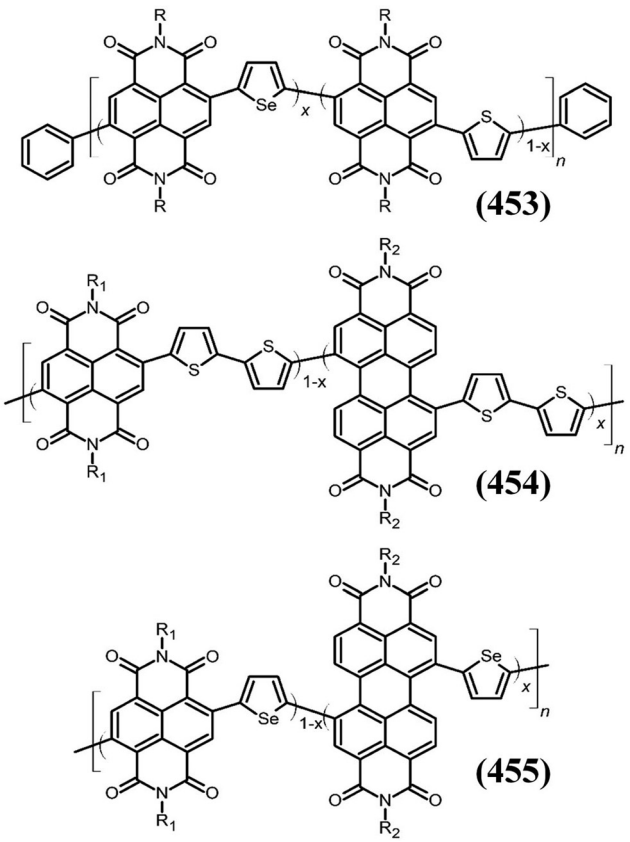

Fig. 97 The structure of NDI-based random thiophene–NDI/selenophene–NDI terpolymer (**453**) for efficient all-polymer solar cells[303,305] and n-type NDI–bithiophene/PDI–bithiophene as a co-acceptor (**454**).[240f,304]

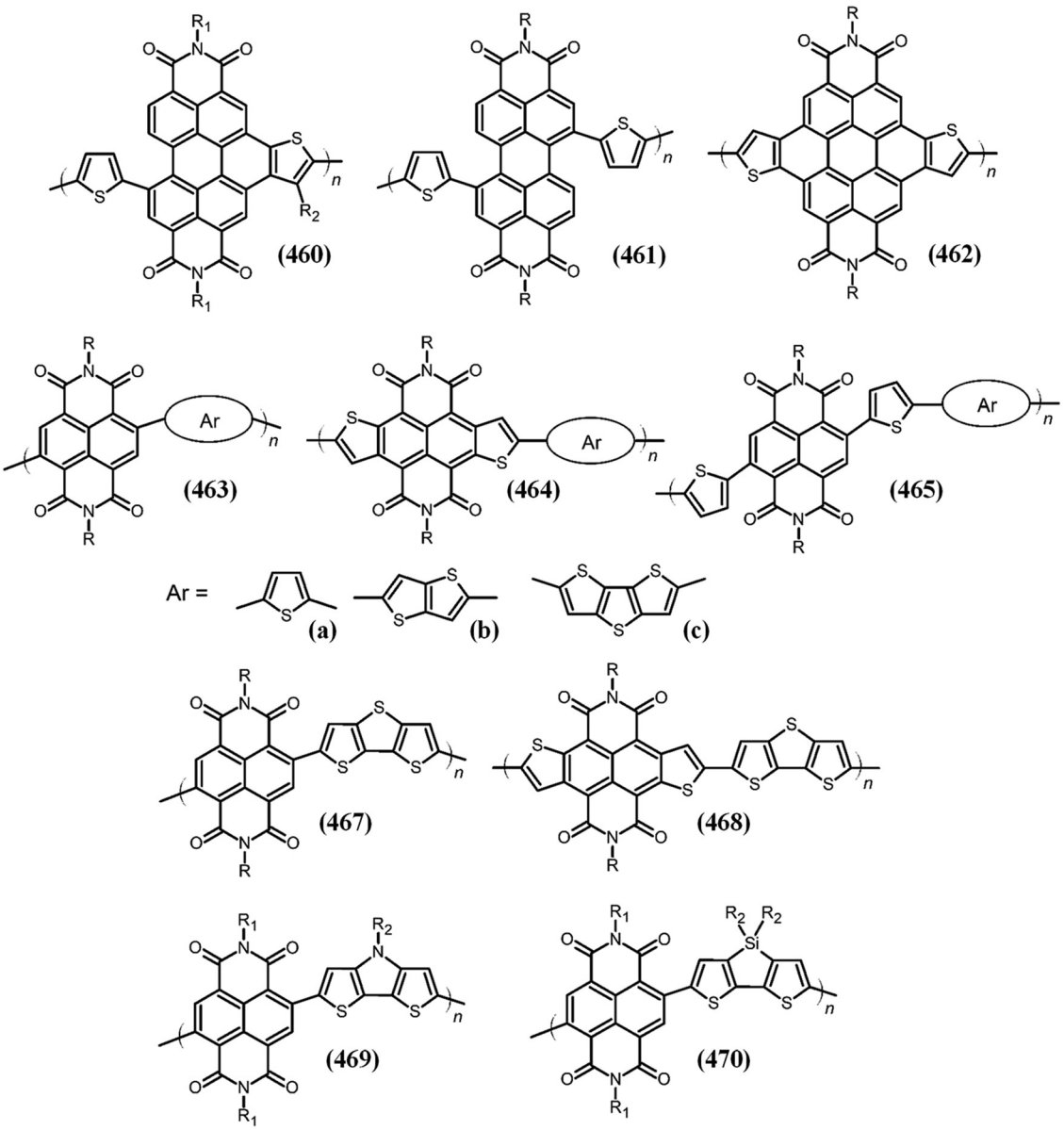

Fig. 98 The chemical structures of n-type polymers based on classic symmetric NDI and PDI building blocks.[10b,308,309] NDI-dithienosilole and dithienopyrrole acceptor copolymers (**469**, **470**).[310]

4.30% obtained from the control copolymer *N,N′*-bis(2-hexyldecyl). Chen and co-workers[317] synthesized another pair of (**320**) acceptor copolymers, namely with *N,N′*-bis(2-octyldodecyl) and *N,N′*-bis(2-hexyldecyl) NDI substitutions. The alkyl chain engineering in NDI resulted in increased solubility in both halogen and non-halogen solvents. The device fabricated in 1,2-dimethylbenzene (1,2-DMB) solvent by pairing either of these polymers with PTB7-Th polymer as a donor resulted in PCEs of 3.88% and 4.94% in the case of larger and smaller alkyl substitutions, respectively.

A cathode interface layer (CIL) based on (**320**) with tertiary amine *N,N′*-substitutions was synthesized by Andersson and co-workers.[318] The photovoltaic device with a TQ1/$PC_{71}BM$ bulk heterojunction layer with the studied polymer interlayer exhibited a high J_{sc} value of 10.5 mA cm^2, a V_{oc} of 909 mV, and a FF value of 68%, leading to a high power conversion efficiency of 6.7%. Zhou and co-workers[309] utilized NDI units connected to thiophene, thienothiophene, or dithienothiophene units *via* a thiophene π-bridge, and three new copolymers (**465a–c**) were synthesized and used in all-PSCs. By increasing the number of copolymerized aromatic rings from (a) to (c), the PCE values decreased gradually from 3.78 to 1.14% to 0.70% when using PBDB-T as the donor polymer. Li and co-workers[319] investigated a series of novel acceptor–donor–acceptor–donor–acceptor (A_2–D–A_1–D–A_2) structured acceptor oligomers with NDI as the centre and acceptor unit (A_1), oligothiophenes ($T = 1, 2, 3, 4$) as π-bridges (D), and 2-(1,1-dicyanomethylene)rhodanine (DCRD) as terminal groups (A_2) (**477**, **478**) using quantum

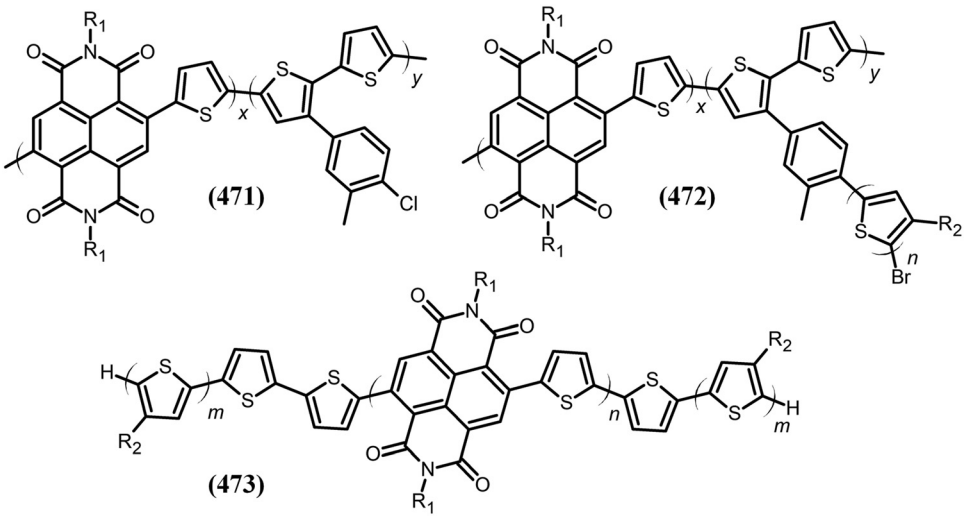

Fig. 99 Chemical structures of (**471**) n-type linear polymer, p–n type graft copolymers (**472**), and p–n–p type triblock polymer (**473**).[311]

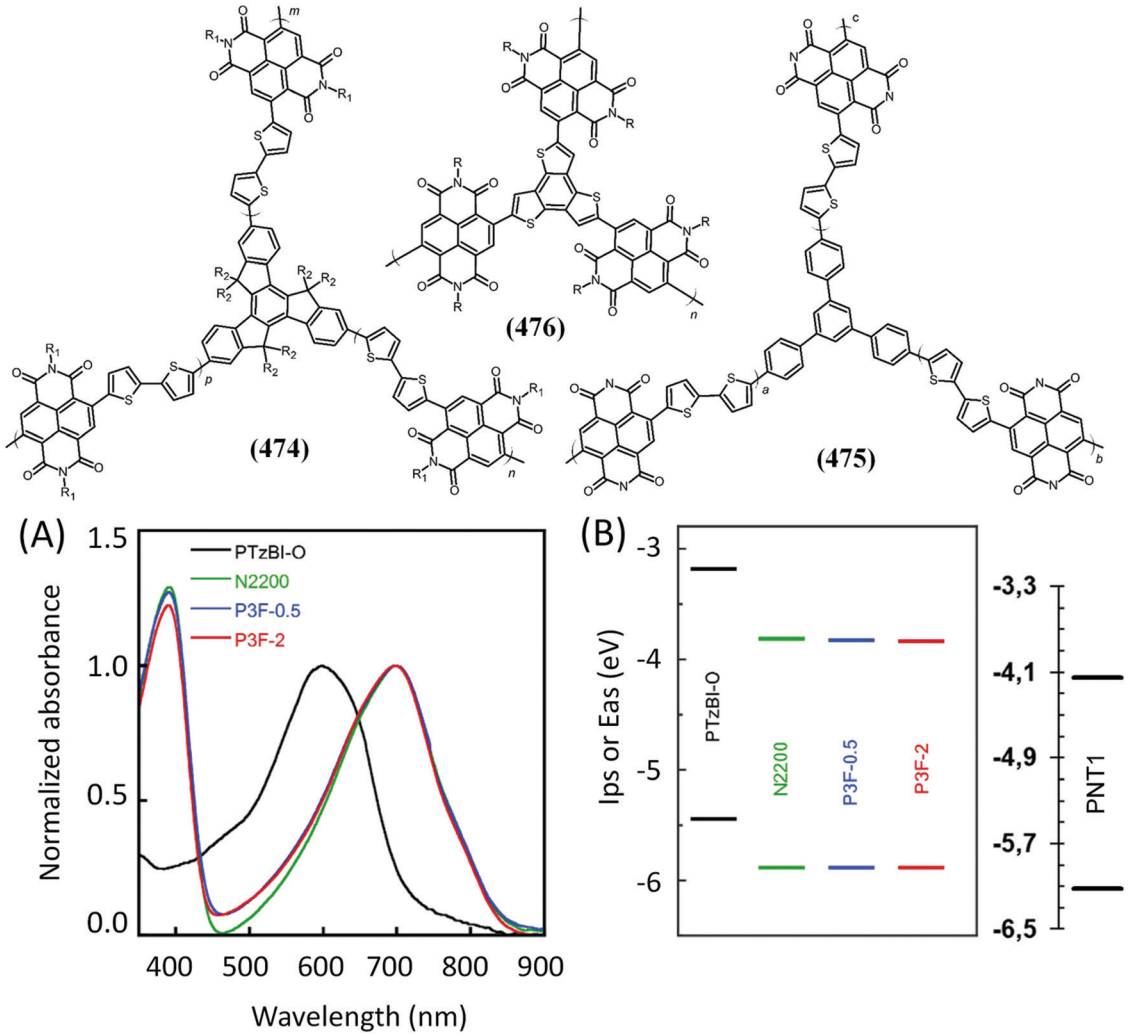

Fig. 100 Star-like n-type conjugated polymers (**474**) based on NDI,[312] (**475**) with 1,3,5-trisphenyl-benzene as the branched unit,[313] (**476**) polymer where benzo[1,2-*b*:3,4-*b*′:5,6-*b*″]trithiophene derivative is used as the A3 knot.[314] (A) absorption spectra of the (**474**) and (**322**) polymers; (B) IPs and EAs of the polymers.[312] This figure has been adapted from ref. 312 with permission from Springer Nature, copyright 2018.

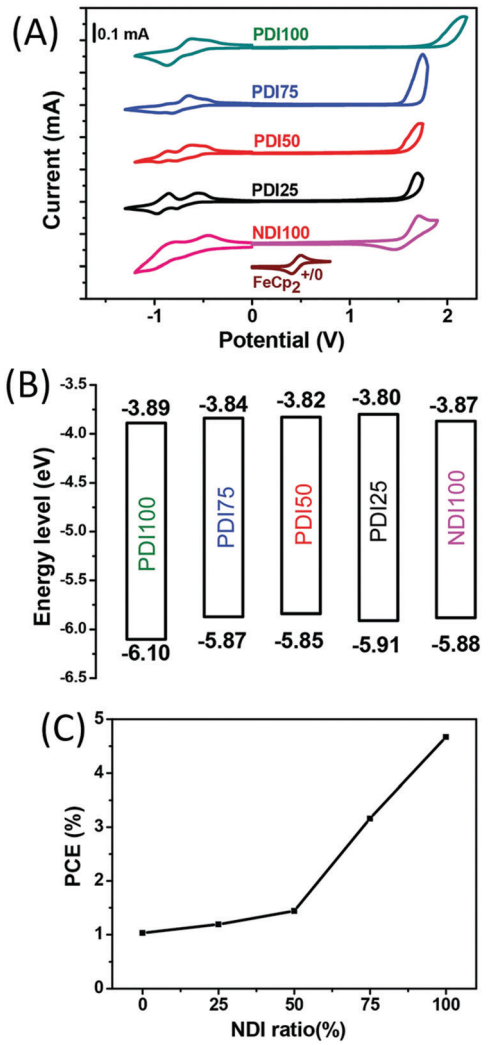

Fig. 101 (A) Cyclic voltammograms, (B) energy alignment, and (C) PCE *vs.* NDI feed ratio for (**454**, x = 1, 0.75, 0.5, 0.25) and (**322**).[315] This figure has been adapted from ref. 315 with permission from John Wiley and Sons, copyright 2016.

chemistry and Marcus theory (Fig. 102). The results indicate that the incorporation of DCRD as the acceptor unit into D–A–D type oligomers has been shown to make them promising candidates for high efficiency acceptor materials for OSCs.

There has been much development to use donor–acceptor, donor–acceptor–donor, and acceptor–acceptor–acceptor polymer systems for solar cell applications, and all the structures

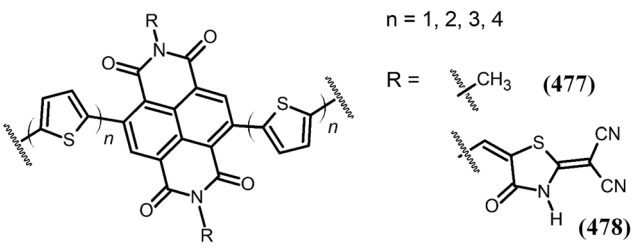

Fig. 102 The chemical structure of oligothiophene–NDI molecules.[319]

are illustrated in Fig. 103, 105, and 106, respectively. To provide details, Tao and co-workers[320] reported a series of A–D_1–A–D_2 type random terpolymer acceptors (**479**) (x = 0, 0.05, 0.10 or 0.20) which were designed by introducing 2D benzodithiophene (BDT) monomers into the N2200 backbone. The average PCSs of 5.80%, 2.81% and 1.41% obtained for the (**479**) at x = 0.10 devices were higher than 5.16%, 2.81% and 1.41% for devices containing the N2200 (**322**) acceptor when using PBDB-T, PTB7-Th and PDCBT as polymer donors, respectively.

Neher and co-workers[323] combined experimental and theoretical approaches to explain the intimate mechanisms in the polythiophene-based donor and rylene diimide-based acceptor polymers (**322**) using density functional theory (DFT). The results point to the roles that geometric deformations and direct-contact intermolecular polarization play in establishing a driving force (energy gradient) for the optoelectronic processes taking place at the interface. Li and co-workers[324] reported two conjugated D–A copolymers (**330**) and (**331**) consisting of NDI acceptor units and thienylene–vinylene–thienylene or furanylene–vinylene–furanylene donor moieties, respectively. PCEs of 6.43% and 5.21% in the case of (**330**) and (**331**), respectively, were recorded. Zhou and co-workers[10b] performed a systematic investigation of the comparative properties of PDI, NDI, and naphthodithiophene diimide (NDTI) molecules with the same alkyl chains and with the dithienothiophene (DTT) unit, resulting in the NDI based compounds (**467**) and (**468**). When these compounds were combined with BDDT to fabricate solar cell devices, they exhibited power conversion efficiencies of 3.49, 2.50, and 5.57% in the case of the PDI based polymer, (**467**) and (**468**), respectively. Zhou and co-workers[321a] synthesized three rylene diimide-based polymers of (**480**) and PDI homologues. PTB7-Th was utilized as the p-type polymer to fabricate photovoltaic devices with the three polymer acceptors. The PTB7-Th:fused PDI acceptor combination realized a PCE of 5.65% in optimized conditions, which was higher than that of the PDI based acceptor (3.74%) and (**480**) based device (0.88%). They have also investigated the effect of symmetry of the copolymerized unit on the properties of NDI based photovoltaic polymers by synthesizing three n-type semiconductor polymers (**481–483**). The (**482**) based all-PSC obtained the highest PCE of 5.99% with PBDB-T as the donor polymer.[325] Wang and co-workers[321b] addressed the low fill factor (normally < 0.65) problem associated with all-PSCs. They synthesized a series of NDI–bithiophene–thiophene random polymers (**484**). The polymer (**484**) with x = 0.1 showed optimal miscibility with the donor PTB7-Th and balanced hole and electron mobility in the blend, which lead to the best performance with a PCE of 7.6% and a FF of 0.71 for the solar cell with a device area of 16 mm^2. Chochos and co-workers,[314] by tuning the reaction and purification conditions of palladium-catalyzed Stille cross-coupling polycondensation, synthesized a new solution processable n-type all conjugated polymer network (**476**). Conventional and inverted BHJ solar cells exhibited PCEs of 0.3% and 1.2%, respectively, when (**476**) was employed as the electron acceptor with PTB7-Th as the electron donor. Li and co-workers[321c] also

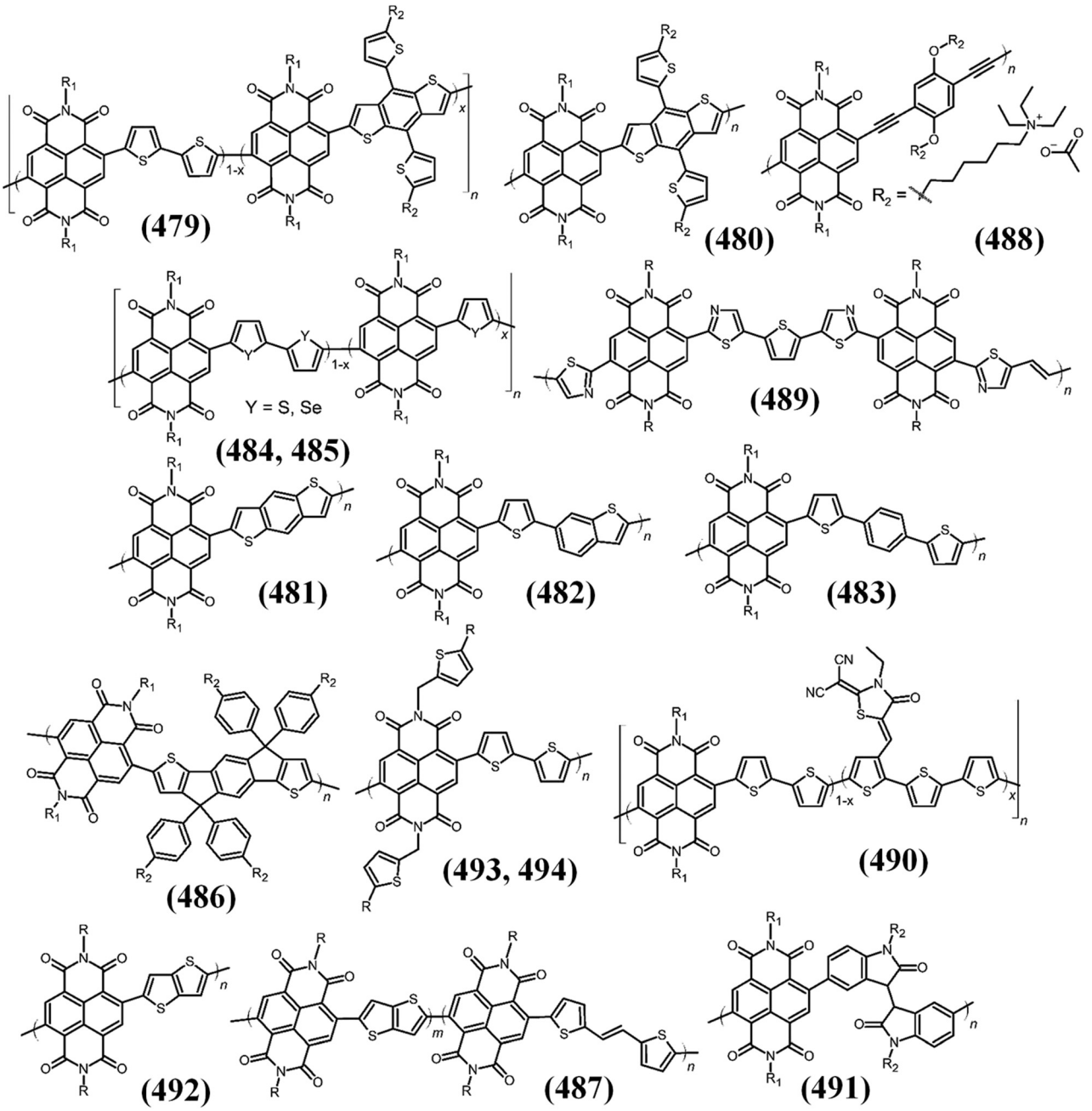

Fig. 103 The structures are of n-type NDI linked with benzodithiophene or biselenophene/selenophene,[240f,320,321] **305**[11] poly(NDI–acetylene–diisoquinoline), having very good solubility in water/alcohol mixture.[322]

reported the synthesis of a novel acceptor polymer (**486**) consisting of indacenodithienothiophene (IDT) and NDI units. This polymer exhibited PCEs of 3.63%, 4.12% and 5.33% when using PTB7-Th, J50 and J51, respectively, as donors, which was attributed to the complementary absorption behaviour of the donor and acceptor polymers (Fig. 104).

In a different approach to optimizing OSC performance, Wang and co-workers[326] investigated the influence of thermal annealing processes on the photovoltaic parameters by using a quinoxaline–thiophene donor (TQ1) and an NDI acceptor polymer (**322**). The power conversion efficiency doubled upon annealing compared to non-annealed devices as a result of higher short-circuit current (J_{sc}) and fill factor (FF), and a lower open circuit voltage (V_{oc}) which was attributed to the improved charge transport and bulk heterojunction characteristics. Chen and co-workers[321d] reported a copolymer (**487**) consisting of NDI as the acceptor and randomly distributed thieno[3,2-*b*]-thiophene (TT) and thienylene–vinylene–thienylene (TVT) as donor units. The organic solar cell device fabricated using a blend of PTB7-Th and (**487**) demonstrated a high power conversion efficiency of 4.86%. The same research group further extended their work[327] and studied the effect of the TT-to-TVT

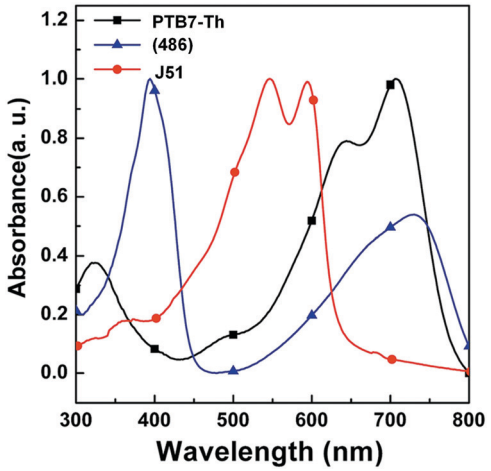

Fig. 104 Film absorption spectra of the polymer acceptor (**486**) and polymer donors (PTB7-Th and J51).[321c] This figure has been adapted from ref. 321*c* with permission from The Royal Society of Chemistry, copyright 2016.

ratio on the absorption pattern, energy levels, charge transport characteristics, morphology and power performance. The solar cell device fabricated using blends of PTB7-Th and (**487**) (with 25% TT and 75% TVT, respectively) exhibited a high power conversion efficiency of 5.27%. McNeill and co-workers synthesized (Fig. 105)[328] and evaluated six NDI molecular acceptors for organic solar cells based on two chemical architectures: (i) star-shaped structures with a triarylamine core flanked by three NDI moieties (**495–497**) and (ii) a linear molecule composed of a bithiophene bridge between two NDI moieties (**498–500**) and the structures are illustrated in Fig. 105. Organic solar cells were fabricated with each acceptor, utilizing PTB7-Th as the donor material in inverted bulk-heterojunction devices. Nitrogen was observed to lower the solar cell performance of these acceptors by significantly reducing the short circuit current density (J_{SC}), while sulphur increased the J_{SC} and in the star configuration led to the highest PCE of 2.8%.

Kim and co-workers[329] enhanced the performance of all-PSCs using a crystalline small-molecule additive, 6,6′-dithiopheneisoindigo (DTI). The DTI additive in a blend of PTB7-Th donor and (**320**) acceptor enhanced the PCE of all-PSCs from 5.8 to 6.8%. They also demonstrated that DTI additive could be applied to other all-PSC systems (PTB7 Th:(**320**) (PCE: 5.90 → 6.81%), PTB7-Th:(**321**) (5.83 → 6.52%), PTB7 Th:(**322**) (5.75 → 6.30%), and PPDT2FBT:(**320**) (3.77 → 4.43%)) with different polymer donors and NDI-based polymer acceptors, where the efficiencies of all-PSCs were enhanced by 10–20%. Park and co-workers[330] designed an NDI-based polymer with the strongly electron withdrawing dicyanothiophene (**342**) as the electron transport layer (ETL) in place of the fullerene-based ETL in inverted perovskite solar cells (Pero-SCs). It is found that (**342**) not only improves the electron extraction ability but also prevents ambient condition interference by forming a hydrophobic ETL surface. The performance of devices based on (**342**) significantly outperforms those based on PCBM from 14.3 to 17.0%. Kim and co-workers[331] synthesised a series of NDI based small molecules (**501–503**), which facilitated π–π stacking interactions and/or hinder excessive aggregation and exhibited different morphological behaviors, such as miscibility or crystallinity, in bulk heterojunction blends, with 7,7′-(4,4-bis(2-ethylhexyl)-4*H*-silolo-[3,2-*b*:4,5-*b*′]dithiophene-2,6-diyl)bis(6-fluoro-4-(5′-hexyl-[2,2′-bithiophen]-5-yl)benzo[*c*] [1,2,5] thiadiazole) (DTS-F) electron donors (Fig. 106). The photovoltaic devices prepared with (**503**) gave the highest power conversion efficiency (PCE) of 3.01%, with an open-circuit voltage (V_{oc}) of 0.75 V, a short-circuit current density (J_{sc}) of 7.10 mA cm^{-2}, and a fill factor of 56.2% (Fig. 106).

Burn and co-workers[321e] synthesized an acceptor polymer (**489**) that comprised the A–A′–A structural motif (where the A′-unit is a naphthalene diimide, while the A groups are thiazoles). When employed as an electron-acceptor material in all-PSCs it was found that the BHJ devices had poorer efficiencies compared to the cells incorporating SD films when

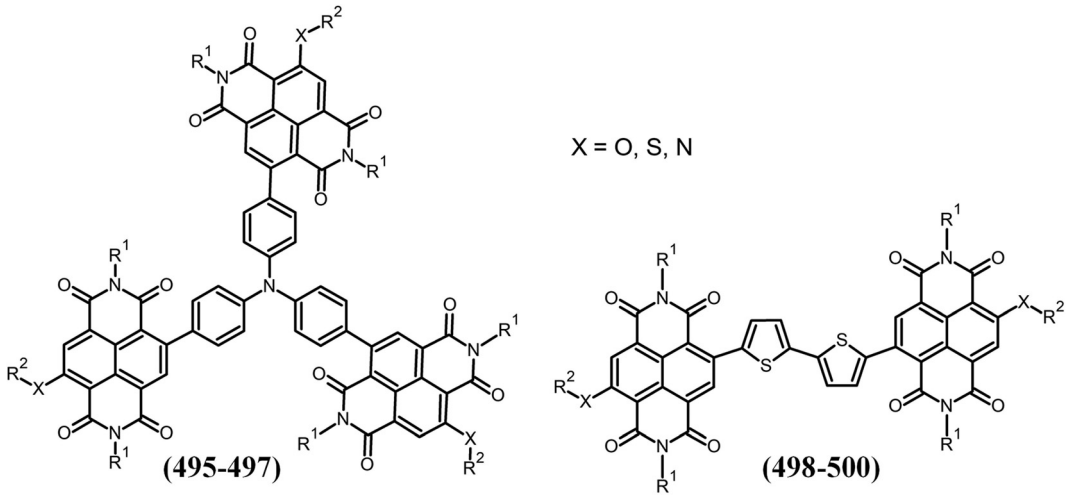

Fig. 105 Chemical structures of triarylamine–NDIs and bithiophene–NDIs.[328]

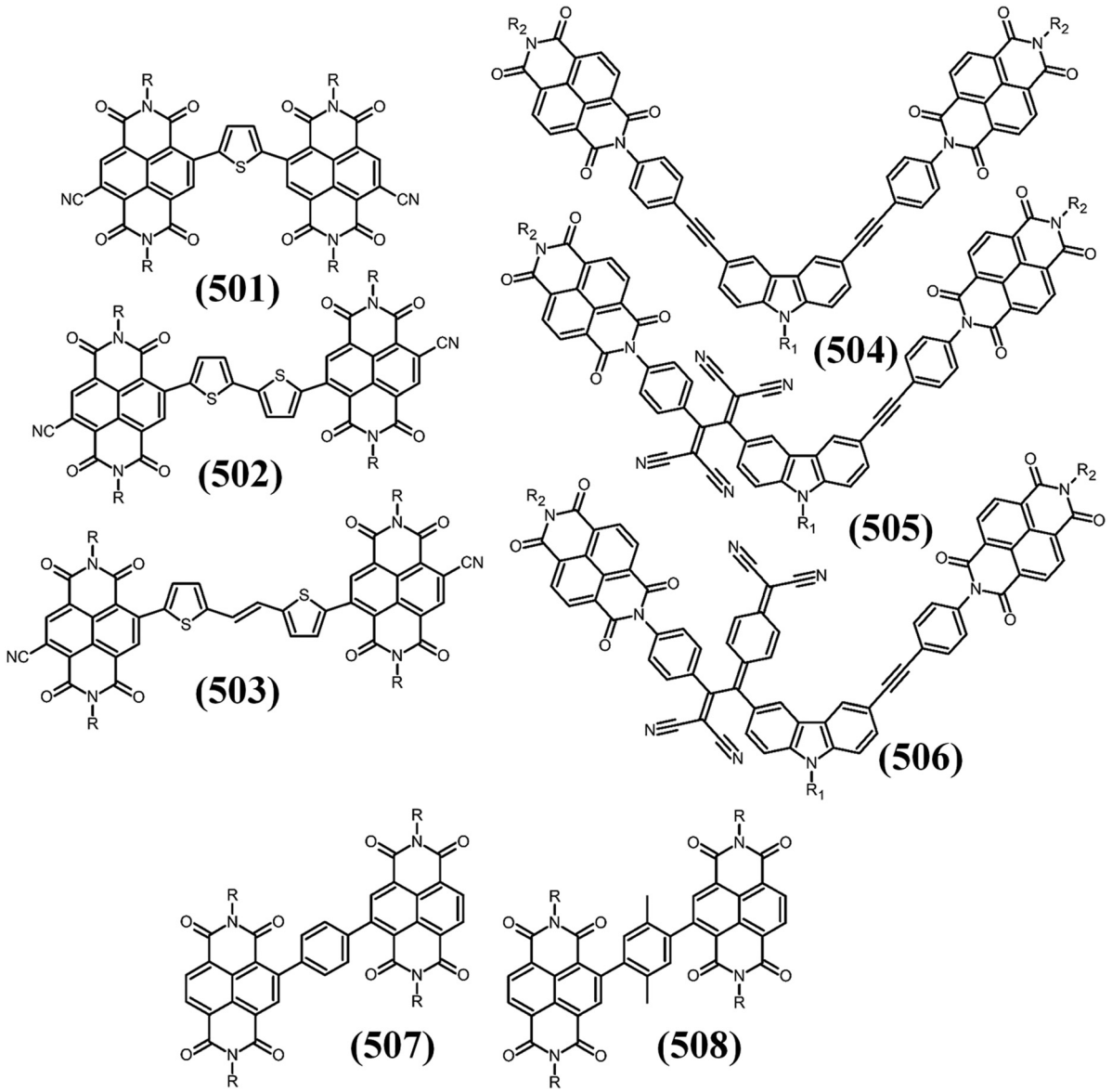

Fig. 106 The chemical structure of NDI–thiophene based small acceptor molecules (**499–501**),[331] V-shaped small molecule non-fullerene NDI based electron acceptors (**499–501**),[332] and NDI dimers with phenyl linkers (**499–501**).[333]

PBDTT-FTTE was used as the donor polymer. The best all-polymer SD device containing the ''high''-molecular weight material gave a PCE of 4.5%. Tan and co-workers[240u] using electron-deficient five-membered heterocycles, 1,3,4-oxadiazole (OZ) or 1,3,4-thiadiazole (TZ) moieties, prepared two A_1–D–A_2–D-type polymer acceptors containing naphthalene diimide, (**343**) and (**344**), for all-polymer solar cells. Employing (**343**) as the acceptor material and PTB7 as the donor material, the all-polymer solar cells based on PTB7/(**343**) (1 : 1, by weight) give the best power conversion efficiency of 2.58% with a short-circuit current density (J_{sc}) of 10.05 mA cm^2, an open-circuit voltage (V_{oc}) of 0.70 V, and a fill factor (FF) of 0.37 due to the formation of a well-optimized, bicontinuous network of the donor and acceptor polymer domains. Wang and co-workers[240o] synthesized an NDI based electron acceptor (**322**) consisting of the double N → B bridged bipyridine (BNBP) unit. A combination of the BNBP unit and selenophene unit (P-BNBP-Se) exhibited a lower LUMO energy of 0.16 eV (similar to that of commercially used PTB7-Th) compared to the two parent compounds. Thus, a high electron mobility of P-BNBP-Se (2.07×10^{-4} cm^2 V^{-1} s^{-1}) and a decent power conversion efficiency (4.26%) of the PTB7-Th:P-BNBP-Se device were recorded. A series of terpolymers, *i.e.* (**453**), were synthesized using NDI in conjugation with two thiophene and selenophene units by Kim and co-workers.[305] They observed an increase in the crystallinity and structural ordering of the terpolymers as a function of sulphur content, thus enhancing the electron mobility. These terpolymers along with a suitable donor demonstrated an increase in power conversion efficiency from 2.50 to 3.60% with the increase in S content. Jenekhe and co-workers[240p] fabricated polymer solar

cells using NDI-biselenophene with 2-octyldodecyl side chains (**324**) and blended with high molecular weight (M_n = 53.7 kDa) PBDB-T donor which lead to an excellent power conversion efficiency of 9.4%. The enhancement in photovoltaic performance was attributed to improved face-on molecular orientation, high electron mobility and balanced charge transport characteristics. Jenekhe and co-workers[321f] designed and synthesized new biselenophene/selenophene linked NDI based copolymer acceptors (**485**) (x = 0.1, 0.2, 0.5) which when combined with PBDB-T as the donor demonstrated a remarkable power conversion efficiency of 10.1% and an internal quantum efficiency of 97%. NDI based polymers with varying degrees of selenium substituents, namely NDI-Se, NDI-BiSe, and NDI-TriSe (**321**, **324**, **327**), were synthesized by Xin and co-workers.[240q] The seleno-polymers demonstrated good thermal stability, high crystallinity and appropriate energy levels similar to perovskites. When these polymers were used as electron transport layers (ETL) in p–i–n type perovskite solar cells, they exhibited a high efficiency of 14.0% in the case of the NDI-TriSe solar cell. Lee and co-workers[240r] demonstrated a small-molecule donor solar cell utilizing BDT2TR as a donor and (**322**) and $PC_{71}BM$ as acceptors. The BDT2TR:$PC_{71}BM$ device showed a high PCE of 8.20%, where the BDT2TR:(**322**) device showed excellent photovoltaic results with a PCE of 4.43%, a V_{OC} of 0.86, a J_{SC} of 7.26 mA cm^2, and a FF of 71%. Ma and co-workers[240s] extended the work on (**322**) both experimentally and theoretically, investigating the effect of tuning the molecular design of building blocks and modifying side chains of the acceptor polymer. Such modifications allowed tuning of the desired energy levels, solubility, crystallinity and coplanarity of the acceptor polymer which improved intermolecular packing in the heterojunction solar cell device, thus resulting in an excellent power conversion efficiency of 6.0%.

The low photocurrent density of most non-fullerene organic solar cells has been a limiting factor so far. In an attempt to address this challenge Wang and co-workers[247c] strategized to increase the dielectric constants (ε_r) of polymer:polymer blends, so that the binding energy of excitons can be reduced and their dissociation efficiency can be increased. To achieve this, they synthesized five fluorinated NDI-based acceptor polymers by varying the fluorine content of these polymers (**405–407**). This led to an increase in the ε_r resulting in an improved photocurrent of 14.7 mA cm^2 and a high power conversion efficiency (PCE) of 7.3% in a PTB7-Th:(**406**, x = 0.1) organic solar cell device. Lee and co-workers[240v] utilised a dual-acceptor strategy to construct NDI based polymers by incorporating variable electron-affinity units, namely, 2,2′-(perfluoro-1,4-phenylene)dithiophene (TF) (**368**), benzothiodiazole (BT) (**340**) and fluorinated benzotriazole (FTAZ) (**408**), respectively, into the N2200 backbone. P1 possessed the largest bandgap affording the most complementary light absorption with PTB7-Th. The device based on PTB7-Th:(**368**) yielded a higher PCE of 3.24% than the other two polymer based devices (2.99% for (**340**) and 1.52% for (**408**)).

The effect of fluorination was further studied by McNeill and co-workers[247d] by combining NDI- and thiophene-flanked phenyl copolymers. Depending on the number of fluorine atoms in the phenyl unit of the copolymers in the (**368**) set, which along with PTB7-Th resulted in an increase in PCE from 3.1 to 4.6% and an increase in short-circuit current from 7.7 to 11.7 mA cm^{-2}. Xu and co-workers[247e] investigated the effect of the number of fluorine atoms on the donor portion of the NDI based donor–acceptor conjugated (**368**) polymer set for use in all-polymer organic solar cells. Compared with a non-fluorinated polymer (1.31%), the monofluorinated polymer (2.35%) and the difluorinated polymer (2.44%) showed higher PSC performance. The synthesis of two difluorobenzene containing NDI polymers (**368**), *i.e.* one regio-random and one regio-regular, was demonstrated by Ong and co-workers.[247f] When bulk heterojunction solar cell devices were fabricated based on these two polymers, the regio-regular one exhibited a higher power conversion efficiency of over 5% compared to the regio-random one (**368**) due to improved crystallinity and greater absorption and electron mobility of the material. A slightly different approach focussing on improving the intermolecular interactions within NDI based polymers was undertaken by Park and co-workers.[247g] A fluorinated copolymer of NDI and (*E*)-1,2-bis(3-fluorothiophen-2-yl)ethene (**352**) was utilized, which exhibited lower crystallinity, greater electron mobility and improved mechanical resilience compared to nonfluorinated (**330**). The (**352**) based solar cell devices exhibited excellent power conversion efficiencies of 5.11–7.14%. Kim and co-workers[240a] developed a series of random copolymer donors possessing complementary light absorption with the naphthalene diimide-based polymer acceptor (**322**) for highly efficient all-PSCs. By controlling the molar ratio of the electron-rich benzodithiophene (BDTT) and electron-deficient fluorinated-thienothiophene (TT-F) units, a series of polymer donors with BDTT : TT-F ratios of 1 : 1 (P1), 3 : 1 (P2), 5 : 1 (P3), and 7 : 1 (P4) were prepared. Copolymer P1 was found to be the optimal polymer donor for fullerene-based solar cells due to its high absorption, whereas the highest power conversion efficiency of 6.81% is achieved for all-PSCs with P3, which has the most complementary light absorption with (**322**). Woo and co-workers[53] studied the photovoltaic and charge dynamic properties of all polymer solar cells consisting of (**322**) and (**405**, X = F). The (**322**) acceptor, when combined with PBDTTTPD as the donor polymer, exhibited a high power conversion efficiency of 6.09% (V_{OC} =1.00 V, J_{SC} = 11.68 mA cm^{-2}, and FF = 0.52) which is approximately 3 times greater than that of a similar device fabricated with (**322**). Thus, fluorination of NDI based polymers serves as a beneficial alternative to improve photovoltaic performance. McNeill and co-workers,[334] using direct arylation, synthesized NDI based acceptor polymers with molecular weights M_n varying from 20 to 167 kDa (**368**). The performance of PTB7-Th:(**368**) solar cells was found to improve with increasing (**368**) molecular weight. With variation of the molecular weight of the acceptor polymer for M_n = 22–167 kDa, an optimum level of phase separation is achieved, accompanied by an increase in charge mobility, balancing charge generation and charge separation.

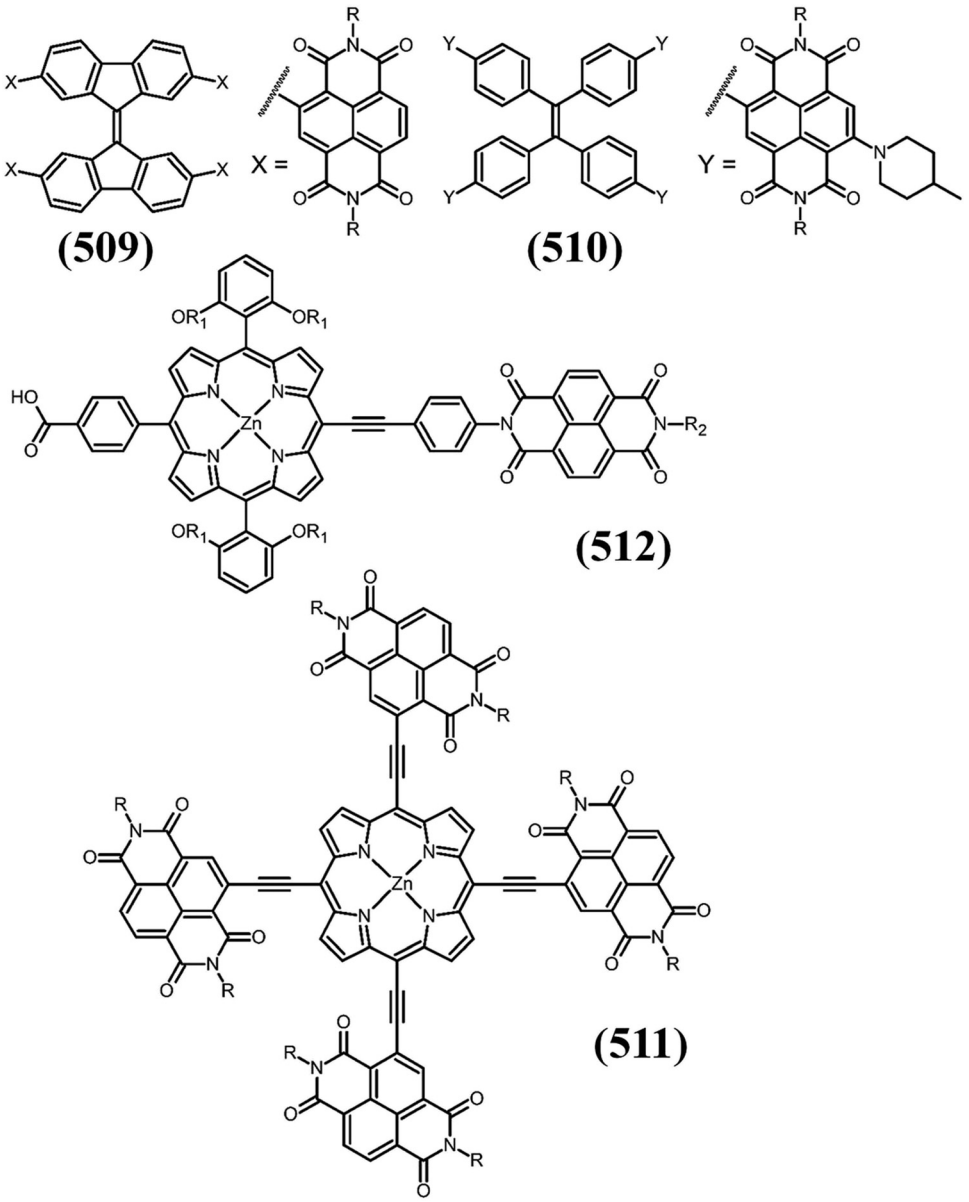

Fig. 107 The chemical structures of bifluorenylidene-NDI_4,[335] tetraphenylethylene-NDI_{4g},[336] the n-type porphyrin-NDI acceptor,[337] and control of electron transfer dynamics of push–pull porphyrin-NDI as sensitizers.[338]

Marder and co-workers[335] synthesized two 9,9′-bifluorenylidene (BF) core based non-fullerene acceptors (BF-PDI_4 and BF-NDI_4 (**509**)) by Suzuki coupling of 2,2′,7,7′-tetrakis (4,4,5,5-tetramethyl-1,3,2-dioxaborolan-2-yl)-BF with PDI-Br and NDI-Br, respectively (Fig. 107). The photovoltaic performance of BF-PDI_4 and BF-NDI_4 as acceptors was investigated by fabricating inverted solar cells with the structure: ITO/ZnO/active layer/MoO_3/Ag. Power conversion efficiencies of 3.64% and 2.28% were achieved using BF-PDI_4 and BF-NDI_4, respectively, as the acceptor in a blend with the polymer PTB7-Th as a donor.

The effect of side chain engineering in NDI was studied by Cao and co-workers[339] by performing side chain modifications of N2200 (**322**) to produce a series of NDI-based conjugated polymers (NOEx) (**513**) using Stille cross-coupling polymerization (Fig. 108). Branched alkyl chains of the NDI unit were replaced by linear oligoethylene oxide (OE) side chains. A PCE of 8.1% with a J_{sc} of 12.9 mA cm^2 and a high FF of 0.75 was obtained for the all-PSCs (PBDT-TAZ:**513** x = 0.1).

The side chain engineering of NDI based molecules and their effects on solar cell performance was further investigated by Chen and co-workers.[321g] They synthesized two novel NDI and 2.2′-bithiophene based polymers (**493** 2-hexyldecyl, **494** 2-octyldodecyl) and modified their electronic properties by inducing thiophene groups in the side chains which resulted in extended absorption from 350 nm to 900 nm compared to N2200 (**322**). The solar cell device of the configuration having ITO/PEDOT:PSS/PTB7-Th:acceptors/2,9-bis(3-

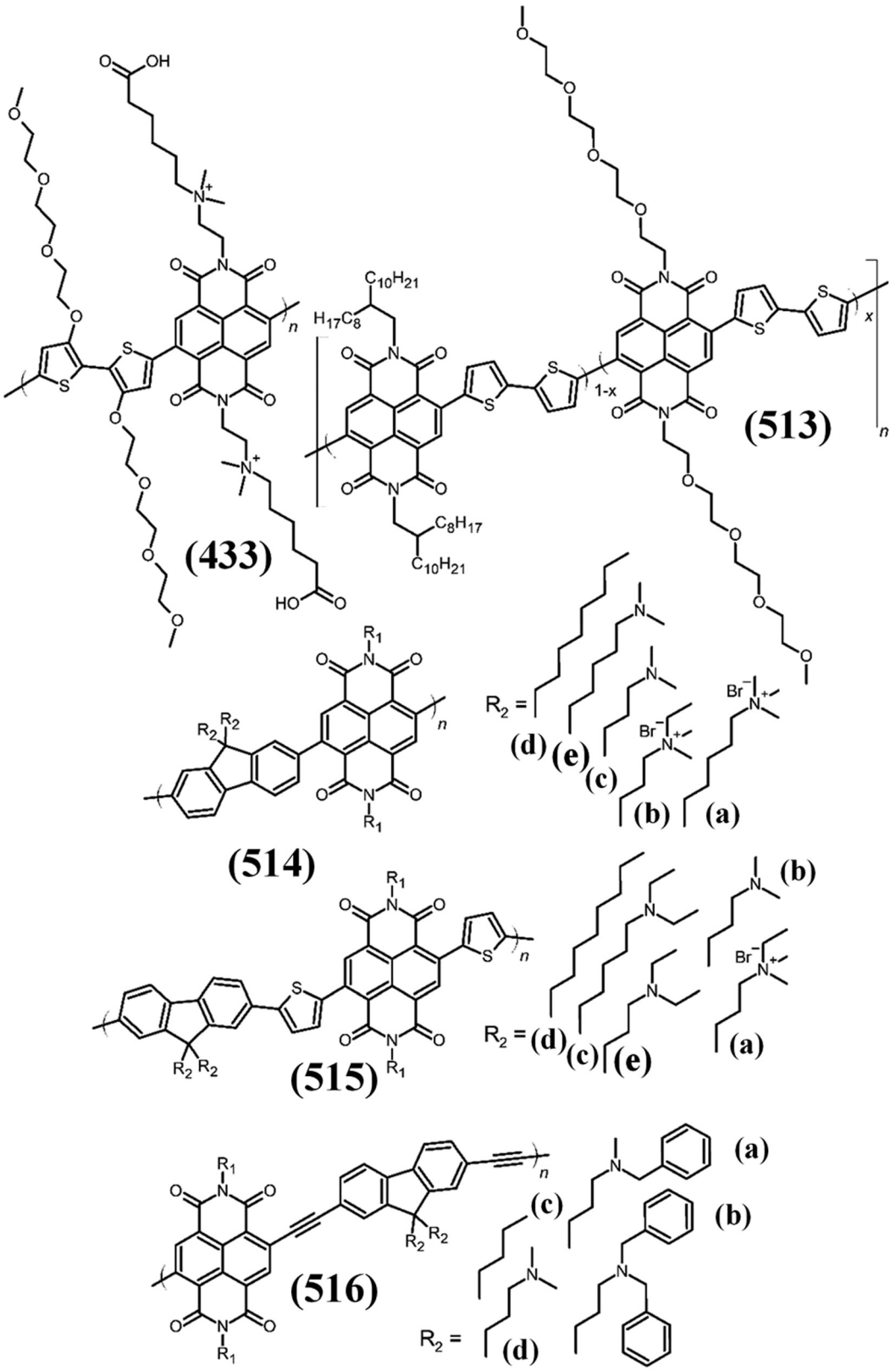

Fig. 108 NDI based polymers with PEG or hydrophobic moieties to control solubility; the chemical structure of the n-type donor–acceptor copolymer with zwitterion side chains on the acceptor units and TEG side chains on the donor units p(ZI-NDI-gT2) (**433**).[285] PEGylated NDI–dithiophene copolymer (**513**),[240f,339] fluorene–NDI,[340] fluorene–NDI–thiophene copolymers,[341] and fluorene–NDI–acetylene spacers.[340b]

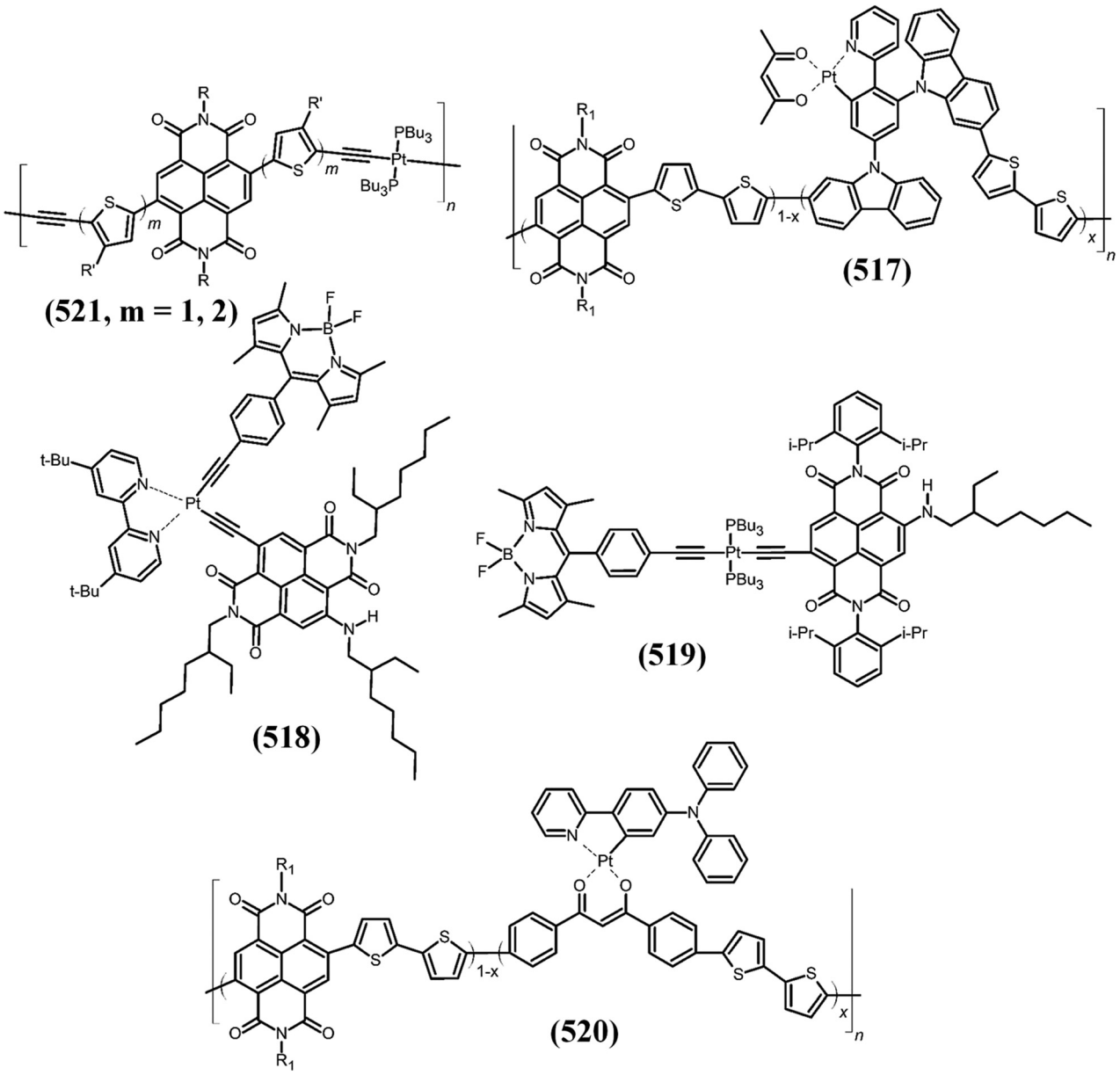

Fig. 109 The chemical structures of Pt(II) complex NDI compounds.[237,342–344]

(dimethylamino)propyl)-PDI (PDIN)/Al exhibited high power conversion efficiencies of 2.73 and 4.75% in the case of (**493**, **494**) based systems, respectively.

Li and co-workers[240b] also demonstrated an all-PSC by synthesizing an n-type conjugated copolymer (**408**) based on NDI and benzotriazole with thiophene π bridges. The (**408**) based all-PSC with wide-band-gap polymer PBDB-T as a donor could achieve a PCE of 6.49% with a high V_{oc} of 0.937 V.

The (**322**) acceptor was modified by incorporating several molar ratios of platinum complexes by Huang and co-workers.[342] Terpolymers (**517**) (x = 0.1, 0.2 and 0.5) demonstrated a partial increase in melting point, crystallization temperature, and HOMO–LUMO energies compared to (**322**). Upon blending with PTB7-Th the solar cell power conversion efficiency increased to 4.51% in the case of (**517**) in comparison to 3.24% in the case of (**322**). Kim and co-workers[343] reported Pt(II) bisacetylide and monoacetylide complexes (**518**, **519**) with heteroleptic acetylide ligands, namely boron-dipyrromethane (BDP) and NDI ligands. The complex (**518**) was examined as broadband light-excitable triplet photosensitizer for triplet–triplet annihilation (TTA) upconversion with an up-conversion quantum yield of 4.1% (Fig. 109).

The importance of having a non-planar conjugated acceptor molecule when designing organic non-fullerene solar cells was demonstrated by Hui Huang and co-workers.[240x] This was achieved by copolymerizing NDI with the non-planar unit triphenylamine (TPA) resulting in two different conjugated nonplanar polymers, namely (**349**; *N,N′*-OD) and (**349**; *N,N′*-HD). The solar

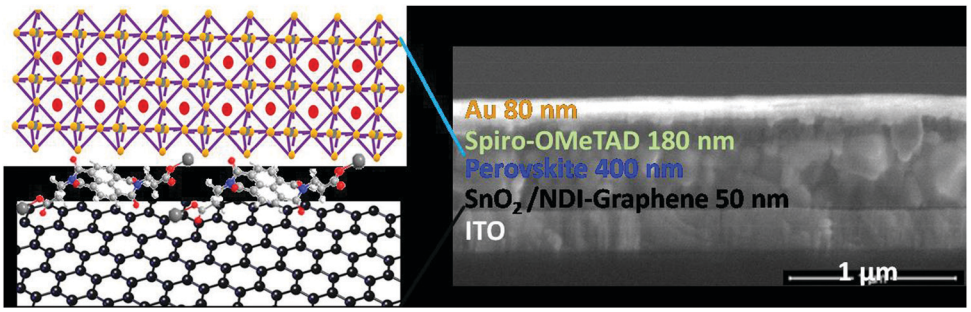

Fig. 110 Schematic architecture of planar perovskite solar cells. The expanded scheme shows the bonding of NDI-graphene with perovskite films in the cross-sectional SEM image of the deposited film on SnO_2–5% G substrates by the one-step spin-coating method.[345] This figure has been adapted from ref. 345 with permission from The American Chemical Society, copyright 2018.

cell device based on the PTB7-Th:(**349**; *N,N′*-HD) system exhibited the highest power conversion efficiency of 2.17%. An inverted polymer solar cell (PSC) consisting of a ZnO layer coated with cationic conjugated NDI based polymer (**514a**) was fabricated by Yoon and co-workers.[340a] The ZnO/(**514a**) surface exhibited uniformity and enhanced hydrophobicity causing a reduction in surface tension, induction of permanent interfacial dipole at the interface and a reduced work function. The inverted device (ITO/ZnO/(**514a**)/PTB7-Th:$PC_{71}BM$/MoO_3/Ag) exhibited slightly elevated V_{oc} values and significantly lower contact resistance with a significantly higher power conversion efficiency (8.65%) compared to bare ZnO films (7.99%). Doping of ZnO with NDI based derivates such as (**515a**) was carried out by Huang and co-workers[341a] to form a hybrid cathode interfacial layer (CIL). As a result of the enhanced conductivity of this organic–inorganic hybrid material, it could be used as a cathode material along with indium tin oxide electrodes. When used in inverted polymer solar cells (PSCs) the material exhibited a significant increase in power conversion efficiency (PCE) of 10.04%, along with improvements in the open circuit voltage, fill factor (FF) and short-circuit current density (J_{SC}). Wang and co-workers[345] synthesized an organic–inorganic hybrid by incorporating modified NDI-graphene onto SnO_2 (Fig. 110). This resulted in an increased surface hydrophobicity and formed van der Waals interactions across the interface between the surfactant and the organic–inorganic hybrid lead halide perovskite, resulting in a remarkable power conversion efficiency of 20.2% and an enhanced fill factor of 82%.

Furthermore, the same research group[313] synthesized two homologues of a star-like NDI based molecular structure, namely (**475**), by incorporating 1,3,5-trisphenyl-benzene branches into the linear (**322**) copolymer. Both homologues exhibited lower melting points and crystallization temperatures, and appreciable miscibility with the commonly used PTB7-Th copolymer. The polymer solar cells formed using PTB7-Th:(**475**) exhibited a high power conversion efficiency (6.87%) and an improved short-circuit current density. Jang and co-workers[337] developed a high-performance porphyrin-based electron acceptor (**511**) for OPVs by substitution of four NDI units at the perimeter of a Zn–porphyrin (P_{Zn}) core using an ethyne linkage. Effective π-conjugation between four NDI wings and the P_{Zn} core significantly broadened Q-band absorption to the near infrared region, thereby achieving a narrow band gap of 1.33 eV. Employing a windmill-structured tetra-NDI substituted P_{Zn}-based acceptor (**511**) and a mid-band gap polymer donor (PTB7-Th), the bulk heterojunction OPV devices achieved a PCE of 8.15% with an energy loss of 0.61 eV. Hammarström and co-workers[338] synthesized porphyrin dyes for use in p-type (NiO) dye sensitized solar cells. One porphyrin was designed with a significant charge transfer character in the excited state because of push–pull effects of the substituents, while another porphyrin had an appended NDI acceptor group. The creation of the push–pull dye ZnP-TPA-NO_2, with a TPA spacer between the porphyrin group and the NiO, led to no significant increase in charge separation lifetime or photovoltaic performance compared to ZnP_{ref}. It is conceivable that the dyes lie flat on the NiO surface, so that molecular control of the location of the excess electrons in the reduced state has no or only little effect. However, charge recombination is slower for (**512**) and the dye with an appended acceptor unit displayed a significantly better photovoltaic performance. Tsao and co-workers[240c] presented an integrated approach to achieve highly efficient and long-term stable methyl ammonium lead iodide ($MAPbI_3$) perovskite nanowire solar cells by combining a N-DPBI doped (**322**; *N,N′*-OD) polymeric film as the electron transport layer (ETL) with an atomic-layer-deposited Al_2O_3-based film as the encapsulation layer. Their results indicate that N-DPBI doping can not only improve the electron extraction capability by minimizing resistive losses, but also improve the surface coverage of the (**322**; *N,N′*-OD) ETL on the $MAPbI_3$ NW layer. With this n-doped ETL, a remarkable power conversion efficiency (PCE) of up to 18.83% was achieved. Im and co-workers[346] reported highly efficient and thermally stable inverted $CH_3NH_3PbI_3$ ($MAPbI_3$) and $HC(NH_2)_2PbI_{3-x}Br_x$ ($FAPbI_{3-x}Br_x$) perovskite planar solar cells demonstrated by using an *N,N′*-bis(phenylmethyl)-NDI (**522**) based electron transport material (ETM) instead of a conventional fullerene-based phenyl-C_{61}-butyric acid methyl ester (PCBM) (**524**) ETM. The $MAPbI_3$ and $FAPbI_{3-x}Br_x$ devices with the (**522**) based ETM exhibited 18.4% and 19.6% power conversion efficiencies under an illumination of 1 sun (100 mW cm^{-2}), respectively, which are comparable to the efficiencies of (**524**) ETM-based

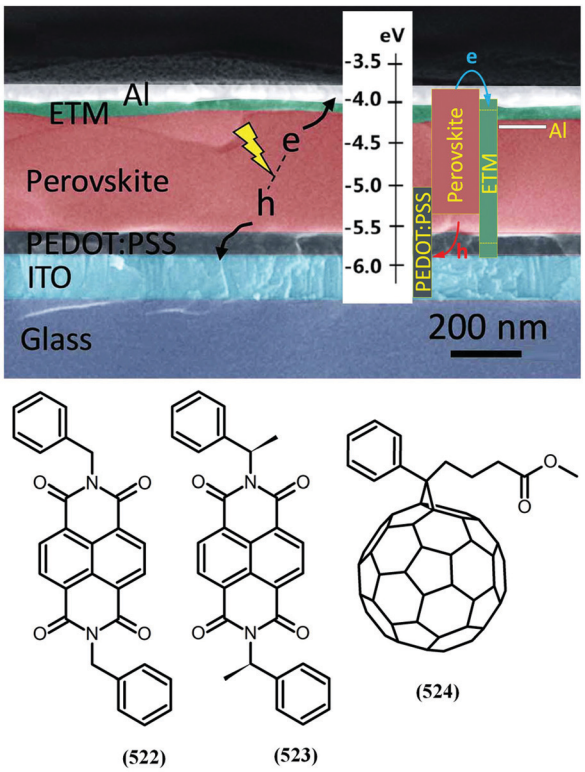

Fig. 111 SEM cross-sectional images of an inverted perovskite solar cell and chemical structures of PCBM (**524**) and *N*,*N*′-bis(phenylmethyl)-NDI (**522**)[346] or *N*,*N*′-bis(*R*)-1-phenylethyl-NDI (**523**)[347] in the ETM layer. This figure has been adapted from ref. 347 with permission from The Royal Society of Chemistry, copyright 2019.

examples (18.9% and 20.0%). The improved thermal stability of NDI-based perovskite solar cells is attributed to much stronger hydrogen bonds in the (**522**) molecular crystals than those in the (**524**) crystals. Kwon and co-workers[347] demonstrated a design strategy wherein homochiral asymmetric-shaped groups were incorporated into electron-transport materials for non-fullerene based perovskite solar cells (PSCs). They synthesized *N*,*N*′-bis[(*R*)-1-phenylethyl]-NDI (NDI-PhE) (**523**) which exhibited good film characteristics and a high power conversion efficiency of up to 20.5%, which is higher than that of the commercial PCBM (**524**) material (Fig. 111). This excellent PSC performance was attributed to the high quality film-forming ability and multi-dimensional isotropic electron transport capability of (**523**).

Jen and co-workers[240d] demonstrated the synthesis and utilization of the (**322**; *N*,*N*′-OD) polymer as an electron-transport layer inverted perovskite solar cell which exhibited a very high power conversion efficiency of 16.8%. This was achieved by modifying (**322**) with PFN-Ox. This device also exhibited good stability even under high humidity conditions. Huang and co-workers[348] synthesized a novel, water/alcohol soluble, NDI functionalized pyridinium salt, *N*,*N*′-bis(1-*n*-hexylpyridinium-4-ylmethyl)-NDI (**525**). This polymer exhibited a high band gap (2.95 eV) and an enhanced electron mobility (7.1×10^{-5} cm^2 V^{-1} s^{-1}) with a LUMO energy level of 4.07 eV. When (**525**) was used as an interface layer and in solar cell devices based on ITO/NiO_x/perovskite/$PC_{61}BM$/(**525**)/Ag device structures, it resulted in a decrease of the cathode work function, thus significantly enhancing solar power conversion efficiency to a value of 17.27% (Fig. 112). While several organic materials have demonstrated their capability for application in organic solar cells as cathode interlayers (CILs), most of them do not allow processing *via* printing techniques, which affects the large-scale production process. Hou and co-workers[349] synthesized the NDI-based compound (*N*,*N*′-dimethylamino) propyl-NDI (**526**) as an easily printable CIL (**526**) which exhibited good film-forming ability along with high crystallinity, enhancing semiconductor electron-transport properties and facilitating processability. Furthermore, a device constructed based on (**526**) and PBDB-T-2F:IT-4F demonstrated a high power conversion efficiency of 13.9%, thus opening new possibilities for designing low cost and efficient organic solar cells.

An interesting work worth mentioning here is by Huang and co-workers, [341b] as they synthesized two novel NDI-based (**515a and b**), self-doped, water/alcohol-soluble conjugated polymers (WSCPs) as highly efficient electron transport layers (ETLs) for high-performance solar cells. The amino groups at the side chain induced self-doping in WSCPs, which resulted in remarkable PCEs of 9.7% and 10.11% in the case of PTB7-Th/PC_{71}BM and PffBT4T-2OD/PC_{71}BM, respectively. Wang and co-workers[351] synthesized four [1]benzoselenopheno[3,2-*b*][1]benzoselenophene (BSBS) derivatives and three [1]benzothieno[3,2-*b*]benzothiophene (BTBT) derivatives and studied the influence of the alkyl side-chains on the packing of NDI derivatives and their effect on the electronic structures. Cao and co-workers[340b] synthesized a series of NDI based n-type conjugated polymers (**516a–d**) with amino-functionalized side groups and backbones and used them as cathode interlayers (CILs) in polymer and perovskite solar cells. The chemical variations of the amine side groups, from dimethylamino to *N*-methylbenzylamino and then to dibenzylamino, led to a decrease in the electron-donating properties and an increase in steric hindrance. When used as CILs, high power conversion efficiencies (PCEs) of 10.1% and 15.2%, respectively, were achieved in polymer and perovskite solar cells. Cao and co-workers[341c] further synthesized an amino-functionalized copolymer with a conjugated backbone composed of fluorene, NDI, and thiophene spacers (**515c–d**), introduced as an alternative electron transport layer (ETL) to replace the commonly used (**524**) in the p–i–n planar-heterojunction organometal trihalide perovskite solar cells. With these dual functionalities, the resulting solar cells outperform those based on (**524**), with the PCE increased from 12.9% to 16.7% based on (**515c–d**). Minchinobu and co-workers[234] synthesized a series of new dual imide-functionalized derivative-based regioregular D–A_1–D–A_2 copolymers with different side chains (**337**, *N*,*N*′-decyltetradecyl, octadecyldodecyl, and hexyldecyl). These new polymers (**337**) showed strong electron affinities with deep lowest unoccupied molecular orbital (LUMO) levels down to −4.01 eV, indicating that they are promising electron transport materials. The (**337**) polymers were used as electron acceptors in all-PSCs. The

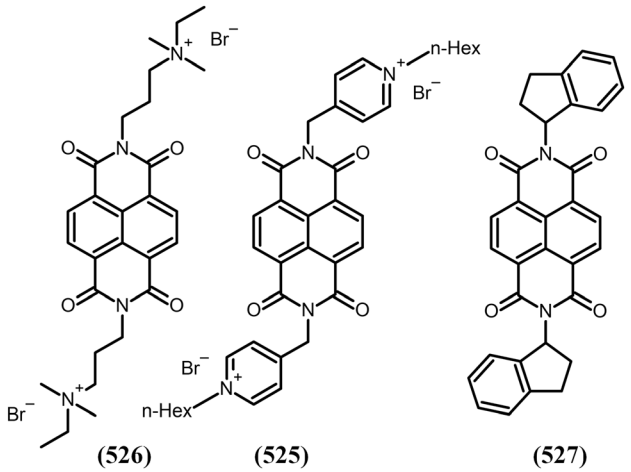

Fig. 112 The chemical structures of *N,N′*-bis(1-*n*-hexylpyridin-1-ium-4-ylmethyl)–NDI (**525**),[348] *N,N′*-dimethylamino propyl–NDI (**526**),[349] and *N,N′*-bis(1-indanyl) NDI (**527**).[350]

highest power conversion efficiency of 6.62% was obtained for the (**337**, *N,N′*-hexyldecyl) blend film due to its excellent short-circuit current (J_{sc}) value (12.07 mA cm^{-2}), which was much higher than that of the (**337**, *N,N′*-decyltetradecyl) and (**337**, *N,N′*-octadecyldodecyl) based all-PSCs (7.67 and 10.19 mA cm^{-2}, respectively). Liang and co-workers[352] studied the effect of substituent functional groups on the frontier molecular orbital energy levels and charge carrier properties of NDI using the CAM-B3LYP/6-31G(d) and TD-B3LYP/6-31+G(d,p) computational methods. By modifying the electron withdrawing or electron donating effect of the substituent groups (**528**) the electron transfer properties could be enhanced, thus assisting in designing efficient acceptors for organic solar cell applications (Fig. 113).

An NDI based polymer consisting of (*E*)-2,3-bis(thiophen-2-yl)acrylonitrile (CNTVT) and NDI (**347**) was synthesized by Zhan and co-workers[240e] *via* a Stille coupling copolymerization process and utilized in organic solar cells (OSCs). Broad absorption around 300–850 nm was observed along with the LUMO and HOMO energy levels of −3.93 eV and −5.83 eV, respectively, for this polymer. The OSC device with PTB7-Th and NDI polymer

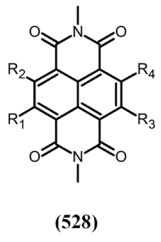

(528)

R_1 = CN	R_1 = C_6H_5
R_1 = R_2 = CN	R_1 = R_2 = C_6H_5
R_1 = R_3 = CN	R_1 = R_3 = C_6H_5
R_1 = R_4 = CN	R_1 = R_4 = C_6H_5
R_1 = OCH_3	R_1 = NO_2
R_1 = R_2 = OCH_3	R_1 = R_2 = NO_2
R_1 = R_3 = OCH_3	R_1 = R_3 = NO_2
R_1 = R_4 = OCH_3	R_1 = R_4 = NO_2
R_1 = CN, R_2 = OCH_3	R_1 = C_6H_5, R_2 = NO_2
R_1 = CN, R_3 = OCH_3	R_1 = C_6H_5, R_3 = NO_2
R_1 = CN, R_4 = OCH_3	R_1 = C_6H_5, R_4 = NO_2

Fig. 113 Chemical structures of core-substituted NDIs evaluated using TD-DFT.[352]

yielded a maximum conversion efficiency of 3.80%. Huang and co-workers[240t] synthesized acceptor molecules based on NDI and dicyanodistyrylbenzene units to give (**348**) with two different *N*-alkyl substitutions. In combination with the donor molecule PBDB-T, these acceptor molecules exhibited power conversion efficiencies of 4.26% for PDCB-NDI812 and 3.43% in the case of PDCB-NDI1014 which was attributed to the higher short-circuit current enhanced charge carrier mobility. Li and co-workers[240w] synthesized a novel copolymer NDI and 1,3,4-thiadiazole (TZ) (**343**). With PTB7-Th as the donor and (**343**) as the acceptor molecule, the device exhibited an appreciable power conversion efficiency of 4.35% and a high short-circuit current density of 13.26 mA cm^{-2}. Bhosale and co-workers[336] synthesized a novel tetraphenylethylene-functionalized non-fullerene electron acceptor (**510**), consisting of acceptor NDI units as terminal groups. This compound exhibited high solubility and thermal stability. A solar cell device constructed with W8 based on [D : A 1 : 1.2 = 5.26% (P3HT); 8.58% (PTB7)] exhibited a high power conversion efficiency of 8.5%. Furthermore, Bhosale and co-workers[301] combined NDI (**448–452**) with rhodanine or 1,3-indanedione functionalities at the terminal ends and synthesized two new electron acceptor compounds, coded as N3 and (**451**). These materials demonstrated good solubility, high thermal stability, and energy levels similar to poly(3-hexyl thiophene) (P3HT). The fabricated bulk heterojunction device (P3HT : (**449**) 1 : 1.2) exhibited a power conversion efficiency of 4.76%. Subsequently, Bhosale and co-workers[302] synthesized non-fullerene electron acceptors (**449**, **450**), composed of a central NDI and two different terminal accepting functionalities, malononitrile and 2-(4- nitrophenyl)acetonitrile, respectively. Both of the new materials (**449**, **450**) displayed high thermal stability and were found to have energy levels matching those of the archetypal electron donor poly(3-hexylthiophene). A simple, solution-processable bulk-heterojunction device afforded a promising power conversion efficiency of 2.24% when (**450**) was used as a non-fullerene electron acceptor along with the conventional donor polymer poly(3-hexylthiophene). In the meantime, dye sensitized solar cells were studied by Odobel and co-workers[353] by synthesizing four new diketopyrrolopyrrole (DPP) based sensitizers to be utilized in p-type dye-sensitized solar cells (p-DSSCs) (**529**, **530**) as shown in Fig. 114. The thienyl DPP core was substituted with thiophene carboxylic (Th) or a 4,4′-[(phenyl)-aza]dibenzoic acid as the anchoring group on one end and the NDI moiety on the other. The photovoltaic device performance revealed that the (**529**) dye is particularly efficient (J_{SC} = 7.38 mA cm^{-2}; V_{oc} = 147 mV; FF = 0.32; h = 0.35%) and exhibits activity even in the low energy region, *i.e.* around 700 nm.

Chen and co-workers[321h] incorporated a rhodanine-based dye molecule into the NDI-polymer (**490**) using a random copolymerization method. This resulted in an enhanced light absorption coefficient and up-shifting of the LUMO energy level, along with a decrease in crystallinity. The fabricated device exhibited an excellent power conversion efficiency of 8.13%. Three conjugated polymers consisting of isoindigo and NDI (**491**) and PDI were designed, and the effect of building blocks and alkyl chains on

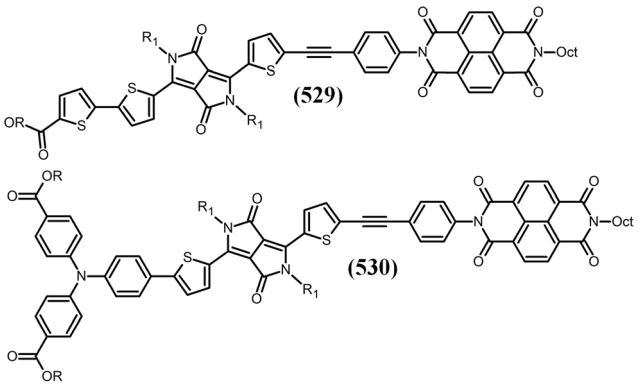

Fig. 114 The molecular structures of diketopyrrolopyrrole (DPP)-NDI based sensitizers for solar cells.[353]

photoresponse performance was studied by Huang and co-workers.[11] The best photovoltaic cell efficiency of 2.68% was reported. The effect of polarizability of NDI based electron acceptors on the device performance was studied by Luo and co-workers.[310] Copolymers of NDI with dithieno[3,2-*b*:20,30-*d*]silole (DTS) (**470**) and *N*-alkyl dithieno[3,2-*b*:20,3-*d*]pyrroles (DTP) (**469**) were synthesized. It was found that a decrease in dipole moment results in an increase in polarizability of the copolymer as a result of the change in the transient fluorescence lifetime, which influenced the power conversion efficiency of the solar cell. Guo and co-workers[240*f*] developed high-performance n-type terpolymers by the introduction of thienopyrroledione (TPD) into the copolymer f-BTI2-FT which resulted in a series of terpolymers (BTI2–*x*TPD) having distinct TPD contents. More importantly, TPD triggers noncovalent S···O interactions, increasing backbone planarity and in-chain charge transport. Such interactions also promote face-on polymer packing. As a result, all polymer solar cells (all-PSCs) based on BTI2–30TPD achieved an optimal power conversion efficiency (PCE) of 8.28% with a small energy loss (0.53 eV).

In the field of organic solar cells (OSCs), tandem structure devices have attractive advantages for improving power conversion efficiency (PCE). Cao and co-workers[341*d*] reported a method for achieving an environmentally friendly solvent processed polymeric ICL by adopting PNDIT-F3N (**515b**) blended with poly(ethyleneimine) (PEI) as the electron transport layer (ETL) and PEDOT:PSS as the hole transport layer. It was found that the modification ability of PNDIT-F3N (**515b**) on PEDOT can be linearly tuned by the incorporation of PEI, which offers the opportunity to study the charge recombination behavior in ICL. Finally, a tandem OSC with the highest PCE of 12.6% was achieved.

Sharma and co-workers[332] synthesized two simple semiconducting acceptor–acceptor$_1$–donor–acceptor (A–A$_1$–D–A) modular, small molecule non-fullerene electron acceptors, NDICz-5 (**505**) and NDICz-6 (**506**), for application in solution-processable bulk-heterojunction solar cells. The optoelectronic and photovoltaic properties of (**505**, **506**) were directly compared with those of a structural analogue, NDICz-4 (**504**), which was designed based on an A–D–A format. All of these new materials were designed to be V-shaped and comprised an electron rich carbazole donor core (D) together with an electron deficient NDI terminal core (A). It was observed that (**505**, **506**) exhibited superior properties, such as light-harvesting, enhanced photocurrent density and overall device performance, when compared with (**504**). Cao and co-workers[322] developed a series of tailor-made n-type water/alcohol soluble-conjugated polymers (n-WSCPs) (**488**) that comprise different conjugated backbones and pendant polar groups. The photoconductive properties of these n-WSCPs were found to correlate strongly with the electron affinities of the conjugated backbones and electron-donating strengths of the polar side chains in n-WSCPs. High performance PSCs (PCE $>10\%$ or $>9\%$) could be obtained when these n-WSCPs were used as ETMs or by using high mobility thick donor polymers and thick ETMs, respectively, indicating the potential ability to fabricate large-area PSCs using R2R processing. Choi and co-workers[333] designed NDI dimer-based electron acceptors with different linkers between NDI moieties (**507**, **508**) and investigated the influence of the linker structure on the device performance of non-fullerene OSCs. Introduction of a processing additive significantly increased the PCEs of both devices ((**508**): 2.08 → 3.11% and (**507**): 0.74 → 1.73%). The higher PCE for the device with (**508**) was attributed to weaker bimolecular recombination and an even surface morphology without large domains. In spite of the non-planar structure of (**508**), this resulted in excellent miscibility between PTB7-Th and (**508**) and high device performance. Kwon and co-workers[350] developed a non-fullerene electron transport material based on NDI-ID (**527**) for high-performance, low-temperature solution-processable PSCs showing both an unprecedented PCE of up to 20.2% and long-term stability. The new (**527**) consisting of an *N*-substituted indane group having simultaneous alicyclic and aromatic characteristics was synthesized by a low-cost, one-step reaction and a facile purification method. The partially flexible characteristics of an alicyclic cyclopentene group on indane groups open up the possibility of low temperature solution processing.

Li *et al.*[354] designed and synthesized rhodanine-bridged and core-extended NDIs. They demonstrated that the rhodanine moiety could act not only as a π-spacer to enlarge the molecular conjugated system, but also as an electron-donating unit to tune the molecular energy levels, to give electron mobilities in the range of 10^{-4}–10^{-3} cm^2 V^{-1} s^{-1}, and the inverted perovskite solar cells provided a power conversion efficiency value of 8.82%.

8 Aggregation-induced emission

In recent years fluorescent probes and bioprobes have received attention due to their significance in various fields such as sensing and environmental monitoring (chemosensing, biosensing, disease diagnosis) and solar cell (OLED, OFET) applications. NDIs and cNDIs have shared this attention; however, due to the planar structure of NDIs and cNDIs many derivatives show aggregation-caused quenching (ACQ) when they are aggregated or assembled, because of π–π interactions.[355] In

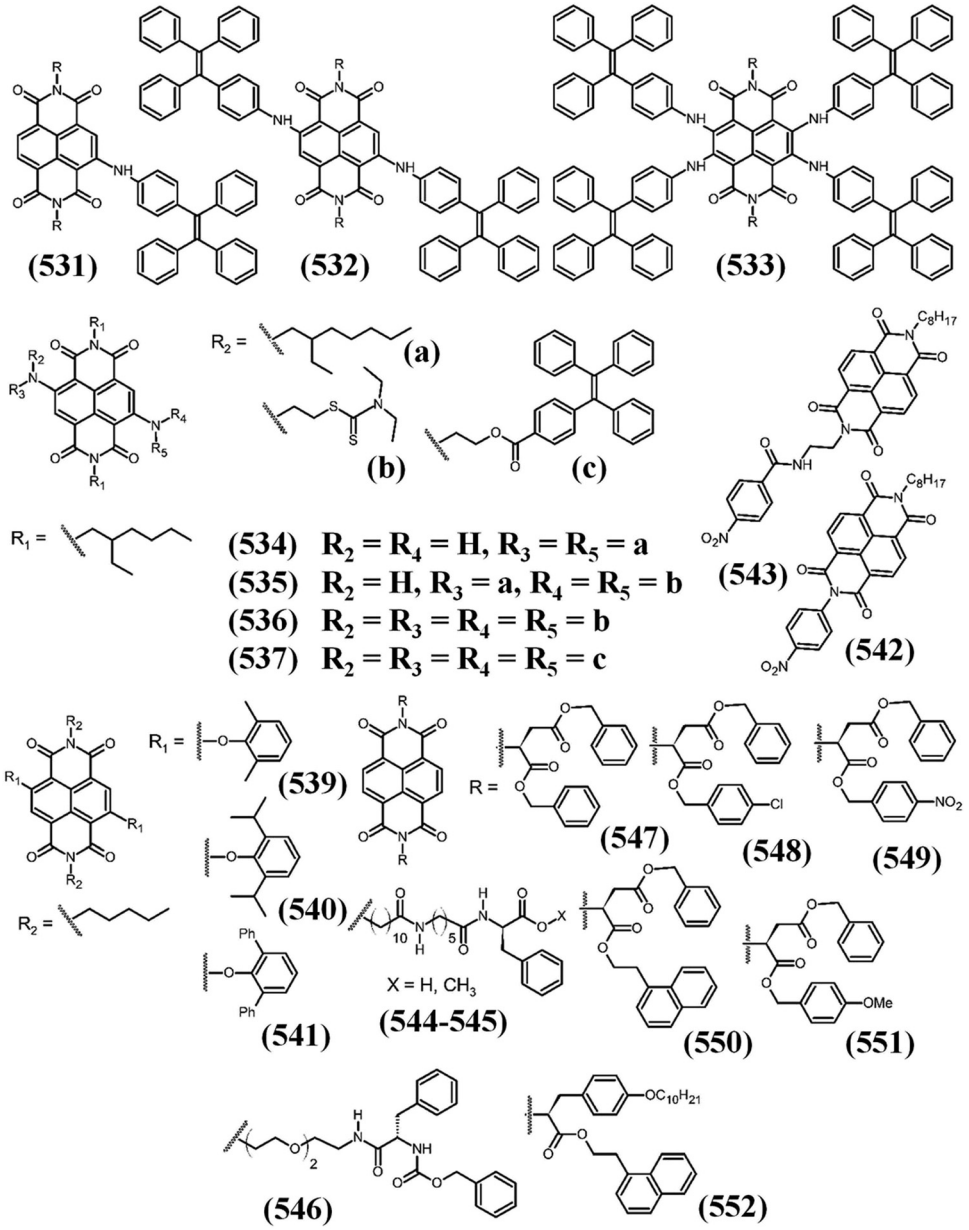

Fig. 115 The molecular structures of NDI derivatives with aggregation induced emission properties.[84,357–359]

2001, the Tang group[356] discovered a new concept – so called aggregation-induced emission (AIE) – in which non-emissive luminogens in solution are induced to emit by aggregate formation, and they outlined various derivatives which show AIE effects, with tetraphenylethylene (TPE) being highly fluorescent upon aggregation (AIE effect), and its various derivatives are illustrated in Fig. 115.

In this regard, we have reported that AIE activity could be imparted onto to non-AIE active NDI molecules by functionalisation with TPE on the core of NDI. We core-substitute NDI with one, two or four TPE molecules to produce 2-TPEcNDI (**531**), 2,6-DTTPEcNDI (**532**) and TTPEcNDI (**533**) by nucleophilic substitution reaction of BrNDI, Br_2NDI and Br_4NDI with amino-TPE, respectively.[357] Typically, all these derivatives were soluble in solvents such as $CHCl_3$, CH_2Cl_2 and THF; however, they precipitated in solvents such as hexane, MeOH and water. Thus, all three derivatives (**531–533**) in THF produced very weak or no emission in dilute/dissolved state in THF, giving an ~0.09 quantum fluorescence yield; however, in THF/water (1 : 9, v/v) self-assembled aggregates produced high fluorescence with quantum yields Φ_f of ~9%, 18% and 29%, respectively. Interestingly, these (**531–533**) derivatives were also highly fluorescent in good/poor solvent mixtures such as $CHCl_3$/hexane and gave comparable quantum yields. This was the first report to show functionalisation of NDI with TPE, not only to induce the AIE effect to the NDI, but also to produce controlled nanostructures such as hollow spheres, fibrils, and leaf like structures.

Later, Li and co-workers synthesised an NDI bearing flexible side chains as well as TPE to suppress the strong π–π interactions, which resulted in NDI derivatives transitioning from ACQ to AIE active in acetone/water with high quantum yields, where core-substitution of the NDI importantly did not disturb the original π system.[358a] In their design principle, they have functionalised the core of the NDI with primary, secondary or tertiary alkyl amines, yielding (**534**), (**535**) and (**536**), respectively. As expected, NDIs bearing secondary amines were highly fluorescent in acetone and quenched upon the addition of water, with decreasing fluorescence quantum yields (Fs) from 16.0% to 0.49% in water, a typical ACQ phenomenon. Similarly, (**535**) bearing two different amine substituents also showed an ACQ effect; however, (**536**) bearing tertiary amines as the substituents produced weak FL (quantum yield of 0.18%) in acetone, which increased to a 9 times higher quantum yield upon the addition of water (AIE activity). Similarly, an NDI functionalised with AIE active TPE produces (**537**), which also displayed induction of AIE activity to the NDI. Lin and co-workers synthesised a cNDI bearing 2,6-diphenoxy substituents having methyl (**539**), isopropyl (**540**) or phenyl (**541**) substituents at both the *ortho*-positions of the phenoxy substituent.[358b] Their findings demonstrated that slipped cofacial π–π stacking of NDI in solid state resulted in the AIE activity. In another study, we reported that the AIE activity of NDI is not only generated by core-substitution but also by functionalising the imide position with electron withdrawing groups. In this study, we synthesised two NDI derivatives (**542**, **543**), one bearing an aromatic NO_2 group at the imide position and another NDI bearing an aromatic NO_2 group with a diethyl spacer along with an amide linkage.[84] AIE activity was investigated by dissolving both the derivatives in $CHCl_3$ and gradually adding methylcyclohexane (MCH). In the titration (**542**) does not show any difference between the diluted and aggregated states. However, (**543**) produces weak emission (Φ_F = 1.3%) and upon the addition of 95% MCH it produces enhanced emission with a high Φ_F = 22.8%, which indicates that (**543**) is AIE active, and this could also be seen by the naked eye under UV light. AIE active (**543**), upon aggregation in $CHCl_3$/MCH (5 : 95, v/v), produced vesicular self-assembled nanostructures from bowl-like structures with an average diameter of 460 nm and a wall thickness of about 70 nm. Narayan and co-workers synthesized the NDI derivatives (**210**) and (**209**), amphiphiles bearing tethering acetylated and deacetylated β-D-glucopyranosides, respectively, *via* azide–alkyne click chemistry. The aggregation induced emission (AIE) properties were investigated by acetylation/deacetylation of the β-D-glucopyranoside unit.[120] Lin and co-workers described the AIE active ONT π-gel using bis-pyridine functionalised NDI (**262**) and functionalized trimeric amide (TCP) (**263**) *via* self-assembly. The gel displayed strong AIE at 468 nm and furthermore this ONT gel could detect and adsorb ferric (Fe^{3+}) or cupric (Cu^{2+}) ions from water as well as in a thin film.[173] Therefore, this study may have future potential for the practical application of AIE gels in multi-analyte detection.

Banerjee designed and synthesised novel NDI-appended peptides, *i.e.* HOOC-Phe-Acp-Und-NDI-Und-Acp-Phe-COOH (**544**, **545**), and studied their aggregation behaviour in water.[359a] Compound (**545**) displayed high yellow fluorescence in aqueous solution as well as solid state. Transmission electron microscopy (TEM) analysis revealed that cross-linked nanofibrillar nanostructures could be formed. Interestingly, (**545**) displayed non-emissive behaviour in basic medium and high emission under acidic conditions, meaning that it may be possible to use this type of derivative to erase and rewrite florescent color codes for verification in the aggregated state in aqueous medium.

Over the last three decades, fluorescence probes have been prepared from a range of materials and their AIE behaviour can be exploited to this end. Das and co-workers synthesised an *N*-substituted, NDI-based, carboxybenzyl-protected, L-phenylalanine-appended bolaamphiphile (**546**) and studied its aggregation. They found that, when the bolaamphiphile (**546**) was dissolved in DMSO–water (1 : 99, v/v) solvent mixtures, spherical organic nanoparticles (ONPs) formed due to self-assembly through π–π stacking, and these NPs were fluorescent through AIE activity, with green-emission of FONPs due to excimer formation in solution as well as in the solid phase.[359b] Furthermore, they have used these green-emitting FONPs (**547–551**) for bioimaging of anticancer drugs inside mammalian cells. In an extension of their work, they synthesised an NDI bearing L-aspartic acid amphiphilic molecules having a benzyl ester group at both terminals with varying substituents.[359c] In this study they revealed that the FONP properties can be tuned with electron-withdrawing groups (EWG) such as nitrobenzene and electron-donating groups (EDG), such as methoxybenzene and naphthalene. All these NDI derivatives were well soluble in dimethyl sulfoxide (DMSO), and upon addition of water J-type aggregation produced FONPs at f_w = 99% in DMSO. All of the derivatives demonstrated AIE activity through excimer formation. Importantly, the emission color of these novel AIE-gens (**548–551**) was tunable from cyan blue, to faint green, to strong green, and finally to bright orange. They used these multicolor-emitting FONPs for bioimaging applications. In another report, they synthesised NDI derivatives appended with L-tyrosine-tagged hydrophobically (**552**) and prepared FONPs in tetrahydrofuran (THF)/water (30/70, v/v) solvent mixtures *via* excimer formation in combination with intramolecular charge transfer (λ_{ex} = 350 nm), yielding orange emissive FONPs[359d] which were used for long-term bioimaging of mammalian cells.

9 NDI based polymers

9.1 NDI based polymers in solar cells

In the last two decades, polymer solar cells have attracted attention due to their potential commercial implementation, mostly because of their unique advantages such as light weight and flexibility. Polymer solar cells are based on p-type conjugated polymer donors and n-type polymer acceptors. Both the polymer donor and polymer acceptor materials have characteristic complementary absorption spectra which can be tuned

accordingly through the molecular energy levels, and require favourable characteristics such as effective charge transfer, good miscibility and thermal stability.[313]

Amongst polymer bearing acceptor units, NDI based polymer acceptors have been used extensively to fabricate polymer solar cells due to their absorption from the visible to near IR region, electron mobility, and thermal stability.[240x] The NDI based polymer acceptor is combined with the polymer donor in the active layer of all-polymer solar cells. Earlier, we[83] and others have reviewed NDI molecules in solar cells in some detail. In this section, we will illustrate recent developments in the field of NDI based polymer acceptors. Yoon and co-workers synthesized electron accepting NDI derivatives containing cationic conjugated polyelectrolytes such as (**514a**) for inverted polymer solar cells (PSCs). This PFTNDI (**514a**) was shown to improve the surface properties of the ZnO layer such as uniformity and hydrophobicity, as well as electron transport properties in inverted PSCs, which leads to a lower surface tension. The permanent dipole moment at the interface of ZnO and PFTNDI (**514a**) is mainly due to the interaction of the trimethyl ammonium bromide salt in PFTNDI and the hydrophilic ZnO surface, which results in a reduced work function of the ZnO layer. To investigate the photovoltaic performance, the inverted device with the configuration of ITO/ZnO/(**514a**)/PTB7-Th:$PC_{71}BM$/MoO_3/Ag was fabricated. The shifting of the vacuum level and reduced work function of the ZnO film led to an increased V_{OC} value, and along with the reduced surface tension the PFTNDI-treated devices exhibited a PCE of 8.65%, higher than that for the plain ZnO based device (7.99%). These results suggested that the NDI-incorporated polyelectrolytes act as an interfacial modifier for the enhanced performance of the inverted polymer solar cells, and after treatment with PFTNDI the 7.99% PCE was enhanced to 8.65%.[340a] In another report the Cao group functionalized the NDI based linear polymer N2200 (**322**) to a star like n-type conjugated homologue polymer (**475**) by incorporating 1,3,5-trisphenyl-benzene as the branched unit. The functionalized (**475**) homologues exhibited comparable energy levels and optical properties to (**322**) but with a decreased crystallization temperature due to reduced rigidity of the molecular backbone. The (**475**) homologues were miscible with the commercially available donor polymer PTB7-Th, and all-PSCs were fabricated using PTB7-Th:(**475**) in the active layer. The device based on PTB7-Th:(**475**, 1% starting component) using chlorobenzene as a processing solvent with 0.3 vol% DBE and 0.2 vol% DIO as additives displayed an excellent PCE of 6.87%, higher than the 5.75% PCE of the (**322**) based device, which was mainly due to the formation of a more favourable film morphology, greater electron mobility and reduced molecular recombination. In contrast, the PTB7-Th:(**475**, 2% starting component) based device exhibited a PCE of 6.07%, lower than that of the (**475**) based device because of higher exciton dissociation.[313] The same group has described two n-type conjugated polymer acceptors for all-PSCs based on dicyanodistyrylbenzene (DCB) and NDI units (**348**). The electrochemical and optoelectronic properties of the (**348**) polymer acceptors were investigated along with thermal properties, charge carrier mobility and morphology. The photovoltaic performance of the all-PSCs was investigated using the medium band gap polymer donor poly[(2,6-(4,8-bis(5-(2-ethylhexyl)-thiophen-2-yl)benzo[1,2-*b*:4,5-*b*′]dithiophene)-co-(1,3-di(5-thiophene-2-yl)-5,7-bis(2-ethylhexyl)benzo[1,2-*c*:4,5-*c*′]dithiophene-4,8-dione)] (PBDB-T). By integrating the polymer acceptors and the PBDB-T donor polymer as a photoactive layer, the (**348**) based devices showed the highest PCEs of 3.03% and 2.85% without any treatment, whereas the same devices exhibited higher PCEs of 4.26% and 3.43%, respectively, after 1 vol% DIO solvent processing and thermal annealing at 100 °C. This enhanced PCE was mainly attributed to the improved short circuit current density, increased charge transfer and greater exciton dissociation in the PBDB-T:(**348**) based blend film.[240t] In another report they synthesized two novel starburst polymer acceptors with 10,15-dihydro-5*H*-diindeno[1,2-*a*:1′,2′-*c*]fluorine (truxene) as the central core unit and NDI–bithiophene as the branched chains (**474**) for all-PSCs. They investigated the optical, electronic and thermal properties of these starburst polymer acceptors and found that they exhibited comparable absorption and electronic properties to the linear polymer N2200 (**322**). The photovoltaic performance of the starburst polymer acceptors was investigated using the polymer donor PTzBI-O and energy levels matching those of the starburst polymer acceptors. All-PSCs were fabricated with these starburst polymer acceptors and the PTzBI-O donor polymer. The device based on (**474**) afforded PCEs of 8.0–7.31%, much higher than that of the widely used (**322**) polymer. The (**322**) polymer acceptor bears alternating NDI and bithiophene units which afforded high electron mobility and suitable ionization potential and electron affinity, making it a good acceptor material in PSCs. The improved performance was mainly due to greater electron and hole mobilities, the formation of favourable film morphology and reduced molecular recombination compared to the (**322**) polymer acceptor. Their findings clearly show that starburst polymer acceptors are a useful tool for the fabrication of high performance all-PSCs.[312] They have also synthesized two novel n-type polymers (**515a** and **b**), water/alcohol-soluble conjugated polymers (WSCPs) composed of conjugated NDI as the main chain and highly polar amino or ammonium functionalized side chains for high performance PSCs. They confirmed that the NDI unit afforded good electron mobility to the polymer acceptors (**515a** and **b**), whereas the polar amino or ammonium side chain enabled processability in alcohol and also enhanced electron collection in the PSCs. They further confirmed the doping effect of WSCPs on $PC_{71}BM$ by ESR and SCLC measurements and revealed the self-doping mechanism between **515a** and **b**. They have used **515a** and **b** as ETLs in PSCs along with polymer donor materials, either PTB7-Th or PffBT4T-2OD and $PC_{71}BM$ as the acceptor. The PSCs showed excellent performance with PCEs of 9.7% and 10.11%, respectively, for PTB7-Th/$PC_{71}BM$ and PffBT4T-2OD/$PC_{71}BM$ devices based on self-doped WSCP ETLs. They also studied the effect of ETL thickness on the performance of the PSCs and found that they were able to improve the PCE by varying the thickness of the ETLs. Interestingly the device based

on PffBT4T-2OD/$PC_{71}BM$ displayed a PCE of 8% when the thickness of ETL was 100 nm. Their findings show that WSCPs as ETLs are encouraging candidates for high performance PSCs.[341b] A new NDI based polymer was developed with optimized nanoscale morphology of the blend film through side chain engineering. They introduced branched alkyl chains on the NDI units in an NDI-based polymer (**322**) by linear oligoethylene oxide (OE) to fine-tune the morphology of the blend and synthesized NDI based polymer acceptors (**513**, x = 0, 0.1, 0.2, 0.3), where x represents the percentage of OE chain substituted NDI units relative to total NDI units. Several factors such as polymer crystallization, charge carrier mobility and donor:acceptor miscibility as well as the favourable morphology of the blend surface can be modulated by introducing the OE side chain into the photoactive material. They also found that the OE introduction impacted the electrochemical and optical properties of the acceptor. The PSCs based on PBDT-TAZ:(**513**, x = 0.1) achieved the highest PCE of 8.1% with a record high FF of 0.75 and a J_{SC} of 12.9 mA cm^{-2}. The group also found that the (**513**, x = 0.1) based device maintained long term thermal stability. Several factors contributed to this high performance, including miscibility with the polymer donor, enhanced polymer packing and nanophase separation with 10% of the OE side chains. They have put forward (**513**, x = 0.1) as an alternative to the commercially available (**322**) polymer acceptor.[339] They have also synthesized NDI based n-type conjugated polymer acceptors composed of fluorene and NDI units with different amine side groups (**514c–d**, **516a–d**) and a polymer backbone as efficient cathode interfacial materials for polymer and perovskite solar cells. The electron transport properties were improved by self-doping between the amine side group and the NDI units which ultimately enhanced the performance of the PSCs in both polymer and perovskite solar cells, and they investigated the impact of the amine group on cathode interfacial effects. All of the NDI based polymer acceptors exhibited self-doping behaviour and excellent charge transfer ability which make them promising components in PSCs. Their findings demonstrated that, with decreasing electron donating ability and increasing steric hindrance, the device performance of perovskite solar cells decreases. They further introduced an acetylene spacer into a backbone which increased the electron transport process when used as a cathode interlayer, and the device based on a PTB7-Th/$PC_{71}BM$ blend afforded a high PCE of 10.1% in PSCs and 15.2% PCE in perovskite solar cells. They investigated the effect of thickness of the cathode interlayer on the device performance, with a 100 nm interlayer thickness achieving a PCE of 8% and 13.5% for polymer and perovskite solar cells, respectively. Their findings revealed that the use of cathode interlayer materials can boost the performance both polymer and perovskite solar cells.[340b] In another report, they functionalized a conjugated polymer with an amino group for use as an electron transport layer (ETL) in high performance perovskite solar cells. They have introduced an NDI based ETL containing fluorine and NDI units with a thiophene spacer to replace the commonly used ETL [6,6]-phenyl-C61-butyric acid methyl ester (PCBM). The incorporation of fluorene resulted in deep HOMO levels, whereas the thiophene spacer enhanced the charge transport properties. They studied the effect of the new ETL on interfacial effects by various techniques such as photoluminescence (PL), time resolved PL decay, and impedance spectroscopy and Kelvin probe measurements. They found that the amine side groups on the polymer enhanced the electron extraction properties by making the surface traps of perovskite solar cells unreactive, and that favourable interfacial dipoles were formed. With these increased electron transport properties, and with (**515c**) as the ETL, the perovskite device exhibited a much higher PCE of 16.7%, whereas for the commonly used PCBM the device showed a maximum PCE of 12.9%, and the (**515d**) based device was poorly performing.[341c]

In another report they described self-doped n-type WSCPs with tailored backbones and polar groups (**488**) to enable favourable charge transport processes for ETLs. They synthesized a series of n-type WSCPs composed of different conjugated backbones and terminal polar ammonium side groups in which the acetylene bridge was introduced *via* a Palladium catalysed Sonogashira polymerization reaction. These WSCPs exhibited self-doping behaviour which was confirmed by UV-Vis absorption and ESR spectroscopy, and confirmed that n-type backbones and polar groups are responsible for doping in WSCPs. The presence of the triple bond contributes to the high mobility and gives planarity to the structure, whereas the polar groups are responsible for the high electron affinity of the resulting polymers. Photoconductivity studies demonstrated different illumination properties depending on the strength of electron donating and polar groups. The PSC exhibited a PCE of greater than 10% for photovoltaic devices with 5–10 nm n-type WSCPs, and a PCE of greater than 9% for 60 nm n-type WSCP photovoltaic devices.[322] They have also synthesized three novel NDI–thiophene skeletons based on n-type conjugated polymers with asymmetric alkyl side chains, namely, (**320a–c**), with varying size *N*-alkyl substitutions for all-PSCs: (**320a**) with *N,N′*-bis(2-hexyldecyl), (**320b**) with *N*-(2-ethylhexyl)-*N′*-(2-decyltetradecyl) and (**320c**) with *N*-(2-butyloctyl)-*N′*-(2-octyldodecyl) side chains. Compared to (**320a**) which has identical side chains, the polymers (**320b**) and (**320c**) demonstrated higher crystallization and melting temperatures and also showed stronger aggregation in solution. All-PSCs were fabricated using these newly synthesized polymer acceptors and the polymer donor PRB7-Th. They found that the device based on the polymer acceptor with two identical alkyl side chains (**320a**) exhibited poor performance with a PCE of 4.30% compared to the (**320b**) and (**320c**) based devices with superior PCEs of 5.88% and 6.89%, respectively. Devices based on all polymer acceptors showed nearly identical open-circuit voltages of 0.77 V. This improved performance of the devices based on asymmetric alkyl side chains was due to the formation of a more favourable blend morphology and a balanced charge transport system. Their findings showed that the introduction of asymmetric alkyl side chains can tune the photovoltaic performance of the all-PSCs.[316]

Chen *et al.*[360] studied all-polymer solar cells with NDI-based polymer acceptors based on (**322**) and (**353**) where the 3,3′-difluoro-2,2′-bithiophene unit is introduced into the N2200 polymer by random copolymerization. This has significantly improved the absorption coefficients of terpolymers, reduce the polymer aggregation, and produce more flexible main chains to favour a closer contact and better miscibility with the crystalline donor. Xie *et al.*[361] designed and synthesized NDI and diethynylbenzo[1,2-*b*:4,5-*b*′]dithiophene (DEBDT) alternating units with different side chains for application in all-PSCs. They were able to fine-tune the photoelectronic properties of the polymers using systematic side chain engineering, but the size of the alkyl side chains on NDI units has minimal impacts on light-harvesting properties and molecular energy levels, while introducing side chain groups into DEBDT units can significantly broaden the absorption profile and tune the lowest unoccupied molecular orbital energy levels of polymers. Sorrentino *et al.*[362] synthesised a cationic NDI-based ionene polymer cathode interlayer with good solubility in alcohol, transparency in the visible range, self-doping behaviour, and good film forming ability for fullerene and non-fullerene polymer solar cells. This has increased the power conversion efficiencies of both fullerene and non-fullerene devices. Lee *et al.*[363] studied the effect of sidechains on the mechanical properties of all-PSCs constructed using (**322**) N2200. The N2200 variant they developed achieved superior power conversion efficiency (PCE) and mechanical robustness of all-PSCs compared to those of N2200-based devices. Zhu *et al.*[364] studied the effect of side chain positions in the (**486**) acceptor polymer and found two polymers with similar narrow bandgaps and electron energy levels. PSCs based on optimized blends of these acceptors with PBZ-C6 display power conversion efficiencies of 5.81% to 5.00%. Zhu *et al.*[365] also studied (**368b**) polymer acceptors in the all-PSC setting and obtained a PCE of 4.49%. In this report they demonstrated that direct (hetero)arylation reaction is a promising tool for building efficient polymer acceptors *via* convenient and low-cost synthesis.

A new way to achieve water/alcohol processed polymeric interconnecting layers (ICL) for conventional tandem OSCs was described, as tandem structure devices are capable of providing superior PCEs. The ICL plays a very important role in achieving high performance tandem solar cells. The ICL generally consists of a hole transport layer and an electron transport layer, with both being responsible for the charge transfer and recombination processes. A new polymeric ICL was developed which was processed with an eco-friendly solvent, by using (**515e**) and poly(ethyleneimine) and PEDOT:PSS as the ETL and hole transport layers, respectively. They used this ICL for the fabrication of tandem OSCs, where they found that the poly(ethyleneimine) tuned the work function of (**515e**) on PEDOT. They also studied the effect of the thickness of the ICL on the device performance and concluded that, with an ICL thickness of 60 nm, the device showed a high PCE of 12.6%. Their findings demonstrated that eco-friendly solvent processed polymeric ICLs can be fabricated, which is advantageous for printing large surface area devices.[341d]

Gao *et al.* have developed a random terpolymer electron acceptor based on cyclometalated Pt complexes for PSCs. They introduced 0, 1, 2, and 5 mol% of cyclometalated Pt complexes to the polymer backbone of (**322**). The terpolymer was composed of three different repeating units as a monomer, and they introduced an organometallic complex monomer for the first time as a polymer acceptor for PSCs. These terpolymers, (**517**) (x = 0.01, 0.02 and 0.05), exhibited similar optical properties to plain (**322**), whereas little difference was observed in the electrochemical properties and HOMO/LUMO energy levels of terpolymers and the Pt free (**322**) polymer. The terpolymer also exhibited a slightly higher melting point and crystallization temperature due to the introduction of the Pt complex into the plain (**322**) polymer, and these terpolymers were thermally stable when characterised by TGA and DSC. For electron and hole mobility measurements they employed the space charge limited current (SCLC) method. When blended with a PTB7-Th polymer donor, the all-PSCs showed an improvement in the device performance compared to the Pt free polymer acceptor (**322**). The PTB7-Th/(**517**, x = 0.01) based inverted and conventional PSCs exhibited the highest PCEs of 4.51% and 3.74%, respectively, much higher than the values of 3.88% and 3.24% for Pt free PTB7-Th/(**517**, x = 0.02) based devices. They further investigated the performance of the (**517**) based device with a higher concentration of cyclometalated Pt complex, and they found that this led to a decreased PCE. They finally concluded that the improved performance of (**517**, x = 0.01) based devices is mainly due to a higher electron and hole transport ability and greater charge separation, as well as nanoscale separated morphology.[342]

The Huang group synthesized three novel n-type triphenylamine-based conjugated polymer acceptors, (**349**; *N,N*′-OD) and (**349**; *N,N*′-HD). These non-planar conjugated polymers were composed of two electron accepting units, isoindigo (IIG) and NDI, and the electron donor triphenylamine (TPA) which was copolymerized with these accepting units. They also changed the building block and acceptor units, as well as the alkyl chain of the polymer backbone to tune the photovoltaic properties. They used a PTB7-Th polymer donor to fabricate PSCs with these polymer acceptors to investigate photovoltaic performance, and they found that the device based on PTB7-Th:(**349**; *N,N*′-HD) exhibited the highest PCE of 2.17%, higher than that of the PTPA-IIG(OD), (**349**; *N,N*′-OD) based devices.[240x] In another report they have synthesized three acceptor–acceptor conjugated polymers based on IIG, NDI and PDI units (**491**) for all-PSCs. They studied the effect of these units and alkyl chains on photovoltaic and photoresponsive devices. They reported the highest PCE of 2.68% for the A-A type conjugated polymer PIIG-PDI OD based device with the PTB7-Th polymer donor. They also reported a polymer photodetector for the first time with high responsivity and detectivity of 0.12 A W^{-1} and 1.2 $\times$ 10^{12} jones, respectively.[11]

Zhang *et al.* reported NDI based terpolymers with high open circuit voltages. They synthesized a series of random terpolymers at various thiophene-NDI/selenophene-NDI ratios in a set of copolymers (**453**) used to fine-tune the photovoltaic

properties. These terpolymers consist of NDI as an acceptor unit with branched octyldecyl chain and thiophene and selenophene donor units. They further studied the optical and electronic properties of (**453**) along with crystallinity and charge transport properties. They used PBDT(T)TPD, a deep energy level polymer donor to fabricate PSCs, and found that the device based on PBDT(T)TPD/0.5-NDI showed improved performance, with a PCE of 5.4%, a J_{SC} of 9.1 mA cm^{-2}, and a V_{OC} of 1.05 V, better than those of PBDT(T)TPD/(**320**) and PBDT(T)TPD/(**321**) based solar cells. The PBDT(T)TPD/(**453**, $x = 0.5$) based device possessed greater charge carrier mobilities and more balanced electron/hole transport properties. The high performance of the PBDT(T)TPD/(**453**, $x = 0.5$) blend was due to the good crystallinity, miscibility with the polymer donor PBDT(T)TPD, and favourable morphology of the blend. Their findings clearly showed that by choosing different polymer compositions the performance of PSCs can be fine-tuned.[303]

Chen and co-workers reported NDI-based non-halogenated solvent processed PSCs. They have synthesized two non-fullerene acceptors composed of 2-octyldodecyl (**320a**) and 2-hexyldecyl alkyl (**320b**) side chains onto NDI backbones with thiophene spacers. The excellent solubility of both the acceptors in halogenated and non-halogenated solvents may be due to a decrease in aggregation in NDI units due to the large dihedral angle between thiophene and NDI. They have employed three non-halogenated solvents, 1,3,5-trimethylbenzene (1,3,5-TMB), 1,2,4-trimethylbenzene (1,2,4-TMB), and 1,2-dimethylbenzene (1,2-DMB), as a processing solvent for the device fabrication and investigated the device performance based on PNDIT-20 and PNDIT-16 and PTB7-Th polymer donor, without any additives or post-treatment. The PTB7-Th polymer donor was chosen because of complementary absorption spectra and exhibited energy levels matching those of the polymer acceptors. Among these non-halogenated solvents, when 1,2-DMB was employed for device fabrication, the all-PSC exhibited the highest PCEs of 3.88% and 4.94% without additives or post-treatment for PTB7-Th:(**320b**) and PTB7-Th:(**320a**) based devices, respectively. They found that this photovoltaic performance in 1,2-DMB solvent was higher when the device was fabricated using a hazardous chlorinated solvent such as 1,2-dichlorobenzene as a processing solvent. Further, they confirmed by SCLC measurements that 1,2-DMB solvent showed more balanced electron and hole transfer ability, ultimately resulting in a higher J_{SC} and formation of a more favourable morphology on the blend surface.[317]

They have also described the synthesis of (**487**) *via* Stille coupling. The novel random copolymer acceptor consists of three building blocks including NDI as an acceptor unit, with randomly distributed thieno[3,2-*b*]-thiophene (TT) and thienylene–vinylene–thienylene (TVT) as a donor unit. They used PTB7-Th as a polymer donor to fabricate PSCs, and found that the device based on PTB7-Th:(**487**) blend showed the highest PCE of 4.86%. This PCE was higher than the PCE obtained for the devices based on (**492**) and (**330**) blends. Their findings show that random copolymerization is an encouraging strategy towards high performance PSCs.[321d]

In another report they have synthesized a series of D–A type random copolymers (**487**) *via* Stille coupling reactions for solar cell applications. (**487**) consists of NDI as the acceptor unit and two donor units, thieno[3,2-*b*]thiophene (TT) and thienylene–vinylene–thienylene (TVT), which are randomly distributed. They further studied the influence of the TT to TVT ratio on the absorption, electrochemical and thermal properties as well as photovoltaic properties. The devices based on random polymers exhibited more balanced electron/hole transport properties and also formed more suitable film morphologies, ultimately achieving higher performance compared to alternating copolymer based polymer devices. The fabricated photovoltaic device based on the PTB7-Th polymer donor and PNDI–TT–TVTs containing 25% of TT and 75% of TVT as the polymer acceptor exhibited a PCE of 5.27%.[327] They have also described the role of side chain engineering of acceptor units in the performance of all-PSCs. They synthesized two novel conjugated polymer acceptors (**493**, **494**), containing side chain thiophene as a donating group and NDI units. They found that, with the introduction of the thiophene group on the side chain, the polymer exhibited improved absorption spectra with a narrow band gap, and this side chain engineering also leads to improved charge transfer ability and formation of favourable morphology of the blend film compared to the (**322**) reference polymer acceptor. The presence of side chain thiophene rings causes steric hindrance and reduces the aggregation effect of NDI units. The photovoltaic device was fabricated with the configuration of ITO/PEDOT:PSS/PTB7-Th:acceptors with 3% of DPE solvent additive and showed maximum PCEs of 4.75% and 2.73% for the (**493**, **494**) based devices, respectively. The higher performance for the (**493**) based device was ascribed to balanced electron/hole transfer, favourable blend morphology, and enhanced J_{SC} and FF compared to the (**322**) polymer acceptor. The poor performance of the (**494**) based device is due to unbalanced charge mobility and poor solubility. Their findings showed that side chain engineering by using an aromatic thiophene group is also an effective strategy for high performance all-PSCs.[321g]

Yan *et al.* reported NDI based polymers for highly efficient perovskite solar cells. They synthesized three NDI based conjugated polymers with the same side chain but different numbers of selenophene units *via* copolymerization of NDI and selenophene (**321**), 2,2′-biselenophene (**324**) or 2,2′:5′,2″-terselenophene (**327**). During the characterization of these NDI-selenophene copolymers, they found that these polymers exhibited strong thermal stability, high crystallinity, and high electron mobility and the energy levels were well matched to those of perovskite absorbers. The SCLC measurements showed increased electron mobility while going from (**321**) to (**324**) to (**327**) as the number of selenophene units increases, and for the (**327**) based polymer they found the highest mobility of 3.0×10^{-4} cm^2 V^{-1} s^{-1}. They have fabricated perovskite solar cells with the configuration of ITO/NiO_x/$MAPbCl_{0.2}I_{2.8}$/ETL/Ag and used these polymers as the single ETL and solution processed ETLs, achieving the highest efficiency of 14.0% from the (**327**) solar cell which is the standard device equivalent PCE using

C_{60}/BCP as the ETL, whereas for (**321**) and (**324**) based devices the PCEs observed were 9.51% and 7.66%, respectively.[240q] Zhan and co-workers synthesized PDI and NDI based two polymer acceptors *via* Stille coupling copolymerization, containing (*E*)-2,3-bis(thiophen-2-yl)acrylonitrile (CNTVT) (**347**) as donor units, and PDI or NDI acceptor units. Both acceptors displayed good solubility, and the NDI based polymer showed stronger pi–pi stacking compared to the PDI based polymer which results in improved charge transfer properties of the NDI based polymer. The binary device based on PTB7-Th:(**347**) exhibited a maximum PCE of 3.80%, much higher than 1.74% for the PTB7-Th:PDI-CNTVT blend. The high performance for the NDI based device was mainly attributed to high electron/hole mobility and charge transport ability leading to higher J_{SC} and FF.[240e] They have also synthesized a series of NDI and PDI based copolymers containing the 2,2′-bithiophene (BT) (**454**) which has electron-donating properties for solar cell applications. The presence of the BT unit imparts high charge transfer ability to the resulting polymer. Furthermore, they employed UV-Vis absorption spectroscopy to investigate the effect of the PDI/NDI ratio on optical and electrochemical properties, and also on the charge transfer ability and morphology of the blend surface, as well as the photovoltaic performance. They found that with a decrease in the PDI ratio these polymers showed enhanced V_{OC}, improved charge transfer ability and improved J_{SC} values. As a result, the PTB7-Th:NDI100 (**322**) based device showed a higher PCE of 4.67%, whereas the device based on the PTB7-Th:(**454**, x = 1) blend exhibited a low PCE of 1.03%, due to very poor charge mobility and very low FF for the PDI based device. The photovoltaic device based on (**454**, x = 1, 0.75, 0.5, 0.25) PDI100, PDI75, PDI50, and PDI25 blends showed relatively low device performance compared to the NDI100 (**322**) based device. This was ascribed to the more balanced charge transport and more favourable morphology formation of the blend surfaces for NDI100 (**322**) based devices.[315]

One of the drawbacks of organic semiconductors that limit their efficiency in organic solar cells is their low dielectric constant. Mohapatra *et al.*,[366] in an attempt to enhance the dielectric constant of NDI-based polymers, synthesized three semiconducting copolymers by combining the thiophene-substituted diketopyrrolopyrrole (TDPP) monomer with three different monomeric units with varying electron donating/accepting strengths including NDI with triethylene glycol (TEG) side-chains. The NDI-based P(gNDI-TDPP) exhibited the highest dielectric constants ($\sim$5) at 1 MHz frequency, with significant contribution from the TEG side chains. Wang and co-workers synthesized five NDI based fluorinated polymer (**405–407**) acceptors for all-PSC applications. The optical and electronic properties of the polymer acceptors were investigated systematically, and it was found that fluorinated polymers exhibited improved dielectric constants which increased the charge generation process in the blend. They have comparatively studied the performance of fluorinated and non-fluorinated polymer acceptors with the PTB7-Th polymer donor. They further investigated the effect of thiophene content on the crystallinity and molecular weights of these polymer acceptors, where they found a reduced crystallinity and increased molecular weights for the polymers with an increase in the number of thiophene units. The device based on PTB7-Th:(**406**, x = 0.1) exhibited a higher PCE of 7.3% with a FF of 0.68 and a high J_{SC} of 14.7 mA cm^{-2} compared to other polymer based devices, which is mainly due to the well defined miscibility of the (**406**, x = 0.1) polymer with PTB7-Th, improved photon harvesting exciton dissociation properties, and lower recombination loss. The J_{SC} of 14.7 mA cm^{-2} for the device was higher than 12.9 mA cm^{-2} for the non-fluorinated (**406**, x = 0.1) based device. They also found that, for the PTB7-Th:(**406**, x = 0.1) based all-PSCs, the high photovoltaic performance was maintained even with a large variation of the D : A ratio. Their findings showed that by fluorinating the polymer acceptor we can fine-tune the crystallinity and improve the dielectric constant.[247c] In another report they have undertaken a systematic study on the effect of thermal annealing on the photovoltaic performance. They selected a PSC based on the poly[2,3-bis(3-octyloxyphenyl)quinoxaline- 5,8-diyl-*alt*-thiophene-2,5-diyl] (TQ1) polymer acceptor and N2200 (**322**) polymer donor to investigate the thermal annealing effect. They found that after annealing the device showed approximately double the PCE of the non-annealed device, and thermal annealing results in improved electron and hole mobilities with enhanced J_{SC} and FF, but a lower V_{OC}. They further used scanning force microscopy techniques, and grazing-incidence wide-angle X-ray scattering to confirm the higher charge mobility and improved interconnected network of the thermally annealed device layer. They have also investigated the performance of the solar cell using the TQ1/N2200 (**322**) based inverted device and found that the PCE increased from 2.4% to 4.4% after thermal annealing, which is mainly due to the higher charge mobility and favourable morphology of the blend surface.[326] They have also synthesized NDI based copolymers of (**553**) at x = 0.1, 0.2, 0.5, where x is the single thiophene percentage relative to the whole donor units, by replacing the number of bithiophene units in the commercially available polymer N2200 (**322**) with a single thiophene unit. They found reduced crystallinity and enhanced solubility when changing the thiophene content. The polymer acceptors showed good miscibility with the donor polymer PTB7-Th, leading to a high performance photovoltaic device. The PTB7-Th:(**553**, x = 0.1) based PSC exhibited a maximum PCE of 7.6% with a FF of 0.71 after solvent annealing which is much higher than that of the PTB7-Th:N2200 (**322**) based device and the structures are illustrated in Fig. 116. The solvent annealing process allows higher exciton dissociation and enhanced charge mobilities with reduced charge recombination. Interestingly for this PSC they found negligible bimolecular recombination, so that the separated charges can be effectively transported and collected by the electrode, a rare phenomenon in all-PSCs. Hence they showed how the synergistic effect of fine-tuned crystallinity and solvent annealing results in high performance all-PSCs.[321b] Kim *et al.* synthesized a series of NDI based n-type random terpolymers (**555**) composed of electron accepting NDI units in conjugation

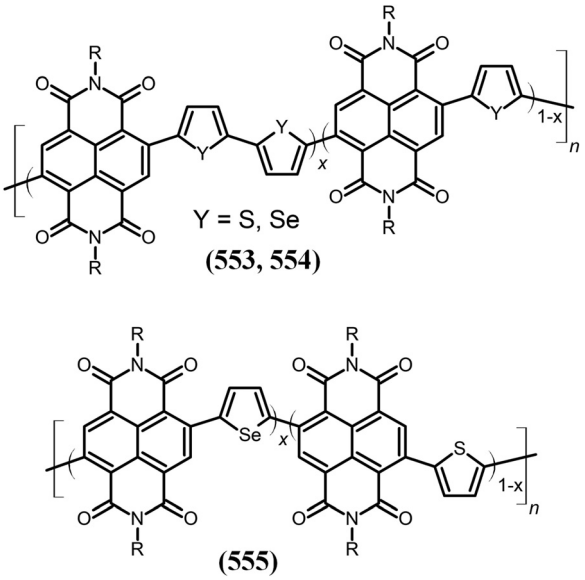

Fig. 116 The chemical structure of NDI-mono- and bithiophene (**553**)[321b] copolymer acceptors, and random terpolymers of NDI, thiophene and selenophene (**555**).[305]

with thiophene (T) and selenophene (S), which are electron donor units. They have synthesized (**555**) copolymers with $x = 1$, 0.8, 0.5, 0.2, 0 T/S ratios, and these different ratios were found to tune the crystallinity of the NDI based polymers. The crystallinity was enhanced by the S content in the polymer acceptor, and hence the structural ordering of the terpolymer acceptor and electron/hole mobility can be enhanced by adding more S units to the polymer backbone. Further, they have studied the effect of different compositions of donor units on the optical, electrochemical and photovoltaic properties of NDI based polymers. The all-PSCs composed of the PTB7 donor polymer and (**555**) polymer acceptor afforded an increased PCE from 2.5% for (**555**, $x = 1$) to 3.60% for (**555**, $x = 0$) with enhanced J_{SC} as the content of S increased. The high PCE for the (**555**, $x = 0$) acceptor is mainly due to the higher charge mobility and formation of a more favourable morphology of the blend surface.[305]

Deshmukh *et al.* reported a systematic investigation of the effect of fluorination on the performance of NDI based polymer acceptors in all-PSCs. They synthesized three polymer acceptors: non-fluorinated, bifluorinated and tetrafluorinated phenyl rings (**368b–d**). In all-PSCs, when blended with the PTB7-Th donor polymer, they found that the fluorinated acceptors showed greatly enhanced performance compared to nonfluorinated ones due to their improved J_{SC} and FF. These increased J_{SC} and FF were mainly ascribed to the improved absorption and charge collection for fluorinated polymers. They found that the V_{OC} gradually decreased as the degree of fluorination increased from 0 to 4, as the LUMO energy levels decreased. The device based on the PTB7-Th:(**368c**) blend exhibited a maximum PCE of 4.8% with an improved J_{SC} compared to 3.1% for the non-fluorinated (**368d**) based device. They found that fluorination improves light absorption, charge mobility and phase separated morphology but will not affect ultrafast charge generation kinetics.[247d] Li and co-workers synthesized NDI-based n-type polymer acceptors (**343**) containing five membered heterocyclic 1,3,4-thiadiazole (TZ) for all-PSC applications. They inserted a TZ unit in between two thiophene rings of the N2200 (**322**) polymer, and the resulting polymer achieved an electron mobility of 0.36 $cm^2\ V^{-1}\ s^{-1}$. The TZ unit in (**343**) was used to adjust the LUMO energy levels (24.02 eV), complementary to the polymer donor PTB7-Th (23.64 eV), suggesting effective exciton dissociation from the donor to the acceptor. They further observed that (**343**) exhibited complementary absorption to the PTB7-Th donor. The all-PSCs using (**343**) as the acceptor and PTB7-Th as the donor were fabricated, and after optimization with 1% DIO additive, the blend microstructure showed a constant D/A interpenetrating network, and the best device based on PTB7-Th:(**343**) showed a maximum PCE of 4.35% with a 13.26 mA cm^{-2} J_{SC}.[240w] Two NDI-based n-type D–A copolymers were synthesized *via* Stille coupling polymerization (**330, 331**). These polymers composed of NDI as the acceptor and thienylene–vinylene–thienylene (TVT) (**330**) or furanylene–vinylene–furanylene (FVF) (**331**) as the donor unit. They introduced TVT and FVF units for the formation of a planar structure and achieved greater electron/hole mobility, where the S and O atoms in thienyl and furanylene units were used to fine-tune the optoelectronic properties of the polymers. They found that (**330**) and (**331**) showed decent solubility, strong thermal stability and wide absorption spectra. The PSCs were fabricated using (**330**) and (**331**) acceptors and the medium band gap donor J51 presented energy levels matching those of the acceptor, with the device configuration of ITO/PEDOT:PSS/J51:polymer acceptor/PDINO/Al. They found that the J51:(**330**) based device showed a PCE of 5.21%, while the device based on the J51:(**331**) blend exhibited the highest PCE of 6.43%. These results suggest that arylene-vinylene-arylene-NDI copolymers are encouraging polymer acceptors for high performance all-PSCs.[324] They have also reported a dye-incorporated NDI based acceptor for high performance all-PSCs by random copolymerization. They introduced the rhodanine dye 2-(1,1′-dicyanomethylene)-4-(3-thienylmethylene) rhodanine (TR) with different percentages into the NDI polymer backbone to give TR : NDI : 2T at 5 : 95 : 100 and 10 : 90 : 100 ratios (**490a and b**). During characterization they observed improved absorption and electronic properties for these newly synthesized NDI based polymers after insertion of the rhodanine dye into the NDI backbone. They also found that the crystallinity and microstructure of the D/A blend were further fine-tuned by random polymerization of the rhodanine dye into N2200 (**322**). These acceptors (**490a**) and (**490b**) were found to mix properly into the polymer donor PBDB-T. The all-PSCs were fabricated using two acceptors and PBDB-T donor, and the additive-free as-cast photovoltaic device PBDB-T:(**490a**) showed the highest PCE of 8.13%, much higher than 5.15% for the (**322**) based device, because of the considerably reduced bimolecular recombination in the (**490a**) based device. The higher performance of the (**490a**) based device is strongly ascribed to the improved J_{SC}, V_{OC} and FF, and also to the better

absorption coefficient and strong miscibility with the polymer donor, as well as phase separation and favourable morphology formation.[321h] They have also synthesized D–A alternating copolymer acceptors composed of indacenodithienothiophene (IDT) and NDI units for all-PSC applications. They inserted an IDT functionality into an NDI building block (**486**) and used it as an acceptor material in all-PSCs. The extended conjugation of the IDT unit in the (**486**) polymer may be advantageous for delocalization of pi-electrons, which ultimately increases the charge transfer mobility, improves absorption and reduces the optical band gap. The highly bulky tetrahexylphenyl group of IDT on the NDI backbone suppressed the intermolecular interactions leading to reduced aggregation in solid state in the active layer of the photovoltaic device. They investigated the optical and electrochemical properties of polymer (**486**) and found a lower optical band gap of 1.51 eV with appropriate HOMO and LUMO energy levels of −5.75 eV and −3.84 eV, respectively, for the (**486**) polymer acceptor. All these factors make the use of this polymer as an acceptor material in all-PSCs possible. The PSCs were fabricated using three different conjugated polymer donors, J50, J51 and PTB7-Th, of medium and low band gaps. The photovoltaic performance using the (**486**) acceptor showed PCEs of 3.63%, 4.12% and 5.33% for PTB7-Th, J50 and J51 donor polymer based devices, respectively. The high performance of the J51:(**486**) based device resulted from the complementary absorption of the donor/polymer, high lying LUMO energy levels, and higher V_{OC}.[321c]

In the next report, they have described a novel high voltage n-type polymer acceptor based on NDI and benzotriazole moiety with a thiophene bridge for all-PSCs. They synthesized the polymer acceptor (**408**) by modifying the conventional polymer acceptor N2200 (**322**), and inserted a benzotriazole unit in between the two thiophene rings. The increased steric effect of the benzotriazole unit causes reduced aggregation of polymer (**408**) in solid state. The optical and electronic properties of (**408**) were investigated and blue-shifted absorption and upshifted LUMO energy levels for the (**408**) polymer compared to N2200 were observed. The all-PSCs were fabricated using the wide band gap polymer donor PBDB-T and the (**408**) acceptor. The photovoltaic properties of the (**408**) acceptor were investigated using the wide band gap polymer donor PBDB-T and compared with an N2200 (**322**) based device. The PBDB-T:(**408**) based device optimized PSC with 1% CN additive exhibited a high PCE of 6.44% with a V_{OC} of 0.937 V. The optimized device based on the PBDB-T:(**408**) blend showed a PCE of 5.85% with a V_{OC} of 0.812 V. The upshifted LUMO energy levels of the (**408**) acceptor result in a higher V_{OC} for the (**408**) based device.[240b] Kolhe *et al.* developed new n-type random copolymers (**485**) (x = 0.1, 0.2, 0.5) based on NDI-biselenophene/NDI-selenophene moieties. The optical, electrochemical, photoluminescence and photovoltaic properties of (**485**) were investigated, and improved charge transport ability, active layer morphology and photovoltaic properties were observed. They found greatly enhanced charge mobility for these random copolymers compared to BSS0, which was ascribed to the face-on orientated molecular packing of random polymers which was further confirmed by GIWAXS measurements. Phase-separated morphology for BSS10 and (**485**)20 based devices was confirmed. When blended with the polymer donor PBDB-T the all-PSC based on (**485**) polymer acceptors showed improved photovoltaic performance compared to BSS0. The PBDB-T:(**485**, x = 0.1) based all-PSC without any additives exhibited a PCE of 10.1% with a low energy loss of 0.59 eV and a high internal quantum efficiency of 97%. On the other hand, the (**485**, x = 0.2) polymer based device showed a PCE of 9.58% with an external quantum efficiency of >85%, and the BSS50 based device afforded a maximum PCE of 9.69%, much higher than 7.38% of the (**485**, x = 0) based device. The improved charge mobilities, reduced crystalline domain size and more favourable morphology formation of blend surfaces resulted in high performance of these random polymer based all-PSCs.[321f] Chen and co-workers used the Kumada catalyst-transfer polycondensation (KCTP) process to synthesize NDI-based block polymers. They synthesized a series of n-type conjugated block and triblock copolymers with flanked chains, p-type grafted polymer P1, n-type linear polymer (**471**) with an n-type backbone and a p-type graft chain, a p–n type graft copolymer (**472**) and a p–n–p type triblock polymer (**473**) with a middle n-type chain and p-type flanked chains. These polymers, when used to fabricate polymer thin film transistors, displayed moderate charge mobilities of 10^{-4} to 10^{-3} cm^2 V^{-1} s^{-1}, and this could be improved by thermal annealing treatment. The fabricated all-PSC for block copolymers as single active components showed a PCE of 0.22%, and when PNDI was used as a surfactant it was 2.28% with V_{OC}, J_{SC}, and FF of 0.61 V, 7.00 mA cm^{-2} and 0.54, respectively.[311]

Jen and co-workers employed the n-type polymer N2200 (**322**) along with PFN-Ox as the ETL with good ambient stability for highly efficient inverted perovskite solar cells. They used the commercially available (**322**) polymer mixed with poly[9,9-bis(6′-(*N*,*N*-diethylamino)propyl)-fluorene-*alt*-9,9-bis (3-ethyl(oxetane-3-ethyloxy)-hexyl) fluorene] (PFN-Ox) as a polymeric additive. They found that when only (**322**) was used the ETL the inverted perovskite device showed a PCE of around 15% and when PFN-Ox was used as the additive the (**322**):PFN-Ox hybrid ETL showed an improved PCE of 16.8%. They also improved the stability of the hybrid ETL compared to only (**322**), with the PFN-Ox additive improving the electronic properties of the (**322**) polymer.[240d] Zhou and co-workers[10b] reported a comparative study between PDI, NDI and naphthodithiophene diimide (NDTI) based polymer acceptors in PSCs. They synthesized three n-type polymer acceptors: PPDI-DTT, (**467**), and (**468**) using the electron rich dithienothiophene (DTT) unit. They found that while going from PDI through NDI to NDTI the absorption shifted towards red, giving a high photoresponse between 400 and 800 nm for the (**468**) based device. Hence, a device based on the BDDT polymer donor and (**468**) polymer acceptor showed the highest PCE of 5.57% with a relatively high J_{SC} value. In contrast the BDDT:PPDI-DTT and BDDT:(**467**) based PSCs exhibited lower PCEs of 3.49% and 2.50% with lower J_{SC} values compared to the (**468**) based device. SCLC measurements showed that the BDDT:(**468**) blend had better charge transfer properties among the three acceptors, whereas

the (**467**) based blend film showed the most unbalanced charge carrier transfer, which resulted in lower performance for the (**467**) based blend. They revealed the reason behind the high performance of the (**468**) based device, the strong absorption in the NIR region, balanced charge transfer, higher EQE value, and higher J_{SC} of 13.68 mA cm^{-2}. In another report they have synthesized three n-type NDI, PDI, and fused PDI-based polymers with alternative backbone structures and benzodithiophene conjugated side groups: PNDI-BDT (**480**), PPDI–BDT, and PFPDI–BDT. The electron rich benzodithiophene group was supposed to enhance the charge carrier mobilities of the resulting polymers. They found deep LUMO energy levels from −3.55 to −3.97 eV for these acceptors. The all-PSCs were fabricated using PTB7-Th, which exhibited matching energy levels and complementary spectra. They found that the PTB7-Th:PFPDI–BDT-based optimized device exhibited the highest PCE of 5.65% with a higher J_{SC} compared to (**480**) and PPDI–BDT based devices which showed PCEs of 0.88% and 3.74%, respectively. The high performance for the PFPDI–BDT-based blend may be ascribed to the higher photoresponse from 350 to 750 nm, less charge recombination, and favourable morphology of the blend film.[321a] In another report they synthesized three n-type polymer acceptors: PDTNDI-T (**465a**), PDTNDI-TT (**465b**), and PDTNDI-DTT (**465c**). They introduced thiophene (T), thienothiophene (TT), or dithienothiophene (DTT) units *via* a thiophene pi-bridge into NDI-*alt*-fused thiophene copolymers and investigated them as acceptors in all-PSCs. An investigation of the photovoltaic performance showed that, with an increase in the number of thiophene units in the DTNDI based polymer, the device performance decreased. The all-PSC based on the PBDB-T donor exhibited PCEs of 3.78%, 1.14% and 0.70% for the devices based on (**465a–c**) blends, respectively, as the number of thiophene rings increased. The same trend was found for the PSCs based on the PTB7 donor polymer. The PCEs observed were 1.53%, 0.68% and 0.27% for the (**465a–c**) based devices, respectively. They stated that this reduction in performance may be attributed to the differing molecular orientations and electron mobilities. Their findings showed that introducing fused aromatic rings into the pi-bridge is not always advantageous to NDI based polymers in all-PSCs.[309] In the next report, they synthesized the asymmetric rylene diimide based n-type polymer acceptor, PTDI-T (**460**) containing asymmetric thianaphthene fused PDI, for all-PSC applications. The electron rich thiophene ring was used to enhance the charge mobility of the resulting polymer. The photovoltaic performance of the (**460**) polymer acceptor was evaluated using two different polymer donors, PTB7-Th and PBDB-T. When blended with PTB7-Th, the (**460**) based device showed a highest PCE of 4.70%, higher than those of the PPDI-2T and PDTCDI based devices. The PBDB-T polymer (**460**) based blend exhibited the highest PCE of 2.89% with a very high V_{OC} of 1.03 V. The PTB7-Th:PTDI-T based blend exhibited higher charge mobility, more uniform surface morphology and higher PL quenching efficiency compared to the PBDB-T:PTDI-T based device, resulting in a higher photovoltaic performance for the PTB7-Th based device.[308]

Deng *et al.* reported the synthesis of two novel polymer acceptors composed of difluorobenzene attached to the NDI backbone *via* a thiophene bridge (**368b**), one random and one regioregular, for all-PSC applications. They examined the structural effects of the random and the regioregular polymers (**368b**) on the optical, electrochemical and photovoltaic properties in all-PSCs. They found that the structurally regioregular polymer shows enhanced thin film crystallinity and higher electron mobility compared to the random polymer, with longer absorption and a stronger absorption coefficient than those of (**368b**). The self-assembly formation of structurally regioregular polymer P2, when processed with DIO additive, leads to highly organized nanofibrillar network structure and molecular ordering in the thin film with a PTB7-Th donor. When blended with the PTB7-Th polymer donor the regioregular (**368b**) based device exhibited a much higher PCE of 5.20% with a higher J_{SC} compared to 1.30% of PCE for the PTB7-Th:random (**368b**) based blend. The high performance of the regioregular (**368b**) based device is ascribed to the greater electron/hole mobility with PTB7-Th.[247f]

Luo and co-workers synthesized four polymer acceptors with broad absorption bands and two polymer donors for all-PSC applications. They used dithieno[3,2-*b*:20,30-*d*]silole (DTS) (**470**) and *N*-alkyl dithieno[3,2-*b*:20,3-*d*]pyrroles (DTP) (**469**) along with PDI and NDI units to synthesize these copolymer acceptors. All the copolymers exhibited excellent thermal stability suitable for device fabrication. The absorption of P2 was observed to be blue-shifted compared to P1 as the fluorine number increased, and they also found a longer fluorescence lifetime for the PDI based polymer compared to the NDI polymer, which is further supported by the polarizability of the polymers. The photovoltaic investigation showed that the P2:PDIDTP based device showed the highest PCE of 4.05% among these all polymer acceptor based devices. They concluded that the PDI based device exhibited the highest polarizability which increases the electron mobility by increasing exciton separation and decreasing coulombic binding energy.[310] The Wang group introduced the amino functionalized copolymer PFN-2TNDI (**515c**) instead of TiO_2 as the ETL in an n–i–p planar heterojunction perovskite device. The conjugated copolymer (**515c**) was composed of an NDI acceptor unit, fluorene and a thiophene spacer and has an amino group in the alkyl amine side chain which can reduce the work function and act as an efficient ETL in PSCs. Appropriate energy levels, favourable charge mobility and suitable film formation made (**515c**) a good ETM for perovskite solar cells. They also found that the good film forming ability of polymer (**515c**) results in high quality film formation. The perovskite device in conjunction with (**515c**) copolymer attained a very good PCE of about 16% under standard illumination conditions. They found that the perovskite device with this ETL showed strong photostability to UV light compared to the TiO_2 based device. 75% of the original efficiency was maintained after irradiation for over 3000 hours, while in contrast the TiO_2 based device showed less than 10% of its original efficiency within 300 hours of irradiation.[341e] Kim *et al.* overcame the problem of large-scale

phase separation caused by large crystal domains in blend films and the mechanical stability of all-PSCs using an NDI based polymer acceptor. They introduced the fluorinated copolymer PNDI–FTVT (**352**) as an acceptor to improve the mechanical stability of flexible all-PSCs and compared with its non-fluorinated analogue PNDI–TVT (**330**). (**352**) was designed to mix well with the donor in blend films and also improve the charge transfer process. The crystallinity and charge carrier mobility of the (**352**) copolymer were investigated and it was found to be relatively crystalline with higher electron mobility compared to the non-fluorinated (**330**) polymer. When blended with the polymer donor PBDB-T, (**352**) displayed small phase separation with strongly mixed morphology due to the reduced crystal domain size, which improved the interactions with the PBDB-T donor polymer and enhanced the charge transport process with mechanical flexibility. They also found that these morphological changes influence the exciton dissociation at the donor/acceptor interface along with charge transport properties, which further improved the J_{SC} and FF for (**352**) based flexible all-PSCs. The PBDB-T:(**352**) based all-PSC exhibited a high PCE of 7.14% with outstanding mechanical stability compared to 5.11% for the non-fluorinated (**330**) polymer based device. The flexible all-PSC based on the PBDB-T:(**352**) blend showed improved mechanical stability, and retained 81% of its initial photovoltaic performance, with a 5.78% PCE observed after 1000 bending cycles at a bending radius of 8.0 nm.[247g]

Leclerc and co-workers synthesized the high molecular weight alternating NDI–bithiophene copolymer P(NDIOD-T2) (**322**) by direct hetero-arylation polymerization (DHAP). Inverted PSCs were fabricated using PNDIOD-T2 as the acceptor and two polymer donors: PBDB-T and PTB7-Th. With PBDB-T as the donor, the PNDIOD-T2 based device showed a high PCE of 7.3% with a J_{SC} of 12.55 mA cm^{-2} and a V_{OC} of 0.90 V with a 0.65 FF for the all-PSC without the use of solvent additives, which are much higher than those of the N2200 polymer based device. The higher performance of the PNDIOD-T2 acceptor was assisted by finer phase separated morphology which resulted from blend film aging. The lower performance of the N2200 based device was attributed to structural bithiophene homocoupling defects.[240g]

Shi *et al.* synthesized a series of NDI-based low band-gap polymer acceptors (**322**, **324** and **321**) P(NDI2OD-T2), P(NDI2OD-Se2), P(NDI2OD-Se), and P(NDI2HD-Se) with different building blocks and side chains. To achieve high performance all-PSCs they substituted the thiophene ring in (**322**) by selenophene and diselenophene groups in order to enhance the light absorption and charge mobility. The optical and electrochemical properties demonstrated that the molecular structures of these new polymers can be tuned effectively. It was found that by changing the coplanarity of the molecule the intermolecular packing of the polymer acceptor can be tuned, and aggregation of these polymers in solution and in solid films induces structural changes in the polymer backbone which affect the photovoltaic performance. The optimized all-PSCs based on the PTP8:P(NDI2HD-Se) (**321**) blend exhibited the highest PCE of 6.0%, resulting from the improved morphology and fine-tuned energy levels. The higher PCE may be due to the favourable crystallinity of the donor/acceptor blend, resulting in ideal phase separated morphology and balanced electron/hole transport.[240s]

Wang and co-workers developed new polymer acceptors named P-BNBP-Se and P-BNBP-T based on electron deficient building blocks containing B to N subunits, and double B to N bridged bipyridine (BNBP). In general, the NDI based polymer electron acceptors (**322**) exhibit low lying E_{LUMO} energy levels resulting in low open circuit voltages for all-PSCs, so to tune their LUMO levels they introduced the BNBP unit to NDI backbones. The optical and electrochemical investigations showed a lower E_{LUMO} for the BNBP unit and selenophene unit based polymer, with that of P-BNBP-Se lower by 0.16 eV than the BNBP unit and thiophene unit based copolymer. As a result of the lower E_{LUMO} the P-BNBP-Se exhibited matching energy levels with the PTB7-Th polymer donor. The PSC based on the PTB7-Th:P-BNBP-Se blend showed a high PCE of 4.26% with a V_{OC} of 1.03 V and a low energy loss of 0.56 eV. The same device based on the P-BNBP-T polymer acceptor showed a moderate PCE of 2.27%. This different performance is mainly attributed to the high electron mobility of the PTB7-Th:P-BNBP-Se based blend compared to the PTB7-Th:P-BNBP-T blend, which was found to be 2.07×10^{-4} cm^2 V^{-1} s^{-1} for P-BNBP-Se, much higher than 7.16×10^{-5} cm^2 V^{-1} s^{-1} for P-BNBP-T.[240o]

Woo and co-workers reported the effect of fluorination of NDI and found that fluorination increases the interfacial interactions between the donor and acceptors as well as charge dynamics. They synthesized NDI-based n-type polymer acceptors P(NDI2OD-T2) (**322**) and P(NDI2OD-T2F) (**353**) for all-PSCs along with the polymer donor PBDTTTPD. The PBDTTTPD:P(NDI2OD-T2)-based PSC exhibited a low PCE of 2.02% but had a high V_{OC} value of 1.03 V, whereas the fluorinated analogue polymer P(NDI2OD-T2F)-based device exhibited an enhanced PCE of 6.09% with increased J_{SC} and FF. Fluorination can thus enhance the electron/hole transport process and provide suitable blend morphology, and it was found that the PBDTTTPD:P(NDI2ODT2F) based blend displayed highly efficient hole transfer and long-lived polarons.[53]
Asha and co-workers synthesized a new series of n-type NDI–bithiophene/PDI–bithiophene random copolymers (**454**). They tuned the optical, electrochemical and semiconducting properties of P(NDI2OD-T2) (**322**) by introducing varying amounts of PDI as co-acceptors *via* Stille coupling copolymerization, along with the NDI unit named NDI-Th-PDIx (x = 15, 30 and 50 mol% of PDI). They observed reduced self-aggregation, enhanced pi-pi stacking distance and reduced crystallinity compared to P(NDI2OD-T2). The ΔH_m value for the random copolymer:PTB7-Th blend was found to be lower than that of the PTB7-Th:P(NDI2OD-T2) blend, suggesting reduced crystallinity and higher PL quenching in random copolymers. NDI-Th-PDIx was investigated using two donor polymers, PTB7 and PTB7-Th, and both donor based devices PTB7-Th:NDI-Th-PDIx and PTB7:NDI-Th-PDIx showed better photovoltaic performance than the reference PTB7-Th:P(NDI2OD-T2) based blend. The PTB7 donor showed a higher PCE of 5.03% with the NDI-Th-

PDI30 polymer acceptor, much higher than the PTB7 based donor. The PTB7-Th:NDI-Th-PDI30 blend exhibited improved charge carrier transport with 4.2×10^{-4} and 1.5×10^{-4} $cm^2 V^{-1} s^{-1}$ hole and electron mobilities, respectively.[304]

Song and co-workers introduced an n-type semiconducting material NDI based acceptor (**437**) onto ITO using 3-bromopropyltrimethoxysilane (**438**) as a coupling agent. The ITO surface in configuration (**440**) was designed to improve the surface modification and device stability of PSCs. The modified ITO showed a decreased WF from 4.70 to 4.23 eV, showing matching LUMO energy levels to the fullerene acceptor. When the modified ITO cathode interlayer was used in PSCs, the inverted PTB7-Th:$PC_{71}BM$ based device showed a high PCE of 5.87%, much higher than that for the same device without the cathode interlayer, which showed a 3.58% PCE. This dramatically improved performance was mainly attributed to the improved open circuit voltage and the strong chemical bond formation between NDI-TMS films. They also found enhanced stability for inverted PSCs due to these chemically bonded interlayers (Fig. 95).[297]

Gao *et al.* synthesized benzodithiophene-modified NDI-based terpolymer acceptors with reduced molecular planarity and crystallinity, to achieve the stable and improved performance of all-PSCs. To adjust the molecular packing and the crystallinity of polymer they synthesised A–D_1–A–D_2 type terpolymer acceptors, PNDI-BDT_x (x = 0.5, 0.1 or 0.2) (**479**), by replacing varying amounts of bithiophene in the N2200 (**322**) backbone with 8-bis[5-(2-ethylhexyl)-2-thienyl]benzo[1,2-*b*:4,5-*b*′]dithiophene (BDT) units. They compared this systematically with its analogue N2200 using three polymer donors: PBDB-T, PTB7-Th and PDCBT to fabricate PSCs, and compared their performance with polymer acceptors, finding that the PNDI-BDT5 and PNDI-BDT10 based devices showed enhanced photovoltaic performance compared to N2200 based devices. The PBDB-T:PNDI-BDT10 based blend exhibited the best average PCE of 5.80%, higher than the value of 5.16% for the PBDB-T:N2200 blend. The other polymer donors PTB7-Th and PDCBT showed relatively lower PCEs of 3.90% and 1.96% for the PNDI-BDT10 acceptor, higher than the values of 2.81% and 1.41% for the N2200 based acceptor, respectively. They also studied the effect of excess BDT content on device performance and found a greatly reduced PCE with the increase in BDT content. The PBDB-T:PNDI-BDT10 based device showed long term thermal stability compared to other acceptor based devices.[320]

Lee and co-workers reported thermally and mechanically stable PSCs from the NDI based polymer acceptor P(NDI-2T) (**322**) with the fullerene acceptor $PC_{71}BM$, along with the small molecule donor BDT2TR. The fullerene acceptor based device BDT2TR:$PC_{71}BM$ showed a high PCE of 8.20%, with the BDT2TR:P(NDI-2T) based device showing a PCE of 4.43% with a high FF of 71%. They found that the BDT2TR:P(NDI-2T) based blend was thermally stable compared to the $PC_{71}BM$ based device, even after exposure to a temperature of 150 °C for 15 h.[240r] In the next report, they have employed a dual acceptor strategy for high performance PSCs. They have incorporated various electron accepting units such as 2,2′-(perfluoro-1,4-phenylene) dithiophene, benzothiadiazole and fluorinated benzotriazole, respectively, into the N2200 (**322**) backbone, and reported three polymer acceptors (**368c**, **340** and **408**). Optical properties showed a strong absorption band in the region from 300 to 800 nm for all three polymer acceptors, while (**368c**) showed an absorption maximum at 530 nm and a large band gap complementary to the polymer donor PTB7-Th. The device based on the PTB7-Th:(**368c**) blend achieved a higher photovoltaic performance compared to (**340**, **408**) based devices, affording a PCE of 3.24%, higher than 2.93% and 1.52% for (**340**, **408**) based devices, respectively.[240v]

Xu and co-workers synthesized four fluorinated D–A polymer acceptors composed of an NDI backbone and fluorinated phenyl units named PNDI-xF-Ph (x = 0, 0.1, 0.2 and 0.4) (**368a–d**). They systematically investigated the effect of fluorine substitution on the optical and electrochemical properties of acceptors and observed multiple effects such as improved light absorption, broadened optical band gap and changes in crystallinity of the polymers. Upon increasing the fluorine number the frontier energy levels (HOMO, LUMO) are lowered and molecular ordering of polymer acceptors was observed. A simple spin coated photovoltaic device was fabricated using the PTB7-Th donor polymer and (**368a–d**) acceptors. The mono- and di-fluorinated polymers (**368a**) and (**368b**) showed higher performance than the respective non-fluorinated polymer PNDI-0F-Ph. In contrast, the tetra-fluorinated polymer (**368c**) showed a very low PCE, lower than that of the non-fluorinated polymer acceptor. The di-fluorinated (**368b**) based device exhibited the highest PCE of 2.50%. Hence their findings show that optimised use of fluorine can be effective in constructing high performance PSCs.[247e]

Cho *et al.* introduced isoindigo-based small molecular additives to improve the performance of all-PSCs. The small molecular additive, 6,6′-dithiopheneisoindigo (DTI), which is highly crystalline in nature was synthesized. The DTI exhibited extended conjugation and could help to maintain effective charge carriers when used in the blend film PTB7-Th:P(NDI2HD-T) (**320**), with the PCE changing dramatically from 5.9% to 6.8%. Their investigation showed that even a small amount of DTI improved the crystallinity without phase separation of the blend surface. They found that the addition of DTI increased the exciton dissociation, charge carrier mobility, and reduced charge recombination to greatly enhance the performance of the PSCs. They have also used the DTI additive in various devices such as PTB7 Th:P(NDI2HD-T) (**320**) (PCE: 5.90/6.81%), PTB7-Th:P(NDI2HD-Se) (**321**) (5.83/6.52%), PTB7-Th:P(NDI2HD-T2) (**322**) (5.75/6.30%), and PPDT2FBT:P(NDI2HD-T) (**320**) (3.77/4.43%) and found that the PCE for each device increased.[329]

Michinobu and co-workers synthesized D–A_1–D–A_2 type polymers (**334–337**) with different side chains such as PNT-R (**337**), R = 2-decyltetradecyl (DT), 2-octadecyldodecyl (OD), and 2-hexyldecyl (HD). They observed that a decrease in the side chain length enhanced the absorption, with deeper LUMO levels, strong electron affinity and well phase separated morphology. The decrease in side chain length enhanced

the packing properties of the polymer with crystalline microstructure in the donor/acceptor blend. This resulted in a high electron mobility for the PNT-HD based polymer of 1.05 cm^2 V s^{-1}. In PSCs with the PBDTTTPD donor polymer the PNT-HD based device showed a high PCE of 6.62% with a very high J_{SC} of 12.07 mA cm^{-2} which is much higher than the J_{SC} values of 7.67 and 10.19 mA cm^{-2} for devices based on PNT-DT and PNT-OD blends, respectively.[234] Fang *et al.* synthesized A–A′–A type PNNT (**489**) polymer acceptors composed of NDI as the A′ unit and thiazoles as the A unit. They found that the polymers exhibited strong absorption, an excellent electron mobility of 10^{-4} cm^2 V^{-1} s^{-1} and an electron affinity of 4.3 eV. When (**489**) was used in PSCs, the BHJ devices afforded very poor PCEs. When PBDTT-FTTE was used as a polymer donor the SD device showed the highest PCE of 4.5%. These results suggest that there was interrupted packing of polymers in BHJ films compared to the SD device.[321e] Zhang *et al.* synthesized a series of new iso-NDI polymers, composed of the iso-NDI backbone and 2,2′-bithiophene (BT) (**556**), 3,3′-difluoro-2,2′-bithiophene (fBT) (**557**) and 2,2′-bithiazole (BTz) (**558**) units, for the copolymerization of the electron deficient iso-NDI unit (Fig. 117). They found that the iso-NDI based polymers exhibited higher E_{LUMO} energy levels by 0.36 eV, which ultimately resulted in greater V_{OC} in all-PSCs compared to the classical polymer electron acceptor N2200 (**322**). They also found that these iso-NDI-based polymers exhibited blue-shifted absorption and lower charge transport, leading to lower photovoltaic performance than that of the reference polymer N2200. When blended with the P3HT donor polymer the iso-NDI based device showed the highest PCE of 0.27%.[367]

Bao and co-workers reported a comparative study of the morphology of P3HT:PCBM based blend in comparison with P3HT:PNDIT (**320**) blend films, to attain high performance PSCs. Very distinct behaviour was observed for the P3HT:PCBM blend compared to P3HT:PNDIT based blend film because of the different mobilities of P3HT in the donor/acceptor blend. Furthermore, PNDIT showed poor affinity compared to PCBM to form mixed phases with P3HT, resulting in inhibition of crystallization of the donor polymer, which creates ideal small phase separation in the active layer between the donor and acceptor polymers.[306] Son and co-workers reported the effect of the molecular orientation of the polymer donor on charge generation and photovoltaic properties in all-PSCs. They synthesized five donor polymers by random copolymerization of 5-fluoro-2,1,3-benzothiadiazole with different concentrations of 2,2′-bithiophene (2T) and dithieno[3,2-*b*;2′,3′-*d*]thiophene (DTT) named P2T, PR1, PR2, PR3, and PDTT, where all the copolymers exhibited different molecular orientations. The PSCs were fabricated using these polymer donors and PNDI (**322**) or $PC_{71}BM$ as the polymer acceptor. They found that the charge transport for PNDI-based PSCs was much more dependent on the molecular orientation of the polymer donor compared to $PC_{71}BM$ based PSCs. In PNDI-based PSCs the polymer donors showed a high number of face-on-oriented crystallites, which results in an increase in the J_{SC} and EQE values and hence the performance of the PSCs. The PR2:PNDI based PSC exhibited an improved PCE of 6.01% compared to 3.11% for the PDTT donor based device. The edge-on orientation of the P2T polymer in the blend film results in decreased EQE and PCE values with the PNDI acceptor, where the PNDI polymer exhibited face-on orientation. On the other hand, the PR2 polymer showed face-on orientation and therefore exhibited high EQE and PCE values with PNDI polymer with a PCE of 6.01%, whereas PR2 with $PC_{71}BM$ exhibited a highest PCE of 7.03% due to the large population of face-on orientation of polymer donors in the blend films.[306]

Weng *et al.* synthesized two new polymer acceptors based on A_1–D–A_2–D using electron deficient five membered heterocyclic rings such as 1,3,4-oxadiazole (OZ) or 1,3,4-thiadiazole (TZ) and an NDI backbone, named PNOZ and PNTZ (**343**, **344**), respectively. They found that both the acceptors exhibited broad absorption spectra and deep LUMO energy levels below −4.0 eV, with phase separated microstructures. The polymer donor PTB7 in the all-PSC containing PNTZ polymer acceptor showed a best PCE of 2.58% with a high J_{SC} of 10.05 mA cm^{-2} due to the phase separated active layer morphology, whereas the PNOZ acceptor based optimized device showed a highest PCE of 1.22%.[240u] Chochos and co-workers synthesized a novel n-type conjugated polymer (**476**) *via* an $A_3 + B_2$ synthetic approach. The bulky side chains were introduced for the solubility of the (**476**) polymer in common organic solvents. They found good thermal stability and a broad absorption spectrum in the visible region for the (**476**) polymer along with reversible redox properties. The solution processable BHJ device PTB7-Th:(**476**) exhibited PCEs of 0.3% and 1.2% for conventional and inverted PSCs, respectively.[314] Kim *et al.* synthesized a new polymer acceptor, P(NDI2DT-TTCN) (**342**), for use as the ETL and replaced fullerene acceptors in inverted perovskite solar cells. The P(NDI2DT-TTCN) has strong electron withdrawing dicyanothiophene groups and an NDI backbone. Electronic and optical properties showed deep LUMO energy levels and the intermolecular interactions between N and S lead to strong electron mobility of (**342**). (**342**) showed enhanced electron extraction properties, and the hydrophobic ETL surface prevents ambient state interference. When compared to fullerene PCBM based ETL the P(NDI2DT-TTCN) ETL based perovskite devices showed good mechanical strength and a high PCE of 17.0% compared to the fullerene based ETL which showed a 14.3% PCE.[330] Further, Kim and co-workers synthesized a series of copolymers containing different compositions of the electron-rich donor unit 2-ethylhexylthienyl substituted benzo[1,2-*b*:4,5-*b*′]dithiophene (BDTT) and the electron-deficient acceptor unit fluorinated thieno[3,4-*b*]thiophene (TT-F). By controlling the molar ratios of BDTT and TT-F they synthesized a series of polymer donors, such as 1 : 1 (P1), 3 : 1 (P2), 5 : 1 (P3), and 7 : 1 (P4), with different BDTT:TT-F ratios. By changing the donor/acceptor ratios in polymers they tuned the absorption properties, and the absorption maxima of polymer donors were gradually blue-shifted from 703 to 548 nm when the donor/acceptor ratio increased from 1 : 1 to 7 : 1, whereas their blends with P(NDI2HD-T2) (**322**) showed increased light absorption. Hence this improved light absorption enhanced

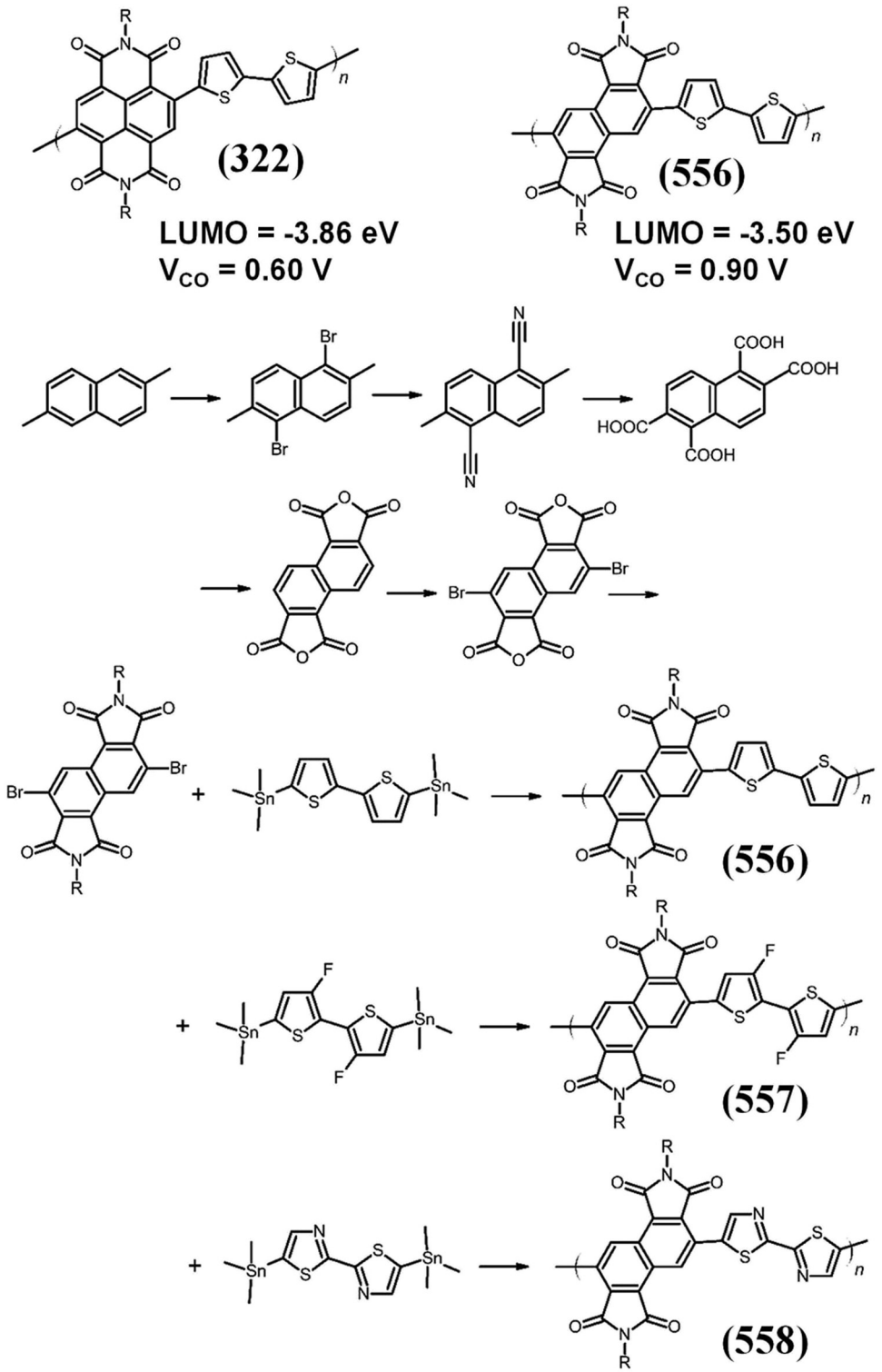

Fig. 117 Schematic illustration of the replacement of the 1,4,5,8-NDI unit with the 1,2,5,6-NDI unit to develop polymer electron acceptors with high-lying E_{LUMO} and enhanced V_{OC}. Synthetic routes of iso-PNDIBT (**556**), iso-PNDI2fBT (**557**), and iso-PNDIBTz (**558**). Reagents and conditions: (i) iron powder, I_2, Br_2, CCl_4, −10 °C, r.t.; (ii) CuCN, DMF, reflux; (iii) $K_2Cr_2O_7$, NaOH, H_2O, 200 °C; (iv) acetic anhydride, reflux; (v) NBS, H_2SO_4, 130 °C; (vi) acetic acid, 2-octyldodecylamine, reflux; and (vii) $Pd_2(dba)_3{\cdot}CHCl_3$, P(o-Tol)$_3$, reflux.[367]

the J_{SC} values and also the performance of the all-PSCs. The performance of the all-PSCs showed that these P series polymer donors exhibited a higher PCE with the P(NDI2HD-T2) polymer acceptor compared to PCBM and fullerene acceptors. Polymer P3 showed a high PCE of 6.81% with a higher J_{SC} of 14.40 mA cm^{-2} with the P(NDI2HD-T2) polymer acceptor compared to 5.58% with

PCBM acceptors. For PCBM based devices as the donor/acceptor ratio of the polymer donor increased from P1 to P4 the PSC exhibited a gradually decreased PCE.[240a]

Sun *et al.* reported the imide-functionalized heteroarene-based n-type terpolymers for additive-free all-PSCs. They synthesized imine-functionalized random terpolymers based on heteroarene units, BTI2-*x*TPD (**564**), containing thienopyrroledione (TPD) (**559**) and f-BTI2 (**561**) as acceptor units and 3,4-difluorothiophene as the donor unit. They introduced the imide functionality in the polymer backbone to maintain favourable balance of crystallinity and miscibility of the polymers in the active layer with high charge mobility. They incorporated different TPD contents into the copolymer f-BTI2-FT (**563**), resulting in different terpolymers BTI2-*x*TPD. The TPD unit activated the intramolecular non-covalent S···O interactions which facilitated the face-on interactions of the polymers, and were also responsible for enhanced molecular planarity and charge transport processes. The additive free all-PSCs were fabricated using the PTB7-Th polymer donor, and it was found that the PTB7-Th:BTI2-30TPD exhibited a highest PCE of 8.28% with a very low energy loss of 0.53 eV, which is greater than the values 4.4% and 6.85% for the corresponding copolymers PTPD[2*F*]T(HD) (**562**) and f-BTI2-FT (**563**), respectively, as shown in Fig. 118. They also reported the stability of the device; after 400 h of aging the same device retained 90% of its initial PCE.[240f]

9.2 Transistors

Ryu *et al.* synthesized two new NDI and 3,3′-dichloro-2,2′-bithiophene (T2Cl2) based chlorinated polymers P(NDI2HD–T2Cl2) and P(NDI2OD–T2Cl2) (**338**) for n-channel semiconductor applications, where chlorine substitution in the polymer backbone lowers the FMO energy levels and widens the band gap of the polymer compared to the non-chlorinated analogue. They found that chlorinated NDI polymer based thin-film-transistors (OTFTs) displayed supressed ambipolarity due to lower HOMO energy levels and exhibited electron mobility approaching 0.1 $cm^2 V^{-1} s^{-1}$. They found that at high humidity or upon submersion in water the chlorinated NDI polymer based OTFTs exhibited much higher stability compared to non-chlorinated polymer based OTFTs. Excellent operational stability of the chlorinated NDI polymer based OTFTs was reported with $<3\%$ degradation after bias-stress tests (Fig. 119).[235]

Jenekhe and co-workers developed non-volatile electronic memory devices using PNDIBS (**324**) as high mobility n-type polymer semiconductors, and exploited charge trapping as a basis for high performance OFET devices (Fig. 120). Using the n-type polymer PNDIBS, OFET memory devices were fabricated and their charge trapping capacity investigated. They found that at 60 V PNDIBS-based OFET devices showed outstanding charge trapping and de-trapping properties. Durability of more than 200 cycles was observed with exceptional data retention, with a large on/off current ratio between two binary memory states. They also reported that when the n-type semiconductor is end-capped with a phenyl group the memory device performance was reduced, which was attributed to a lower trap density as well as charge trapping capability.[238]

Yan *et al.* synthesized two new metallopolyyne copolymers, composed of an electron deficient NDI spacer with different numbers of thiophene units functionalized with platinum (**521**, m = 1, 2). The absorption, electronic, thermal and charge transport properties were investigated to study the effect of the different numbers of thiophene units on the NDI backbone.

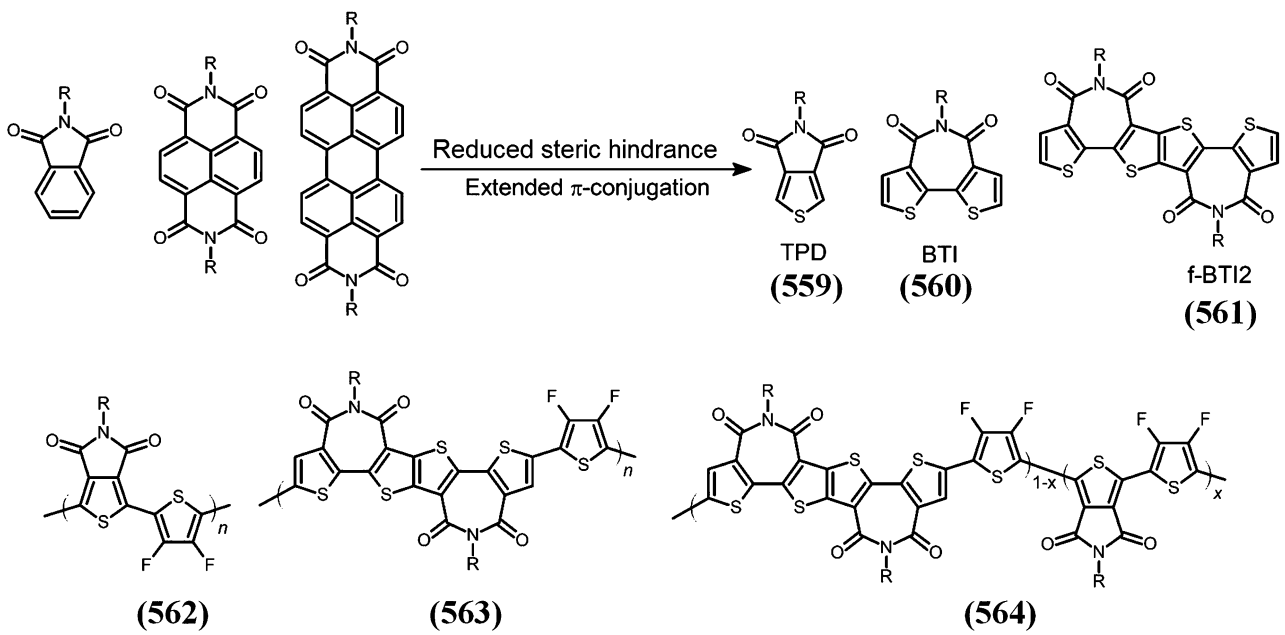

Fig. 118 Chemical structures of imide-functionalized arenes and heteroarenes, and imide-functionalized heteroarenes TPD and f-BTI2-based copolymer acceptors together with the derived terpolymers for all-polymer solar cells.[240f]

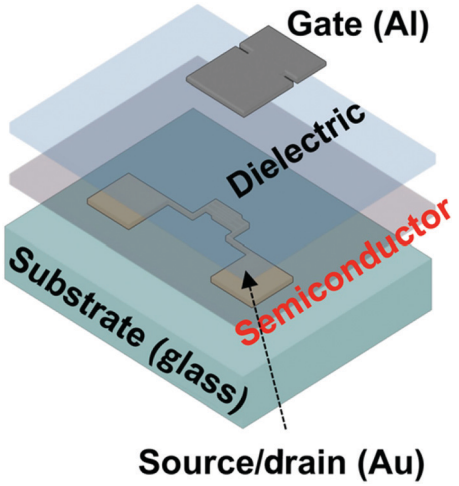

Fig. 119 Schematic of a TG/BC TFT architecture for NDI-based polymeric semiconductors to study the effect of chlorine incorporation and n-channel transistors operating in water.[235]

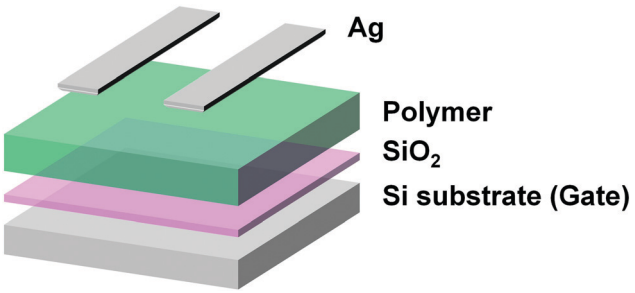

Fig. 120 Schematic of the charge-trapping organic field-effect transistor memory devices where NDI-based n-type polymer semiconductors (PNDIBS and ePNDIBS) are used.[238]

Interestingly, the solution processable polymers (**521**, m = 1, 2) showed π-channel FET properties, observing unipolar p-type transport compared to other NDI based polymers. They have demonstrated that these polymer (**521**, m = 1, 2) based OFETs are suitable for printable electronics.[237] Higashihara and co-workers reported the synthesis and OFET characteristics of NDI-based polymers (**279–282**) containing ambipolar semiconducting materials such as benzodithiophene or dithienopyrrole units. Later, they incorporated the 3-hexylthiophene (3HT) spacer between NDI and donor units, observing extended absorption with increased intramolecular charge transfer (ICT). (**281**, **282**) demonstrated a 250 nm red shift for ICT compared to (**279**, **280**) due to increased HOMO energy levels. Furthermore (**280**, **282**) showed ordered crystalline structures due to pi–pi stacking of the planar backbone, which increased due to the introduced 3HT spacer. The fabricated FET device using (**279–282**) polymers showed dominant n-type transistor characteristics, whereas the FET based on the (**281**, **282**) polymer showed higher electron mobility and higher I_{on}/I_{off} up to 1.5×10^{-2} cm^2 V^{-1} s^{-1} and 10^5, respectively, compared to the (**279**, **280**) polymer.[198]

Bao and co-workers synthesized high performing NDI-based n-type conjugated polymers attached with polystyrene (PS) side chains (**385**) by terminating the living anionic polymerization. The effect of PS side chains with 0–20 mol% on the conjugated polymer backbone and its electrical properties were investigated and it was found that all the polymers showed a high electron mobility of around ≈0.2 cm^2 V^{-1} s^{-1} (Fig. 80). Interestingly the FET device with 20 mol% of PS showed strongly improved electron mobility and improved transistor device stability for several weeks compared to the polymer with a lower PS concentration. The improved stability was attributed to the covalently bonded PS side chain encapsulating layer around the semiconducting polymer backbone. Furthermore they found that crystallinity decreases with an increase in PS side chain content.[253] Kim and co-workers synthesized two NDI-based copolymers *via* Stille coupling with different alkyl side chains, *i.e.*, P(NDI-T2VT2)-24 and P(NDI-T2VT2)-28 (**345**, **346**). The P(NDI-T2VT2) polymer has NDI as electron accepting and bithiophene vinylene bithiophene as electron donating units. n-Type transistor characteristics were observed for both the polymers with an electron mobility of 0.015 cm^2 V^{-1} s^{-1} for (**345**) and 0.019 cm^2 V^{-1} s^{-1} for (**346**). The slightly higher mobility of (**346**) OFETs was mainly due to better solubility and crystallinity compared to the (**345**) polymer.[240k] Liang *et al.* reported the conjugated polymer poly(NDI-vinylene) (PNV) (**397**), which exhibited red emission in solid state and good semiconducting properties for transistors. The conjugated polymer was synthesized by connecting a vinyl unit to the NDI group. The hydrogen bonding C–H–O between the carbonyl group of NDI and vinyl led to a slightly twisted structure which was explained by DFT calculations, and this hydrogen bonding was a promising factor for enhanced emission in both solid and solution states. The strong red emission in the solid state led to 33.4% PL efficiency with electron mobility up to 1.5×10^{-3} cm^2 V^{-1} s^{-1} for the fabricated OFETs based on (**397**).[260] Hamburger and co-workers reported the NDI based n-type semiconducting polymers (**565–567**). The side chains were thermally cleavable at curing temperatures between 180 and 220 °C, resulting in strongly reduced solubility. The OFETs based on these polymers showed satisfactory device performance, and cleavage of side chains results in decreased device performance, whereas the increased OFET mobilities can be attained by improving non-cleavable side groups (Fig. 121).[368]

Maria *et al.*[369] investigated the use of hydrophobic propyl and hexyl spacers to minimize detrimental swelling close to the conjugated backbone and balance the mixed ionic and electronic conduction properties of n-type materials in aqueous electrolytes. They found that polymers functionalized with alkyl spacers outperform their analogue bearing EG-only side chains in OECTs.

Sung *et al.* reported the donor–acceptor NDI-based polymer containing selenophene vinylene selenophene as a donor unit P(NDI–SVS) (**332**). The P(NDI–SVS) polymer exhibited decreased energy band gap and marginally lower LUMO energy levels of 1.31 eV and −3.98 eV, respectively, compared to the reference

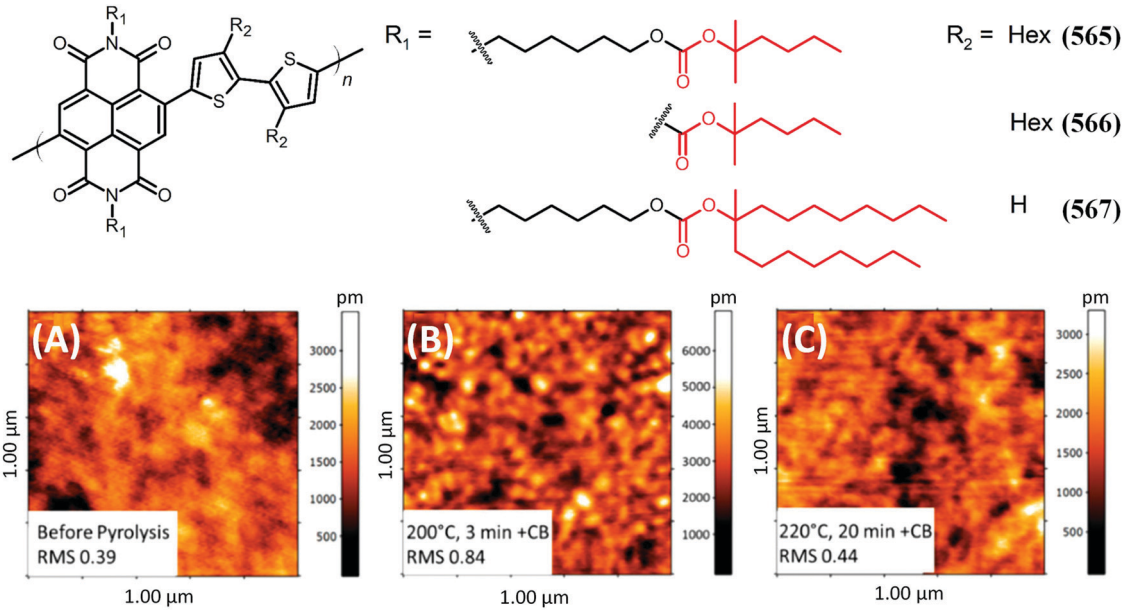

Fig. 121 The chemical structure of the NDI–bithiophene based polymers with thermally cleavable side chains (red) and the atomic force measurements of polymer 3 based films (A) before pyrolysis, (B) after pyrolysis at 200 °C for 3 min and CB, and (C) after pyrolysis at 220 °C for 20 min and CB.[368] This figure has been adapted from ref. 368 with permission from The American Chemical Society, copyright 2016.

copolymer P(NDI2OD-T2) (**322**). The solution processed OFET optimized device based on P(NDI–SVS) showed a high field-effect mobility of 2.4 $cm^2\ V^{-1}\ s^{-1}$ with excellent ambient stability. Improved crystallinity was observed by annealing at temperatures above 180 °C, whereas the high electron mobility for the PNDI–SVS based OFET was already achieved at 150 °C, supporting plastic-based flexible circuit applications of the P(NDI–SVS) polymer.[240m] Jin and co-workers reported various π-conjugated polymers NDI-T-1FP-T, NDI-T-2FP-T, and NDI-T-4FP-T (**368b–d**) synthesized by fluorination of NDI polymers with different fluorine atom contents (1F, 2F, and 4F). The significant effect of various amounts of fluorine atoms on the charge transfer properties of NDI based polymers was investigated. They found remarkable differences in their electronic properties including energy levels, ground and excited state dipole moments ($\Delta\mu_{ge}$), exciton lifetimes, dihedral angles, and charge transport behaviour of NDI polymers with different fluorine contents. As the fluorine content increases a reduced $\Delta\mu_{ge}$ and charge transfer properties were observed. The optimized OFET devices using n-type π-conjugated polymers showed high electron mobilities of 0.35, 0.18, and 0.16 $cm^2\ V^{-1}\ s^{-1}$, respectively, which considerably increased to 0.51, 0.34, and 0.26 $cm^2\ V^{-1}\ s^{-1}$, respectively, upon doping of a very low amount of polyethylenimine (PEI). (**368d**) exhibited unipolar n-channel behaviour in OFETs due to the presence of the maximum number of fluorine atoms, whereas ambipolar behaviour was observed for (**368b**) and (**368c**) polymers with hole mobilities of 0.08 and 0.05 $cm^2\ V^{-1}\ s^{-1}$, respectively (Fig. 122).[51]

Zhang *et al.* reported the thiazole flanked NDI polymers, PTzNDI-2FT, PTzNDI-T, PTzNDI-Se, and PTzNDI-2T (**380–384**), containing TzNDI and four different donor units. These polymers exhibited coplanar conformation and deep lying HOMO energy levels mainly due to the presence of the TzNDI unit. The OFETs based on all the TzNDI-based polymers exhibited unipolar n-type transport characteristics with $\sim 10^{-9}$–10^{-8} A off

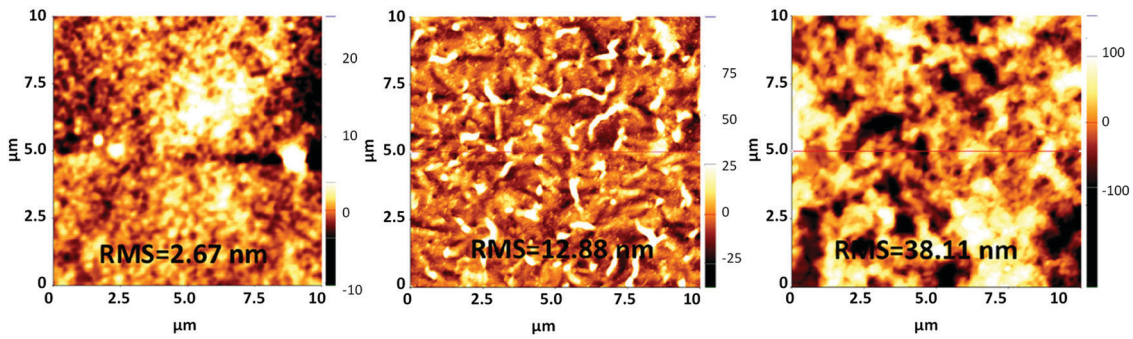

Fig. 122 AFM images (10 µm × 10 µm) of NDI-T-1FP-T (**368b**), NDI-T-2FP-T (**368c**), and NDI-T-4FP-T (**368d**) films coated from chlorobenzene solution.[51] This figure has been adapted from ref. 51 with permission from The American Chemical Society, copyright 2018.

current and 10^4–10^7 on–off current ratios. The near-ideal transfer curves with kink-free transfer characteristics were observed for all polymer based OFETs with suppressed hole transport. The PTzNDI-2FT based OFET exhibited the highest electron mobility of 0.57 $cm^2\ V^{-1}\ s^{-1}$ among all the polymers, which was also greater than that of the N2200 (**322**) based OFET, which displayed a 0.41 $cm^2\ V^{-1}\ s^{-1}$ electron mobility.[252a]

Liu and co-workers reported a simple and efficient side-chain engineering strategy to develop a new NDI-based n-type polymer PNDI2T-DTD (**322**) with a bithiophene backbone to fabricate flexible high performance thin-film transistors. They demonstrated that branching/linear side-chain engineering also leads to improved charge transport properties of the transistor. Replacing the branched alkyl chain by a linear alkyl group in the P(NDI2T-DT) polymer gave P(NDI2T-DTD), an n-type NDI–bithiophene polymer. The P(NDI2T-DTD) polymer, containing flexible side chains compared to P(NDI2T-DT), showed short π–π stacking distances and improved lamellar packing of the polymeric chain, leading to enhanced thin-film crystallinity. The improved pre-aggregation behaviour of P(NDI2T-DTD) was investigated by absorption spectroscopy. The fabricated FET device (Fig. 123) based on P(NDI2T-DTD) showed a high electron mobility of 1.52 $cm^2\ V^{-1}\ s^{-1}$ on flexible poly(ethylene terephthalate) (PET) substrates, very much higher than that of the P(NDI2T-DT) based FET. The P(NDI2T-DTD) based device when exposed to air for 100 days showed a 1.50 $cm^2\ V^{-1}\ s^{-1}$ maximum electron mobility, indicating strong air stability.[240h]

Park *et al.* synthesized two new NDI-based polymers by modifying the vinylene position with two different donor units P(NDI-VTV) and P(NDI-VSV) (**350**, **351**) and studied their effect on electron transport properties. The effect of the vinylene position on the electron transport properties of NDI-based polymers was investigated using an additional two polymers (**330**, **332**) along with (**350**, **351**). They found that the incorporation of a vinylene group between thiophene and selenophene units leads to a higher backbone planarity for (**350**, **351**) polymers compared to PNDI–TVT and PNDI–SVS polymers. The grazing incidence X-ray diffraction measurements showed that polymers (**350**, **351**) with shorter acceptor monomer units exhibited strong face-on orientation, whereas the polymers (**330**, **332**) exhibited mixed face-on and edge-on orientations with higher crystallinity due to the presence of longer monomer units. The optimized OFET device based on (**350**, **351**) polymers showed electron mobilities of 0.043 and 0.7 $cm^2\ V^{-1}\ s^{-1}$, respectively, which are much lower than those of (**330**, **332**) polymer based OFETs.[240n]

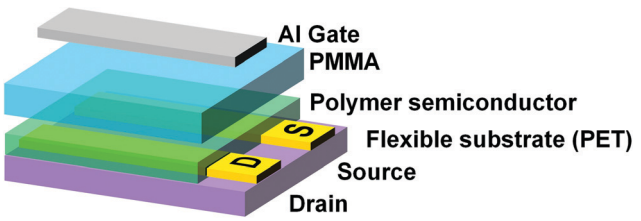

Fig. 123 Schematic illustration of the top-gated FET device structure for the study of n-type organic NDI–bithiophene based polymeric semiconductors.[240h]

Kim *et al.* reported flexible and durable polymer FETs fabricated using flow-coating DPP and NDI based polymers named P(DPP2DT-T2), P(DPP2DTTT), P(DPP2DT-DTT), P(NDI2OD-T2) (**322**), P(NDI2OD-F2T2) (**353**), and P(NDI2OD-Se2) (**324**). These polymers exhibited very high carrier mobilities and very high on/off ratios. There were no noticeable changes observed in the electrical characteristics of these polymer based FETs even after a 300-cycle bending test. All the polymers showed high performance in FET devices, with greater than 10^7 on/off current ratios. The highly crystalline nature of the polymer films was responsible for this high performance. Furthermore, they found that 150 °C annealing temperature was ideal for controlling the polymer film morphology. The device performance showed that the highest electron mobility of 0.85 $cm^2\ V^{-1}\ s^{-1}$ was exhibited by the (**324**) based FET.[240l] Wang *et al.* reported N-doped polymer FETs with improved electron transport and reduced contact resistance. The dimeric air-stable dopant $(RuCp^*Mes)_2$ (**401**) was applied to OFETs based on the n-type P(NDI–DPP) polymer (**400**). It was found that R_{con} and V_{th} can be adequately tuned by dopant concentration, and increased electron transport and large on/off ratios were observed in n-doped OFETs with a lower concentration of the $(RuCp^*Mes)_2$ dopant. The n-doping with $(RuCp^*Mes)_2$ was confirmed by up-shifted Fermi levels, whereas the different concentration of dopant was exposed by XPS spectroscopy. After doping the electron transport was increased, leading to improved OFET mobility, whereas enlarged off-state current was observed.[263]

9.3 Other NDI-based polymers

Lapkowski and co-workers synthesized novel PTCDA and NTDA based polymers with polyetheramine. The new polymers exhibited low lying LUMO levels, with electron affinity ranging from −4.28 to −4.14 eV, and this can be beneficial for the polymers to be used in air operating devices. Furthermore, all the new polymers exhibited strong solubility in organic solvents and were fully soluble in $CHCl_3$, CH_2Cl_2 and NMP at room temperature. EPR measurements showed that radical anion formation results from the reduction of the polymers. The fluorescence properties of (**570**, **571**) showed significant fluorescence leading to high quantum yields of 0.46 and 0.68, respectively. For the blends of (**570**, **571**) with PMMA the quantum yields observed were 0.04 and 0.15, respectively.[64]

Chen *et al.* synthesized (**572**, **573**) NDI and pyromellitic diimide homologue polymers for memory devices. They found different electrical switching effects for (**572**) and (**573**), where both (**572**, **573**) were able to form a number of charge transfer complexes due to dissimilar π–π* conjugations (Fig. 124). The memory device investigation demonstrated the dynamic random access memory characteristics for Al/(**573**)/indium tin oxide (ITO) based device, whereas for the Al/(**572**)/ITO based device showed rewritable (FLASH) memory characteristics. Their results suggested that the memory performance can be

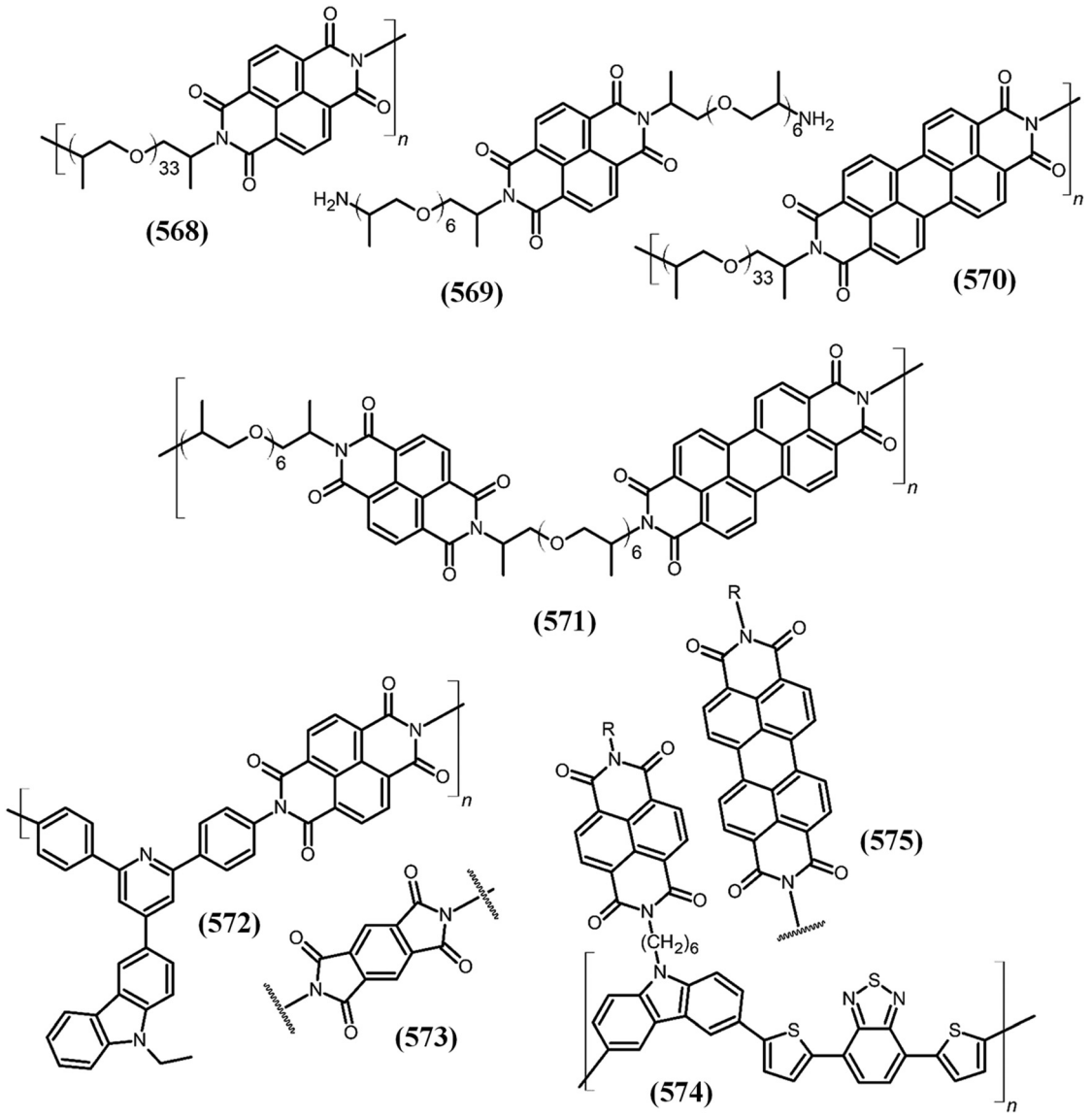

Fig. 124 The chemical structures of PDI and NDI *N,N′*-polymers and copolymers.[41,64,193]

affected by the electric field induced charge transfer materials.[193] Ledwon *et al.* have synthesized a new class of donor–acceptor type polymers containing two acceptor units with NDI and PDI side chains attached to a benzothiadiazole central unit (**574, 575**). They showed the independent reduction of the central polymer chain and NDI/PDI side groups. The separated charge was observed on the main polymer chain and on PDI/NDI side groups, with independent UV-Vis spectra for the main polymer chain and for the aromatic PDI/NDI side groups. (**575**) showed an electron affinity of 4.1 eV, whereas (**574**) showed a shifted electron affinity of 4.2 eV. They observed quite poor solar cell performance for these conjugated polymers.[41] Ledwon *et al.* synthesised a series of NDI based n-type conjugated polymers (**576–579**) and observed that radical anion formation occurs in the first reduced state which is then delocalized on NDI units (Fig. 125). The second reduced state forms a spinless species, and characterisation showed that the interactions between NDI units as well as stacking leads to aggregate formation. They have also applied these polymers in BHJ photovoltaic device applications, fabricated OSCs using P3HT as the donor polymer and demonstrated quite weak photovoltaic performance for these synthesized polymers.[370]

Ba and co-workers synthesized NDI based fully conjugated copolymers P(NDI–CZL) (**580**) and P(NDI–TTL) (**581**) with imine-bridged structures. Both the copolymers exhibited interesting absorption and electronic properties and very weak fluorescence (Fig. 126). It was also found that both the copolymers were thermally stable, with good solubility and solution processability. The observed M_n values for P(NDI–CZL) and P(NDI–TTL) were 18.9×10^3 g mol^{-1} and 26.0×10^3 g mol^{-1}, respectively. The HOMO energy levels for P(NDI–CZL) and P(NDI–TTL) were −5.47 eV and −5.68 eV, respectively. They further suggested that these copolymers can be used as acceptor materials to investigate the photovoltaic performance.[371]

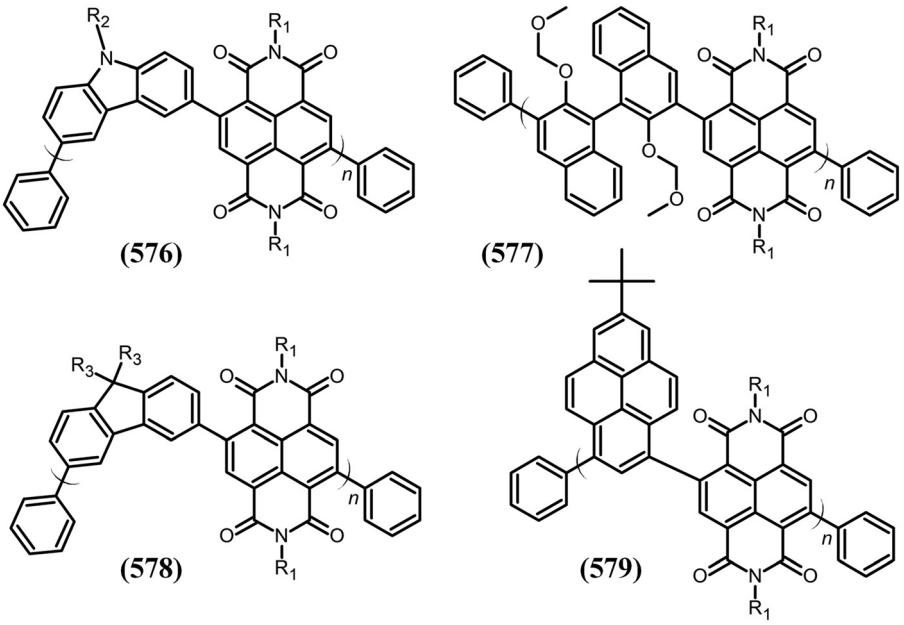

Fig. 125 The chemical structures of n-type conjugated polymers containing NDI acceptor units.[370]

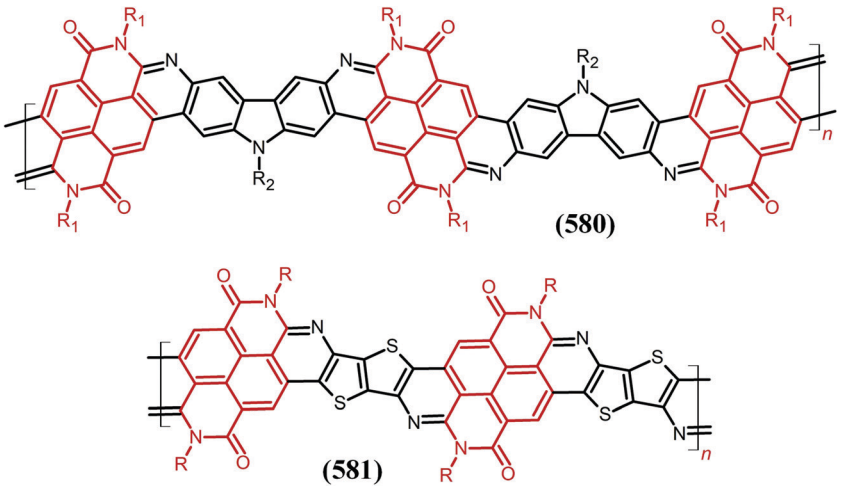

Fig. 126 Fully conjugated ladder NDI copolymers.[371]

Sommer and co-workers synthesized P(NDI-T2) (**322**) *via* direct arylation polymerization, where they optimised the thionation reaction with Lawesson's reagent (LR). They showed that out of four only two carbonyl groups of the NDI polymer react with LR, giving a regioregular thionated product with trans configuration. Even the use of excess LR reagent gives only gives the same dithionated product due to steric hindrance. They revealed the effect of thiocarbonyl groups on properties and stated that the 2*S*-*trans*-P(NDI-T2) (**328**) exhibited strong aggregation, slightly red-shifted absorption, low solubility, thermal stability and also a lower LUMO level by 0.22 eV when compared to PNDIT2.[231]

Horatz *et al.* reported two amorphous fluorene-NDI copolymers P(TNDIT-Fl(C_4C_2)) and P(TNDIT-Fl($C_{10}C_8$)) (**515**). The amorphous nature of the P(TNDIT-Fl(C_4C_2)) and P(TNDIT-Fl($C_{10}C_8$)) were observed by XRD with a high absorption spectrum in the range suitable for MALDI laser systems. For low molecular-weight compounds (LMWCs) they have used these copolymers as MALDI matrices, and compared them with P(NDI-T2) semi-crystalline polymer matrix. The amorphous matrices compared to semi-crystalline P(NDI-T2) polymer matrices give higher signal intensities resulting from the analyte insertion in the amorphous polymer matrix.[341f] Beverina and co-workers reported the synthesis of alternating naphthalene dianhydride (NDA) bithiophene copolymer P(NDA-T2) (**582**) as shown in Fig. 127. They found that P(NDA-T2) is insoluble in organic solvents. P(NDA-T2) exhibited a similar LUMO energy level to NDI analogues and showed a −3.9 eV LUMO energy level. They reported an alternative electron acceptor copolymer, insoluble P(NDA-T2), the oxo-

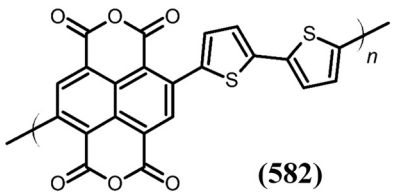

Fig. 127 The chemical structure of the naphthalene dianhydride bithiophene copolymer.[372]

analogue of NDI, which was synthesized by direct thermal treatment of soluble tetra-ester PNTET2.[372]

Zhang *et al.* functionalized the n-type copolymer P(NDI-T2) (**322**) with polyethylene glycol (PEG) and *N,N′*-alkyl chains (**583**), and investigated their potential applications in lipid bilayers. From synthetic lipid vesicles they formed a lipid bilayer on the surface of the P(NDI-T2) copolymer backbone. They used various compositions of EG and found that the EG concentration greatly affects vesicle/film interactions resulting in changes in the surface energy of the films (Fig. 128). The interactions of these surfaces with fluorophore-labelled liposomes were investigated by fluorescence microscopy. They observed different reproducible patterns from interactions between zwitterionic vesicles and high electron transport copolymer P(NDI-T2), indicating the wettability of the film. They also described the type of surface necessary for the lipid bilayer formation, and the liposomes favour the EG rich region forming the lipid bilayer.[373]

Tan *et al.* prepared and investigated the aggregation behaviour of an NDI based polymer, synthesized by reacting *N,N′*-*ω*-dialkenyl NDI with 2,5-dialkoxy-1,4-diiodobenzene (**584–588**), in the presence of $Pd(OAc)_2$-NaOAc catalyst (Fig. 129). The polymers exhibited strong absorption spectra and the light scattering measurement showed the aggregation of polymer with a 48 nm hydrodynamic radius. They also observed the elastic nature of the NDI based polymers, which, on heating at 110–122 °C temperature, becomes insignificant.[374]

Karpov *et al.* reported an isoindigo functionalized NDI based polymer, synthesized by a radical mechanism using activated Zn without addition into the C–Br bond. EPR measurements showed paramagnetic behaviour. They have synthesized the heteropolymer P(TiIT-*co*-TNDIT) (**589**) by copolymerising isoindigo and NDI based homopolymers (Fig. 130). They developed a simple polymerization approach at room temperature, whereas for poly-condensation, Suzuki and Stille reactions at prolonged high temperature were required.[375]

Gowd and co-workers described the three component hierarchical self-assembly of the electron donor pyrenebutyric acid (PBA), with the strong electron acceptor NDI and a block polymer. They synthesized the block copolymer supramolecule containing two small molecules and one polystyrene-*block*-poly(4-vinylpyridine) (PS-*b*-P4VP) *via* a self-assembly approach.

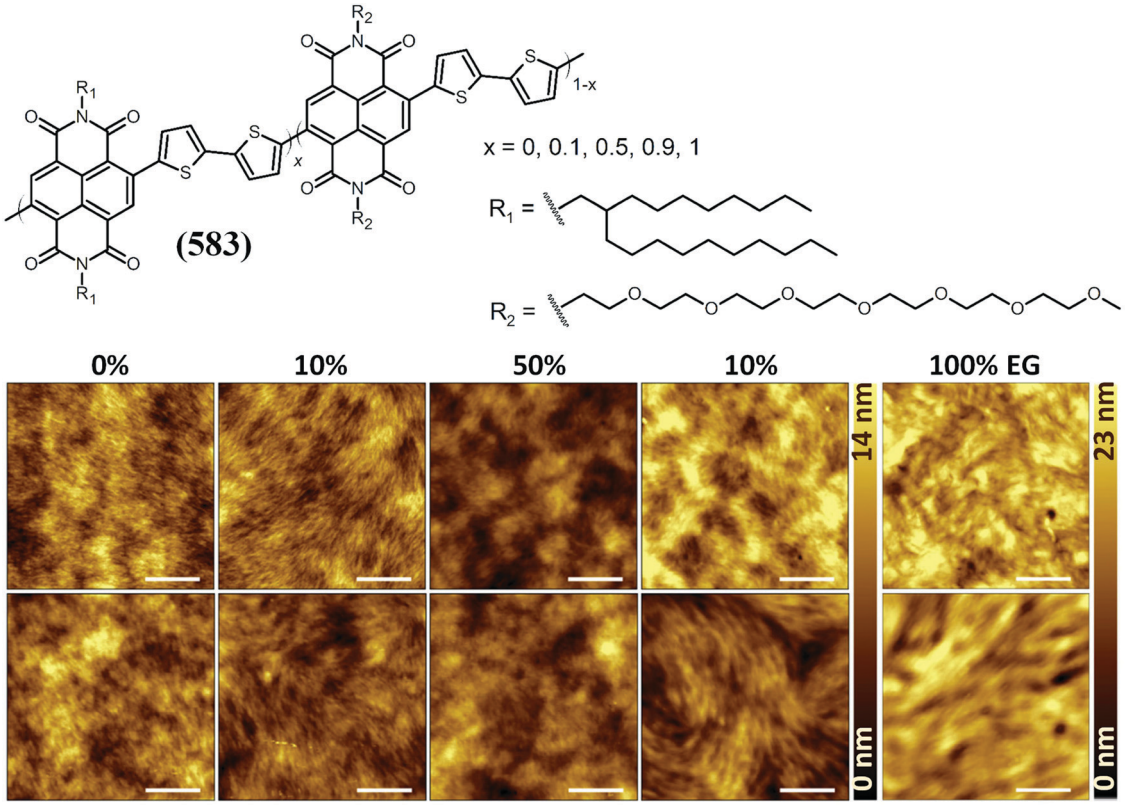

Fig. 128 Chemical structure of five NDI-dithiophene copolymers with 0, 10, 50, 90, and 100% EG chain percentages, and the AFM topography images of the polymer films characterized in air (upper panel) and in PBS (lower panel).[373] This figure has been adapted from ref. 373 with permission from The American Chemical Society, copyright 2018.

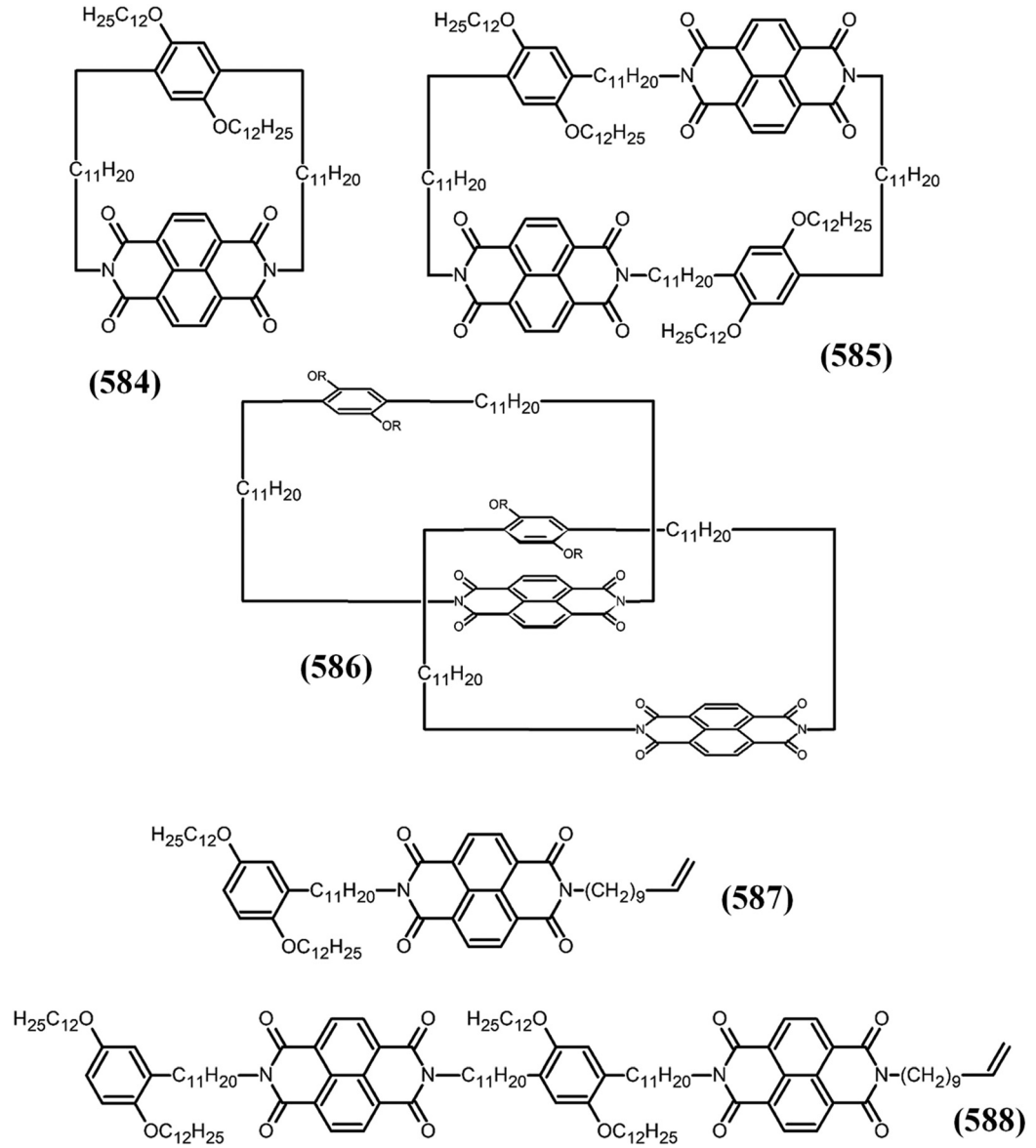

Fig. 129 Chemical structures of poly(arylene alkenylene)s and poly(arylene alkylene)s having dialkoxyphenylene and aromatic diimide groups.[374]

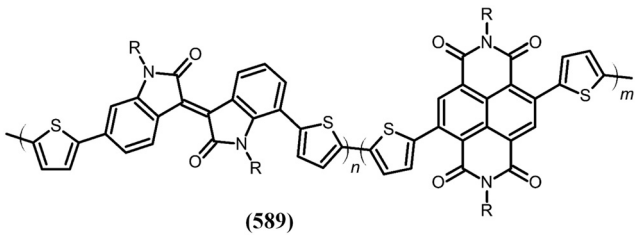

Fig. 130 The chemical structure of the NDI–thiophene-isoindigo-based copolymer.[375]

The hydrogen bonding between PBA and P4VP in solid state leads to cylindrical morphology in the bulk by aromatic–aromatic interactions, and CT complexes formed after further addition of NDI. They observed hierarchical structure formation between PBA and NDI due to organization of PBA and NDI in the polymer microdomain. The high charge carrier mobility of the PS-*b*-P4VP (PBA + NDI) supramolecule was confirmed by SCLC.[91] Kang *et al.* synthesized NDI based high electron mobility polymers P(NDIF-TVT) and P(NDIF-T2) (**410**, **411**), functionalized with semifluorinated alkyl side chains. They compared the microstructural organization of air-stable semiconducting polymers P(NDIF-TVT) and P(NDIF-T2) having semifluorinated alkyl side chains with their branched alkyl analogues. They found that both the polymers displayed high crystalline order, and self-organization of semifluorinated alkyl side chains induced rigidity in the resulting polymer forming a superstructure containing side-chain and backbone crystals. These polymers also exhibited high electron mobility and can be used as field-effect transistor materials, with unipolar n-channel transport. Specifically, P(NDIF-T2) showed an electron

mobility and an on–off current ratio of 6.5 $cm^2 V^{-1} s^{-1}$ and 10^5, respectively, higher than those of branched alkyl chain polymers.[247h] Nava *et al.* reported NDI based high electron transport copolymers, synthesized by substituting the two imide oxygens with sulphur, named 2*S-trans*-P(NDI-T2) (**328**), to fabricate flexible, air stable thermoelectric generators. The thionated 2*S-trans*-P(NDI-T2) exhibited lower LUMO energy levels and higher electrical conductivity compared to P(NDI-T2) (**322**), which leads to enhanced air stability. The n-type doped thionated copolymer (**328**) was stable to air for over 16 h. (**328**) and when doped with N-DPBI had higher electrical conductivity and power fraction than (**322**) doped films. An electrical conductivity of 6×10^{-3} S cm^{-1} and a high power fraction of 4.9×10^{-2} μW m^{-1} K^{-2} were observed for the (**328**) doped polymer.[240i] Park and co-workers have used fluorinated NDI based polymers to increase electron transport. They synthesized two NDI-based polymers P(NDI–TVT) (**330**) and fluorinated P(NDI–FTVT) (**352**). These two polymers exhibited major differences after thermal annealing. At elevated temperatures, the (**330**) film showed very poor electrical connectivity due to large crystalline domains, formed *via* self-assembly of the NDI moiety, whereas for the (**352**) polymer the robust aggregation of FTVT unit harvests the interconnected domain with extreme stability of the film morphology, improved electron mobility and enhanced electrical connectivity at high temperatures. The robust aggregation formation occurs due to improved intermolecular interactions between the FTVT unit and the polymer chain.[239] Liu *et al.* described two inorganic–organic hybrid coordination polymers containing semiconductive components for controlled photo-induced electron transfer. They synthesized coordination polymers from NDI and CuI or PbI_2 clusters, namely $[Cu_2I_2(DPNDI)]_n$ (a) and $[PbI_2(DPNDI)]_n$ (b) in Fig. 131 (where DPNDI = *N,N′*-di-(4-pyridyl)-NDI). Both the polymers exhibited comparable 2D heterostructures but showed different photo-induced electron transport properties. Compared to polymer (b), polymer (a) only undergoes intramolecular electron transfer reactions easily due to the greater HOMO energy level of $[Cu_2I_2]_n$ compared to $[PbI_2]_n$ giving a long-lived charge separated state for polymer (a).[376]

Medina *et al.* described how MO localization controls the bandgap for region (i-/r-) regular NDI- and PDI–bithiophene based copolymers. They reported two regular and irregular polymer acceptors based on NDI and PDI backbones, named i-P(NDI-2T) and r-P(PDI-2T) (**322**), respectively. The regio(ir)regular NDI- and PDI–bithiophene based acceptors showed similar absorption spectra even in the presence of cross conjugation. DFT calculations showed the frontier MO localization, where the FMO was localized on the PDI unit for the P(PDI-2T) copolymer, whereas FMO was mostly localized in the donor/acceptor units of the P(NDI-2T) copolymer.[240j] Frontera and co-workers demonstrated that inorganic–organic hybrid magnetic nanoparticles can adsorb volatile organic compounds (VOCs). The experimental and theoretical investigations showed that NDI based magnetite supported inorganic–organic hybrid nanoparticles are candidates to adsorb aromatic and non-aromatic VOCs, and were used to fabricate sorbent tubes (Fig. 132). The adsorption values were determined for various VOCs, and DFT-D3 calculations showed the correlation between the electron accepting ability of NDI and VOC adsorption capacity of the tubes. The desorbed sorbent tubes went without losing their properties and can be reused more than 200 times.[377]

Bao and co-workers reported the n-doping of NDI and PDI based polymers by the dimeric dopant $(2\text{-Cyc-DMBI})_2$,

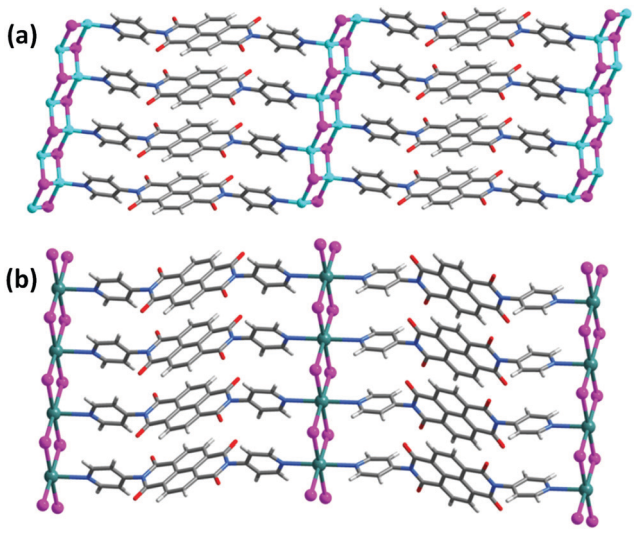

Fig. 131 Views of two-dimensional networks of (a) $[Cu_2I_2(DPNDI)]_n$ and (b) $[PbI_2(DPNDI)]_n$, (DPNDI = *N,N′*-di-(4-pyridyl)-NDI). Aqua, Cu; green, Pb; gray, C; blue, N; pink, I.[376] This figure has been adapted from ref. 376 with permission from The Royal Society of Chemistry, copyright 2016.

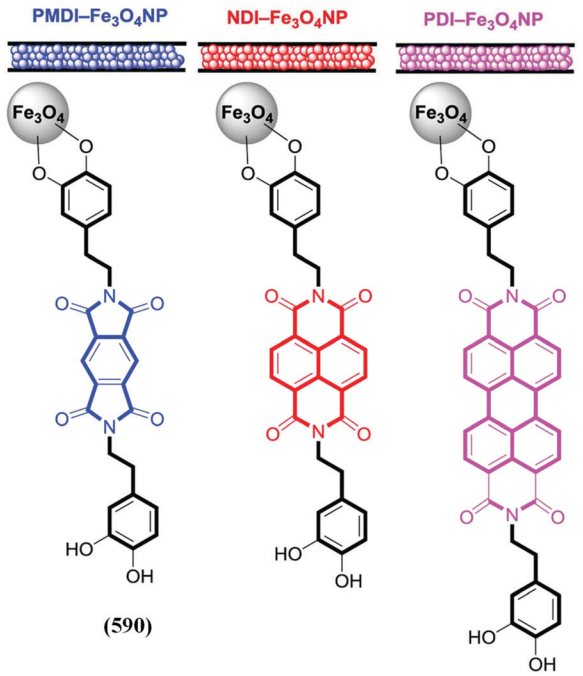

Fig. 132 Schematic representation of the sorbent tubes and magnetite supported organic–inorganic hybrids of perylene diimide (PDI), NDI, and pyromellitic diimide (PMDI).[377]

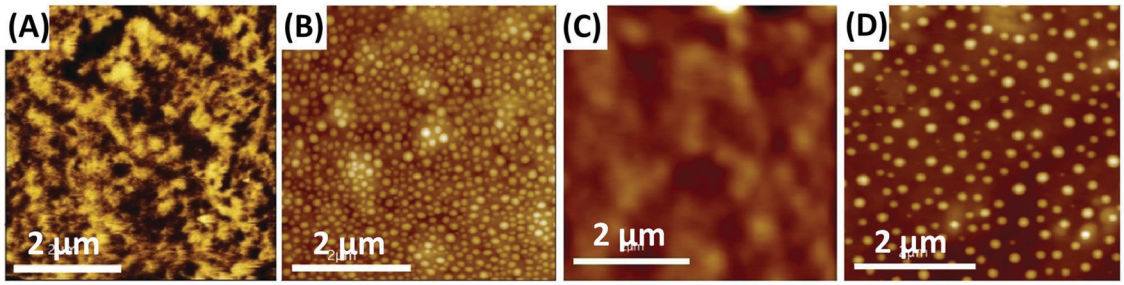

Fig. 133 AFM height images of (A) pristine PNDIT2, (B) doped PNDIT2, (C) pristine P(NDI-*alt*-[T270-*co*-TPT30]), and (D) doped P(NDI-*alt*-[T270-*co*-TPT30]). The doping concentration was 23 wt% in both cases.[232] This figure has been adapted from ref. 232 with permission from John Wiley and Sons, copyright 2018.

which was further copolymerized with ethynylene, ethylene, and bithiophene. They found that, for the ethynylene-linked polymer, the reduced species are delocalized on the polymer backbone compared to the bithiophene-linked polymer. Conductivity measurements showed that the ethynylene-linked polymers exhibited much higher conductivities compared to the bithiophene-linked polymer. The NDI based polymer P(NDI2OD-T2) (**322**) exhibited a conductivity of higher than 4×10^{-3} S cm^{-1}.[207] Shin *et al.* synthesized P(NDI-*alt*-[T2-*co*-TPT]) (**333**) type ternary copolymers with different concentrations of the *meta* substituted monomer TPT ranging from 0 to 100 mol%. The miscibility of the dopant with the polymer is a major limitation for high doping efficiency. To overcome this problem, they introduced TPT, a kinked monomer, into the NDI based polymer and observed improved miscibility of an n-type dopant with an NDI–bithiophene copolymer, leading to more effective doping. The DSC measurement showed a decrease in crystallinity of the P(NDI-*alt*-[T2-*co*-TPT]) (**333**) polymer with an increase in TPT concentration up to 5 mol%; afterward, it increases with TPT content. The miscibility of the dopant 4-(1,3-dimethyl-2,3-dihydro-1*H*-benzoimidazol-2-yl)-*N*,*N*-diphenylaniline was also observed to be increased with (**333**), whereas the lower charge mobility of (**333**) films caused by TPT units decreases the electrical conductivity compared to P(NDI-T2) (**322**). The introduction of TPT causes the conjugation breakdown which ultimately results in lower electron mobility (Fig. 133).[232]

Mei and co-workers synthesized n-type NDI based semiconducting polymers, where the polymer consists of a conjugation break spacer with 3–7 methylene units (NDI-C_m) (**590**). They observed that the NDI-C_m exhibited very low melting points (55–105 °C) due to the absence of pi-aggregation and crystallinity and very poor charge transport was observed for (**590**). By using 5% complementary semiconducting polymer blends of P(NDI2OD-T2) (**322**), they observed increased performance for NDI-C_m polymer transistors up to 100-fold compared to the pure matrix.[378]

Hao *et al.* used a positional isomerism strategy and synthesized two 1-D coordination polymers containing Zn and NDI units, named $[ZnCl_2(3\text{-DPNDI})]\cdot H_2O$ and $[ZnCl_2(4\text{-DPNDI})]\cdot$DMA where 3/4-DPNDI = (3/4-pyridyl)-NDI and DMA = dimethylacetamide. Both the polymers showed different 1-D coordinations, different supramolecular networks due to lone pair–pi interactions, and also totally different photochromic and photoinduced electron transfer properties. For different positional isomeric 3/4-DPNDI ligands the distinct number and strength of lone pair–pi interactions lead to a linear shape chain for $[ZnCl_2(3\text{-DPNDI})]\cdot H_2O$ and a zigzag shaped chain for $[ZnCl_2(4\text{-DPNDI})]\cdot$DMA. Compared to $[ZnCl_2(4\text{-DPNDI})]\cdot$DMA, $[ZnCl_2(3\text{-DPNDI})]\cdot H_2O$ exhibited exceptional photochromic behaviour with a very fast photoresponsive rate due to a higher number of lone pair–pi interactions which strengthens the donor and acceptor units.[380] Wang *et al.* synthesized two Zn-based coordination polymers using NDI as a primary ligand and aromatic di-carboxylic acids as secondary ligands *via* a solvothermal process, named $[Zn(3\text{-NDI})_{0.5}(NDC)(DMF)]_n$ and $([Zn_{1.5}(3\text{-NDI})_{0.5}(BDC)_{1.5}]\cdot 2.5DMF)_n$. Both the polymers exhibited photochromic behaviour due to the different spatial arrangements of the two different acids. $[Zn(3\text{-NDI})_{0.5}(NDC)(DMF)]_n$ exhibited a 2-D structure, whereas the polymer $([Zn_{1.5}(3\text{-NDI})_{0.5}(BDC)_{1.5}]\cdot 2.5DMF)_n$ showed a 3-D structure with hex topology. Both of the complexes exhibited photochromism and photo-controlled luminescence upon irradiation with a xenon lamp at 300 W.[381] Kawan *et al.* synthesized an NDI based n-type semiconducting polymer (**591**) with supported lipid bilayers (SLBs) for organic electrochemical transistors (OECT). They introduced a lysine side chain to improve surface properties and to facilitate bulk cation charging. Furthermore, the lysine chain enabled vesicle adsorption as it helps the formation of zwitterionic lipid vesicle assembly into SLBs, where the NDI-T2 was shown to be a promising channel material for OECT.[379a] Chen *et al.* developed a new electron deficient building block, a thienopyridine-fused naphthaleneamide, TPNA, for π-extension of NDI based polymers at the diagonal position, and they have synthesized several TPNA based polymer acceptors (**592–595**). TPNA extends pi-conjugation compared to NDI and also leads to higher electron delocalization, a planar conformation and reduced steric hindrance compared to NDI. 2D GIWAXS measurements showed that the TPNA based polymers exhibited hierarchically ordered microstructures leading to lamellar diffraction (*h*00), and also exhibited very close pi–pi stacking, with a short stacking distance of 3.5 to 3.6 Å. The homo-TPNA (**592**) and TPNA-BTz (**594**) polymers possessed lower FMO energy levels. The thin film

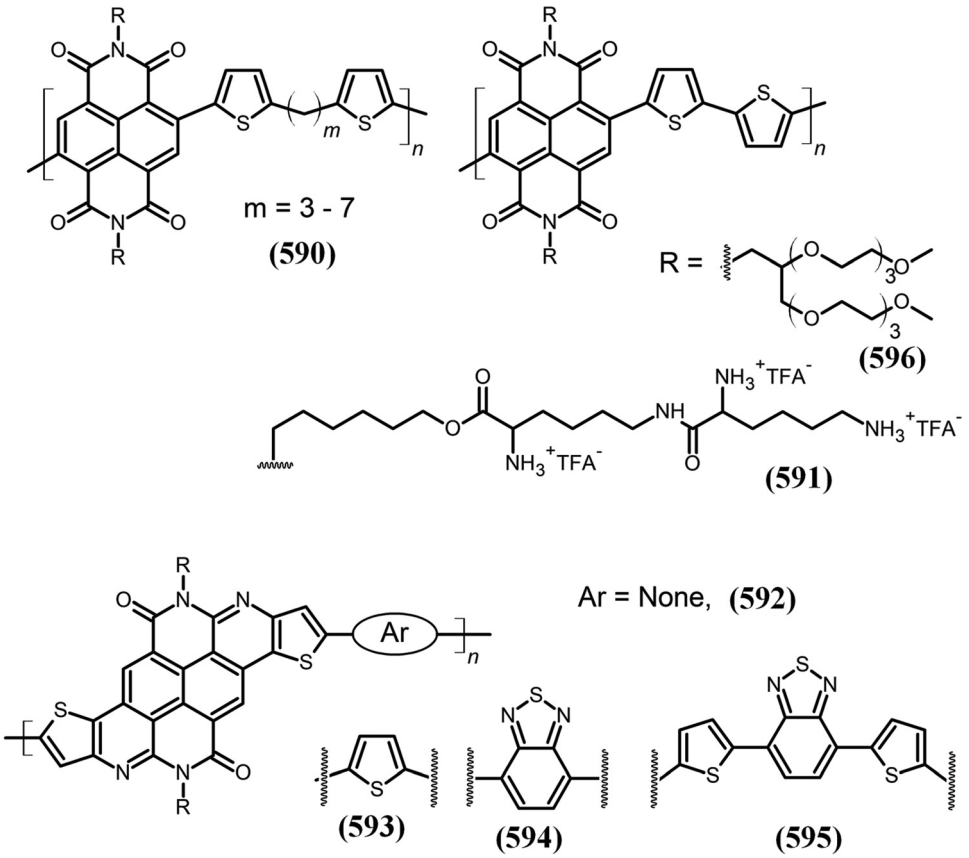

Fig. 134 The molecular structures of NDI based polymers, where the effect of backbone rigidity and structure on the thermomechanical and semiconducting properties was studied.[378,379]

transistor properties showed that the TPNA-BTz (**594**) polymer exhibited strong n-channel performance with a highest electron mobility of 0.19 $cm^2 V^{-1} s^{-1}$ (Fig. 134).[379b]

Sommer and co-workers synthesized the NDI–bithiophene copolymer P(EO-NDI-T2) (**596**) with ethylene oxide, where the ether based side chains were stable to base, giving high solubility to the polymer. The P(EO-NDI-T2) polymer, due to its amphiphilic nature, exhibited good solubility with aggregation, especially in chlorobenzene where controlled backbone aggregation was observed. They observed electrical conductivities higher than $\sim 10^{-2}$ S cm^{-1} by using the benzimidazole-based N-DiPrBI dopant with a doping level of 1–2% and a power factor value of 0.11 μW $m^{-1} K^{-2}$.[379c] Sommer *et al.* synthesized five different NDI-based copolymers (**322**, **380**, **597–599**), with changed HOMO and LUMO energy levels, and investigated their influence on the electron transfer reactions both photochemical and thermally induced from SM NDI with a DMAP side chain (**600**).[347] The lower LUMO levels allowed air stability for electron transfer reactions, and they further characterized the molecules by DFT calculations and absorption and ESR spectroscopy. The cyanated NDI copolymers (**598**, **599**) showed radical anion formation; for thermally activated P($NDICN_2$-T2) the concentration of radical anion was found to be 40 times higher than its noncyanated analogue. The thermally induced electron transfer to the LUMO of the NDI copolymer from the

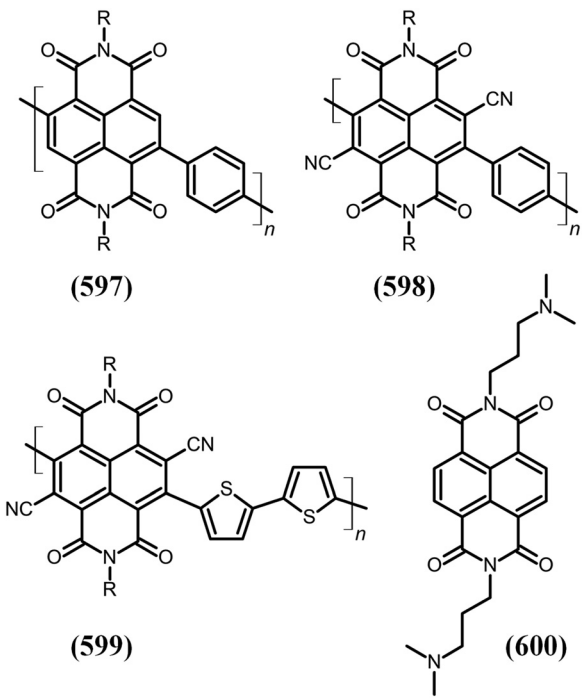

Fig. 135 The molecular structures of NDI copolymers n-doped with NDI tertiary amine.[382]

HOMO of the DMAP side chain results in decreased radical stability, whereas from DMAP to the NDI copolymer the photoinduced electron transfer was governed by the position of the HOMO level. Even with high radical anion concentrations and strong air stability, the cyanated NDI copolymers (**598**, **599**) exhibited limited electric conductivity due to localization of radical anions and strong backbone torsion (Fig. 135).[382]

Gu and co-workers incorporated conjugation break spacers (CBSs) of different lengths into the NDI based n-type polymer (**590**), and investigated their role in thermo-mechanics. They also explained the role of backbone flexibility on the thermomechanical properties of the polymers by introducing flexible CBS with zero to seven carbon alkyl spacers. They found that with addition or increasing length of CBS the backbone flexibility was increased, which was further supported by reduction in the glass-transition temperature, melting point and elastic modulus upon increasing the CBS length. They observed decreased thermomechanical properties with increasing CBS length, whereas the elastic modulus and Tg were observed to be decreased. The PNDI-C4 polymer showed high, unusual ductility which may be due to increasing entanglements and disruption of crystallization.[379d]

10 Artificial photosynthesis

The photosynthetic reaction center (PRC) of purple bacteria forms long-lived charge separated states upon photoexcitation with sunlight. PRC has several membrane proteins that fixate the chlorophyll components used to absorb light along an axis through a membrane within a 12-yoctolitre volume (12×10^{-24} L).[78] The light absorbed by chlorophylls is passed onto adjacent pigments. The PRC in the both photosystems I and II harnessing solar photons to power chemical reactions for artificial photosynthesis by capturing energy upon photoexcitation of pigments which transfer through antennae *via* oxidation–reduction potential. PRC is based on various features such as photoredox donor–acceptor molecules that are non-covalently connected. To understand this phenomenon many researchers have focused on preparing donor–acceptor systems to study photoinduced charge separation reactions, *i.e.* capturing/storing solar energy using covalent and non-covalent strategies.[383] In the last three decades, NDI and cNDI have made significant contributions to our understanding in this area not only because of their easy synthesis, but also due to their capability of tuning the properties by functionalising NDI to make it either an electron-donating and/or an electron-accepting component.[384] The Osuka group synthesised fixed-distance triads bearing zinc porphyrin as a donor, free base porphyrin as a spacer, and an NDI moiety as an electron-acceptor, and they observed photoinduced long-lived charge separation (0.14–80 μs) between various triads with fixed distances, *i.e.* 13 and 17.2 Å, respectively.[385] Later, the Wasielewski group described picosecond photoinduced electron transfer within a triad system in which NDI was used as an electron acceptor.[386] Sessler and co-workers synthesised the first non-covalent rigid dyad systems made up of porphyrin and NDI through hydrogen-bonding and studied steady-state fluorescence quenching.[131] Fukuzumi found long lived charge separation (450 μs) within zinc-porphyrin and NDI covalently and non-covalently linked in solution. In 2006, Matile and co-workers described a breakthrough, where they created for the first time an artificial photosynthetic reaction centre within a lipid bilayer using octaphenyl-rod functionalised with cNDIs, which produced ultrafast charge separation across a lipid membrane.[82] Later, that group also prepared zipper and layer-by-layer assembly of colourful cNDIs for artificial photosystems.[387] In this section, we outline a few early important examples from our group (see Fig. 136). In earlier work, we reported the synthesis of a series of rigid and planar donor–acceptor structures bearing either porphyrin or tetrathiafulvalene (TTF) as a donor and cNDI as an acceptor, connected *via* either a diaza rigid bridge, an amine, an amide or carbon–carbon linkage. Further, we have studied photoinduced electron/energy transfer between these systems by means of electrochemical and photophysical methods, *i.e.* time-resolved spectroscopy. Interestingly, the cNDI-TTF (**601**)[388] system shows excellent redox behavior and a strong photoinduced intramolecular charge transfer, in which the formation of cation radical was observed at 852 nm $(\text{cNDI-TTF})^{\bullet+}$ upon chemical oxidation with $FeCl_3$ due to significant π–π interaction, and a near-IR absorption (1270 nm) band was observed. In another example, a cNDI bearing dyad with zinc-tetraphenylporphyrin was produced (**602**)[389] *via* a 2,3-annulated linkage, and upon photoexcitation of the porphyrin in DCM, the charge separation (CS) from the ZnTPP to the cNDI unit was in the range of 1–3 ps. We also synthesised two triads (**603**)[390] bearing NDI as a central moiety functionalised on the core by either free base or zinc porphyrin by means of Suzuki coupling reactions. After photoexcitation, charge separation takes place from porphyrin to cNDI in tetrahydrofuran and benzonitrile solvents, with charge separation of ~1 ps and ~25 ps time constants in the ZnP and FbP triads, respectively, and charge recombination with time constants of about ~7 and 16 ps. Later, we synthesised multichromophoric systems, *i.e.* pentads (**604**, **605**), made up of cNDI as a center core and four ZnP or FbP substituted on the core *via* aniline bridges.[391] Ultrafast spectroscopy in a polar solvent revealed that charge recombination in the charge-separated state and the ground state occurs within a few picoseconds. In another report, we synthesised a donor–acceptor dyad bearing porphyrin as a donor and cNDI as an acceptor connected through an amide linkage (**606**).[392] Interestingly, the porphyrin having zinc metal with cNDI in a polar solvent was shown to be ~5 orders of magnitude faster due to the charge separation, followed by recombination; however, much less solvent dependence is observed with free base dyads. An important fact in this dyad is that excitation energy transfer takes place from cNDI to the porphyrin, and the structures are illustrated in Fig. 136.

The details of this study have been reviewed by us,[3b] the Matile group[62] and also discussed in detail in our earlier review.[2b] In this review, we explore recent examples of donor–

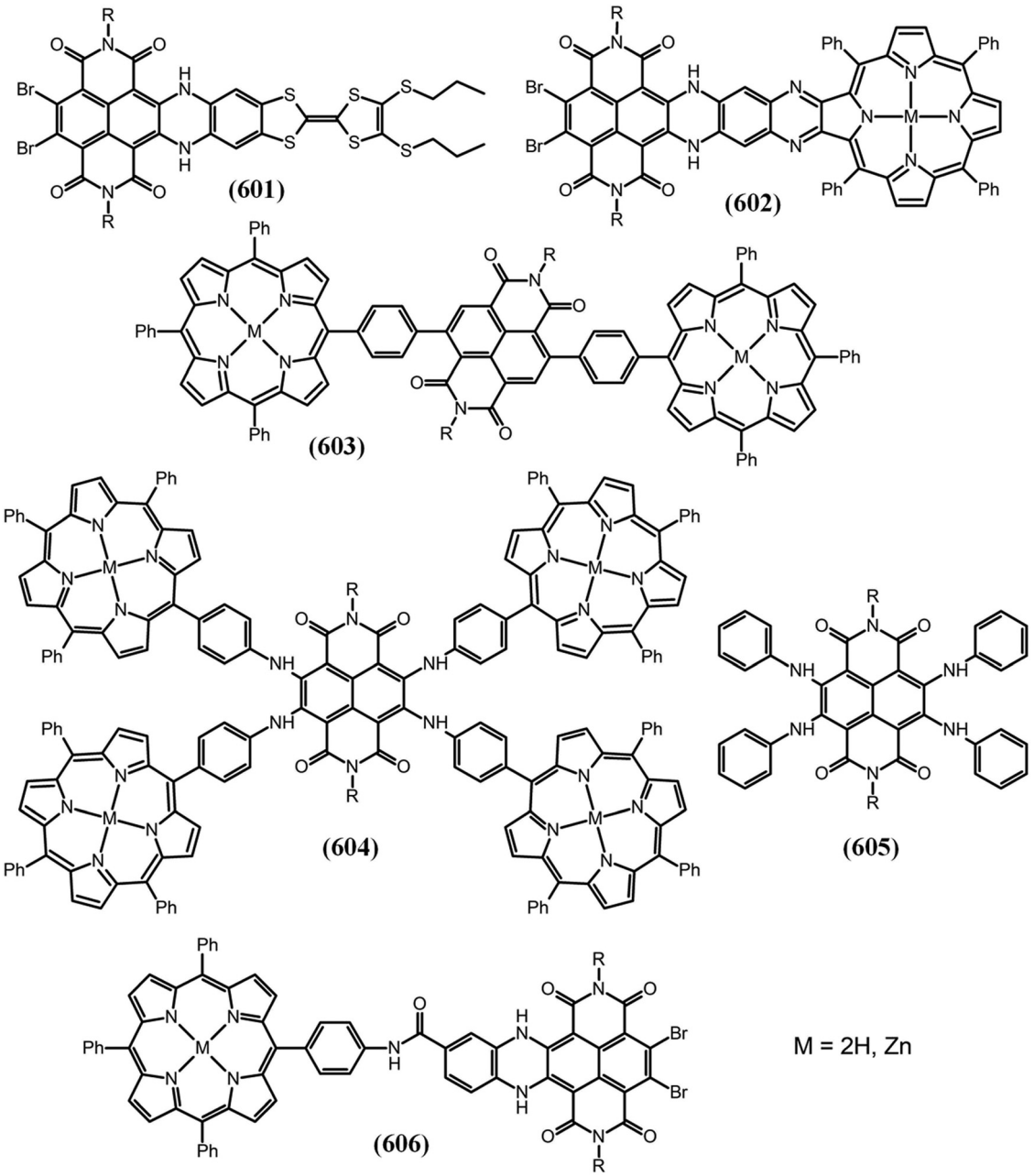

Fig. 136 The molecular structures of NDI based dyads, triads, tetrads and pentads.[388–392]

acceptor systems based on NDI/cNDI used in artificial photosynthesis. The Schubert group synthesised photoredox-active acceptor–photosensitizer dyads based on NDI (**607**) as a hydrophilic acceptor polymer by incorporating triethylene glycol or poly(ethylene glycol) side chains in the monomer units, and performed nitroxide-mediated polymerization (NMP).[393] The kinetic study of the polymerization showed controlled chain growth, as well as a narrow molar mass distribution due to the functional NMP initiator, and a single Ru(II) photosensitizer unit is readily attached at the terminus of the polymer chains (**607**) by a modular approach to construct water soluble dyads. Steady-state absorption and emission spectroscopy revealed efficient quenching of the Ru(II) fluorescence due to intramolecular charge transfer from the complex to the acceptor polymer. These results demonstrated side chain modification to synthesise water-processible photoredox-active architectures (Fig. 137).

Joint work by the Lin and Huang groups described two semiconductive inorganic–organic hybrid coordination polymers with similar 2D heterostructures, *i.e.* iodide-NDI coordination network compounds $[Cu_2I_2(DPNDI)]_n$ and $[PbI_2(DPNDI)]_n$.[376] However, both had different photo-induced electron-transfer properties. Coordinating polymers were prepared upon slow diffusion of methanol in *N,N′*-

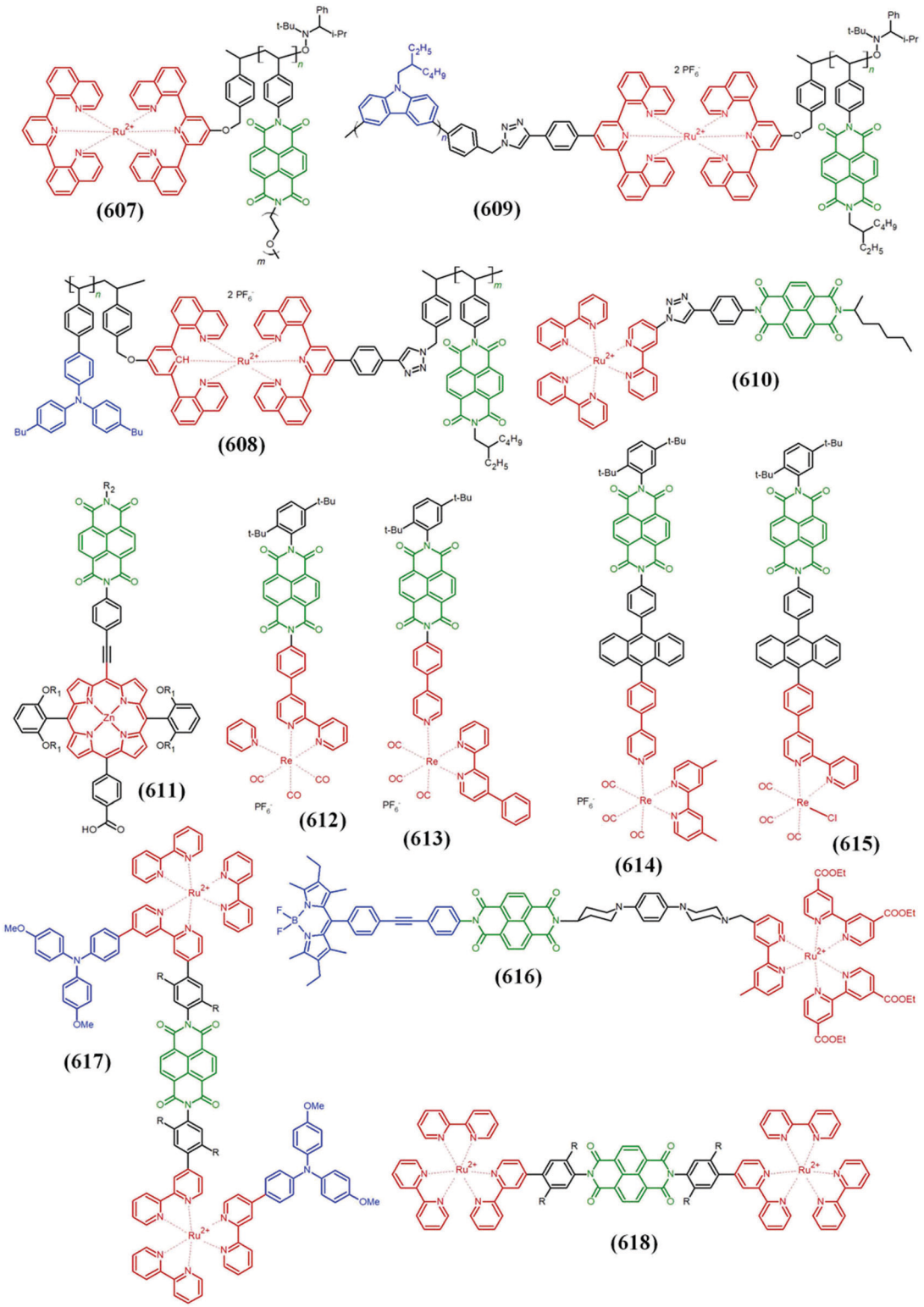

Fig. 137 Hydrophilic poly(naphthalene diimide)-based acceptor–photosensitizer dyad (**607**),[393] multi-donor–photosensitizer–multi-acceptor triads (**608**, **609**),[394] a sensitizer–acceptor dyad (**407**),[395] electron transfer dynamics of push–pull porphyrins–NDI as sensitizers,[338] molecular structures of the NDI–Ru^{II}(bipyridine)$_3$ tetrad (**616**),[396] NDI based radical anions and dianions to Re(bpy)(CO)$_3$ (**612**),[397] NDI radical anion to electrocatalytically active Re(bpy)(CO)$_3$Cl in a molecular triad (**612–614**),[398] and NDI based triad and pentad photosensitized by [Ru(2,2′-bipyridine)$_3$]$^{2+}$ (**617**, **618**).[399]

dimethylformamide solution bearing *N,N′*-di-(4-pyridyl)-NDI (DPNDI), HI and CuI in a crystallisation tube, which resulted in crystalline black needles of $[Cu_2I_2(DPNDI)]_n$; similarly, $[PbI_2(DPNDI)]_n$ produced dark red needle crystals, by only

replacing CuI with PbI_2. Interestingly, upon photoexcitation, only hybrid heterostructures undergo intramolecular electron transfer to form a long-lived charge separated state due to a higher HOMO energy level of the $[Cu_2I_2]_n$ chain compared than that of the $[PbI_2]_n$ cluster, and thus $[Cu_2I_2(DPNDI)]_n$ may be implicated in artificial photosynthesis (see Fig. 131). Joint work by Jager and Schubert described the multidonor–photosensitizer–multiacceptor (D_n–P–A_m) triad (**608**) with photosensitizer polymer-based architecture for long-lived charge separation. In this triad, triarylamine and NDI were used as donor and acceptor units, respectively, with a Ru(II) photosensitizer.[394a] The Ru(II) photosensitizer was equipped with pendant polymer chains bearing multiple triarylamine and NDI units, and the sensitizer can be selectively excited in the visible light region. Thus, D_n–P–A_m architecture assures directional and long-lived charge transport. Upon photoexcitation >95% charge separation (CS) was observed including similar CS lifetimes (400 ns) and longer-lived CS components (2400 ns, 30%), indicating multiple contributing pathways. In another report, they prepared a D_n–P–A_m triad of poly(triarylamine) block architectures, in which they replaced D_n, *i.e.* triarylamine, with a new conjugated poly(3,6-*N*-alkylcarbazole) but keeping the same A_m (**609**), *i.e.* styrenic poly-NDI segments.[394b] Upon visible light excitation, electron transfer was initiated from D_n to A_m with CS >95% of several tens of microseconds, and the recombination was reduced to the earlier D_n–P–A_m non-conjugated system.[394a] They believe that this novel D_n–P–A_m system can be used in related fields such as OFETs, OLEDs or to transduce the optical stimulus for long-lived redox-chemical and or redox-mechanical responses.

Schanze and co-workers synthesised a series of NDI-end-capped thiophene oligomers (**619**) and studied photoinduced electron transfer, in which oligomers were used as electron donors and NDI was used as the electron acceptor (Fig. 138).[400] NDI was used as an electron acceptor because NDI has a low reduction potential (−1.10 V *vs.* Fc/Fc^+),[383,401] and because of ground state overlap of absorption between NDI and the oligothiophenes, allowing selective excitation of the donor. NDI absorbs in the visible region, making it easy to characterise NDI radical anions.[383] The phenyl group between NDI and thiophene oligomer units leads to a weak electronic coupling between the donor and acceptor, and thus photoinduced electron transfer (PET) forward and recombination are in the nonadiabatic regime. Characterisation of T_4NDI_2 by ultrafast femtosecond–picosecond transient absorption confirmed that intramolecular electron transfer reactions occur with $k > 10^{11}$ s^{-1}, which is the highest value observed in oligomers. The Schanze group in collaboration with the Mohammed group studied PET in a series of π-conjugated oligo(phenylene ethynylenes) (OPEs) as backbones in combination with end-capped NDI dyads as acceptors (**620**, **621**), and they also investigated the effect of conjugation length in long-lived CS.[402] The OPE backbone had 4 to 8 phenylene ethylene units (coded as PE_n-NDI, where n = 4, 6 and 8). Transition fluorescence and absorption spectroscopy show that intermolecular charge transfer from OPE to NDI is the main pathway for disabling the excited states of the PE_n-NDI oligomers with an efficiency >97%. They also found that CS and CR are strongly exothermic ($\Delta G^0_{CS} \sim -1.10$ and $\Delta G^0_{CR} \sim -2.00$ eV). To demonstrate the usefulness of NDI, they studied PET in the presence of methyl viologen, demonstrating that regardless of the length of the oligomer the absorption of the cation radical state $OPE^{\bullet+}$ remains constant ($\lambda \sim 575$ nm). Nevertheless, charge separation occurs within 1–10 ps with rates slightly decreasing with increasing length of oligomers, which may be because of a decrease in the electronic coupling between the donor and acceptor. CR decreases in the sequence PE_4-NDI > PE_6-NDI ~ PE_8-NDI.

In this direction, the group of Quaranta and Aukauloo described multiple-charge accumulation in a sensitizer–acceptor dyad of NDI linked to a $[Ru(bpy)_3]^{2+}$ (bpy = bipyridine) chromophore (**610**).[395] Upon photoexcitation photo-induced electron transfer produces long-lived two-electron charge accumulation with a life time of ~200 μs with a 100% quantum yield. In a proof-of-concept that demonstrates a man-made molecular system can be used for mimicking nature as well

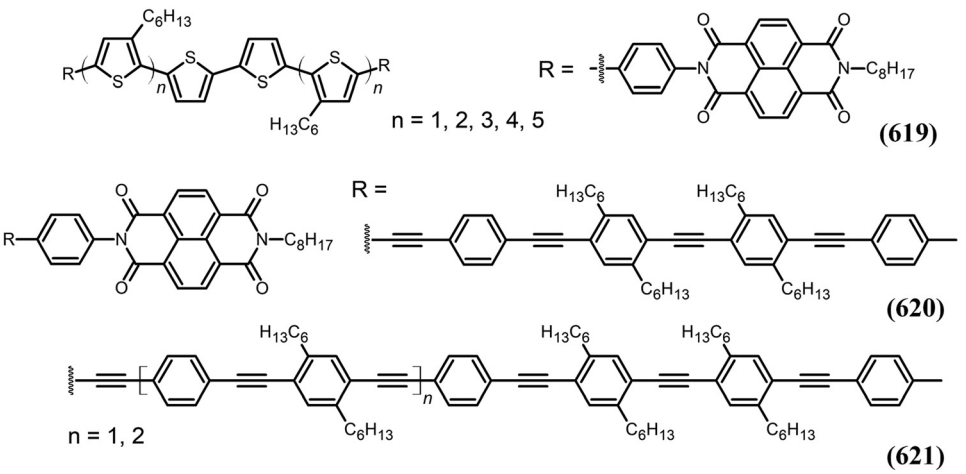

Fig. 138 NDI end-capped thiophene oligomers[400] and π-conjugated oligomer–acceptor dyads.[402]

as for solar cell development, the Odobel and Hammarström group synthesised three different porphyrin dyes with push–pull characteristics. The synthesised zinc-porphyrin with an NO_2 pull component using triphenyl amine as the donor (push), *i.e.* ZnP–TPA–NO_2 (**611**), when compared with the reference dye zinc porphyrin, ZnP–TPA–NO_2, exhibited improved efficiency in solar cells.[338] In another porphyrin, they replaced the NO_2 acceptor with NDI. The NiO based dye sensitized solar cell gave better performance than ZnP–TPA–NO_2 and the reference ZnP. In another report, they synthesised a molecular tetrad to mimic the Z-scheme. The molecular tetrad, *i.e.* Bodipy–NDI–TAPD–Ru, composed of NDI as an acceptor, was connected with 4,4-difluoro-1,3,5,7-tetramethyl-2,6-diethyl-4-bora-3*a*,4*a*-diaza-*s*-indacene (Bodipy) and a Ru(II)(bipyridine)$_3$ at two different diimide positions along with the electron donor tetraalkylphenyldiamine (TAPD) (**616**).[396] Upon photoexcitation, Biodipy was oxidised and Ru reduced, and the charge separated state was higher than that of reference dyes Biodipy-NDI and TADP-Ru alone, with life time increased to 850 ns with a quantum yield of the CS state of ~24%.

NDI is a good acceptor because its radicals absorb in the visible region, with photoinduced electron transfer studied using donors such as porphyrins, TTF, oligomers, and triphenyl amines with NDI as an acceptor.[3b] Wasielewski and co-workers described the use of PET for the first time[403] and prepared a series of diradicals in which both radicals are anions ($NDI^{\bullet -}$) covalently linked with or without a series of benzene spacers.[404] They demonstrated that only the singlet ground state (not the corresponding triplet) can undergo PET upon excitation of one of the $NDI^{\bullet -}$ radicals to produce the NDI^0-NDI^{2-} moieties. These results suggest that using photoexcitation by manipulating the spin states of diradicals for QIS applications may be possible in the future. In another report, they synthesised two dyads bearing NDI and PDI as acceptors and a Re(bpy)(CO)$_3$ component as the electron donor attached through either a bipyridine ligand or directly to the Re centre *via* a pyridine ligand (**612**).[397] Both the complexes resulted in photoreduction of Re(bpy)(CO)$_3$ using visible (>600 nm) or near-IR (950 nm) light. They found that electron transfer is slower with the NDI/PDI attached directly to the Re centre when compared with the spacer bipyridine ligand, and thus this study suggests that the acceptor-pyridine-ligated chromophore will be of less utility than the acceptor-byp-ligated chromophore for the design of future catalytic systems. They synthesised a series of triads, *i.e.* $[Re(dmb)(CO)_3(Py\text{-}DPA\text{-}NDI)]^+PF_6^-$ (**614**), $[Re(bpy\text{-}NDI)(CO)_3]^+PF_6^-$ (**612**) and $[Re(bpy)(CO)_3(Py\text{-}NDI)]^+ PF_6^-$ (**613**), and investigated electron transfer from the NDI radical anion to Re(bpy)(CO) where the quantum yield of the electron transfer step was ~90%, and they also studied CO_2 reduction catalysis, with the use of a 9,10-diphenanthracene acceptor (**614**).[398,405] They studied photoexcited NDI anion linked with Zr(IV)-based UiO-NDI metal–organic frameworks (MOF).[406] The photoreducing power of the reduced MOF, *i.e.* formation of $UiO\text{-}NDI^{\bullet -}$, was evidenced by the photodegradation of CH_2Cl_2. Wenger and co-workers synthesised two novel triads $[Ru(bpy)_3]^{2+}$-NDI-$[Ru(bpy)_3]^{2+}$ (**617**, **618**) composed of the NDI acceptor connected with two $[Ru(bpy)_3]^{2+}$ (bpy = 2,2′-bipyridine) sensitizers at both of the diimide positions.[399] Photoexcitation of Ru donor produces intra- and intermolecular electron transfer events to generate NDI^{2-} with a lifetime of 120 ns in CH_3CN in the presence of excess trimethylamine. Therein and co-workers studied the effect of changes in dielectric constants (ε_s) within a protein matrix upon the PET reaction between a donor–bridge–acceptor molecule, with zinc porphyrin (ZnP) donor, phenyl (Ph) ring as a spacer, and NDI as an acceptor

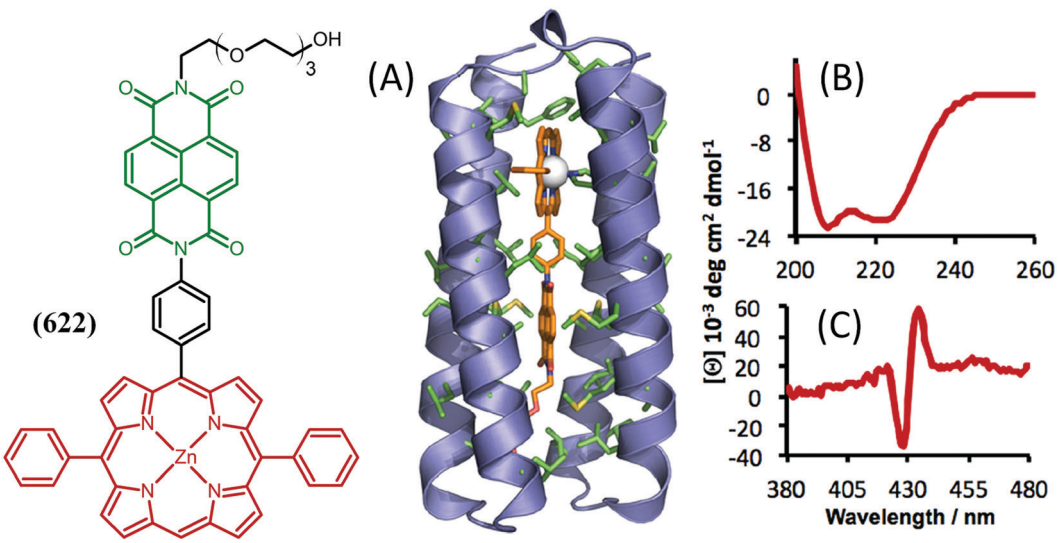

Fig. 139 (A) Model of SCPZnI3 showing interior hydrophobic residues (green) surrounding PZn–Ph–NDI (orange). (B,C) Circular dichroism spectra of SCPZnI3 holoprotein. (B) Molar ellipticity per residue is consistent with a helical structure. (C) Molar ellipticity (Cotton effect) in the visible region indicates that the achiral cofactor resides in a structured, chiral environment.[407] This figure has been adapted from ref. 407 with permission from The American Chemical Society, copyright 2016.

within the triad, *i.e.* ZnP–Ph–NDI (**622**).[407] They studied the dynamics as a function of dielectric constant of the solvent and designed a protein, SCPZnI3, to bind PZn–Ph–NDI into a protein interior, in which SCPZnI3 undergoes a switch in the effective dielectric constant from $\varepsilon_s \approx 8$ to $\varepsilon_s \approx 3$ upon the PET process (Fig. 139).

11 Medical, biomedical applications, and diagnostics

This is a multidisciplinary research field which comprises fast moving, innovative technologies with the main aim to develop small organic molecules for medical and biomedical applications in diagnostics and treatments.

11.1 G-quadruplex binding

Naphthalene diimides showed significant anticancer activity in animal models, with therapeutic potential related to their ability to strongly interact with G-quadruplexes. G-quadruplexes provide scaffolding for two-dimensional organic frameworks of four-stranded nucleic acid structures due to the strong hydrogen-bonding ability of guanine-rich sequences. G-quadruplexes can be formed from telomeric repeats in various organisms both *in vitro* and *in vivo*. Importantly, the human telomeric repeat is made up of the repeated sequences CGTTAG, and for therapeutic purposes binding of molecules within the G-quadruplex to specific sequences of DNA with high affinity and stability is an important goal of biological chemists for the transcription factor proteins to modulate the transcription of genes. Thus, researchers have been working to elucidate the complex regulation of mammalian gene expression, as well as to develop targeted diagnostics and generic aberrations in the field of medicine. Among the planar aromatic molecules, NDI has been shown to be versatile due to high affinity and selectivity for G-quadruplex binding.

A series of core-substituted NDIs and unsubstituted NDIs have been studied because of their promising biophysical and biological features. The Richer group has written a short review on the selectivity of NDI with G-quadruplex.[408] In this section we present the latest developments on NDIs and their mode of binding with quadruples and their consequent anticancer activity. Earlier work by Neidle and co-workers gave confirmation of the binding of a G-quadruplex with a tetra-substituted NDI ligand (**624**) complex with two human telomeric DNA quadruplexes,[409] and since then many researchers have been using NDIs or cNDIs for binding with G-quadruplex. Recently, the same group synthesised trisubstituted NDI derivatives (**626**), which contain two side chains terminating in morpholino groups at the diimide positions (**625**) and a third side chain terminating in a protonated pyrrolidino group.[410] They have used this trisubstituted NDI derivative for the treatment of human pancreatic ductal adenocarcinoma cancer genes having over-representation of G-quadruplexes and shown a superior profile compared to the commonly used therapy 'gemcitabine'. This type of NDI molecule may thus be appropriate for use in the treatment of currently hard-to-treat cancers. In another report, they used *N,N′*-bis(2-(pyrrolidin-1-yl)ethylamino)-2,6-bis(2-(pyrrolidin-1-yl)ethylamino)-NDI (**623**), which shows micromolar inhibition of cell growth in a wild-type patient-derived GIST cell line and also shows a sub-micromolar activity in two distinct patient-derived imatinib-resistant gastrointestinal cancer cell lines.[411] This NDI derivative strongly stabilises both G-quadruplexes, which include one from the BCL-2 promoter DNA and another from quadruplex from its 50-UTR region of the RNA (Fig. 140).

The Morales and Galan group reported divalent NDI ligands bearing charged sugars (glucose and mannose) at both the diimide positions (**627**), which show high selectivity towards the hybrid-type topology of the K^+ human telomeric G-quadruplex (Fig. 140).[412] Interestingly, among the sugar-based NDIs, imidazolium containing mannoside-conjugates were the most selective ligands towards the F21T K^+ quadruplex sequence. The methylpiperazine-substituted NDI derivative was shown to be more toxic to HeLa cancer cells than the regularly used doxorubicin (DOX), and also showed less toxicity towards fetal lung fibroblasts WI-38. This finding demonstrates that charged carbohydrates act as binding motifs that interact with G-quadruplex grooves.

Takenaka and co-workers synthesised seven NDI ligands (**628–634**) by varying the chain length between NDI and a ferrocenyl group (FNDI).[413] In their study, they found that the FNDI binds to tetraplex DNA with high selectivity and affinity ($>10^5$ M^{-1} in 0.10 M AcOK-AcOH containing 0.10 M KCl) compared to either single- or double-stranded DNA. Based on this assay, they found that FNDI ligands can be categorised into three main categories for inhibition of both telomerase and Taq polymerase (*Thermus aquaticus*, *i.e.* thermostable DNA polymerase), inhibition of telomerase alone, or inhibition of none of them. In another report, they prepared two new NDI carrying four ferrocenyl substituents (**637**, **638**), derived from (**635**, **636**), respectively, for electrochemical indication of tetraplex DNA.[414] Among the derivatives NDI bearing four ferrocenyl on a tetraplex DNA immobilized electrode gave a signal 13.5 times higher than that of the single stranded DNA-immobilised electrode with a 1 : 2 binding ratio. The Estrela group synthesised an NDI containing a ferrocenyl group with an oligoethylene chain as a spacer as an intercalation unit for the development of an electrochemical DNA biosensor with a peptide nucleic acid (PNA) sequence to monitor the DNA recognition, where ferrocene oxidation was used for the quantification of DNA recognition (see Fig. 56).[184] Interestingly, this novel NDI derivative demonstrated good DNA recognition with a limit of detection of 11.68 fM. In this report, the group synthesised three cyclic NDI dimers with varying alkyl chains (n = 3, 5 or 7) between the linkers and used them to bind G-quadruplex. Their findings demonstrated that all of the cNDI dimers show recognition of G-quadruplex, preferably with higher thermal stability compared to cNDI monomers. These NDI dimers also exhibited stronger inhibition toward telomerase activity, and stop telomere DNA elongation compared to the monomer, as well as show improved anticancer potential. Thus, these types of cNDI

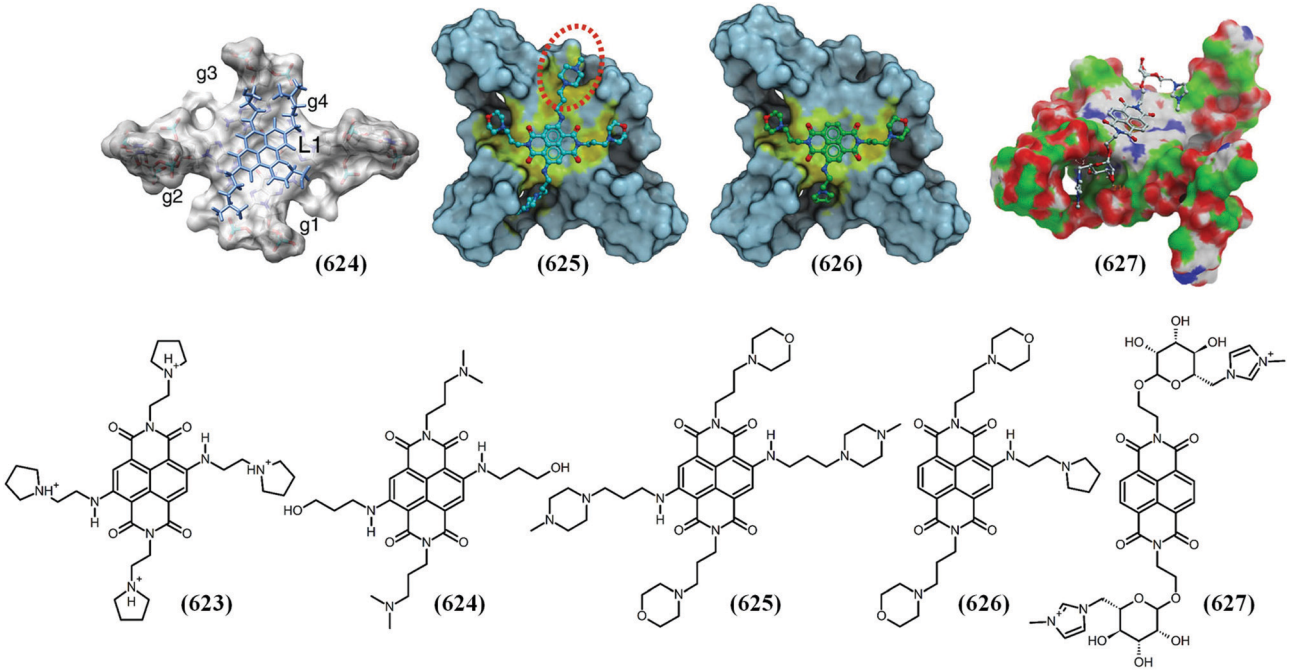

Fig. 140 Surface representation of the 12-mer bimolecular quadruplex highlighting the central positioning of a ligand molecule over the 3′ G-tetrad (**624**) and the orientation of the ligand substituents away from the grooves, g1–g4.[409] The molecular model of MM41 bound to a human telomeric G4, following docking and minimization, and using the *co*-crystal (PDB 3UYH) as a starting point, and the molecular model of CM03 bound to the native parallel human telomeric G4 structure (PDB 1KF1) following docking and minimization (**625**, **626**).[410] This figure has been adapted from ref. 410 with permission from The American Chemical Society, copyright 2018. The structure of the compound (*N*,*N*′-bis(2-(pyrrolidin-1-yl)ethylamino)-2,6-bis(2-(pyrrolidin-1-yl)ethylamino)-NDI (**623**).[411] This figure has been adapted from ref. 411 with permission from Elsevier, copyright 2018. Model of (**627**) bound to the parallel K^+ human telomeric G-quadruplex (based on PDB ID: 4DA3). See the ESI for further details.[412] This figure has been adapted from ref. 412 with permission from John Wiley and Sons, copyright 2017.

dimers may be useful for future anticancer applications. In another report they have synthesised cNDI dyads with alkyl chain spacers (C = 4–7) (**639**), where the C_7 linker showed low IC_{50} values at <10 nm conc. (Fig. 141). For cancer cell lines, however the dyad with C_4 linker was shown to be much less effective, with IC values increased up to 1 μm.[415] These results demonstrate that the chain length between dyads plays the main role. The group has synthesised a new NDI bearing a Cu(II) complex coded as NDI–Cu–DETA (**641**)) which acts as a G-quadruplex cleaving agent with higher selectivity when compared to the structure without Cu(II).[416] The NDI–Cu–DETA complex formed a hydroxyl radical upon binding to G-quadruplex DNA even in the presence/absence of H_2O_2 (see Fig. 142).

The Doria and Freccero group synthesised a series of NDI dyads containing coumarin with varying spacers (**642**) as red emitting probes for G-quadruplex nucleic acids (Fig. 143).[417] Their findings revealed that medium and short chains (<7 carbon atoms) provided energy transfer from NDI to coumarin; however, longer alkyl spacers enhanced the sensing efficiency upon excitation of the NDI. They also observed that hydrophilic tertiary amines are more efficient compared with quaternary ammonium salt analogues and polyethyleneglycol spacers. The Freccero group[418] also synthesised a series of eighteen NDI water-soluble core extended red-NIR fluorophore dyes (**643**) for sensing of G-quadruplex nucleic acids. These new NDIs are soluble in water which quenches their emission; however, upon the addition of G-quadruplex in solution all of the NDIs switch on fluorescence emission at above 600 nm due to groove-like interactions of NDI with G-quadruplex. They also prepared a series of carbohydrate functionalised NDI (**644–649**) chromophores and employed them to investigate their potential application for selective G-quadruplex binding and cell penetration.[419] However, carb-NDI showed some selectivity towards DNA duplexes rather than G-quadruplex due to higher stabilization of the polymorphic human telomere G-quadruplex structures. Nevertheless, global G-quadruplex was shown to be affected depending on the different sugar units attached to NDI. Their further studies revealed that (**649**) had significantly different toxicity to both HT-29 and MCF-cells than (**644–648**), showing that cancerous cell lines interact differently with NDI as a function of the sugar attached.

The Mergny group[420] synthesised core-extended NDIs (c_{ex}-NDIs) (**650–654**) and used these derivatives as G4 light-up sensors. The sensing mechanism relied on the shift of the aggregate-monomer equilibrium towards the bright monomeric state upon G4 binding. These c_{ex}-NDIs (**650–654**) were shown to be selective and sensitive compared with other ligands previously used for light-up sensors. This study provides a rational basis to design NDI scaffolds for G4 ligand binding preference and opens up new paths for light-up sensors for G4 ligands in biology.

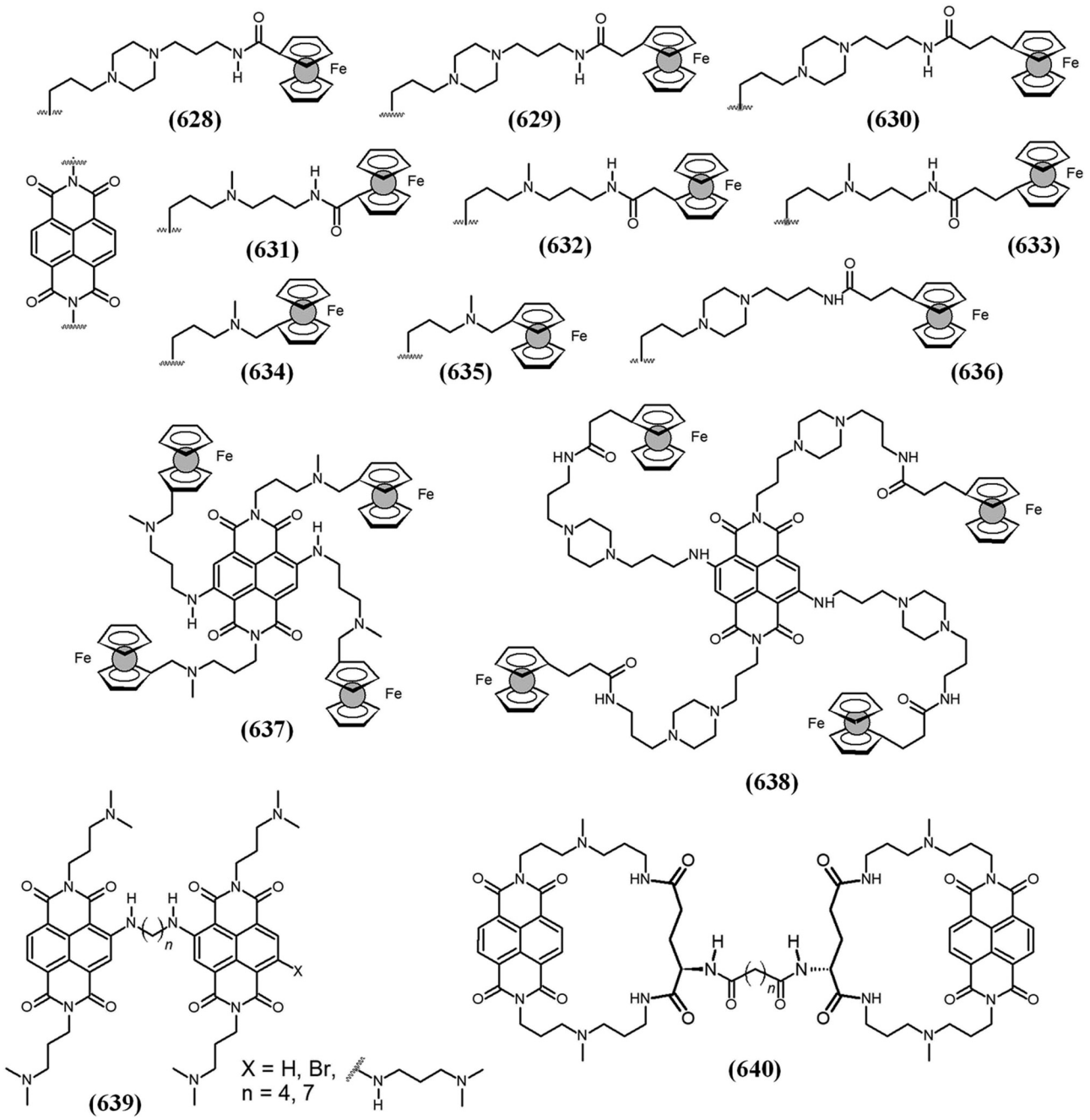

Fig. 141 Chemical structures of ferrocenyl–NDIs as tetraplex DNA binders,[413,414] and cNDI-dimers with varying linker chain lengths (n = 3, 5, or 7), and 1,7-diaminoheptane or 1,4-diaminobutane NDI dyads with N^1,N^1-dimethylpropane-1,3-diamine (**639**).[31,415]

The Freccero and Richter group synthesised c_{ex}-NDIs bearing NO_2 and COOH (**652**, **655**, **656**), which upon aggregation become non-emissive; however, upon binding with G-quadruplex red-NIR emission occurred, and these c_{ex}-NDIs were also capable of fast cellular nucleolar localisation.[421] Importantly, c_{ex}-NDIs demonstrated anti-HIV-1 activity due to their ability to bind viral G-quadruplex with higher affinity than the cellular G-quadruplexes. In another report, Muoio *et al.* prepared three NDI based ligands H-NDI-Tyr (**657**), H-NDI-NMe_2 (**658**), and tetra-NDI-NMe_2 (**659**) and evaluated an *in vitro* model of glioblastoma to evaluate the G-quadruplex 3,11-difluoro-6,8,13-trimethyl-8*H*-uino[4,3,2-*kl*]acridinium methosulfate (RHPS4) ligand.[422] The NDIs showed a lower specificity for telomere targeting compared to RHPS4; however, they were effective in blocking cell proliferation even at nM concentrations, demonstrating NDI G4-ligands are powerful antiproliferative agents. Doria *et al.* synthesised a set of core-substituted NDIs with p-extended rigid arylethynyl groups (**660**, **661**) to study their G-quadruplex binding properties.[423] The G-quadruplex NDI (**660d**, **660e**, **661d**) ligands bearing a

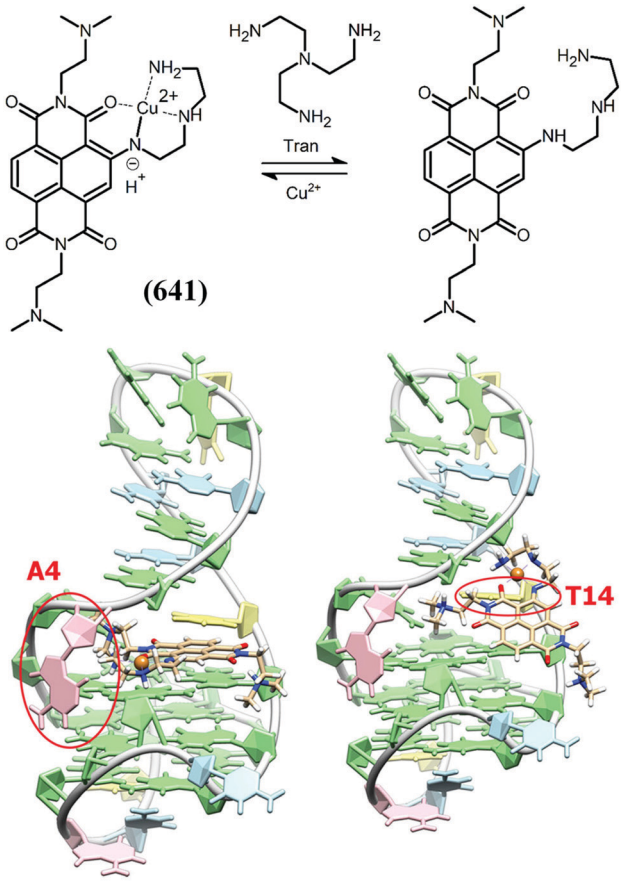

Fig. 142 Selective scissoring molecular tool for quadruplex nucleic acids and the NDI-Cu-DETA titration reaction using Tren.[416] This figure has been adapted from ref. 416 with permission from The American Chemical Society, copyright 2018.

Mannich base with a diethylaminomethyl functional group on the arylethynyl show good selectivity for parallel G-quadruplex and (**661d**) acts as a most powerful ligand toward c-myc, bcl-2 and parallel-induced hTel. Molecular modelling demonstrated that π–π-stacking of the NDI core, along with formation of hydrogen bonds between hydroxyl groups and dimethylaminoethyl moieties, led to favorable interactions to stabilize G4 hTel. Therefore, this study demonstrated that water soluble NDI ligands are most promising for G-quadruplex binding and may be useful for the treatment of various cancers. In another report, they synthesised four types of NDI ligands: (i) 4 di- and tri-cationic-substituted NDIs (1–3, 5), (ii) a mono-cationic tetra-substituted NDI (**661b**), (iii) two core-extended NDIs (**660d**, **661c**) and (iv) 2 novel polycation NDIs (**660e**, **661d**), which were used for G-quadruplexes within the androgen receptor (AR) gene (which is castration resistant prostate cancer (CRPC)).[31] Among the NDI screened derivatives for stabilization of AR G-quadruplex, the core-substituted NDI (**660d**) was the most powerful ligand, as such AR-positive cells show high sensitivity to (**660d**) in comparison with AR-negative CRCP or normal prostate epithelial cells and also (**660d**) induced remarkable weakening of AR mRNA and protein amounts and significant perturbations in the expression levels of KLK3 (Fig. 143).

Platella *et al.*[424] reported the first intensive NMR study on the interaction of trifunctionalized NDI with G-quadruplex models with various topology structures, *i.e.* the parallel-type and the hybrid-type, with complementing measurements of dynamic light scattering, circular dichroism and fluorescence analysis to monitor the binding process. This study showed preferential binding of the NDI derivative at the outer G-quartets, with the initial binding events occurring at both 5′- and 3′-ends in the case of the parallel G-quadruplex and at the 5′-end for the hybrid G-quadruplex. Hao *et al.*[425] reported that the Tel26 in human telomeres undergo dynamic conformational conversion from hybrid-2 topology to parallel topology under the influence of NDI ligand in K^+ buffer, even at the cellular physiological temperature of 37 °C. Ahmed *et al.*[426] reported that the G-quadruplex-binding small molecule of (**626**) and the HDAC inhibitor SAHA (Vorinostat) act synergistically to inhibit gemcitabine-sensitive and resistant pancreatic cancer cells. Their study suggests that a CM03-SAHA combination can be a potential candidate for a human clinical evaluation trial, both as a first-line therapy and as a second-line therapy for gemcitabine-relapsed (chemo-resistant) patients.

So far, we have seen that planar NDI can be used to intercalate between G-quadruplexes; however, the Wasielewski and Wu group prepared G-quadruplex 2D frameworks of electron-accepting NDI (**662**) and PDI end-capped with two electron-rich donors (see Fig. 144).[427] These molecules form G-quadruplex *via* strong hydrogen-bonding along with π–π-interactions of NDI/PDI stacking between 2D layers. Time-resolved resonance spectroscopies revealed long-lived charge separation and mobile charges on NDI/PDI and recombination kinetics typical of dissociated charge carriers. They have also shown that these organic G-quadruplexes are applicable as cathode materials in a Li-ion battery due to their structural stability and electrical conductivity. A recent study demonstrated the preparation of 2D G-quadruplex organic frameworks of the electron-rich donor 2,7-diaryl pyrene containing two terminal guanine building blocks due to strong hydrogen bonding between the guanine molecules.[140] The resulting guanine-pyrene based 2D frameworks had large optical band gaps with a high lying HOMO, and thus may be useful for photocatalytic reactions. Interestingly, when guanine-pyrene was co-crystallized with guanine functionalised NDI[427] CT complexes were generated.

11.2 Anticancer agents

Hepatocellular carcinoma (HCC) is the third most common cause of cancer death, but there are only a few drugs available for its treatment. NDI has been used as an anticancer agent and shown to be effective for selective binding of double-strand DNA or G-quadruplex. An NDI bearing polyamine groups has shown potent inhibition of cancer cells both *in vitro* and *in vivo*. Learning from this, Freccero and Manet synthesised a water-soluble NDI containing tetracationic quaternary ammonium functional groups (**663**, **664**) which were used for theranostic applications (Fig. 145).[428] They found that these new NDI

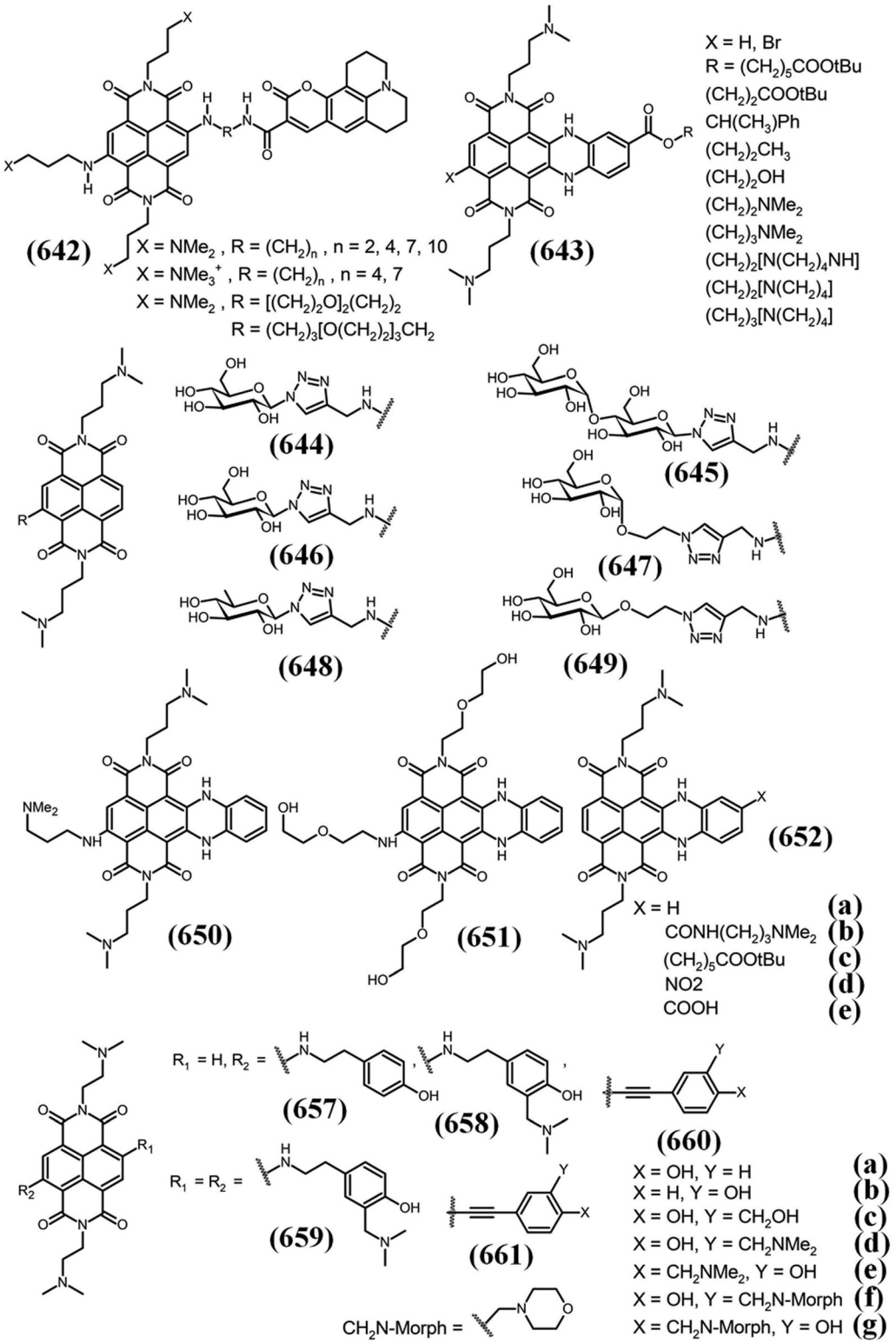

Fig. 143 The molecular structures of dyads investigated as G-quadruplex nucleic acid sensors,[417] core-extended NDIs used for G-quadruplex fluorescence sensing,[418,421] G-quadruplex ligands based on carbohydrate NDI conjugates,[419] core-extended NDI exploited as a G4 light-up sensor,[420] and mono- and di-core-substituted NDI G4 ligands.[422,423]

derivatives selectively bind to G-quadruplex DNA over double-stranded DNA. They have also studied sensitizing ability, cellular uptake, cytotoxicity and photocytotoxicity. Overall, these near-IR red fluorescence emitters accumulate into cell

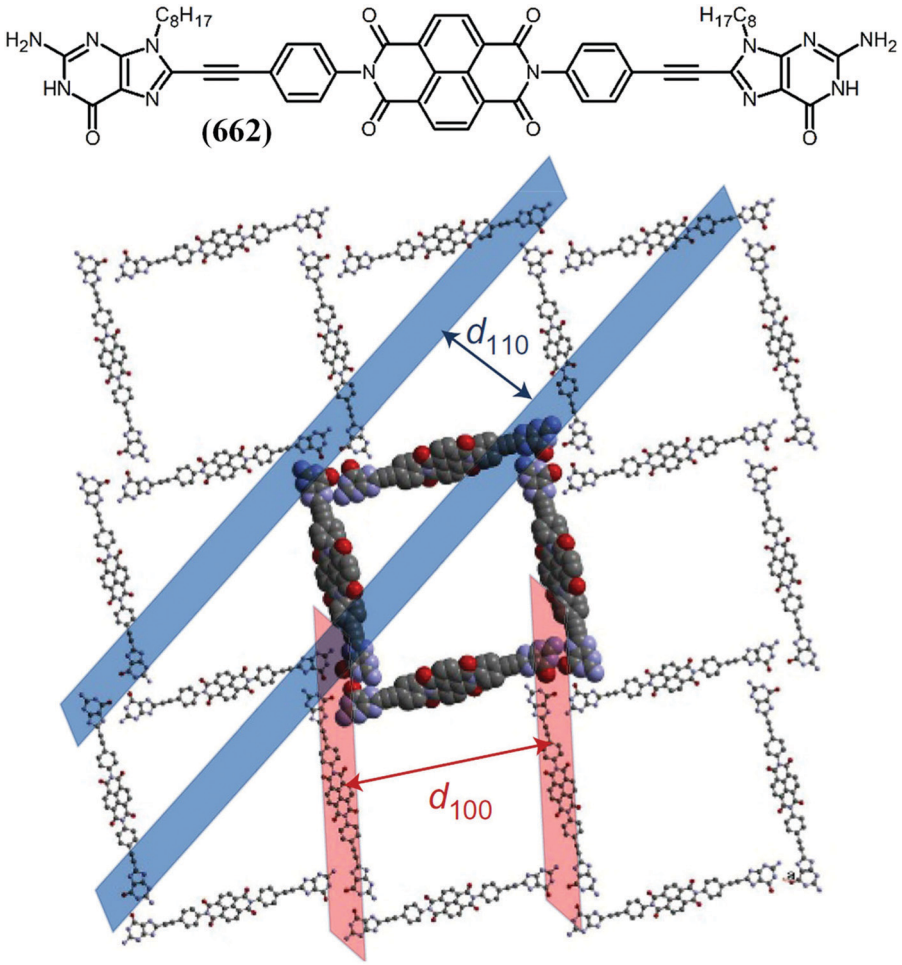

Fig. 144 G-quadruplex organic frameworks through a two-step process that consists of a cross-coupling reaction, and one layer of ordered π stacks simulated G-quadruplex framework structures.[140,427] This figure has been adapted from ref. 427 with permission from Springer Nature, copyright 2018.

nuclei and upon irradiation of NDI cell viability was reduced > 40% and cell expression of γH2AX foci was enhanced, indicating DNA damage at μM concentrations in conjugation with low dark cytotoxicity. The study shows for the first time that charged tetracationic NDI with intense emission in the red/NIR upon irradiation might induce DNA damage in specific sites, perhaps leading to development of new NDIs for HCC treatment in the future. The Milelli group [429] synthesised NDI derivatives bearing polyamine functional groups, *i.e.* *o*-methoxybenzylamino-propyl moiety on one imide and a spermine functional group on the other (**665a–e**), which show cell phenotype-reprogramming properties, demonstrating prevention of the epithelial to mesenchymal transition in cancer cells. When they compared G-quadruplex binding with various NDI derivatives of varying chain lengths between the amino group and the NDI core, as well as the number of amino groups, they revealed an interesting trend: $3 < 4 \approx 5 \ll 6$. Using a similar strategy, Dai and Luo synthesised new asymmetric NDI derivatives and employed them for anticancer activities, and they found that the activity is significantly affected by the substituent groups at the NDI diimide positions (**665f–q**).[430] The NDI derivative bearing alkyl chains at one end and an ammonium group at the other end (**665g**) showed a stronger inhibitory effect on hepatoma cells SMMC-7721 and Hep G2 with IC_{50} values of 1.48 ± 0.43 μM and 1.70 ± 0.53 μM, respectively, as compared to non-cancer cells QSG-7701 with an IC_{50} value of 7.11 ± 0.08 μm. Importantly, treatment of SMMC-7721 cells and Hep G2 cells with (**665g**) gives apoptotic cells with values of 52.1% and 67.8% at 3 μm of (**665g**), respectively. This is evidence that (**665g**) induced autophagy and suppressed the migration of hepatoma cells depending on the concentration of produced ROS, and thus this molecule may be used as a potent anticancer agent in future. Mondal and co-workers described the synthesis of NDI-bis-hydrazimide (**665s**) which showed antineoplastic properties which negatively affected the cell viability of three cancer cell lines (AGS, HeLa and PC3) and also induced S phase cell cycle arrest along with SubG0/G1 accumulation.[431] This new NDI derivative showed the highest sensitivity towards a gastric cancer cell line, in which NDI induced extensive DNA double strand breaks causing p53 activation to transcription for target gene p21 in AGS cells *via* ROS upregulation.

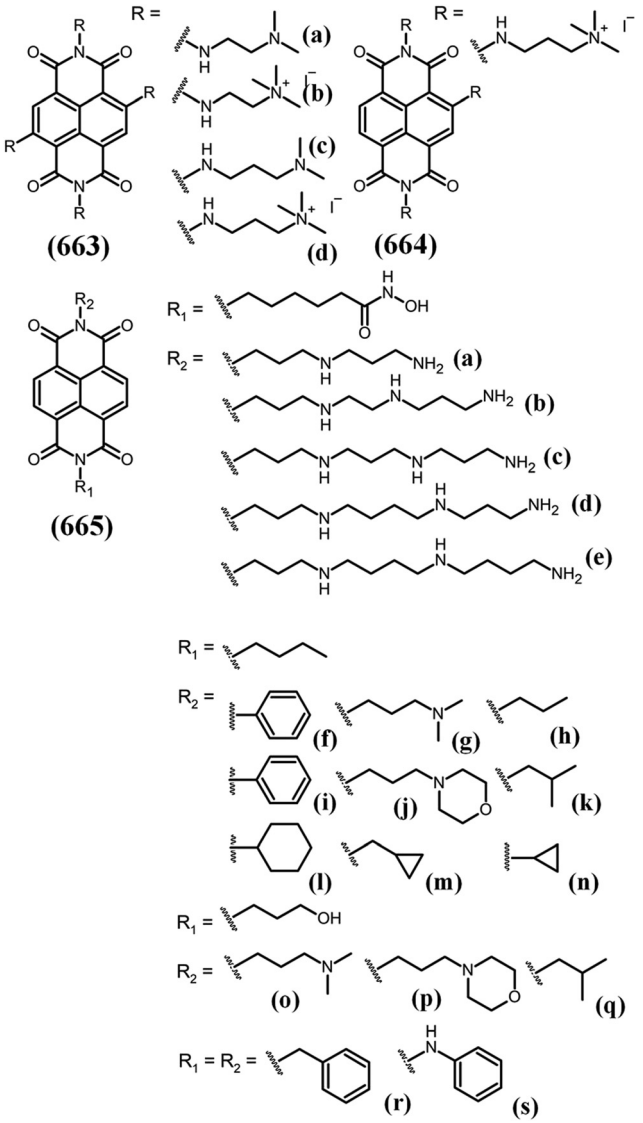

Fig. 145 NDI derivatives with theranostic applications,[428] asymmetric NDI based anticancer agents,[430] NDI derivatives downregulating c-Myc and p21 expression in gastric adenocarcinoma cells,[431] polyamine-NDI conjugates targeting histone deacetylases and DNA for cancer phenotype reprogramming.[429]

11.3 Antiparasitic drugs

Antiparasitic drugs are commonly used for the treatment of parasitic diseases caused by parasites of different classes such as helminths, amoeba, parasitic fungi and protozoa. Pérez-Victoria and co-workers synthesised a series of carbohydrate NDI-derivatives (**666–670**) as G4-binders.[432] They found that carb-NDI was selective toward G4s including hTel and could bind EBR1 selectively over double-stranded DNA. These ligands show excellent antiparasitic activity with IC_{50} values in the nM range against *T. brucei*, *L. major*, and *P. falciparum*, and were shown to be highly selective against MRC-5 human cells. Furthermore, cytotoxicity and zebrafish toxicity studies demonstrated that carbohydrate reduces the intrinsic toxicity of NDIs. In another report, they synthesised 24 new carb-NDI derivatives (**671–674, a–c**) and used them as antiparasitic agents (Fig. 146).[433] Flow cytometry and confocal microscopy showed that the carb-NDI derivatives exhibit excellent uptake into *T. brucei* parasites and were localised in the nuclei and kinetoplasts, giving excellent antiparasitic activity and selectivity against control mammalian cells.

11.4 Antimicrobial activity

Ghosh and co-workers synthesised four unsymmetric cationic bola-shaped NDI-based π-amphiphiles (**675–679**).[434] These amphiphiles have a central NDI core with a hydrophilic wedge and a head group (pyridine) with amine and hydrazine head groups, which allowed directional self-assembly *via* strong hydrogen-bonding, and these derivatives were used as bacteria mimic lipid vesicles as well as antimicrobials. Interestingly, both (**677**) and (**678**) containing the same pyridine head group but with a different location of the hydrazide group led to pyridyl groups being located on outer or inner walls of vesicles. (**677**) assembled with bacterial membrane by mimicking DPPE liposome ($\Delta G = -6.35$ kcal mol^{-1}); however NDI-2a assembled structures did not interact at all. ITC studies demonstrated the interaction of three assembled NDI-derivatives with DPPE liposome in the order of (**675**) > (**677**) > (**676**). Furthermore, the antimicrobial activity was studied and showed that (**677**) is selective against Gram-positive bacteria, while (**678**) did not show any activity. (**676**) with an amine head group exhibited moderate activity but no selectivity to the erythrocytes; however, (**675**) with the tertiary amine head group was shown to have outstanding antimicrobial activity with high selectivity over erythrocytes and very low minimum inhibitory conc. values of 15.8 and 62 μg mL^{-1} for *Staphylococcus aureus* and *Escherichia coli*, respectively. In another report, they have shown stimuli-responsive directional vesicular assembly of a series of non-symmetrical NDI-derived bola-amphiphiles (**680–684**) with tuneable functionality (Fig. 147).[435] With the varying nature of the ionic head-groups at the NDI imide position the impact of charge delocalization on the membrane curvature was seen. The formed anionic vesicles were further used for enzyme inhibition. They believe that stimuli-responsive self-assembled vesicular structures could be of interest for triggered release of drug molecules by thermal control in biomedical applications.

12 Metal–organic frameworks and NDI ligand–metal complexes

Metal–organic frameworks (MOFs) are organic–inorganic hybrid materials that form 1-, 2-, or 3-D (dimensional) structures with are often porous in nature with a high surface area, and have been used for various applications such as ion exchange, catalysis, and adsorption of gases and vapors, to name a few.

12.1 Organic–inorganic crystals

In this section, we will explore various MOF structures based on NDI. Although metal ions and organic ligands form the main

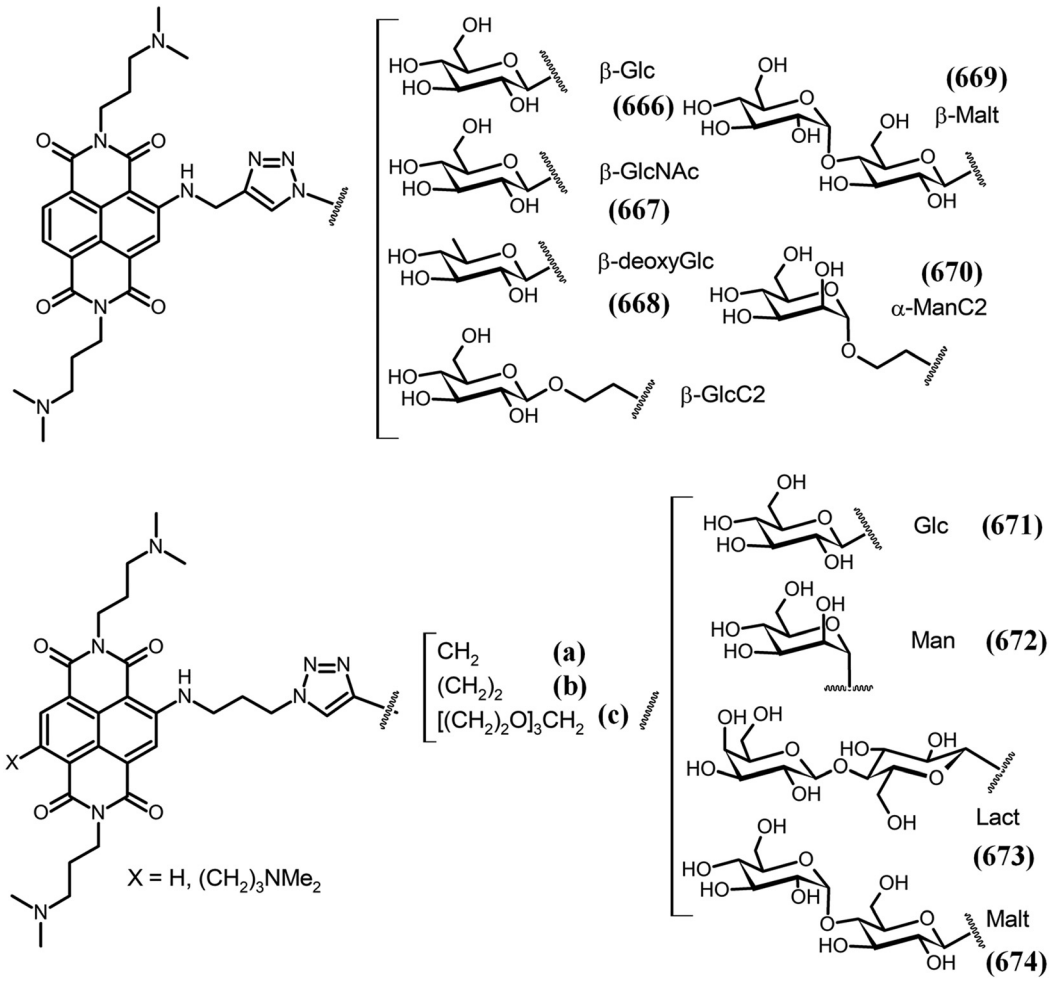

Fig. 146 The carbohydrate–NDI conjugate family of G-quadruplex ligands studied as new antiparasitic agents.[432,433]

body of MOFs, anions also play a role in regulating structures, so called anion-directed coordination systems. In this regard, Zheng and co-workers studied coordination of *N,N*-di-(5-tetrazol)-NDI (H2dtNDI) (**685–689**) with Cd and produced a mixture of two types of components, *i.e.* $([Cd(dtNDI)(DMF)_{2.5}]\cdot DMAc)_n$ (**a**) and $([Cd_2(dtNDI)_2(DMAc)_2]\cdot DMAc)_n$ (**b**). When they treated H2dtNDI with CdX_2 (x = ClO_4^-, NO_3^- and I^-) it afforded the $([Cd(dtNDI)(H_2O)_{2.5}]\cdot DMAc)_n$ (**c**) single coordination polymer.[436] They also found that the mixture of (**a**) and (**b**) can be converted into a pure compound (**c**) by an anion-exchange process, which can be monitored by powder X-ray diffraction (Fig. 148). Similar anion-controlled formation of various architectures and photochromism of cadmium-NDI coordination polymers were reported by Liu and co-workers.[437] The Zhang and Xiang group synthesised the $([Zn(L)_{0.5}(bpy)(H_2O)]\cdot 3.5H_2O)$ MOF based on Zn(II), carboxylate-NDI (**689**) and 4,4′-bipyridine (bpy), which is a unique doubly interpenetrated 3D open framework having **mog** topology.[438] This MOF displayed excellent chemical stability and also featured reversible photochromic behaviour with a color change from yellowish to brown, and could be tuned with UV light, heat and pH. This suggests that NDI may contribute in the future to photochromic MOD materials for photochemical processes *via* photoinduced electron transfer. Niu and co-workers synthesised polyoxometalates (POM) incorporating the zinc-NDI based MOF, *i.e.* $([Zn(HPYI)_3]_2(DPNDI))[BW_{12}O_{40}]_2$, i.e., ZnW–DPNDI–PYI, which they use for photocatalytic oxidation of benzylamine and olefin epoxidation *via* photo-induced electron transfer (conPET) processes in air under visible-light.[439] In another report, the Liu group synthesised photochromic switchable NDI based coordination MOFs, *i.e.* $[Zn_2(DPNDI)(TPDC)_2]$ and $[Cd_6(DPNDI)(TPDC)_6(DMF)_6]$, and these two derivatives showed photoinduced electron transfer and also naked-eye detectable photochromic effects, where the luminescence of both derivatives can be tuned by switching with UV-Vis light in air.[204] Park and co-workers synthesised carboxylic-functionalised organic nanocrystals (ONC) based on NDI which was shown to be highly selective as a uranium sorbent, where the adsorption of uranyl ions with the carboxyl and hydroxyl groups of the ONCs removed up to ~97.5 and ~73% of U(VI), respectively.[440]

12.2 MOFs

Zhang and co-workers synthesised a 2D zinc based MOF, *i.e.* $[Zn(H_2O)_2(2,6\text{-NDC})(\text{NDI-A})]\cdot 2H_2O$ (**691**), in which NDI was used

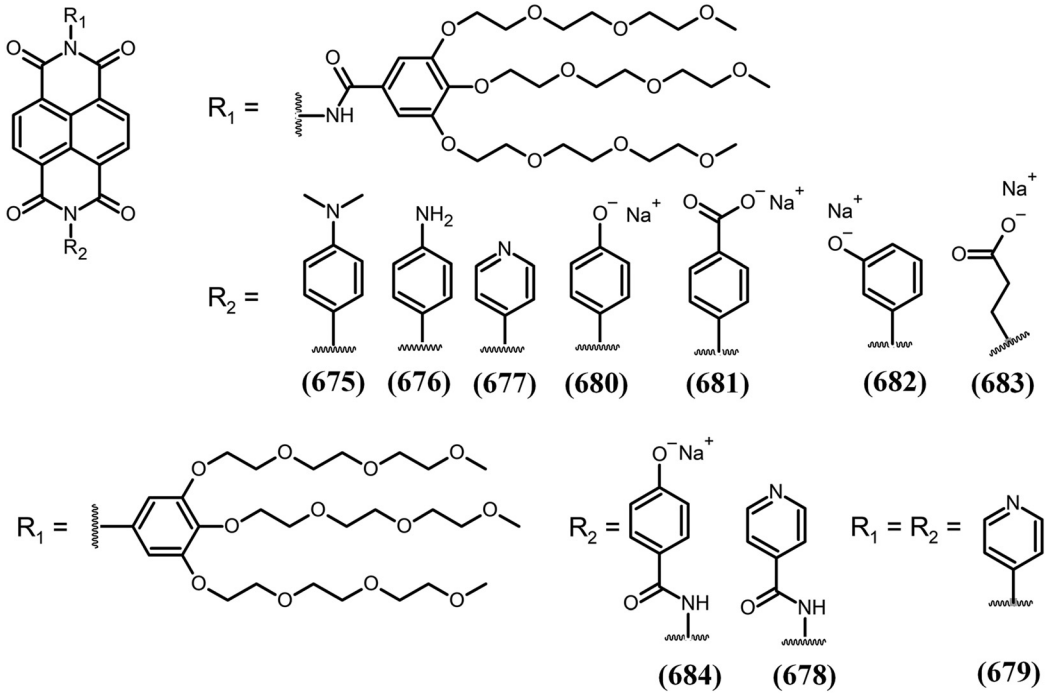

Fig. 147 Structure of hydrazide-containing cationic NDI amphiphile molecules giving vesicular self-assemblies with tunable surface functionality and antimicrobial activity,[434] and anionic amphiphile molecules with similar self-assemblies for enzyme inhibition activity.[435]

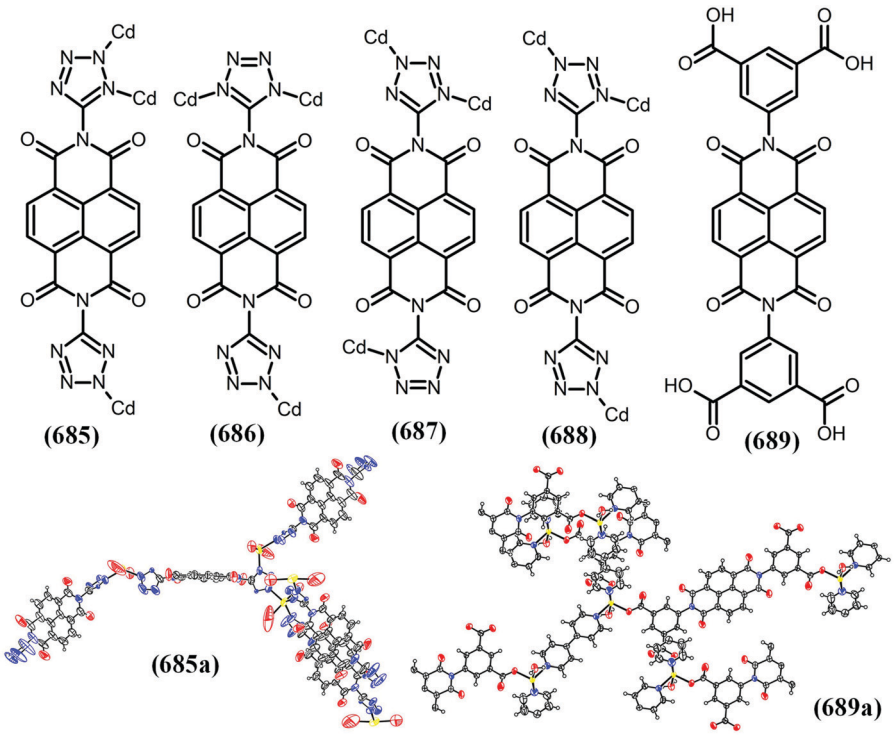

Fig. 148 The coordination modes and environment of Cd(II) ions with the *N,N*-di-(5-tetrazol)-NDI ligand,[436] and the coordination environments of the Zn atoms with 4,4′-bipyridine and carboxylate based NDI to give MOFs.[438] This figure has been adapted from ref. 438 with permission from Elsevier, copyright 2018.

as an acceptor and 2,6-NDC (2,6-naphthalene dicarboxylic group) as a donor (**690**).[441] The formed MOF was shown to be thermally stable and exhibited reversible photochromic behaviour and photo-controlled quenching of fluorescence, *i.e.* the formation of NDI-A radicals was observed due to photoinduced electron transfer. Dinča and co-workers reported

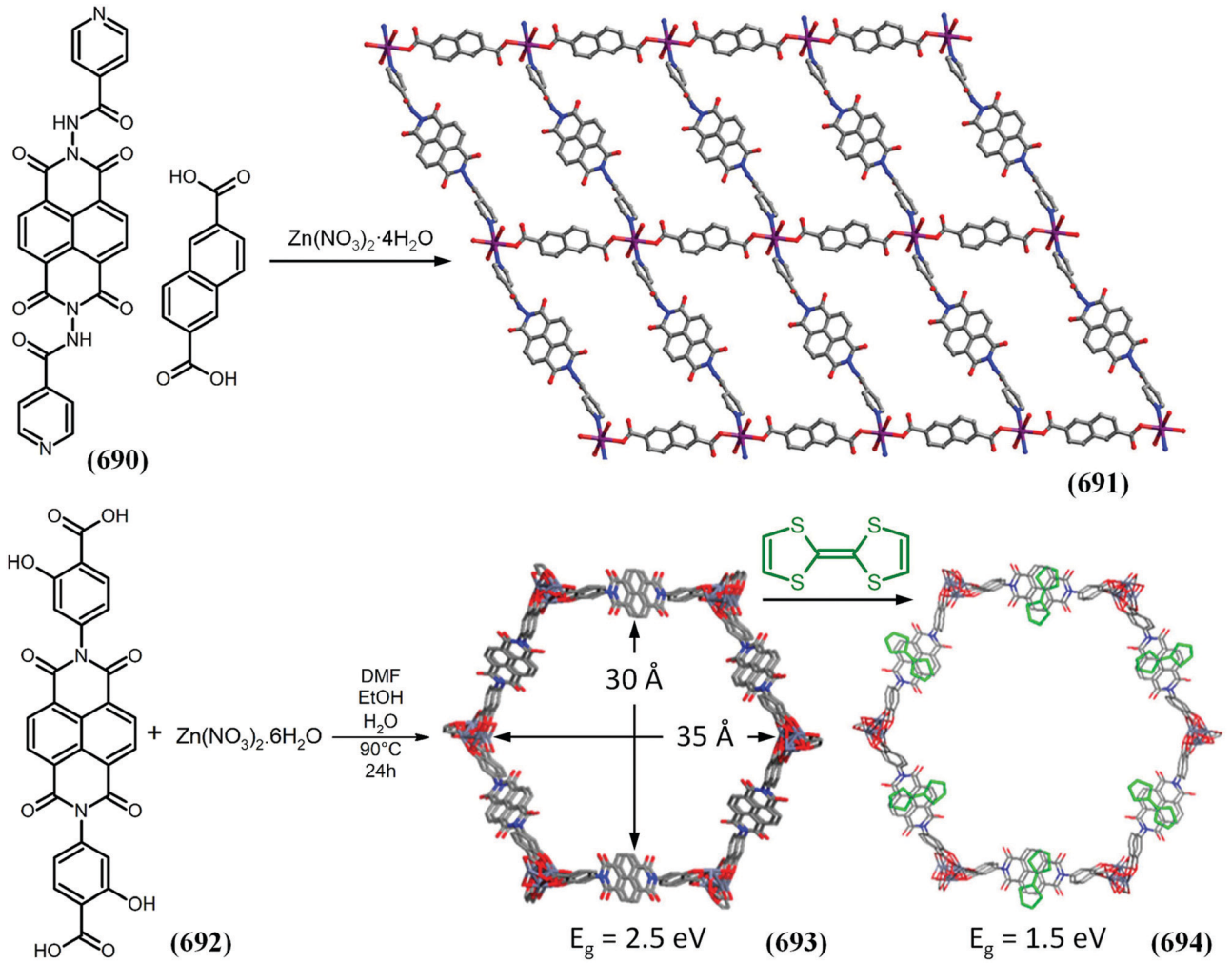

Fig. 149 The 2D photochromic zinc-NDI based MOF, where every two NDI ligands and two 2, 6-NDC2− ligands are symmetrically connected by one Zn(II) ion and each Zn(II) ion is also linked by two water molecules perpendicular to the 2D network.[441] The structure of a DSNDI-zinc ion based MOF-74 architecture, where the π-intercalation of electron-rich planar tetrathiafulvalene (TTF) guests between the NDI ligands stacked along the walls lowers the electronic band gap.[443] These figures have been adapted from ref. 441 and 443 with permission from The American Chemical Society, copyright 2018 and 2017, respectively.

the immobilization of redox-active NDI onto a mesoporous MOF-74 structure to produce an electrochromic MOF, which can be switched from transparent-to-dark (Fig. 64).[205b,442] Furthermore, they showed that these materials produce different morphologies in solid thin films from Mg^{2+} and Ni^{2+} when deposited on fluorine-doped tin-oxide glass, as these films show quasi-reversible redox events due to the [NDI]/[NDI]$^{\bullet-}$ and [NDI]$^{\bullet-}$/[NDI]$^{2-}$ redox couples which are responsible for the electrochromic switching. These materials may be useful in the future for potential applications in smart windows. Using the same MOF structures the Campbell group reported the rapid and selective detection of fluoride anions in solution, observable by the naked eye by a color change in aqueous solution.[174] The Shou and Saha group prepared similar MOFs (**693**) from an NDI bearing salicylic acid groups (**692**) and further studied π-intercalation of planar tetrathiafulvalene (TTF) as an electron-rich guest between the NDI ligands (**694**).[443] This material showed improved electron delocalisation through the TTF-mediated π-donor/acceptor stacks, which led to diminished bad gaps in the doped material and improved electrical conductivity as shown in Fig. 149. The D'Alessandro group demonstrated charge transfer (CT) complexation with donor–acceptor characteristics in a tetrathiafulvalene-NDI based semiconducting MOF under applied electrochemical bias and pressure using *in situ* Raman spectroscopic techniques.[444]

The Castaldelli, Silva and Demets group has synthesised a Co(II) based MOF (**696**) containing *N,N′*-bis(4-pyridyl)-NDI (**695**) as the primary ligand and terephthalic acid as a supporting ligand in the monoclinic space group *C*2/*c* (Fig. 150).[445] They studied its semiconductivity and found that this new MOF shows dual photoconductive behaviour as well as photoresistivity, with a very high responsivity of 2.5×10^5 A W^{-1}.

Goswami *et al.* have synthesised a UiO-type MOF (**698**) containing a Zr_6 metal node and *N,N′*-bis(2,6-dimethyl-4-benzoic acid)-NDI (**697**), and this MOF was shown to be highly

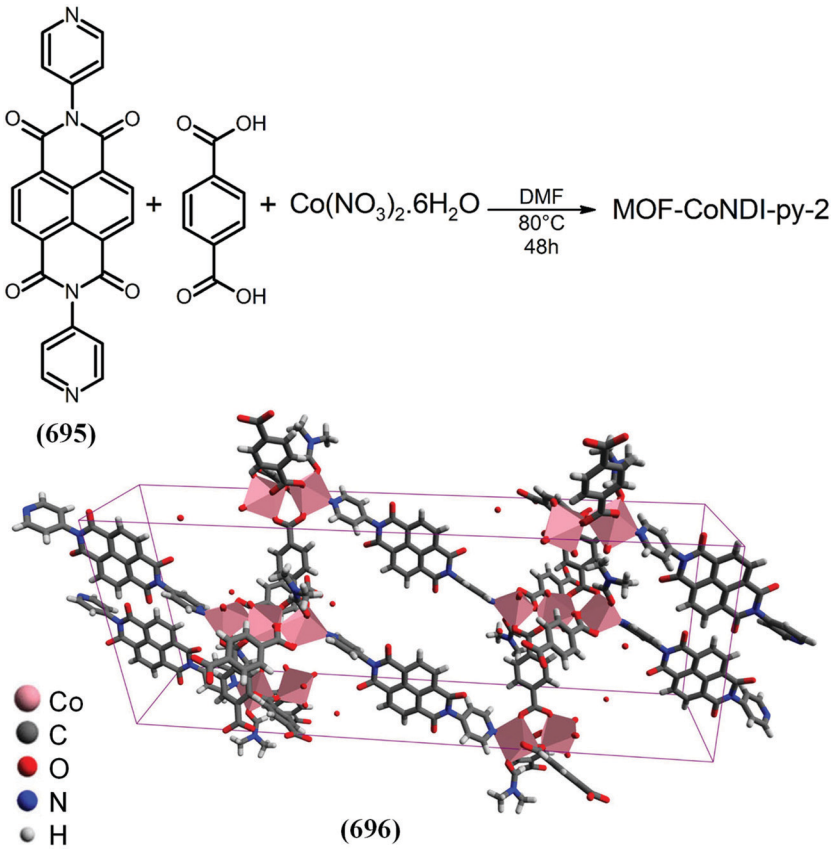

Fig. 150 The MOF-CoNDI-py-2 crystal unit cell structure obtained by single-crystal XRD.[445] This figure has been adapted from ref. 445 with permission from Springer Nature, copyright 2017.

stable, with 2,6-dimethyl groups on the NDI providing high solubility (Fig. 151).[406] They reduced the MOF to generate UiO-NDI$^{\bullet-}$. Using the UiO concept, the Ott group prepared the UiO MOF, *i.e.* Zr(dcphOH-NDI) (**700**), with a redox-active NDI bearing an OH group (**699**) to facilitate proton transfer.[446] They functionalised FTO with Zr(dcphOH-NDI) to produce Zr(dcphOH-NDI)@FTO UiO-type of MOF which showed reversible electrochromic behaviour due to one-electron reductions of the redox-active NDI linkers. This Zr(dcphOH-NDI)@FTO UiO-type MOF displayed a high surface area and a large pore size.

The Zhang and Chen group synthesised a three dimensional porous MOF (FJU-101) (**702**) containing *N,N′*-bis(5-isophthalic acid)-NDI (**701**) and $Cu(NO_3)_2$ under solvothermal conditions. FJU-101 showed a high methane (CH_4) storage capacity of 212 (or 181) cm^3 (STP) cm^{-3}, and this storage capacity is significantly higher than those of isoreticular MFM-130a and UTSA-40a (Fig. 152).[447] They concluded that the polar carbonyl sites within FJU-101 were responsible for strong electrostatic interactions with methane molecules.

The Lin and Huang group studied the host–guest encapsulation of DAN into the weakly fluorescent MOF $ZnSiF_6(DPNDI)_2$ (**703**), which led to orange emission (**704**).[448] Furthermore, they used this luminescent MOF as a colorimetric probe for the detection/sensing of strongly basic amines and also used it as a photochromic probe for weakly basic *N*-methyl-2-pyrrolidone (NMP) and *N,N′*-dimethylformamide (DMF) molecules (Fig. 153).

Zhang and Xiang prepared cadmium-based photochromic MOFs (FJU-67, FJU-68, and FJU-69) using the NDI-related pyrazolate ligand (H_2NDI: 2,7-bis(3,5-dimethyl) dipyrazol-NDI) and dicarboxylic acids (H_2BDC : 1,4-dicarboxybenzene; NH_2-H_2 BDC : 2-aminoterephthalic acid; H2NDC : 2,6-naphthalenedicarboxylic acid), which produced 3D networks interpenetrated with the net topology.[449] In further studies, they found that, upon light irradiation, FJU-67 was bright yellow and FJU-69 was pale yellow with both showing reversible photochromic properties, which may be due to photoinduced free radical generation of the NDI units. This finding may provide a new concept for the design of MOFs with solid crystalline hybrid materials to study structure–photoresponse relationships in the future. Xu *et al.*[450] synthesized two new Co(II) coordination polymers based on monoquats/NDI derivatives and dicyanamide with photo- and thermo-chromism properties. These chromism properties are due to electron transfer and radical formation processes occurring during solvent removal. Li *et al.*[451] constructed the POMOF $\{Cu_4(C_{26}H_{16}N_4O_4)_4(-CH_3CN)_2[SiW_{12}O_{40}]\}\cdot 4H_2O$ *via* self-assembly of the catalytic oxidant Keggin-type $[SiW_{12}O_{40}]^{4-}$ anion, a photosensitizer *N,N′*-bis(4-pyridyl-methyl)-NDI (DPNDI) ligand, and a Cu(I) cation. This MOF showed good efficiency as a heterogeneous

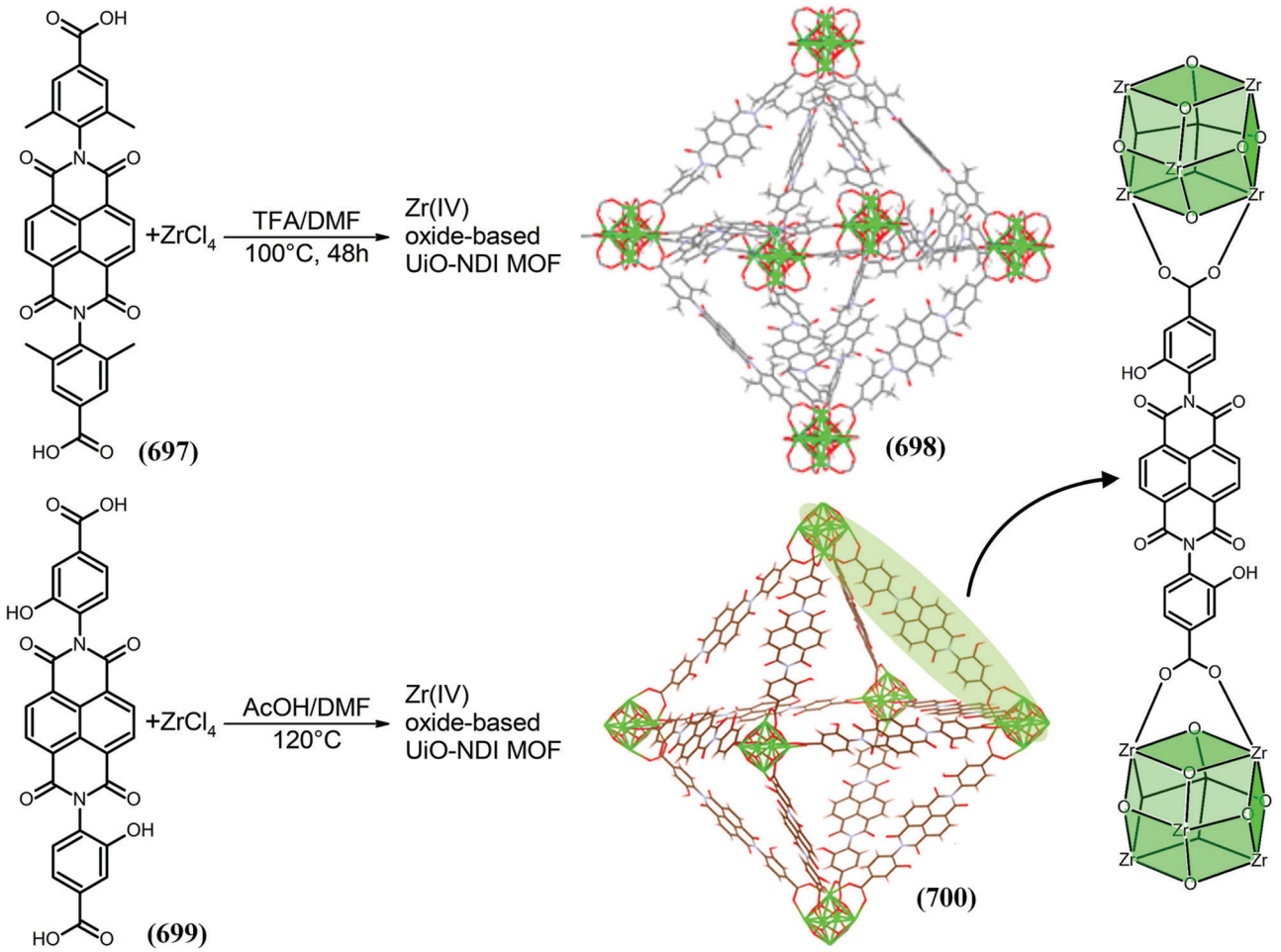

Fig. 151 Synthesis of UiO-NDI and the schematic representation of the octahedron cage in the MOF.[406,446] This figure has been adapted from ref. 406 and 446 with permission from The American Chemical Society, copyright 2018.

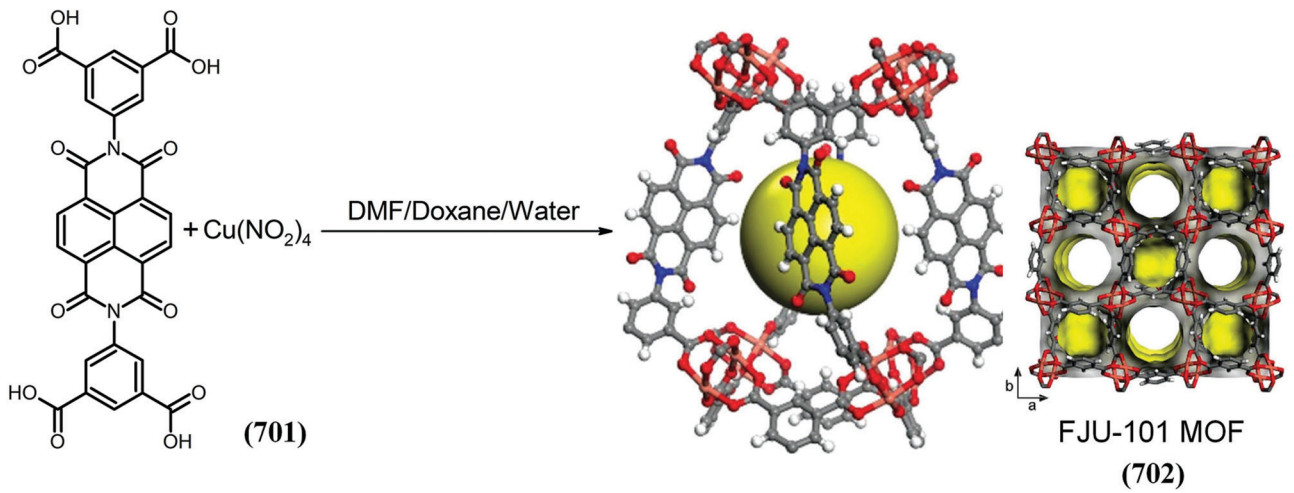

Fig. 152 The structure of the $Cu1_6(L)_4$ nano-sized cage of the FJU-101 MOF; a spherical and 3D framework structure with a 1D cylindrical channel viewed along the crystallographic *c*-axis.[447] This figure has been adapted from ref. 447 with permission from The Royal Society of Chemistry, copyright 2019.

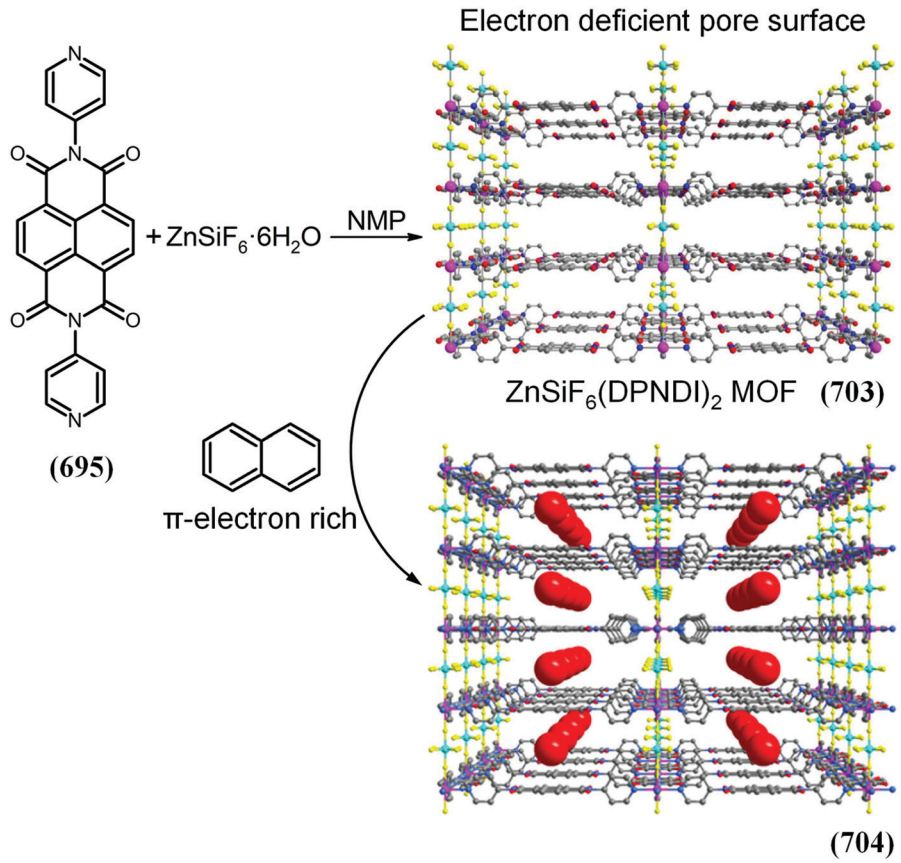

Fig. 153 Encapsulation of naphthalene into the Zn-*N,N′*-di(4-pyridyl)-NDI MOF.[448] This figure has been adapted from ref. 448 with permission from The American Chemical Society, copyright 2016.

photocatalyst in the oxidation process of amines to imines without a co-catalyst under mild conditions. Another set of MOFs with catalytic oxidation properties were synthesized and characterized by Tran *et al.*[452] Isostructural lanthanide MOFs (Ln-MOF-589, Ln = La^{3+}, Ce^{3+}) were formed solvothermally from Lewis acid $[Ln_2(–COO)_6(–COOH)_2(H_2O)_6]$ units and the NDI core, and showed catalytic activity for the oxidation of olefins.

12.3 Complexes and crystals

In the past two decades, coordination polymers have attracted attention due to potential applications in various fields such as fluorescent probes, gas adsorption, catalysis and sensing. In this regard, NDI is a promising ligand due to its planar structure as well as tendency to form π–π interactions. Liu and co-workers synthesised the complexes ($[Co(4\text{-pmntd})(H_2O)_4\cdot Co(4\text{-pmntd})(H_2O)_4]\cdot 4(NO_3)\cdot 3(H_2O))_n$ (**705**) and ($[Mn(4\text{-pmntd})(SCN)_2]\cdot 2(C_2H_5OH))_n$ (**706**), based on (4-pmntd = *N,N′*-bis(4-pyridylmethyl)-NDI) (**227**).[453] The complex (**705**) produces a 1D zigzag chain arrangement in a cross-like fashion by hydrogen bonding; however, the complex (**706**) was a (4,4)-sql 3D supramolecular framework with 1D quadrangle channels formed by strong π–π interactions and hydrogen bonding. Importantly, both the complexes (**705**) and (**706**) exhibited blue emission in DMF, and interestingly complex (**706**) showed enhanced fluorescence intensity at 420 nm upon the addition of 2 equiv. of SCN^- (Fig. 154).

Groot and co-workers undertook structural determination of a bioinspired *para*-crystalline optical material using a fused zinc-NDI-salphen-phenazine (**707**) prototype light-harvesting compound.[131,454] The Wei and Lin group constructed a supramolecular π-gel (ONT) (**709**) displaying aggregation induced emission (AIE) at 468 nm, employing *N,N′*-di(4-pyridinyl) functionalized NDI (**695**) with tri-(4-pyridinyl) functionalized trimesic amide (TCP) (**708**) *via* non-covalent interactions.[173] They found that ONT could be used to remove ferric (Fe^{3+}) or cupric (Cu^{2+}) ions (**710**) from water. They also prepared a thin film of ONT which was used to detect Fe^{3+} or Cu^{2+}, indicating potential for detection and separation of cationic substances *via* fluorescence in the future. Wade and co-workers[455] described photoreduction of *N,N′*-bis(2,6-diisopropylphenyl)-NDI (**712**) in the presence of monovalent Li^+ and divalent Mg^{2+} as illustrated in Fig. 155. Thus, cation–anion interactions of Li^+ and Mg^{2+} with [$Dipp_2$NDI] facilitated efficient photoreduction to $[Dipp_2NDI]^{2-}$ in THF solution leading to a dimeric Mg^{2+} complex (**713**) of $[Dipp_2NDI]^{2-}$ *via* chemical reduction. Lacroix and co-workers described the synthesis of molecular junctions using donor–acceptor strategies, in which an NDI bearing bis-terpyridine was used as an electron acceptor which was covalently bound to ruthenium at one side with

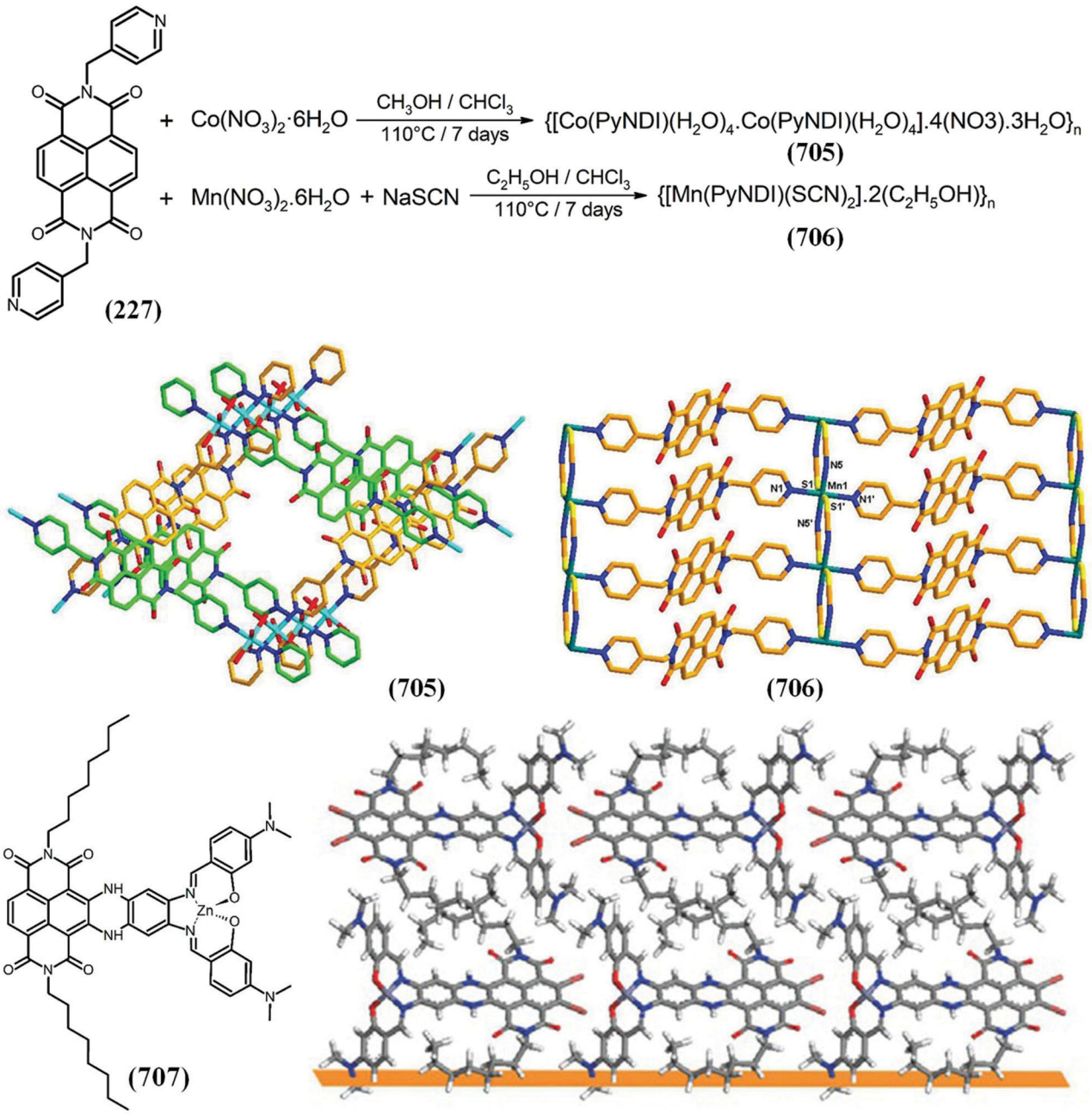

Fig. 154 The MOF synthesis and the coordination environments of Co^{2+} and Mn^{2+} ions in (**705**) and (**706**) of the (4, 4)-sql network structure, and the proposed possible assembly of the supramolecular AIE π-gel ONT.[173] All hydrogen atoms and disordered atoms have been omitted for clarity. The simulated diffraction pattern of the DATZnS(3′-NMe) obtained with the NMR-derived geometry in the *P*2/*c* space group solid-state structure of (**707**).[131,454] These figures have been adapted from ref. 131, 173 and 454 with permission from The Royal Society of Chemistry, copyright 2019, and John Wiley and Sons, copyright 2017, respectively.

the other side functionalised with a phenylamine terminal group (**714**), which can be converted *in situ* to a diazonium cation and grafted onto various substrates.[456] They showed that films on glassy carbon showed five redox states by cyclic voltammetry.

Chiral self-discrimination is challenging with multicomponent mixtures; in this regard, the Kwak and Oh group constructed multifunctional homochiral and heterochiral chiral supramolecular biocoordination polymers (SBCPs) with alanine-functionalized NDIs as organic linkers. AlaNDI-Zn (**716**, **717**) was composed of an NDI ligand with alanine termini (AlaNDI) (**715**) and Zn ions, which was used for chirality transcription of amino acids in biocoordination polymers (Fig. 156).[159] Among the SPCPs, homochiral SBCP was shown to selectively detect chiral napoxen, which can be confirmed by quenching of fluorescence. They also studied

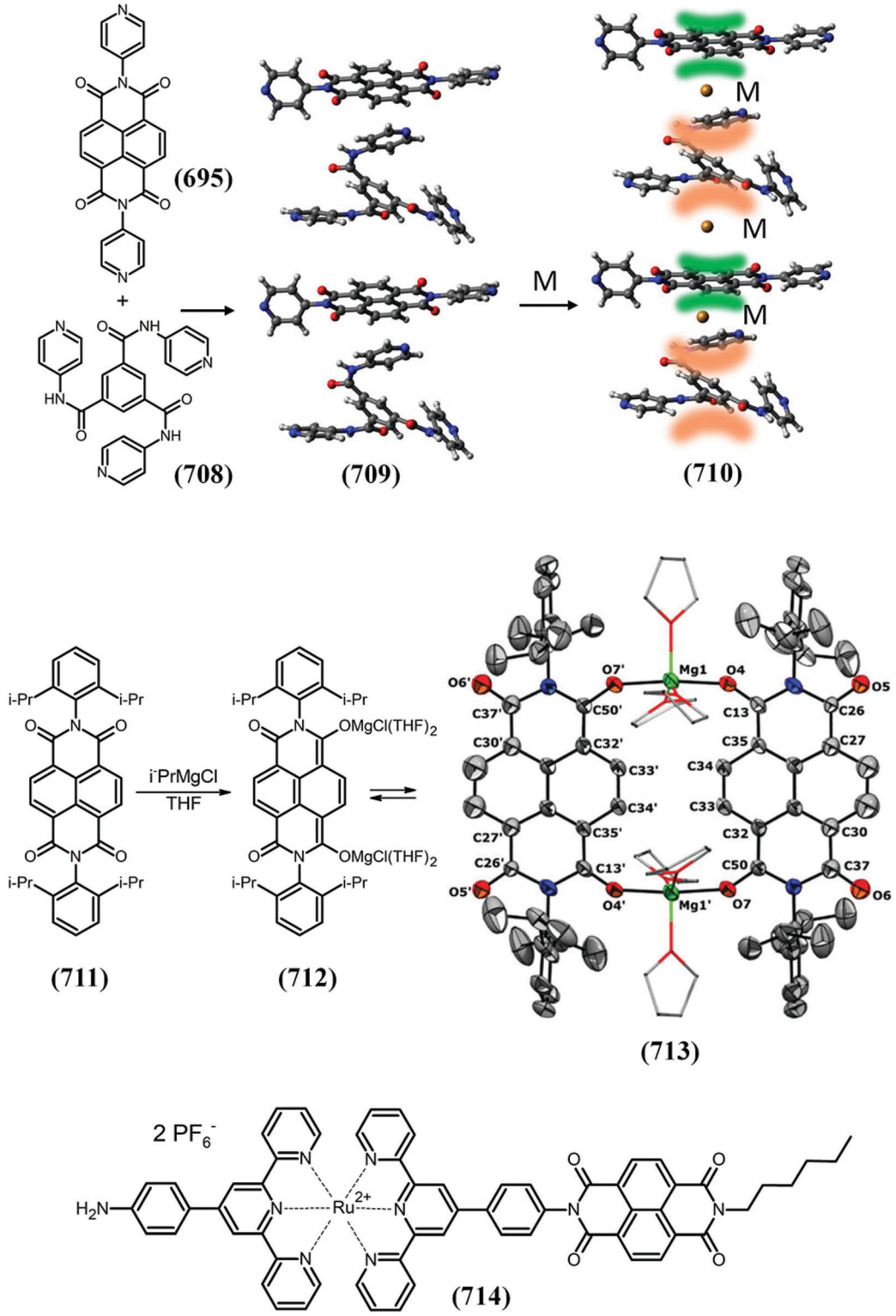

Fig. 155 The π-gel (ONT) (**709**) supramolecular structure and metal complexing of the supramolecular[173] synthesis of Mg complexes of (**712**) and the solid-state structure of (**713**),[455] and the chemical structure of the (**714**) dyad.[455] These figures have been adapted from ref. 173 and 455 with permission from The Royal Society of Chemistry, copyright 2017 and 2019, respectively.

the use of SBCPs for sensing of electron-rich VOCs such as ethanol and aniline. SBCPs detected aniline with a limit of detection up to 16 ppm, comparable to ammonia or amines using conductive CPs. In another report, they described the synthesis of heterochiral supramolecular coordination networks (SCNs) by a solvothermal reaction of NDI with cadmium

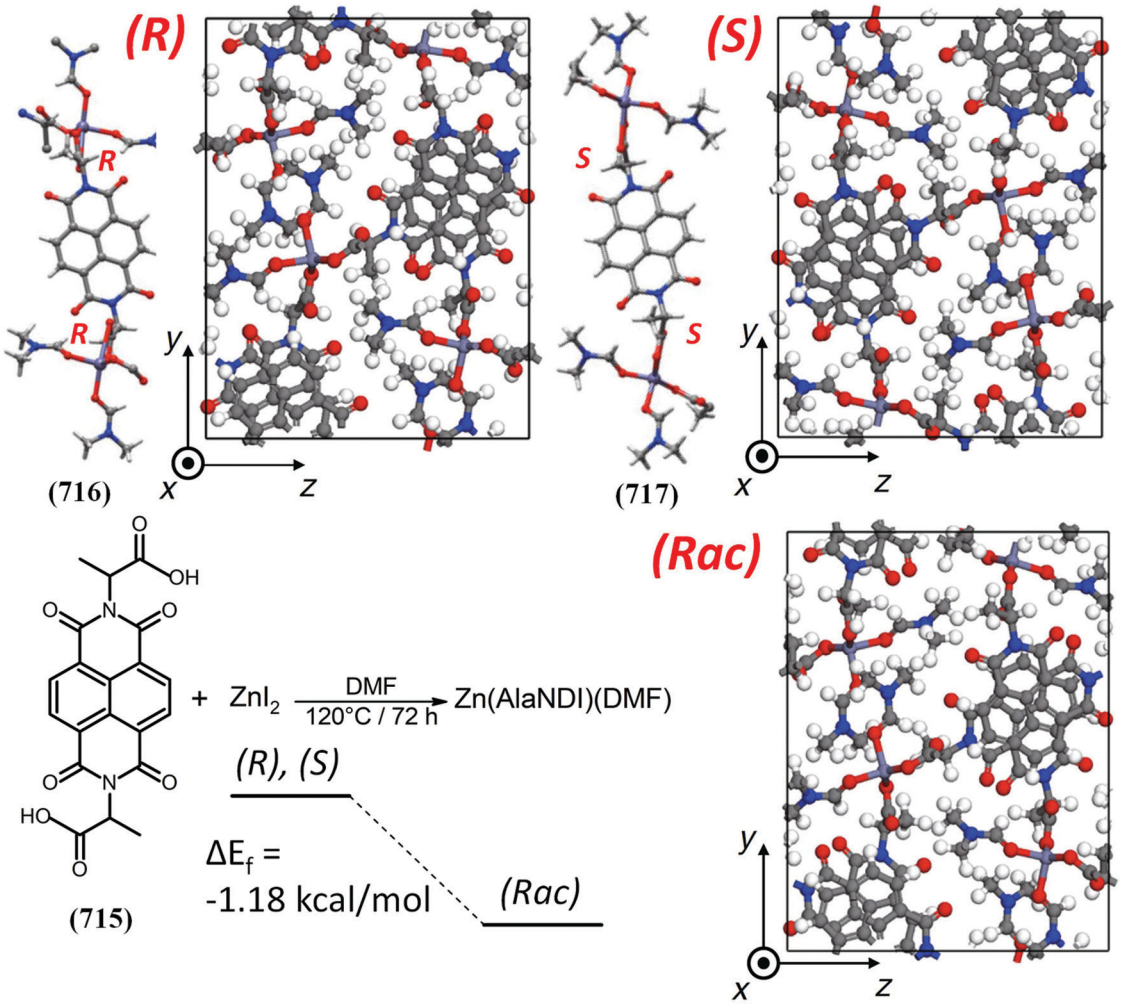

Fig. 156 Formation energy (ΔE_f) calculation results for chiral discrimination phenomena in heterochiral SBCPs. The carbon, hydrogen, oxygen, nitrogen, and zinc atoms of AlaNDI-Zn SBCPs are colored in gray, white, red, blue, and thin-purple, respectively.[159] This figure has been adapted from ref. 159 with permission from Springer Nature (NPG), copyright 2018.

iodide.[203] These newly prepared heterochiral doped SCNs displayed photochromic and photodetection properties, with enhanced conductivity and photoresponsivity in the presence of hydrazine due to electron transfer from hydrazine to SCNs. These SPCPs and SCNs developed in their study show potential for use as versatile sensors (photoactive, chemiresistive) and chiral sensing, as well as for nano/micro-optoelectronic applications.

In another report the Pan group described structural tuning of coordination polymers of an NDI bearing flexible pyridyl arms coordinated with Cu(II), Cd(II) and Zn(II) resulting in 2D bat-like or dumbbell-like (4,4)-sql topological or 3D type building units, with structural tuning of the cavity size by introducing pillar anions.[457] Sun and co-workers used an NDI-ammonium molecule to synthesise a 2D lead-iodine based hybrid single crystal perovskite, in which the lead-iodide skeleton works as a sandwich type template to induce the NDI-A cation to a 1D π-stack, and demonstrate charge transfer between the lead-iodide and 1D NDI chains with a narrowed bandgap (Fig. 157).[458] This NDI-containing perovskite crystal was highly stable and showed ambipolar transport with a mobility of more than 5×10^{-3} $cm^2 V^{-1} s^{-1}$ without hysteresis. This study demonstrated the use of lead-iodine-NDI hybrid materials for the next generation photovoltaic and other optoelectronic devices in future.

Lu's group[459] produced for the first time polyoxometalate (POMs)-NDI (anion–π, donor–acceptor) charge transfer hybrid materials with room-temperature phosphorescence photochromism properties. The non-covalent anion–π interactions between the POMs and NDI effectively induce the formation of an alternate arrangement in a crystalline superstructure, providing efficient charge-transfer pathways to bridge the large singlet–triplet energy gap in the NDI *via* emissive transition from the $^3\pi$–π^* excited state. Lin's group[460] synthesised a porous cuboid 3D H-bonded anion–π coordinated framework using (**695**), by slow diffusion of a methanol solution of tri(tetraphenyl phosphonium) hexacyanoferrate, $(Ph_4P)_3Fe(CN)_6$, into a DMF solution of (**695**) and a small amount of HI with a buffered layer of MeOH and DMF in solution in a long thin test tube. In similar works by the same group,

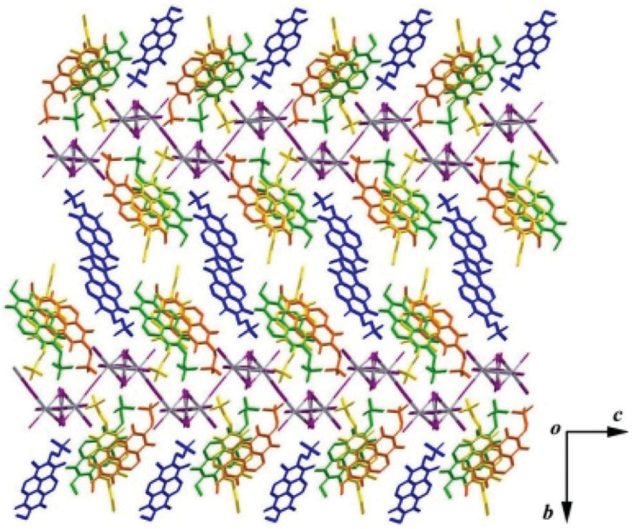

Fig. 157 The view of the $(NDIA)_4Pb_3I_{10}$ crystal structure down the *a*-axis showing infinite stacks of NDIA molecules, with a large overlap in a trimer (NDIA in yellow, orange, and green color) and between the neighbor trimers.[458] This figure has been adapted from ref. 458 with permission from The American Chemical Society, copyright 2018.

they[461] showed that the combination of *N,N′*-dipyridyl NDI tectons (**695**) with three POM anions ($SiW_{12}O_{40}^{4-}$, $PW_{12}O_{40}^{3-}$ or $PMo_{12}O_{40}^{3-}$) gave three isostructural D–A hybrid heterostructures with an alternate arrangement of segregated POM anions and 1D H-bonded NDI networks, with enhanced photochromic speeds and switch-on room-temperature phosphorescence emissions. The quantum yields of these three compounds increased with increasing anion–π interactions.

12.4 Metallomacrocycles

The Turner group described the formation of two homochiral metallomacrocycles (**718**) and the formation of rotaxanes by dipyridyl co-ligands passing through metallomacrocycles (4,4-bipyridine, dipyridylethene and dipyridyl-NDI), with coordination polymers of L-alanine substituted NDI. Multiple parallel π-interactions were observed with the exception of one material in which a 1D chain interpenetrates in a 1D → 2D manner (Fig. 58).[462] Two of the reported coordination polymers containing dipyridyl-NDI (4PyNDI) did not show π-interactions

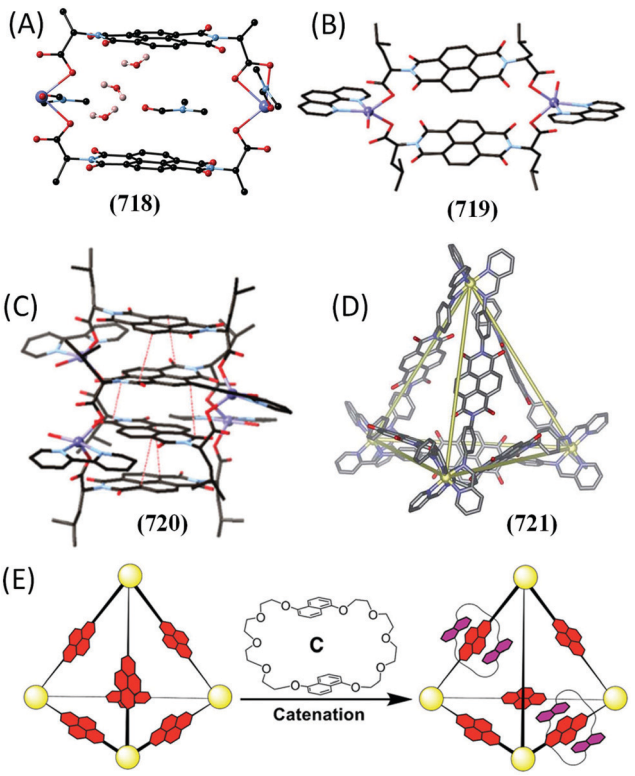

Fig. 158 (A) One macrocycle of the 1D chains of alternating $Cd_2(AlaNDI)_2$ metallomacrocycles and 4PyNDI showing the associated solvent (the DMF and one water residing within the macrocycle).[462] (B and C) The crystallographically determined structures of $[Cd_2(LeuNDI)_2\text{-}(1,10\text{-phen})_2(OH_2)_2]$ and $[Cd_2(LeuNDI)_2(2,2'\text{-bipy})_2(OH2)_2]_2$.[463] (D) The crystal structures of Zn_4L_6 tetrahedra, where the yellow lines connect Zn^{II} centres to highlight the tetrahedral frameworks. (E) The summary of the host–guest of the homoleptic cages (**721**) with crown ether C.[464] These figures have been adapted from ref. 462–464 with permission from The Royal Society of Chemistry, copyright 2016, 2017 and 2019, respectively.

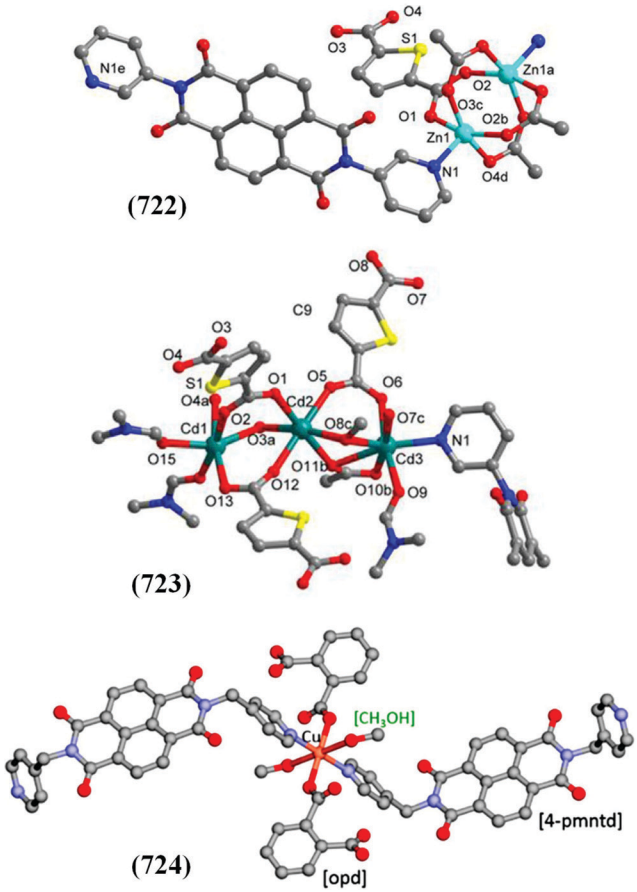

Fig. 159 View of the coordination environment of the Zn(II) ions in $[Zn_2(DPNDI)(TPDC)_2]$ (**722**) and Cd(II) in $[Cd_6(DPNDI)(TPDC)_6(DMF)_6]$ (**723**).[204] This figure has been adapted from ref. 204 with permission from Elsevier, copyright 2019. Coordination environments of the Cu(II) ion in the compound $[Cu_2(4\text{-pmntd})_2(CH_3OH)_4(opd)_2]_n{\cdot}MeOH$ (**724**).[466] This figure has been adapted from ref. 466 with permission from The American Chemical Society, copyright and 2019.

between the 4PyNDI ligands, instead interacting with the macrocycles. They concluded that metallomacrocycles may be promising synthons for future crystal engineering applications. In another report, they synthesised metallomacrocycles and [2]-catenanes based on a leucine substituted NDI organic (**719**, **720**), which demonstrated the formation of an excimer and exciplex emission in solution.[463] Similarly, the Sanders and Nitschke group described the synthesis of two Zn_4L_6 cages (**721**) bearing either diamine NDI or porphyrin. They formed different supramolecular structures, in which the electron poor NDI ligand with an electron-rich crown-ether macrocycle produced mechanically-interlocked species up to a [3]catenane and the porphyrin based cage (see Fig. 158(E)) acted as a receptor for a C_{70} guest molecule.[464] They also demonstrated a dynamic combinatorial library (DCL) of seven constitutionally distinct mixed-ligand Zn_4L_6 cages when mixing these species.

12.5 Metallopolymers or coordination polymers

π-Conjugated coordination polymers/metallopolymers based on NDI units have attracted considerable attention because these polymers act as n-type acceptors and also allow low-cost, flexible and light-weight device fabrication. π-conjugated coordination polymers (CPs) with electron-deficient NDI building blocks have low energy levels which, when combined with light absorption properties, make them useful for solar cells, light emitting diodes and transistors. π-Conjugated coordination polymers where NDI is functionalised with pyridyl/benzoic acid substituents through the diimide site are able to coordinate with d-metal ions. The Turner group has reported homochiral coordination polymers using flexible acid chains.[462,463] Kiriy and co-workers have prepared the coordination polymer *N,N′*-(diIJ2-picolyl)-NDI by reacting 2-picolylamine with NDA and further coordination polymers were prepared using $ZnCl_2$ in acetone. They also studied the coordination chemistry and supramolecular properties both in the crystalline phase and in solution.[133] In another report, they described the polymerisation of isoindigo-based monomers and their polymerisation with zinc-based NDI monomers at room temperature, which is difficult even with Stille, Suzuki and direct arylation polycondensation reactions.[375]

Liu and workers described the photochromic properties of *N,N′*-di(3-pyridyl)-NDI (DPNDI) and thiophene-2,5-dicarboxylic acid (H2TPDC) in the presence of Zn^{2+}/Cd^{2+} ions (**722**, **723**) under solvothermal conditions, where different structures were observed because of different coordination modes.[204] Both of these CPs were photochromic electron-transfer complexes with reversible photochromic behaviour. Typically, upon excitation of DPNDI at 350 nm photoinduced electron transfer and a change in luminescence at 467 and 496 nm occurs, which may be due to π–π* transitions of the ligand. This emission gradually decreases and is quenched when the sample is kept in the dark after 5 min irradiation. This study demonstrates a new strategy for the synthesis of light-responsive smart materials for future applications. Another report by the Liu group demonstrated that *N,N′*-bis(3-carboxyphenyl)-NDI coordinated to magnesium(II) produces a 1-D coordination polymer under solvothermal conditions and displays reversible photochromic behaviour in the dark and under visible light.[465] Wang and co-workers synthesised for the first time two metallopolyynes using a platinum(II) donor coordinated with an NDI acceptor to produce D–A-based copolymers, and further demonstrated p-

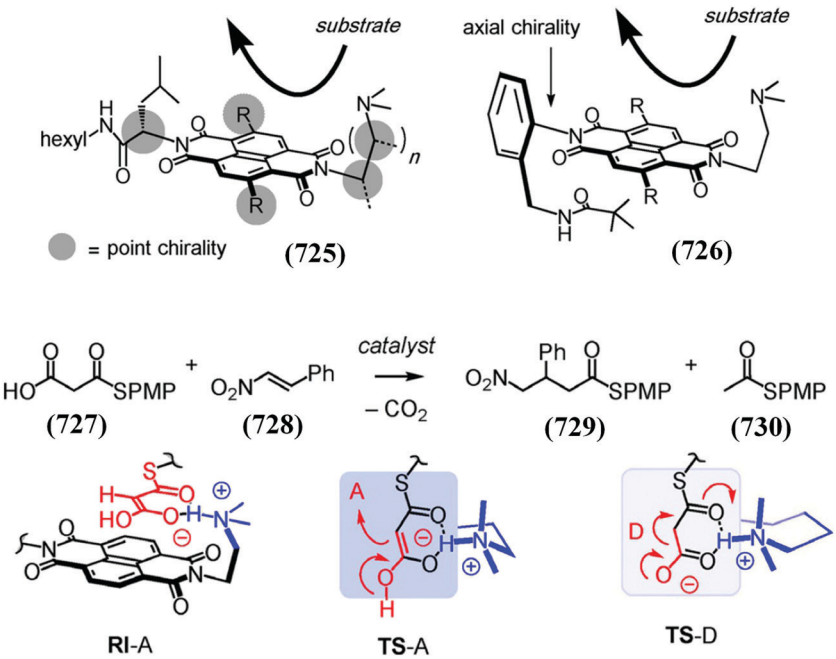

Fig. 160 Anion–π catalyst (**726**) with axial chirality (*P* enantiomer, R = SO_2-octyl), compared to the previously reported anion–π catalyst (**725**) with point chirality. Anion–π catalysts accelerate the addition of (**727**) to (**728**), yielding (**729**), and decelerate the intrinsically favored decarboxylation of (**727**), yielding (**730**), presumably by discriminating the planar reactive intermediate RI-A and transition state TS-A from the twisted TS-D on their π-acidic aromatic surface.[469]

channel field-effect charge transport characteristics on Si/SiO_2 substrates, which is the opposite to other organic NDI-based coordination polymers. Unipolar p-type transport with values between $\mu_h = 3.84 \times 10^{-4}$ and 2.89×10^{-4} cm^2 V^{-1} s^{-1} for OFETs was observed for both of the polymers.[344] This report showed that NDI based polymers can not only can be used for n-type semiconductors but, when functionalised with thiophene, can also show promising p-channel characteristics, and may be useful for printable electronics in the future. Tao and co-workers described a series of heavy metal-containing terpolymer acceptors by conjugating a Pt complex into a PNDIT2 polymer backbone through an ancillary ligand, and upon increasing the amount of Pt metal the average power-conversion efficiency (OCE) increases 3.16%/4.14%, 3.39%/4.54% and 3.88%/4.91%, respectively. These results show that the introduction of Pt metal in the terpolymer acceptor complex provides a simple and efficient method to enhance the PCE of all-PSCs. The Yang group prepared NDI-based coordination polymers with Cu^{2+} (**724**) and this coordination network exhibited selective separation of ethanol over acetonitrile at room temperature (see Fig. 159).[466]

13 Catalysis

Anion–π interactions, *i.e.* non-covalent interactions between electron rich ions and an electron poor aromatic NDI π-system, have opened up new opportunities for various applications such as sensing and catalysis.[431] Anion–π interactions have a crucial role in controlling the selectivity and increasing the π-acidity of the catalyst. The details of this work have been reviewed by the Matile group in 2018.[467] For example, the Matile group used the π-acidic surface of an NDI to develop catalysts for the stereoselective addition of aldehydes to nitroolefins. In another study, they reported the use of anion–π interactions for the Kemp elimination reaction. The Matile group has used anion–π interaction within enolate enamine and iminium chemistry for the catalytic cyclization and cycloaddition and further these they and others have used these interactions not as an artificial enzyme but also in

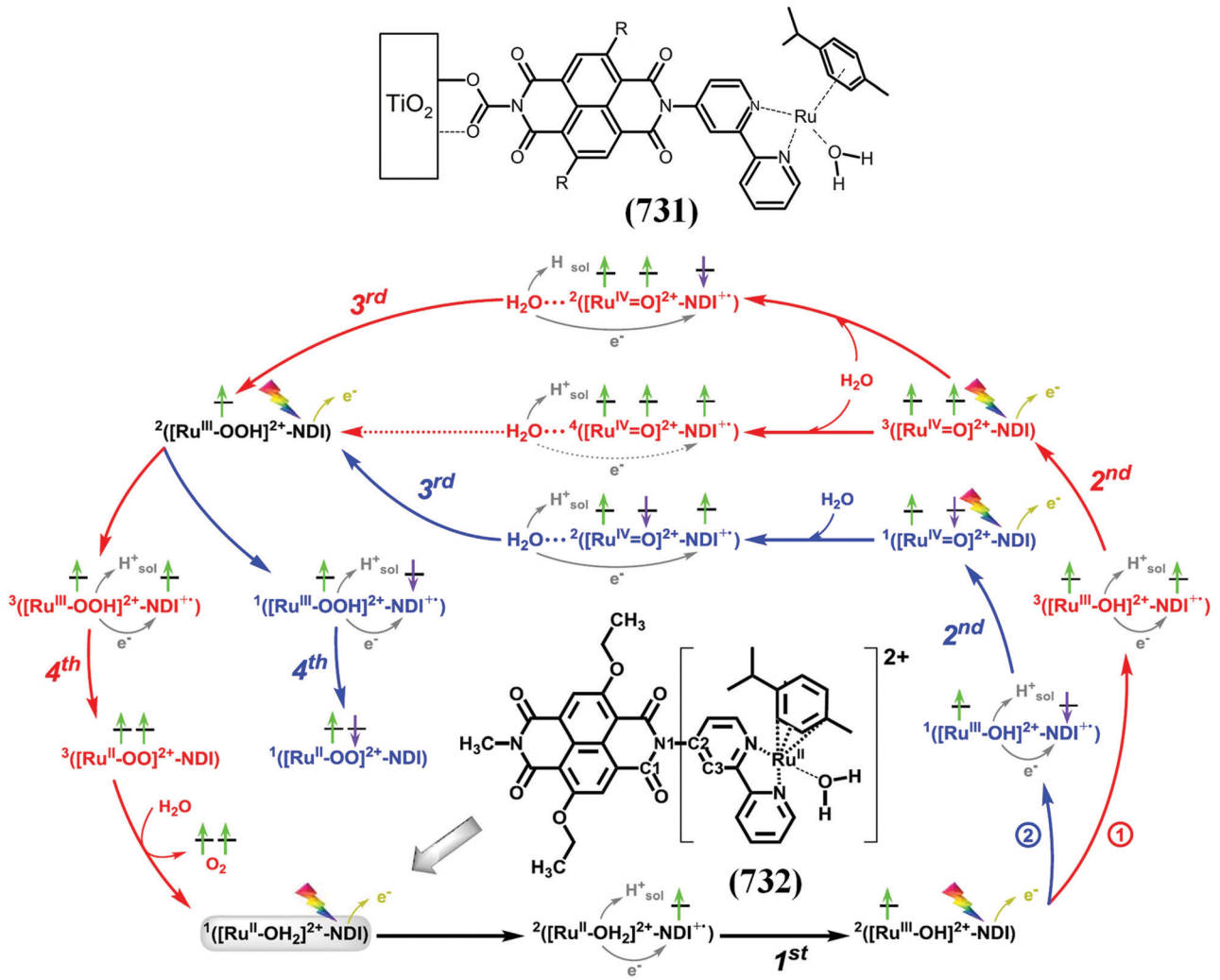

Fig. 161 Schematic representation of the proposed photoanode (**731**) including the acceptor–semiconductor (TiO2), the NDI based chromophore, and the Ru-based water oxidation catalyst;[474] and the proposed photocatalytic water splitting cycle by a Ru-based WOC–dye system, consisting of four catalytic steps.[475]

π-stacked foldamers, and fullerene-centered triads. Details of all the above reactions using anion–π interactions and use of the π aromatic surface are covered in a review article by the Matile group.[467]

In a recent work, they have described the use of π-acidity of the catalyst for epoxide opening ether cyclizations without the addition of an activating agent. They have also used other anion–π–acidic surfaces such as benzene, PDIs and NDI for comparison.[468] NDI is one of the most studied systems for anion–p catalysts because the NDI aromatic surface provides the π–acidic aromatic plane [467] where catalysis occurs. However, for the asymmetric anion–π catalysis, one needs to break the symmetry of these planes, thus axial chirality is the main requirement. The Matile group introduced the first anion–π catalysts with axial chirality, using bifunctional NDI catalysts with a tertiary amine next to the π–acidic NDI plane bearing a bulky aromatic substituent in the imide position to produce separable atropisomers (Fig. 160).[469] In their study they used malonic thioester (**727**) and the enolate acceptor (**728**) using anion–π catalysis on axially chiral π–aromatic surfaces. However, the expected chiral enolate addition product (**729**) was not produced instead the enolate decarboxylation product (**730**) was observed. Therefore, this enantioselectivity was introduced for the first time with a small-molecule anion π catalyst.

The organic–inorganic donor–acceptor hybrids are a new class of complexes composed of semiconductive organic dyes and inorganic pigments. These materials demonstrated optoelectronic and photocatalytic properties. Li *et al.*[470] synthesised two organic–inorganic hybrids from dipyridyl-NDI tecton (DPNDI) with CuI or $AgOOCF_3$ to give 1D $[Cu_8I_{14}]^{6-}$ or $[Ag_8I_{14}]^{6-}$ polyanions coordinated by an interwoven network of *in situ N*-methylated DPNDI cations. The compact arrangement of these two semiconductive constituents was produced by the charge-assisted anion–π and C–H···I hydrogen-bonding interactions, and the obtained hybrid materials display high chemical stability and efficiency and moderate stability in the photoreduction of Cr(VI) upon visible light irradiation. In another example of NDI based complex with photocatalytic activity, Liu *et al.*[471] constructed two organic–inorganic hybrids from the protonated NDI derivative *N*,*N*′-bis(4-pyridylmethyl)-NDI (DPMNI) and various metal halides to give $(H_2DPMNI)\cdot(Cu_4I_6)\cdot(CH_3CN)$ and $(H_2DPMNI)\cdot(Pb_2I_6)\cdot(DMF)$. The electron transfers between the one-dimensional metal halides and the protonated DPMNI components in these hybrids induced photocatalytic activity for degrading RhB in the presence of visible light.

Solar energy conversation into storable chemical energy is an area of renewable chemistry that relies on catalysis.[472] Nature converts waters into molecular oxygen and high-energy-density molecular compounds.[473] Dyes have been used for photoinduced charge separation processes which can be used for catalytic water splitting to mimic nature. Buda and co-workers used *ab initio* molecular dynamics simulations to design simpler structures for the solar to fuel conversion by water splitting, where they used a TiO_2 substrate functionalised with a supramolecular complex involving covalently bound NDI to a mononuclear Ru-based water oxidation catalyst.[474] Their

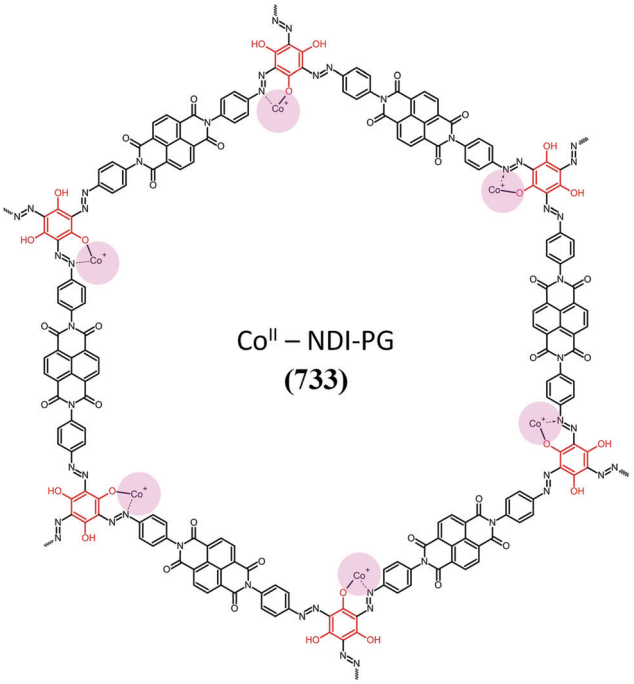

Fig. 162 The chemical structure of the Co^{II}–NDI–PG complex.[476]

study showed photoinduced electron transfer from the NDI to the semiconductor, which activates the Ru catalyst (**731**), and the detailed mechanistic pathway is illustrated in Fig. 161.

In another report, density functional theory (DFT)–*ab initio* molecular dynamic (AIMD) simulations were used for a mononuclear Ru-based water oxidation catalyst along with an NDI dye (**732**) that can be used for fast photoinduced electron injection into the conduction band of the TiO_2 semiconductor anode, *i.e.* $[Ru^{II}(H_2O)]_2^{+}$–NDI complex.[475] In the complete process, oxidized NDI provides the driving force for the whole

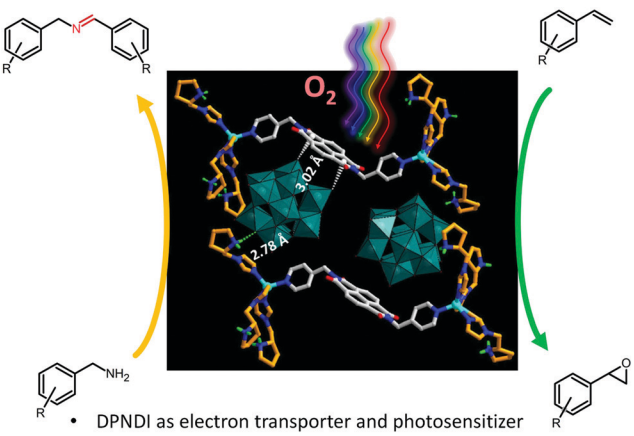

Fig. 163 The schematic diagram of the catalytic site distribution in the ZnW–DPNDI–PYI catalyst, showing the interactions of the catalytic sites.[439] This figure has been adapted from ref. 439 with permission from The Royal Society of Chemistry, copyright and 2019.

photocatalytic water splitting cycle as illustrated in Fig. 160. These two studies may provide clear guidelines for future optimization in the field of dye-sensitized photoelectrochemical cells (DS-PEC) used for splitting of water molecules. In recent years, porous organic polymers (POPs) have emerged as interesting materials because of their applications in sensing, separation and catalysis. Maji and co-workers synthesised stable, low-cost, metallated azo-NDI based active porous organic polymer catalysts for water splitting (Fig. 162).[476] They used diamine-NDI with phloroglucinol, in which the azo nitrogen of diamine of NDI and one of the phenolic oxygen atoms of the POP were used to coordinate to Co^{II}, resulting in a Co^{II}–NDI–PG complex (**733**). The complex with ~8% metal loading showed the best electrocatalytic activity for water oxidation in alkaline medium at pH 13.6 and a 1 mA cm^{-2} catalytic current density was achieved at an overpotential of 340 mV. They replaced NDI with benzidine (BD) for the oxidation of water and found that NDI exhibits better performance because of the redox active moiety and delocalised π-electrons with no loss of activity even after 500 cycles.

Niu and co-workers developed a ternary supramolecular photocatalytic oxidation system with polyoxometalates (PMOs) incorporating a metal–organic framework (POMOF) bearing the Zn(II) ion, $[BW_{12}O_{40}]^{5-}$ anion, *N,N′*-bis(4-pyridylmethyl)-NDI (DPNDI), and pyrrolidine-2-yl-imidazole (PYI) within a single framework, *i.e.* $([Zn(HPYI)_3]_2(DPNDI))[BW_{12}O_{40}]_2$, also called as (ZnW–DPNDI–PYI).[439] DPNDI is a component having electron transfer properties, with high redox π-acidity, PYI is a strong electron donor to improve electron transfer, and the POM acceptor was shown to be very stable against oxidative degradation. Upon visible irradiation, DPNDI can form a radical anion, $DPNDI^{-}$, and contribute to the activation of O_2 through a photoinduced electron transfer process. In this study, they performed oxidative homocoupling of benzyl amine and also extended their study to various primary amines; except for aniline, all the other derivatives gave excellent quantitative yields (see Fig. 163).

Another report by the Ott group described a new type of metal–organic framework (MOF), Zr(dcphOH-NDI), for electrocatalysis, in which redox-active NDI is used as a linker in a UiO-type framework, and the hydroxyl groups incorporated on the dcphOH-NDI linker facilitate proton transport through the material.[446] Zr(dcphOH-NDI) was placed on FTO as a redox-active 1 μm thin film cathode material of Zr(dcphOH-NDI)@FTO. Zr(dcphOH-NDI)@FTO showed sequential one-electron reduction of the NDI linker and ~97% NDI sites were

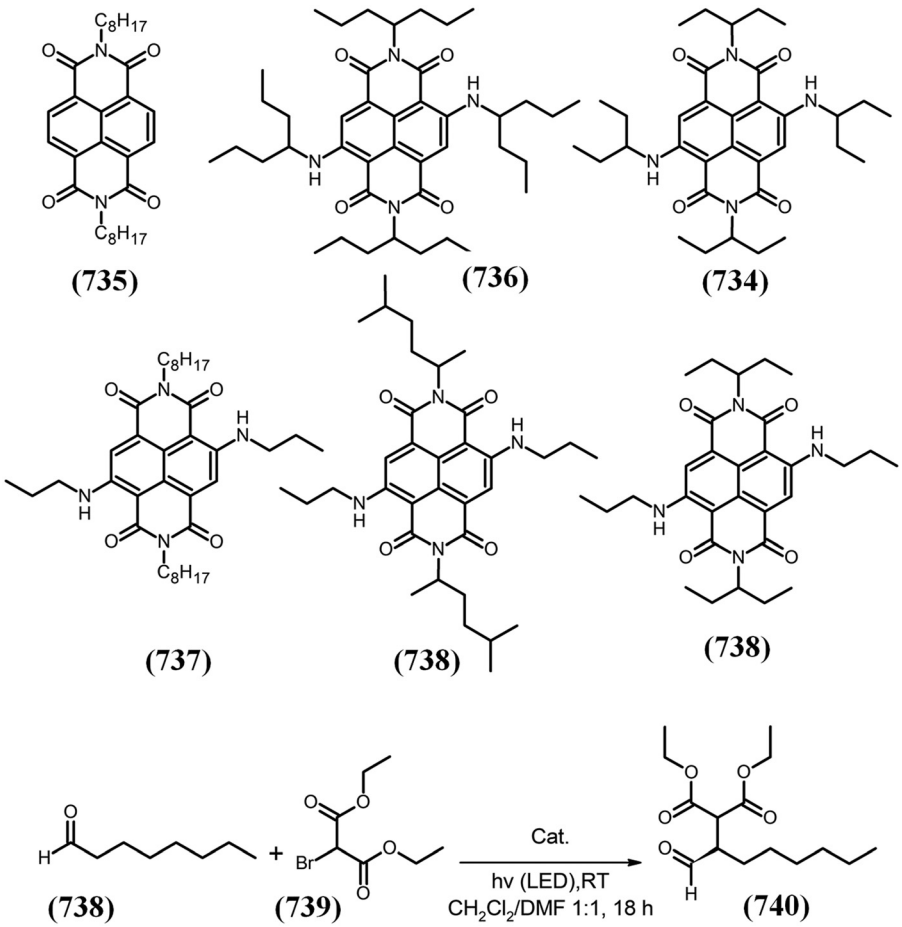

Fig. 164 The chemical structures of NDI derivatives with improved solubility for visible light photoredox catalysis, and the organo/photocatalytic α-alkylation reaction of octanal.[477]

electrochemically active in aqueous solution. The Zr(dcphOH-NDI)@FTO thin film showed characteristics of a diffusion (D_e) controlled process through a linker-to-linker hopping mechanism with charge balanced by electrolyte transport. D_e was measured directly by UV-vis spectroelectrochemistry and shown to be decreased by 1 order of magnitude.

Wagenknecht and co-workers synthesised five new core-substituted NDIs bearing various dialkylamino groups (**734**–**738**) and studied visible light photoredox catalysis with core-unsubstituted NDI as a reference molecule (Fig. 164).[477] These core-substituted NDIs differ from each other by the alkyl groups at the imide nitrogens, as well as the two substituents at the core, in order to improve their solubility in DMF. Among the substituents, the 1-ethylpropyl group at the diimide position and the unbranched *n*-propyl group at the core amines produced the highest solubility. Nevertheless, diaminoalkyl substituents at the core of NDI increased the charge-transfer of their photoexcited states, shifting their UV-vis absorption to the visible region (*i.e.* 500–650 nm) with the excited state reduction potential estimated to be approximately +1.0 V (vs SCE) in comparison with non-substituted NDI, making them excellent candidates for photocatalysis applications. The catalytic activity of cNDI (**738**) in comparison with (**735**) was evaluated using the MacMillan benchmark, in which cNDI (**738**) was much ''cleaner'' than (**735**). Furthermore, they studied the use of cNDI (**738**) for the photocatalytic α-alkylation of 1-octanal (**738**) with diethyl 2-bromomalonate (**739**) in the presence of an organocatalyst and 500 mM of 2,6-lutidine and (**735**) or cNDI (**738**). Upon irradiation with LED light where cNDI absorbed in the visible region which produced a better yield compared to (**735**), and this yield varies with the variation of the structure, which as shown in Fig. 164. This study suggests that, in future studies, researchers should not only depend on photoredox catalysis for tuning their optical and electrochemical properties, but also photophysical dynamics to improve the catalytic activity.

14 Conclusion and outlook

In this review we have taken a comprehensive look at recent applications of NDI in key areas, and shown that the outlook in many emerging technologies is promising due to the key features of NDI derivatives that make them so versatile and functional. Synthetic versatility afforded by recent advances in substitution at the core and traditional functionalisation of NDI through the imide nitrogen atoms allows exploitation of π-stacking, as well tuning of electronic, charge transfer and optical properties. Depending on the functional group appended, we have seen that access to supramolecular and polymer chemistry is possible which is almost unrivalled for a class of substances based on one primary building block. The details and diversity of the applications described in each of the sections outlined in this review are a testament to the fact that NDI and its derivatives will continue to grow in applications that such a building block can provide.

The next step in the development of NDI derivatives is advancement into practical applications. Up until now, although advances have been made in so many areas, our understanding of this class of molecules is ever increasing, and a maturity is being reached which will allow scientists to design, synthesise, and tailor NDI derivatives to a unique application where it is class leading, and this may come in almost any of the areas described above. Due to the tools and background that the field now has as its disposal, the authors feel that this breakthrough will not be too far away.

Conflicts of interest

All the authors declare no conflicts of interest.

Acknowledgements

S. V. B. (GU) acknowledges UGC-FRP for financial support and a professorship, and the Council of Scientific & Industrial Research (CSIR), India for providing support, code No. 02(0357)/19/EMR-II. R. W. J. acknowledges UGC for financial support under a UGC-NET senior research fellowship.

References

1 X. Zhan, A. Facchetti, S. Barlow, T. J. Marks, M. A. Ratner, M. R. Wasielewski and S. R. Marder, *Adv. Mater.*, 2011, **23**, 268–284.
2 (*a*) M. B. Avinash and T. Govindaraju, *Acc. Chem. Res.*, 2018, **51**, 414–426; (*b*) S. V. Bhosale, C. H. Jani and S. J. Langford, *Chem. Soc. Rev.*, 2008, **37**, 331–342.
3 (*a*) Y. Fukutomi, M. Nakano, J.-Y. Hu, I. Osaka and K. Takimiya, *J. Am. Chem. Soc.*, 2013, **135**, 11445–11448; (*b*) M. Al Kobaisi, S. V. Bhosale, K. Latham, A. M. Raynor and S. V. Bhosale, *Chem. Rev.*, 2016, **116**, 11685–11796.
4 (*a*) C. Yan, S. Barlow, Z. Wang, H. Yan, A. K. Y. Jen, S. R. Marder and X. Zhan, *Nat. Rev. Mater.*, 2018, **3**, 18003; (*b*) A. Nowak-Król, K. Shoyama, M. Stolte and F. Würthner, *Chem. Commun.*, 2018, **54**, 13763–13772; (*c*) G. D. Fallon, M. A. P. Lee, S. J. Langford and P. J. Nichols, *Org. Lett.*, 2004, **6**, 655–658; (*d*) J. G. Hansen, N. Feeder, D. G. Hamilton, M. J. Gunter, J. Becher and J. K. M. Sanders, *Org. Lett.*, 2000, **2**, 449–452; (*e*) D. A. Vicic, D. T. Odom, M. E. Núñez, D. A. Gianolio, L. W. McLaughlin and J. K. Barton, *J. Am. Chem. Soc.*, 2000, **122**, 8603–8611; (*f*) H. N. Lee, Z. Xu, S. K. Kim, K. M. K. Swamy, Y. Kim, S.-J. Kim and J. Yoon, *J. Am. Chem. Soc.*, 2007, **129**, 3828–3829.
5 D. B. Amabilino and J. F. Stoddart, *Chem. Rev.*, 1995, **95**, 2725–2828.
6 S.-L. Suraru and F. Würthner, *Angew. Chem., Int. Ed.*, 2014, **53**, 7428–7448.
7 (*a*) S. V. Bhosale, S. V. Bhosale and S. K. Bhargava, *Org. Biomol. Chem.*, 2012, **10**, 6455–6468; (*b*) A. Insuasty, S. Maniam and S. J. Langford, *Chem. – Eur. J.*, 2019, **25**, 7058–7073; (*c*) S. Maniam, H. F. Higginbotham,

T. D. M. Bell and S. J. Langford, *Chem. – Eur. J.*, 2019, **25**, 7044–7057.
8 F. Würthner, S. Ahmed, C. Thalacker and T. Debaerdemaeker, *Chem. – Eur. J.*, 2002, **8**, 4742–4750.
9 H. Vollmann, H. Becker, M. Corell and H. Streeck, *Justus Liebigs Ann. Chem.*, 1937, **531**, 1–159.
10 (*a*) F. Würthner and M. Stolte, *Chem. Commun.*, 2011, **47**, 5109–5115; (*b*) J. Yang, B. Xiao, K. Tajima, M. Nakano, K. Takimiya, A. Tang and E. Zhou, *Macromolecules*, 2017, **50**, 3179–3185.
11 X. Wang, L. Lv, L. Li, Y. Chen, K. Zhang, H. Chen, H. Dong, J. Huang, G. Shen, Z. Yang and H. Huang, *Adv. Funct. Mater.*, 2016, **26**, 6306–6315.
12 (*a*) A. Diac, M. Matache, I. Grosu and N. D. Hădade, *Adv. Synth. Catal.*, 2018, **360**, 817–845; (*b*) M. Liu, G. Ouyang, D. Niu and Y. Sang, *Org. Chem. Front.*, 2018, **5**, 2885–2900.
13 W. S. Horne, N. Ashkenasy and M. R. Ghadiri, *Chemistry*, 2005, **11**, 1137–1144.
14 B. Koz, S. Demic and S. Icli, *Asian J. Chem.*, 2016, **28**, 2755–2758.
15 K. Cai, J. Xie and D. Zhao, *J. Am. Chem. Soc.*, 2014, **136**, 28–31.
16 K. Cai, J. Xie, X. Yang and D. Zhao, *Org. Lett.*, 2014, **16**, 1852–1855.
17 C. Li, W. Jiang, X. Zhu and Z. Wang, *Asian J. Org. Chem.*, 2014, **3**, 114–117.
18 C. Li, C. Xiao, Y. Li and Z. Wang, *Org. Lett.*, 2013, **15**, 682–685.
19 C. Li, Z. Lin, Y. Li and Z. Wang, *Chem. Rec.*, 2016, **16**, 873–885.
20 W. Yue, J. Gao, Y. Li, W. Jiang, S. Di Motta, F. Negri and Z. Wang, *J. Am. Chem. Soc.*, 2011, **133**, 18054–18057.
21 A. Takai and M. Takeuchi, *Bull. Chem. Soc. Jpn.*, 2018, **91**, 44–51.
22 W. Yue, Y. Zhen, Y. Li, W. Jiang, A. Lv and Z. Wang, *Org. Lett.*, 2010, **12**, 3460–3463.
23 W. Yue, A. Lv, J. Gao, W. Jiang, L. Hao, C. Li, Y. Li, L. E. Polander, S. Barlow, W. Hu, S. Di Motta, F. Negri, S. R. Marder and Z. Wang, *J. Am. Chem. Soc.*, 2012, **134**, 5770–5773.
24 Q. Ye, J. Chang, K.-W. Huang and C. Chi, *Org. Lett.*, 2011, **13**, 5960–5963.
25 P. Pahlavanlu, A. J. Tilley, B. T. McAllister and D. S. Seferos, *J. Org. Chem.*, 2017, **82**, 12337–12345.
26 K. Takimiya and M. Nakano, *Bull. Chem. Soc. Jpn.*, 2018, **91**, 121–140.
27 M. Nakano, D. Hashizume and K. Takimiya, *Molecules*, 2016, **21**, 981.
28 W. Chen, M. Nakano, J.-H. Kim, K. Takimiya and Q. Zhang, *J. Mater. Chem. C*, 2016, **4**, 8879–8883.
29 R. Matsidik and K. Takimiya, *Chem. – Asian J.*, 2019, **14**, 1651–1656.
30 C. Gu, Y. Li, L. Xiao, H. Fu, D. Wang, L. Cheng and L. Liu, *J. Org. Chem.*, 2017, **82**, 12806–12812.
31 M. Tassinari, G. Cimino-Reale, M. Nadai, F. Doria, E. Butovskaya, M. Recagni, M. Freccero, N. Zaffaroni, S. N. Richter and M. Folini, *J. Med. Chem.*, 2018, **61**, 8625–8638.
32 Y. Tachapermpon, S. Maniam, N. Wanichacheva and S. J. Langford, *Asian J. Org. Chem.*, 2017, **6**, 47–53.
33 S. Maniam, S. Sandanayake, E. I. Izgorodina and S. J. Langford, *Asian J. Org. Chem.*, 2016, **5**, 490–493.
34 N. A. Young, S. C. Drew, S. Maniam and S. J. Langford, *Chem. – Asian J.*, 2017, **12**, 1668–1675.
35 T. L. D. Tam and J. W. Xu, *Chem. Commun.*, 2019, **55**, 6225–6228.
36 T. L. D. Tam, C. K. Ng, X. Lu, Z. L. Lim and J. Wu, *Chem. Commun.*, 2018, **54**, 7374–7377.
37 L. Hu, J. Li, J. Huang and J. Yin, *Chin. J. Chem.*, 2017, **35**, 93–97.
38 T. Maeda, J. Zhou, Y. Oda, H. Nakazumi and S. Yagi, *Res. Chem. Intermed.*, 2018, **44**, 4783–4795.
39 C. K. Ng, T. L. D. Tam, F. Wei, X. Lu and J. Wu, *Org. Chem. Front.*, 2019, **6**, 110–115.
40 E. Schab-Balcerzak, M. Grucela, G. Malecki, S. Kotowicz, M. Siwy, H. Janeczek, S. Golba and A. Praski, *J. Mol. Struct.*, 2017, **1128**, 462–470.
41 A. Drewniak, M. D. Tomczyk, L. Hanusek, A. Mielanczyk, K. Walczak, P. Nitschke, B. Hajduk and P. Ledwon, *Polymers*, 2018, **10**, 487.
42 T. Nakazato, T. Kamatsuka, J. Inoue, T. Sakurai, S. Seki, H. Shinokubo and Y. Miyake, *Chem. Commun.*, 2018, **54**, 5177–5180.
43 S. Quinn, E. S. Davies, C. R. Pfeiffer, W. Lewis, J. McMaster and N. R. Champness, *ChemPlusChem*, 2017, **82**, 489–492.
44 M. Kremer, M. Kersten and S. Höger, *Org. Chem. Front.*, 2018, **5**, 1825–1829.
45 Y. Li, C. Li, W. Yue, W. Jiang, R. Kopecek, J. Qu and Z. Wang, *Org. Lett.*, 2010, **12**, 2374–2377.
46 A. Weißenstein, V. Grande, C. R. Saha-Möller and F. Würthner, *Org. Chem. Front.*, 2018, **5**, 2641–2651.
47 S.-L. Suraru and F. Würthner, *J. Org. Chem.*, 2013, **78**, 5227–5238.
48 S. B. Schmidt, T. Biskup, X. Jiao, C. R. McNeill and M. Sommer, *J. Mater. Chem. C*, 2019, **7**, 4466–4474.
49 R. Matsidik, A. Luzio, Ö. Askin, D. Fazzi, A. Sepe, U. Steiner, H. Komber, M. Caironi and M. Sommer, *Chem. Mater.*, 2017, **29**, 5473–5483.
50 R. Matsidik, M. Giorgio, A. Luzio, M. Caironi, H. Komber and M. Sommer, *Eur. J. Org. Chem.*, 2018, 6121–6126.
51 K. Kranthiraja, D. X. Long, V. G. Sree, W. Cho, Y.-R. Cho, A. Zaheer, J.-C. Lee, Y.-Y. Noh and S.-H. Jin, *Macromolecules*, 2018, **51**, 5530–5536.
52 C. Lu, M. Fujitsuka, A. Sugimoto and T. Majima, *J. Phys. Chem. C*, 2017, **121**, 4558–4563.
53 M. A. Uddin, Y. Kim, R. Younts, W. Lee, B. Gautam, J. Choi, C. Wang, K. Gundogdu, B. J. Kim and H. Y. Woo, *Macromolecules*, 2016, **49**, 6374–6383.
54 Z. Fei, Y. Han, J. Martin, F. H. Scholes, M. Al-Hashimi, S. Y. AlQaradawi, N. Stingelin, T. D. Anthopoulos and M. Heeney, *Macromolecules*, 2016, **49**, 6384–6393.
55 A. Singh, A. Ganesh Kumar, S. Bisoi and S. Banerjee, *New J. Chem.*, 2017, **41**, 6849–6856.

56 P. S. Rao, A. Gupta, D. Srivani, S. V. Bhosale, A. Bilic, J. Li, W. Xiang, R. A. Evans and S. V. Bhosale, *Chem. Commun.*, 2018, **54**, 5062–5065.
57 D. Srivani, A. Agarwal, S. V. Bhosale, A. L. Puyad, W. Xiang, R. A. Evans, A. Gupta and S. V. Bhosale, *Chem. Commun.*, 2017, **53**, 11157–11160.
58 D. S. Pal and S. Ghosh, *Chem. – Eur. J.*, 2018, **24**, 8519–8523.
59 G. Andric, J. F. Boas, A. M. Bond, G. D. Fallon, K. P. Ghiggino, C. F. Hogan, J. A. Hutchison, M. A.-P. Lee, S. J. Langford, J. R. Pilbrow, G. J. Troup and C. P. Woodward, *Aust. J. Chem.*, 2004, **57**, 1011–1019.
60 C.-H. Lai, S. Muhammad, A. G. Al-Sehemi and A. R. Chaudhry, *J. Mol. Graphics Modell.*, 2019, **87**, 68–75.
61 J. R. Mulder, C. F. Guerra, J. C. Slootweg, K. Lammertsma and F. M. Bickelhaupt, *J. Comput. Chem.*, 2016, **37**, 304–313.
62 B. Schulze Lammers, R. Ebeling, E. Dirksen, T. J. J. Müller and S. Karthäuser, *J. Phys. Chem. C*, 2019, **123**, 9860–9867.
63 L. Gonzalez, C. Liu, B. Dietrich, H. Su, S. Sproules, H. Cui, D. Honecker, D. J. Adams and E. R. Draper, *Commun Chem. Commun.*, 2018, **1**, 77, DOI: 10.1038/s42004-018-0075-2.
64 S. Pluczyk, K. Laba, E. Schab-Balcerzak, K. Bijak, S. Kotowicz and M. Lapkowski, *J. Electroanal. Chem.*, 2017, **795**, 90–96.
65 K. Cai, Q. Yan and D. Zhao, *Chem. Sci.*, 2012, **3**, 3175–3182.
66 P. Pahlavanlu and D. S. Seferos, *Phosphorus, Sulfur Silicon Relat. Elem.*, 2019, **194**, 664–668.
67 S. Lee, F. Miao, H. Phan, T. S. Herng, J. Ding, J. Wu and D. Kim, *ChemPhysChem*, 2017, **18**, 591–595.
68 S. K. Mohan Nalluri, J. Zhou, T. Cheng, Z. Liu, M. T. Nguyen, T. Chen, H. A. Patel, M. D. Krzyaniak, W. A. Goddard, M. R. Wasielewski and J. F. Stoddart, *J. Am. Chem. Soc.*, 2019, **141**, 1290–1303.
69 S. K. M. Nalluri, Z. Liu, Y. Wu, K. R. Hermann, A. Samanta, D. J. Kim, M. D. Krzyaniak, M. R. Wasielewski and J. F. Stoddart, *J. Am. Chem. Soc.*, 2016, **138**, 5968–5977.
70 D. Chen, A.-J. Avestro, Z. Chen, J. Sun, S. Wang, M. Xiao, Z. Erno, M. M. Algaradah, M. S. Nassar, K. Amine, Y. Meng and J. F. Stoddart, *Adv. Mater.*, 2015, **27**, 2907–2912.
71 K. Zaugg, J. Velasco, K. A. Robins and D.-C. Lee, *ACS Omega*, 2019, **4**, 5434–5441.
72 M. Zerson, M. Neumann, R. Steyrleuthner, D. Neher and R. Magerle, *Macromolecules*, 2016, **49**, 6549–6557.
73 G. Bélanger-Chabot, A. Ali and F. P. Gabbaï, *Angew. Chem., Int. Ed.*, 2017, **56**, 9958–9961.
74 S. Shokri, J. Li, M. K. Manna, G. P. Wiederrecht, D. J. Gosztola, A. Ugrinov, S. Jockusch, A. Y. Rogachev and A. J.-L. Ayitou, *J. Org. Chem.*, 2017, **82**, 10167–10173.
75 M. K. Gish, A. L. Jones, J. M. Papanikolas and K. S. Schanze, *J. Phys. Chem. C*, 2018, **122**, 18802–18808.
76 R. Ebeling, S. Tsukamoto, E. Dirksen, V. Caciuc, T. J. J. Müller, N. Atodiresei and S. Karthäuser, *J. Phys. Chem. C*, 2017, **121**, 26916–26924.
77 J.-M. Lehn, *Supramolecular chemistry: Concepts and perspectives*, Wiley-VCH Verlag GmbH & Co., Weinheim, 1995, p. 281.
78 S. V. Bhosale and S. J. Langford, *Chem. Soc. Rev.*, 2012, **41**, 1637–1651.
79 C. J. Pedersen, *Angew. Chem., Int. Ed.*, 1988, **27**, 1021–1027.
80 D. J. Cram, *Angew. Chem., Int. Ed.*, 1988, **27**, 1009–1020.
81 (*a*) L. L. Miller and K. R. Mann, *Acc. Chem. Res.*, 1996, **29**, 417–423; (*b*) H. E. Katz, A. J. Lovinger, J. Johnson, C. Kloc, T. Siegrist, W. Li, Y. Y. Lin and A. Dodabalapur, *Nature*, 2000, **404**, 478–481.
82 S. Bhosale, A. L. Sisson, P. Talukdar, A. Fürstenberg, N. Banerji, E. Vauthey, G. Bollot, J. Mareda, C. Röger, F. Würthner, N. Sakai and S. Matile, *Science*, 2006, **313**, 84–86.
83 D. S. Pal, H. Kar and S. Ghosh, *Chem. Commun.*, 2018, **54**, 928–931.
84 N. V. Ghule, D. D. La, R. S. Bhosale, M. Al Kobaisi, A. M. Raynor, S. V. Bhosale and S. V. Bhosale, *ChemistryOpen*, 2016, **5**, 157–163.
85 S. P. Goskulwad, D. D. La, R. S. Bhosale, M. Al Kobaisi, L. A. Jones, S. V. Bhosale and S. V. Bhosale, *ChemistrySelect*, 2018, **3**, 1460–1465.
86 S. P. Goskulwad, D. D. La, R. S. Bhosale, M. Al Kobaisi, S. V. Bhosale and S. V. Bhosale, *RSC Adv.*, 2016, **6**, 39392–39395.
87 S. M. Wagalgave, D. DucLa, R. S. Bhosale, M. A. Kobaisi, L. A. Jones, S. V. Bhosale and S. V. Bhosale, *New J. Chem.*, 2018, **42**, 6785–6793.
88 A. Sikder, J. Sarkar, T. Sakurai, S. Seki and S. Ghosh, *Nanoscale*, 2018, **10**, 3272–3280.
89 M. Al Kobaisi, R. S. Bhosale, M. E. El-Khouly, D. D. La, S. D. Padghan, S. V. Bhosale, L. A. Jones, F. Antolasic, S. Fukuzumi and S. V. Bhosale, *Sci. Rep.*, 2017, **7**, 16501.
90 K. Pérez de Carvasal, N. Aissaoui, G. Vergoten, G. Bellot, J.-J. Vasseur, M. Smietana and F. Morvan, *Chem. Commun.*, 2021, **57**, 4130–4133.
91 K. Deepthi, R. R. B. Amal, V. R. Rajeev, K. N. N. Unni and E. B. Gowd, *Macromolecules*, 2019, **52**, 2889–2899.
92 A. M. Sanders, T. J. Magnanelli, A. E. Bragg and J. D. Tovar, *J. Am. Chem. Soc.*, 2016, **138**, 3362–3370.
93 S. Chakraborty, D. Ray, V. K. Aswal and S. Ghosh, *Chem. – Eur. J.*, 2018, **24**, 16379–16387.
94 H. Kar, D. W. Gehrig, N. K. Allampally, G. Fernández, F. Laquai and S. Ghosh, *Chem. Sci.*, 2016, **7**, 1115–1120.
95 M. Zangoli, M. Gazzano, F. Monti, L. Maini, D. Gentili, A. Liscio, A. Zanelli, E. Salatelli, G. Gigli, M. Baroncini and F. Di Maria, *ACS Appl. Mater. Interfaces*, 2019, **11**, 16864–16871.
96 T. Sakurai, Y. Tsutsui, K. Kato, M. Takata and S. Seki, *J. Mater. Chem. C*, 2016, **4**, 1490–1496.
97 P. Pramanik, D. Ray, V. K. Aswal and S. Ghosh, *Angew. Chem., Int. Ed.*, 2017, **56**, 3516–3520.
98 A. Sikder, D. Ray, V. K. Aswal and S. Ghosh, *Angew. Chem., Int. Ed.*, 2019, **58**, 1606–1611.
99 P. Dey, P. Rajdev, P. Pramanik and S. Ghosh, *Macromolecules*, 2018, **51**, 5182–5190.
100 A. Das and S. Ghosh, *Chem. Commun.*, 2016, **52**, 6860–6872.
101 T. Choisnet, D. Canevet, M. Sallé, E. Nicol, F. Niepceron, J. Jestin and O. Colombani, *Chem. Commun.*, 2019, **55**, 9519–9522.
102 A. K. Jeevan and K. R. Gopidas, *ChemistrySelect*, 2019, **4**, 506–514.

103 N. Nandi, K. Gayen and A. Banerjee, *Soft Matter*, 2019, **15**, 3018–3026.
104 K. Samanta, E. Zellermann, M. Zähres, C. Mayer and C. Schmuck, *Soft Matter*, 2017, **13**, 8108–8112.
105 K. Samanta, M. Ehlers and C. Schmuck, *Chem. – Eur. J.*, 2016, **22**, 15242–15247.
106 F. Billeci, F. D'Anna, S. Marullo and R. Noto, *RSC Adv.*, 2016, **6**, 59502–59512.
107 Z. Guo, P. Yu, K. Sun, W. Wang, Y. Wei and Z. Li, *Chem. – Asian J.*, 2017, **12**, 1104–1110.
108 X. Shen, B. Li, T. Pan, J. Wu, Y. Wang, J. Shang, Y. Ge, L. Jin and Z. Qi, *Beilstein J. Org. Chem.*, 2019, **15**, 1203–1209.
109 T. Nakamura, N. Shioya, T. Shimoaka, R. Nishikubo, T. Hasegawa, A. Saeki, Y. Murata, R. Murdey and A. Wakamiya, *Chem. Mater.*, 2019, **31**, 1729–1737.
110 S. R. Nelli, J.-H. Lin, T. N. A. Nguyen, D. T.-H. Tseng, S. K. Talloj and H.-C. Lin, *New J. Chem.*, 2017, **41**, 1229–1234.
111 S. Bartocci, J. A. Berrocal, P. Guarracino, M. Grillaud, L. Franco and M. Mba, *Chem. – Eur. J.*, 2018, **24**, 2920–2928.
112 S. Datta, S. Samanta and D. Chaudhuri, *J. Mater. Chem. A*, 2018, **6**, 2922–2926.
113 P. Chen, J. H. Mondal, Y. Zhou, H. Zhu and B. Shi, *Polym. Chem.*, 2016, **7**, 5221–5225.
114 N. Singha, P. Gupta, B. Pramanik, S. Ahmed, A. Dasgupta, A. Ukil and D. Das, *Biomacromolecules*, 2017, **18**, 3630–3641.
115 P. Rajdev, S. Chakraborty, M. Schmutz, P. Mesini and S. Ghosh, *Langmuir*, 2017, **33**, 4789–4795.
116 H. Kar, G. Ghosh and S. Ghosh, *Chem. – Eur. J.*, 2017, **23**, 10536–10542.
117 T. B. F. Moraes, M. F. R. A. Schimidt, R. Bacani, G. Weber, M. J. Politi, B. Castanheira, S. Brochsztain, F. D. A. Silva, G. J. F. Demets and E. R. Triboni, *J. Lumin.*, 2018, **204**, 685–691.
118 S. V. Shinde, M. Kulkarni and P. Talukdar, *RSC Adv.*, 2016, **6**, 30690–30694.
119 G. Markiewicz, M. M. J. Smulders and A. R. Stefankiewicz, *Adv. Sci.*, 2019, **6**, 1900577.
120 R. Kumar, S. N. Ugale, A. M. Kale, R. S. Bhosale and R. Narayan, *ChemistrySelect*, 2018, **3**, 9393–9401.
121 A. Sarkar, S. Dhiman, A. Chalishazar and S. J. George, *Angew. Chem., Int. Ed.*, 2017, **56**, 13767–13771.
122 G. Ghosh, M. Paul, T. Sakurai, W. Matsuda, S. Seki and S. Ghosh, *Chem. – Eur. J.*, 2018, **24**, 1938–1946.
123 Y. Li, L. Li, Y. Wu and Y. Li, *J. Phys. Chem. C*, 2017, **121**, 8579–8588.
124 Y. Gao, T. Gao, L. Wang, X. Ma, R. Jin, C. Kang and L. Gao, *New J. Chem.*, 2021, **45**, 5093–5098.
125 S. P. Goskulwad, M. Al Kobaisi, D. D. La, R. S. Bhosale, M. Ratanlal, S. V. Bhosale and S. V. Bhosale, *Chem. – Asian J.*, 2018, **13**, 3947–3953.
126 D. B. Shaikh, R. S. Bhosale, D. D. La, M. Al Kobaisi, S. V. Bhosale and S. V. Bhosale, *Chem. – Asian J.*, 2018, **13**, 3268–3273.
127 M. Kumar, N. L. Ing, V. Narang, N. K. Wijerathne, A. I. Hochbaum and R. V. Ulijn, *Nat. Chem.*, 2018, **10**, 696–703.
128 S. Leret, Y. Pouillon, S. Casado, C. Navío, Á. Rubio and E. M. Pérez, *Chem. Sci.*, 2017, **8**, 1927–1935.
129 G. Li-Destri, L. Fichera, A. Zammataro, G. Trusso Sfrazzetto and N. Tuccitto, *Nanoscale*, 2019, **11**, 14203–14209.
130 H. Zhu, P. Hao, Q. Shen, J. Shen, G. Li, G. Zhao, H. Xing and Y. Fu, *CrystEngComm*, 2021, **23**, 3356–3363.
131 B. Thomas, J. Rombouts, K. B. S. S. Gupta, R. V. A. Orru, K. Lammertsma and H. J. M. de Groot, *Chem. – Eur. J.*, 2017, **23**, 9346–9351.
132 J.-J. Liu, T. Liu, S.-B. Xia, C.-X. He, F.-X. Cheng, M.-J. Lin and C.-C. Huang, *Dyes Pigm.*, 2018, **149**, 59–64.
133 J. I. Lovitt, C. S. Hawes and T. Gunnlaugsson, *CrystEngComm*, 2019, **21**, 207–217.
134 S. Kumar, V. Malik, J. Shukla, Y. Kumar, D. Bansal, R. Chatterjee and P. Mukhopadhyay, *Chem. – Eur. J.*, 2019, **25**, 4740–4750.
135 F. Billeci, F. D'Anna, I. Chiarotto, M. Feroci and S. Marullo, *New J. Chem.*, 2017, **41**, 13889–13901.
136 S. Kuila, K. V. Rao, S. Garain, P. K. Samanta, S. Das, S. K. Pati, M. Eswaramoorthy and S. J. George, *Angew. Chem., Int. Ed.*, 2018, **57**, 17115–17119.
137 G.-B. Li, Q.-Y. Yang, R.-K. Pan, S. Liu and Y.-W. Xu, *New J. Chem.*, 2017, **41**, 6160–6166.
138 G. R. Krishna, R. Devarapalli, G. Lal and C. M. Reddy, *J. Am. Chem. Soc.*, 2016, **138**, 13561–13567.
139 D. Taura, X. Wang, M. Ito and E. Yashima, *Org. Chem. Front.*, 2021, **8**, 2551–2555.
140 Y.-L. Wu, N. S. Bobbitt, J. L. Logsdon, N. E. Powers-Riggs, J. N. Nelson, X. Liu, T. C. Wang, R. Q. Snurr, J. T. Hupp, O. K. Farha, M. C. Hersam and M. R. Wasielewski, *Angew. Chem., Int. Ed.*, 2018, **57**, 3985–3989.
141 Y. Ma, L. Luo, C. Yang, W. Wang, X. Liu, J. Zhang and W. Huang, *Macromol. Rapid Commun.*, 2021, **42**, 2000655.
142 A. Mizuno, Y. Shuku, M. M. Matsushita, M. Tsuchiizu, Y. Hara, N. Wada, Y. Shimizu and K. Awaga, *Phys. Rev. Lett.*, 2017, **119**, 057201.
143 W. Ali, G. Ning, M. Hassan and W. Gong, *Asian J. Org. Chem.*, 2019, **8**, 74–78.
144 K. Liu, C. Wang, Z. Li and X. Zhang, *Angew. Chem., Int. Ed.*, 2011, **50**, 4952–4956.
145 L. Yang, P. Langer, E. S. Davies, M. Baldoni, K. Wickham, N. A. Besley, E. Besley and N. R. Champness, *Chem. Sci.*, 2019, **10**, 3723–3732.
146 R. Djemili, L. Kocher, S. Durot, A. Peuronen, K. Rissanen and V. Heitz, *Chem. – Eur. J.*, 2019, **25**, 1481–1487.
147 B. M. Schmidt, T. Osuga, T. Sawada, M. Hoshino and M. Fujita, *Angew. Chem., Int. Ed.*, 2016, **55**, 1561–1564.
148 S. Cui, G. Zhuang, J. Wang, Q. Huang, S. Wang and P. Du, *Org. Chem. Front.*, 2019, **6**, 1885–1890.
149 T. A. Barendt, I. Rašović, M. A. Lebedeva, G. A. Farrow, A. Auty, D. Chekulaev, I. V. Sazanovich, J. A. Weinstein, K. Porfyrakis and P. D. Beer, *J. Am. Chem. Soc.*, 2018, **140**, 1924–1936.
150 T. A. Barendt, A. Docker, I. Marques, V. Félix and P. D. Beer, *Angew. Chem., Int. Ed.*, 2016, **55**, 11069–11076.

151 T. A. Barendt, S. W. Robinson and P. D. Beer, *Chem. Sci.*, 2016, **7**, 5171–5180.
152 N. She, D. Moncelet, L. Gilberg, X. Lu, V. Sindelar, V. Briken and L. Isaacs, *Chem. – Eur. J.*, 2016, **22**, 15270–15279.
153 R. Khurana, J. Mohanty, N. Barooah and A. C. Bhasikuttan, *J. Mol. Liq.*, 2021, **334**, 116023.
154 H.-G. Li and G.-W. Wang, *J. Org. Chem.*, 2017, **82**, 6341–6348.
155 S. Sato, Y. Nishi and S. Takenaka, *Electroanalysis*, 2019, **31**, 1988–1993.
156 A. Spinello, G. Barone and J. Grunenberg, *Phys. Chem. Chem. Phys.*, 2016, **18**, 2871–2877.
157 T. Mondal and S. Ghosh, *Polym. Chem.*, 2016, **7**, 6735–6743.
158 A. Mukherjee, T. Sakurai, S. Seki and S. Ghosh, *ChemNanoMat*, 2018, **4**, 860–866.
159 X. Shang, I. Song, G. Y. Jung, W. Choi, H. Ohtsu, J. H. Lee, J. Y. Koo, B. Liu, J. Ahn, M. Kawano, S. K. Kwak and J. H. Oh, *Nat. Commun.*, 2018, **9**, 3933.
160 S. V. Bhosale, S. V. Bhosale, M. B. Kalyankar and S. J. Langford, *Org. Lett.*, 2009, **11**, 5418–5421.
161 W. Hughes, A. Rananaware, D. D. La, L. A. Jones, S. Bhargava and S. V. Bhosale, *Sens. Actuators, B*, 2017, **244**, 854–860.
162 R. V. Hangarge, D. D. La, M. Boguslavsky, L. A. Jones, Y. S. Kim and S. V. Bhosale, *ChemistrySelect*, 2017, **2**, 11487–11491.
163 R. P. Cox, S. Sandanayake, D. L. A. Scarborough, E. I. Izgorodina, S. J. Langford and T. D. M. Bell, *New J. Chem.*, 2019, **43**, 2011–2018.
164 L. Zong, Y. Song, Q. Li and Z. Li, *Sens. Actuators, B*, 2016, **226**, 239–244.
165 L. Zong, Y. Xie, Q. Li and Z. Li, *Sens. Actuators, B*, 2017, **238**, 735–743.
166 L. Zong, C. Wang, Y. Song, Y. Xie, P. Zhang, Q. Peng, Q. Li and Z. Li, *Sens. Actuators, B*, 2017, **252**, 1105–1111.
167 L. Zong, C. Wang, Y. Song, J. Hu, Q. Li and Z. Li, *RSC Adv.*, 2019, **9**, 12675–12680.
168 P. Praikaew, S. Maniam, A. Charoenpanich, J. Sirirak, V. Promarak, S. J. Langford and N. Wanichacheva, *J. Photochem. Photobiol., A*, 2019, **382**, 111852.
169 L. Zong, M. Zhang, Y. Song, Y. Xie, J. Feng, Q. Li and Z. Li, *Sens. Actuators, B*, 2018, **257**, 882–888.
170 Q. Lin, P.-P. Mao, L. Liu, J. Liu, Y.-M. Zhang, H. Yao and T.-B. Wei, *RSC Adv.*, 2017, **7**, 11206–11210.
171 Q. Lin, L. Liu, F. Zheng, P.-P. Mao, J. Liu, Y.-M. Zhang, H. Yao and T.-B. Wei, *RSC Adv.*, 2017, **7**, 38458–38462.
172 L. E. Solís-Delgado, A. Ochoa-Terán, A. K. Yatsimirsky and G. Pina-Luis, *Anal. Lett.*, 2016, **49**, 2301–2311.
173 T.-B. Wei, Q.-P. Zhang, Y.-Q. Fan, P.-P. Mao, J. Wang, X.-W. Guan, Y.-M. Zhang, H. Yao and Q. Lin, *Soft Matter*, 2019, **15**, 6530–6535.
174 H. C. Wentz and M. G. Campbell, *Polyhedron*, 2018, **154**, 309–313.
175 A. Kalita, S. Hussain, A. H. Malik, U. Barman, N. Goswami and P. K. Iyer, *ACS Appl. Mater. Interfaces*, 2016, **8**, 25326–25336.
176 G.-B. Li, Z. Zhang, L.-S. Liao, R.-K. Pan and S.-G. Liu, *Spectrochim. Acta, Part A*, 2021, **254**, 119588.
177 B. S. Kavitha, S. Sridevi, P. Makam, D. Ghosh, T. Govindaraju, A. S and A. K. Sood, *Sens. Actuators, B*, 2021, **333**, 129550.
178 T. Ono, Y. Tsukiyama, S. Hatanaka, Y. Sakatsume, T. Ogoshi and Y. Hisaeda, *J. Mater. Chem. C*, 2019, **7**, 9726–9734.
179 P. Mukhopadhyay, Y. Iwashita, M. Shirakawa, S.-I. Kawano, N. Fujita and S. Shinkai, *Angew. Chem., Int. Ed.*, 2006, **45**, 1592–1595.
180 J. Fan, X. Chang, M. He, C. Shang, G. Wang, S. Yin, H. Peng and Y. Fang, *ACS Appl. Mater. Interfaces*, 2016, **8**, 18584–18592.
181 S. Ali, M. A. Jameel, A. Gupta, S. J. Langford and M. Shafiei, *Synth. Met.*, 2021, **275**, 116739.
182 N. V. Ghule, R. S. Bhosale, K. Kharat, A. L. Puyad, S. V. Bhosale and S. V. Bhosale, *ChemPlusChem*, 2015, **80**, 485–489.
183 F. Doria, A. Oppi, F. Manoli, S. Botti, N. Kandoth, V. Grande, I. Manet and M. Freccero, *Chem. Commun.*, 2015, **51**, 9105–9108.
184 H. Gaiji, P. Jolly, S. Ustuner, S. Goggins, M. Abderrabba, C. G. Frost and P. Estrela, *Electroanalysis*, 2017, **29**, 917–922.
185 T. Himuro, S. Sato, S. Takenaka and T. Yasuda, *Electroanalysis*, 2016, **28**, 1448–1454.
186 Z. Tian, H. Cui, H. Liu, J. Dong, H. Dong, L. Zhao, X. Li, Y. Zhang, Y. Huang, L. Song, L. Bian, Y. Wang, X. Xu and C. Wang, *MedChem. Commun.*, 2017, **8**, 2079–2092.
187 D. Chakraborty, D. Sarkar, A. K. Ghosh and P. K. Das, *Soft Matter*, 2021, **17**, 2170–2180.
188 K. Zhang, L. Lv, X. Wang, Y. Mi, R. Chai, X. Liu, G. Shen, A. Peng and H. Huang, *ACS Appl. Mater. Interfaces*, 2018, **10**, 1917–1924.
189 L. Hu, J. Han, W. Qiao, X. Zhou, C. Wang, D. Ma, Y. Li and Z. Y. Wang, *Polym. Chem.*, 2018, **9**, 327–334.
190 W. Xu, Y. Guo, X. Zhang, L. Zheng, T. Zhu, D. Zhao, W. Hu and X. Gong, *Adv. Funct. Mater.*, 2018, **28**, 1705541.
191 L. Hu, W. Qiao, J. Han, X. Zhou, C. Wang, D. Ma, Z. Y. Wang and Y. Li, *Polym. Chem.*, 2017, **8**, 528–536.
192 J. Qin, F. Lin, D. Hubble, Y. Wang, Y. Li, I. A. Murphy, S.-H. Jang, J. Yang and A. K. Y. Jen, *J. Mater. Chem. A*, 2019, **7**, 6773–6783.
193 H. Chen, L. Wu, X. Xiao, H. Wang, J. Jiang, L. Wang, Q. Xu and J. Lu, *Sci. China: Chem.*, 2017, **60**, 237–242.
194 S. Kumar, J. Shukla, K. Mandal, Y. Kumar, R. Prakash, P. Ram and P. Mukhopadhyay, *Chem. Sci.*, 2019, **10**, 6482–6493.
195 M. V. Vener, O. D. Parashchuk, O. G. Kharlanov, D. R. Maslennikov, D. I. Dominskiy, I. Y. Chernyshov, D. Y. Paraschuk and A. Y. Sosorev, *Adv. Electron. Mater.*, 2021, **7**, 2001281.
196 W. Xie, W. Huang, L. Tu, H. Shi and H. Liu, *J. Mater. Chem. C*, 2021, **9**, 3620–3625.
197 A. Mukhopadhyay, V. Paulino, K. Liu, C. L. Donley, B. Bernard, A. Shomar, C. Liu and J.-H. Olivier, *ACS Appl. Mater. Interfaces*, 2021, **13**, 4665–4675.
198 S. Fukuta, H.-C. Wu, T. Koganezawa, Y. Isshiki, M. Ueda, W.-C. Chen and T. Higashihara, *J. Polym. Sci., Part A: Polym. Chem.*, 2016, **54**, 359–367.

199 M. Korzec, S. Kotowicz, K. Łaba, M. Łapkowski, J. G. Małecki, K. Smolarek, S. Maćkowski and E. Schab-Balcerzak, *Eur. J. Org. Chem.*, 2018, 1756–1760.
200 H. F. Higginbotham, P. Pander, R. Rybakiewicz, M. K. Etherington, S. Maniam, M. Zagorska, A. Pron, A. P. Monkman and P. Data, *J. Mater. Chem. C*, 2018, **6**, 8219–8225.
201 W. Zhang, H. Wang, J. Miao, Y. Zhu, M. Umair Ali, T. Xu, L. Zhao, D. Zhang, G. He and H. Meng, *Org. Electron.*, 2018, **59**, 301–305.
202 N. Nandi, S. Basak, S. Kirkham, I. W. Hamley and A. Banerjee, *Langmuir*, 2016, **32**, 13226–13233.
203 X. Shang, I. Song, J. H. Lee, W. Choi, H. Ohtsu, G. Y. Jung, J. Ahn, M. Han, J. Y. Koo, M. Kawano, S. K. Kwak and J. H. Oh, *ACS Appl. Mater. Interfaces*, 2019, **11**, 20174–20182.
204 T. Liu, Y. Chen, Z.-L. Sun, J. Liu and J.-J. Liu, *J. Solid State Chem.*, 2019, **277**, 216–220.
205 (*a*) C. R. Wade, M. Li and M. Dincă, *Angew. Chem., Int. Ed.*, 2013, **52**, 13377–13381; (*b*) K. AlKaabi, C. R. Wade and M. Dincă, *Chem*, 2016, **1**, 264–272.
206 M. Schwarze, B. D. Naab, M. L. Tietze, R. Scholz, P. Pahner, F. Bussolotti, S. Kera, D. Kasemann, Z. Bao and K. Leo, *ACS Appl. Mater. Interfaces*, 2018, **10**, 1340–1346.
207 B. D. Naab, X. Gu, T. Kurosawa, J. W. F. To, A. Salleo and Z. Bao, *Adv. Electron. Mater.*, 2016, **2**, 1600004.
208 T. L. D. Tam and J. Xu, *J. Mater. Chem. A*, 2021, **9**, 5149–5163.
209 W. Wu, Z. Zhao, J. Li, M. Chen and X. Gao, *Asian J. Org. Chem.*, 2018, **7**, 2279–2284.
210 D. Zheng, M. Zhang and G. Zhao, *Phys. Chem. Chem. Phys.*, 2017, **19**, 28175–28181.
211 K. Rundel, Y. Liang, A. Welford, D. Prendergast and C. R. McNeill, *J. Chem. Phys.*, 2019, **150**, 104302.
212 F. N. Miros and S. Matile, *ChemistryOpen*, 2016, **5**, 219–226.
213 H. T. Black, N. Yee, Y. Zems and D. F. Perepichka, *Chem. – Eur. J.*, 2016, **22**, 17251–17261.
214 D. Zhang, L. Zhao, Y. Zhu, A. Li, C. He, H. Yu, Y. He, C. Yan, O. Goto and H. Meng, *ACS Appl. Mater. Interfaces*, 2016, **8**, 18277–18283.
215 J. T. Ly, E. K. Burnett, S. Thomas, A. Aljarb, Y. Liu, S. Park, S. Rosa, Y. Yi, H. Lee, T. Emrick, T. P. Russell, J.-L. Brédas and A. L. Briseno, *ACS Appl. Mater. Interfaces*, 2018, **10**, 40070–40077.
216 Z. Yao, Y. Sun and C. Kang, *Nano LIFE*, 2016, **06**, 1642007.
217 N. Renaud, M. A. Harris, A. P. N. Singh, Y. A. Berlin, M. A. Ratner, M. R. Wasielewski, F. D. Lewis and F. C. Grozema, *Nat. Chem.*, 2016, **8**, 1015–1021.
218 T. N. Kopylova, S. Y. Nikonov, E. N. Telminov, R. M. Gadirov, K. M. Degtyarenko and V. Burtman, *J. Appl. Phys.*, 2018, **124**, 125501.
219 G. Wu, Z.-G. Zhang, Y. Li, C. Gao, X. Wang and G. Chen, *ACS Nano*, 2017, **11**, 5746–5752.
220 Y. Liu, D. R. Villalva, A. Sharma, M. A. Haque and D. Baran, *ACS Appl. Mater. Interfaces*, 2021, **13**, 411–418.
221 G. Zuo, Z. Li, E. Wang and M. Kemerink, *Adv. Electron. Mater.*, 2018, **4**, 1700501.
222 N. Pearce, E. S. Davies, R. Horvath, C. R. Pfeiffer, X.-Z. Sun, W. Lewis, J. McMaster, M. W. George and N. R. Champness, *Phys. Chem. Chem. Phys.*, 2018, **20**, 752–764.
223 J. Schäfer, M. Holzapfel, A. Schmiedel, U. E. Steiner and C. Lambert, *Phys. Chem. Chem. Phys.*, 2018, **20**, 27093–27104.
224 A. Ganesh Kumar, D. Bera, S. Banerjee, R. Veerubhotla and D. Das, *Eur. Polym. J.*, 2016, **83**, 114–128.
225 A. G. Kumar, S. Saha, H. Komber, B. R. Tiwari, M. M. Ghangrekar, B. Voit and S. Banerjee, *Eur. Polym. J.*, 2019, **118**, 451–464.
226 Z. Yue, Y.-B. Cai and S. Xu, *J. Membr. Sci.*, 2016, **501**, 220–227.
227 K. Takimiya, M. Nakano, H. Sugino and I. Osaka, *Synth. Met.*, 2016, **217**, 68–78.
228 H. Ran, X. Duan, R. Zheng, F. Xie, L. Chen, Z. Zhao, R. Han, Z. Lei and J.-Y. Hu, *ACS Appl. Mater. Interfaces*, 2020, **12**, 23225–23235.
229 Y. H. Ha, J. G. Oh, S. Park, S.-K. Kwon, T. K. An, J. Jang and Y.-H. Kim, *Org. Electron.*, 2018, **63**, 250–256.
230 A. Ohyama, J. Miyazawa, Y. Yokota, N. Hirata, N. Oguma and M. Ichikawa, *Org. Electron.*, 2018, **58**, 231–237.
231 Y.-h. Shin, A. Welford, H. Komber, R. Matsidik, T. Thurn-Albrecht, C. R. McNeill and M. Sommer, *Macromolecules*, 2018, **51**, 984–991.
232 Y. Shin, M. Massetti, H. Komber, T. Biskup, D. Nava, G. Lanzani, M. Caironi and M. Sommer, *Adv. Electron. Mater.*, 2018, **4**, 1700581.
233 R. Porrazzo, A. Luzio, S. Bellani, G. E. Bonacchini, Y.-Y. Noh, Y.-H. Kim, G. Lanzani, M. R. Antognazza and M. Caironi, *ACS Omega*, 2017, **2**, 1–10.
234 Y. Wang, S. W. Kim, J. Lee, H. Matsumoto, B. J. Kim and T. Michinobu, *ACS Appl. Mater. Interfaces*, 2019, **11**, 22583–22594.
235 G.-S. Ryu, Z. Chen, H. Usta, Y.-Y. Noh and A. Facchetti, *MRS Commun.*, 2016, **6**, 47–60.
236 B. Nketia-Yawson, G. D. Tabi and Y.-Y. Noh, *Org. Electron.*, 2018, **52**, 257–263.
237 L. Yan, C. Li, L. Cai, K. Shi, W. Tang, W. Qu, C.-L. Ho, G. Yu, J. Li and X. Wang, *J. Organomet. Chem.*, 2017, **846**, 269–276.
238 N. M. Murari, Y.-J. Hwang, F. S. Kim and S. A. Jenekhe, *Org. Electron.*, 2016, **31**, 104–110.
239 M. Kim, W.-T. Park, S. U. Ryu, S. Y. Son, J. Lee, T. J. Shin, Y.-Y. Noh and T. Park, *Chem. Mater.*, 2019, **31**, 4864–4872.
240 (*a*) S. W. Kim, J. Choi, T. T. T. Bui, C. Lee, C. Cho, K. Na, J. Jung, C. E. Song, B. Ma, J.-Y. Lee, W. S. Shin and B. J. Kim, *Adv. Funct. Mater.*, 2017, **27**, 1703070; (*b*) Q. Ma, X. Xue, L. Zhong, I. Angunawela, S. Chen, H. Ade, L. Huo, Z. Zhang and Y. Li, *J. Mater. Chem. C*, 2019, **7**, 9031–9037; (*c*) C.-Y. Chang, B.-C. Tsai, M.-Z. Lin, Y.-C. Huang and C.-S. Tsao, *J. Mater. Chem. A*, 2017, **5**, 22824–22833; (*d*) Z. Zhu, C.-C. Chueh, G. Zhang, F. Huang, H. Yan and A. K.-Y. Jen, *ChemSusChem*, 2016, **9**, 2586–2591; (*e*) S.-x. Dai, S.-m. Zhang, Q.-d. Ling and X.-w. Zhan, *Chin.*

J. Polym. Sci., 2017, **35**, 230–238; (*f*) H. Sun, B. Liu, C. W. Koh, Y. Zhang, J. Chen, Y. Wang, P. Chen, B. Tu, M. Su, H. Wang, Y. Tang, Y. Shi, H. Y. Woo and X. Guo, *Adv. Funct. Mater.*, 2019, **29**, 1903970; (*g*) A. Robitaille, S. A. Jenekhe and M. Leclerc, *Chem. Mater.*, 2018, **30**, 5353–5361; (*h*) J. Ma, Z. Zhao, Y. Guo, H. Geng, Y. Sun, J. Tian, Q. He, Z. Cai, X. Zhang, G. Zhang, Z. Liu, D. Zhang and Y. Liu, *ACS Appl. Mater. Interfaces*, 2019, **11**, 15837–15844; (*i*) D. Nava, Y. Shin, M. Massetti, X. Jiao, T. Biskup, M. S. Jagadeesh, A. Calloni, L. Duò, G. Lanzani, C. R. McNeill, M. Sommer and M. Caironi, *ACS Appl. Energy Mater.*, 2018, **1**, 4626–4634; (*j*) B. Milián-Medina, M. Wykes, Z. Chen, A. Facchetti and J. Gierschner, *J. Mater. Chem. C*, 2016, **4**, 9405–9410; (*k*) Y. Ha, E.-Y. Shin, S.-K. Kwon and Y.-H. Kim, *Sci. Adv. Mater.*, 2017, **9**, 2004–2012; (*l*) M. J. Kim, A. R. Jung, M. Lee, D. Kim, S. Ro, S.-M. Jin, H. D. Nguyen, J. Yang, K.-K. Lee, E. Lee, M. S. Kang, H. Kim, J.-H. Choi, B. Kim and J. H. Cho, *ACS Appl. Mater. Interfaces*, 2017, **9**, 40503–40515; (*m*) M. J. Sung, A. Luzio, W.-T. Park, R. Kim, E. Gann, F. Maddalena, G. Pace, Y. Xu, D. Natali, C. de Falco, L. Dang, C. R. McNeill, M. Caironi, Y.-Y. Noh and Y.-H. Kim, *Adv. Funct. Mater.*, 2016, **26**, 4984–4997; (*n*) K. Park, E.-Y. Shin, X. Jiao, C. R. McNeill, Y.-H. Kim, S.-K. Kwon and Y.-Y. Noh, *ACS Appl. Mater. Interfaces*, 2019, **11**, 35185–35192; (*o*) Z. Ding, X. Long, C. Dou, J. Liu and L. Wang, *Chem. Sci.*, 2016, **7**, 6197–6202; (*p*) N. B. Kolhe, H. Lee, D. Kuzuhara, N. Yoshimoto, T. Koganezawa and S. A. Jenekhe, *Chem. Mater.*, 2018, **30**, 6540–6548; (*q*) W. Yan, Z. Wang, Y. Gong, S. Guo, J. Jiang, J. Chen, C. Tang, R. Xia, W. Huang and H. Xin, *Org. Electron.*, 2019, **67**, 208–214; (*r*) S. Oh, S. Badgujar, D. H. Kim, W.-E. Lee, N. Khan, M. Jahandar, S. Rasool, C. E. Song, H. K. Lee, W. S. Shin, J.-C. Lee, S.-J. Moon and S. K. Lee, *J. Mater. Chem. A*, 2017, **5**, 15923–15931; (*s*) S. Shi, J. Yuan, G. Ding, M. Ford, K. Lu, G. Shi, J. Sun, X. Ling, Y. Li and W. Ma, *Adv. Funct. Mater.*, 2016, **26**, 5669–5678; (*t*) B. He, Q. Yin, J. Zhang, T. Jia, X. Yang, X.-F. Jiang, F. Huang and Y. Cao, *Chin. J. Chem.*, 2018, **36**, 406–410; (*u*) C. Weng, Z. Liu, H. Guo and S. Tan, *Macromol. Chem. Phys.*, 2017, **218**, 1700094; (*v*) D. Tu, X. Liu, J. Zhang, Q. Yang, S. Yu, X. Guo and C. Li, *ACS Sustainable Chem. Eng.*, 2018, **6**, 16005–16010; (*w*) C. Weng, L. Gao, Z. Zhang, Z. Liu, S. Tan and Y. Li, *J. Polym. Sci., Part B: Polym. Phys.*, 2017, **55**, 990–996; (*x*) X. Wang, L. Lv, W. Gu, X. Wang, T. Dong, Z. Yang, H. Cao and H. Huang, *Dyes Pigm.*, 2017, **140**, 141–149; (*y*) S. Sharma, R. Soni, S. Kurungot and S. K. Asha, *Macromolecules*, 2018, **51**, 954–965.

241 A. Welford, S. Maniam, E. Gann, L. Thomsen, S. J. Langford and C. R. McNeill, *Org. Electron.*, 2018, **53**, 287–295.

242 Y. Peng and Z. Li, *Mater. Chem. Phys.*, 2018, **214**, 260–264.

243 Z. Yuan, Y. Ma, T. Geßner, M. Li, L. Chen, M. Eustachi, R. T. Weitz, C. Li and K. Müllen, *Org. Lett.*, 2016, **18**, 456–459.

244 H. E. Katz, J. Johnson, A. J. Lovinger and W. Li, *J. Am. Chem. Soc.*, 2000, **122**, 7787–7792.

245 L. Zhao, D. Zhang, Y. Zhu, P. Sen, H. Meng and W. Huang, *J. Mater. Chem. C*, 2017, **5**, 848–853.

246 C. An, H. Makowska, B. Hu, R. Duan, W. Pisula, T. Marszalek and M. Baumgarten, *RSC Adv.*, 2018, **8**, 16464–16469.

247 (*a*) Y.-Y. Hsu, S.-C. Yeh, S.-H. Lin, C.-T. Chen, S.-H. Tung and R.-J. Jeng, *React. Funct. Polym.*, 2016, **108**, 86–93; (*b*) G. E. Purdum, N. Yao, A. Woll, T. Gessner, R. T. Weitz and Y.-L. Loo, *Adv. Funct. Mater.*, 2016, **26**, 2357–2364; (*c*) X. Xu, Z. Li, J. Wang, B. Lin, W. Ma, Y. Xia, M. R. Andersson, R. A. J. Janssen and E. Wang, *Nano Energy*, 2018, **45**, 368–379; (*d*) K. D. Deshmukh, R. Matsidik, S. K. K. Prasad, N. Chandrasekaran, A. Welford, L. A. Connal, A. C. Y. Liu, E. Gann, L. Thomsen, D. Kabra, J. M. Hodgkiss, M. Sommer and C. R. McNeill, *ACS Appl. Mater. Interfaces*, 2018, **10**, 955–969; (*e*) X. Li, X. Liu, P. Sun, Y. Feng, H. Shan, X. Wu, J. Xu, C. Huang, Z.-K. Chen and Z.-X. Xu, *RSC Adv.*, 2017, **7**, 17076–17084; (*f*) P. Deng, C. H. Y. Ho, Y. Lu, H.-W. Li, S.-W. Tsang, S. K. So and B. S. Ong, *Chem. Commun.*, 2017, **53**, 3249–3252; (*g*) M. Kim, H. I. Kim, S. U. Ryu, S. Y. Son, S. A. Park, N. Khan, W. S. Shin, C. E. Song and T. Park, *Chem. Mater.*, 2019, **31**, 5047–5055; (*h*) B. Kang, R. Kim, S. B. Lee, S.-K. Kwon, Y.-H. Kim and K. Cho, *J. Am. Chem. Soc.*, 2016, **138**, 3679–3686.

248 S.-L. Suraru, U. Zschieschang, H. Klauk and F. Würthner, *Chem. Commun.*, 2011, **47**, 11504–11506.

249 J. Li, Y.-H. Hu, C.-W. Ge, H.-G. Gong and X.-K. Gao, *Chin. Chem. Lett.*, 2018, **29**, 423–428.

250 D. X. Long, E.-Y. Choi and Y.-Y. Noh, *Dyes Pigm.*, 2017, **142**, 323–329.

251 H. S. Ryu, M. J. Kim, M. S. Kang, J. H. Cho and H. Y. Woo, *Macromolecules*, 2018, **51**, 8258–8267.

252 (*a*) L. Zhang, Z. Wang, C. Duan, Z. Wang, Y. Deng, J. Xu, F. Huang and Y. Cao, *Chem. Mater.*, 2018, **30**, 8343–8351; (*b*) Z. Yuan, C. Buckley, S. Thomas, G. Zhang, I. Bargigia, G. Wang, B. Fu, C. Silva, J.-L. Brédas and E. Reichmanis, *Macromolecules*, 2018, **51**, 7320–7328.

253 T. Kurosawa, Y.-C. Chiu, Y. Zhou, X. Gu, W.-C. Chen and Z. Bao, *Adv. Funct. Mater.*, 2016, **26**, 1261–1270.

254 X. Gao, C.-a. Di, Y. Hu, X. Yang, H. Fan, F. Zhang, Y. Liu, H. Li and D. Zhu, *J. Am. Chem. Soc.*, 2010, **132**, 3697–3699.

255 F. Zhang, Y. Hu, T. Schuettfort, C.-A. Di, X. Gao, C. R. McNeill, L. Thomsen, S. C. B. Mannsfeld, W. Yuan, H. Sirringhaus and D. Zhu, *J. Am. Chem. Soc.*, 2013, **135**, 2338–2349.

256 M. Ichikawa, K. Iwasaki, A. Ohyama, J. Miyazawa, Y. Yokota, N. Hirata and N. Oguma, *Jpn. J. Appl. Phys.*, 2017, **56**, 111601.

257 A. Welford, S. Maniam, E. Gann, X. Jiao, L. Thomsen, S. J. Langford and C. R. McNeill, *Org. Electron.*, 2019, **75**, 105378.

258 S. Nam, S. G. Hahm, D. Khim, H. Kim, T. Sajoto, M. Ree, S. R. Marder, T. D. Anthopoulos, D. D. C. Bradley and Y. Kim, *ACS Appl. Mater. Interfaces*, 2018, **10**, 12921–12929.

259 A. Ohyama, N. Hirata, N. Oguma and M. Ichikawa, *Org. Electron.*, 2018, **63**, 300–304.

260 X. Liang, L. Tan, Z. Liu, Y. Ma, G. Zhang, L. Wang, S. Li, L. Dong, J. Li and W. Chen, *Chem. Commun.*, 2017, **53**, 4934–4937.

261 M. M. Nahid, A. Welford, E. Gann, L. Thomsen, K. P. Sharma and C. R. McNeill, *Adv. Electron. Mater.*, 2018, **4**, 1700559.
262 Z.-C. Chen, R.-R. Fang, Y.-Y. Yu, J.-H. Gao and J.-H. Wan, *J. Appl. Polym. Sci.*, 2019, **136**, 46926.
263 R. Wang, Y. Guo, D. Zhang, H. Zhou, D. Zhao and Y. Zhang, *Macromol. Rapid Commun.*, 2018, **39**, 1700726.
264 Y. Yamashita, S. Jhulki, D. Bhardwaj, E. Longhi, S. Kumagai, S. Watanabe, S. Barlow, S. R. Marder and J. Takeya, *J. Mater. Chem. C*, 2021, **9**, 4105–4111.
265 A. Lv, Y. Li, W. Yue, L. Jiang, H. Dong, G. Zhao, Q. Meng, W. Jiang, Y. He, Z. Li, Z. Wang and W. Hu, *Chem. Commun.*, 2012, **48**, 5154–5156.
266 I. Song, S.-C. Lee, X. Shang, J. Ahn, H.-J. Jung, C.-U. Jeong, S.-W. Kim, W. Yoon, H. Yun, O. P. Kwon and J. H. Oh, *ACS Appl. Mater. Interfaces*, 2018, **10**, 11826–11836.
267 S. S. Birajdar, S. Brixi, P. S. Rao, R. S. Bhosale, M. Al Kobaisi, A. Gupta, B. H. Lessard, S. V. Bhosale and S. V. Bhosale, *ChemistryOpen*, 2021, **10**, 414–420.
268 H.-R. Yang and Y.-Y. Lai, *Adv. Electron. Mater.*, 2021, **7**, 2000939.
269 D. Ohayon, A. Savva, W. Du, B. D. Paulsen, I. Uguz, R. S. Ashraf, J. Rivnay, I. McCulloch and S. Inal, *ACS Appl. Mater. Interfaces*, 2021, **13**, 4253–4266.
270 J. G. Oh, Y. H. Ha, J.-H. Kim, S.-K. Kwon, T. K. An, Y.-H. Kim and J. Jang, *Org. Electron.*, 2021, **89**, 106032.
271 (*a*) Y. Henderson, *Science*, 1915, **41**, 910–911; (*b*) J. R. Owen, *Chem. Soc. Rev.*, 1997, **26**, 259–267; (*c*) L. F. Nazar, M. Cuisinier and Q. Pang, *MRS Bull.*, 2014, **39**, 436–442.
272 (*a*) S. Nishida, Y. Yamamoto, T. Takui and Y. Morita, *ChemSusChem*, 2013, **6**, 794–797; (*b*) W. Huang, Z. Zhu, L. Wang, S. Wang, H. Li, Z. Tao, J. Shi, L. Guan and J. Chen, *Angew. Chem., Int. Ed.*, 2013, **52**, 9162–9166; (*c*) Y. Hanyu and I. Honma, *Sci. Rep.*, 2012, **2**, 453.
273 A. E. Lakraychi, K. Fahsi, L. Aymard, P. Poizot, F. Dolhem and J. P. Bonnet, *Electrochem. Commun.*, 2017, **76**, 47–50.
274 M. Veerababu, U. V. Varadaraju and R. Kothandaraman, *Electrochim. Acta*, 2016, **193**, 80–87.
275 V. Medabalmi, N. Kuanr and K. Ramanujam, *J. Electrochem. Soc.*, 2017, **164**, A6147–A6153.
276 Y. Shi, H. Tang, S. Jiang, L. V. Kayser, M. Li, F. Liu, F. Ji, D. J. Lipomi, S. P. Ong and Z. Chen, *Chem. Mater.*, 2018, **30**, 3508–3517.
277 S. Maniam, K. Oka and H. Nishide, *MRS Commun.*, 2017, **7**, 967–973.
278 Y. Sasada, S. J. Langford, K. Oyaizu and H. Nishide, *RSC Adv.*, 2016, **6**, 42911–42916.
279 F. Xu, H. Wang, M. Wu, J. Nan, T. Li and S.-A. Cao, *Mater. Chem. Phys.*, 2018, **214**, 120–125.
280 F. Xu, H. Wang, J. Lin, X. Luo, S.-A. Cao and H. Yang, *J. Mater. Chem. A*, 2016, **4**, 11491–11497.
281 K. T. Sarang, A. Miranda, H. An, E.-S. Oh, R. Verduzco and J. L. Lutkenhaus, *ACS Appl. Polym. Mater*, 2019, **1**, 1155–1164.
282 H. Zhang, Y. Xie, X. Chen, T. Jia, W. Huang, S. Luo, Q. Hou, R. Zeng and Z. Sun, *J. Electrochem. Soc.*, 2017, **164**, A290–A294.
283 S. Perticarari, Y. Sayed-Ahmad-Baraza, C. Ewels, P. Moreau, D. Guyomard, P. Poizot, F. Odobel and J. Gaubicher, *Adv. Energy Mater.*, 2018, **8**, 1701988.
284 S. Perticarari, T. Doizy, P. Soudan, C. Ewels, C. Latouche, D. Guyomard, F. Odobel, P. Poizot and J. Gaubicher, *Adv. Energy Mater.*, 2019, **9**, 1803688.
285 D. Moia, A. Giovannitti, A. A. Szumska, I. P. Maria, E. Rezasoltani, M. Sachs, M. Schnurr, P. R. F. Barnes, I. McCulloch and J. Nelson, *Energy Environ. Sci.*, 2019, **12**, 1349–1357.
286 M. Chen, C. Yang, Z. Xu, Y. Tang, J. Jiang, P. Liu, Y. Su and D. Wu, *RSC Adv.*, 2016, **6**, 13666–13669.
287 F. de Araújo Silva, R. S. Cicolani, G. Lima, F. Huguenin and G. Jean-François Demets, *RSC Adv.*, 2018, **8**, 24029–24035.
288 A. V. Mumyatov, A. F. Shestakov, N. N. Dremova, K. J. Stevenson and P. A. Troshin, *Energy Technol.*, 2019, **7**, 1801016.
289 S. Jhulki, C. H. Feriante, R. Mysyk, A. M. Evans, A. Magasinski, A. S. Raman, K. Turcheniuk, S. Barlow, W. R. Dichtel, G. Yushin and S. R. Marder, *ACS Appl. Energy Mater*, 2021, **4**, 350–356.
290 Y. Wang, H. Wu and J. F. Stoddart, *Acc. Chem. Res.*, 2021, **54**, 2027–2039.
291 A. Roy, S. Mondal, A. Halder, A. Banerjee, D. Ghoshal, A. Paul and S. Malik, *Eur. Polym. J.*, 2017, **93**, 448–457.
292 J. Lv, Y.-X. Tan, J. Xie, R. Yang, M. Yu, S. Sun, M.-D. Li, D. Yuan and Y. Wang, *Angew. Chem., Int. Ed.*, 2018, **57**, 12716–12720.
293 M. R. Biradar, A. V. Salkar, P. P. Morajkar, S. V. Bhosale and S. V. Bhosale, *New J. Chem.*, 2021, **45**, 9346–9357.
294 G. Wang, N. Chandrasekhar, B. P. Biswal, D. Becker, S. Paasch, E. Brunner, M. Addicoat, M. Yu, R. Berger and X. Feng, *Adv. Mater.*, 2019, **31**, 1901478.
295 J. Yang, B. Xiao, A. Tang, J. Li, X. Wang and E. Zhou, *Adv. Mater.*, 2019, **31**, 1804699.
296 Z.-G. Zhang and Y. Li, *Angew. Chem., Int. Ed.*, 2021, **60**, 4422–4433.
297 Z. Li, Y. Liu, K. Zhang, Z. Wang, P. Huang, D. Li, Y. Zhou and B. Song, *Langmuir*, 2017, **33**, 8679–8685.
298 Y. Bentounsi, K. Seintis, S. Diring, E. Vauthey and F. Odobel, *ACS Appl. Energy Mater*, 2021, **4**, 2629–2636.
299 U. Ali, A. Javed, A. Tallat, J. Iqbal and A. Raza, *J. Mol. Model.*, 2019, **25**, 50.
300 M. J. Sung, M. Huang, S. H. Moon, T. H. Lee, S. Y. Park, J. Y. Kim, S.-K. Kwon, H. Choi and Y.-H. Kim, *Sol. Energy*, 2017, **150**, 90–95.
301 D. Srivani, A. Gupta, S. V. Bhosale, A. L. Puyad, W. Xiang, J. Li, R. A. Evans and S. V. Bhosale, *Chem. Commun.*, 2017, **53**, 7080–7083.
302 D. Srivani, A. Gupta, A. M. Raynor, A. Bilic, J. Li, S. V. Bhosale and S. V. Bhosale, *RSC Adv.*, 2016, **6**, 38703–38708.
303 T. Zhang, M. Lu, W. Wang, W. Lv, J. Cui, W. Feng and Q. Ling, *Dyes Pigm.*, 2017, **146**, 169–177.
304 S. Sharma, N. B. Kolhe, V. Gupta, V. Bharti, A. Sharma, R. Datt, S. Chand and S. K. Asha, *Macromolecules*, 2016, **49**, 8113–8125.

305 Y. Kim, H.-H. Cho, K. Taesu, K. Liao and B. Kim, *Polym. J.*, 2016, **48**, 517–524.
306 X. Gu, H. Yan, T. Kurosawa, B. C. Schroeder, K. L. Gu, Y. Zhou, J. W. F. To, S. D. Oosterhout, V. Savikhin, F. Molina-Lopez, C. J. Tassone, S. C. B. Mannsfeld, C. Wang, M. F. Toney and Z. Bao, *Adv. Energy Mater.*, 2016, **6**, 1601225.
307 J. W. Jo, J. W. Jung, H. Ahn, M. J. Ko, A. K.-Y. Jen and H. J. Son, *Adv. Energy Mater.*, 2017, **7**, 1601365.
308 J. Yang, F. Chen, H. Ran, J.-Y. Hu, B. Xiao, A. Tang, X. Wang and E. Zhou, *Macromol. Rapid Commun.*, 2018, **39**, e1700715.
309 J. Yang, B. Xiao, S. W. Heo, K. Tajima, F. Chen and E. Zhou, *ACS Appl. Mater. Interfaces*, 2017, **9**, 44070–44078.
310 M. Li, Y. Qin, W. Dai and X. Luo, *RSC Adv.*, 2018, **8**, 3809–3815.
311 J. Wang, C. Lu, T. Higashihara and W.-C. Chen, *Microsyst. Technol.*, 2017, **23**, 1183–1189.
312 K. Li, R. Xie, W. Zhong, K. Lin, L. Ying, F. Huang and Y. Cao, *Sci. China: Chem.*, 2018, **61**, 576–583.
313 B. He, Z. Li, T. Jia, J. Xin, L. Ying, W. Ma, F. Huang and Y. Cao, *Dyes Pigm.*, 2018, **159**, 85–91.
314 H. Bildirir, D. Di Carlo Rasi, M. M. Wienk, R. A. J. Janssen, A. Avgeropoulos, V. G. Gregoriou, S. Allard, U. Scherf and C. L. Chochos, *Macromol. Rapid Commun.*, 2018, **39**, 1700629.
315 S. Dai, S. Huang, H. Yu, Q. Ling and X. Zhan, *J. Polym. Sci., Part A: Polym. Chem.*, 2017, **55**, 682–689.
316 T. Jia, Z. Li, L. Ying, J. Jia, B. Fan, W. Zhong, F. Pan, P. He, J. Chen, F. Huang and Y. Cao, *Macromol. Rapid Commun.*, 2018, **39**, 1700765.
317 G. Shen, X. Li, X. Wu, Y. Wang, H. Shan, J. Xu and X. Liu, Z.-x. Xu, F. Chen and Z.-K. Chen, *Org. Electron.*, 2017, **46**, 203–210.
318 J. M. Bjuggren, A. Sharma, D. Gedefaw, S. Elmas, C. Pan, B. Kirk, X. Zhao, G. Andersson and M. R. Andersson, *ACS Appl. Energy Mater*, 2018, **1**, 7130–7139.
319 X. Tang, X. Liu, W. Shen, W. Hu, R. He and M. Li, *RSC Adv.*, 2016, **6**, 102159–102171.
320 X. Gao, J. Gao, Z. Xue, H. Wang, J. Wang, Y. Cheng, Z. Li, F. Zhu, S. Huettner, H. Li and Y. Tao, *J. Mater. Chem. C*, 2019, **7**, 10338–10351.
321 (*a*) J. Yang, Y. Yin, F. Chen, Y. Zhang, B. Xiao, L. Zhao and E. Zhou, *ACS Appl. Mater. Interfaces*, 2018, **10**, 23263–23269; (*b*) Z. Li, X. Xu, W. Zhang, X. Meng, W. Ma, A. Yartsev, O. Inganäs, M. R. Andersson, R. A. J. Janssen and E. Wang, *J. Am. Chem. Soc.*, 2016, **138**, 10935–10944; (*c*) L. Xue, Y. Yang, Z.-G. Zhang, X. Dong, L. Gao, H. Bin, J. Zhang, Y. Yang and Y. Li, *J. Mater. Chem. A*, 2016, **4**, 5810–5816; (*d*) X. Li, P. Sun, Y. Wang, H. Shan, J. Xu and X. Song, Z.-x. Xu and Z.-K. Chen, *J. Mater. Chem. C*, 2016, **4**, 2106–2110; (*e*) Y. Fang, H. Jin, A. Raynor, X. Wang, P. E. Shaw, N. Kopidakis, C. R. McNeill and P. L. Burn, *ACS Appl. Mater. Interfaces*, 2018, **10**, 24046–24054; (*f*) N. B. Kolhe, D. K. Tran, H. Lee, D. Kuzuhara, N. Yoshimoto, T. Koganezawa and S. A. Jenekhe, *ACS Energy Lett.*, 2019, **4**, 1162–1170; (*g*) X. Wu, Y. Tang, Y. Wang, X. Liu, C. Liu, X. Zhang, Y. Yang, X. Gao, F. Chen, X. Guo and Z.-K. Chen, *J. Polym. Sci., Part A: Polym. Chem.*, 2017, **55**, 3679–3689; (*h*) D. Chen, J. Yao, L. Chen, J. Yin, R. Lv, B. Huang, S. Liu, Z.-G. Zhang, C. Yang, Y. Chen and Y. Li, *Angew. Chem., Int. Ed.*, 2018, **57**, 4580–4584.
322 Z. Hu, Z. Chen, K. Zhang, N. Zheng, R. Xie, X. Liu, X. Yang, F. Huang and Y. Cao, *Sol. RRL*, 2017, **1**, 1700055.
323 G. Sini, M. Schubert, C. Risko, S. Roland, O. P. Lee, Z. Chen, T. V. Richter, D. Dolfen, V. Coropceanu, S. Ludwigs, U. Scherf, A. Facchetti, J. M. J. Fréchet and D. Neher, *Adv. Energy Mater.*, 2018, **8**, 1702232.
324 L. Xue, Y. Yang, H. Bin, Z.-G. Zhang, J. Zhang, Y. Yang and Y. Li, *J. Polym. Sci., Part A: Polym. Chem.*, 2017, **55**, 1757–1764.
325 J. Yang, F. Chen, B. Xiao, S. Sun, X. Sun, K. Tajima, A. Tang and E. Zhou, *Sol. RRL*, 2018, **2**, 1700230.
326 Y. Xia, C. Musumeci, J. Bergqvist, W. Ma, F. Gao, Z. Tang, S. Bai, Y. Jin, C. Zhu, R. Kroon, C. Wang, M. R. Andersson, L. Hou, O. Inganäs and E. Wang, *J. Mater. Chem. A*, 2016, **4**, 3835–3843.
327 X. Li, P. Sun, Y. Wang, H. Shan, J. Xu, C. You, Z.-X. Xu and Z.-K. Chen, *Polym. Chem.*, 2016, **7**, 2230–2238.
328 K. Rundel, S. Maniam, K. Deshmukh, E. Gann, S. K. K. Prasad, J. M. Hodgkiss, S. J. Langford and C. R. McNeill, *J. Mater. Chem. A*, 2017, **5**, 12266–12277.
329 H.-H. Cho, G. Han, R. Younts, W. Lee, B. R. Gautam, S. Lee, C. Lee, T. Kim, F. S. Kim, K. Gundogdu and B. J. Kim, *J. Mater. Chem. A*, 2017, **5**, 21291–21299.
330 H. I. Kim, M.-J. Kim, K. Choi, C. Lim, Y.-H. Kim, S.-K. Kwon and T. Park, *Adv. Energy Mater.*, 2018, **8**, 1702872.
331 J. Hong, Y. H. Ha, H. Cha, R. Kim, Y. J. Kim, C. E. Park, J. R. Durrant, S.-K. Kwon, T. K. An and Y.-H. Kim, *ACS Appl. Mater. Interfaces*, 2017, **9**, 44667–44677.
332 P. S. Rao, V. G. More, A. D. Jangale, S. V. Bhosale, R. S. Bhosale, A. L. Puyad, J.-Y. Chen, J.-L. Li, S. V. Bhosale, A. Gupta and G. D. Sharma, *Dyes Pigm.*, 2019, **171**, 107677.
333 J. T. Oh, Y. H. Ha, S.-K. Kwon, S. Song, J. Y. Kim, Y.-H. Kim and H. Choi, *Macromol. Rapid Commun.*, 2018, **39**, 1800108.
334 K. D. Deshmukh, R. Matsidik, S. K. K. Prasad, L. A. Connal, A. C. Y. Liu, E. Gann, L. Thomsen, J. M. Hodgkiss, M. Sommer and C. R. McNeill, *Adv. Funct. Mater.*, 2018, **28**, 1707185.
335 Y. Fan, S. Barlow, S. Zhang, B. Lin and S. R. Marder, *RSC Adv.*, 2016, **6**, 70493–70500.
336 S. M. Wagalgave, S. V. Bhosale, R. S. Bhosale, A. L. Puyad, J.-Y. Chen, J.-L. Li, R. A. Evans, A. Gupta and S. V. Bhosale, *Mater. Chem. Front*, 2019, **3**, 1231–1237.
337 W. T. Hadmojo, U.-H. Lee, D. Yim, H. W. Kim, W.-D. Jang, S. C. Yoon, I. H. Jung and S.-Y. Jang, *ACS Appl. Mater. Interfaces*, 2018, **10**, 41344–41349.
338 L. Zhang, L. Favereau, Y. Farre, A. Maufroy, Y. Pellegrin, E. Blart, M. Hissler, D. Jacquemin, F. Odobel and L. Hammarström, *RSC Adv.*, 2016, **6**, 77184–77194.
339 X. Liu, C. Zhang, C. Duan, M. Li, Z. Hu, J. Wang, F. Liu, N. Li, C. J. Brabec, R. A. J. Janssen, G. C. Bazan, F. Huang and Y. Cao, *J. Am. Chem. Soc.*, 2018, **140**, 8934–8943.

340 (*a*) S. Y. Nam, E. Y. Choi, C. E. Song, C. Lee, I. H. Jung and S. C. Yoon, *J. Inf. Disp.*, 2016, **17**, 17–24; (*b*) T. Jia, C. Sun, R. Xu, Z. Chen, Q. Yin, Y. Jin, H.-L. Yip, F. Huang and Y. Cao, *ACS Appl. Mater. Interfaces*, 2017, **9**, 36070–36081.

341 (*a*) S. Dong, K. Zhang, X. Liu, Q. Yin, H.-L. Yip, F. Huang and Y. Cao, *Sci. China: Chem.*, 2019, **62**, 67–73; (*b*) Z. Wu, C. Sun, S. Dong, X.-F. Jiang, S. Wu, H. Wu, H.-L. Yip, F. Huang and Y. Cao, *J. Am. Chem. Soc.*, 2016, **138**, 2004–2013; (*c*) C. Sun, Z. Wu, H.-L. Yip, H. Zhang, X.-F. Jiang, Q. Xue, Z. Hu, Z. Hu, Y. Shen, M. Wang, F. Huang and Y. Cao, *Adv. Energy Mater.*, 2016, **6**, 1501534; (*d*) K. Zhang, B. Fan, R. Xia, X. Liu, Z. Hu, H. Gu, S. Liu, H.-L. Yip, L. Ying, F. Huang and Y. Cao, *Adv. Energy Mater.*, 2018, **8**, 1703180; (*e*) D. Li, C. Sun, H. Li, H. Shi, X. Shai, Q. Sun, J. Han, Y. Shen, H.-L. Yip, F. Huang and M. Wang, *Chem. Sci.*, 2017, **8**, 4587–4594; (*f*) K. Horatz, K. Ditte, T. Prenveille, K.-N. Zhang, D. Jehnichen, A. Kiriy, B. Voit and F. Lissel, *ChemPlusChem*, 2019, **84**, 1338–1345.

342 X. Gao, M. Wang, X. Cao, J. Yang, Y. Zhong, Z. Zhang, C. Li, S. Huettner, Y. Tao, Y. Li and W. Huang, *J. Polym. Sci., Part A: Polym. Chem*, 2018, **56**, 105–115.

343 P. Wang, Y. H. Koo, W. Kim, W. Yang, X. Cui, W. Ji, J. Zhao and D. Kim, *J. Phys. Chem. C*, 2017, **121**, 11117–11128.

344 X. Gao, D. Shi, M. Wang, Z. Xue, Y. Hu, Y. Tao and W. Huang, *J. Mater. Chem. C*, 2018, **6**, 9903–9913.

345 X. Zhao, L. Tao, H. Li, W. Huang, P. Sun, J. Liu, S. Liu, Q. Sun, Z. Cui, L. Sun, Y. Shen, Y. Yang and M. Wang, *Nano Lett.*, 2018, **18**, 2442–2449.

346 J. H. Heo, S.-C. Lee, S.-K. Jung, O. P. Kwon and S. H. Im, *J. Mater. Chem. A*, 2017, **5**, 20615–20622.

347 S.-K. Jung, J. H. Heo, D. W. Lee, S.-H. Lee, S.-C. Lee, W. Yoon, H. Yun, D. Kim, J. H. Kim, S. H. Im and O.-P. Kwon, *ChemSusChem*, 2019, **12**, 224–230.

348 S. Peng, J. Miao, I. Murtaza, L. Zhao, Z. Hu, M. Liu, T. Yang, Y. Liang, H. Meng and W. Huang, *J. Mater. Chem. C*, 2017, **5**, 5949–5955.

349 Q. Kang, L. Ye, B. Xu, C. An, S. J. Stuard, S. Zhang, H. Yao, H. Ade and J. Hou, *Joule*, 2019, **3**, 227–239.

350 S.-K. Jung, J. H. Heo, D. W. Lee, S.-C. Lee, S.-H. Lee, W. Yoon, H. Yun, S. H. Im, J. H. Kim and O.-P. Kwon, *Adv. Funct. Mater.*, 2018, **28**, 1800346.

351 Z. Ma, H. Geng, D. Wang and Z. Shuai, *J. Mater. Chem. C*, 2016, **4**, 4546–4555.

352 S. Tang, X. Lv, D. Liu, Z. Li, S. Li, G. Chen, L. Kang, D. Liang and R. Jin, *J. Taiwan Inst. Chem. Eng.*, 2017, **76**, 35–43.

353 Y. Farré, M. Raissi, A. Fihey, Y. Pellegrin, E. Blart, D. Jacquemin and F. Odobel, *ChemSusChem*, 2017, **10**, 2618–2625.

354 J. Li, J. Li, C. Ge and X. Gao, *Org. Mater.*, 2020, **2**, 165–172.

355 J. Mei, N. L. C. Leung, R. T. K. Kwok, J. W. Y. Lam and B. Z. Tang, *Chem. Rev.*, 2015, **115**, 11718–11940.

356 B. Z. Tang, X. Zhan, G. Yu, P. P. Sze Lee, Y. Liu and D. Zhu, *J. Mater. Chem.*, 2001, **11**, 2974–2978.

357 A. Rananaware, D. D. La, S. M. Jackson and S. V. Bhosale, *RSC Adv.*, 2016, **6**, 16250–16255.

358 (*a*) L. Zong, Y. Xie, C. Wang, J.-R. Li, Q. Li and Z. Li, *Chem. Commun.*, 2016, **52**, 11496–11499; (*b*) X. Fang, H. Ke, L. Li and M.-J. Lin, *Dyes Pigm.*, 2017, **145**, 469–475.

359 (*a*) S. Basak, N. Nandi, S. Paul and A. Banerjee, *ACS Omega*, 2018, **3**, 2174–2182; (*b*) P. Choudhury, K. Das and P. K. Das, *Langmuir*, 2017, **33**, 4500–4510; (*c*) P. Choudhury, S. Sarkar and P. K. Das, *Langmuir*, 2018, **34**, 14328–14341; (*d*) P. Choudhury and P. K. Das, *Langmuir*, 2019, **35**, 10582–10595.

360 D. Chen, S. Liu, J. Liu, J. Han, L. Chen and Y. Chen, *ACS Appl. Polym. Mater.*, 2021, **3**, 1923–1931.

361 R. Xie, Y. Liang, J. Jing, J. Chen, R. Li and K. Zhang, *Dyes Pigm.*, 2021, **189**, 109246.

362 R. Sorrentino, M. Penconi, A. Andicsová-Eckstein, G. Scavia, H. Švajdlenková, E. Kozma and S. Luzzati, *Energies*, 2021, **14**, 454.

363 J.-W. Lee, N. Choi, D. Kim, T. N.-L. Phan, H. Kang, T.-S. Kim and B. J. Kim, *Chem. Mater.*, 2021, **33**, 1070–1081.

364 B. Zhu, L. Guo, P. Deng and S. Liu, *J. Mater. Chem. C*, 2021, **9**, 2198–2204.

365 B. Zhu, Y. Feng, Q. Zhang, P. Deng and J. Yuan, *Org. Electron.*, 2021, **89**, 106051.

366 A. A. Mohapatra, Y. Dong, P. Boregowda, A. Mohanty, A. Sadhanala, X. Jiao, A. Narayan, C. R. McNeill, J. R. Durrant and S. Patil, *J. Phys. Chem. C*, 2021, **125**, 6886–6896.

367 S. Zhang, J. Liu, Y. Han and L. Wang, *Macromol. Chem. Phys.*, 2017, **218**, 1600606.

368 S. Hillebrandt, T. Adermann, M. Alt, J. Schinke, T. Glaser, E. Mankel, G. Hernandez-Sosa, W. Jaegermann, U. Lemmer, A. Pucci, W. Kowalsky, K. Müllen, R. Lovrincic and M. Hamburger, *ACS Appl. Mater. Interfaces*, 2016, **8**, 4940–4945.

369 I. P. Maria, B. D. Paulsen, A. Savva, D. Ohayon, R. Wu, R. Hallani, A. Basu, W. Du, T. D. Anthopoulos, S. Inal, J. Rivnay, I. McCulloch and A. Giovannitti, *Adv. Electron. Mater.*, 2021, **31**, 2008718.

370 P. Ledwon, D. Ovsiannikova, T. Jarosz, S. Gogoc, P. Nitschke and W. Domagala, *Electrochim. Acta*, 2019, **307**, 525–535.

371 F. Liu, Y. Wu, C. Wang, J. Ma, F. Wu, Y. Zhang and X. Ba, *Polymers*, 2018, **10**, 790.

372 A. Sanzone, S. Cimò, S. Mattiello, R. Ruffo, I. Facchinetti, G. E. Bonacchini, M. Caironi, M. Sassi, M. Sommer and L. Beverina, *ChemPlusChem*, 2019, **84**, 1346–1352.

373 Y. Zhang, A. Savva, S. Wustoni, A. Hama, I. P. Maria, A. Giovannitti, I. McCulloch and S. Inal, *ACS Appl. Bio Mater.*, 2018, **1**, 1348–1354.

374 L. Y. Tan, Y. Tsuchido, K. Osakada, Z. Cai, Y. Takahashi and D. Takeuchi, *Macromolecules*, 2019, **52**, 1642–1652.

375 Y. Karpov, J. Maiti, R. Tkachov, T. Beryozkina, V. Bakulev, W. Liu, H. Komber, U. Lappan, M. Al-Hussein, M. Stamm, B. Voit and A. Kiriy, *Polym. Chem.*, 2016, **7**, 2691–2697.

376 J.-J. Liu, Y. Chen, M.-J. Lin, C.-C. Huang and W.-X. Dai, *Dalton Trans.*, 2016, **45**, 6339–6342.

377 M. D. L. N. Piña, M. S. Gutiérrez, M. Panagos, P. Duel, A. León, J. Morey, D. Quiñonero and A. Frontera, *RSC Adv.*, 2019, **9**, 24184–24191.

378 W. W. McNutt, A. Gumyusenge, L. A. Galuska, Z. Qian, J. He, X. Gu and J. Mei, *ACS Appl. Polym. Mater.*, 2020, **2**, 2644–2650.

379 (*a*) M. Kawan, T. C. Hidalgo, W. Du, A.-M. Pappa, R. M. Owens, I. McCulloch and S. Inal, *Mater. Horiz.*, 2020, **7**, 2348–2358; (*b*) J. Chen, X. Zhuang, W. Huang, M. Su, L.-W. Feng, S. M. Swick, G. Wang, Y. Chen, J. Yu, X. Guo, T. J. Marks and A. Facchetti, *Chem. Mater.*, 2020, **32**, 5317–5326; (*c*) Y.-h. Shin, H. Komber, D. Caiola, M. Cassinelli, H. Sun, D. Stegerer, M. Schreiter, K. Horatz, F. Lissel, X. Jiao, C. R. McNeill, S. Cimò, C. Bertarelli, S. Fabiano, M. Caironi and M. Sommer, *Macromolecules*, 2020, **53**, 5158–5168; (*d*) L. A. Galuska, W. W. McNutt, Z. Qian, S. Zhang, D. W. Weller, S. Dhakal, E. R. King, S. E. Morgan, J. D. Azoulay, J. Mei and X. Gu, *Macromolecules*, 2020, **53**, 6032–6042.

380 P. Hao, H. Zhu, Y. Pang, J. Shen and Y. Fu, *CrystEngComm*, 2020, **22**, 3371–3377.

381 Y.-J. Wang, S.-Y. Wang, Y. Zhang, B. Xia, Q.-W. Li, Q.-L. Wang and Y. Ma, *CrystEngComm*, 2020, **22**, 5162–5169.

382 S. B. Schmidt, M. Hönig, Y. Shin, M. Cassinelli, A. Perinot, M. Caironi, X. Jiao, C. R. McNeill, D. Fazzi, T. Biskup and M. Sommer, *ACS Appl. Polym. Mater.*, 2020, **2**, 1954–1963.

383 S. J. Langford, M. J. Latter and C. P. Woodward, *Photochem. Photobiol.*, 2006, **82**, 1530–1540.

384 S. P. Adiga and D. Shukla, *J. Phys. Chem. C*, 2010, **114**, 2751–2755.

385 O. Atsuhiro, Z. Run-Ping, M. Kazuhiro, O. Takeshi and N. Koichi, *Bull. Chem. Soc. Jpn.*, 1993, **66**, 3773–3782.

386 U. Heinen, T. Berthold, G. Kothe, E. Stavitski, T. Galili, H. Levanon, G. Wiederrecht and M. R. Wasielewski, *J. Phys. Chem. A*, 2002, **106**, 1933–1937.

387 R. Bhosale, J. Míšek, N. Sakai and S. Matile, *Chem. Soc. Rev.*, 2010, **39**, 138–149.

388 M. Jaggi, B. Schmid, S.-X. Liu, S. V. Bhosale, S. Rivadehi, S. J. Langford and S. Decurtins, *Tetrahedron*, 2011, **67**, 7231–7235.

389 N. Banerji, S. V. Bhosale, I. Petkova, S. J. Langford and E. Vauthey, *Phys. Chem. Chem. Phys.*, 2011, **13**, 1019–1029.

390 D. Villamaina, S. V. Bhosale, S. J. Langford and E. Vauthey, *Phys. Chem. Chem. Phys.*, 2013, **15**, 1177–1187.

391 D. Villamaina, M. M. A. Kelson, S. V. Bhosale and E. Vauthey, *Phys. Chem. Chem. Phys.*, 2014, **16**, 5188–5200.

392 O. Yushchenko, R. V. Hangarge, S. Mosquera-Vazquez, S. V. Boshale and E. Vauthey, *J. Phys. Chem. B*, 2015, **119**, 7308–7320.

393 R. Schroot, T. Schlotthauer, M. Jäger and U. S. Schubert, *Macromol. Chem. Phys.*, 2017, **218**, 1600534.

394 (*a*) T. Schlotthauer, R. Schroot, S. Glover, L. Hammarström, M. Jäger and U. S. Schubert, *Phys. Chem. Chem. Phys.*, 2017, **19**, 28572–28578; (*b*) R. Schroot, T. Schlotthauer, B. Dietzek, M. Jäger and U. S. Schubert, *Chem. – Eur. J.*, 2017, **23**, 16484–16490.

395 S. Mendes Marinho, M.-H. Ha-Thi, V.-T. Pham, A. Quaranta, T. Pino, C. Lefumeux, T. Chamaillé, W. Leibl and A. Aukauloo, *Angew. Chem., Int. Ed.*, 2017, **56**, 15936–15940.

396 L. Favereau, A. Makhal, Y. Pellegrin, E. Blart, J. Petersson, E. Göransson, L. Hammarström and F. Odobel, *J. Am. Chem. Soc.*, 2016, **138**, 3752–3760.

397 N. T. La Porte, J. F. Martinez, S. Hedström, B. Rudshteyn, B. T. Phelan, C. M. Mauck, R. M. Young, V. S. Batista and M. R. Wasielewski, *Chem. Sci.*, 2017, **8**, 3821–3831.

398 J. F. Martinez, N. T. La Porte and M. R. Wasielewski, *J. Phys. Chem. C*, 2018, **122**, 2608–2617.

399 M. Skaisgirski, X. Guo and O. S. Wenger, *Inorg. Chem.*, 2017, **56**, 2432–2439.

400 A. L. Jones, M. K. Gish, C. J. Zeman, J. M. Papanikolas and K. S. Schanze, *J. Phys. Chem. A*, 2017, **121**, 9579–9588.

401 C. Thalacker, C. Röger and F. Würthner, *J. Org. Chem.*, 2006, **71**, 8098–8105.

402 J. Jiang, A. Alsam, S. Wang, S. M. Aly, Z. Pan, O. F. Mohammed and K. S. Schanze, *J. Phys. Chem. A*, 2017, **121**, 4891–4901.

403 N. T. La Porte, J. A. Christensen, M. D. Krzyaniak, B. K. Rugg and M. R. Wasielewski, *J. Phys. Chem. B*, 2019, **123**, 7731–7739.

404 N. T. La Porte, J. F. Martinez, S. Chaudhuri, S. Hedström, V. S. Batista and M. R. Wasielewski, *Coord. Chem. Rev.*, 2018, **361**, 98–119.

405 J. F. Martinez, N. T. La Porte, C. M. Mauck and M. R. Wasielewski, *Faraday Discuss.*, 2017, **198**, 235–249.

406 S. Goswami, J. N. Nelson, T. Islamoglu, Y.-L. Wu, O. K. Farha and M. R. Wasielewski, *Chem. Mater.*, 2018, **30**, 2488–2492.

407 N. F. Polizzi, M. J. Eibling, J. M. Perez-Aguilar, J. Rawson, C. J. Lanci, H. C. Fry, D. N. Beratan, J. G. Saven and M. J. Therien, *J. Am. Chem. Soc.*, 2016, **138**, 2130–2133.

408 V. Pirota, M. Nadai, F. Doria and S. N. Richter, *Molecules*, 2019, **24**, 426.

409 G. N. Parkinson, F. Cuenca and S. Neidle, *J. Mol. Biol.*, 2008, **381**, 1145–1156.

410 C. Marchetti, K. G. Zyner, S. A. Ohnmacht, M. Robson, S. M. Haider, J. P. Morton, G. Marsico, T. Vo, S. Laughlin-Toth, A. A. Ahmed, G. Di Vita, I. Pazitna, M. Gunaratnam, R. J. Besser, A. C. G. Andrade, S. Diocou, J. A. Pike, D. Tannahill, R. B. Pedley, T. R. J. Evans, W. D. Wilson, S. Balasubramanian and S. Neidle, *J. Med. Chem.*, 2018, **61**, 2500–2517.

411 M. Gunaratnam, G. W. Collie, A. P. Reszka, A. K. Todd, G. N. Parkinson and S. Neidle, *Bioorg. Med. Chem.*, 2018, **26**, 2958–2964.

412 S. T. G. Street, D. N. Chin, G. J. Hollingworth, M. Berry, J. C. Morales and M. C. Galan, *Chem. – Eur. J.*, 2017, **23**, 6953–6958.

413 S. Sato and S. Takenaka, *J. Inorg. Biochem.*, 2017, **167**, 21–26.

414 S. Sato, A. Kajima, H. Hamanaka and S. Takenaka, *J. Organomet. Chem.*, 2019, **897**, 107–113.

415 F. Doria, E. Salvati, L. Pompili, V. Pirota, C. D'Angelo, F. Manoli, M. Nadai, S. N. Richter, A. Biroccio, I. Manet and M. Freccero, *Chem. – Eur. J.*, 2019, **25**, 11085–11097.

416 M. Nadai, F. Doria, M. Scalabrin, V. Pirota, V. Grande, G. Bergamaschi, V. Amendola, F. R. Winnerdy, A. T. Phan, S. N. Richter and M. Freccero, *J. Am. Chem. Soc.*, 2018, **140**, 14528–14532.

417 M. Zuffo, S. Ladame, F. Doria and M. Freccero, *Sens. Actuators, B*, 2017, **245**, 780–788.
418 M. Zuffo, F. Doria, S. Botti, G. Bergamaschi and M. Freccero, *Biochim. Biophys. Acta, Gen. Subj.*, 1861, **2017**, 1303–1311.
419 M. Arévalo-Ruiz, F. Doria, E. Belmonte-Reche, A. De Rache, J. Campos-Salinas, R. Lucas, E. Falomir, M. Carda, J. M. Pérez-Victoria, J.-L. Mergny, M. Freccero and J. C. Morales, *Chem. – Eur. J.*, 2017, **23**, 2157–2164.
420 M. Zuffo, A. Guédin, E.-D. Leriche, F. Doria, V. Pirota, V. Gabelica, J.-L. Mergny and M. Freccero, *Nucleic Acids Res.*, 2018, **46**, e115.
421 F. Doria, M. Nadai, M. Zuffo, R. Perrone, M. Freccero and S. N. Richter, *Chem. Commun.*, 2017, **53**, 2268–2271.
422 D. Muoio, F. Berardinelli, S. Leone, E. Coluzzi, A. di Masi, F. Doria, M. Freccero, A. Sgura, M. Folini and A. Antoccia, *FEBS J.*, 2018, **285**, 3769–3785.
423 F. Doria, M. Nadai, G. Costa, G. Sattin, C. Gallati, G. Bergamaschi, F. Moraca, S. Alcaro, M. Freccero and S. N. Richter, *Eur. J. Org. Chem.*, 2016, 4824–4833.
424 C. Platella, M. Trajkovski, F. Doria, M. Freccero, J. Plavec and D. Montesarchio, *Nucleic Acids Res.*, 2020, **48**, 12380–12393.
425 X. Hao, C. Li, Y. Wang, F. Zhang, J. Hou, C. Kang and L. Gao, *Chem. Res. Chin. Univ.*, 2021, **37**, 795–800.
426 A. A. Ahmed and S. Neidle, *Molecules*, 2020, **25**, 5407.
427 Y.-L. Wu, N. E. Horwitz, K.-S. Chen, D. A. Gomez-Gualdron, N. S. Luu, L. Ma, T. C. Wang, M. C. Hersam, J. T. Hupp, O. K. Farha, R. Q. Snurr and M. R. Wasielewski, *Nat. Chem.*, 2017, **9**, 466–472.
428 E. Salvati, F. Doria, F. Manoli, C. D'Angelo, A. Biroccio, M. Freccero and I. Manet, *Org. Biomol. Chem.*, 2016, **14**, 7238–7249.
429 A. Pasini, C. Marchetti, C. Sissi, M. Cortesi, E. Giordano, A. Minarini and A. Milelli, *ACS Med. Chem. Lett.*, 2017, **8**, 1218–1223.
430 X. Xu, S. Wang, Y. Chang, C. Ge, X. Li, Y. Feng, S. Xie, C. Wang, F. Dai and W. Luo, *MedChem. Commun.*, 2018, **9**, 1377–1385.
431 S. K. Gurung, S. Dana, K. Mandal, P. Mukhopadhyay and N. Mondal, *Chem.-Biol. Interact.*, 2019, **304**, 106–123.
432 E. Belmonte-Reche, M. Martínez-García, A. Guédin, M. Zuffo, M. Arévalo-Ruiz, F. Doria, J. Campos-Salinas, M. Maynadier, J. J. López-Rubio, M. Freccero, J.-L. Mergny, J. M. Pérez-Victoria and J. C. Morales, *J. Med. Chem.*, 2018, **61**, 1231–1240.
433 M. Zuffo, A. Stucchi, J. Campos-Salinas, M. Cabello-Donayre, M. Martínez-García, E. Belmonte-Reche, J. M. Pérez-Victoria, J. L. Mergny, M. Freccero, J. C. Morales and F. Doria, *Eur. J. Med. Chem.*, 2019, **163**, 54–66.
434 A. Sikder, J. Sarkar, R. Barman and S. Ghosh, *J. Phys. Chem. B*, 2019, **123**, 7169–7177.
435 A. Sikder, D. Ray, V. K. Aswal and S. Ghosh, *Langmuir*, 2018, **34**, 868–875.
436 T.-T. Li, Y.-M. Liu, T. Wang and S.-R. Zheng, *Inorg. Chem. Commun.*, 2017, **84**, 5–9.
437 J.-J. Liu, S.-B. Xia, Y.-L. Duan, T. Liu, F.-X. Cheng and C.-K. Sun, *Polymers*, 2018, **10**, 165.
438 F. Wei, Y. Ye, W. Huang, Q. Lin, Z. Li, L. Liu, S. Chen, Z. Zhang and S. Xiang, *Inorg. Chem. Commun.*, 2018, **93**, 105–109.
439 J. He, Q. Han, J. Li, Z. Shi, X. Shi and J. Niu, *J. Catal.*, 2019, **376**, 161–167.
440 J. Park, J. Bae, K. Jin and J. Park, *J. Hazard. Mater.*, 2019, **371**, 243–252.
441 M.-L. Wang, C. Fu, L. Li and H. Zhang, *Inorg. Chem. Commun.*, 2018, **94**, 142–145.
442 S. Furukawa and J. Ashburne, *Chem*, 2016, **1**, 186–188.
443 Z. Guo, D. K. Panda, M. A. Gordillo, A. Khatun, H. Wu, W. Zhou and S. Saha, *ACS Appl. Mater. Interfaces*, 2017, **9**, 32413–32417.
444 P. M. Usov, C. F. Leong, B. Chan, M. Hayashi, H. Kitagawa, J. J. Sutton, K. C. Gordon, I. Hod, O. K. Farha, J. T. Hupp, M. Addicoat, A. B. Kuc, T. Heine and D. M. D'Alessandro, *Phys. Chem. Chem. Phys.*, 2018, **20**, 25772–25779.
445 E. Castaldelli, K. D. G. Imalka Jayawardena, D. C. Cox, G. J. Clarkson, R. I. Walton, L. Le-Quang, J. Chauvin, S. R. P. Silva and G. J.-F. Demets, *Nat. Commun.*, 2017, **8**, 2139.
446 B. A. Johnson, A. Bhunia, H. Fei, S. M. Cohen and S. Ott, *J. Am. Chem. Soc.*, 2018, **140**, 2985–2994.
447 Y. Ye, R.-B. Lin, H. Cui, A. Alsalme, W. Zhou, T. Yildirim, Z. Zhang, S. Xiang and B. Chen, *Dalton Trans.*, 2020, **49**, 3658–3661.
448 J.-J. Liu, Y.-B. Shan, C.-R. Fan, M.-J. Lin, C.-C. Huang and W.-X. Dai, *Inorg. Chem.*, 2016, **55**, 3680–3684.
449 Z. Li, J. Guo, F. Xiang, Q. Lin, Y. Ye, J. Zhang, S. Chen, Z. Zhang and S. Xiang, *CrystEngComm*, 2018, **20**, 7567–7573.
450 W.-J. Xu, K.-P. Chen, Y. Zhang, Y. Ma, Q.-W. Li and Q.-L. Wang, *J. Mol. Struct.*, 2021, **1231**, 129948.
451 J. Li, B. Chang, H. Zhao, Q. Meng, M. Li and Q. Han, *J. Mater. Sci.*, 2021, **56**, 6676.
452 Y. B. N. Tran and P. T. K. Nguyen, *New J. Chem.*, 2021, **45**, 2090–2102.
453 G.-B. Li, J.-H. Shi, R.-K. Pan and S.-G. Liu, *Inorg. Nano-Met. Chem.*, 2017, **47**, 1017–1022.
454 B. Thomas, J. Rombouts, G. T. Oostergetel, K. B. S. S. Gupta, F. Buda, K. Lammertsma, R. Orru and H. J. M. de Groot, *Chem. – Eur. J.*, 2017, **23**, 3280–3284.
455 B. R. Reiner, B. M. Foxman and C. R. Wade, *Dalton Trans.*, 2017, **46**, 9472–9480.
456 D. Frath, V. Q. Nguyen, F. Lafolet, P. Martin and J.-C. Lacroix, *Chem. Commun.*, 2017, **53**, 10997–11000.
457 C. Li, Z. Wei, M. Pan, H. Deng, J. Jiang and C. Su, *Chin. Chem. Lett.*, 2019, **30**, 1297–1301.
458 X. Li, J. Yang, Z. Song, R. Chen, L. Ma, H. Li, J. Jia, J. Meng, X. Li, M. Yi and X. Sun, *ACS Appl. Energy Mater.*, 2018, **1**, 4467–4472.
459 (*a*) J.-Z. Liao, L. Meng, J.-H. Jia, D. Liang, X.-L. Chen, R.-M. Yu, X.-F. Kuang and C.-Z. Lu, *Chem. – Eur. J.*, 2018, **24**, 10498–10502; (*b*) X.-Y. Wu, H.-L. Zhang, S.-S. Wang, W. Wu, L. Lin, X.-Y. Jiang and C.-Z. Lu, *Dalton Trans.*, 2020, **49**, 3408–3412.

460 M.-H. You, M.-H. Li, Y.-F. Liu, H.-H. Li and M.-J. Lin, *CrystEngComm*, 2019, **21**, 6688–6692.
461 M.-H. You, M.-H. Li, Y.-M. Di, Y.-W. Wang and M.-J. Lin, *Dyes Pigm.*, 2020, **173**, 107943.
462 S. A. Boer and D. R. Turner, *CrystEngComm*, 2017, **19**, 2402–2412.
463 S. A. Boer, R. P. Cox, M. J. Beards, H. Wang, W. A. Donald, T. D. M. Bell and D. R. Turner, *Chem. Commun.*, 2019, **55**, 663–666.
464 S. P. Black, D. M. Wood, F. B. Schwarz, T. K. Ronson, J. J. Holstein, A. R. Stefankiewicz, C. A. Schalley, J. K. M. Sanders and J. R. Nitschke, *Chem. Sci.*, 2016, **7**, 2614–2620.
465 J. J. Liu, T. Liu and C. C. Huang, *Acta Crystallogr., Sect. C: Struct. Chem.*, 2017, **73**, 437–441.
466 G.-B. Li, B.-Q. Song, S.-Q. Wang, L.-M. Pei, S.-G. Liu, J.-L. Song and Q.-Y. Yang, *ACS Omega*, 2019, **4**, 1995–2000.
467 Y. Zhao, Y. Cotelle, L. Liu, J. López-Andarias, A.-B. Bornhof, M. Akamatsu, N. Sakai and S. Matile, *Acc. Chem. Res.*, 2018, **51**, 2255–2263.
468 X. Zhang, X. Hao, L. Liu, A.-T. Pham, J. López-Andarias, A. Frontera, N. Sakai and S. Matile, *J. Am. Chem. Soc.*, 2018, **140**, 17867–17871.
469 C. Wang and S. Matile, *Chem. – Eur. J.*, 2017, **23**, 11955–11960.
470 M.-H. Li, Y.-M. Di, Y.-W. Wang, M.-H. You and M.-J. Lin, *Dyes Pigm.*, 2021, **187**, 109146.
471 J.-J. Liu, S.-B. Xia, T. Liu, C.-X. He, H. Suo and J. Liu, *J. Solid State Chem.*, 2021, **295**, 121900.
472 D. Gust, T. A. Moore and A. L. Moore, *Acc. Chem. Res.*, 2009, **42**, 1890–1898.
473 Y. Tachibana, L. Vayssieres and J. R. Durrant, *Nat. Photonics*, 2012, **6**, 511–518.
474 A. Monti, J. M. de Ruiter, H. J. M. de Groot and F. Buda, *J. Phys. Chem. C*, 2016, **120**, 23074–23082.
475 Y. Shao, J. M. de Ruiter, H. J. M. de Groot and F. Buda, *J. Phys. Chem. C*, 2019, **123**, 21403–21414.
476 S. A. Bhat, C. Das and T. K. Maji, *J. Mater. Chem. A*, 2018, **6**, 19834–19842.
477 B. Reiß and H.-A. Wagenknecht, *Beilstein J. Org. Chem.*, 2019, **15**, 2043–2051.

